THE GEOCHEMISTRY OF THE RONEVAL ANORTHOSITE, SOUTH HARRIS, SCOTLAND

by

Graham John Witty B.Sc. (London)

A thesis submitted for the degree
of Doctor of Philosophy in the
University of London

Royal School of Mines,
Imperial College
LONDON, S.W.7.

June 1975

Abstract

The Roneval anorthosite complex forms a wedge-shaped mass of approximately 9.5 Km^2 within the Lewisian of South Harris. The anorthosite complex can be described in terms of a central layered anorthosite body and a narrow partially layered gabbroic envelope. The gabbroic envelope of the complex is thought to represent an early sill-like intrusion, parts of which have assimilated considerable amonts of the quartzose paragneisses into which the body was intruded. The central anorthosite represents a later basin or sill-like intrusion. The overall structure of the complex is that of a large isoclinal syncline, the anorthosite forming the observed core to this fold.

The whole-rock XRF analyses of the layered rocks of the anorthosite complex indicate that they are the differentiation products of two basaltic magmas. The differentiation patterns have been studied using Pearce variation diagrams. In the case of the anorthosite body the results demonstrate that the sequence of layered rocks present can be ascribed to the fractional crystallization of plagioclase feldspar (plus clinopyroxene in the lowest part of the intrusion) from a high-alumina calc alkalic parent magma. The chemistry of the layered rocks of the gabbroic envelope (the banded ultramafites and mafic gabbros) can be ascribed to the fractional crystallization of plagioclase feldspar, clinopyroxene and ilmenite from a basic alkalic magma. It is emphasised that all of these rocks have been thoroughly recrystallized by high grade regional metamorphism. The fact that igneous differentiation trends can still be found within these rocks suggests that metamorphism has been isochemical, both on the scale of the complex and also on the scale of individual layers within it.

Three major rock suites are recognized in the Outer Hebrides. Rocks of alkalic and high-alumina calc alkalic type are present in southern South Harris, and throughout the remainder of the Outer Hebrides and the Scottish mainland tholeiitic 'Scourie dykes' are abundant. The significance of this association and its bearing upon the interpretation of South Harris as an Archean arc system is discussed.

List of Contents

	Page
Abstract	1
List of Contents	2
List of Figures	5
List of Tables	9
List of Plates	11
Acknowledgement	14
Chapter 1 Introduction	
1.1 General features of the Lewisian complex... ...	16
1.2 A brief historical account of the geological investigations into the anorthosite complex and associated meta-igneous rocks of South Harris ...	19
1.3 Geological investigations into the economic potential of the South Harris anorthosite body...	24
1.4 Igneous rock terminology	25
1.5 The rock types of southern South Harris - An introduction	28
1.6 Methods of study...	31
1.7 Format	32
Chapter 2 The Anorthosite Complex	
2.1 General introduction	34
2.2 The anorthosite	35
2.2.1 Mineralogical and textural variations within the anorthosite	38
2.2.2 The lower zone of banded anorthosites.. ...	50
2.2.3 The middle zone of banded anorthosites ...	59
2.2.4 The Upper zone of schlieren anorthosites ...	62
2.2.5 Saussuritised anorthosite..	67
2.2.6 Crushed and saussuritised anorthosite.. ...	69
2.2.7 Summary..	69
2.3 The gabbroic rim of the anorthosite..	72
2.3.1 Banded ultramafites and mafic gabbros.. ...	74
(1) Field relations..	74
(2) Petrology..	77
(i) Ultramafite units..	80
(ii) Mafic gabbro units	82
(iii) Mineral assemblages	85
(3) Epidote veining..	90
2.3.2 The quartz gabbros...	93
2.3.3 Summary..	96
2.4 Minor intrusives...	97
2.4.1 Ultramafic and mafic gabbro dykes and sheets.	97

Page

2.4.2 Hornblendite intrusions 99

(1) Hornblendite dykes 99
(2) Hornblendite lenses 100

2.4.3 Breccias and associated minor ultramafic and anorthositic intrusions from the anorthosite/quartz gabbro contact 100

(1) Type 'A' breccias 104

(i) Description of the brecciated area north-east of the Abhainn Easean Chais stream 104
(ii) Petrology of the ultramafites.. ... 108
(iii) Origin of type 'A' breccias 108

(2) Type 'B' breccias 110
(3) Summary 113

2.4.4 Anorthositic-gabbro dykes and trondhjemitic pegmatites 115
2.4.5 Unmetamorphosed basic dykes 120

Chapter 3 The Meta-Igneous Rocks Associated with the Anorthosite Complex

3.1 Introduction 123
3.2 The gabbro-diorite 125

3.2.1 Field relations 125
3.2.2 Petrology 130

3.3 The norite... 130

3.3.1 Field relations 130
3.3.2 Petrology 132

3.4 Mafic gabbro sheets 133

3.4.1 Field relations 133
3.4.2 Petrology 133

3.5 Ultramafite lenses in the Langavat meta-sedimentary belt 134
3.6 Ultramafite lenses in the Leverburgh meta-sedimentary belt 136

3.6.1 Peridotites 136
3.6.2 Pyroxenites 137

3.7 Pyroxenite dykes... 138
3.8 History of igneous intrusive activity in southern South Harris 143

Chapter 4 The Structural and Metamorphic History of the Anorthosite Complex

4.1 The regional structure of the Outer Hebrides ... 146
4.2 The structure of the anorthosite complex - An introduction 146
4.3 F_1 deformation 148

4.3.1 The relationship of early gabbroic dykes to the F_1 deformation... 157

4.4 Pre-F_1 banding 160
4.5 Folding of the anorthosite complex (F_2 deformation).. 165

Page

4.6 F_3 deformation (early Laxfordian?)... 166
4.7 F_4 deformation (late Laxfordian?) 167
4.8 The coastal thrusting 170
4.9 F_5 deformation (Tertiary) 177
4.10 The metamorphism of the anorthosite complex - An introduction 177
4.11 M_1 metamorphism 178
4.12 M_2 metamorphism 181
4.13 M_3 metamorphism 182
4.14 Summary 183

Chapter 5 The Geochemistry of the Anorthosite Complex and of the associated meta-igneous rocks

5.1 General introduction 189
5.2 Aims of geochemical study 190
5.3 General chemistry of the anorthosite complex ... 193
5.3.1 The anorthosite 193
5.3.2 The banded ultramafites and mafic gabbros ... 205
5.3.3 The quartz gabbros... 205
5.4 Metamorphism of the anorthosite complex 209
5.5 The differentiation of the anorthosite complex... 217
5.6 General chemistry of the South Harris igneous rocks 257
5.7 The significance of the meta-igneous rock suites of South Harris 271

Chapter 6 Mineral Geochemistry of the Anorthosite Complex and associated meta-igneous rocks

6.1 General introduction 275
6.2 Clinopyroxenes 276
6.3 Orthopyroxenes 282
6.4 Garnets 286
6.5 Amphiboles... 293
6.5.1 Classification of the amphiboles 295
6.5.2 Element variations within the amphiboles ... 301
6.6 Plagioclase feldspars 305
6.7 Epidotes 310
6.8 Chemical distributions between co-exisiting minerals 310

Summary and Conclusions 318

References 321

Appendix 1 - Whole-rock and mineral analyses 328

Appendix 2 - Sample localities for analysed rocks ... 393

List of Figures

		Page
1.1	Geological map of southern South Harris...	29
1.2	The relative proportions of the main rock types exposed in southern South Harris	30
2.1	The anorthosite complex	36
2.2	Lower zone banded anorthosite, west slope of Ha-Cleit	51
2.3	Lower zone banded anorthosite, measured section Y-Z, mineral assemblages	55
2.4	The gabbroic rim of the anorthosite complex	73
2.5	Diagramatic sections across the contacts of the ultramafite/mafic gabbro pods	76
2.6	Banded ultramafites and mafic gabbros, Abhainn Easean Chais pod..	78
2.7	Measured sections from the Abhainn Easean Chais ultramafite/mafic gabbro sequence...	79
2.8	Banded ultramafites and mafic gabbros, measured section A-B, mineral assemblages	91
2.9	Breccias and associated ultramafite and anorthosite intrusions, north-east end of anorthosite complex ...	101
3.1	Pyroxenite dyke, 600 metres E.N.E. of Rudh'an Teampuill...	140
3.2	Mineralization of pyroxenite dyke...	141
4.1	Schematic map illustrating the arrangement of Laxfordian antiforms and synforms in the Outer Hebrides ...	147
4.2	Composite diagram illustrating the effects of the F_1^1 plastic deformation and the F_1^2 brittle deformation ..	154
4.3	The distribution of foliations and banding in the north-eastern part of the anorthosite complex... ...	158
4.4	The disposition of the compositional banding in the ultramafites and mafic gabbros of the Abhainn Easean Chais pod...	162
4.5	The distribution of major shears and faults effecting the rocks at the north-eastern end of the anorthosite complex	168
4.6	Rose diagrams illustrating the predominant trends of (a) the early Laxfordian shears; (b) the late Laxfordian shears; and (c) the Tertiary faults	169
4.7	The coastal thrust zone in the anorthosite complex ...	171
4.8	The thrust zone,360 metres south-east of Loch Na H-uamh	172
4.9	An interpretation of the overall structure of southern South Harris.	185
4.10	Block-diagram to illustrate the style of folding within and adjacent to the anorthosite complex...	186
5.1	AFM projections for the rocks of the anorthosite complex	194
5.2	Oxide variation diagram for two gravity stratified units from the lower zone banded 'anorthosites' (measured section Y-Z)	199
5.3	Variation of normative molecules, within a single gravity stratified unit from the lower zone banded 'anorthosites'	201

		Page
5.4	Variation of normative molecules, within a single gravity stratified unit (continued).	202
5.5	Variation of total iron as FeO/total iron as FeO+ MgO with structural height, for the rocks of the anorthosite body	204
5.6	AFM projection to demonstrate the chemical effects of assimilation of the quartzose paragneisses by the meta-igneous rocks of the anorthosite complex... ...	206
5.7	The relation between wt% Na_2O and wt% SiO_2 for the banded ultramafites/mafic gabbros, quartz gabbros and quartzose paragneisses from the gabbroic rim of the anorthosite complex	207
5.8	The relation between the total modal % garnet + amphibole and the % difference between total normative feldspar and modal feldspar, for the analysed samples from gravity stratified units 2 & 3	211
5.9	The contrast between :- A the observed variation in rock type within a single gravity stratified unit (unit 3) based on the modal mafic index; and B the original (pre-metamorphic) variation in rock type based on the normative mafic index..	215
5.10	Harker variation diagrams (A-F) for the rocks of the anorthosite complex	219
5.11	Harker variation diagrams (G-L) for the rocks of the anorthosite complex	220
5.12	(a) CaO : SiO_2 and (b) Al_2O_3 : SiO_2 iron ratio diagrams (molecular) for those rocks of the anorthosite sequence which contain 80% or more normative feldspar	229
5.13	(a) Na_2O : SiO_2 and (b) K_2O : SiO_2 iron ratio diagrams (molecular) for those rocks of the anorthosite sequence which contain 80% or more normative feldspar.	230
5.14	(a) FeO + MgO : SiO_2 and (b) MgO : SiO_2 potash ratio diagrams (molecular) for all the rocks of the anorthosite sequence	234
5.15	MnO : SiO_2 potash ratio diagram (molecular) for all the rocks of the anorthosite sequence	235
5.16	TiO_2 : SiO_2 potash ratio diagram (molecular) for all rocks of the anorthosite sequence...	236
5.17	Al_2O_3 : SiO_2 potash ratio diagram (molecular) for all the rocks from the anorthosite sequence	238
5.18	Na_2O : SiO_2 potash ratio diagram (moelcular) for all the rocks from the anorthosite sequence...	239
5.19	The theoretical variation of absolute amounts of CaO and SiO_2 during fractionation of plagioclase feldspar from the liquid pm. (-the parent magma for the anorthosite)	243
5.20	A. The variation in absolute amounts of CaO and SiO_2 in unit 3 from the base of the lower zone of the anorthosite sequence. B. An interpretation of the rock types from unit 3	245
5.21	MgO : SiO_2 potash ratio diagram (molecular) for the banded ultramafites and mafic gabbros from the gabbroic rim of the anorthosite complex	247
5.22	FeO + MgO : SiO_2 potash ratio diagram (molecular) for the banded ultramafites and mafic gabbros from the gabbroic rim of the anorthosite complex...	248
5.23	TiO_2 : SiO_2 potash ratio diagram (molecular) for the banded ultramafites and mafic gabbros from the gabbroic rim of the anorthosite complex...	249
5.24	CaO : SiO_2 potash ratio diagram (molecular) for the banded ultramafites and mafic gabbros from the gabbroic rim of the anorthosite complex...	251

Page

5.25 Na_2O : SiO_2 potash ratio diagram (molecular) for the banded ultramafites and mafic gabbros from the gabbroic rim of the anorthosite complex... 254
5.26 Al_2O_3 : SiO_2 potash ratio diagram (molecular) for the banded ultramafites and mafic gabbros from the gabbroic rim of the anorthosite complex... 255
5.27 AFM projection for the rocks of the South Harris igneous suite 259
5.28 AFM projection of the South Harris igneous rocks. Only those rocks from the anorthosite which are thought to approximate in composition to the parent magma, are plotted on this projection 262
5.29 Weight % Al_2O_3 vs. An/An + Ab for the calc-alkalic and tholeiitic rock types from South Harris 264
5.30 Distribution of normative feldspar compositions for the South Harris meta-igneous rocks. 266
5.31 Differentiation index variation diagrams for the rocks of the anorthosite complex, the gabbro-diorite and the norite... 268
5.32 Differentiation index variation diagrams for the rocks of the anorthosite complex, the gabbro-diorite and the norite (continued).. 269

6.1 Compositions of pyroxenes, plotted on the En - Fs - Wo triangle 277
6.2 Major element variations across two clinopyroxene grains 278
6.3 The relation between the ferrosilite (Fs) component of the clinopyroxenes and wt% a)CaO; b)TiO_2 and c)Na_2O... 280
6.4 Plot of mol % jadeite against Tschermaks molecule for the South Harris clinopyroxenes 281
6.5 (a) - the relation between the atomic ratio Fe/Fe + Mg of the clinopyroxenes and their respective host rocks.
(b) - the relation between the atomic ratio Fe/Fe + Mg of the orthopyroxenes and their respective host rocks. 283
6.6 (a) - the relation between wt% CaO and wt% FeO in the orthopyroxenes.
(b) - the relation between wt% FeO + MgO and Al_2O_3 in the orthopyroxenes 284
6.7 Garnets from the anorthosite complex, plotted in terms of their three major end member molecules : pyrope, almandine and grossular 288
6.8 Major element variations across individual garnet grains 289
6.9 (a) - the relation between the atomuc ratio Fe/Fe + Mg of the garnets and their respective host rocks.
(b) - the relation between the atomic ratio Fe/Fe + Mg of the amphiboles and their respective host rocks.. 292
6.10 Classification of the amphiboles with respect to the diagram given by Leake (1968) 296
6.11 Classification of the amphiboles with respect to the number of tetrahedral Al and (Na+K) atoms (after Deer et al., 1963) 298
6.12 Classification of the amphiboles with respect to a diagram given by Ernst (1968) and modified by Windley and Smith (1974) 300
6.13 (a) - the relation between wt% SiO_2 and Al_2O_3 in the amphiboles.
(b) - the relation between wt% MgO and FeO in the amphiboles 302

Page

6.14 The relation between wt% FeO and MnO in the amphiboles.. 303

6.15 (a) - the relation between wt% Cr_2O_3 and FeO in the amphiboles.
(b) - the relation between wt% TiO_2 and FeO in the amphiboles.. 304

6.16 The relation between wt% Fe_2O_3, Al_2O_3 and retardation (estimated from interference colours) in the epidotes... 311

6.17 Distribution of iron and magnesium (expressed as the atomic ratio Fe/Fe + Mg) between orthopyroxene, clinopyroxene and garnet, with respect to co-existing amphibole... 313

6.18 The relation between Al, Cr, Ti and Mn atoms in the clinopyroxenes, orthopyroxenes, garnets and co-existing amphiboles 316

List of Tables

		Page
1.1	Regional Lewisian chronology - Hebrides and mainland	17
1.2	Igneous rock terminology...	26
1.3	Equivalence of igneous rock terminology used in this work, with that of earlier workers	27
2.1	Summary of mineralogical and textural variations, with respect to structural environment, within the anorthosite body	48
2.2	Summary of the petrology and mineralogy of the anorthosite. The mineralogical data in this table summarizes the variations shown by the early (M_1) granulite facies minerals	49
2.3	Basic unmetamorphosed dykes from the anorthosite complex..	121
3.1	Proposed intrusive history of the South Harris igneous rock types, with particular reference to the anorthosite complex...	144
4.1	The relations between the F_1 deformational events, early basic intrusives and migmatization in the anorthosite	156
4.2	Proposed sequence of events for the coastal thrust zone	176
4.3	A geological history for southern South Harris ...	184
5.1	Key to symbols used in plots of rock data	192
5.2	Averaged analyses of the main rock types of the anorthosite complex	195
5.3	Correlation coefficients for oxides from the rocks of the anorthosite complex. A - the anorthosites; B - the banded ultramafites and mafic gabbros ...	218
5.4	Gradients of regression lines and correlation coefficients of the potash, iron and magnesia molecular ratios calculated for the anorthosites and banded ultramafites and mafic gabbros..	225
5.5	A - element ratios for two theoretical, stoichiometric, bytownite feldspars B - average element ratios of the analysed clinopyroxenes and orthopyroxenes from the mafic gabbros at the base of the lower zone of the anorthosite sequence	232
5.6	Chemical variations due to the fractionation and removal of plagioclase crystals..	241
5.7	Chemical variations due to the fractionation and accumulation of plagioclase crystals - plagioclase cumulate rocks	242
5.8	Average element ratios of the analysed clinopyroxenes and plagioclase feldspar from the banded ultramafites and mafic gabbros..	252

Page

5.9 Summary of phases controlling crystallization in the differentiated rock types of the anorthosite complex.. 258

6.1 The compositions of the analysed plagioclase feldspars from the rocks of the anorthosite complex ... 307
6.2 Non-stoichiometry in the analysed plagioclase feldspars 309
6.3 A - The distribution of Mg and Fe^{2+} between co-existing pyroxenes
B - Temperature estimates from co-existing pyroxenes, using the method of Wood and Banno (1973) 315

List of Plates

		Page
2.1	Plagioclase feldspar; showing straight or gently curved grain boundaries and triple point junctions...	41
2.2	Plagioclase feldspar; showing highly sutured grain boundaries..	41
2.3	Mortar texture	42
2.4	Myrmekite developing along plagioclase - plagioclase grain boundaries..	42
2.5	Myrmekite developing along plagioclase - clinopyroxene grain boundary...	43
2.6	Polygonal texture.	43
2.7	Amphibole - plagioclase feldspar - magnetite symplectite after M_1 garnet	45
2.8	Symplectite rimmed by zones of magnetite granules ...	45
2.9	Hornblende - clinozoisite aggregate after M_1 clinopyroxene	46
2.10	Hornblende - clinozoisite - plagioclase aggregate; mafic schlieren from an upper zone anorthosite.. ...	46
2.11	Gabbro with mafic gabbro horizons; base of lower zone, 120 metres east of Loch na Cachlaidh	53
2.12	23cm. mafic gabbro horizon; base of lower zone, 270 metres south-west of Ha-Cleit summit...	53
2.13	Orthopyroxene - bearing mafic gabbro horizon; 95 metres above base of lower zone, west slope of Ha-Cleit	57
2.14	Banded gabbroic anorthosite; base of lower zone ...	57
2.15	Diffuse amphibole - clinopyroxene band from gabbroic anorthosite; base of lower zone	58
2.16	Clinopyroxene band from gabbroic anorthosite; top of lower zone	58
2.17	Gabbro; 85 metres above base of middle zone	61
2.18	Gabbro; 340 metres above base of middle zone	61
2.19	Schlieren anorthosite; upper zone, 160 metres W.S.W. of the anorthosite quarry	65
2.20	Schlieren anorthosite; upper zone, 320 metres N.E. of Beinn na H-aire	65
2.21	Schlieren anorthosite; upper zone, 310 metres east of Beinn na H-aire	65
2.22	Schlieren anorthosite; upper zone, 10 metres south-west of the anorthosite quarry	65
2.23	Schlieren anorthosite; upper zone, 730 metres north of Loch na Cachlaidh	65
2.24 2.25 2.26	Examples of the interbanding of mafic gabbro and ultramafite, from the lower portions of several mafic gabbro units: Abhainn Easean Chais pod, S.W. flank of anorthosite complex	84
2.27	270cm. mafic gabbro layer, sandwiched between two ultramafite horizons; base of mafic gabbro unit. ...	86
2.28	Mafic gabbro, showing the development of large circular xenoblastic garnets...	86
2.29	Opaque iron oxide inclusions in M_1 amphibole	88
2.30	Rutile inclusions in M_1 garnet	89
2.31	Garnet - clinopyroxene intergrowth..	89
2.32	Interbanding of paragneiss and banded ultramafite/mafic gabbro; 136 metres north-west of Ha-Cleit summit	92

		Page
2.33	Epidote veins cutting the banded ultramafites and mafic gabbros, 110 metres W.N.W. Ha-Cleit summit ...	92
2.34 2.35 2.36 2.37	Brecciated blocks of foliated and banded gabbroic anorthosite within a massive ultramafite matrix; type 'A' breccia	102 & 103
2.38 2.39	Modified type 'A' breccias	107
2.40	Anorthosite and ultramafite xenoliths in a massive anorthosite matrix; type 'B' breccia	111
2.41	Finely banded anorthosite xenolith in a massive anorthosite matrix; type 'B' breccia	111
2.42	Xenolithic block of foliated quartz gabbro, intruded by anorthosite; type 'B' breccia	114
2.43	Xenolithic block of foliated quartz gabbro, intruded by anorthosite; type 'B' breccia	114
2.44 2.45 2.46	Sequence of plates showing the progressive deformation of a type 'A' breccia	116
2.47	Anorthositic-gabbro dyke; cutting a lower zone gabbro.	119
2.48	Anorthositic-gabbro dyke (enlargement)	119
2.49	Anorthositic-gabbro dyke; cutting a banded ultramafite	119
2.50	Gismondine	122
3.1	Ultramafite net veining gabbro-diorite	129
3.2	Mafic gabbro/ultramafite net veining gabbro-diorite...	129
3.3	Dendritic pyrrhotite	142
3.4	Pyrrhotite rimming euhedral pyrite..	142
4.1 4.2 4.3	Photo-mosaics: contorted and migmatised anorthositic gabbros and gabbros from the lower zone of the anorthosite sequence	151 152 153
4.4	F_1^1 intrafolial fold	155
4.5	Banded gabbro sequence injected by quartzo-feldpathic veins...	155
4.6	Early D_1 gabbroic dyke showing the development of an F_1 foliation	159
4.7	Early D_1 gabbroic dyke involved in an F_1^1 fold.. ...	159
4.8	Zone of flinty crush rock (pseudotachylite) lining a subsiduary thrust plane	173
4.9	Vein of flinty crush rock (pseudotachylite) intruding hornblendite	173
4.10	Xenolithic strip of saussuritised anorthosite in hornblendite	174
4.11	Fine anastomosing shears developed throughout the hornblendites	174

Loose Maps in Back Pocket:

Map 1 The anorthosite complex; north-east of Roneval (1:5000)

Map 2 The anorthosite complex; east and south-east of Ha-Cleit summit (1:88)

Map 3 800 metre section of the gabbroic rim of the anorthosite complex; north-east of the Abhainn Easean Chais (1:88)

Map 4 The anorthosite; sample localities on the east and south-east slopes of Ha-Cleit (1:88)

Acknowledgements

I would like to thank Dr. Gloria Borley who supervised this research project and criticised the final manuscript.

My thanks go also to the following:

Mr. & Mrs. Macleod of Dunmore Crescent, Leverburgh for their hospitality during field-work;

Mr. A. Hill, Mr. J. Bullen and Mr. D. Bailey for technical assistance;

Mr. J. Blount and Mr. J. Maddox for thin section preparation;

Mr. J. Gee and Mrs. H. Richardson for photographic services;

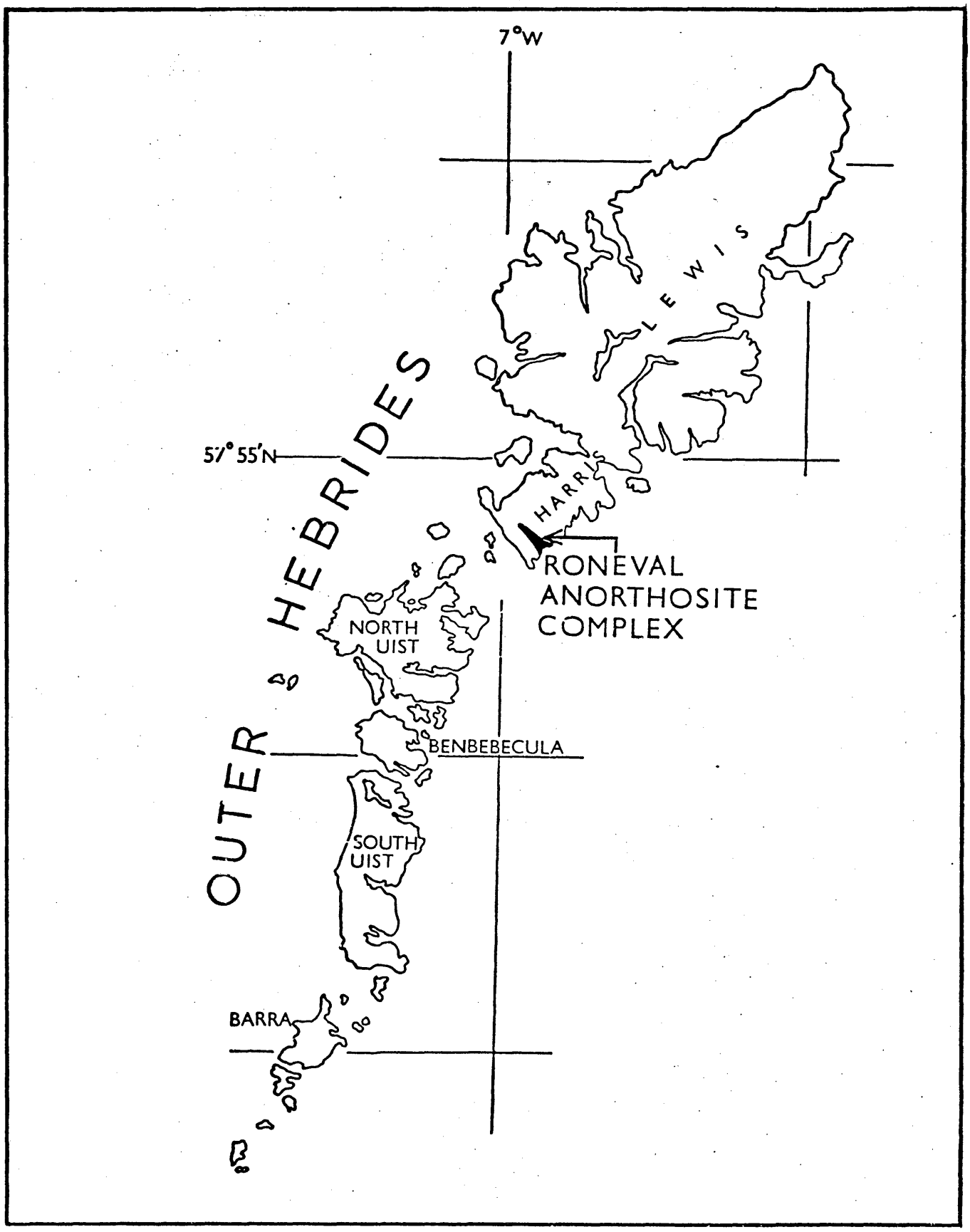
Miss S. Witty for typing the final script;

Mr. Paul Suddaby for his help with operating the microprobe and to Dr. Janet Watson and Mr. Alan Heyes for many helpful discussions.

I would like to thank Robertson Research and Powell Duffrhyn Limited, for their permission to inspect reports, maps and borehole core relating to the anorthosite.

This work was undertaken during the tenure of a NERC Research Studentship, which I gratefully acknowledge.

I would also like to thank my wife for her financial support which enabled me to complete this thesis.


7°W
LEWIS
HARRIS
57° 55'N
OUTER HEBRIDES
RONEVAL
ANORTHOSITE
COMPLEX
NORTH
UIST
BENBECULA
SOUTH
UIST
BARRA

CHAPTER 1

INTRODUCTION

1.1 General Features of the Lewisian Complex

It was first noted by Dearnley* that the Lewisian of the Outer Hebrides was the product of cyclic reworking. An early phase of Scourian gneiss formation (approximately 2800 million years) was characterised by widespread granulitic facies metamorphism. The term Badcallian has been proposed by Park (1970) for this early part of the Scourian. On a regional scale the most obvious structural features were produced during a period of regeneration following the early gneiss-forming period. This Laxfordian tectonic and metamorphic regeneration continued until about 1600 to 1500 million years ago and was responsible for the development of new mineral assemblages, mainly of amphibolite facies. The main Laxfordian series of events was preceded by the intrusion of a swarm of basic dykes, the Scourie dykes, which were variously affected by subsequent Laxfordian reworking. Granite injection and migmatization occurred in both the Scourian and Laxfordian.

Evans (1965) and Tarney (1964) have established the occurrence of a pre-Scourie dyke amphibolite facies metamorphism and associated major folding affecting the Scourian gneisses near Lochinver (Scottish mainland). This event has been termed the Inverian and has been given the status of an orogeny by Bowes (1968). The Inverian metamorphism has been dated at 2200 million years, by Evans (1965).

The principle rock groups observed in the Outer Hebrides are:-

a) Narrow belts, usually less than 2 km in width, of metamorphosed supracrustal rocks (e.g. southern South Harris, North Harris and North Lewis). These belts have been described in detail by Coward et al (1969). The main bulk of the rocks forming these belts are considered to be sedimentary in origin and are characterized by a highly variable sequence of lithologically

*Dearnley (1962)

	Intrusive Rocks	Phases of deformation, metamorphism and migmatization
LAXFORDIAN 2.2 - 1.5 b.y.	Emplacement of granite-gneiss sheets and pegmatites	Polyphase deformation, metamorphism and local migmatization. Reworking of Scourian complex (with Scourie dykes). Mainly amphibolite facies metamorphism
	Scourie dyke swarm - Basic tholeiitic dykes	
SCOURIAN 2.8 - 2.2 b.y.	Potash pegmatites 2.6-2.4 b.y. of N.E. trend	INVERIAN EVENT - localized deformation and metamorphism BADCALLIAN EVENT approx 2.8 b.y. Regional gneiss forming metamorphism, granulite or amphibolite facies. Produces structures of N.E. - S.W. trend. Interleaving of supracrustal, intrusive and granite gneiss layers.
	Deposition of supracrustal rocks of Hebrides and Scottish mainland with associated ultra-basic, basic and anorthositic intrusives	
PRE-SCOURIAN		Formation of early granite-gneiss basement 2.8 - 3.0 b.y. (?) - metamorphic complex perhaps comparable with oldest rocks of Godthabs-Fjord region of West Greenland.

Table 1.1. Regional Lewisian chronology - Hebrides and mainland (after Watson, in press)

distinct types, including quartzites, pelites, semi-pelites and limestones. These rock types are almost universally associated with amphibolites, hornblende schists, pyroxenites and serpentinites which are considered to have been of meta-volcanic origin (Watson and Lisle, 1973).

In southern South Harris the metasediments of the Leverburgh and Langavat belts are associated with a variety of intrusive igneous bodies, referred to by Dearnley (1959, 1963) as the 'South Harris Igneous Complex'. These include tonalitic noritic and anorthosite bodies, sheets of metagabbro and a variable suite of minor intrusives.

b) Banded or grey quartzo-feldspathic gneisses, which make up approximately 80% of the area, and are of granodioritic, tonalitic or granitic composition. Some parts of the grey gneisses are thought to represent transformed portions of the supracrustal assemblage described above. Others appear to represent a pre-Scourian gneiss basement, reworked during both Scourian and Laxfordian cycles, on which this supracrustal assemblage was deposited. Alternatively it is proposed that the grey gneiss may have been derived from tonalitic intrusions pre-dating or coeval with the early Scourian event.

Myers (1968, 1970) considers that the earliest features of the grey gneisses, of western North Harris, originated in Scourian episodes when the supracrustals were already in existence. He concludes that both the grey gneisses and the supracrustals originated as part of a single cover sequence resting on a pre-Scourian gneiss basement. Much of this cover was transformed into gneiss during the Scourian, parts of this cover sequence which resisted the gneiss forming processes survived as isolated supracrustal remnants within the grey gneiss. Thus a basement-cover junction, if it exists, must be drawn within the gneisses, to separate those of a supracrustal parentage formed during the Scourian cycle and those which represent regenerated gneiss formed during a pre-Scourian cycle. Coward et al (1970) regard the eastern gneisses of the southern Outer Isles as possibly representing such a pre-Scourian gneiss basement.

The supracrustal belt of southern South Harris defines a major anomolous zone in the Lewisian complex of the Outer Isles. The north-westerly structural trend of this zone is at a high angle to that of other parts

of the Outer Hebrides. This belt is also the site of important geophysical anomolies. The regional gravity map for the Outer Hebrides reveals a general N.N.E. trend of the isogals. A well defined gravity high (+60 milligals), with a north-west trend occurs over southern South Harris. A pronounced positive magnetic anomoly also with a north-west trend is situated over South Harris (Westbrook, 1974). It may be no coincidence that this supracrustal belt and anomolous zone is also the site of a major Lewisian plutonic (and possibly volcanic) igneous centre.

The present investigation is primarily concerned with the nature of the anorthosite complex (defined as the anorthosite body plus its gabbroic rim) which forms a small but distinctive part of this suite of igneous rocks. A detailed petrological account of the rocks of the anorthosite complex is given in Chapter 2. A brief account of the petrology and field relations of the associated meta-igneous rocks given in Chapter 3. This account is basically a resumé of previous work and ideas on these rocks, supplemented by some new data from the present investigation. The structural, metamorphic and intrusive history of the anorthosite complex is discussed in Chapter 4. A detailed structural analysis of the anorthosite body is at present being made by A. Heyes (Chelsea College, University of London).

1.2 A Brief Historical Account of the Geological Investigations into the Anorthosite Complex and Associated Meta-igneous Rocks of South Harris

The rocks of South Harris consist solely of high grade metamorphic gneisses of Pre-Cambrian age, termed the Lewisian complex. The 19th century geological map of Scotland, prepared by Sir Archibald Geikie, depicts the whole of South Harris as being made up of Lewisian gneiss. It was not until 1923-1924 when T. J. Jehu and R. M. Craig made a reconnaissance survey of the Outer Hebrides, that differentiaition of the various rock types occurring in South Harris was put on a systematic basis. In their account of the geology of South Harris (Jehu and Craig, 1927) they described the main gneiss types, distinguishing both orthogneisses and paragneisses, and provided the earliest geolocial map of the area, on a scale of 1.5 cms - 1 mile. On this map they mark the

approximate positions of two N.W.-S.E. paragneiss belts (equivalent to the Leverburgh and Lanagavat belts of later workers), indicating some bands of marble and serpentinite within these paragneisses. Between these two belts they recognized, and roughly delimited, a large gabbro-diorite body forming the peaks of Bleaval, Mula, Greval, Beinn Tharsuinn and Sletteval. To the South of the gabbro-diorite body they described a mainly labradorite rock or anorthosite gneiss, occurring as a wedge shaped body with vertical contacts forming the greater part of Roneval and Beinn na h-Aire. They suggested that the anorthosite gneiss and the gabbro-diorite were intrusive into the paragneiss.

Davidson (1943) published a detailed petrological account of the rocks in the Rodil district. From this area he described the occurrence within the Leverbrugh paragneisses, of lensoid bodies of peridotite and websterite. He also described and mapped two extensive metagabbro sheets, one forming a rim to the south-west flank of the anorthosite, and the second forming an extensive sheet along the south coast bordering the Sound of Harris (the pyroxene granulite or norite of later workers).

These metagabbroic rocks are characterised by the absence or rarity of quartz and in this way differ from the gabbro-diorites, described by Jehu and Craig, to the north-east of this area. Davidson considered that the peridotites and websterites, together with the metagabbros, were contemporaneous and comagmatic with the anorthosite and gabbro-diorite. He regarded the whole of the orthogneiss complex as a single highly differentiated intrusion, to which the anorthosite forms a central core margined by gabbro-diorite to the north and gabbro to the south. He likened this suite of rocks to those of the Adirondack complex.

Davidson also distinguished two major metamorphic events affecting the rocks of this area;

a) An early high grade garnet producing event

and b) A later retrograd event, with alteration of the early assemblages and the production of kelyphytic rims around the early garnets.

Dearnley (1959, 1963) described the geochemistry and petrology of the orthogneisses and produced both a lithological (scale 1:25000) and structural map of South Harris. He recognised an igneous suite comprising of anorthosite, tonalite (equivalent to the gabbro-diorite of Jehu and Craig), metagabbro, ultramafites and ultrabasites, and trondhjemitic pegmatites. Dearnley termed this association of igneous rocks 'The South Harris Igneous Complex' and considered that the close field association of the various rocks of this suite reflected a common genesis.

He compared the geochemistry of the South Harris igneous suite to that of the Scourie dykes and suggested that the former may represent '..... a plutonic centre related to the widespread non-orogenic minor intrusives of the Outer Hebrides and to the Scourie dykes of the Scottish mainland.' A basic tholeiitic parent magma for this suite of rocks was proposed by Dearnley.

He considered the rocks of the igneous suite to have been affected by two Laxfordian metamorphic and deformational events. Firstly, an early Laxfordian granulite facies metamorphism, associated with a major phase of regional deformation which produced a series of isoclinal folds about north-west south-east trending axial planes. This was followed by a late Laxfordian amphibolite facies metamorphism associated with cross folding along north-east south-west axes. Dearnley regarded the metagabbros bordering the Sound of Harris (which he termed "pyroxene granulites") to be also of igneous origin, but predating and not comagmatic with the rocks of the igneous suite. Within the pyroxene granulites and adjacent paragneisses he recognised relic textures of a pre-Laxfordian granulite facies metamorphism and deformation. Dearnley suggested that

the pyroxene granulites represent a slice of older basement thrust into its present position after the Laxfordian folding of the igneous suite.

A detailed account of the petrology and geochemistry of the ultrabasic and ultramafic lenses from the Leverburgh and Langavat paragneiss belts was given by Livingstone (1963). He concluded that the ultrabasites and ultramafites from either belt were genetically different.

Graham (1969), as an extension to his work in North Uist, made a structural study of southern South Harris. He considered that the pyroxene granulite was contemporaneous with the anorthosite and tonalite, all of which he regarded as of Scourie dyke age.

The structural and geochemical study of South Harris by Palmer (1971) produced widely differing conclusions to those of Dearnley. Palmer considered, on structural, chemical and petrological evidence, that the pyroxene granulite forms an integral part of the South Harris igneous suite. In line with this conclusion he abandons the term pyroxene granulite in favour of the igneous term norite.

Palmer regarded the igneous suite as calc-alkaline in affinity. The anorthosite, norite and tonalite (quartz-diorite) are shown to exhibit a linear alkali enrichment trend, corresponding to the calc-alkaline trend of Nockolds (1954). He concludes that it is unlikely that the South Harris igneous suite was coeval or comagmatic with the Scourie dykes (which are of tholeiitic affinity) as suggested by Dearnley. Alternatively he suggested that the igneous suite is synorogenic and that its intrusion pre-dated the early Scourian granulite facies metamorphism.

Palmer also noted that the observed intrusive sequence of the igneous rocks is consistently the reverse of a normal differentiation sequence. He suggested also that the regional deformation in South Harris was determined by the highly viscous homogeneous nature of the three major igneous plutons (the anorthosite, tonalite and norite). He argued that the three igneous plutons have all suffered differing

degrees of flattening and passive rotation within the inhomogeneous, less viscous, paragneiss matrix.

The most recent account of the metamorphic history of South Harris is given by Dickinson (1974). She describes four tectono-metamorphic events, the earliest of these being Scourian (Badcallian) and characterised by granulite facies assemblages. A second high grade, early Laxfordian, metamorphism transitional between amphibolite and granulite facies, is proposed. The third and fourth metamorphic events are late Laxfordian and characterised by lower amphibole facies assemblages.

With regard to the South Harris igneous suite, there are two main areas of disagreement among earlier workers:-

a) The Age of the Igneous Suite

(i) Dearnley (1959, 1963) concluded that the rocks of the igneous suite are contemporaneous and comagmatic with the Scourie dykes. But he regarded the pyroxene granulite as a distinct intrusion of pre - or early Scourian age.

(ii) Myers (1968) considered the tonalite intrusion predates the Scourian migmatisation exhibited by the paragneisses of the Langavat belt. This would suggest an early Scourian age for this intrusion.

(iii) Graham (1969) proposed that the pyroxene granulite was contemporaneous with the rest of the igneous suite and ascribed a Scourie dyke age to these rocks.

(iv) An early age for the complex is proposed by Palmer (1971) who suggested that the anorthosite, norite (pyroxene-granulite) and tonalite, followed by the metagabbros and ultrabasites are intruded into the supracrustals pre - or coeval with the early Scourian granulite facies metamorphic event.

b) The Nature of the Igneous Suite

The igneous suite is thought to have either:-

(i) Tholeiitic affinities - Dearnley (1959, 1963)

or(ii) Calc-alkaline affinities - Palmer (1971)

Throughout all previous work no detailed study of the anorthosite has been made.

1.3 Geological Investigations into the Economic Potential of the South Harris Anorthosite Body

Anorthosite has many potential uses. It may provide a source for alumina (Al_2O_3 contents approaching and in excess of 30%), or in the case of the South Harris anorthosite and its gabbroic rim, a source of abrasive garnet. The anorthosite may also be used as a roadstone aggregate, a filler or abrasive, and as a source of feldspar for use in the ceramic industry.

A detailed mapping and sampling programme of the anorthosite was undertaken by Robertson's Research between 1963 - 1966. (Newman, 1971). Mapping on a scale of 25 inches to 1 mile, was concentrated in the south-eastern part of the body (Howley, 1966; Westoll, 1967). In conjunction with this a proton magnetometer survey of the whole of the anorthosite and the adjacent gabbros was undertaken. A small quarrying operation in the anorthosite was initiated in 1966, but suspended in mid-1967 due to a decline in the roadstone market. Approximately 1350 feet of core was recovered from a number of drill holes in the anorthosite. Initially diamond drilling was concentrated around the quarry area, in the south-eastern part of the body. But in mid-1967 a small drilling programme was commenced in the north-east of the body. This latter drilling programme was directed towards the location of possible ilmenite deposits that may have been present at the contact of the anorthosite and its gabbroic envelope. However, no highly titaniferous rocks were encountered.

The economic potential of the anorthosite has been recently re-evaluated and a small scale quarrying operation was recommenced in mid-1973.

1.4 Igneous Rock Terminology

A rationalisation of the igneous rock terminology adopted by previous workers (Table I.3) has been attempted. The meta-igneous rock types present in South Harris have been divided into classes depending on their percentage content of mafic minerals. The definitions of rock types used in this work (Table I.2) are taken in part from Windley et al (1973). This classificatory scheme has proved useful for field classification, by visual estimate of the percentage of mafic minerals, and for more precise work using modal analyses. The former method often proved more reliable than modal analysis when dealing with heterogenous rock types.

It should be stressed that the mineral assemblages of all of the rocks in question are metamorphic in origin. Strictly speaking the prefix meta- should be added to the rock terms used. However, this leads to a clumsy terminology and has not been followed in this thesis.

The equivalence of the rock terminology used in this work to that of previous workers in this area is shown in Table I.3. The terms gabbro-diorite (as used by Jehu and Craig, 1927) and norite (as used by Palmer, 1971) are retained pending a more thorough investigation of these two bodies.

The term anorthosite is used in this thesis in two ways:-

a) In the strict sense defined in Table I.2.

and b) 'Anorthosite', written thus and used in a general way, has been retained to describe a variety of rocks. These range from mafic gabbro to anorthosite, and constitute a major part or whole of the anorthosite body delimited in Fig 1.1.

Minor modifications to this classificatory scheme have been made in the description of the gabbroic rocks from the envelope of the anorthosite. Here the term quartz gabbro has been introduced to distinguish mafic

ROCK TYPE	PERCENTAGE OF MAFIC MINERALS	MINERALOGY	
ANORTHOSITE	0 - 10%		
GABBROIC ANORTHOSITE	10 - 20%		
ANORTHOSITIC GABBRO	20 - 35%		
GABBRO	35 - 65%		
MAFIC GABBRO	65 - 90%		
ULTRAMAFITES	90 - 100%	1) DUNITE	Olivine 90 - 100%
		2) PERIDOTITE	Olivine + Pyroxene 90 - 100% Olivine < 90% Pyroxene < 90%
		3) PYROXENITE	Pyroxene 90 - 100%
		4) AMPHIBOLE DUNITE	Amphibole 10 - 50%; Olivine + Amphibole 90 - 100%
		5) AMPHIBOLE PERIDOTITE	Amphibole 10 - 50%; Olivine + Pyroxene 50 - 90%; Olivine, Pyroxene < 90%
		6) AMPHIBOLE PYROXENITE	Amphibole 10 - 50%; Pyroxene + Amphibole 90 - 100%
		7) HORNBLENDITE	Amphibole (not necessarily hornblende) 50 - 100%
		8) GARNETITE	Garnet 50 - 100%

Table 1.2. Igneous Rock Terminology (in part after Windley et al, 1973)

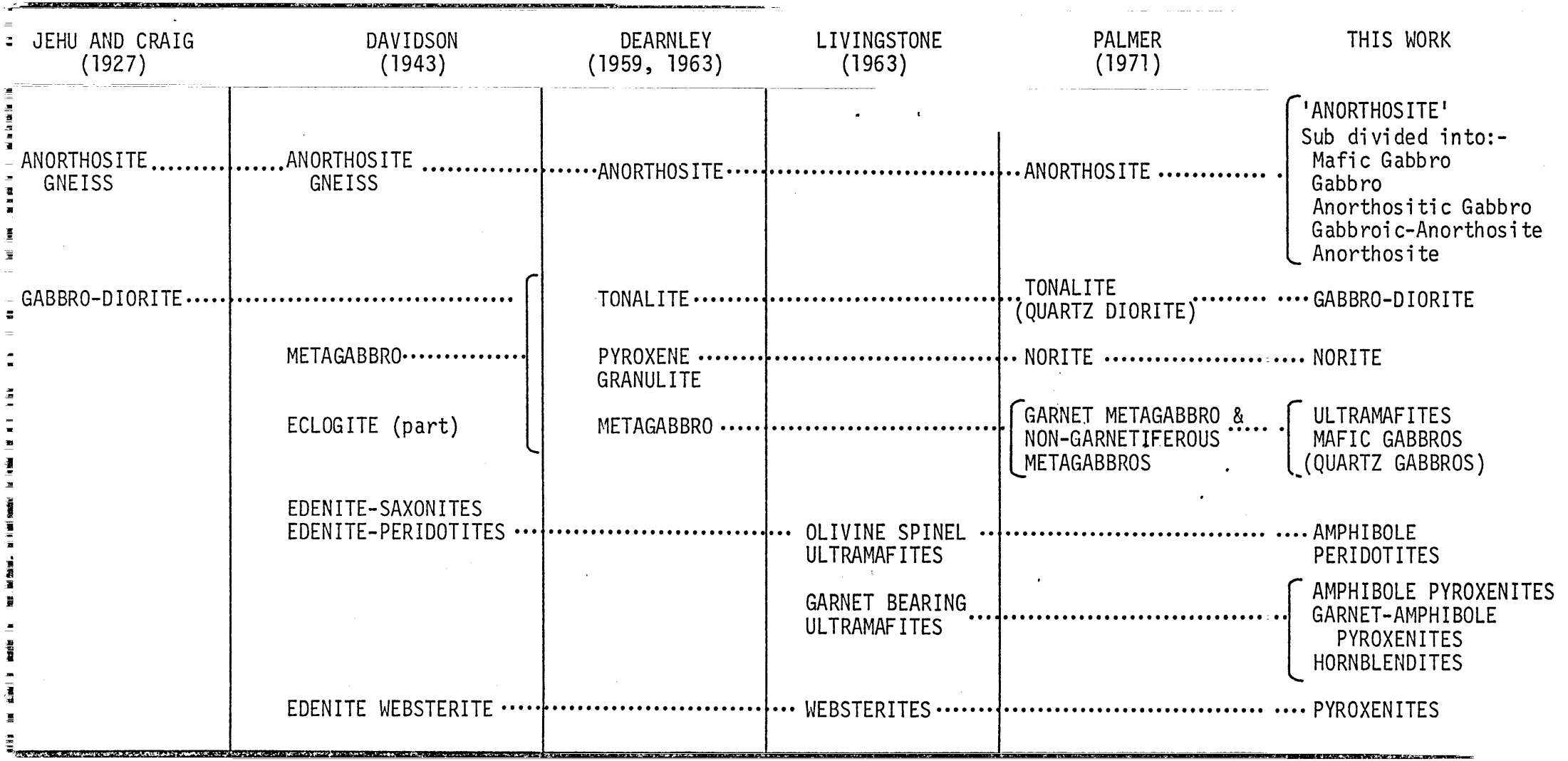


Table **1.3.** Equivalence of Igneous Rock terminology used in this work, with that of earlier workers

gabbros with an appreciable quartz content from those more normal mafic gabbro types with little or no modal quartz.

In detailed descriptions of the ultramafites from the gabbroic rim of the anorthosite, it was necessary to adopt a slightly different scheme. Here individual rocks have been named after their predominant mineral phase, and prefixed to take into account the subordinate major mineral phases. For example, an ultramafite yielding the following mode:-

Garnet 22.5%, clinopyroxene 49%. amphibole 9%,

Amphibole/plagioclase symplectite (after garnet) 19%

- has been termed a garnet clinopyroxenite.

1.5 The Rock Types of Southern South Harris - An Introduction

Our present knowledge of the distribution of the various rock types of southern South Harris, results mainly from the work of Dearnley. His lithological map (Fig 1.1) of this area, although elaborated upon by more recent workers, remains essentially unchanged. A broad division into paragneisses and orthogneisses can be made.

a) The paragneisses (metasediments and metavolcanics) occur in two N.W. - S.E. trending belts - the Langavat and Leverburgh belts. A description of the paragneisses is beyond the scope of this work, but good accounts of these rocks have been given by Davidson (1943), Dearnley (1963), Palmer (1971) and Dickinson (1974).

b) The orthogneisses (meta-igneous rocks) are generally agreed to be intrusive into the paragneisses. The igneous suite of rocks comprises three large plutons:-

i) the gabbro-diorite

ii) the norite

and iii) the anorthosite

Associated with these are a diverse suite of minor intrusives.

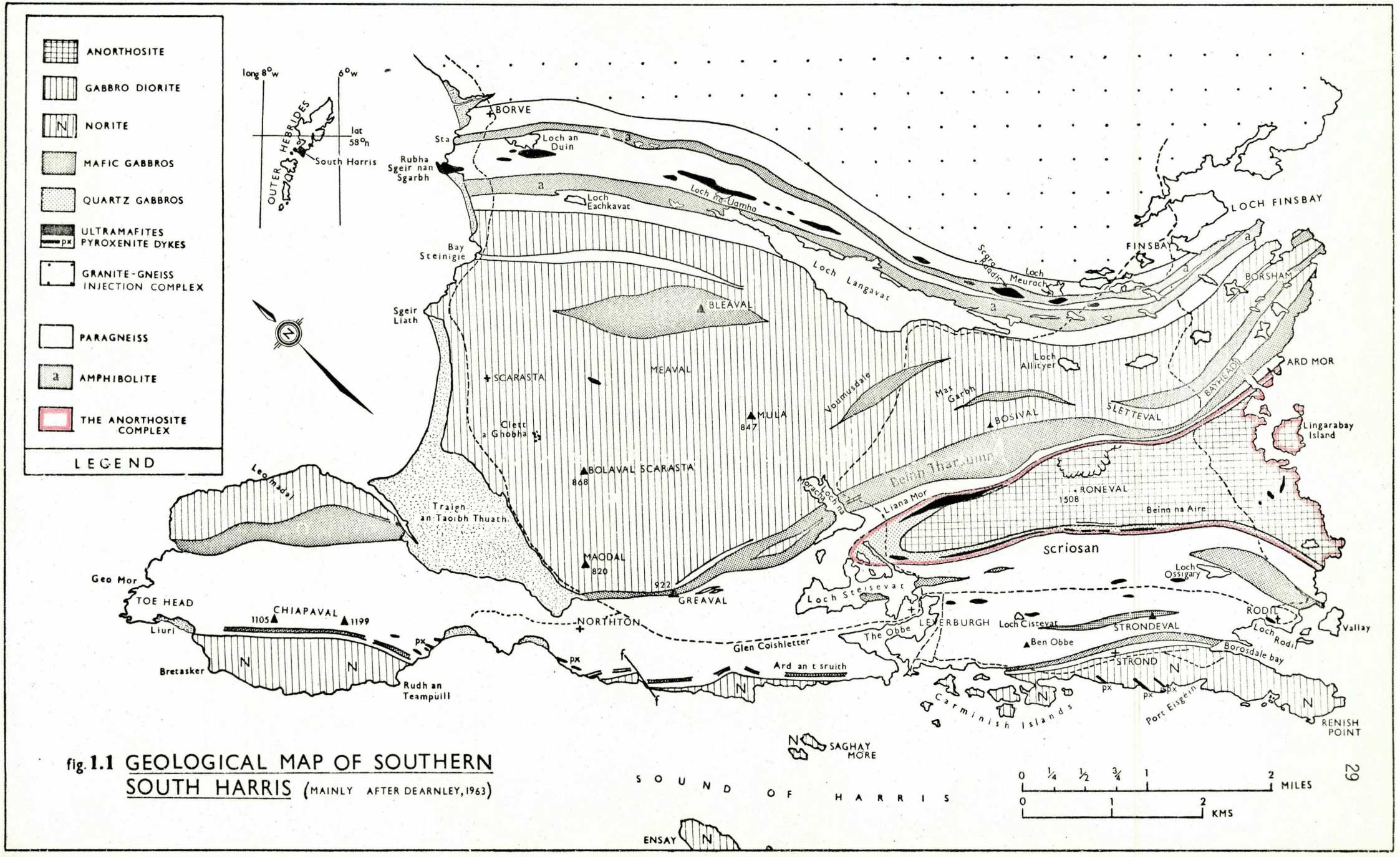


fig. 1.1 GEOLOGICAL MAP OF SOUTHERN SOUTH HARRIS (MAINLY AFTER DEARNLEY, 1963)

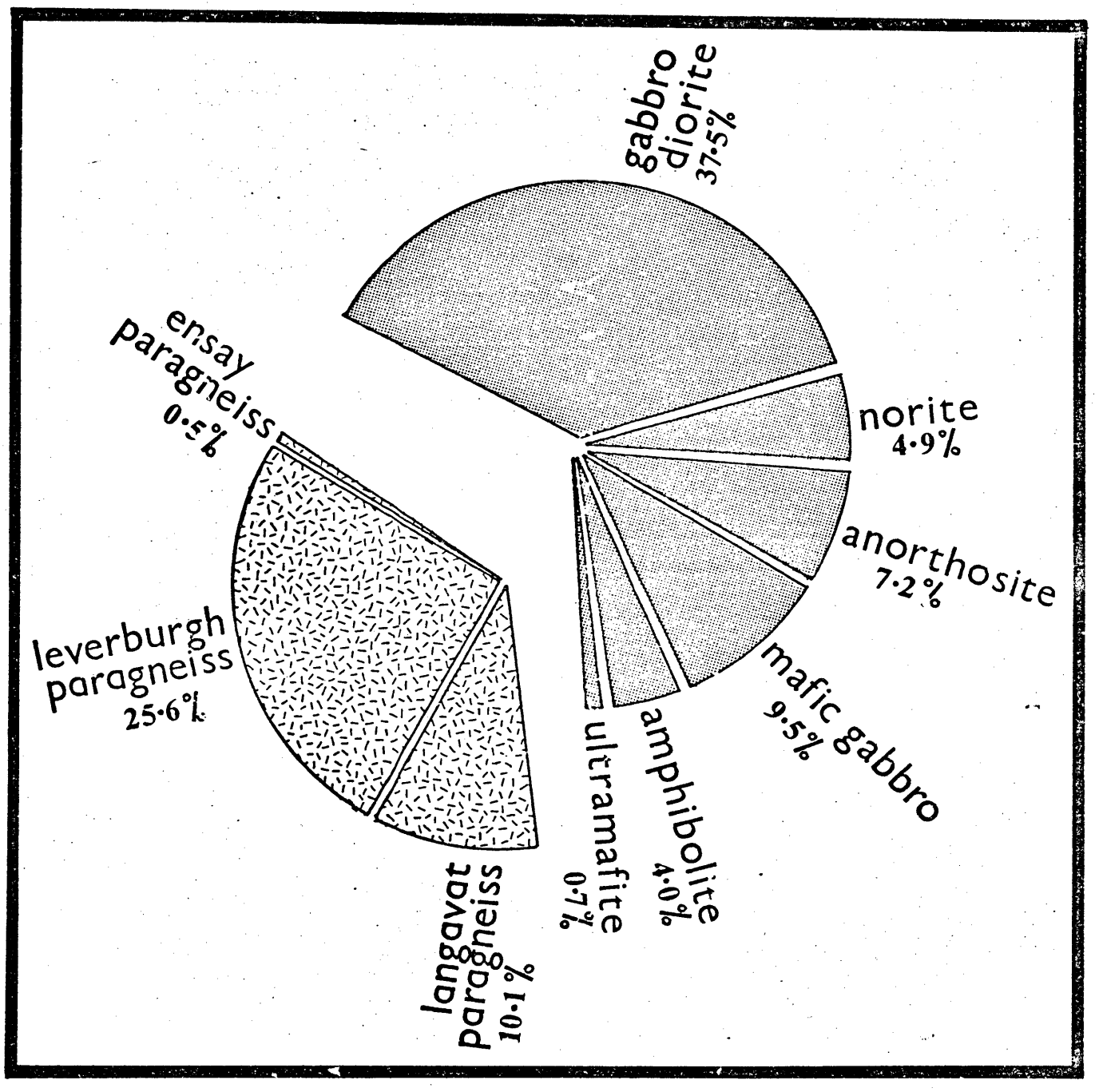


fig. 1.2 The relative proportions of the main rock types exposed in southern South Harris. Note the preponderance of metaigneous rock types (strippled). The approximate proportions of the meta-igneous rocks are:-
Gabbro-diorite 58.8%; Norite 7.7%; Anorthosite 11.2; Mafic gabbro (and amphibolite) 21.2% and ultramafite 1.1%

These comprise:-

i) Mafic gabbros, occurring as extensive sheets rimming the three major plutons and as smaller sheets within the paragneisses and gabbro-diorite. Small dyke or sill-like bodies of mafic gabbro occur intrusive into all three plutons.

ii) Ultramafites, occurring as small concordant lensoids in the paragneisses of the Langavat and Leverburgh belts and as dykes and irregular bodies intrusive into the three plutons.

These rocks are also cut by quartz veins and feldspar/quartz pegmatites of Scourian and Laxfordian age, and by a number of unmetamorphosed basic dykes, mainly of Tertiary age.

The relative proportions of the main rock types occuring in southern South Harris is shown in Fig 1.2.

1.6 Methods of Study

Previous mapping of the anorthosite was mainly concerned with delimiting its extent. At the initiation of this study very little was known of the internal nature of the anorthosite body. Thus, before embarking on a sampling programme, it was necessary to determine the main structural elements and to produce a lithological map of the anorthosite complex. Initial mapping of the complex was of a reconnaisance type and had two main aims. The first aim was to determine the large scale variations in rock type and structure within the complex, and the second to aid in the selection of small areas suitable for further detailed mapping. A total of ten reconnaisance traverses were made across the width of the complex and a single traverse along its length. In situ exposure of the complex varies greatly and was one of the major factors in determining the location of the areas for further detailed study.

In situ exposure is often poor, since glaciation has left a great deal of detrius which obscures the solid geology and is often misleadingly

'solid' itself. Indeed the problem of deciding whether a particular exposure is in place or not is often acute. In many areas it appears that boulders of anorthosite are derived directly from the underlying 'in situ' anorthosite and it may be that much of the detrius in this area was produced by a permafrost action rather than having been glacially transported and dumped. Exposure at the summit of Roneval is particularily poor. Although large flat table-like exposures are present in this area these are infrequent and appear as small disconnected islands in a sea of scree. The area to the north of Leverburgh is largely free from glacial scree and in situ exposure here varies from 30-70%.

An area of approximately 1.25 Km^2, between Roneval and Leverburgh, was exposure mapped on a scale of 1:5000 (Map 1). From within this area, two sections of the gabbroic rim of the complex were exposure mapped on a scale of 1:88 (Maps 2 & 3). Also an area of approximately 0.15 Km^2 of anorthosite from 190 metres south-west of Ha-Cleit summit was mapped on the same scale (Map 2).

Laboratory work involved the study of approximately 140 thin sections of the rocks of the anorthosite complex. Thin sections, borrowed from Dr. J. Tarney (Institute of Geological Sciences), and from the collections of other Imperial College workers were also examined. In all 155 whole rock analyses and 111 mineral analyses have been made. These, plus additional analyses culled from the literature (which includes 25 previously unpublished analyses from the anorthosite), are presented in Appendix 1.

1.7 Format

All measurements referred to in this thesis are in the metric system. Diagrams and maps bound into the thesis are referred to as figures and are numbered sequentially within each chapter. Photographs and tables are respectively referred to as plates and tables and are again numbered sequentially within each chapter. Maps in the back pocket are termed

maps. The numbers of the thin sections which appear in photographs and diagrams refer to the thin section numbers in the Imperial College collection.

CHAPTER 2

THE ANORTHOSITE COMPLEX

2.1 General Introduction

The anorthosite complex forms a wedge-shaped mass of approximately 9.5Km^2 stretching from the east coast, between Ard Mor and Rudha Vallarip, to Leverburgh.

For ease of description the complex is divided into three categories:-

a) The 'Anorthosite' - a banded sequence of rocks ranging from gabbro to anorthosite (s.s.) in composition and forming the central part of the complex.

b) The gabbroic rim of the complex, composed predominantly of mafic gabbro and further subdivided into:-

i) Banded ultramafites and mafic gabbros

ii) Quartz gabbros

The gabbroic rim also includes numerous lenses and strips of paragneiss.

c) Minor intrusives. A variable suite of rocks comprising:-

i) Ultramafic and mafic gabbro dykes and sheets.

ii) Ultramafite and anorthosite intrusions associated with brecciation, along the 'anorthosite' contact.

iii) Hornblendite dykes and lenses

iv) Anorthositic gabbro dykes and trondhjemitic pegmatites.

v) Unmetamorphosed basic dykes.

The overall structure of the anorthosite complex is that of a large isoclinal fold, the 'anorthosite' forming the observed core to this fold. The axis of the fold is vertical and present exposure of the complex reveals a cross section in a plane perpendicular to the fold axis.

2.2 The 'Anorthosite'

The term 'anorthosite' is here used in a general way to include a highly banded sequence of rocks ranging from gabbro to anorthosite (s.s.). A threefold division of the 'anorthosite' has been adopted (fig. 2.1).

Traversing from the margin of the 'anorthosite' (the contact of the 'anorthosite' with the gabbroic rim of the complex), inwards these three divisions are:-

a) A lower zone of banded 'anorthosites' - characterised by a small scale banding.

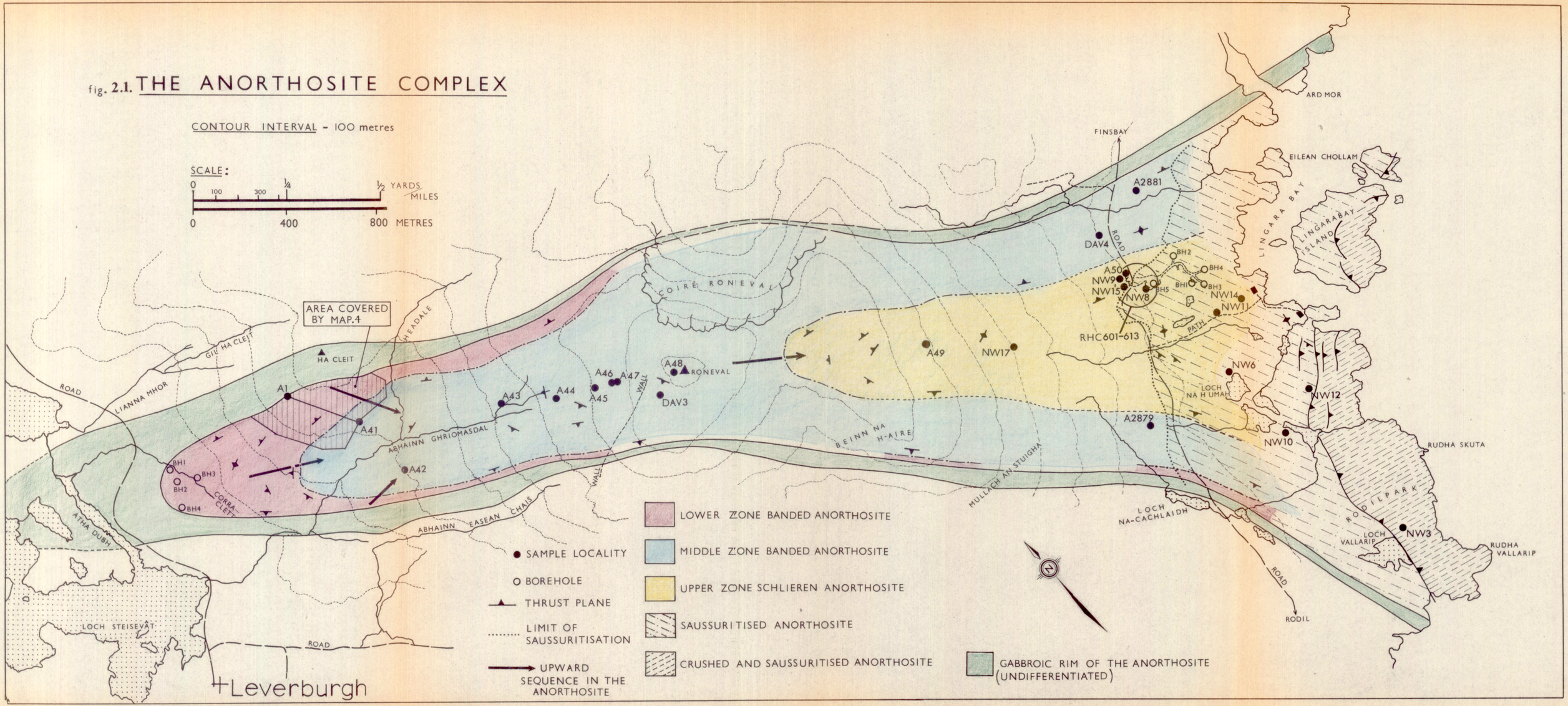
b) A middle zone of banded 'anorthosites' - characterised by a larger scale banding.

c) An upper zone of schlieren 'anorthosites'

The lower zone is thought to represent the original base of the 'anorthosite' body and the upper zone the exposed top of the 'anorthosite'. The identification of the original base of this sequence depends on observations discussed in this thesis. These are briefly summarised below:-

I) Field observations - Although the earliest recognizable mineral assemblages, within the anorthosite, are metamorphic these appear to preserve a presumably igneous gravity stratification in the body. Both the lower and middle zones are composed of a number of gravity stratified units. A complete succession, from base to top of one of these units, shows a gradation from gabbro (with minor mafic gabbro horizons) - anorthositic gabbro - gabbroic anorthosite - anorthosite. Assuming that the gabbroic portion of these units represents the base of an original igneous gravity stratified unit these have been used as an indicator of the 'way up' of the 'anorthosite' sequence. In all cases a facing direction from the margin to the centre of the body is indicated. This agrees with an overall gradation within the 'anorthosite' body from a predominantly gabbroic marginal facies to a central anorthositic facies.

fig. 2.1. THE ANORTHOSITE COMPLEX



II) Chemical evidence - From the presumed base (margin) to the top (centre) of the anorthosite sequence and from the base to the top of any one gravity stratified unit within this sequence, the following variations are apparent:-

i) an overall increase in normative feldspar content.

ii) an overall increase in the FeO/FeO+MgO ratio- indicative of an iron enrichment trend.

iii) an increase in the differentiation index (which is effectively a measure of the acidity of the rock type).

The fact that these chemical trends are preserved also suggests that the metamorphisms affecting the anorthosite body (and the associated meta-igneous rocks) were essentially isochemical.

Folding of the anorthosite has resulted in the repetition, with slight assymetry, of the above succession on either flank of the body. The style of the isoclinal fold, to which the anorthosite forms a core, is that of a neutral antiformal syncline (Fleuty, 1964). The anorthosite sequence is thus everywhere inverted. Folding has also produced intense tectonic thinning of the above zones along the fold limbs. The most complete succession for each zone, allowing for the affects of later deformation, can be found along the axial trace of the fold.

Two further 'anorthosite' types are also considered:-

d) Saussuritised anorthosite

e) Crushed and saussuritised anorthosite

Both types occur at the south east end of the anorthosite complex. The saussuritised anorthosite lies mainly to the east of the Rodil-Finsbay Road and the crushed and saussuritized anorthosite to the east of the major coastal thrust plane (fig. 2.1).

The contact of the 'anorthosite' with the rocks of the gabbroic rim is variable in character. In many cases an intervening strip of paragneiss is found along this contact (e.g. S.W. slope of Roneval, west slope of Ha-Cleit) partial assimilation of this paragneiss, by the anorthosite, can often be observed. In other areas the nature of this contact is futher obscured by later brecciation and intrusion (Section 2.4.3). However, where a straightforward contact is observed, it is very abrupt. The banding in the 'anorthosite' is in all cases concordant to this contact.

2.2.1 Mineralogical and Textural Variations within the 'Anorthosite'

Mineral variations within the 'anorthosite' are the result of a variety of factors. The earliest recognisable mineral assemblages, are the result of a high grade granulite facies metamorphism (M_1), and comprise:-

$$\text{plag} \pm \text{cpx} \pm \text{gt} \pm \text{amp} \pm (\text{opx}) \pm \text{ilm} \pm \text{qtz}$$

Orthopyroxene (hypersthene) is a rare phase in the 'anorthosite', having only been found at one locality.

The amphibole of these early assemblages appears to be of two types:-

a) A ferroan pargasite, pleochroism: X yellow green; Y brown green; Z dark brown. This occurs abundantly within the lower zone 'anorthosites', but is not common outside this zone.

b) A pargasitic hornblende - edenite, pleochroism: X pale green-straw; Y green; Z blue green. This occurs mainly in gabbroic rocks from the lower and middle zones.

Both types occur in texturally stable, granoblastic intergrowths with the other members of the early (M_1) assemblage.

The four main phases of this early (M_1) assemblage show systematic variations:-

a) On a small scale, within each anorthosite zone. Such variations produce a complex mineralogical or compositional banding in the lower and middle zone anorthosites. The nature of this banding is described in detail in the sections dealing with the petrology of these zones.

and b) On a large scale, from the base to the top of the 'anorthosite' succession. These variations can be summarised as follows:-

(i) an overall increase in modal clinopyroxene

(ii) an overall increase in modal plagioclase feldspar

(iii) an overall decrease in modal garnet

(iv) an overall decrease in modal amphibole

(v) Ilmenite shows a slight overall decrease

The net result of these variations is to produce a gradation from amphibole and garnet rich gabbros at the base of the 'anorthosite' body (lower zone), to clinopyroxene rich anorthosites at the top (upper zone).

The amphibole, and to a lesser extent the clinopyroxene, of this early (M_1) assemblage, show some degree of orientation. Such a mineral orientation defines a foliation in these rocks. This foliation is in all cases parallel (or subparallel) to the compositional banding in the anorthosite.

The mineralogical variations shown by the early (M_1) metamorphic assemblage are overprinted by the effects of:-

a) Localized retrogression, producing amphibolitised assemblages. This is observed in association with numerous shear zones transversing the 'anorthosite', and also along the fold limbs of the major isoclinal fold. The latter variation leads to a change in mineralogy of individual horizons,

within the anorthosite succession, when these are traced from the fold hinge to the fold limbs. A textural contrast within the rocks from these two areas also exists. Plagioclase textures from the hinge zone of the fold indicate textural equilibrium, with gently curved grain boundaries and 120^{o} triple point junctions (Plate 2.1). Superimposed on these equilibrium textures, are weak strain phenomena such as undulose extinction and bent twin lamella.

However, within anorthosites from the fold limbs these coarse grained equilibrium textures are replaced by textures indicative of post-crystallization strain. Feldspar grain boundaries become highly sutured, and mortar textures are common (Plates 2.2 & 2.3). Many grains show bent twin lamella and in more extreme cases, mechanical fracturing. In addition, the development of myrmekitic zones (Plates 2.4, 2.5) along plagioclase - plagioclase and plagioclase-clinopryoxene grain boundaries can sometimes be observed. The occurence of such myrmekites may indicate an attempt to maintain equilibrium within the rock mass by some degree of solid state reaction.

Anorthosites from shear zones show polygonal textures (Plate 2.6). Here all the grains are of approximately equal size, grain boundaries are straight or gently curved, and grains tend to be hexagonal in shape.

The above textural changes, involving the breakdown and recrystallization of the plagioclase feldspar, are accompanied by the formation of scapolite along feldspar grain boundaries, a breakdown of the garnet to an amphibole/plagioclase symplectite, and the replacement of clinopyroxene by a pale green sieved hornblendic amphibole. Clinozoisite, zoisite, chlorite, biotite, calcite and epidote may all appear in



Plate 2.1 Interlocking granoblastic meshwork of coarse grained, well twinned, plagioclase feldspar.

Note 120^{o} triple point junctions and straight to gently curved grain boundaries. Upper zone 'anorthosite' from central area of anorthosite body (fold core). X80. Crossed polarised light. Slide no. 38115.

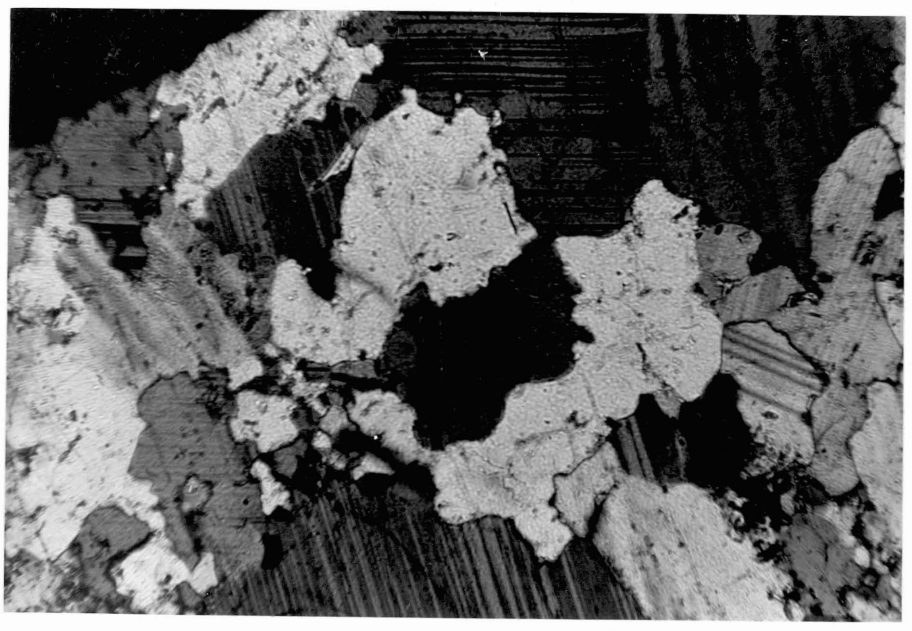


Plate 2.2 Plagioclase grains showing highly sutured grain boundaries. Lower zone 'anorthosite' from the margin of the anorthosite body (fold limb). X80. Crossed polarised light. Slide no. 39999.

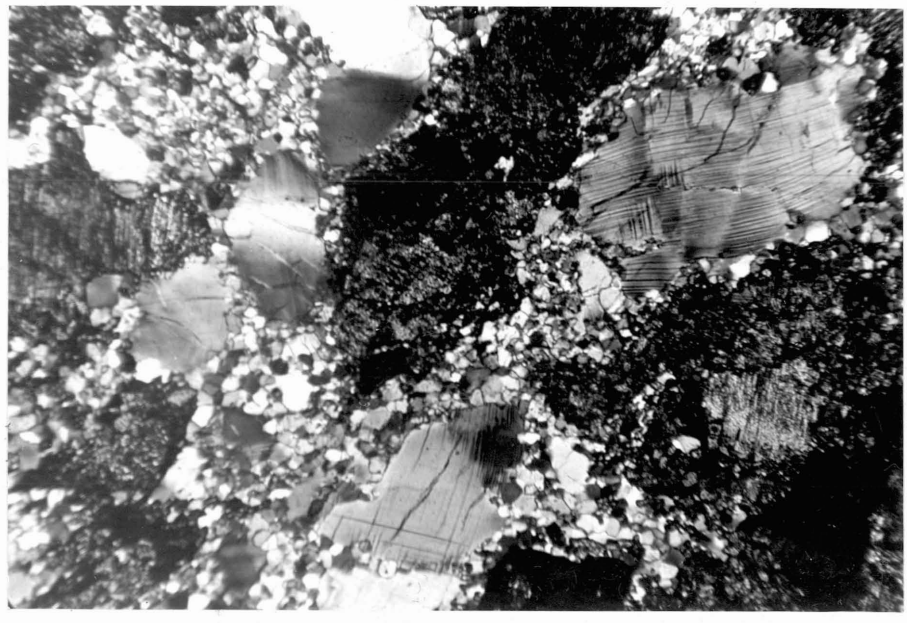


Plate 2.3 Mortar texture - characterised by the occurrence of large, rounded to ovoid grains, surrounded and seperated from each other by tiny strain free grains. Note the large plagioclase grain (top right) showing undulatory extinction and bent twin lamellae. Lower zone anorthositic-gabbro from margin of anorthosite body (fold limb). X80. Crossed polarised light. Slide no. 38459.

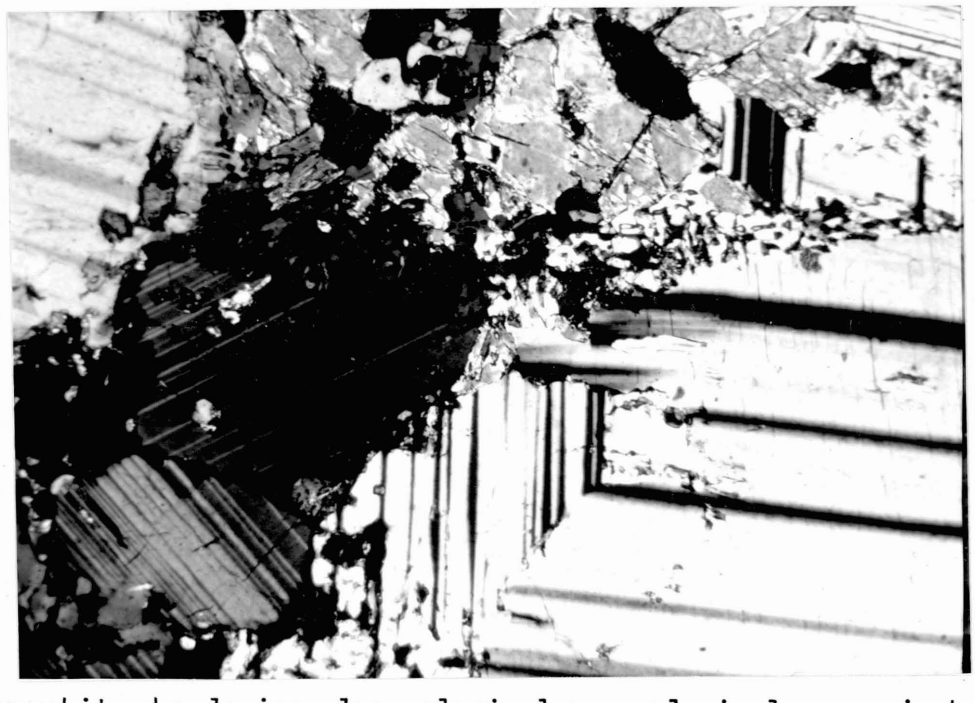


Plate 2.4 Myrmekite developing along plagioclase - plagioclase grain boundaries. Lower zone 'anorthosite' from margin of the anorthosite body (fold limb) X80. Crossed polarised light. Slide no. 40843

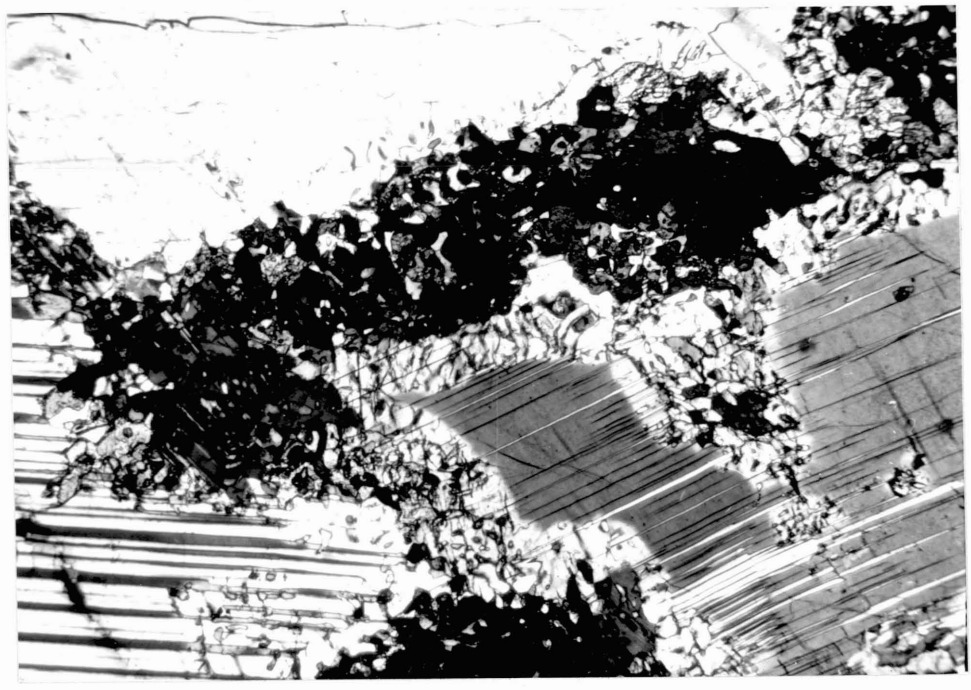


Plate 2.5 Myrmekite developing along plagioclase-clinopyroxene grain boundary. Lower zone 'anorthosite' from margin of anorthosite body (fold limb). X80. Crossed polarised light. Slide no. 40843.

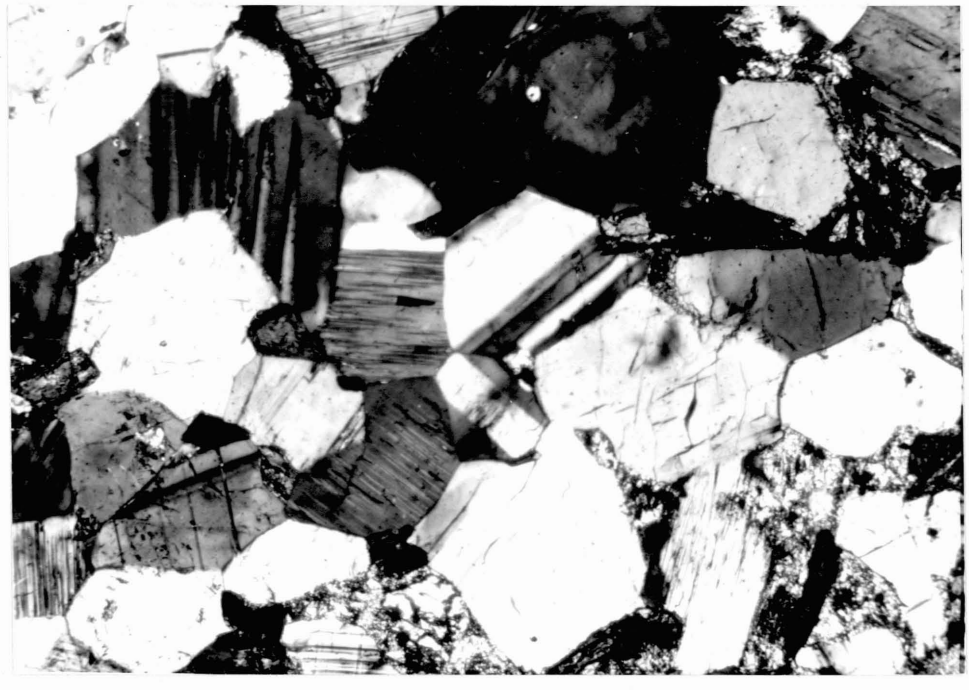


Plate 2.6 Polygonal texture. Anorthosite from a Laxfordian shear. Crossed polarised light. X80. Slide no. 40841

intensely sheared mafic anorthosites.

b) Regional retrogression - particularly apparent in the vicinity of late Laxfordian (F4) shears, but patchily developed throughout the complex. The degree of retrogression appears to be greater in the south-eastern part of the 'anorthosite', between Roneval and the Rodil-Finsbay Road. This appears to coincide with an increase in frequency of late Laxfordian shears in this region. Throughout the 'anorthosite' sequence the effects of this retrogression are more apparent within the leucocratic gabbroic anorthosites and anorthosites.

The most noticeable effect of retrogression is the development of symplectite rims around the garnets, (Plate 2.7). The symplectite rims are composed of a radial intergrowth of pale green amphibole and plagioclase. The garnets may also be traversed by sets of parallel cracks along which a similar intergrowth, or more rarely a quartzo-feldspathic intergrowth may occur. The symplectite rims may develop against plagioclase, clinopyroxene or amphibole, but are usually better developed in the latter two cases. A zone of magnetite granules often marks the outer margin of the symplectite (Plate 2.8). These magnetite granules often appear to be arranged in a euhedral outline and probably delimit the original extent of the garnet grain.

The amphibole of the early (M_1) assemblages may alter to a pale hornblende and thence to biotite, or more commonly directly to biotite. The clinopyroxene in all slides shows some degree of alteration to a pale green hornblende. Initially this alteration occurs marginally or preferentially along the clevage. In more highly retrogressed rocks, the clinopyroxene



Plate 2.7. Symplectite - radial intergrowth of plagioclase feldspar and amphibole - rimming a garnet. X140. Crossed polarised light. Slide no. 39308

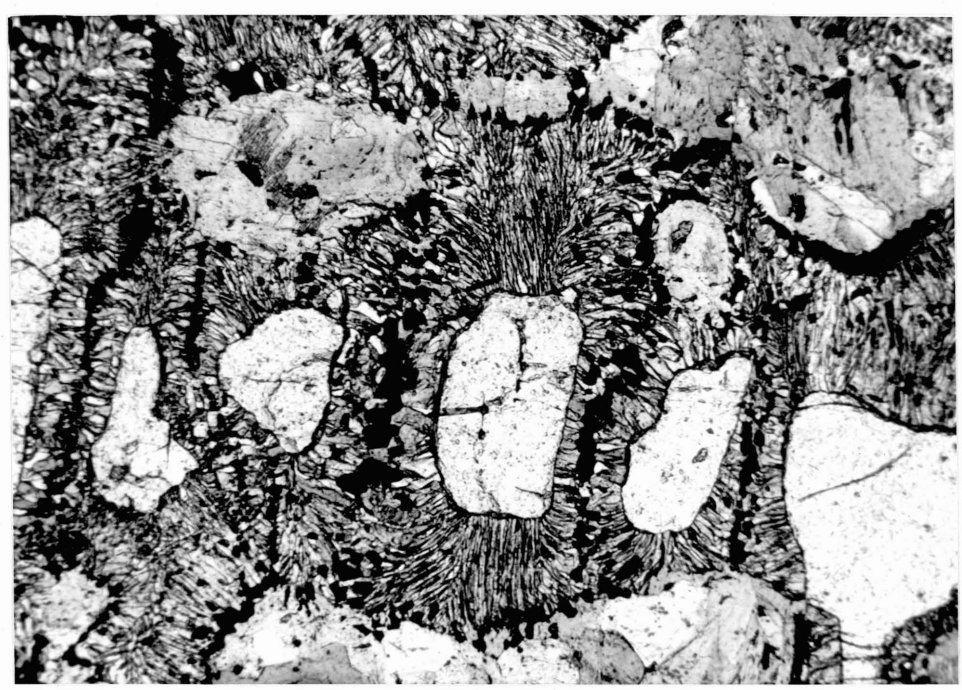


Plate 2.8. Symplectite rims outlined by zones of small magnetite granules. X80. Plane polarised light. Slide no. 41334

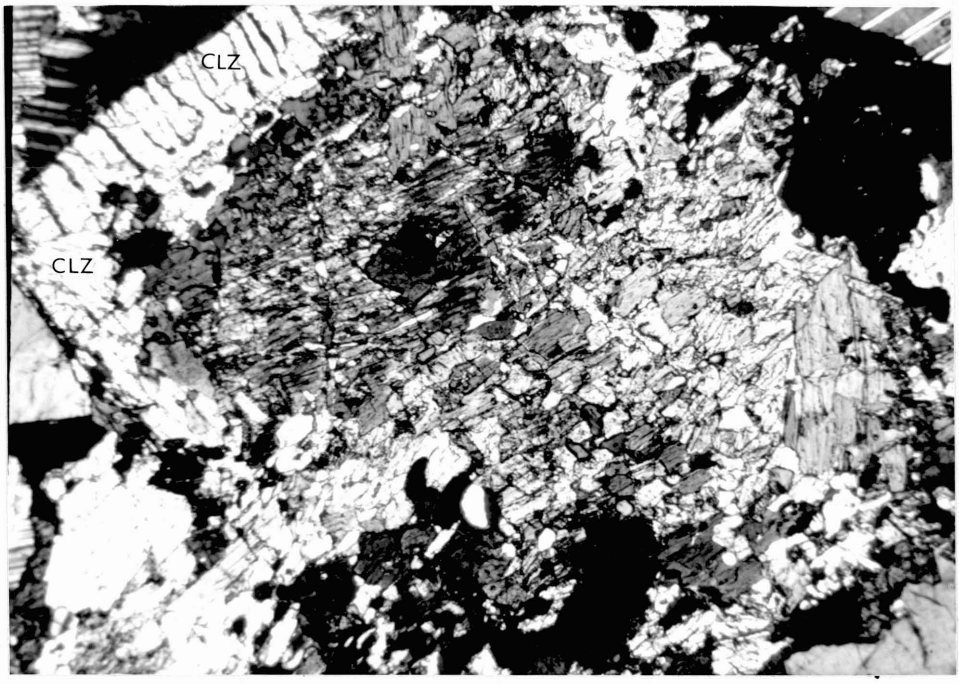


Plate 2.9 Partial retrogression of granulite facies clinopyroxene to a blue-green hornblende. The hornblende aggregate is sheathed by elongate laths of clinozoisite. X 80. Crossed polarised light. Slide no. 38113.

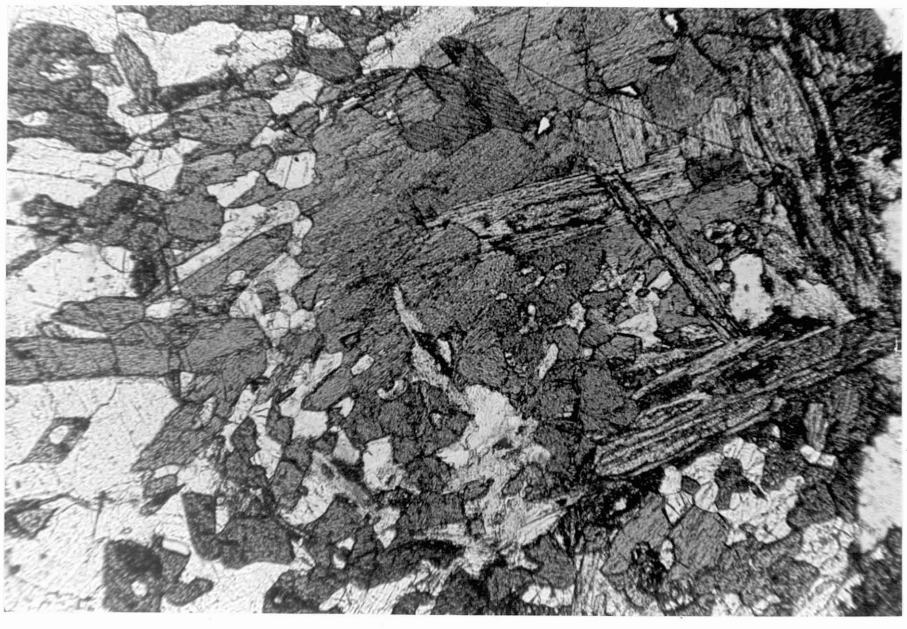


Plate 2.10 Hornblende - clinozoisite - plagioclase feldspar aggregate. Remnants of M_1 clinopyroxene also occur (centre, right), from which it is thought the amphibole and clinozoisite are derived. Semi-diffuse mafic schlieren from the upper zone of the anorthosite sequence. X 60. Plane polarised light. Slide no. 38115.

alters completely to a sieved hornblende, enclosing blebs of plagioclase. The hornblende in this case is commonly sheathed by elongate laths of clinozoisite (Plate 2.9). Ilmenite is often seen in the progress of alteration to sphene.

c) Local dynamic retrogression associated with thrusting has given rise to a zone of saussuritised anorthosites at the south-east end of the complex. The changes in mineralogy brought about by this dynamic retrograd metamorphism are outlined in Section 2.2.5.

The foliation defined by the amphibole (and clinopyroxene) of the early (M_1) assemblages is in some cases overgrown by a second generation of garnet. (The first generation garnet of the M_1 assemblage occurs within this foliation). This second generation garnet occurs as large euhedral grains surrounded by a well developed 'depletion rim' of plagioclase feldspar. Between this depletion rim and the garnet a narrow zone of amphibole/plagioclase symplectite can often be observed. The development of these garnets, throughout the anorthosite and at any one exposure, is very patchy. The significance of this second generation garnet and the evidence for a second, early, high grade metamorphic event (M_2) is discussed in chapter 4.

The petrology of the lower, middle and upper zone anorthosites is now considered in more detail. This is followed by a description of the modified, saussuritised and saussuritised and crushed anorthosites from the south-east end of the body.

STRUCTURAL ENVIRONMENT			
	(A) HINGE ZONE OF ISOCLINAL FOLD	(B) LIMBS OF ISOCLINAL FOLD	(C) SHEAR ZONES
TEXTURES	Within the hinge zone of the fold, equilibrium textures, produced during the early Scourian (M_1) granulite facies metamorphism, are preserved. Plagioclase feldspars show 120° TRIPLE POINT JUNCTIONS with STRAIGHT OR GENTLY CURVED GRAIN BOUNDARIES. Only weak post-crystallization strain phenomena, are present. Plates 2.1, 2.15 & 2.16	Textures indicative of post-crystallization strain. Plagioclase feldspar grain boundaries become highly SUTURED. Individual grains show UNDULOSE EXTINCTION, BENT TWIN LAMELLA and the effects of MECHANICAL FRACTURING. MORTAR TEXTURES are common. In some cases MYMEKITIC ZONES develop along plagioclase-plagioclase and plagioclase-clinopyroxene grain boundaries. Plates 2.2, 2.3, 2.4, and 2.5	POLYGONAL TEXTURES. Mortar textures less common. Plate 2.6.
MINERALOGY	Granulite facies (M_1) metamorphic mineral assemblages. plag ± – Andesine (An_{37}) → Bytownite (An_{75}) ..... Anorthite content of plagioclase feldspar varies with modal colour index of rock cpx ± – Diopside → Salite → Augite ..... amp ± – Mafic rocks (C.I. > 65) Ferroan pargasite → Ferroan pargasitic hornblende ..... Felsic rocks (C.I. < 65) edenite gt ± – Almandine-pyrope garnet (grossular component up to 35%) ..... opx ± – (rare) – Hypersthene En_{63} ..... ilm ..... Variations in the relative concentration of the four main mineral phases (plag, amp, cpx and gt) of this early (M_1) assemblage, produce a complex mineralogical (or compositional) banding of rock types ranging from ultramafite (C.I. 95) to anorthosite (C.I. 5).	Retrogression of early M_1 mineral assemblages. ..... Breakdown and recrystallization of plagioclase feldspar. SCAPOLITE develops along plagioclase-plagioclase grain boundaries. ..... Clinopyroxene is partially or totally replaced by a pale green/blue MAGNESIO-HORNBLENDE — sometimes sheathed by laths of clinozoisite. ..... Partial or total breakdown of (M_1) amphibole to a pale green/blue MAGNESIO-HORNBLENDE and/or BIOTITE ..... Partial breakdown of garnet to an amphibole (magnesio-hornblende)/plagioclase/magnetite SYMPLECTITE-radial intergrowth around garnet ..... ? ? ? ..... Partial breakdown of ilmenite to SPHENE	Localized retrogression of mineral assemblages (limited to shear and a narrow zone either side of shear). ..... Breakdown and recrystallization of plagioclase feldspar. (Breakdown of plagioclase to a zoisite aggregate + minor calcite and scapolite*) Mafic minerals replaced by a complex intergrowth of epidote, chlorite, biotite, magnesio-hornblende, amphibole/plagioclase symplectite (+ magnetite), and sphene. (Mafic minerals replaced by an aggregate of clinozoisite, epidote, chlorite and colourless amphibole-actinolite? *) Assemblages bracketed and marked with an asterix are from saussuritized anorthosites, within and adjacent to early Laxfordian (F_3) shears. These saussuritised assemblages are usually intruded by numerous anastomosing veins of pseudotachylite.

Table 2.1. Summary of mineralogical and textural variations, with respect to structural environment, within the 'anorthosite' body. These variations are further over-printed by a late Laxfordian regional retrogression (M_3) which produces modified assemblages similar to those described under (B). The saussuritisation of anorthosite in some shear zones (C*) produces mineral assemblages similar to those of the saussuritised anorthosites, to the south-east of the Rodil-Finsbay road. The latter are thought to be a result of local dynamic retrogression associated with the coastal thrusting.

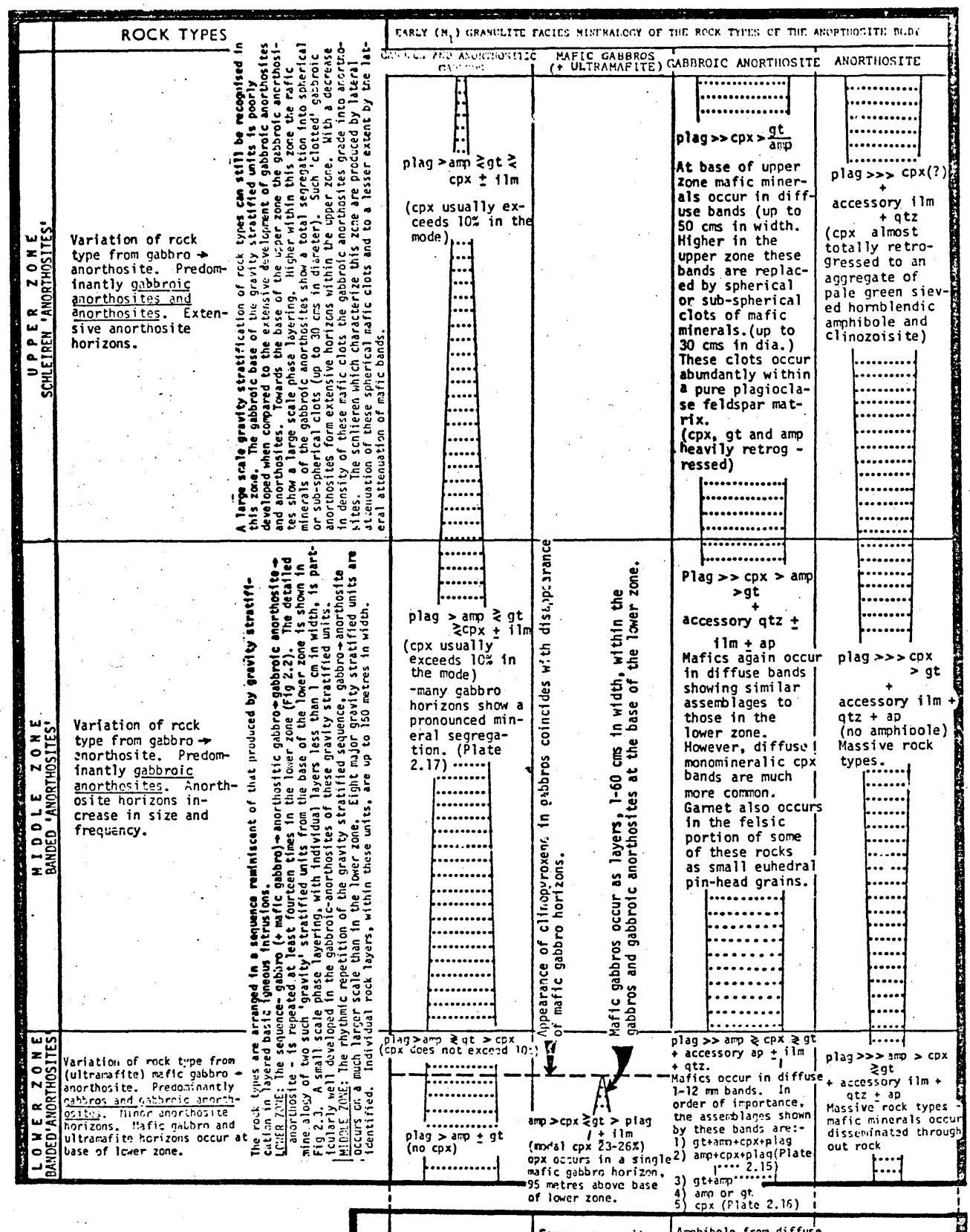


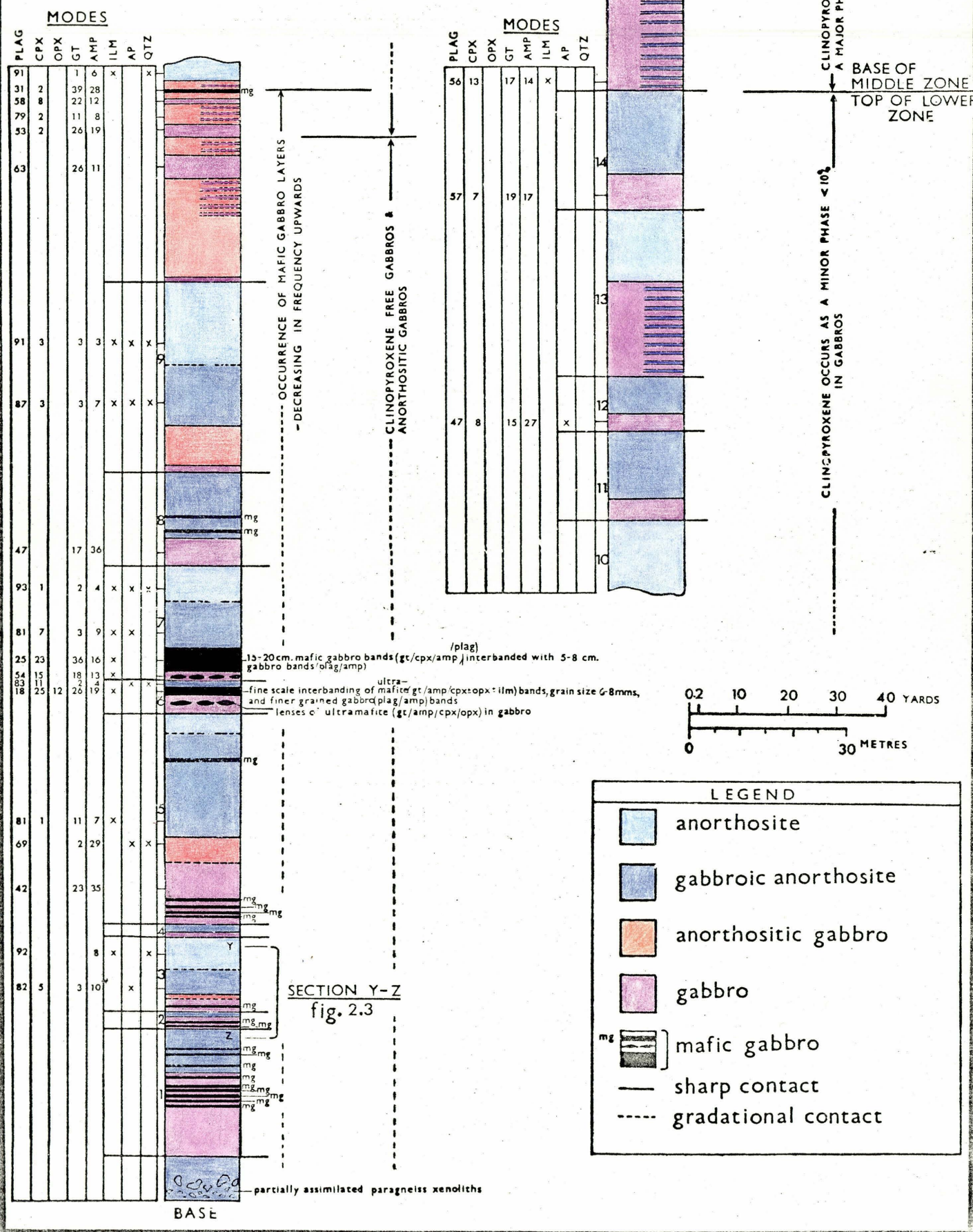
Table 2.2. Summary of the petrology and mineralogy of the 'anorthosite'. The mineralogical data presented in this table summarizes the variations shown by the early (M_1) granulite facies minerals. These assemblages show varying degrees of retrogression. In general, the more felsic types (gabbroic anorthosites and anorthosites) show the greatest effects of retrogression.

2.2.2 The Lower Zone of Banded 'Anorthosites'

This zone varies in width from 68-600 metres. It is thickest in the area north-east of Leverburgh - the nose of the isoclinal fold. Here the most complete succession across this zone has been recorded and it is described in detail below. Considerable tectonic thinning of this zone occurs along both fold limbs, where condensed and incomplete versions of the succession established in the 'nose' area are observed.

The 'anorthosite' rocks of the lower zone exhibit a compositional banding resulting form variations in the relative concentrations of garnet, clinopyroxene, amphibole, plagioclase, feldspar and orthopyroxene. Although this compositional banding or layering is now defined by metamorphic mineral assemblages, it is thought to have been founded upon a primary igneous layering. It is argued that the present banded succession represents an original rhythmically layered igneous sequence. Individual units within this sequence appear to preserve a primary gravity stratification. Such gravity stratified units vary in width from 3 to 42 metres, and in general show a gradation from gabbro (base of unit) - anorthositic gabbro - gabbroic anorthosite - anorthosite (top of unit). Any member of this unit may be absent. The contacts between gabbro and anorthositic gabbro, and gabbroic anorthosite and anorthosite are in all cases gradational over 25-40 cms. All other contacts in these units are sharp. The lower zone is composed of fourteen of these units. A composite section across this zone, from the west slope Ha-Cleit, is shown in fig.2.2. The mineralogy of two gravity stratified units from the base of the lower zone is considered in detail in fig.2.3. The following account is a summary of the main mineralogical features exhibited by the figured, banded succession from the west slope of Ha-Cleit.

fig. 2.2. LOWER ZONE BANDED ANORTHOSITE, WEST SLOPE OF HA-CLEIT



The gabbro layers (colour index 35-65) which form the base of the gravity stratified units are fine grained (grain size 1-2mms), granoblastic rocks typified by the assemblages amphibole/garnet/plagioclase feldspar and amphibole/plagioclase feldspar. The amphibole occurs as small laths and lozenges showing a pleochroic scheme: X pale green-straw; Y green; Z blue/green. Clinopyroxene is entirely absent from these gabbros, until just below the top of the lower zone, where it appears as a minor phase (not exceeding 10%). The arbitary division between lower and middle zones is based on the appearance of clinopyroxene as a major phase in these gabbros. Plagioclase feldspar within these horizons is an andesine (An_{44-48}) and is typically white in hand specimen. With an increase in modal plagioclase these rocks grade into anorthosite gabbro (colour index 20-35).

Mafic gabbros (colour index 65-90) occur as layers 1-30 cms in width within the gabbros (and also the gabbroic anorthosites) of the lower zone (Plates 2.11 & 2.12). These are particularly common at the base of the lower zone, decreasing in frequency upwards, until they finally disappear approximately 120 metres from the top of the lower zone. The mafic gabbros are characterised by an amphibole/clinopyroxene/garnet/plagioclase feldspar/ilmenite assemblage. Garnet (almandine-pyrope) and clinopyroxene (augite-salite) occur in coarse grained (2-3mm), sub-circular clots, up to 9 mms in diameter, within a finer grained amphibole/feldspar (Andesine An_{37}-An_{39}) minor clinopyroxene matrix. In some cases these garnet-clinopyroxene clots can be observed to decrease in diameter (and the garnet to decrease in grain size) towards the top of the mafic gabbro layer (Plate 2.12). The amphibole of the mafic gabbros is a ferroan pargasitic hornblende - ferroan pargasite with pleochroism: X yellow-green; Y brown-green; Z dark brown. These mafic gabbro layers occur within the gabbro



Plate 2.11 Gabbro containing numerous mafic gabbro horizons. Base of lower zone, 120 metres east of Loch na Cachlaidh on the east side of the Rodil-Finsbay road. Upward sequence from right to left.



Plate 2.12 23 cm mafic gabbro horizon. Base of lower zone, 270 metres south-west of Ha-Cleit summit. Upwards sequence right to left.

horizons and not at their base, as one might expect. Up to eight mafic gabbro layers have been recorded from a single 'host' gabbro. In a simple case where one mafic gabbro layer is present, the gabbro immediately below such a layer shows a gradual increase in modal colour index (% of mafic minerals) from its base upwards. This increase in colour index culminates with the mafic gabbro layer and thence gradually decreases within the overlying part of the 'host' gabbro, which often shows a gradational transition to anorthositic gabbro. This variation in colour index is largely brought about by variations in the amount of modal garnet. Modal plagioclase shows an inverse relationship to the colour index. Amphibole, however, shows a decrease from the base of the gabbro upwards and into the mafic gabbro layer. After an initial enrichment immediately above the mafic gabbro layer, the amphibole again shows an overall decrease towards the top of the gabbro horizon (Fig.2.3).

Such a systematic variation in mineralogy is characteristic of all the mafic gabbro bearing gabbro horizons at the base of the lower zone. However, minor modifications to this scheme may occur due to the absence of one or more members of the gravity stratified units (which may be a primary or tectonic feature). At the base of the lower zone, clinopyroxene is entirely absent from the gabbros, but occurs abundantly in mafic gabbro layers within these gabbros. It is interesting to note that the disappearance of mafic gabbro layers from the gabbros near the top of the lower zone, is coincident with the appearance of clinopyroxene as a minor phase in these gabbros. Above this point the amount of clinopyroxene in the gabbro horizons gradually increases with structural height.

Orthopyroxene is a rare phase in the 'anorthosite' and has only been observed from a single mafic gabbro layer in the lower zone. This mafic gabbro occurs approximately 95 metres above the base of

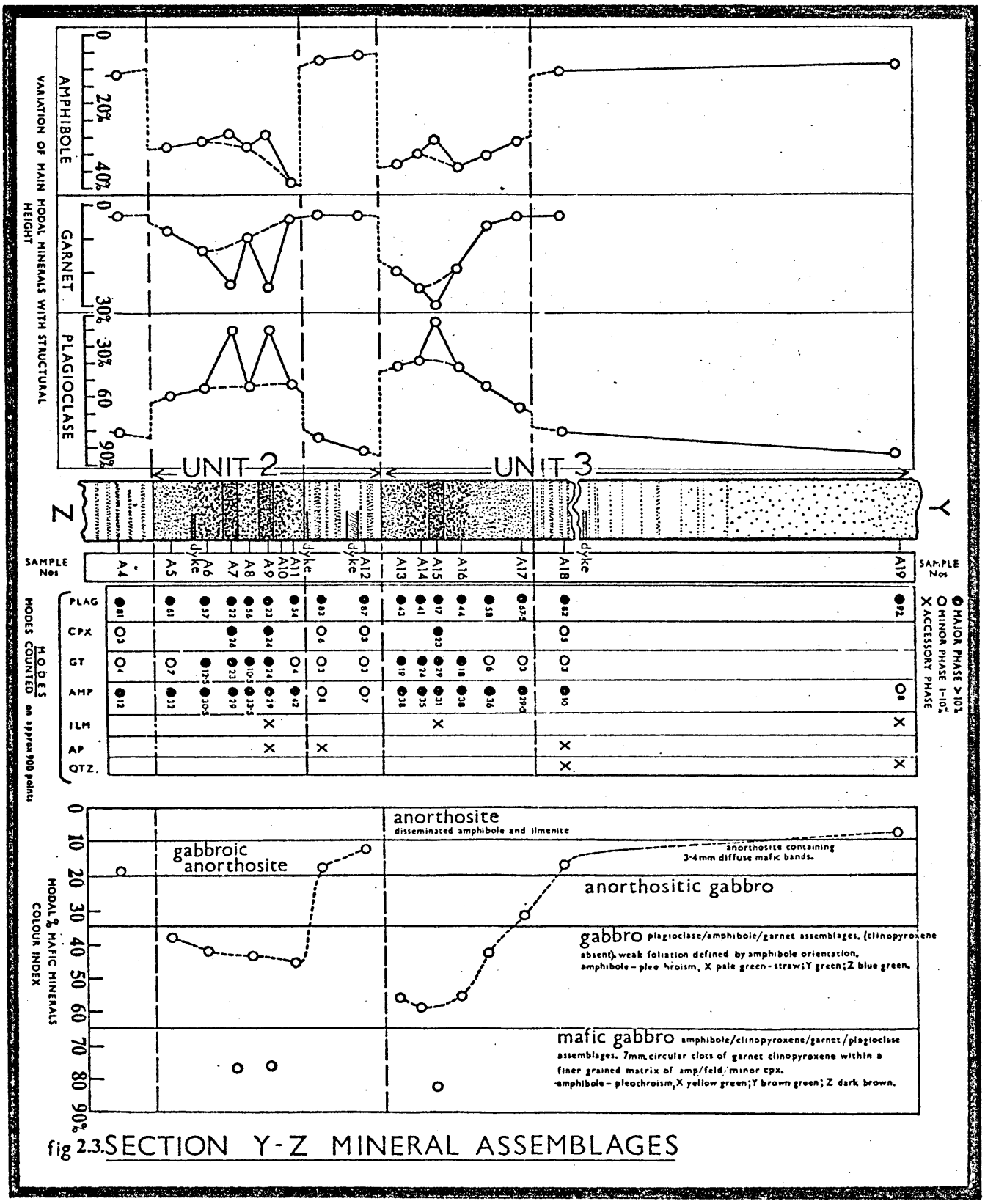


fig 2.3. SECTION Y-Z MINERAL ASSEMBLAGES

the lower zone, in the section studied, and differs markedly in appearance to those previously described. It comprises of an interbanded sequence of coarse grained ultramafite layers and finer grained gabbro layers. (Plate 2.13) The ultramafite layers show a variety of mineral assemblages, two of which are orthopyroxene (hypersthene) bearing:-

gt + amp + cpx + opx + ilm
gt + amp + cpx
amp + cpx + ilm
amp + cpx + opx + ilm
gt + amp

Although gabbros may grade imperceivably into anorthositic gabbros the junction between either of the former with the gabbroic anorthosite member of the gravity stratified units is usually sharp.

The gabbroic anorthosites also contain 14-60 cm wide, parallel-sided mafic gabbro layers. However, unlike the gabbros, no systematic change in mineralogy of the gabbroic anorthosites has been found adjacent to these mafic gabbro layers. The gabbroic anorthosites are essentially anorthosites (s.s.) containing a high proportion of diffuse, 1-12 mm wide, mafic bands (Plate 2.14). The mineralogy of these mafic bands is variable. The commonest type show amphibole/garnet/clinopyroxene/ilmenite/minor plagioclase assemblages. Also of common occurrence are monomineralic garnet, clinopyroxene and amphibole bands, usually of only a single grain's width. Apatite is a common accessory in the felsic parts of the gabbroic anorthosites. With the gradual decrease in density and frequency of the diffuse mafic bands, the gabbroic anorthosites grade into massive anorthosites. Anorthosite (colour index 0-10) forms the top of many of the gravity stratified units. It is in general a massive rock type containing small disseminated grains of amphibole



Plate 2.13 Orthopyroxene bearing mafic gabbro horizon (small scale interbanding of ultramafite and gabbro), 95 metres above the base of the lower zone. - West slope of Ha-Cleit.



Plate 2.14 Banded gabbroic anorthosite. Base of lower zone - West slope of Ha-Cleit.

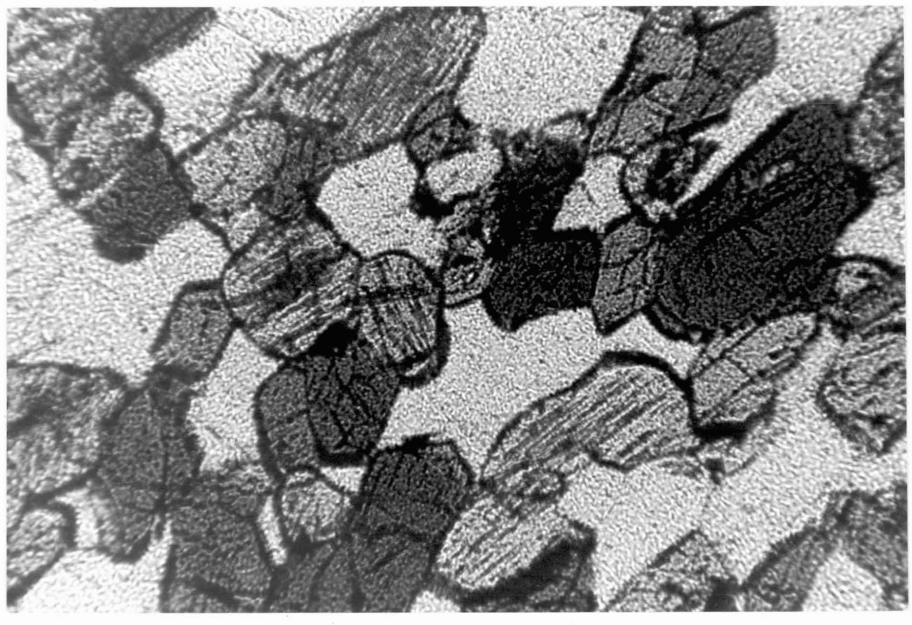


Plate 2.15. Diffuse amphibole (dark) clinopyroxene (grey), plagioclase (white) band from a gabbroic anorthosite. Base of lower zone. X80. Plane polarised light. Slide no. 40827

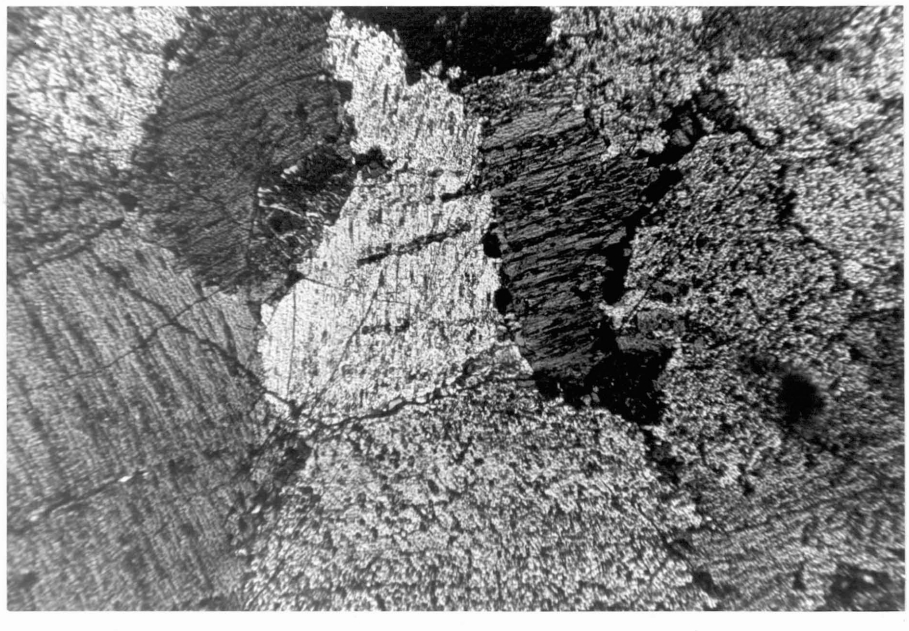


Plate 2.16. 4mm clinopyroxene band from a gabbroic anorthosite. Top of lower zone.
Note 120^{o} triple point junctions and curved grain boundaries.
X80. Crossed polarised light. Slide no. 39994

and clinopyroxene. Accessory ilmenite and quartz are often observed in these rocks.

The plagioclase feldspar of the gabbroic anorthosites (labradorite An_{56-59}) and anorthosites (Labradorite An_{64-68}) may vary in colour from purple - pink - mottled pink/white - white. Davidson (1943) has suggested that the pink colouration of the feldspars is due to small brownish-red rutile rods scattered throughout the feldspar. Such rod-like inclusions are frequently orientated parallel to (010) - the composition plane of the albite twin lamellae. - and often show a zonation.

Probe analyses of these inclusions have detected only small amounts of titanium. It is thought, as previously suggested by Westoll (1967), that the inclusions, within the feldspars, are of haematite (and possibly of rare titanohaematite).

No systematic change in the colour of the feldspars of the gabbroic anorthosites and anorthosites has been observed. Colour variations often take place laterally along any one horizon and frequently hand specimens of these rocks will exhibit feldspars of varying colour. It should be noted, however, that the andesine feldspars of the mafic gabbros, gabbros and anorthositic gabbros are always white.

2.2.3 The Middle Zone of Banded 'Anorthosites'

The most complete section across the middle zone banded 'anorthosites' is patchily exposed on the north-west slopes of Roneval, over approximately 2 kms. The rhythmically banded sequence of gravity stratified 'anorthosites' of the lower zone is repeated, with minor mineralogical differences and, on a much larger scale, in the middle zone. The rocks of the middle zone again vary from gabbro to anorthosite in composition. Mafic gabbro layers, characteristic of the base of the lower zone, are absent.

The most conspicuous features of this zone are the gabbro horizons. Dearnley (1963) referred to these when he described the occurrence, from this area, of large patches (up to 100 yards across) of garnetiferous anorthosite. Eight major gabbro horizons, 55-120 metres in width, have been recorded in addition to numerous minor gabbro bands 1-30 metres in width. The typical assemblage of these gabbro is:-

plag (Andesine-Labradorite, An_{48-52}) > amp $\gtrless$ gt > cpx $\pm$ ilm

Clinopyroxene occurs in all of these gabbros as a major phase(>10%). The relative proportions of the four major phases of the gabbros, show no systematic change with structural height and appear remarkably constant. However, texturally, two types of gabbro can be distinguished:-

a) Fine grained, uniform, garnetiferous gabbros, similar in hand specimen to those found in the lower zone. (Plate 2.17A). This type forms the minor gabbroic horizons (up to 30 metres in width) in the middle zone.

b) Coarser grained gabbros showing a pronounced mineral segregation (Plate 2.18)* These show a well-developed segregation into irregular patches of:-

   i) amp/white plagioclase feldspar/minor cpx

   ii) gt/cpx/pink plagioclase feldspar

In general this type forms the major gabbroic horizons in the middle zone. However, within these horizons, it may merge laterally and vertically into gabbros of the first type.

In the anorthosites or gabbroic anorthosites, immediately below the major gabbro horizons, circular or oval clots of mafics occur. Mineralogically these clots are similar to the gabbros. Good examples of such mafic clots can be examined, 230 metres E.N.E. of Roneval summit (the 'orbicular' rocks of Dearnley) and 390 metres S.W. of

* see also Plate 2.17B



Plate 2.17. Gabbro - 85 metres above base of middle zone.
Left: fine grained garnetiferous gabbro (A)
Right: coarse grained gabbro showing a pronounced mineral segregation (B) - see also Plate 2.18.

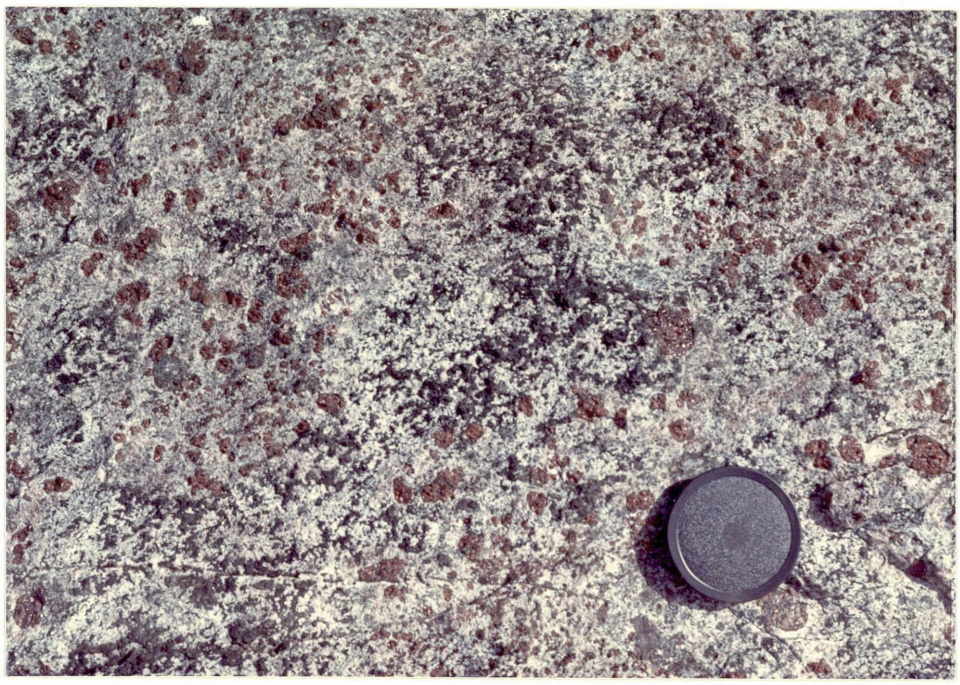


Plate 2.18. Gabbro - 340 metres above base of middle zone.
Note pronounced mineral segregation.

Ha-Cleit summit. These clots rarely exceed 30 cms in diameter, and first appear 8-20 metres below the base of the gabbros.

The gabbro horizons are overlain by gabbroic anorthosites. These are essentially anorthosites containing diffuse 1-2 cm bands of clinopyroxene, and to a lesser extent clinopyroxene and amphibole. Diffuse clots and irregular patches of clinopyroxene (plus minor scapolite and plagioclase), up to 20 cms in diameter, occur in many gabbroic anorthosite horizons.

Garnet is rare in these mafic bands and clots and develops preferentially as small euhedral pin head grains in the felsic portion of the gabbroic anorthosite. The plagioclase of these rocks is a labradorite An_{64-69}, occasionally sieved by numerous inclusions of quartz.

With a decrease in the percentage of mafics the gabbroic anorthosites grade into anorthosites. These are massive rocks composed predominantly of a white/pink bytownite feldspar (An_{69-72}), Clinopyroxene and garnet (plus minor ilmenite) are the main mafic phases in the anorthosites.

Throughout the anorthosites and gabbroic anorthosites of the middle zone, clinopyroxene appears to be the predominant mafic phase. The clinopyroxene may show all stages in alteration to a pale green amphibole, sieved by abundant plagioclase inclusions.

2.2.4 The Upper Zone of Schlieren Anorthosites

This zone is characterised by the predominance of schlieren anorthosites, which are exposed over most of the south-eastern slope of Roneval. Within the upper zone, horizons of massive pure anorthosite (s.s.) are more common and more extensive than in either of the two preceeding zones. Clinopyroxene bearing gabbro horizons, although still in evidence, show a marked decrease in size and frequency.

The schlieren anorthosites, which comprises 65-70% of this

zone, are mainly gabbroic anorthosites (10-20% mafic minerals) but vary according to the density of mafic schlieren. The schlieren or 'fish' in any one horizon are uniform in orientation, but vary considerably in size and shape, both laterally and vertically, in the succession. In plan view there is a gradation in shape from perfectly circular schlieren to highly elongate lensoid schlieren. Circular schlieren vary in size from 20 cms to 30 cms in diameter. Lensoid types show a greater variation in size, but are usually from 25 cms to 70 cms in length and 5 cms to 12 cms in width.

Many of the schlieren must have formed by the lateral extension of original mafic bands. This process, in many cases, can be observed in the field. The degree of lateral extension and the original thickness of the bands must both influence the subsequent shape of the schlieren. However, not all the schlieren appear to be derived in this way. The deformation of a band, for instance, could in no way produce circular or sub circular schlieren. Also one would expect the lateral extension of a band or banded sequence to produce parallel trains of schlieren, individual schlieren being set end upon end. However this is hardly ever the case, the schlieren more commonly showing an 'en echelon' relationship. This type of relationship could be better explained if one evoked the lateral attenuation of a number of randomly scattered circular or sub-circular mafic clots. Such circular clots would be preserved in areas of low deformation.

There are two main types of schlieren:-

a) Highly diffuse, nebulous types: These, in all cases, occur as elongate lensoids, showing a plagioclase, clinopyroxene, amphibole, garnet assemblage. They usually occur interlayered with diffuse mafic bands, from which they are derived. Examples of these schlieren can be found 360 metres due north of Beinn Na H-Aire.

Upper Zone Schlieren Anorthosites

Plate 2.19. 160 metres W.N.W. of the anorthosite quarry, Rodil/Finsbay road.

Plate 2.20. 320 metres N.E. of Beinn na h-Aire.

Plate 2.21. 310 metres east of Beinn na h-Aire.

Plate 2.22. 10 metres S.W. of anorthosite quarry, Rodil/Finsbay road.

Plate 2.23. 730 metres north of Loch na Cachlaidh.











b) Semi-diffuse or non-diffuse types: (Plates 2.19 - 2.23). These are the most commonly occurring schlieren and vary in shape from circular to lenticular (Circular and spheroidal schlieren of this type can be found in exposures 350 metres north-east of Beinn Na H-Aire). This type of schlieren is thought to be almost always derived from original circular mafic clots. The schlieren are dark green in colour and in the majority of cases are composed of a pale green/blue sieved amphibole, enclosing blebs of plagioclase and associated with elongate laths of clinozoisite and anhedral grains of sphene. Plagioclase (An_{65-72}) occurs disseminated throughout the schlieren. Garnet and clinopyroxene (from which the sieved amphibole is derived) are rare phases in these schlieren.

The schlieren anorthosites, in general, show an almost total segregation of the mafic minerals into the schlieren. Only minor amounts of sieved amphibole occur disseminated throughout the anorthosite host. The plagioclase of the host anorthosite is a pink/white labradorite-bytownite, forming an interlocking granoblastic meshwork of coarse grained well twinned crystals. The schlieren anorthosites grade into massive anorthosites by a decrease and final disappearance of the mafic schlieren.

2.2.5 Saussuritised Anorthosites

At the south-east end of the anorthosite complex, the 'anorthosites' of the lower, middle and upper zones are saussuritised. The saussuritised anorthosites are characterized by a buff/white chalky appearance in hand specimen. The division between unsaussuritised and saussuritised rocks is a sharp one and can usually be defined within 30-60 cms. The area of saussuritised anorthosite is delimited in fig.2.1. However, within this area both large and small, irregular areas of unsaussuritised rock occur. In particular many thick gabbro bands in this area tend to have unsaussuritised cores.

The process of saussuritisation mainly involves the alteration of the plagioclase feldspar to a zoisite aggregate. The degree of saussuritisation increases towards the coast. The plagioclase feldspars of the least saussuritised anorthosites (from the quarry area, and from the west side of the Rodil-Finsbay road)show only a partial alteration to zoisite. Alteration appears to start in the centre of the feldspar grain, possibly because the calcium rich zoisite forms more easily from an anorthite rich feldspar. However, many of the feldspars of these rocks also show a preferential alteration to zoisite along individual albite twin lamellae, which is obviously not compositionally controlled. Samples from north of Loch Vallarip and north-east of Loch na H-Uama, show a more complete replacement of the feldspar by zoisite. In some slides no fresh feldspar remains. The zoisite is fine grained, laths rarely exceeding 0.5 mm in length. The original outlines of the feldspar grains are in some cases outlined by flakes of a colourless sericitic mica. The replacement of the plagioclase feldspar by zoisite must release the alkali component of the feldspar. As the potash content of the anorthositic feldspars is very low, this would be mainly sodium and the colourless mica, in all probability, would be a paragonite.

Zoisite may occasionally be associated with small amounts of calcite. Scapolite occurs infrequently in the saussuritised anorthosites.

The process of saussuritisation also releases a certain amount of free quartz. Superimposed on any previous variation in the modal quartz content of these rocks is an increase in modal quartz (maximum values 15-16%) with increase in the degree of saussuritisation.

The density of the saussuritised anorthosites ranges from 2.9 - 3.3 as compared to an average value of 2.75 for the unsaussuritised anorthosites. This fact is easily explained by the replacement of plagioclase feldspar, average density 2.71 by zoisite, density 3.15 - 3.27.

The mafic minerals of the 'anorthosites' are altered to an aggregate of:-

Epidote + clinozoisite + chlorite $\pm$ zoisite $\pm$ colourless amphibole.

Garnet tends to show the greatest resistance to saussuritisation and may often be found in the highly saussuritised anorthosites adjacent to the coast. Frequent examples of altered symplectite rims around unaltered garnets are observed.

Dearnley (1963) noted the occurrence of saussuritised anorthosites in this area, and attributed the process by which these were formed to dynamic retrograde metamorphism associated with movement along the coastal thrust. In this connection it should be re-emphasized that the degree of saussuritisation does increase towards the thrust zone. Also the front of saussuritisation can be seen to roughly parallel the trend of the thrust zone.

Saussuritised rocks are by no means confined to this area. Saussuritisation of the anorthosite develops throughout the complex in association with early Laxfordian (F_3) and late Laxfordian (F_4) shears. In this case it is a very localized phenomenon, usually confined to a 2 metre wide zone either of the shear, and usually associated with minor pseudotachylite veining.

2.2.6 Crushed and Saussuritised Anorthosites

Anorthosites of this type are found above the coastal thrust zone. They are white flinty rocks in hand specimen and give the appearance of having been crushed and mylonitized. These rocks are highly saussuritised, little or no feldspar remaining, but differ from those saussuritised types to the west of the thrust zone in several ways:-

a) The grain size of the zoisite and paragonite, in these rocks, is considerably smaller.

b) Paragonite is much more abundant.

c) Quartz is much more abundant, but rarely visible in hand specimen.

In more gabbroic varieties, quartz may completely pseudomorph garnet grains.

The crushed and saussuritised anorthosites are apparently derived from the south-east, having been thrust into their present position at a very late stage in the evolution of the complex. Internal crushing of this overthrust slice of anorthosite is much in evidence. Late Laxfordian alkali pegmatites, intruded into these rocks prior to thrusting, have been 'streaked out' into thin bands and lenses.

2.2.7 Summary

A number of conclusions, regarding the nature of the anorthosite body, can be made at this stage:-

a) The present mineral assemblages of the anorthositic rocks reflect both the nature of the metamorphisms within the area and the original bulk chemistry of the rocks.

b) The 'anorthosite' is clearly an intrusive body. Small angular xenolithic blocks of the quartzose paragneiss (supracrustals) can be observed within anorthosites, north of Loch Na Cachlaidh and

north of Rubha Skuta.

c) The anorthosite is a highly banded intrusion. The observed compositional banding is thought to have been founded upon an original igneous banding. Both the lower and middle zones of the anorthosite are thought to comprise a rhymically banded sequence of gravity stratified rocks ranging from gabbro to anorthosite in composition. The upper zone, in contrast, comprises mainly massive anorthosites. The mafic minerals in these massive anorthosites occur originally as spheroidal clots.

d) From field observations, the upward sequence within the 'anorthosite' is from the margin to the centre of the body. As the major isoclinal fold, involving the anorthosite complex, is antiformal this sequence is inverted on both fold limbs.

e) Anorthosite (0-10% mafic minerals) forms a number of horizons within this body, but is subordinate to the more gabbroic members of the sequence. The average composition of the 'anorthosite' body approaches that of a gabbroic anorthosite.

The 'anorthosite' body is thought to represent a folded and metamorphosed basin or sheet like stratiform intrusion, formed by gravity differentiation of a gabbroic anorthosite magma. The earliest recognizable textures and mineral assemblages date from the Scourian high grade metamorphic event. No primary igneous textures (or minerals) have been observed.

It is debatable whether any primary igneous textures are mimetically preserved. Igneous textures preserved by simple replacement (pseudomorphing) have not been found. If, as has been inferred, gravity differentiation was a factor in the formation of this banded sequence of rocks, then one might expect some degree of orientation of the original igneous minerals. It is tentatively suggested that the orientation of these older igneous crystals may have controlled the

growth of newer metamorphic ones. This may, to some extent, accout for the well developed foliation (which is everywhere parallel or subparallel to the compositional band'ng) in these rocks.

2.3 The Gabbroic Rim of the 'Anorthosite'

The 'anorthosite' is completely surrounded by a gabbroic rim of varying width. North of Leverburgh, this rim attains its maximum width of 120-350 metres. To the south-east of this region it thins out and rarely exceeds 40 metres in width. A section of the gabbroic rim 3.2 Kms in length from the north-west end of the complex has been mapped in detail. The general distribution of the rock types within this section of the rim is shown in fig.2.4. A section of the gabbroic rim, from the west slope of Ha Cleit and a 750 metre section of the rim to the north of the Abhainn Easean Chais stream, are shown respectively in maps 2 & 3.

Three major lithological types within this gabbroic rim can be recognized:-

a) Banded ultramafites and mafic gabbros, occurring as large podiform bodies usually situated centrally within the quartz gabbros (b). These account for approximately 25-30% of the rim.

b) Quartz gabbros constitute approximately 55-60% of the rim. These contain abundant small torpedo-shaped bodies of ultramafite/mafic gabbro and equally numerous lenses and strips of quartzose paragneiss.

c) Quartzose paragneisses, lithologically and chemically similar to those found rimming the anorthosite complex, occur in a variety of modes within the gabbroic rim:-

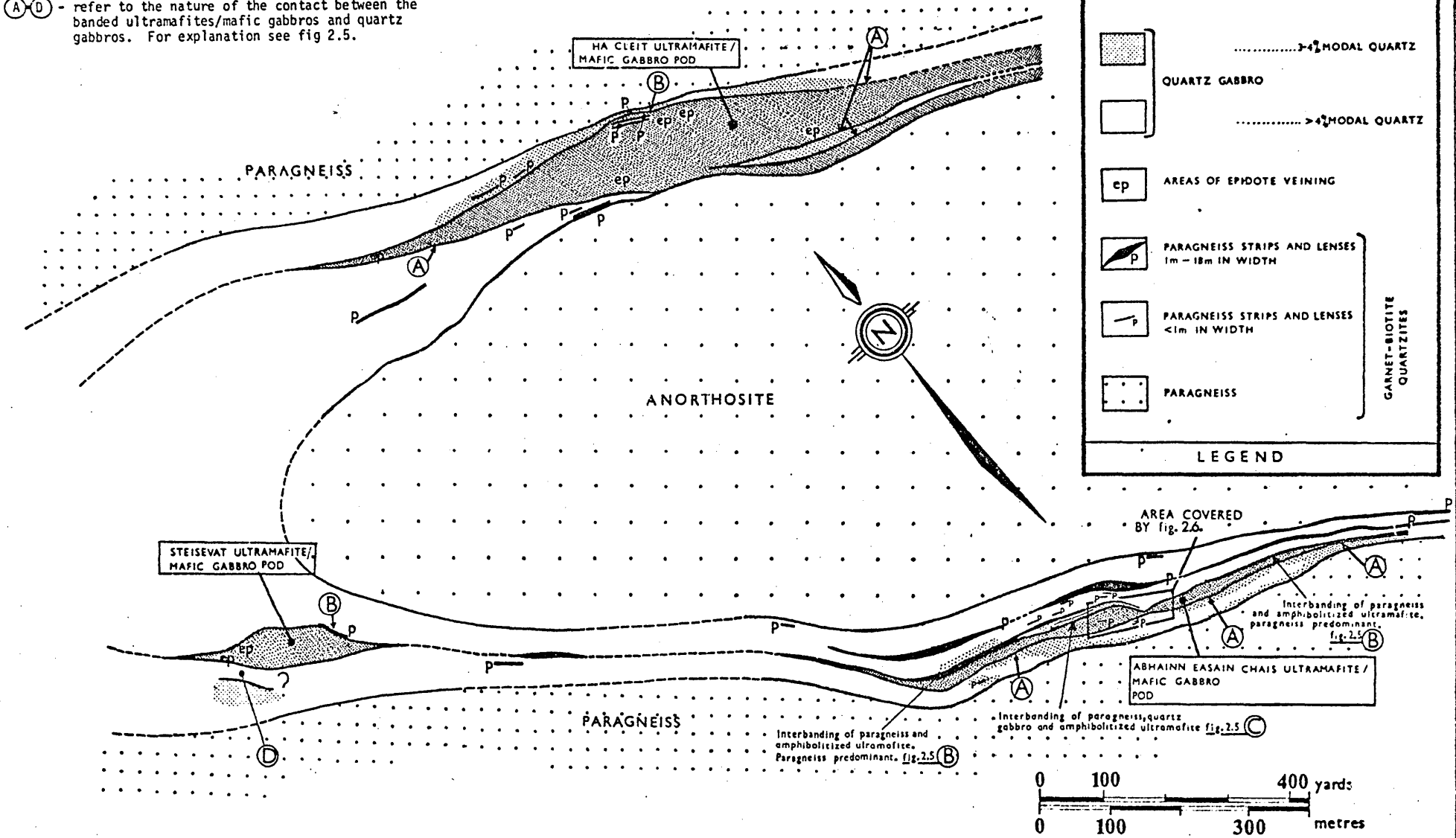
I) As discontinuous paragneiss strips occurring along the quartz gabbro - 'anorthosite' contact. Partial assimilation of this paragneissic material by the 'anorthosite' immediately adjacent to these strips has been observed.

II) Paragneiss strips occur along many of the quartz gabbro

Fig. 2.4.

THE GABBROIC RIM OF THE ANORTHOSITE COMPLEX

Ⓐ-Ⓓ - refer to the nature of the contact between the banded ultramafites/mafic gabbros and quartz gabbros. For explanation see fig 2.5.



- ultramafite/mafic gabbro contacts and also within the ultramafite/mafic gabbro pods.

III) A whole host of paragneiss strips and lenses of variable dimensions are found within the quartz gabbros. Along the southern gabbroic rim of the 'anorthosite', a series of paragneiss lenses, the largest of which is 270 metres in length and 18 metres in width, are traceable over 4 Kms. At the margins of these lenses an interbanding of smaller paragneiss strips and quartz gabbros is apparent. In all cases, the contacts between paragneiss and quartz gabbro are sharp and well defined.

Estimates of the percentage of paragneissic material within the gabbroic rim vary from 10-20%.

The paragneisses are, in all cases, garnet-biotite quartzites, with minor amounts of plagioclase (oligoclase) and potash feldspar (microcline). In some, the oligoclase feldspar carries small anti-perthitic blebs of an alkali feldspar. Quartz is the dominant mineral, occurring as somewhat elongate grains up to 1 cm long. Trains of bubbles are common in the quartz grains and undulatory extinction is prominent.

2.3.1 Banded Ultramafites and Mafic Gabbros

1. Field Relations

The ultramafites and mafic gabbros occur in large podiform bodies, usually situated centrally within the quartz gabbros. Three large pods at the north-west end of the complex have been mapped and sampled in detail (fig.2.4). Similar pods of ultramafite and mafic gabbro occur within the quartz gabbros along both contacts to the coast.

Centrally the ultramafite/mafic gabbro pods show a compositional layering or banding. This banding is lost towards the margins of the

pod where the rocks become amphibolitized and develop a deformational (L-S) fabric.

The marginal relationships of the ultramafite/mafic gabbro pods are highly complex. Four types of contact are described below (fig.2.5). The nature of any one contact may vary along its length.

a) Where the amphibolitized ultramafites/mafic gabbros are in direct contact with the quartz gabbros, the contact is sharp. A high proportion of small lenses of ultramafite/mafic gabbro characterize the quartz gabbros adjacent to such a contact.

b) An intervening strip (or strips) of quartzose paragneiss often occur(s) along this contact (North contact of Easean Chais Pod, Map 3). Individual paragneiss strips vary in width from 3-30 metres. In these areas, immediately adjacent to the margin of the pod, there is a very fine interbanding of paragneiss and amphibolitized ultramafite/mafic gabbro. (Plate 2.32)

c) Less frequently all three components of the gabbroic rim can be seen interbanded along the contacts of these pods. Each component, quartz gabbro, paragneiss and amphibolitized ultramafite/mafic gabbro, occurs as discrete strips. The ultramafite/mafic gabbro often also occurs as small (up to 1 metre in length) lenses within the quartz gabbros and paragneisses, of such an interbanded sequence.

d) Adjacent to the southern contact of the Steisevat Pod, large lenses of partially amphibolitized ultramafite/mafic gabbro occur in a massive hybridized matrix. Within this hybridized matrix patches of quartz gabbro and quartzose paragneiss can be found. However, the main bulk of the matrix material appears to be an admixture of these two types.

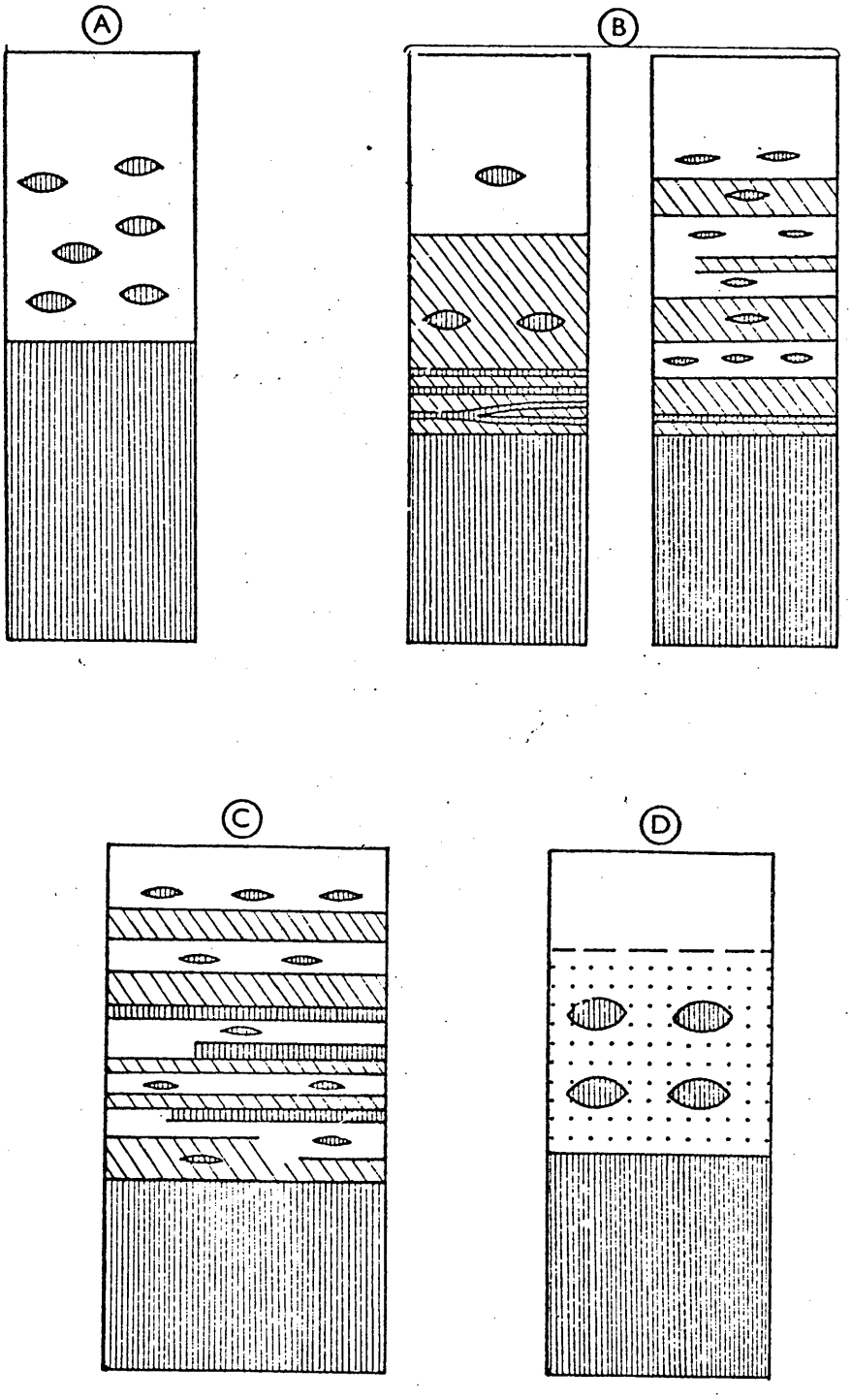


fig.2.5DIAGRAMATIC SECTIONS ACROSS THE CONTACTS OF THE ULTRAMAFITE/ MAFIC GABBRO PODS

UNORNAMENTED – QUARTZ GABBRO : CROSS HATCHED – PARAGNEISS
VERTICAL HATCHING – ULTRAMAFITE/MAFIC GABBRO : DOTTED – HYBRIDIZED ROCKS

Paragneiss strips also occur within the ultramafite/mafic gabbro pods. Where these occur towards the margin of the pod they are orientated parallel to the deformational (L-S) fabric of the host rocks. Elongate lenses and strips of paragneiss occur centrally within these pods, orientated parallel to the compositional banding.

2. Petrology

These rock types invariably show both a large scale and small scale lithological banding. The disposition of this banding is shown in figs. 4.3 & 4.4. In most cases the strike of the banding shows a large angular discordance with the margins of the ultramafite/mafic gabbro pods. The ultramafites and mafic gabbros are medium to fine grained rocks, the grain size ranges up to about 6 mms, often with great variation due to the development of large xenoblastic garnets in some horizons. A granular texture of mostly equidimensional grains is prevalent in these rocks, although there is usually a weak amphibole orientation lying in the plane of the banding. Such a lithological banding or layering is a characteristic feature of all the ultramafites and mafic gabbros studied, but is particularly well preserved in exposures north-east of the Abhainn Easean Chais on the southern flank of the anorthosite complex. The nature of the banding in this area is shown in fig. 2.6 and two detailed measured sections through this banding are shown in fig. 2.7. The description of the banding given below is largely based on observations taken from the figured area, but in general these observations apply to all the banding developed within these rocks.

The minerals within the ultramafites and mafic gabbros appear to belong to a high grade metamorphic assemblage (M_1 granulite facies), but structures and textures reminiscent of primary igneous features may be observed. The figured banding in the Easean Chais pod is thought to represent a metamorphosed and inverted sequence of gravity stratified gabbros and ultrabasics, showing a large scale rock

fig. 2.6.

BANDED ULTRAMAFITES AND MAFIC GABBROS ABHAINN EASEAN CHAIS POD

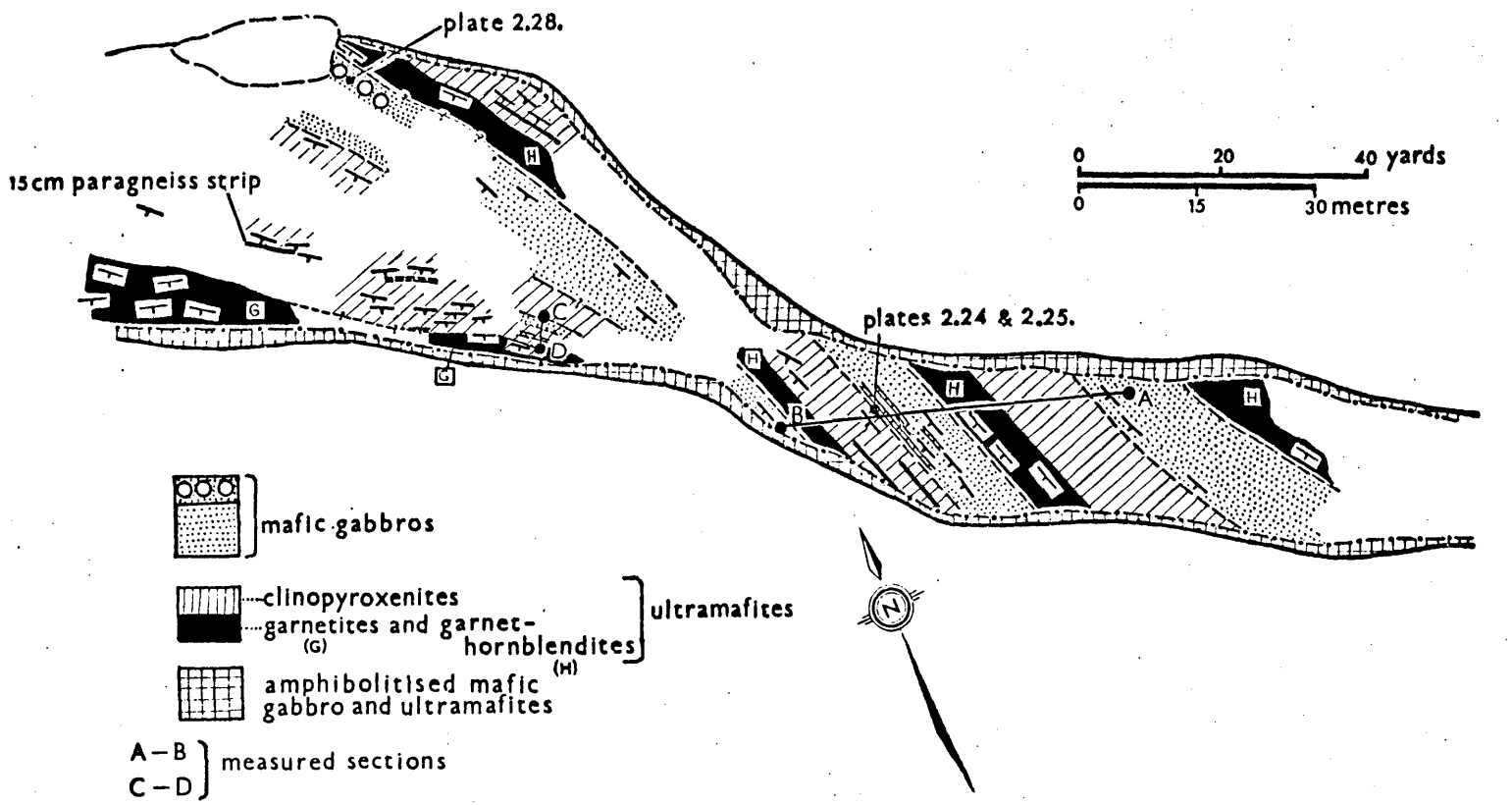


fig. 2.7. MEASURED SECTIONS–EASEAN CHAIS BANDED ULTRAMAFITE/MAFIC GABBRO SEQUENCE

mafic gabbro >10% plagioclase feldspar

ultramafite
- clinopyroxene predominant phase
- amphibole and/or garnet predominant phase(s)

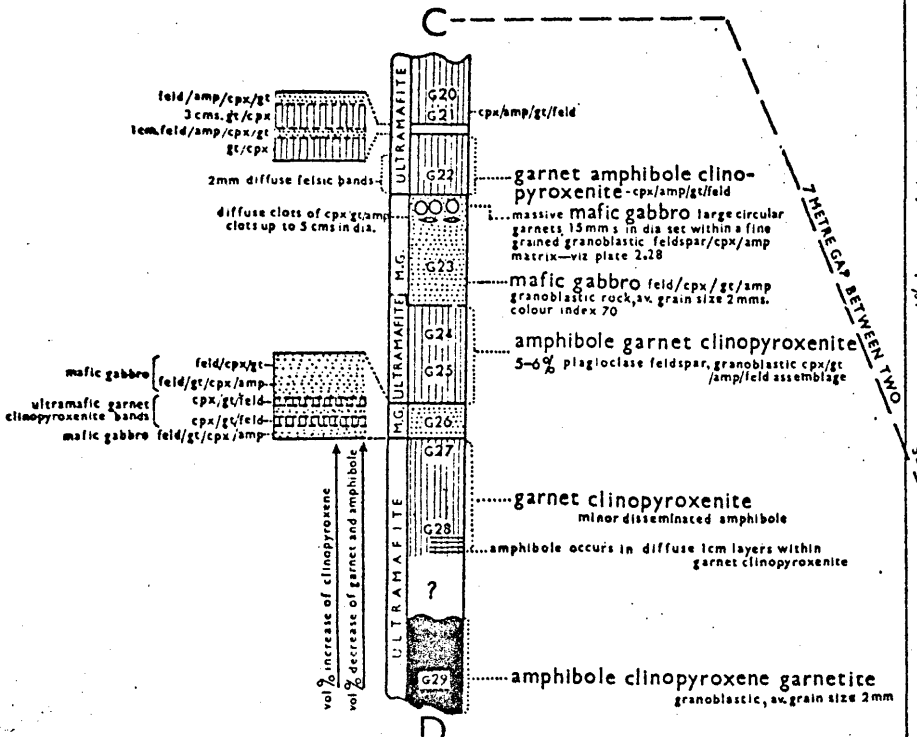
opx	orthopyroxene
feld	plagioclase feldspar
gt	garnet
cpx	clinopyroxene
amp	amphibole
m.g.	mafic gabbro

mineral assemblages–minerals listed in decreasing order of importance

SECTION C-D

length of section 2·6 metres

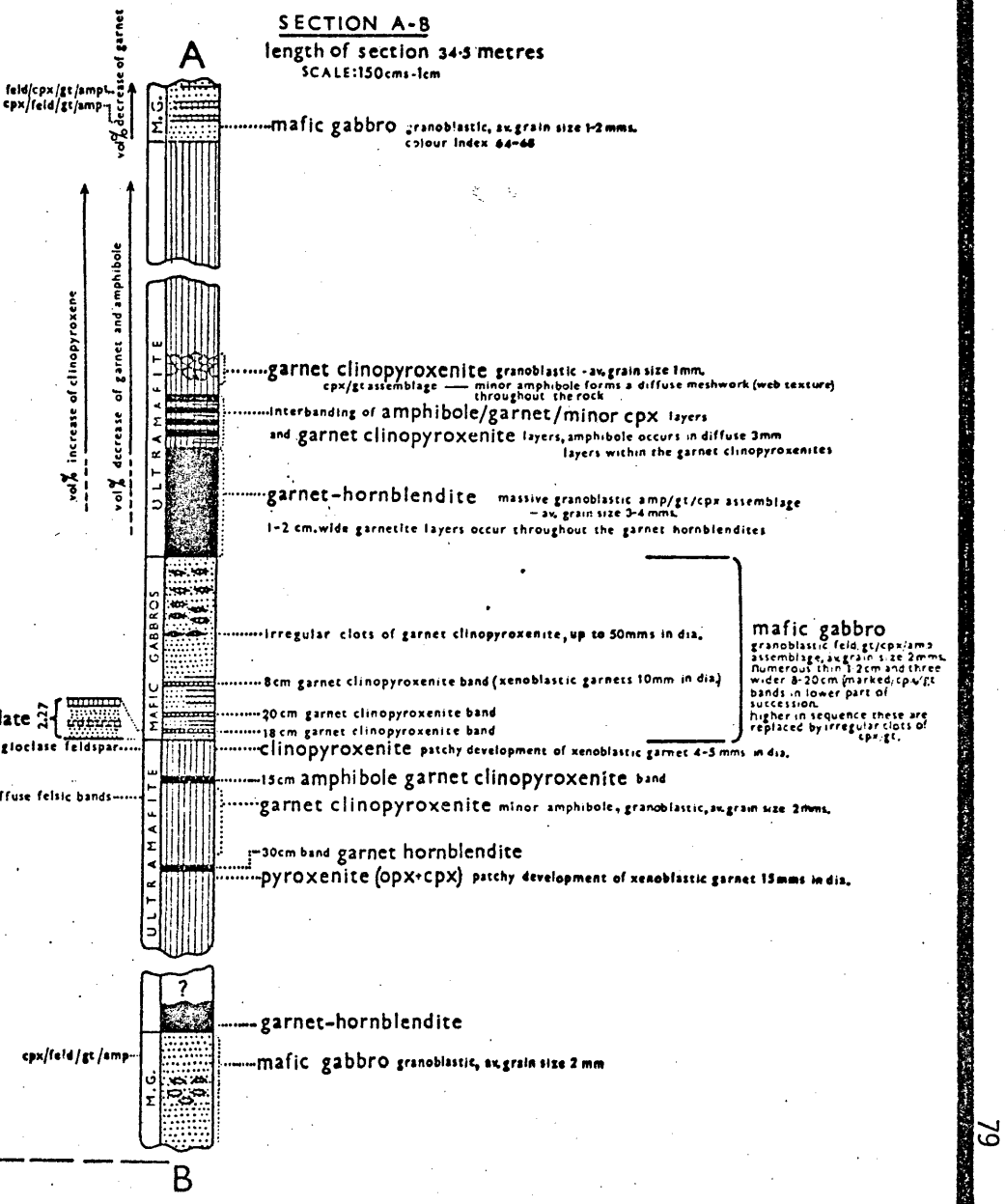
SCALE: 20cms-1cm



SECTION A-B

length of section 34·5 metres

SCALE: 150cms-1cm



layering and small scale rhythmic layering.

The banding in these rocks is a result of variaitions in the relative concentrations of garnet, clinopyroxene, amphibole and plagioclase feldspar. A large scale banding (rock layering) is defined by the alternation of ultramafic units (colour index 90-100) and mafic gabbro units (colour index 65-90). Within these large units, which vary from 15-30 metres in width, a small scale banding (rhythmic layering) with individual layers ranging from 1-30 cms in width is commonly developed.

i) Ultramafite Units

The ultramafite units are dark green-red weathering bands, up to 30 metres in width. A threefold division of these units is possible:-

a) A lower 'basal zone', 4-5 metres in width, of massive garnet/amphibole rock. - garnet hornblendites and amphibole garnetites.

b) A 'transitional zone' of interbanded garnet/amphibole rock and garnet clinopyroxenites.

c) An 'upper zone', 6-9 metres in width, of garnet clinopyroxenites and clinopyroxenites.

The lower zone of the ultramafite units is characterized by a massive granoblastic (average grain size 3-4 mms) garnet/amphibole rock. Within the ultramafite units which are low in the figured sequence, garnet is the major phase of the rocks of this zone (amphibole - garnetites.) However, in ultramafite units which are higher in this sequence, amphibole predominates over garnet in this zone. In the latter case the rocks are garnet - hornblendites and often show a fine banding due to the occurrence of minor, 1-2 mm wide, amphibole-garnetite layers. Clinopyroxene is always present as a subordinate phase.

Upwards from the base of this zone, the volume percent of clinopyroxene increases, with a complementary decrease in the volume

percent of both amphibole and garnet. Approximately 4-5 metres above the base of the ultramafite unit a very fine scale interbanding of amphibole/garnet rock and garnet clinopyroxenite is observed. This interbanding is emphasized by the differing grain size of the two components, the garnet clinopyroxenite being finer grained, having an average grain size of 1-2 mm. Near the base of each unit, individual garnet clinopyroxenite bands are from 5-10 mms in width, but increase upwards in both width and frequency until garnet clinopyroxenite is the predominant rock type. Amphibole is a subordinate phase within the garnet clinopyroxenites and shows a gradual decrease in abundance through the upper zone but is never entirely. absent. Garnet clinopyroxenites, within and just above the transitional zone, show a faint banding due to the occurrence of diffuse amphibole layers, usually no more than a few millimetres in thickness. Higher within the upper zone the garnet clinopyroxenites become massive, amphibole occurs somewhat patchily within these rocks, but in many instances it can be seen to form a diffuse meshwork throughout the rock, delimiting sub -circular areas, approximately 4-5 cms in diameter, of fine grained garnet and clinopyroxene.

A gradual decrease in the volume percent of garnet from the base of the ultramafite unit becomes more pronounced in the upper zone garnet clinopyroxenites. Towards the top of the upper zone the remaining garnet develops as large scattered xenoblastic grains (10-15 mms in diameter), commonly enclosing small grains of clinopyroxene and less commonly sphene, set within a groundmass of polygonized clinopyroxene.

Plagioclase feldspar, occasionally occurring as diffuse bands, appears as a phase towards the top of the upper zone. The amount of plagioclase increases towards the top of this zone but nowhere exceeds 5-6% of the total volume of these rocks.

The contact with the overlying mafic gabbros is usually sharp, but may be gradational over approximately 20 cms.

The alternation of thin amphibole and amphibole/garnet layers with anhydrous clinopyroxene/garnet layers, in the transitional zone poses problems regarding the nature of the amphibole. If the amphibole is entirely metamorphic in origin it would be very difficult to envisage a mechanism which would effectively confine it to certain thin layers only. Windley et al. (1973) have also noted an intimate interlayering of amphibole free and amphibole bearing assemblages from the meta-igneous rocks of the Fiskenaesset complex, west Greenland. Several lines of reasoning have lead them to the belief that some primary amphibole existed in the original igneous rocks.

ii) Mafic Gabbro Units

The mafic gabbros are green-grey weathering rocks forming bands which are up to 10 metres in width.

These rocks are, in general, fine grained (average grain size 1-2 mms) granoblastic plagioclase feldspar, clinopyroxene, garnet, amphibole rocks. At the base of this unit the mafic gabbros often show a very fine interbanding with ultramafic garnet-clinopyroxenites. (containing 2-3% plagioclase feldspar and minor amphibole). Individual bands of both rock types usually do not exceed 30 cms in width. Occasional larger garnet-clinopyroxenite bands, from 50-75 cms in width, occur within this sequence. Examples of the layering within the lower part of the mafic gabbro units are shown in Plates 2.24, 2.25 & 2.26. Higher in the mafic gabbro sequence these garnet-clinopyroxenite bands are replaced by irregular diffuse clots, up to 5 cms in diameter, of garnet and clinopyroxene. Within both the bands and clots of garnet-clinopyroxenite, the garnet forms large xenoblastic grains (15 mms in diameter) set within a polygonized clinopyroxene groundmass, containing minor amounts of feldspar and amphibole. These rocks, both texturally and mineralogically, resemble those

Plates 2.24, 2.25 & 2.26. Examples of the interbanding of mafic gabbro and ultramafite, from the lower portions of several mafic gabbro units. Ultramafite bands weather proud as narrow ridges.

Plates 2.24 & 2.25 - fine scale interbanding - ultramafite bands vary from 5-20 cms in width.

Plate 2.26 - coarser interbanding - ultramafite bands vary from 50-75 cms in width.

All examples are from the Abhainn Easean Chais pod, on the south-western flank of the anorthosite complex.

Plate 2.24



Plate 2.25



Plate 2.26



found at the top of the ultramafite unit.

A very distinctive rock type develops at the top of mafic gabbro units low in the sequence. This is essentially a massive mafic gabbro. However, the garnet in this rock occurs as large 15-20 mm circular xenoblastic grains, contained within a granoblastic clinopyroxene, feldspar and amphibole matrix (Plate 2.28). Invariably this rock type also includes small diffuse clots of garnet clinopyroxenite. From the base to the top of the mafic gabbro units, there is an overall increase in the volume percent of plagioclase feldspar and a complementary decrease in the amount (and grain size) of garnet. This overall variation is shown many times over within individual mafic gabbro layers throughout this unit. (Plate 2.27). The overall sequence of rocks, within the Easean Chais Pod is summarized in fig. 2.6. Without further detailed mapping of these rocks it cannot be known what fraction of the entire sequence this figured sequence represents.

iii) Mineral Assemblages

ULTRAMAFITES

gt + cpx
cpx + amp
gt + cpx + amp + ilm + symp + mag
cpx
amp + symp + ep
(plag) + gt + cpx + ilm + sph
(plag) + gt + cpx + amp + ilm + sph
gt + cpx + opx + amp
(plag) + gt + cpx + opx
(plag) + cpx + amp + ilm + symp + mag + ep + sph

MAFIC GABBROS

plag + gt + cpx + amp + symp + (ep)
plag + gt + cpx + amp + ilm + symp + mag
plag + gt + cpx + amp + ilm + symp + mag + ep + ap
plag + amp + symp + ep + bi
plag + amp + ep



Plate 2.27. 270 cm. Mafic gabbro layer (centre) sandwiched between two ultramafite horizons. Base of mafic gabbro unit. Upward sequence; bottom to top. Note the decrease in grain size and modal % of garnet and complementary increase in plagioclase feldspar, from bottom to top of mafic gabbro layer.

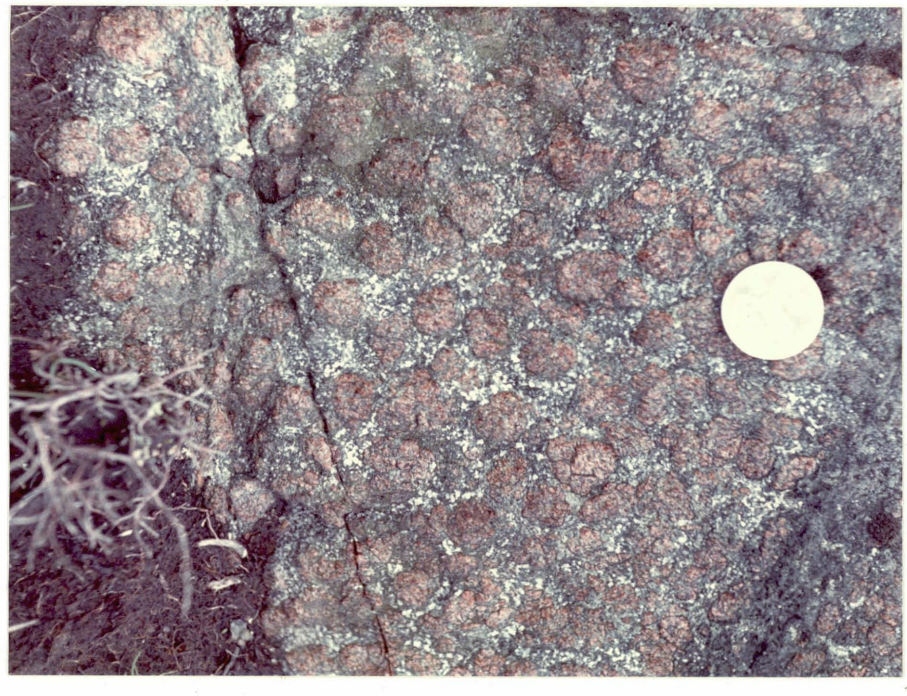


Plate 2.28. Mafic gabbro, showing development of large circular xenoblastic garnets. Top of mafic gabbro unit, Abhainn Easean Chais ultramafite/mafic gabbro pod. (Metamorphic texture possibly founded upon an original igneous 'troctolitic' texture??)

The amphibole of these rocks is an olive green, ferroan pargasite. It occurs as large euhedral to subhedral plates (up to 15 mms) showing a strong pleochroism, X yellow-green; Y brown-green; Z dark brown. The amphibole may often poikilitically enclose smaller clinopyroxene and garnet grains and contain abundant inclusions of iron oxide. (Plate 2.29)

Clinopyroxenes, in both mafic gabbros and ultramafites, are feebly pleochroic augites and salites.

Orthopyroxene is a relatively rare component of these rocks. A highly pleochroic hypersthene (En_{65}) has been observed in several of the clinopyroxene rich ultramafites, but it appears to be entirely absent from the mafic gabbros. A pale pink, weakly zoned, almandine-pyrope garnet is ubiquitious. It frequently occurs as large xenoblastic grains containing smaller grains of clinopyroxene and sphene. The garnet infrequently contains abundant needle-like inclusions of rutile (Plate 2.30). These rutile needles are orientated in three directions to form an intersecting triangular network. In one slide, where orthopyroxene coexists with such inclusion filled garnets, the orthopyroxene also contains rutile inclusions arranged in a similar manner.

Large xenoblastic garnets have been observed to develop consistently in certain horizons within the established ultramafite/mafic gabbro sequence. Elsewhere in the sequence the garnet occurs as small anhedral grains, usually intergrown with clinopyroxene, and containing rounded blebs of quartz. (Plate 2.31).

Plagioclase feldspar occurs as a major phase within the mafic gabbros. Point analyses across many of the feldspars show that they are weakly zoned. Grain boundaries are gently curved and 120^{o} triple point junctions are common. The feldspars without exception show lamellartwinning. A compositional range from bytownite (An_{85}) to andesine/labradorite (An_{46-58}) occurs, from the base to the top of

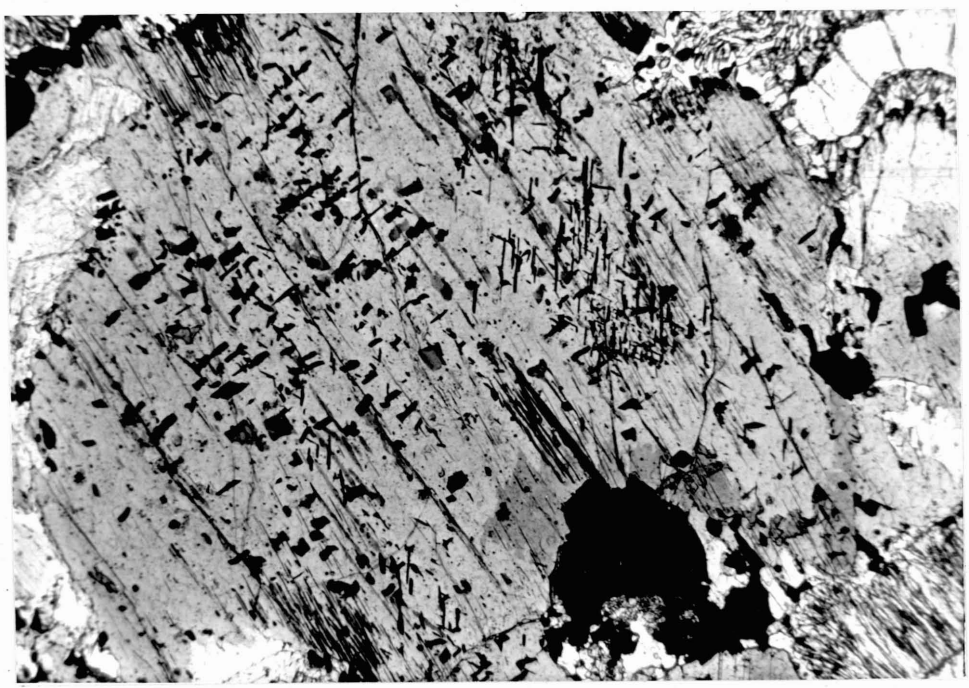
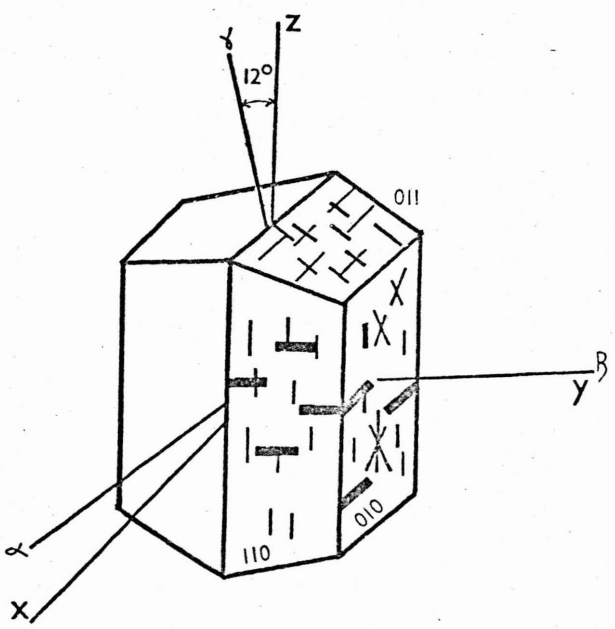


Plate 2.29 Opaque iron oxide inclusions in olive-green (M_1) amphibole. X 80. Crossed polarised light. Slide no. 42582



Orientation of iron oxide inclusions in amphibole.

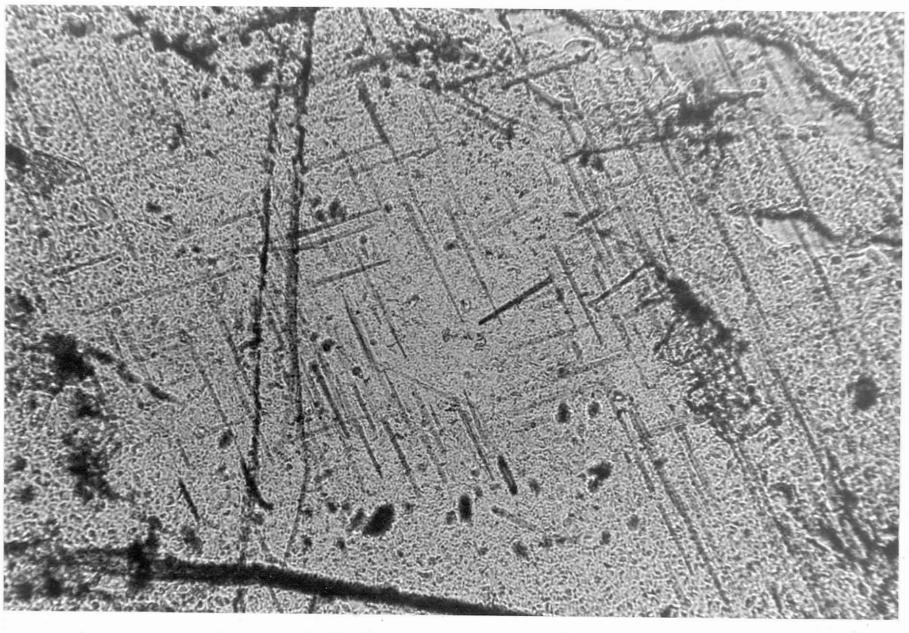


Plate 2.30. Needle-like inclusions of rutile in garnet. Garnet-clinopyroxenite. X140. Plane polarised light. Slide no. 43101

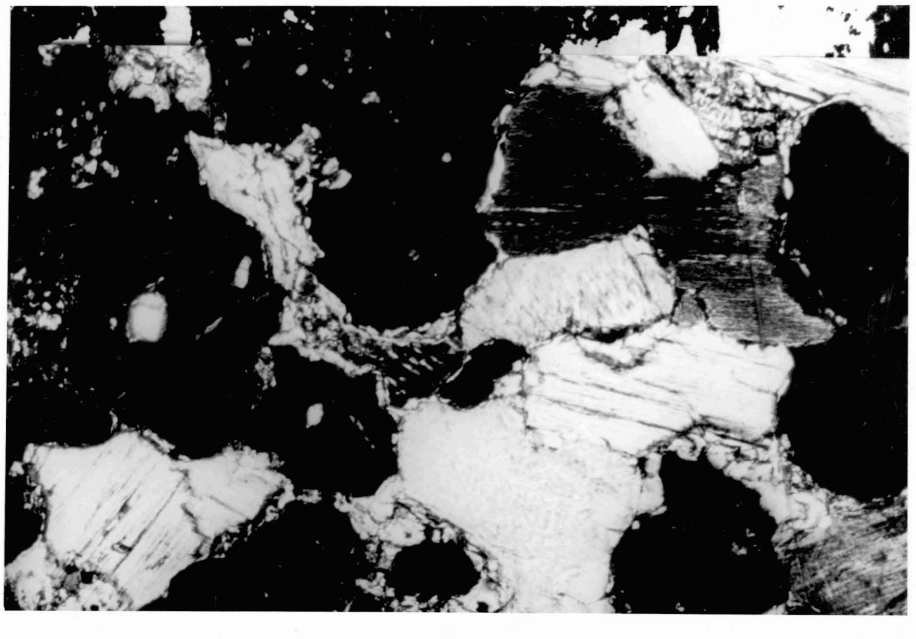


Plate 2.31. Coarse grained intergrowth of garnet and clinopyroxene. The garnet contains numerous rounded blebs of quartz. Garnet-amphibole-clinopyroxenite. X50. Crossed polarised light. Slide no. 39299.

the mafic gabbro units.

The effects of retrogression are most marked in the mafic gabbros. However, even the freshest rocks show alteration of the clinopyroxene to a pale green-blue/green hornblendic amphibole. Garnet alters to a sympectite of plagioclase and amphibole, usually in the form of a radial intergrowth of these two minerals. The amphibole, in large sections of the symplectite rim, often extinguishes simultaneously under crossed nicols. This indicates that, despite the appearance of random radial intergrowth, parts of the rim have grown in optical continuity with each other. The outer margin of the symplectite is often outlined by a zone of magnetite granules. It is thought that this zone of magnetite delimits the original outline of the garnet. The olive-green amphibole may remain fresh or may alter to either a pale green hornblendic amphibole and thence to biotite, or directly to biotite.

The minerology of the measured section A-B is summarized in fig. 2.8.

3. Epidote Veining

The banded ultramafites and mafic gabbros are in places, cut by a number of small epidote veins (Plate 2.33). These may occur in en echelon sets of straight veins (orientated roughly east-west), as single sygmoidal veins, or as a set of irregular anastomosing veins. Such veins are composed of large (8-10 mm), anhedral grains of a highly zoned epidote, associated with minor amounts of calcite and clinozoisite. The epidote poikilitically encloses small aggregates of sericitised plagioclase feldspar, scapolite and ilmenite. Ilmenite often forms a core to these aggregates, around which the plagioclase laths are arranged in a radiating pattern.

fig. 2.8 BANDED ULTRAMAFITES AND MAFIC GABBROS.
MEASURED SECTION A—B
MINERAL ASSEMBLAGES MODES COUNTED ON > 900 POINTS

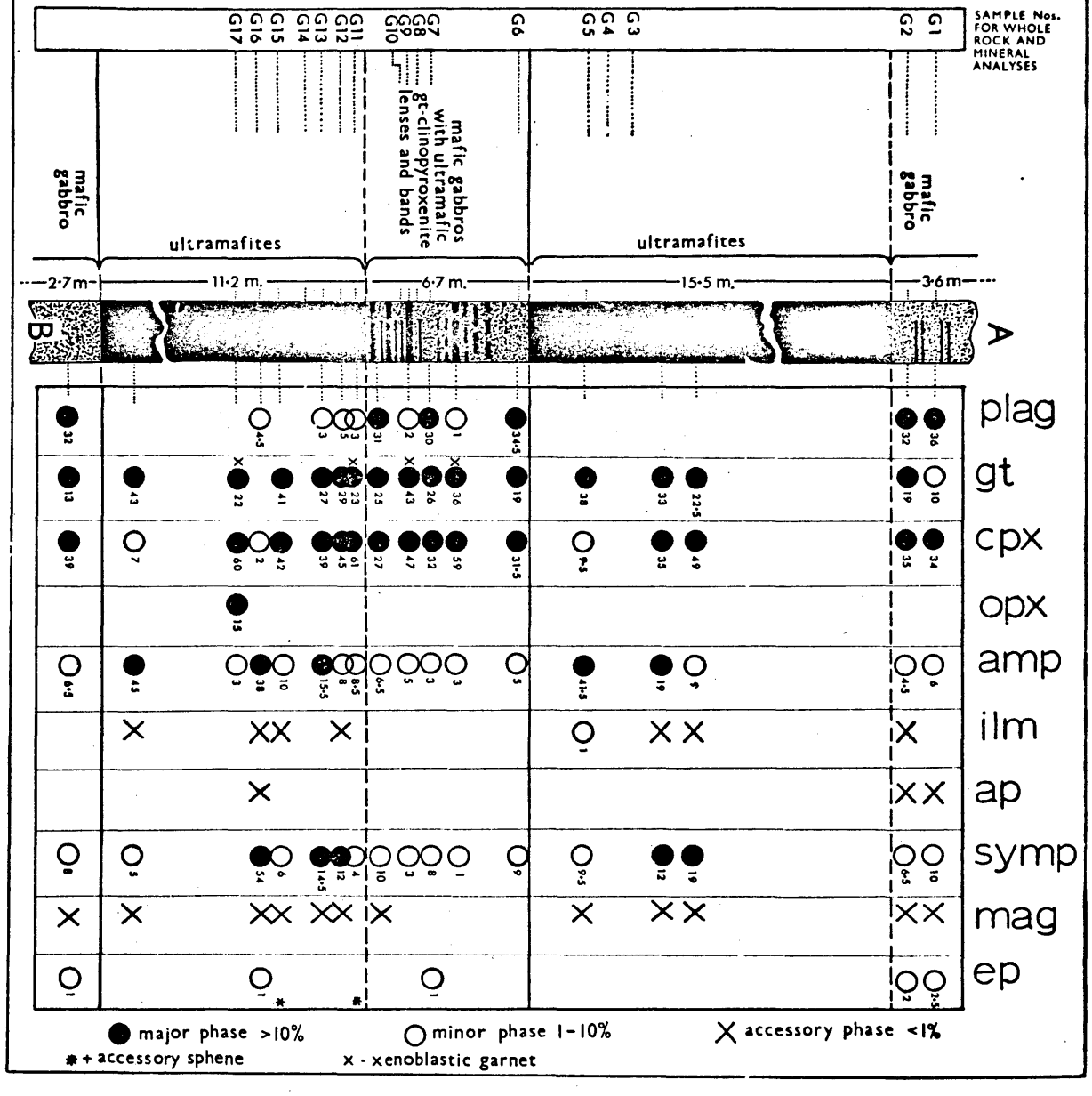




Plate 2.32 Interbanding of paragneiss (garnet-biotite quartzite) and ultramafite/mafic gabbro. Northern contact of the Ha-Cleit ultramafite/mafic gabbro pod, 135 metres N.W. of Ha-Cleit summit.



Plate 2.33 Epidote veins cutting the banded ultramafites and mafic gabbros, 110 metres W.N.W. of Ha-Cleit summit.

2.3.2 The Quartz Gabbros

The quartz gabbros comprise 55-60% of the gabbroic rim of the anorthosite. Unlike the previously described ultramafites and mafic gabbros, the quartz gabbros are uniform rock types showing no evidence of a compositional banding. For the most part they show a deformational (L-S) fabric (fig. 4.3), but may be patchily massive. The quartz gabbros contain a high proportion of included material. These inclusions comprise strips and lenses of quartzose paragneiss and torpedo shaped lenses of partially or totally amphibolitized ultramafite/mafic gabbro. The latter increase in frequency approaching the large ultramafite/mafic gabbro pods. Contacts between the included material and the quartz gabbros are always sharp.

The quartz gabbros include rocks ranging from gabbro - mafic gabbro (colour index 45-85) containing 3-12% modal quartz. The percentage of modal quartz and the type of modal feldspar has been used to subdivide the quartz gabbros into two groups:-

a) Quartz gabbros containing 3-4% modal quartz, and 45-55% labradorite (An_{53-56}) feldspar. Apart from their quartz content, these rocks mineralogically resemble the mafic gabbros of the banded ultramafite/mafic gabbro pods. A typical assemblage for this type is:-

   plag + cpx + amp + gt + qtz + ap + symp

   Quartz gabbros of this type are developed somewhat patchily along both contacts of the ultramafite/mafic gabbro pods (Fig.2.4).

b) Quartz gabbros containing 4-12% modal quartz and 15-50% oligoclase (An_{14-30}) and minor microcline feldspar. These quartz gabbros occupy the remainder of the gabbroic rim. In places the quartz occurs in bands and lenses giving weathered exposures a fluted or ribbed appearance.

Mineral assemblages observed from this type are:-

	plag	+ cpx	+ opx	+ amp	+		qtz	+ bi	+ ilm			
	plag	+ cpx	+ opx	+ amp	+ gt	+	qtz	+ bi	+ ilm	+ ap	+	symp
	plag	+ cpx	+	amp	+ gt	+	qtz	+ bi	+ ilm	+ ap	+	symp
	plag	+ cpx	+	amp	+ gt	+	qtz	+ bi	+ ilm		+	symp
	plag	+ cpx	+		gt	+	qtz	+	ilm		+	symp
mcline +	plag	+ cpx	+	amp	+ gt	+	qtz		+ ilm	+ ap	+	symp
mcline +	plag	+		amp	+			bi +	ilm		+	symp

The oligoclase feldspar shows a faintly developed albite twinning. Undulatory extinction is common and bent twin lamellae are frequently observed. Microcline occurs somewhat infrequently in these rocks. Garnet occurs as small anhedral grains, usually sieved by abundant quartz inclusions. A pale green clinopyroxene (augite-salite) is ubiquitous. However, orthopyroxene (hypersthene, En_{62}) has only been found in two slides. The amphibole of these rocks is a strongly pleochroic, olive-green, ferroan pargasite, similar to that found in the banded ultramafites and mafic gabbros. Biotite, in these assemblages, appears to be partially, if not totally, derived from the amphibole.

Quartz may often show a pronounced segregation into elongate aggregates. Within such aggregates the quartz forms elongate, square ended grains arranged end upon end to form a ribbon type texture. Quartz may also occur as small anhedral unstrained grains in a mortarted texture. Here it occurs with small grains of oligoclase and microcline, which surround and separate large rounded grains of strained feldspar.

The contact of the quartz gabbros with the paragneisses, which surround the anorthosite complex, is usually sharp, but may be gradational over 1-2 metres. The deformational (L-S) fabric observed in the bulk of the quartz gabbros is particularly strongly developed along this contact. The foliation in the paragneisses is in all cases parallel to that in the adjacent quartz gabbros. There is some evidence from the present

study that several paragneiss types are in contact with the quartz gabbros along the south-west contact of the anorthosite complex. It is suggested, from a preliminary investigation of the paragneisses adjacent to the anorthosite complex, that original lithological boundaries within the paragneisses may run obliquely to the present foliation in these rocks.

2.3.3 Summary

The relationship between the two major components of the gabbroic rim, the quartz gabbros and the banded ultramafites/mafic gabbros, is of obvious importance. Superimposed on any primary differences between these two rock types is the fact that they have reacted in differing ways to later deformation. The ultramafites/mafic gabbros preserve a compositional banding, which may be founded upon an original igneous layering. Such a compositional banding is demonstrably earlier then the deformational (L-S) fabric developed throughout most of the quartz gabbros and marginally along the ultramafite/mafic gabbro pods. (Chapter 4). The quartz gabbros show no signs of ever having possessed a compositional banding equatable with that in the ultramafite/mafic gabbro pods.

The major petrological differences between these two rock types are summarised below:-

a) The presence or absence of modal quartz. Quartz occurs as a major phase (up to 12%) in the quartz gabbros but is rare or entirely absent in the banded ultramafites/mafic gabbros.

b) The difference in composition of the feldspar. The plagioclase of the quartz gabbros are considerably more sodic than that of the ultramafites/mafic gabbros. A potash feldspar (microcline) also occurs infrequently in the quartz gabbros.

The quartz gabbros also contain a high proportion of included material. It is of interest to note that the bulk composition of the quartz gabbros lies between that of the included quartzose paragneiss and ultramafite/mafic gabbro. Although the established field relations between these rock types may be open to several interpretations, it is suggested, from a consideration of both the chemistry and field relations of these rocks, that the quartz gabbros represent hybridized equivalents of the ultramafites/mafic gabbros. This

hypothesis will be further investigated when the chemistry of these rocks is considered.

The original form of the gabbroic rim may have been that of a large (ultrabasic/gabbroic) sill or sheet like body. Along both the upper and lower surfaces of such a body, assimilation of the host supracrustals (quartzose paragneisses) occurred, producing a hybridized sheath of quartz gabbro. Centrally, the unmodified magma differentiated under the influence of gravity to produce a layered sequence. Subsequent deformation may be responsible for 'cleaning up' many of the original contacts in such a model. It is also concluded that, although the gabbros of the gabbroic rim and the anorthosites show a close spatial relationship, they are derived from two separate intrusions. As small xenolithic blocks of quartz gabbro have been observed, at one locality, within the lower zone anorthosites (approximately 80 metres above the contact) it is thought likely that the intrusion of the sill, or sheet of ultrabasite/gabbro (now represented by the gabbroic rim), preceded that of the intrusion of the anorthosite.

2.4 Minor Intrusives

2.4.1 Ultramafic and Mafic Gabbro Dykes and Sheets

A suite of ultramafic and mafic gabbro dykes represent the earliest recognisable minor intrusives into the 'anorthosite'. These dykes are most abundant in the lower zone banded 'anorthosites' where two types can be distinguished:-

a) Relatively large parallel sided dykes (D^1 dykes), parallel to the compositional banding (and the earliest foliation) in the lower zone 'anorthosites'. These dykes can exceed 7 metres in width but are usually in the order of 1-2 metres wide. The larger dykes can be traced laterally from 45-70 metres. Minor discordancies can be often seen at the margins of these dykes but they are notable for their

large scale concordance (Plates 4.6 and 4.7).

b) Far less numerous than the D^1 dykes are a second set of smaller D^2 dykes, petrologically similar to, but slightly later than the D^1 dykes. These show a broad concordance to the compositional banding (and the earliest foliation) in the 'anorthosite', but are characterised by their tendency to net-vein the 'anorthosites' (Plate 4.1 and fig. 4.2).

The number of dykes in the middle zone and upper zone 'anorthosites' decreases markedly. This decrease in abundance is accompanied by an increase in the relative frequency of discordant parallel sided D^1 dykes, particularly characteristic of the upper zone 'anorthosites'. The reasons underlying such a change. and the overall relationship of the early mafic gabbro and ultramafite dykes to the early deformational events in the 'anorthosite' is discussed in Chapter 4.

Several large sheets of mafic gabbro occur in the saussuritised anorthosites at the south-east end of the complex. One such sheet occurring along the south-east coast of Lingarabay Island, in the crushed and saussuritised anorthosites, is obviously discordant and intrusive.

This large mafic gabbro sheet, approximately 170 metres in length by 30 metres in width, is saussuritised as are the surrounding anorthosites. Large angular xenolithic blocks of crushed and saussuritised anorthosite occur within the mafic gabbro. Despite the abundance and diversity of form of these early intrusives, they show a remarkably constant mineralogy. The characteristic assemblage of these rocks is:-

gt > cpx > amp > plag > ilm

Garnet is the predominant phase in all of these rocks. It occurs as large anhedral grains, poikilitically enclosing smaller clinopyroxene grains, and frequently containing highly birefringent needle-like inclusions of rutile. Large plates of an olive-green ferroan

pargasitic amphibole in turn enclose the garnet and clinopyroxene.

The plagioclase of these rocks is an andesine (An_{37-44}). A slight variation (8-15%) in modal plagioclase content is observed.

The effects of retrogression in the dykes are often shown marginally, the central part of the dyke preserving a completely unretrogressed granulite facies (M_1) assemblage.

2.4.2 Hornblendite Intrusions

Both small dykes and larger lensoid bodies of hornblendite are intrusive into the anorthosite complex. Despite their petrological similarity these two intrusive types are not thought to be contemporaneous.

1) Hornblendite Dykes:-

Ten dykes of this type have been found within the anorthosite complex. They are characterisitically thin (not exceeding 20cms in width), parallel sided dykes occurring in en echelon sets of up to four dykes. The dykes trend between E - W and E.N.E. - W.S.W. and cut obliquely across the compositional banding (and early foliation) in the anorthosites. Several of these dykes develop a weak foliation parallel to their contacts.

The dykes are composed predominantly of a dark green amphibole, associated with minor amounts of epidote, biotite, plagioclase, microcline (derived from the plagioclase?), quartz and apatite. Occasional large clinopyroxene grains can be observed within this finer grained matrix. The clinopyroxenes show all stages of alteration into a biotite/chlorite aggregate.

From their field relations it appears that these hornblendite dykes are chronologically distinct from the previously described mafic gabbro dykes and constitute a separate later phase of basic dyke intrusion. Palmer (1971) has reported similar hornblendite dykes intrusive into the gabbro-diorite between Bay Steinigie and Sgeir Liath.

2) Hornblendite Lenses:-

Three lensoid bodies of hornblendite have been found intruded into the saussuritised anorthosites at the south-east end of the anorthosite complex (fig. 4.7). Westoll (1967) reports a similar intrusion from the marginal gabbros, south-west of Sletteval, on the northern flank of the complex. Numerous smaller occurrances of hornblendite have been observed along the whole length of the coastal thrust, from Loch Vallarip to Lingarabay Island.

The largest of the three bodies found occurs 370 metres south-east of Loch Na H-Uamh. This body is elongate N.E. - S.W. and is bounded to the north-west and south-east by two major thrust planes. The hornblendite contains abundant xenolithic strips of saussuritised anorthosite (Plate 4.10), and is cut by numerous pale green injection veins of flinty crush rock (pseudotachylite) containing small rounded inclusions of the hornblendite (Plate 4.9). In thin section the rock is seen to be composed entirely of a paragasitic-amphibole, pleochroism, light green; green; straw. The whole intrusion is cut by an anastomosing series of very fine shear planes (Plate 4.11), along which a biotite, epidote, sphene assemblage develops from the amphibole. Further discussion of these hornblendite lenses is reserved until a description of the associated thrusting has been given in Chapter 4.

2.4.3. Breccias and Associated Minor Ultramafite and Anorthosite Intrusions from the Anorthosite/Quartz Gabbro Contact

The occurrence of intermittent brecciation along, and adjacent to the anorthosite/quartz gabbro contact, is as yet a previously undescribed feature of this complex (fig. 2.9). Such breccias fall into two categories:-

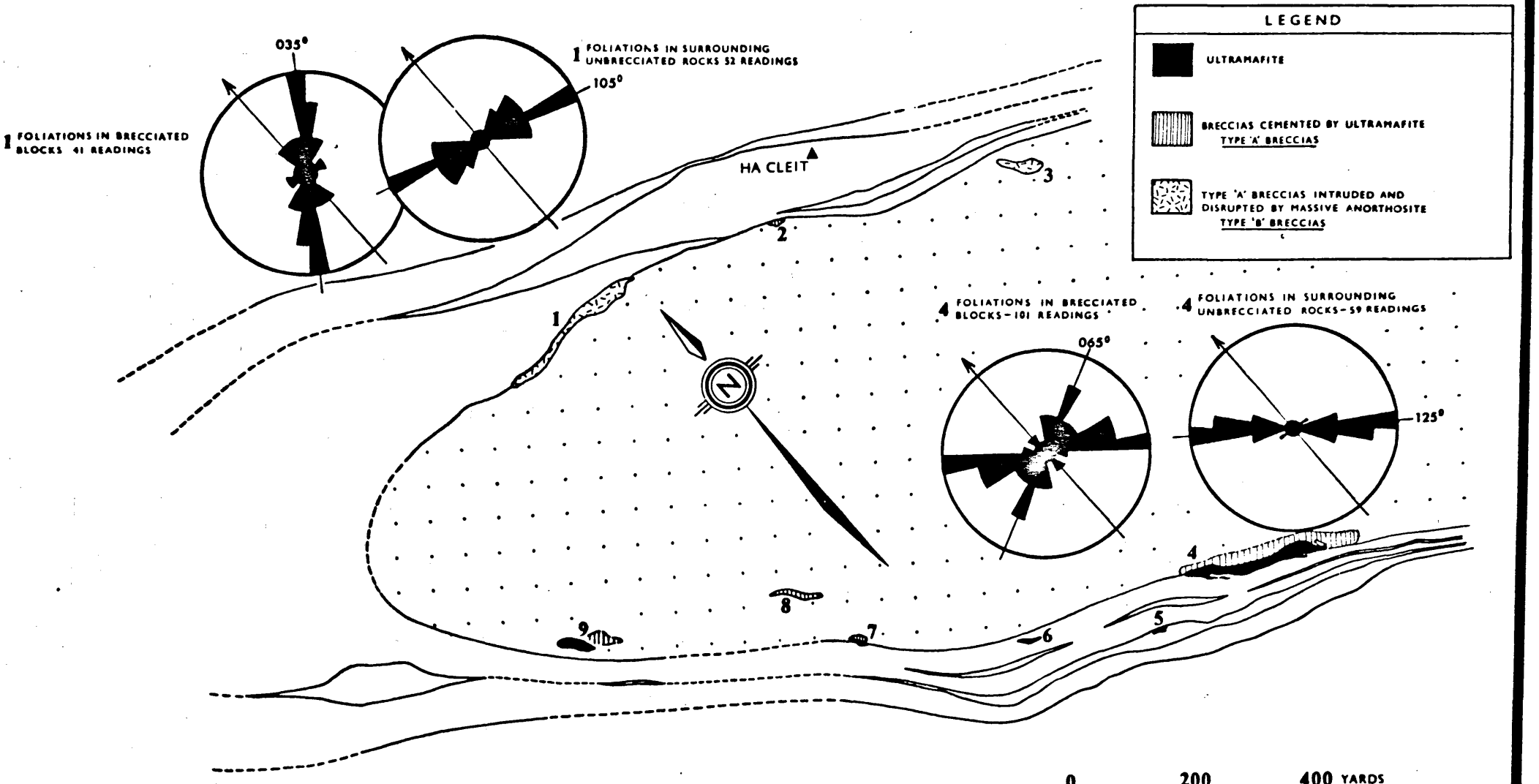


fig. 2.9 BRECCIAS AND ASSOCIATED ULTRAMAFITE & ANORTHOSITE INTRUSIONS, NORTH EAST END OF ANORTHOSITE COMPLEX.



Plate 2.34 Brecciated blocks of foliated and banded gabbroic anorthosite within a massive ultramafite matrix. Note the diffuse patches of garnetite within the ultramafic (clinopyroxenite) matrix. Type 'A' breccia. Location: fig. 2. 9, area 4.

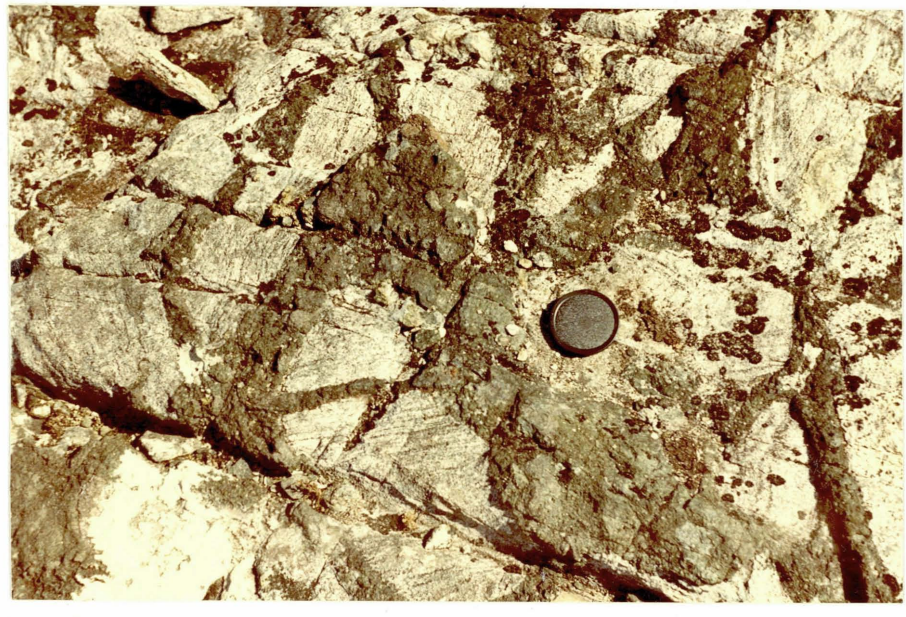


Plate 2.35 Brecciated blocks of foliated and banded gabbroic anorthosite within a massive ultramafite (clinopyroxenite) matrix. Type 'A' breccia. Location: fig. 2.9, area 8.



Plate 2.36 Type 'A' breccia. Location: Fig. 2.9, area 4.



Plate 2.37 Type 'A' breccia. Location: Fig. 2.9, area 4.

TYPE 'A' - Breccias 'cemented' by ultramafite and usually associated with small lenticular ultramafite intrusions (fig 2.9 , Areas 4, 7, 8 and 9).

TYPE 'B' - As type 'A' breccias but subsequently intruded and disrupted by anorthosite (fig. 2.9 , Areas 1, and 3).

1) Type 'A' Breccias

Breccias of this type occur mainly along the south-western flank of the 'anorthosite' and are well exposed in areas north-east of the Abhainn Easean Chais, north of Loch Na Cachlaidh and on the south-eastern slopes of Beinn Na-H-Aire. The overall structure of these areas is characterized by a mosaic of interlocking, angular foliated and banded anorthosite blocks of widely differing orientations which are 'cemented' by narrow interconnecting veins of ultramafite (Plates 2.34 ⩾ 2.37). Small intrusive bodies of massive ultramafite occur in association with many of these brecciated areas. The main effects of the brecciation are seen within the lower zone of banded 'anorthosites'. Minor brecciation of the quartz gabbros is also observed. Marker horizons within the basal 'anorthosite' sequence can be traced through these brecciated areas, via zones of disrupted angular blocks. Only minor lateral displacements of these horizons is noted and it appears that the major effect of disruption was rotation, in both a horizontal and vertical plane, of blocks which remained essentially in their original positions. A number of small isolated ultramafite intrusions (fig.2.9 , areas 5 and 6) have also been observed along the southern flank of the anorthosite. These are petrologically similar to and are thought to be contemporaneous with, the ultramafites associated with the brecciated areas.

(i) Description of the Brecciated Area N.E. of the Abhainn Easean Chais (fig.2.9 ; Area 4, Map 3)

A threefold division of this area is possible:-

a) Intruded along the 'anorthosite' - quartz gabbro contact is

a large irregular body of massive ultramafite, 220 metres in length and from 3-36 metres in width. Contacts between the ultramafite body and the quartz gabbros, to the south-west, are in all cases vertical. Abundant small rounded to subrounded xenoliths of foliated and banded anorthosite and foliated quartz gabbro occur throughout this intrusion. These xenoliths are elongated parallel to their foliation and vary from 6-30 cms in length. Irregular diffuse patches and streaks and discrete non diffuse nodules of a highly garnetiferous ultramafite (garnetite) are distributed somewhat patchily throughout the ultramafite body. It is thought from a consideration of the chemistry of these garnetiferous patches and nodules, that they possibly represent cognate xenoliths of the ultramafite.

b) Adjacent to the north-east contact of ultramafite body the 'anorthosite' is brecciated into large blocks, ranging in size from 10 metres^2 to 100 cms^2. In general the larger blocks are angular, whilst the smaller blocks vary from sub-angular to sub-rounded. This zone is characterized by a high degree of rotational disruption of the 'anorthosite' blocks. Veins and irregular patches of ultramafite, which form a matrix to the breccia, are abundant and tend to dip vertically. Irregular patches and nodules of garnetite, similar to those described above, are seen in the veining ultramafites. (Plate 2.34). Locally within this zone the anorthosite blocks are seen to lose their fine foliation and become massive. It is known from the study of other areas that no massive anorthosites occur in this part of the sequence. Accompanying the loss of foliation in the 'anorthosite' blocks is a gradual blurring of the previously established veining relationships. Initially the ultramafite veins become discontinuous and less distinct. (Plate 2.38) Ultimately the ultramafite is seen to form irregular lumps within a massive anorthositic matrix. However, even at this stage the ultramafite still shows some semblance of its original veining mode (Plate 2.39). Immediately adjacent to these areas, the ultramafites and brecciated anorthosites are cut by narrow discordant anorthosite veins and stringers.

c) Within this zone brecciation and veining by ultramafic material is still apparent. However, the degree of disruption of the brecciated 'anorthosite' blocks is minimal. Veins of ultramafite are narrower and less numerous and tend in the majority of cases, to dip south-westwards.

Plates 2.38 and 2.39 Modified type 'A' breccias.

These modified type 'A' breccias appear to represent a transitional stage between the type 'A' and type 'B' breccias.

Plate 2.38 Note the loss of foliation and banding in the anorthosite blocks. The veins of ultramafite appear also to be discontinuous and less distinct.

Plate 2.39 Again the anorthosite shows no foliation or banding. The ultramafite occurs as irregular lumps within a massive anorthosite matrix.



Plate 2.38



Plate 2.39

ii) Petrology of the Ultramafites

Mineral Assemblages:-

Ultramafites	cpx +			scap					
	cpx +			scap +				symp	
Garnetite Nodules	cpx +	gt +	amp +		ilm				
	cpx +	gt +	amp +		ilm +	plag +	symp +	sphene	
	cpx +		amp +	scap +			symp		

The ultramafites are almost monomineralic clinopyroxene rocks. The clinopyroxene is a pale green weakly pleochroic augite, containing fine rods of exsolved iron oxide. Without exception the clinopyroxene shows a partial alteration to a pale gree/blue hornblendic amphibole. Minor amounts of amphibole/plagioclase symplectite and scapolite, also containing rod-like inclusions of iron oxide, occur. Garnet occurs in the ultramafites in diffuse patches and streaks. A concentration of garnet is also often apparent where the ultramafites are adjacent to 'anorthosite'.

Throughout the ultramafites abundant non-diffuse nodules of garnetite and garnet clinopyroxenite occur. An almandine-pyrope garnet constitutes 30-70% of these nodules. It occurs as large xenoblastic grains, enclosing smaller grains of clinopyroxene and sphene. The garnet, in this case, may often be discontinuously rimmed by small plagioclase feldspar grains. An olive-green, highly pleochroic ferroan-pargasitic amphibole also occurs as small poikilitic plates within these nodules.

iii) Origin of Type 'A' Breccias

Brecciation is usually accompanied by minor intrusions of ultramafite, which also forms a matrix to the breccias. For the reasons stated below it appears unlikely that brecciation was solely a result of the intrusion of the ultramafite, although these two events must have been closely related:-

a) On a large scale the degree of disruption, in many areas, appears

to be out of all proportion to the observed amount of ultramafite 'brecciating' material.

b) The structure of these areas, described as a mosaic of closely interlocking foliated and banded anorthosite blocks of widely differing orientations, seems incompatable with a magmatic brecciation unless a subsequent compaction and 'squeezing' out of the ultramafic 'brecciating' material is evoked.

It is suggested that the brecciation and disruption was produced by an explosive gas action. This was followed by a general upwelling of gabbroic magma (now represented by the ultramafite). The gabbroic magma in this case, would serve to heal the gaps in such an explosively produced breccia and would not itself be the brecciating agent.

Brecciation by an explosive upsurge of volatiles may explain the observed contrast in rounding between large and small blocks, within the breccias. Large blocks may initially be carried upwards in the gas stream and thence resettle or subside, probably into or near their original positions (and possibly having undergone some degree of rotation in the process). They may break up into smaller blocks, but the net result is that they remain angular. Smaller blocks, however, may be picked up by the gas stream and become abraided and subsequently rounded.

The ultramafite matrix appears in some areas to be vesiculated (Plate 2.35). However, this may possibly be a secondary weathering effect.

2) Type 'B' Breccias

Breccias of this type have been found, 450 metres due west and 300 metres south-east of Ha-Cleit summit. (fig. 2.9 , Areas 1 and 3; Map 2). Very complex relationships, between the differing rock types, are developed in these areas. However, it is possible to recognize three main associations of rock types:-

a) The most wide-spread association within these areas is the occurrence of small xenoliths of foliated and banded anorthosite, foliated quartz gabbro and ultramafite, in a matrix of massive anorthosite (Plates 2.40 and 2.41). The massive anorthosite is an almost pure plagioclase feldspar rock, where uncontaminated, which tends to offer far less resistance to weathering than the included xenoliths. Thus the xenoliths weather proud of the matrix material and in many cases give the appearance of having been 'stuck onto' the surface of the exposure. The foliated anorthosite xenoliths range in size from approximately 200 cms^2 down to as little as a few square centimetres and are angular to sub-rounded in shape. Ultramafite xenoliths,from 20 to 30 cms in diameter usually show a greater degree of rounding and in some cases develop narrow (5-10 mm) epidotic reaction rims.

b) A subordinate association is characterized by the occurrence of foliated and banded anorthosite and foliated quartz gabbro xenolithic blocks within an ultramafite matrix. These areas resemble the breccias described previously from the south-west flank of the 'anorthosite'. Such areas are of limited extent and their relationship to the association described above is obscure. However, it appears that these areas may themselves represent large xenolithic rafts which are at least partly, if not totally, engulfed within a massive anorthositic matrix. In agreement with this view is the occurrence of 'composite' xenoliths, within the massive anorthosites. These being of two types:-



Plate 2.40. Anorthosite and ultramafite xenoliths in a massive anorthosite matrix. Type 'B' breccia, 405 metres west of Ha-Cleit summit (fig. 2.9 , Area 1).

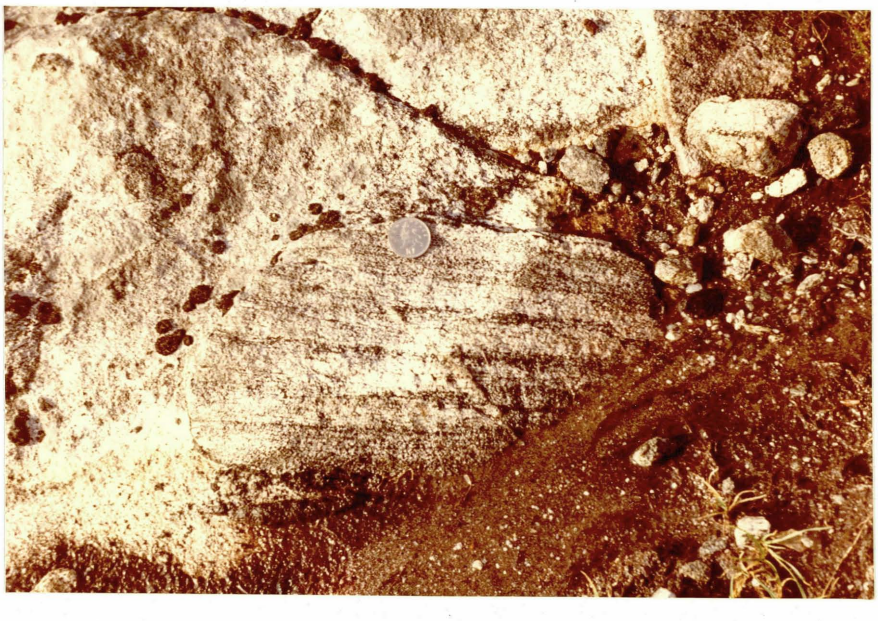


Plate 2.41. Finely banded anorthosite xenolith in massive anorthosite matrix. 300 metres E.S.E. of Ha-Cleit summit (fig. 2.9 , area 3).

I) xenoliths of foliated anorthosite, continuously or discontinuously rimmed by ultramafite.

II) xenoliths composed of two or more foliated anorthosite blocks, cemented together by ultramafite, and contained as a whole within a massive anorthosite.

c) Irregular bodies of massive ultramafite also occur within these areas. These ultramfite intrusions contain small foliated anorthosite and quartz gabbro xenoliths and are themselves intruded by veins and tongues of massive anorthositic material. Partial assimilation by the intruding anorthosite is apparent at many localities.

It is thought that two major events are recorded in these areas. The earlier event involved disruption and brecciation of the anorthosite and quartz gabbro. This was associated with the intrusion of small irregular bodies of ultramafite and a 'healing' of the breccia by ultramafite material. At this stage these areas would resemble the previously described breccias occurring along the south-west flank of the anorthosite.

This breccia has in turn been disrupted by an intrusion of anorthosite. This has obscured many of the primary relationships developed during the initial brecciation. However, rafts and small xenoliths of the original breccia are preserved. Much of the original ultramafite matrix material now occurs as rounded xenoliths within the massive anorthosite. Some degree of reaction between this ultramafic material and the massive anorthosite seems to be indicated by the occurrence of epidotic reaction rims around the former. Apart from small veinlets and stringers of anorthosite found intruding the surrounding banded anorthosites and quartz gabbros, the intrusion of massive anorthosite is confined to the area of the ealier brecciation. The close spatial (and temporal) association of these earlier breccias and the intruding anorthosites may suggest that they are genetically related. It is possible that the anorthosite 'magma'

was generated at a lower crustal level, as must have been the earlier gabbroic magma, and subsequently intruded into the earlier breccias. However, it is thought more likely that the anorthosite 'magma' formed more or less in situ by partial melting of the foliated and banded anorthosites involved in the earlier breccias. An early arrested stage in such a partial melting process may be exhibited by small areas within the previously described type 'A' breccias, north-east of the Abhainn Easean Chais stream (Plates 2.38 and 2.39). The chemistry of the massive anorthosites would also suggest that these are partial melt products.

Partial melting may have been initiated by rapid heat loss from the intrusion of gabbroic magma. However, from field observations it appears likely that melting of the anorthosite occurred somewhat later than the solidification of the gabbros (now ultramafites). It is proposed that a later renewed upsurge of super-heated volatiles, within these previously active areas, may be responsible for the initiation of melting. In either case a volatile rich environment would facilitate the melting of the anorthosite. The massive anorthosites exhibit many features consistent with normal igneous intrusion (Plates 2.42 and 2.43). As already stated the anorthosite intrusions are confined to areas which have suffered an earlier brecciation. Within these areas the anorthosite is packed with xenolithic blocks of ultramafite, banded anorthosite, quartz gabbro and composite xenoliths of the early breccia. Small veins and stringers of the anorthosite intrude into the surrounding unbrecciated rocks for approximately 30 metres.

3) Summary

Breccias of the type described, together with their associated ultramafite and anorthosite intrusions, appear to be peculiar to the marginal areas of the anorthosite. From nowhere else within the South

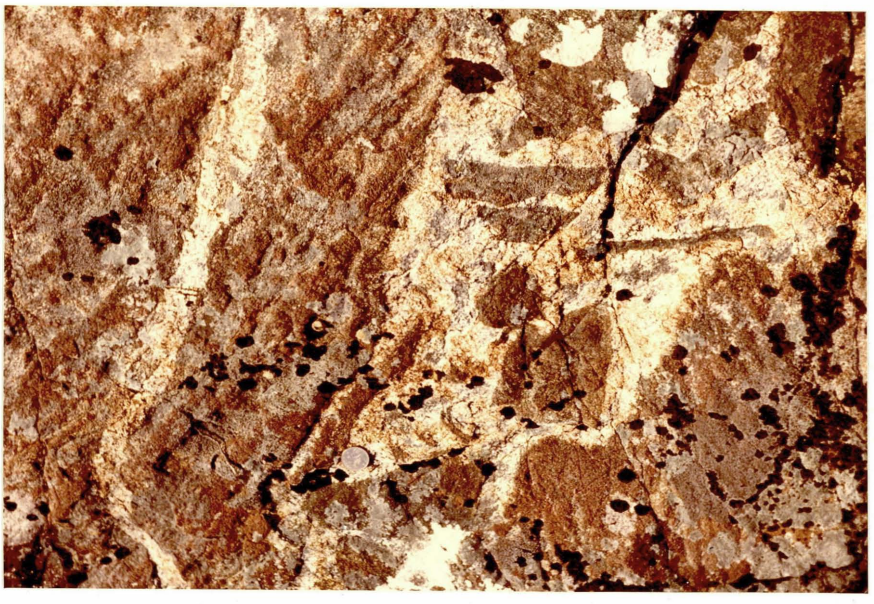


Plate 2.42. Large xenolithic block of foliated quartz gabbro, intruded by anorthosite. Note how the anorthosite has intruded by a 'stoping' mechanism. Type 'B' breccia, 400 metres W.N.W. Ha-Cleit summit.



Plate 2.43. Xenolithic block of quartz gabbro intruded by anorthosite. The anorthosite also contains small xenolithic fragments of ultramafite (centre, left) Location:- as plate 2.42.

Harris igneous rocks are comparable breccias reported. The fact that they are so common along both flanks of the anorthosite may suggest that some 'special feature' of the anorthosite is responsible for their siting.

An altogether inexplicable feature of all the breccias studied is that although, at first glance, the orientation of the brecciated blocks appears random, when studied further the larger blocks, in such breccias, appear to show a preferred orientation. Rose plots showing the orientations of brecciated blocks from two areas are shown in fig.2.9 . From the area 450 metres due west of Ha-Cleit summit, the foliations within the brecciated blocks show a maximum at 035^{o}, an angular discordance of 070^{o} to the regional foliation and almost perpendicular to the anorthosite - quartz gabbro contact. Foliations from brecciated blocks within the area north-east of the Abhainn Easean Chais stream, show two maxima, one coinciding with the regional foliation and the second at 065^{o}, and angular discordance of 060^{o} to the regional foliation. It is not inconceivable that some or possibly all of the blocks within these breccias may have undergone rotation during later deformation.

2.4.4 Anorthositic-Gabbro Dykes and Trondhjemitic Pegmatites

A number of straight, parallel-sided, anorthositic-gabbro dykes occur with the 'anorthosites' at the north-west end of the complex (Plates 2.47 and 2.48). Dykes of this type have also been found within the banded ultramafites and mafic gabbros of the gabbroic rim (Plate 2.49). These dykes are usually no more than 25 cms in width and can be traced laterally up to 36 metres. They cut obliquely across the compositional banding (and early foliation) in the 'anorthosites' and are themselves cut and displaced by early Laxfordian shears. The mafic minerals of these dykes occur in elongate clots, which often show some degree of orientation oblique to the dyke margin. A conspicuous



Plate 2.44



Plate 2.45



Plate 2.46

Sequence of plates showing the progressive shearing (left - right) of a type 'A' breccia. Area 2, fig. 2.9; 130 metres W.S.W. of Ha-Cleit summit.

feature, possessed by all of these dykes, is the occurrence of a central mafic-enriched zone.

The dykes are composed predominantly of a coarse-grained, pink, andesine feldspar (An_{32-38}). Individual feldspar grains may be from 15-20 mms in size. This contrasts with the finer grained nature (average grain size 2-5 mms) of the feldspars from the surrounding anorthosites. The andesine feldspar occasionally occurs in a coarse intergrowth with quartz. Mafic minerals occur in diffuse elongate aggregates. The major mafic phase of these aggregates is a pale green amphibole, sieved by quartz and plagioclase feldspar. Remnants of clinopyroxene sometimes occur centrally within the amphibole intergrowth. Garnet is patchily distributed throughout these aggregates but is noticeably more abundant in those dykes cutting the banded ultramafites and mafic gabbros.

Textures within these dyke rocks suggest some degree of post-crystallization strain. Mortar textures are prevalent. Large anhedral feldspar grains show bent twin lamellae and undulose extinction.

Dearnley (1963) describes similar rock types, occurring as cross cutting veins and dyke-like bodies, from the Rodil park area, at the south-east end of the complex. These he referred to as trondhjemitic pegmatites. Plagioclase feldspar (An_{46-25}) comprises approximately 80% of these pegmatites. However, much of the feldspar shows alteration to zoisite, as these rocks fall within the zone of saussuritisation. Apart from their higher plagioclase feldspar content and their partial saussuritisation, these rocks are mineralogically and texturally similar to the anorthositic-gabbro dykes. Dearnley regards the trondhjemitic pegmatites as late stage differentiates of the anorthosite.

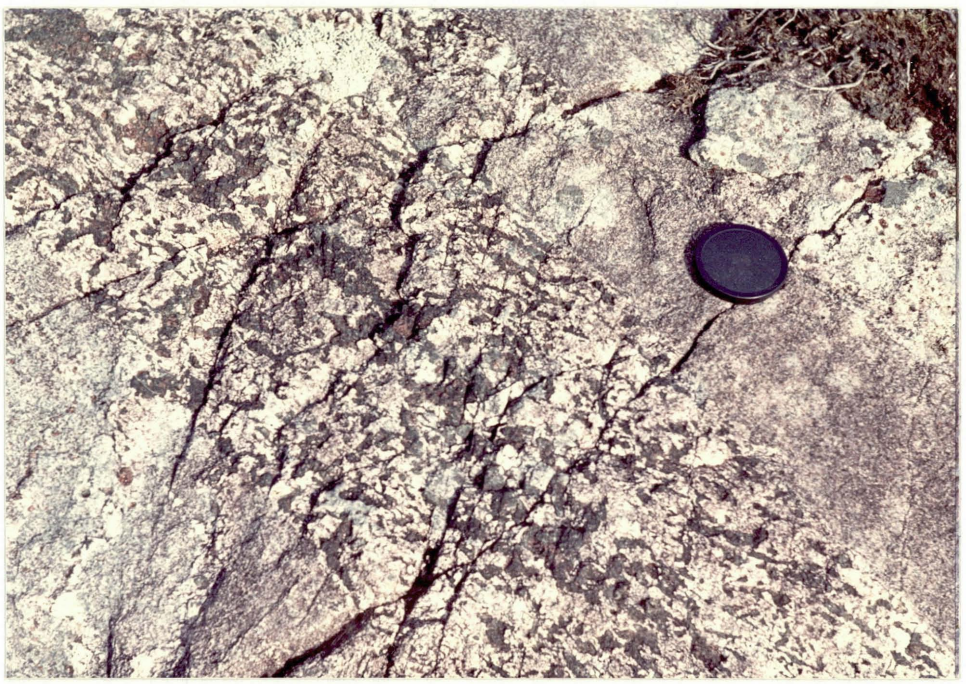
However, it is thought that these dykes are derived by segregation from the surrounding rocks. In this connection it should be mentioned that the basicity of these dykes varies with the basicity of the host rocks.

Plate 2.47. Anorthositic-gabbro dyke, cutting a gabbro horizon from the lower zone of the anorthosite. The hammer handle shows the direction of the foliation within the gabbro.

Plate 2.48. Anorthositic-gabbro dyke - detail of dyke shown in plate 2.47. Note the central mafic enriched zone and the elongate mafic clots arranged obliquely to the dyke margins. (the orientation shown by these mafic clots is also oblique to the foliation in the country rock)

Plate 2.49. Anorthositic-gabbro dyke, cutting a banded ultramafite, from the gabbroic rim of the anorthosite. The pencil shows the direction of banding in the ultramafite.







2.4.5. Unmetamorphosed Basic Dykes

A variety of basic unmetamorphosed dykes occur intrusive into the anorthosite complex. The petrology and field relations of these dykes are summarized in Table 2.3. The olivine free 'tholeiitic' dykes and the olivine dolerite/basalt dykes are thought to be of Tertiary age. The former being intruded prior to the main phase of Tertiary faulting. Gismondine occurs as an amygdale mineral in the olivine free 'tholeiitic' dykes. This is thought to be the first reported occurrence, from Scotland, of this mineral, although it has been recorded from many localities in the Tertiary basalts of Iceland and Ireland (Walker, 1962). The highly vesicular nature of the olivine free 'tholeiitic' dykes would suggest that they were emplaced within 100 metres of the surface. The zeolite assemblage of these dykes also suggests a high level of emplacement (within 200-1000 metres of the surface.)

Dyke Type	Relationship of dykes to structure	Examples	Mineralogy	Amygdale minerals	Remarks
AUGITE LAMPROPHYRE DYKES	Intruded along E-W late Laxfordian (F_4) shears. Displaced by N.N.E.-S.S.W. Tertiary faults	i) 110 metres due west Ha Cleit summit ii) N.E. of Roneval summit (Jehu and Craig 1927)	Phenocryst phases:- major phenocryst phase is augite, occuring in large (3-4mm) euhedral, pale brown-green grains - show hour glass zoning Minor phenocryst phase is plagioclase, occuring in 1-2mm laths. Groundmass:- small needles of plagioclase/olivine(?)/calcite/biotite/opaque iron oxides	QUARTZ CALCITE occur in amygdales from 1-2mms in diameter	
OLIVINE FREE 'THOLEIITIC' DYKES	Intruded along N.N.W.-S.S.E. Early Laxfordian (F_3) shears. Displaced by NNE-SSW and N-S Tertiary faults.	i) 400 metres south west of Ha Cleit summit ii) 235 metres north east of Abainn Easean Chais stream iii) Eilean Quidnish and Aird Harnasaig Loch Grosebay (Jehu & Craig, 1927)	Phenocryst phases:- plagioclase is the only phenocryst phase. Groundmass:- composed of large poikilitic plates of augite, enclosing small laths of plagioclase. Abundant interstitial brown glass occurs in the groundmass.	GISMONDINE (Plate 2.50) THOMPSONITE CHABAZITE occur in amygdales from 3-4cms in diameter	
OLIVINE DOLERITE-OLIVINE BASALT DYKES	Intruded along N.N.E.-S.S.W. and N-S Tertiary faults	i) Lingarabay Island (Fig) ii) 90 metres N.W. of Ha Cleit summit iii) Anorthosite quarry - Rodil-Finsbay Road	Phenocryst phases:- major phenocryst phase is plagioclase (An_{70}, CORE; An_{32} RIM) occuring in laths up to 4mms in length. Augite and olivine occur as minor phenocryst phases. Olivine is usually partially or totally serpentinized Groundmass:- Small laths of plagioclase (An_{36-28})/augite/opaque iron oxides.		Chilled margins of dykes usually slightly sheared. Dykes sometimes show a star jointing.

Table **2.3.** Basic unmetamorphosed dykes from the anorthosite complex



Plate 2.50 Fern-like aggregate of gismondine. X50.Crossed polarised light. Slide no. 43330.

CHAPTER 3

THE META-IGNEOUS ROCKS ASSOCIATED WITH THE ANORTHOSITE COMPLEX

3.1 Introduction

A consideration of the anorthosite of South Harris would not be complete without some comment on the associated meta-igneous rocks. Anorthosites from many areas of the world exhibit a close spatial relationship with rocks of intermediate to silicic composition. These rock types have been variously referred to as mangerites, charnockites, adamellites, quartz syenites and syenites. All of these rock types have been considered to constitute an anorthositic suite because of their close spatial association. Field evidence often indicates that the silicic and intermediate rock types of this suite intrude the anorthositic types. Other than this there is no general agreement as to the petrological relationships between these rock types, or as to whether these rocks constitute a co-magmatic series.

The meta-igeous rocks found in association with the South Harris anorthosite vary in composition from basic to intermediate. No highly silicic types are present. The two major plutons are of (i) gabbro-diorite (with minor tonalitic facies) and (ii) norite. These two bodies, together with the anorthosite, from discrete plutons. Intrusive relations between these three rock types are not observed. Both the gabbro-diorite and norite bodies show a metamorphic and structural history comparable to that of the anorthosite complex, and all three intrusions are assumed to be of approximately the same age. The gabbro-diorite and norite appear to be relatively homogeneous intrusions and do not show a compositional banding comparable to that displayed by the rocks of the anorthosite complex.

Associated with these three plutons are:-

a) Large sheet-like bodies of mafic gabbro, which often exhibit a complex compositional banding. These occur:-

i) rimming the three major plutons. Both flanks of the anorthosite are rimmed by mafic gabbros and a similar rim is found along the southern contact of the gabbro-diorite and the northern contact of the norite. The northern contact of the gabbro-diorite is directly with the paragneisses of the Langavat belt. This relationship is mirrored by the norite whose southern contact is directly with the paragneisses of the Ensay belt. An intervening (discontinuous) strip of paragneiss often occurs between these mafic gabbro sheets and the rocks of the three plutons.

ii) as sheets within the paragneisses of the Leverburgh belt. The two extensive sheets of amphibolite within the Langavat paragneisses may represent highly retrogressed mafic gabbros. Small dyke or sill-like bodies of mafic gabbro occur intrusive into all three plutons.

b) Small concordant lensoid bodies of ultramafite (ultrabasite) occur within the Leverburgh and Langavat paragneisses. These show a variable mineralogy and are dunites, peridotites, pyroxenites and hornblendites. Pyroxenites and hornblendites are also found intrusive into the major plutons.

The earliest recognizable mineral assemblages, in all of these rocks, are the result of an early Scourian granulite facies metamorphism (M_1).

These meta-igneous rocks are cut by quartz-feldspar pegmatites and quartz veins of Scourian and Laxfordian age. The most notable of these are the late Laxfordian alkali pegmatites which occur throughout the Outer Hebrides. The mineralogy and distribution of the South Harris alkali pegmatites has been described by von Knorring and Dearnley, (1960) and by Dearnley (1963).

A description of the field relations and petrology of the meta-igneous rock types associated with the anorthosite complex, is now given. It should be stated that no detailed investigation of these rock types has been made during the present study and the following account is basically a resumé of the observations and ideas of previous workers in this area.

3.2 Gabbro Diorite

3.2.1 Field Relations

The gabbro-diorite is the largest igneous body in South Harris, covering approximately 32 Km^2. The term 'tonalite' has been used by Dearnley to describe this intrusion. However, this term, when applied to the body as a whole, is misleading. Possibly not more than 15% of this body is truly tonalitic. (R. Horsley, pers. comm.)

The gabbro-diorite is in general a uniform body. A large scale variation from leucocratic dioritic and minor tonalitic facies, to melanocratic gabbroic facies may represent a primary igneous feature. Several large lenticular bodies of mafic gabbro (garnet metagabbro of Dearnley and Palmer) occur within the gabbro-diorite, the distribution of these is shown in Fig. 1.1. The entire southern margin of the gabbro-diorite is also rimmed by a sheet of mafic gabbro. Dearnley notes that the contacts between gabbro-diorite and mafic gabbro are in all cases gradational. Hybrid rocks are of common occurrence along such contacts and are especially well developed near the contact of the Bayhead-Sletteval mafic gabbro sheet. In the contact zone between Loch na Moracha and Greval, scattered garnets occur in the gabbro-diorite up to 18 metres from the contact. The amount of garnet increases towards this contact where the rock takes on a hybridized appearance before the final transition to mafic gabbro. Similar relationships have been observed along this contact, from Loch na Moracha to Bosival, during the present study. Throughout the mafic

gabbro rim, strips and lenses of dioritic material are common, the rock often appearing to be an intimate admixture of the two types.

Dearnley proposed that the gabbro-diorite is intrusive into the mafic gabbros, the mafic gabbro lenses of Bleaval, Voumusdale, Mas Garbh and Sletteval representing large disrupted xenolithic 'rafts'. In favour of this relationship he cited the occurrence, in Sletteval quarry, of disorientated angular blocks of mafic gabbro within a hybridized matrix. Such hybridized rocks, which consist of plagioclase (andesine), amphibole, garnet and quartz, grade out into 'normal' gabbro-dicrites and are regarded as essentially contaminated gabbro-diorites that have assimilated much mafic gabbro material.

Myers (1968) also described the occurrence of small lenticular xenoliths of mafic gabbro and the patchy development of hybridized rocks, within the gabbro-diorites immediately adjacent to the Bleaval mafic gabbro sheet.

Palmer (1971), however, regarded these mafic gabbro lenses and strips as comagmatic with the gabbro-diorite and representing an original heterogeneity within the intrusion.

Strips of paragneiss also occur within the gabbro-diorite. The largest of these occurs at Bay Steinigie on the north-west coast. This 70 metre wide strip of paragneiss is parallel to the northern margin of the intrusion and can be traced inland for approximately 4 Kms. On the south-east coast at Borsham a band of similar paragneiss occurs, again parallel to the northern margin of the gabbro-diorite and extending inland for 1 Km.

Paragneisses lithologically similar to those found within the Bay Steinigie and Borsham strips, occur on the north-east side of the Langavat paragneiss belt between Sta Point and Scara Ruadh.

To the north-east of the Bay Steinigie paragneiss strip, Myers (1968) described numerous small angular and lenticular paragneiss xenoliths, many of which show signs of assimilation by the gabbro-

diorite. Already foliated and folded paragneiss xenoliths have also been reported from the gabbro-diorite in this area.

Both Dearnley and Myers regarded these paragneiss strips as xenolithic. An alternative hypothesis is offered by Palmer, who recognized an apparent synformal structure to the Bay Steinigie paragneiss strip and proposed that this strip may represent a 'pinched in' syncline (Ramsey, 1967) of paragneiss.

Narrow discontinuous strips of paragneiss also occur between the gabbro-diorite and mafic gabbro along the southern margin of the intrusion.

Dearnley noted that unaltered gabbro - diorite is very similar in field appearance to the norite (pyroxene granulite).

A variety of rock types occur, which are intrusive into the gabbro-diorite. These fall into four categories:-

a) Quartz/plagioclase pegmatites and quartz veins. The gabbro-diorite is traversed by abundant small veins of this type. These were thought by Dearnley to represent late stage differentiates of the gabbro-diorite. However, Myers regarded many of these veins and pegmatites as products of an early Scourian migmatization.

b) Metamorphosed lamprophyric dykes. Dykes of this type have been reported by Myers and can be found in coastal exposures between Sgeir Liath and Bay Steinigie. They are composed of a granular intergrowth of pale amphibole and plagioclase, containing large poikilitic plates of a deep brown biotite. The biotite show an allignment parallel to the margins of the dykes. The exact age of these dykes is uncertain, but Myers recorded instances where these dykes are cut by deformed quartz veins of the type described above.

c) 'Early' mafic gabbro dykes (Palmer 1971). Dykes of this type occur in two modes:-

i) Sets of straight parallel-sided dykes, cutting obliquely across the earliest recognizable (Scourian) foliation in the gabbro diorite. e.g. north of Chiapaval Hill and on the Greaval-Maodal ridge.

Or as ii) mafic gabbro dykes and sheets net veining the gabbro-diorite. In this instance small angular foliated blocks of gabbro diorite are contained within a massive mafic gabbro matrix. Similar relationships have been observed, north of Sgeir Liath, during the present investigation. Here the gabbro-diorite is patchily veined by ultramafite (Plates 3.1 and 3.2).

It would appear that both these intrusive events post-date the formation of the earliest foliation in the gabbro-diorite. However, Palmer argued that these intrusions infact pre-date this foliation and that these dykes were homogeneously deformed during the period of deformation which produced this foliation. Mineralogically these dykes are similar to the mafic gabbros rimming the southern contact of the gabbro-diorite.

d) Late basic dykes. Palmer also reported the occurrence of a number of thin parallel-sided basic dykes. These dykes trend north-south and occur in en echelon intrusion patterns, cutting obliquely across the early foliation in the gabbro diorite. Palmer described instances where these dykes cut across, and are thus later than, thin pegmatitic veins which he observed to cut the mafic gabbro dykes (c). Fresh examples of these late basic dykes show a clinopyroxene/microcline/apatite assemblage, whilst highly retrogressed types are characterised by amphibole/epidote/microcline assemblages.

Dearnley (1963) has reported the occurrence of ultramafic pods within

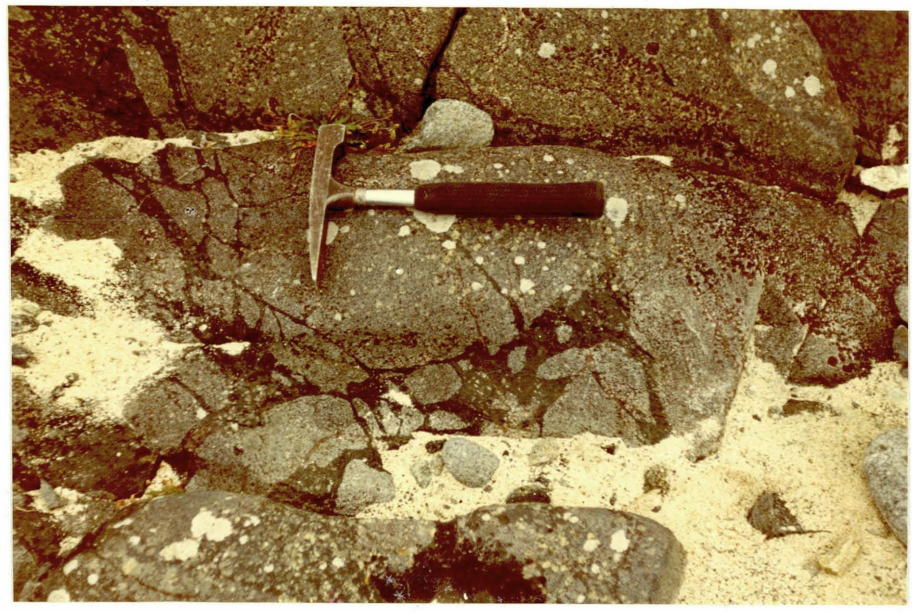


Plate 3.1 Ultramafite net veining gabbro-diorite. Coastal exposure 65 metres north-west of Sgeir Liath.



Plate 3.2 Ultramafite/mafic gabbro net veining gabbro-diorite. Location as for plate 3.1. Note the concentration of abundant large white plagioclase crystals in the central area of the larger vein (centre-left). These decrease in abundance with the decrease in width of the veins, and are completely absent from the very thin anastomosing vein shown in plate 3.1.

the gabbro-diorite. He described a two pyroxene / amphibole / spinel rock from 500 metres north-west of Meaval and reported similar rocks, some containing small amounts of plagioclase, occurring as irregular (xenolithic?) inclusions in the gabbro-diorite at Clett a' Ghobha.

3.2.2 Petrology

The gabbroic facies of the gabbro-diorite intrusion is represented by a dark coloured, fine - medium grained rock characterized by the assemblage:-

opx + cpx + (gt) + plag ± qtz

The less basic, dioritic facies, is slightly coarser grained. In general, orthopyroxene is absent from these rocks, its place being taken by an olive-green amphibole. Typical assemblages of the dioritic facies are:-

amp + gt + plag + qtz

amp + cpx + gt + plag + qtz

The percentage of modal quartz varies from 3-12%.

These assemblages, however, are atypical of the intrusion as a whole, as the vast proportion of the body shows the effects of late Laxfordian retrogression. Dearnley reported that the degree of retrogression increases to the north-east, as the granite-gneiss injection complex of northern South Harris is approached. He defined four north-west south-east zones within the gabbro-diorite, based on the degree of retrogression shown by these rocks (Dearnley 1963, p. 265).

3.3 Norite

3.3.1 Field Relations

The norite or 'pyroxene granulite' was considered by Dearnley (1959) to represent an upthrust wedge of gneiss, older than the other members of the igneous suite. Palmer, (1971) however, regarded the norite as an integral part of the South Harris igneous suite - an association which is substantiated by the present work.

A large part of the norite is below sea level, but the northern contact of the body is well exposed on the north-east coast of South Harris between Renish Point and Bretasker. A small section of the southern contact is exposed on Ensay. The northern contact of the body is rimmed by a narrow discontinuous mafic gabbro strip (maximum width 90 metres), similar to that seen along the southern contact of the gabbro-diorite. A thin strip of paragneiss, from 3-15 metres in width, consistently occurs between this mafic gabbro sheet and the norite body. The southern contact of the norite lacks such a mafic gabbro strip and, as such,the marginal relationships of the norite seem to mirror those of the gabbro-diorite. The sparodic development of large garnets along the northern contact zone of the norite invites comparison with such a development of garnet along the southern contact of the gabbro-diorite, adjacent to the marginal mafic-gabbro sheet.

Palmer's observation of angular xenoliths of paragneiss within the norite at Rudh'an Teampuill appears to be the only direct evidence of an intrusive relationship between the norite and the Leverburgh paragneisses.

In areas where the effects of late retrograde metamorphism are slight the norites are seen to take on the typical 'greasy' appearance of basic charnockites.

Palmer (1971) reported the occurrence of a suite of pyroxenite dykes intrusive into the norite body north-west of Port Eisgein. Individual dykes are up to 9 metres in width and show a preferred orientation, parallel to the north-south foliation in the norite. Such dykes invariably develop complex net-vein relationships at their margins. These coarse grained pyroxenites consist of a granoblastic intergrowth of clinopyroxene and subordinate orthopyroxene. The occurrence of large euhedral clinopyroxenes surrounded by smaller polygonal clinopyroxene and orthopyroxene grains, is thought by Palmer to reflect only partial recrystallization of these dykes.

Dearnley (1963) has also described narrow veins of websterite

(pyroxenite) cutting the norite in coastal exposures at the north end of Ensay House Beach, Ensay. These websteritic veins show a two pyroxene assemblage with minor amounts of plagioclase, amphibole and biotite.

In addition to these pyroxenite dykes, examples of mafic gabbro dykes similar to the early mafic gabbro dykes intrusive into the gabbro diorite, have been observed within the norite. Cutting obliquely across all of these basic dykes is a suite of hornblende - pegmatites (the"basic pegmatites"of Davidson, 1943). These vary in width from 2-90 cms and are most commonly encountered in coastal exposures between Strond and Renish Point. They consist of coarse grained andesine feldspar and amphibole. The amphibole occurs in prismatic crystals up to 6 cms in length, and is frequently orientated perpendicular to the pegmatite walls. Palmer described the occurrence of basified margins to these pegmatites, where the adjacent norite shows a pronounced depletion in plagioclase feldspar. He proposed a segregational origin for these pegmatites. There are many similarities between these pegmatites and the anorthositic-gabbro dykes and trondhjemitic pegmatites cutting the rocks of the anorthosite complex.

3.3.2 Petrology

Early mineral assemblages within the norite are characterized by the associations:-

cpx + opx + plag + amp ± qtz

gt + cpx + plag + amp ± qtz

gt + cpx + opx + plag + amp

Plagioclase (andesine) and quartz constitute approximately 50% of the rock A primary olive-green amphibole occurs but is less common than in the gabbro-diorite. An inverse relationship between orthopyroxene and garnet is noted by Palmer; where garnet is common, orthopyroxene is rare or absent.

A similar relationship between garnet and orthopyroxene has been observed by Livingstone in the Leverburgh ultramafic rocks. The effects of late Laxfordian retrogression are patchily developed.

3.4 Mafic Gabbro Sheets

3.4.1 Field Relations

The distribution of the mafic gabbro sheets is shown in Fig 1.1 and summarized in the introduction to this chapter. The most notable feature of these sheets is the development of an internal compositional or lithological banding. This banding may be orientated parallel to the margins of the sheet. However, in most cases the strike of the banding shows a large angular discordance with the sheet margins.

Where the mafic gabbro sheets are in contact with paragneiss this contact is characterized by an interbanding of the two rock types. There is some evidence to suggest that the mafic gabbro sheets found within the Leverburgh paragneisses are intruded along lithological boundaries within these rocks. Dearnley (1959, 1963) has suggested that the mafic gabbro sheet, south-east of Loch Ossigary is intruded along the contact of the rocks of the Rodil series (mainly pelites, semi-pelites and calc silicates rocks) with those of the Ben Obbe quartzite series (mainly quartzites).

3.4.2 Petrology

The main early assemblages shown by these rocks are:-

	gt	+	cpx	+	plag	+	amp	± qtz
	gt	+	cpx	+	plag			
	gt	+	cpx	+			amp	
	gt	+	cpx					
opx	+ gt	+	cpx	+	plag	+		± qtz
	gt	+			plag	+	amp	+ qtz

The plagioclase feldspar of these assemblages is an andesine (An_{40-49}). Amphibole occurs as sub-idioblastic grains with pleochroism:

X yellow green; Y brown green; Z dark brown.

The banding in these rocks is due to:-

i) The presence or absence of plagioclase feldspar. This produces a large scale rock layering of ultramafic and mafic gabbro (+ subordinate gabbro) rock types.

ii) The presence of elongate lensoid clots or bands of a coarse grained garnet/clinopyroxene intergrowth (ultramafite) within a finer grained groundmass of plagioclase, clinopyroxene and amphibole (mafic gabbro) defines a small scale layering within the large mafic gabbro bands. Everywhere this small scale layering is parallel to the large scale rock layering described above.

iii) The relative concentration of garnet defines a small scale layering within the large ultramafite rock layers.

Where amphibole is present in these rocks it shows a weak orientation in the plane of the compositional banding.

3.5 Ultramafic Lenses in the Langavat Metasedimentary Belt

Ultramafic (ultrabasic) rocks associated with the Langavat paraneisses were first noted by Heddle (1878) and later mapped by Jehu and Craig (1927) and Dearnley (1959, 1963). More recently these rocks have been the subject of a detailed geochemical study by Livingstone (1963), who recorded eight whole-rock analyses of these ultramafites.

The ultramafite rocks occur as a series of isolated lenses (individual lenses varying in length from a few metres to one kilometre), situated centrally within the paragneiss belt and outcropping from Rudha Sgeir Nan Sgarbh on the north-west coast to Loch Meurach. Individual lenses are elongated N.W.-S.E., parallel to the foliation in the surrounding gneisses. In all cases the contacts of the ultramafite lenses are concordant to this foliation. However, these lenses are not confined to the same paragneiss horizon throughout the length of the

Langavat belt (Fig 1.1).

Myers (1968), who considered the structure and lithology of these ultramafite lenses, recognized the occurrence of four main rock types:-

a) Serpentine/tremolite rocks - Massive rock types (dunites & amphibole peridotites) composed of strongly serpentinized olivine set within an unorientated network of tremolite laths. Olivine determinations by Livingstone show a compositional range from $Fo_{90.5} \rightarrow Fo_{84.5}$.

b) Enstatite/anthophyllite rocks - Massive rock types (pyroxenites) composed of radiating clusters of anthophyllite set within a matrix of large enstatite grains, from which the amphibole is partly derived.

c) Actinolite/chlorite rocks - Bright green rocks with a strong linear fabric deformed by small chevron folds (early Laxfordian F_2 folds of Myers, 1968)

d) Green/purple hornblendites occurring as an outer rim to the ultramafite lenses and as small isolated lenses up to 20 metres in length.

These rock types are cross cut by narrow veins of tremolite - Scara Ruadh lens - and veins, up to 6 metres long and 15 cms wide, of fibrous talc and asbestos - Loch Meurach lens - (Dearnley, 1963).

Within individual ultramafite lenses the four rock types (a-d) show a zonal arrangement and occur in the same sequence, in relation to each other and to the structure, in all the ultramafite lenses. Myers has demonstrated that the serpentine/tremolite rocks occur in the cores of tight antiformal folds, enclosed by enstatite/anthophyllite rocks. These are in turn surrounded by actinolite/chlorite rocks and thence rimmed by hornblendites.

It has been proposed, by Myers, that the ultramafite lenses

represent a series of originally sub-concordant layered pyroxenite/peridotite intrusions, of 'alpine type.' The present zonal arrangement of rock types within these bodies is thought, in part, to reflect an interference pattern due to tight interfolding of the originally layered intrusions by two sets of folds. (late Scourian and early Laxfordian, F_1 and F_2 of Myers, 1968).

Both Livingstone and Myers have reported the occurrence of small scale banding, of possible igneous origin, within the Scara Ruadh lens. This banding consists of a series of sharply defined alternating horizons of serpentine/tremolite/magnetite and enstatite/anthophyllite/chlorite and may reflect an original igneous layering of olivine rich and pyroxene rich horizons.

3.6 Ultramafic Lenses in the Leverburgh Metasedimentary Belt

A number of small ultramafite lenses occur between Leverburgh and Rodil, associated with the paragneisses of the Leverburgh belt, and apparently confined to paragneisses of the 'Rodil mixed group' (Palmer, 1971). The margins of these ultramafite lenses are unexposed and their field relations to the adjacent paragneisses are uncertain. The mineral assemblages of the Leverburgh ultramafites differ from those described for the Langavat rocks. The ultramafites of the Leverburgh belt are divided into two groups: Peridotites and pyroxenites.

3.6.1 Peridotites

Amphibole peridotites have been described by Livingstone (1963) and Davidson (1943) from lensoid bodies: north-east of Loch Ossigary; west of the Leverburgh - Rodil Road, 320 metres north of the Rodil - Strond boundary fence; and from south of Leverburgh, 300 metres south of Leverburgh post office. Livingstone termed these rocks 'olivine - spinel ultrabasites' and recorded, from these rocks, a stable assemblage:-

opx (En_{78-84}) > cpx (diopside) > pargasitic amphibole > olivine (Fo_{84}) > spinel (pleonaste + magnetite)

However, textural studies by Palmer (1971) indicate that the spinel, of this assemblage, may be a product of the resorption of the olivine. He envisaged the present mineral assemblage as being the result of the reaction:-

$$ol + plag \xrightarrow{H_2O} opx + cpx + spinel + amp$$

(olivine being in excess of plagioclase in the original assemblage) Davidson (1943) described the petrology of these rocks terming the Loch Ossigary ultramafite, as edenite saxonite and those ultramafites occurring to the south of Leverburgh, as edenite peridotites. The amphibole of these rocks, however, is a pargasite (from analyses by Livingstone) and not an edenite, as suggested by Davidson.

The occurrence of a garnet amphibole peridotite, from a small pod on the east shore of Loch Rodil, due west of St. Clements Church, has been noted by Livingstone (1967).

The mineral assemblage shown by this rock is:-

opx (En_{85}) > colourless amphibole (cummingtonite?) > olivine (Fo_{84}) > garnet > spinel

3.6.2 Pyroxenites (or Websterites)

Both Davidson and Livingstone have described websteritic rocks from two localities near Rodil Village: from a small quarry 270 metres N.N.W. of Rodil Hotel; and from a pit beside the footbridge to Rodil School House. These are essentially two pyroxene rocks, with abundant magnetite and brown spinel, and minor amounts of amphibole, biotite and serpentinized olivine. The amphibole of these assemblages is a pale yellow-green actinolitic-hornblende and appears to be totally derived from the clinopyroxene. The websterites merge laterally into black clinopyroxene bearing amphibolites which are patchily garnetiferous, and thence into plagioclase amphibolites.

Davidson drew attention to this association of amphibolites and

two pyroxene rocks and recalled that such a combination also exists at Scourie (Scottish mainland). Sorensen (1953) also referred to this association when he described ' ..... brecciated ultrabasic rocks at Rodil, in which hypersthene masses up to 2 ft. across are surrounded by amphibolite.'

Amphibole pyroxenites and garnet amphibole pyroxenites have been described from three small lenses between Rodil and Leverburgh; 460 metres south-east of Leverburgh Post Office, on the west slope of Glen Strondeval; from the east shore of Loch Cistevat; and east of the Rodil - Leverburgh Road, 460 metres north of the Rodil - Strond boundary fence. Livingstone referred to these rocks as 'the garnet bearing ultramafites'. In contrast to the peridotites, garnet occurs abundantly within these rocks, but olivine and spinel are absent. The typical assemblage of the garnetiferous amphibole pyroxenites is:-

$$\underset{\text{(salite)}}{\text{cpx}} > \text{gt} > \underset{\text{amphibole}}{\text{pargasitic}} > \underset{(En_{69-77})}{\text{opx}}$$

Livingstone noted that in rocks where modal orthopyroxene exceeds 20%, garnet is usually absent from the assemblage. Apatite and plagioclase (oligoclase - andesine) are common accessory minerals. The amphibole of these rocks is again pargasitic, but shows slightly higher iron and titanium values than the amphibole from the olivine bearing peridotites.

Livingstone has described a small scale banding within these rocks. This banding is defined by the alternation of garnet/clinopyroxene layers (4 mms in width) and amphibole (plus small quantites of garnet and clinopyroxene) layers.

3.7 Pyroxenite Dykes

Pyroxenite dykes intrusive into the norite body have already been described. Similar dykes also occur intrusive into the metasediments south-west of Northton and north-east of Rudh'an Teampuill.

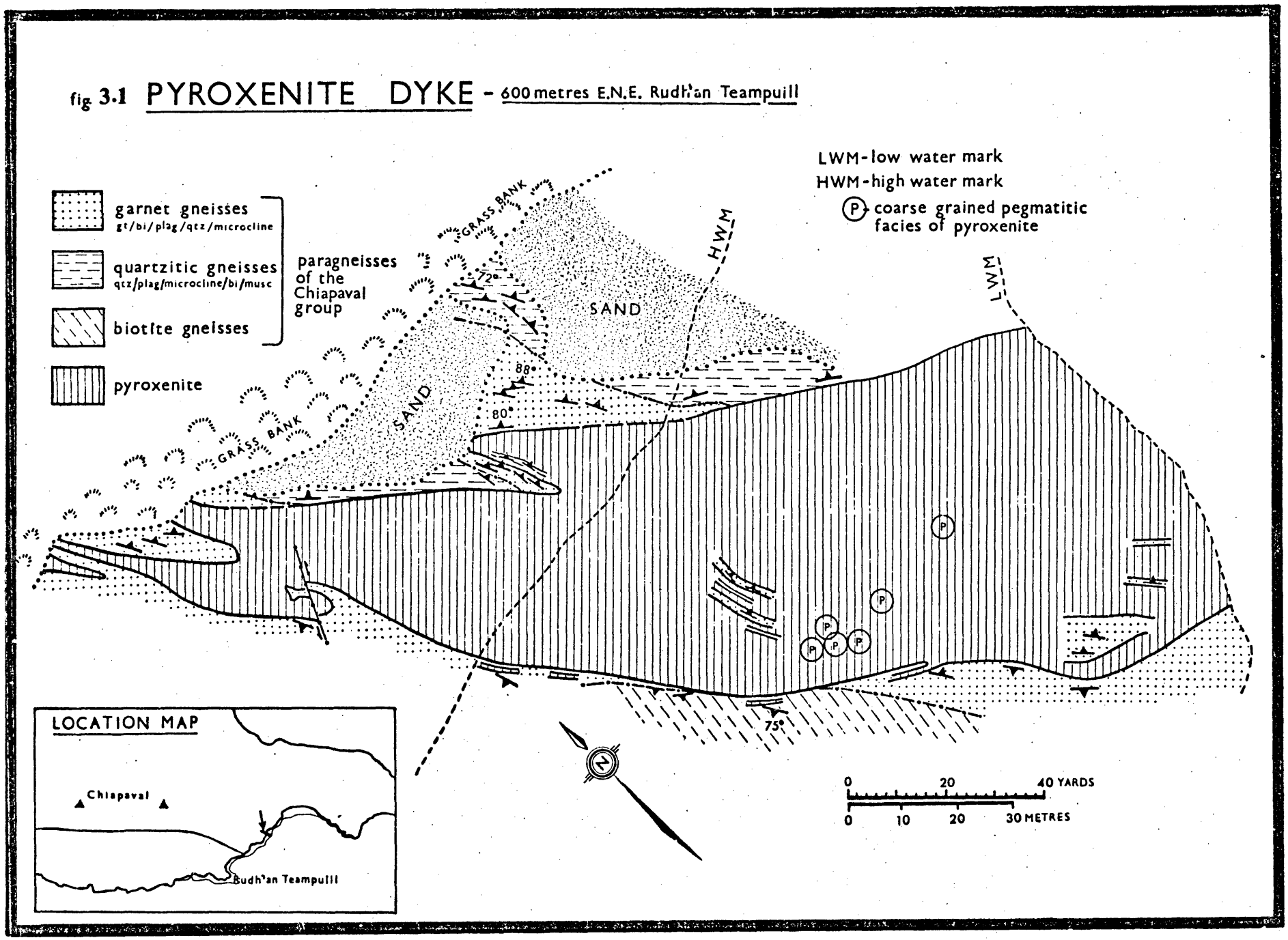
These intrusive bodies appear to be confined to the southern coastline of South Harris. During the present study three large dyke-like bodies, north-east of Rudh'an Teampuill, have been mapped. The largest of these is shown in fig 3.1. All of these dykes are orientated north-west, south-east and are sub-parallel to the foliation in the surrounding metasediments. Marginal areas of the pyroxenite dykes are crowded with small xenolithic strips of metasediment, showing all stages of assimilation by the dyke material. Rafts of metasediment, up to 15 metres in length in the figured example, also occur throughout these bodies.

The pyroxenites are essentially clinopyroxene, orthopyroxene (in ratio of approximately 5:1) rocks with accessory plagioclase feldspar and ilmenite. The abundance of garnet, biotite, kyanite and quartz in the pyroxenites adjacent to the dyke margins (and adjacent to the large metasedimentary rafts within these dykes) is thought to be a direct result of assimilation of the metasedimentary country rocks.

All of the dykes of this type studied show some degree of sulphide mineralization. Pyrrhotite, usually intergrown with minor amounts of chalcopyrite, is the main sulphide phase observed in these rocks. It typically occurs in a branching dendritic form (Plate 3.3). Occassionally the pyrrhotite can be seen to rim small euhedral pyrite crystals (Plate 3.4). Both the pyrite and pyrrhotite are cross cut by narrow veins of chalcocite. These sulphide minerals constitute an estimated 15% of the volume, of the exposed portion, of the figured pyroxenite dyke. The degree of mineralization falls off markedly in the metasediments surrounding this dyke. Also there is very little mineralization of the xenolithic rafts of metasedimentary material within the dyke.

It is suggested that these pyroxenite dykes are contemporaneous with those which intrude the norite.

fig 3.1 PYROXENITE DYKE - 600 metres E.N.E. Rudh'an Teampull



(a)

	PYRITES				PYRRHOTITES			
	POINT 1	POINT 2	POINT 3	POINT 4	POINT 5	POINT 6	POINT 7	
Fe	47.30	47.05	45.56	46.30	60.13	59.62	59.36	Fe
Ni	0.20	0.23	0.39	0.38	0.73	0.70	0.71	Ni
Co	0.05	0.06	0.06	0.11	0.20	0.19	0.24	Co
Mn	0.12	0.09	0.10	0.09	0.13	0.12	0.12	Mn
S	52.32	52.55	53.88	53.16	38.92	39.48	39.74	S
TOTAL	99.99	99.98	99.99	100.04	100.11	100.11	100.17	TOTAL

(b)

	PYRITE	PYRRHOTITE	
	av.20	av.18	
Fe	46.75	60.13	Fe
Ni	0.23	0.70	Ni
Co	0.07	0.21	Co
Mn	0.07	0.12	Mn
S	52.90	38.98	S
TOTAL	100.02	100.14	TOTAL

(c)

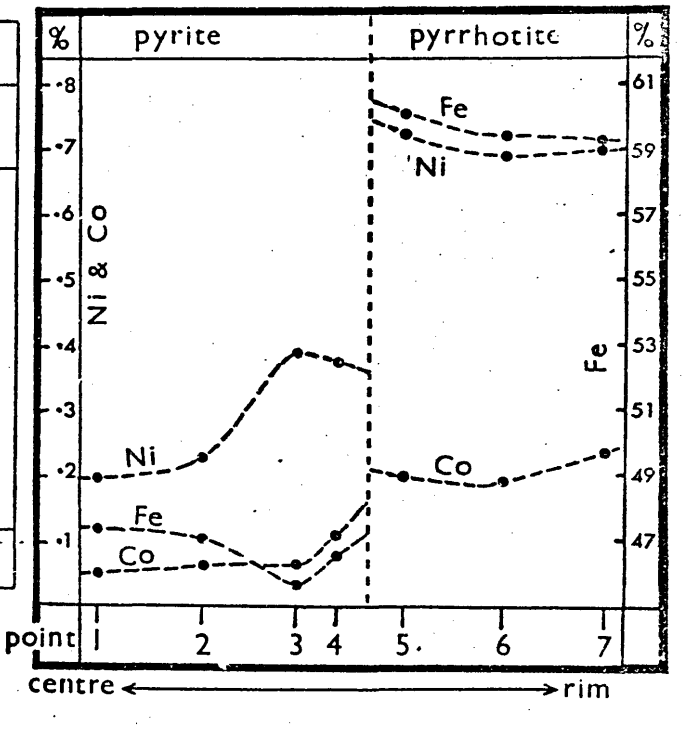


fig 3.2 Mineralization of pyroxenite dyke, 600 metres E.N.E. of Rudh'an Teampuill.
a) 7 point traverse across pyrite/pyrrhotite grain (Plate 3.4). Sulphur values were calculated by difference.
b) Average of 20 pyrite analyses and 18 pyrrhotite analyses
c) Variation of iron, nickel and cobolt along the 7 point traverse. Note the inverse relationship between iron and nickel in the pyrite.

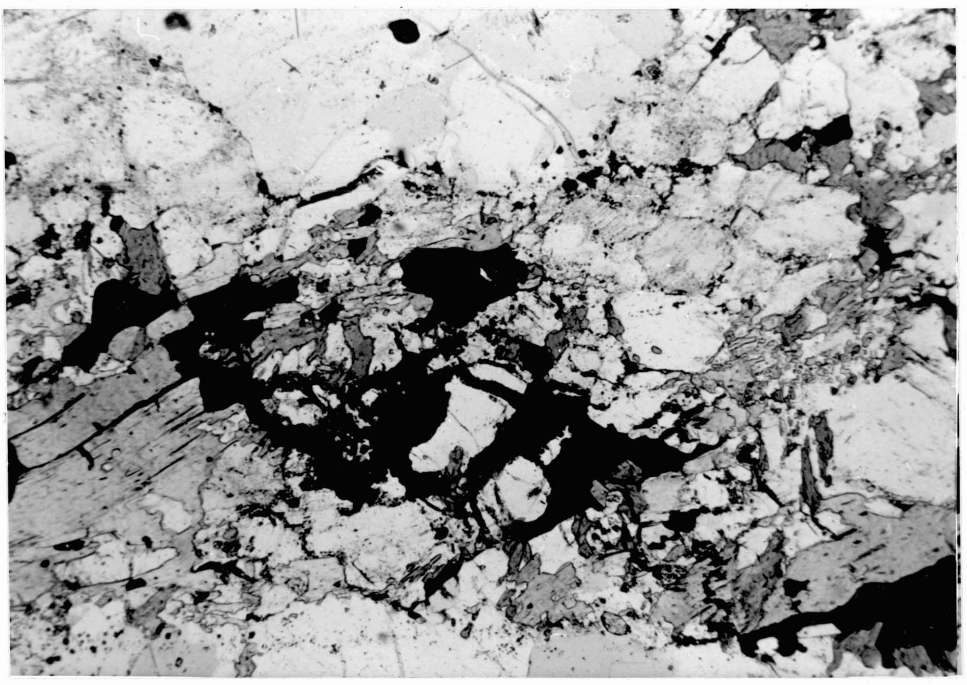


Plate 3.3 Dendritic pyrrhotite. Pyroxenite dyke, 600 metres E.N.E. of Rudh'an Teampuill. x 50

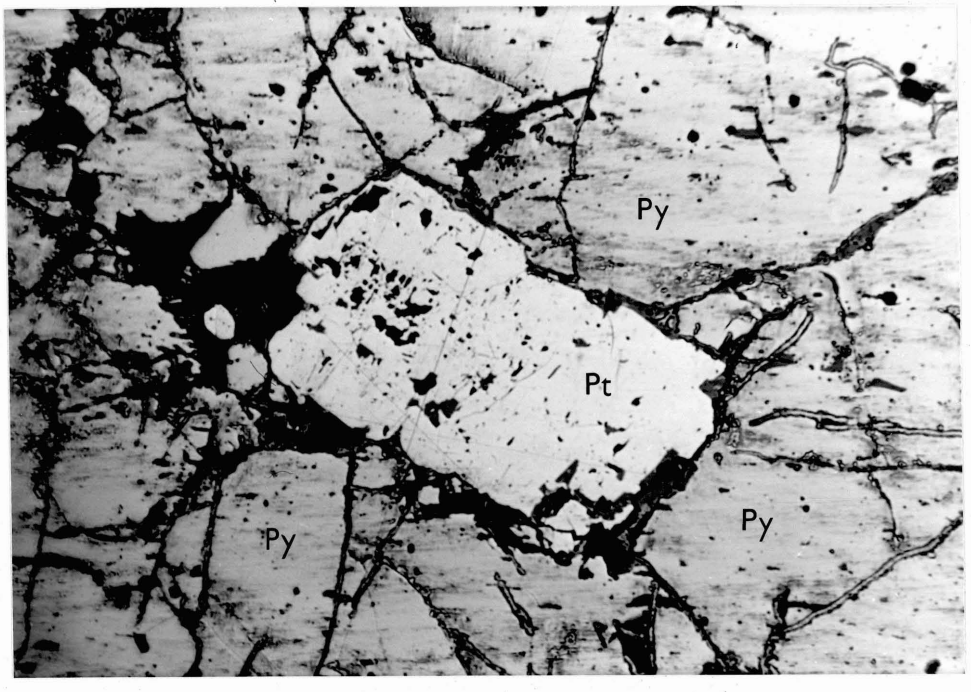


Plate 3.4 Pyrrhotite rimming pyrite. Pyroxenite dyke, 600 metres E.N.E. of Rudh'an Teampuill. x 50 Py - pyrrhotite; Pt - pyrite.

3.8 History of Igneous Intrusive Activity in Southern South Harris

Many intrusive relationships, between the meta-igneous rock types of this area, have already been described. These are presented in a summarized form below and a proposed history of intrusive activity for this area is given in Table 3.1.

a) the gabbro-diorite, norite and anorthosite are all intrusive into and contain xenolithic blocks of the associated paragneisses.

b) the gabbro-diorite and the anorthosite appear to be younger than, and intrusive into, the mafic gabbro sheets which rim them.

c) the gabbro-diorite, norite and anorthosite are intruded by a variety of small basic dykes and sills.

d) no intrusive relations between the gabbro-diorite, norite and anorthosite have been observed.

There appears to be no certainty that mineralogically and compositionally similar bodies are of the same age and correlations that have been made on this basis by previous workers are misleading.

The history of intrusive activity in southern South Harris appears to be that of continued intrusion of ultrabasic and basic material, yielding a variety of ultramafites and mafic gabbros. The earliest intrusives (pre or early Scourian) are represented by the extensive banded mafic gabbro sheets and possibly also by the ultramafites which now form isolated lensoid bodies within the Leverburgh and Langavat meta-sedimentary belts. The amount of ultrabasic and basic igneous activity thence tails off through the remainder of Scourian and Laxfordian. All of these ultrabasites and basites are intruded as large sill-like bodies or as small dykes and sills.

The intrusion of the less basic gabbro-diorite and norite plutons and the stratiform anorthosite body marks an early departure from this pattern of intrusion. The implications of this are discussed

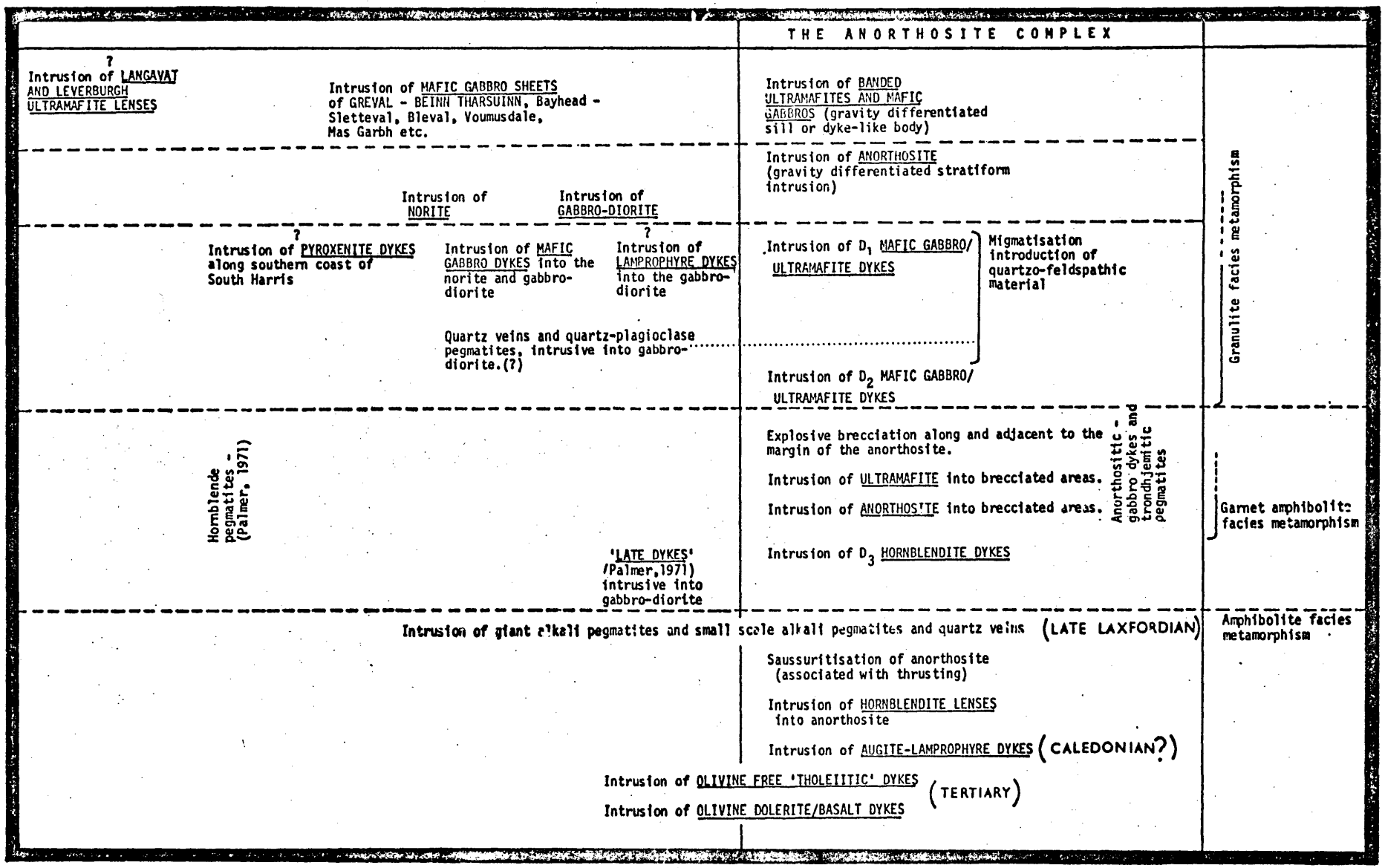


Table 3.I. Proposed intrusive history of South Harris igneous rock types, with particular reference to the anorthosite complex

at greater length elsewhere in this thesis. However, it should be stated at this point that the gabbro-diorite and norite are thought to be genetically related to the anorthosite.

CHAPTER 4

THE STRUCTURAL AND METAMORPHIC HISTORY OF THE ANORTHOSITE COMPLEX

4.1 The Regional Structure of the Outer Hebrides

The pre-Laxfordian structure of the Lewisian is difficult to determine owing to the effects of Laxfordian reworking. When allowances have been made for the modifying effects of later deformation it appears that structures produced during the early Scourian (2,900 - 2,600 million years; Moorbath et al., 1969) had a north-north-easterly trend, which is reflected in the trend of the bouguer gravity contours.

Laxfordian deformation occurred in up to four phases (Coward et al., 1970), the most important of which was responsible for the large scale (F_3) fold structures (fig. 4.1) of the Outer Isles. This major phase of Laxfordian deformation was remarkably heterogeneous in its effects. It produced broad, open, antiformal areas of weak deformation and weak tectonite fabrics of linear type. Within these areas the main Scourian structures can still be recognised and intrusions of 'Scourie dyke' type retain primary igneous intrusive features. In contrast to the antiformal areas, the complimentary Laxfordian synforms are tight, highly deformed structures with strongly planar tectonite fabrics. Within the synforms the Scourian structures are flattened and Scourie dykes are boudinaged and concordant with the gneisses. It has been suggested that South Harris occupies such a Laxfordian synformal zone (Coward et al., 1970; Palmer, 1971).

4.2 The Structure of the Anorthosite Complex - An Introduction

In this chapter a brief survey of the main structural elements of the South Harris anorthosite complex is presented. A determination of the main structures was thought necessary for both sampling purposes and also to determine an overall chronology for the anorthosite complex

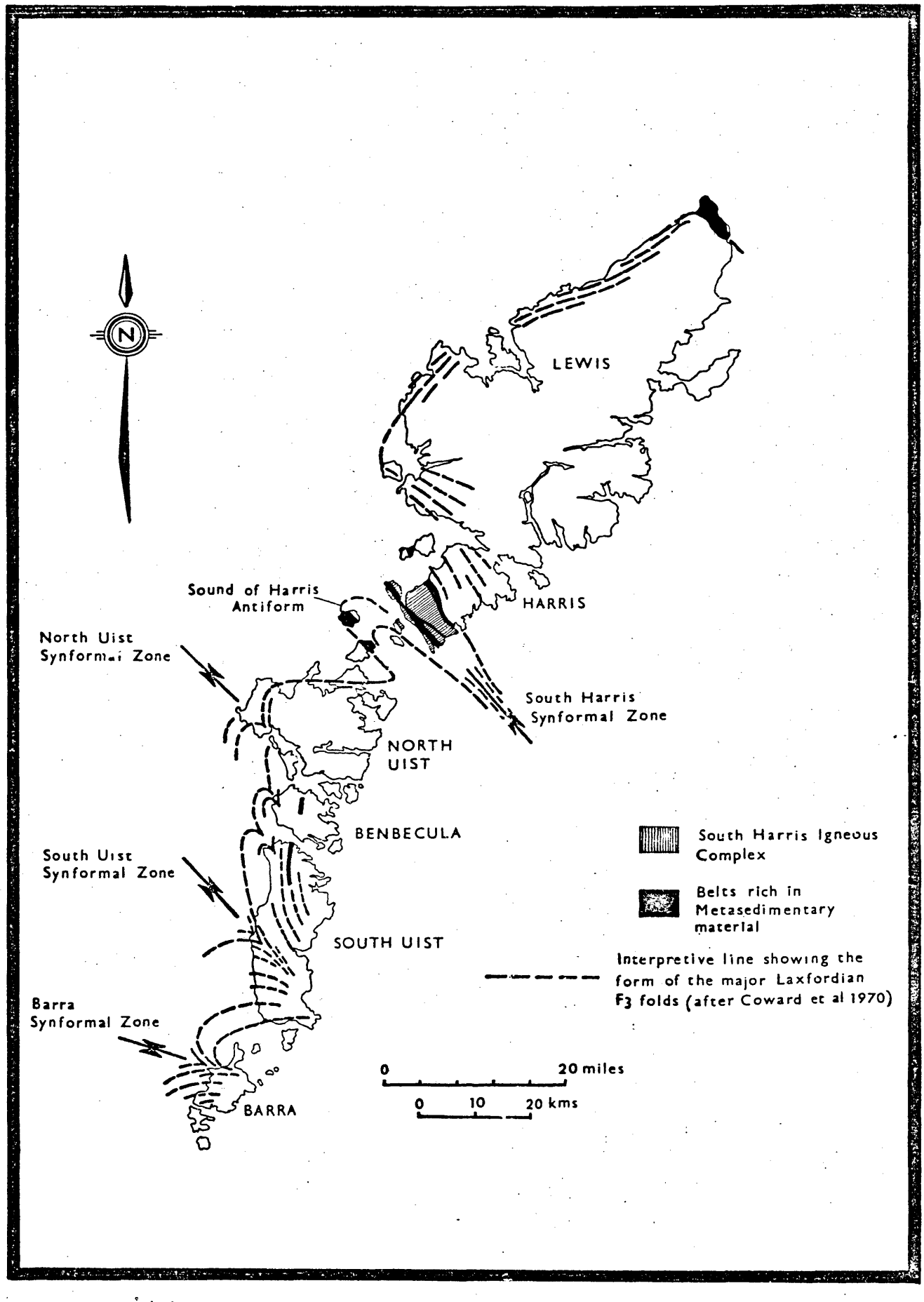


Fig 4.1 . Schematic map illustrating the arrangement of Laxfordian (F_3) antiforms and synforms in the Outer Hebrides (after Coward et al, 1970).

and its environs. The effects of each deformational phase on the anorthosite and its gabbroic envelope are discussed and a summary is presented in the last section of the chapter.

The anorthosite body is thought to have been originally a sheet like mass, intruded into the meta-sedimentary cover sequence, now represented by the Leverburgh, Langavat and Ensay belts. The present work on the anorthosite complex suggests that it pre-dates (or perhaps is coeval with) the early part of the Scourian granulite facies metamorphism and deformation. The associated bodies of gabbro-diorite and norite are also regarded as of this age, but their relationship, both temporally and chemically, to the anorthosite is problematical.

The overall structure of the southern South Harris appears to be that of a large isoclinal fold, or a series of such folds. The anorthosite body forms the observed core to a neutral antiformal syncline, the fold limbs of which include meta-sediments of the Leverburgh supracrustal belt. An aeromagnetic interpretation of this area, presented by Westbrook (1974), suggested that this fold (or one of a series of such folds) may possibly extend north-westwards for at least 22 Kms and extend in depth for at least 7 Kms. This early fold (or folds) is thought to have been refolded and the whole area flattened during the major Laxfordian folding phase.

4.3 F_1 Deformation

The earliest deformational (L-S) fabric observed, in the rocks of of the anorthosite complex has been designated F_1. Pre-dating this F_1 foliation is a compositional banding; a structure defined by lithological layering and characterized by a granoblastic fabric with no linear element. Such a lithological banding is preserved in ultramafite/mafic gabbro pods within the gabbroic envelope of the anorthosite. The nature and arrangement of this banding is discussed in detail in a later section.

The overall disposition of the F_1 foliation within the anorthosite complex is shown in fig. 4.3. It appears that this foliation is sub-parallel or parallel to, and superimposed on, an original compositional banding in the anorthosite. At a later date this F_1 foliation (and banding) has been folded.

All observed structural elements produced during the first recorded phase of deformation (F_1) are small scale.

In some areas within the anorthosite it is possible to recognise, an early plastic phase and a later brittle phase of F_1 deformation (Table 4.1). The early plastic phase of deformation (F_1^1) has given rise to a great deal of contortion and small scale folding. The distribution of such 'intrafolial' folds is shown in fig. 4.3. The degree of folding and contortion increases adjacent to intensely migmatized areas.

Plastic deformation was followed by a phase of brittle deformation (F_1^2) along parallel sets of very fine shear planes, rarely seen to exceed 10mm in width. These two phases of F_1 deformation are illustrated in Plates 4.1, 4.2, 4.3 and 4.4 and fig. 4.2.

The F_1 deformational phase is associated with a period of high-grade (granulite facies) metamorphism (M_1) and migmatization. As previously mentioned the areas of greatest F_1 deformation are usually spatially associated with early migmatization, which is somewhat patchily developed within the anorthosite. This migmatization may be temporally equatable with the 'early' migmatizatization noted in the Leverburgh metasediments by Palmer (1971) and Dickinson (1974).

The main period of migmatization occurred early within the F_1 deformational period, prior to or contemporaneous with the plastic deformational phase (F_1^1). The buff coloured quartzo-feldspathic material occurs in bands and lenses, concordant with the F_1 foliation (Plate 4.5) and occasionally involved with the early small scale plastic folding. A later, minor episode of migmatization is demonstrated

Plate 4.1 Contorted and migmatised anorthositic gabbro/gabbro sequence. Note in particular the small scale F_1^1 plastic folding (right) and the late D_2 mafic gabbro dyke (left and centre.) An interpretive sketch of this photograph is given in fig. 4.2.

Plate 4.2 Contorted and migmatised anorthositic gabbro. Note the disrupted remnants (central) of an early D_1 mafic gabbro dyke.

Plate 4.3 Contorted and migmatised anorthositic gabbro/gabbro sequence.

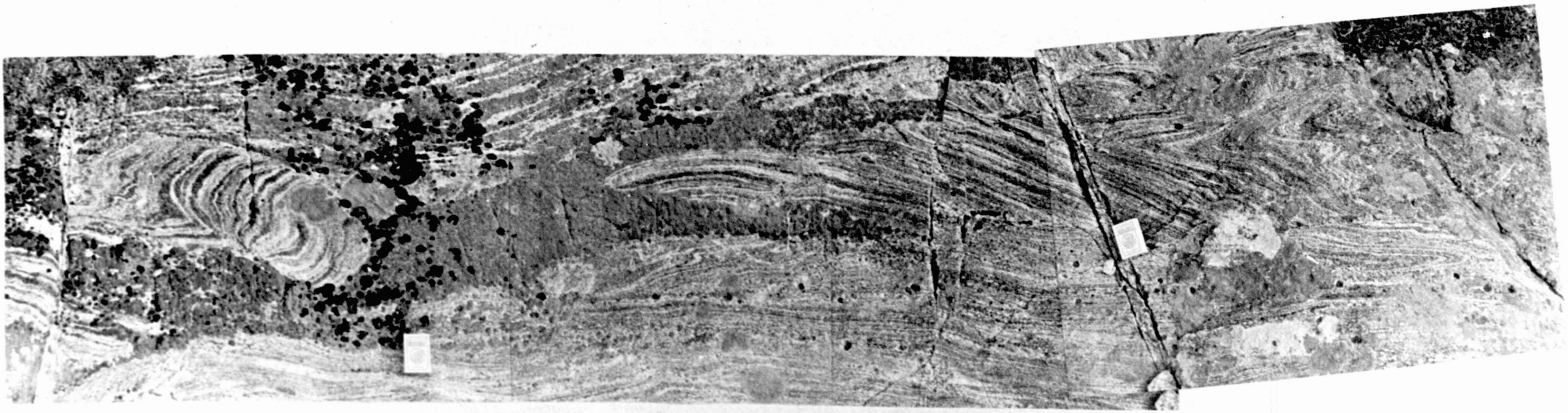


Plate **4.1**



Plate **4.2**

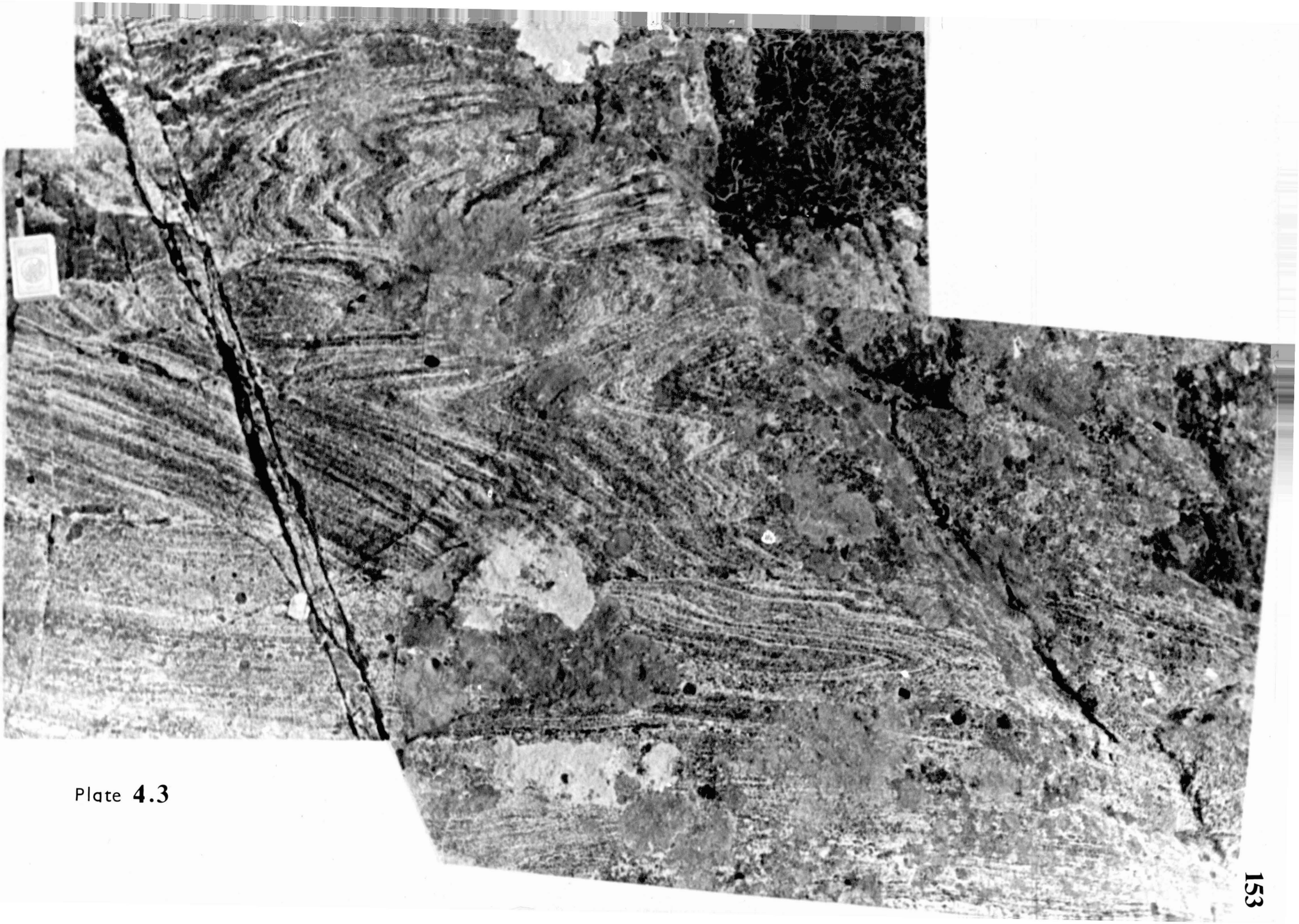


Plate **4.3**

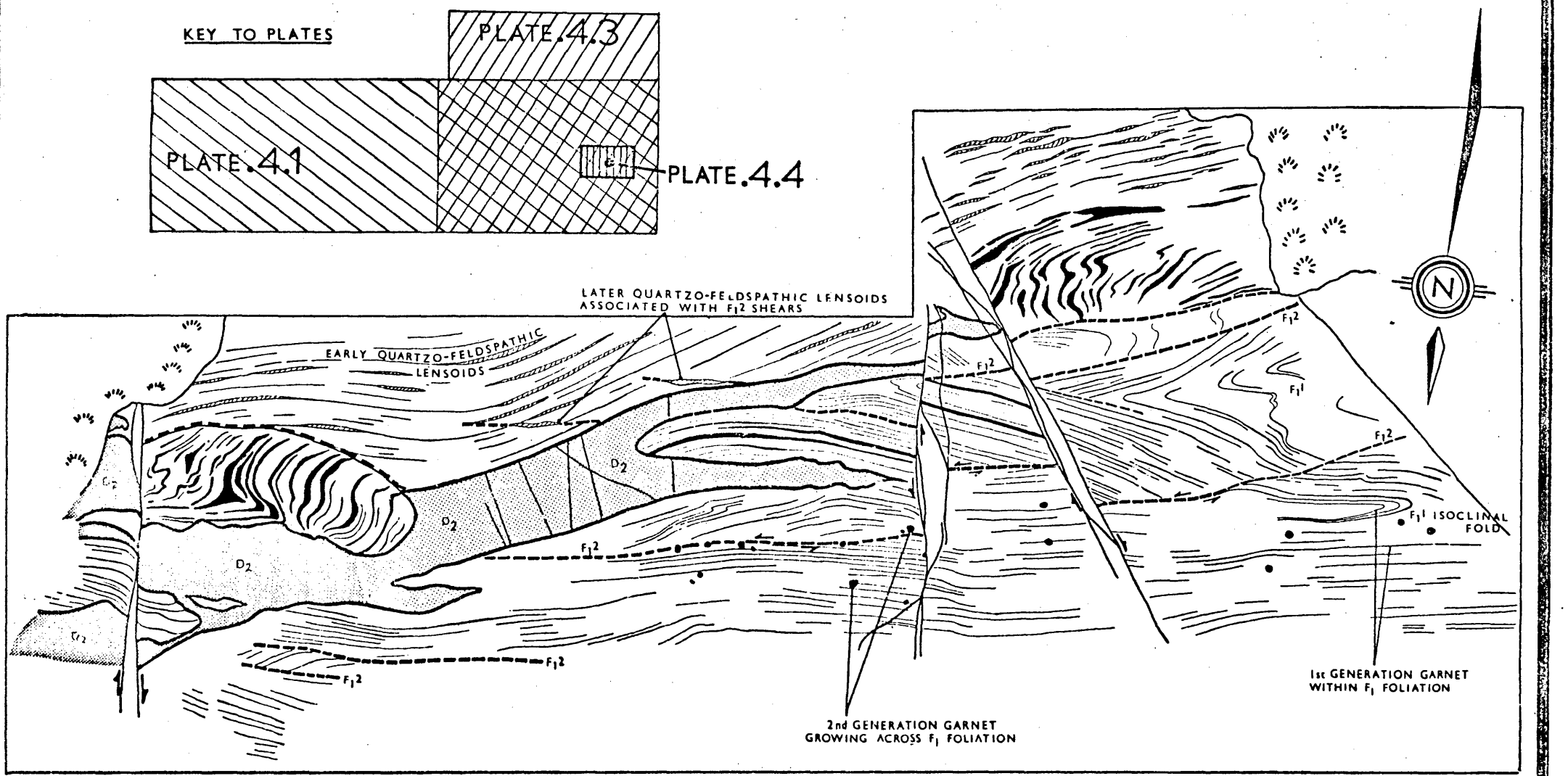


Fig 4.2. Composite diagram from plates 4.1 and 4.3. - showing the effects of both the early (F_1^1) plastic deformation and the later (F_1^2) brittle deformation. Note the two generations of garnet and the discordant (d_2) mafic gabbro dyke. Exposure: 405 metres due west of Ha-Cleit summit. Scale 1:15



Plate 4.4 F_1^2 intrafolial fold. Note the large garnets which grow across the F_1 foliation.



Plate 4.5 Foliated and banded gabbro sequence intruded by D_1 mafic gabbro dykes and injected by cream-buff quartzo-feldspathic veins.

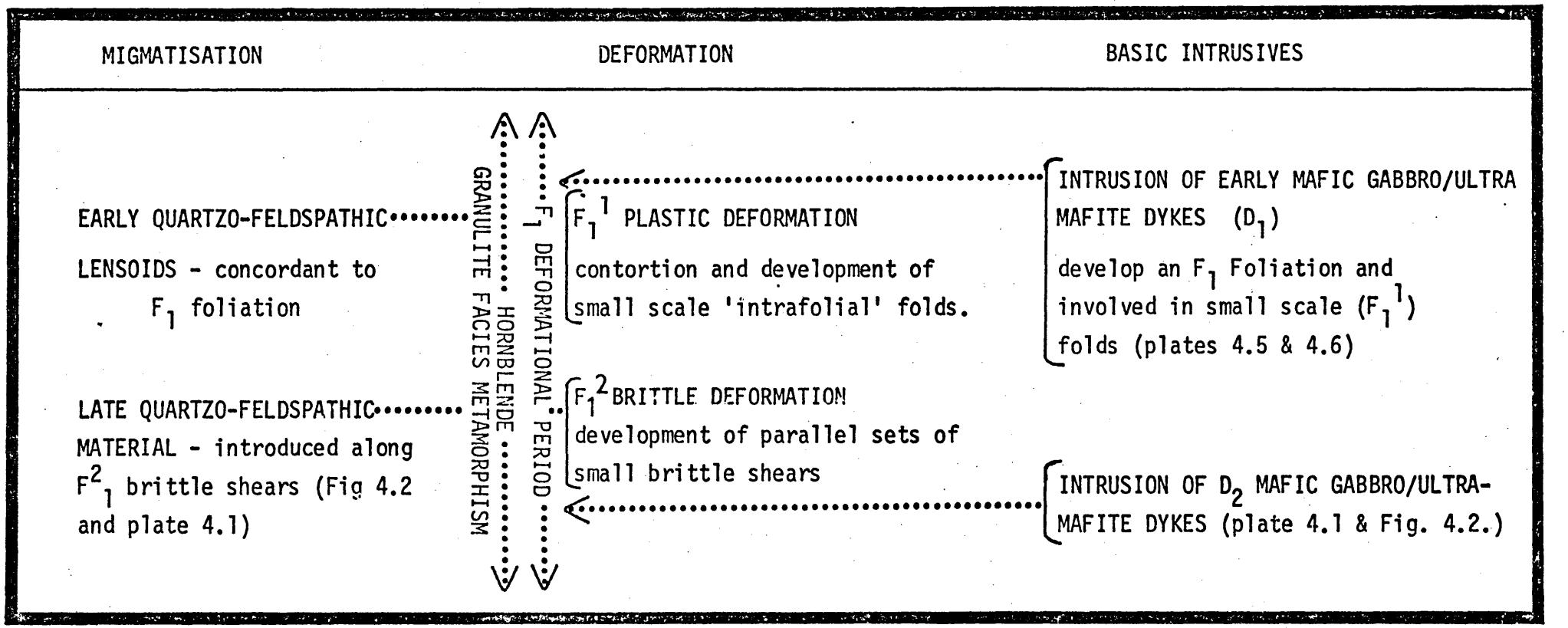


Table 4.1 The relations between the F_1 deformational events, early basic intrusives and migmatization in the anorthosite.

by the occurrence of small discordant quartzo-feldspathic lenses injected along the F_1^2 brittle shears (Fig. 4.2,Plate 4.1).

4.3.1 The Relationship of Early Gabbroic dykes to the F_1 Deformation

Two early mafic gabbro dyke suites (D_1 and D_2), intrusive into the 'anorthosite' are recognized. The proposed relationships of these dykes to the F_1 deformational phases is shown in Table 4.1. Both sets of dykes show remants of a granulite facies mineralogy. The early D_1 gabbroic dykes, show a large scale concordance to the F_1 foliation, although minor discordances can be seen along their margins. In some cases these early D_1 dykes develop a foliation, defined by thin impersistant felsic streaks, which is parallel to the F_1 foliation in the surrounding rocks (Plate 4.6). Also in Plate 4.6 several discordant stringers from the dyke margin can be seen to have been 'pulled out' into parallelism with the F_1 foliation. The D_1 dykes also appear to have been folded in with the anorthosite during the early plastic (F_1^1) deformational phase (Plate 4.7). It is thought that the early gabbroic (D_1 dykes) were intruded prior to, or contemporaneous with, the onset of the F_1 deformational period. Their large scale concordance may be an effect of either tectonic or lithological control.

The D_2 dykes show a broad concordance in that their lengths are parallel or sub-parallel to the F_1 foliation in the rocks which they intrude, but on a small scale they are markedly discordant and show a tendancy to 'net vein' the anorthosite (Fig. 4.2 and Plate 4.1). These dykes appear to post-date the F_1^2 brittle shears and are thought to have been intruded towards the end of the F_1 deformational period.

Both D_1 and D_2 dykes contain a prominent oblique joint pattern, with joints orientated at between 70 - 90° to the dyke margins, at which they usually terminate. In general the less deformed the dyke (i.e. D_2 dykes) the less abundant the joints and the more near perpendicular these joints become to the dyke margins. It is thought that these are tension

fig. 4.3 The Distribution of foliations and Banding in the north-eastern part of the Anorthosite Complex.

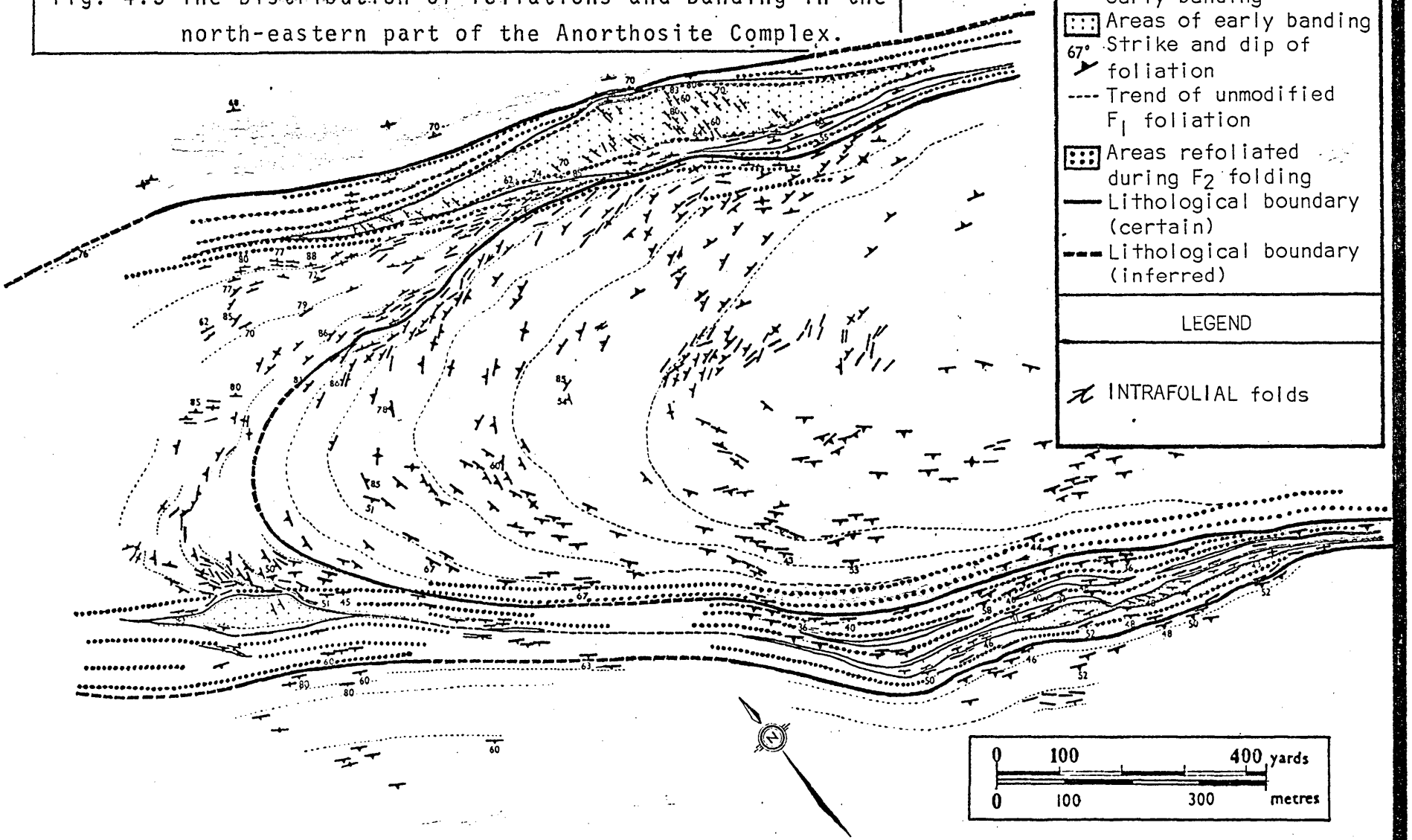




Plate 4.6 Mafic gabbro dyke (D_1). Note the foliation developed within this dyke (F). The dyke also shows evidence of a small scale discordance (dis).
tj - tension joints
s - discordant stringers from the dyke margin.
Location: 405 metres west of Ha-Cleit summit.



Plate 4.7 Mafic gabbro dyke (D_1) involved in an F_1 fold.
Location: 230 metres south-west Ha-Cleit summit.

joints.

Most D_1 and D_2 mafic gabbro dykes occur in the lower zone of the anorthosite sequence; relatively few dykes occur in the middle and upper zones. Mafic gabbro dykes in the upper zone are in some cases oblique to the early foliation and banding, cutting it at up to 30^o. Palmer (1971) has described similar oblique dykes from the anorthosite, which develop a weak segregational foliation parallel to the foliation outside of these dykes - and hence oblique to the dyke margin. It is thought that these oblique dykes in the upper zone are part of the D_1 dyke suite. It is possible that lithological control is the predominant factor in determining whether the D_1 dykes will be concordant or discordant. The occurrence of discordant dykes in the upper zone of the anorthosite sequence may thus simply reflect the more massive type of host rock which occurs at this level.

4.4 The Pre-F_1 Banding

The central parts of the ultramafite/mafic gabbro pods show a compositional or lithological banding, interpretted as possibly an essentially unmodified igneous banding. Marginally these pods become highly sheared, developing an F_1 deformational foliation concordant with the margins of the pods. The sheared rocks are totally amphibolitized and a zone of amphibolitization, varying from 1-4 metres in width, also affects the unsheared ultramafites and mafic gabbros adjacent to the deformed margin of the pods. The lithological banding within the ultramafite/mafic gabbro pods usually shows a large angular discordance to the pod margins and in some cases deflects into the marginal shear foliation.

The ultramafites and mafic gabbros are thought to have formed an originally continuous horizon, subsequently boudinaged during the F_1 deformational period. In the area north-east of Leverburgh (fig. 4.3) three large pods occur; the Ha-Cleit pod on the north-eastern flank of the anorthosite and the Steisevat and Abhainn Easean Chais pods on the south-western flank.

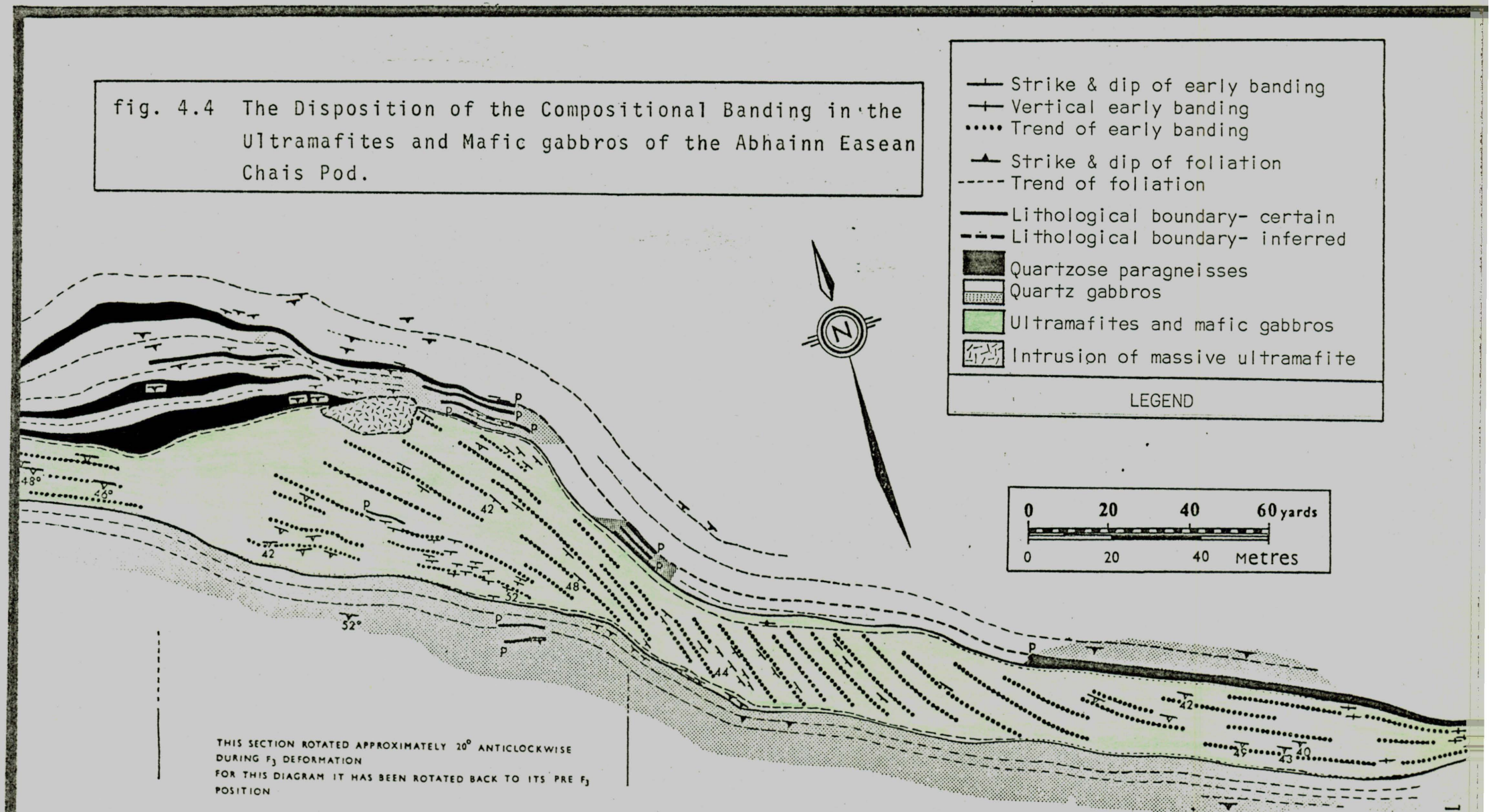
a) The Ha-Cleit ultramafite/mafic gabbro pod is elongated N.W. - S.E. and is approximately 1 Km in length. At the summit of Ha-Cleit it attains a maximum width of 120 metres. The banding in this pod is at 170-190° (approx. N-S) dipping 60-80° east. The regional F_1 deformational foliation on both sides of the pod is at 110-130° dipping constantly N.E. at 60-70°. This discordance, of approximately 60°, between the strike of the banding and the marginal F_1 foliation applies not only to the widest areas of the pod but still holds good when the pod thins to 8m in a north-westerly direction.
Marginally the banding either swings into the F_1 foliation, or terminates against the F_1 foliation with no apparent deflection.

b) The Abhainn Easean Chais pod is again elongated N.W.-S.E. and has been mapped in detail for over 1 Km. It can be traced through intermittent exposure, as a narrow strip 8 metres in width for a further 0.5 Km to the south-western slope of Roneval. It is very much thinner than the Ha-Cleit pod, attaining a maximum width of 45 metres. At the north-west end of the pod the banding is parallel to the margins of the pod and also to the F_1 deformational foliation and dips S.S.W. at 40-50°. In a south-easterly direction the pod thickens out and the banding becomes increasingly oblique to the pod margins. A maximum discordance of 35° is reached before the banding starts to swing back into parallelism with the pod margins and F_1 foliation. Fig. 4.4 is a large scale map of the central part of the pod, showing the variation in the attitude of the banding to the F_1 foliation in the surrounding rocks.

c) The Steisevat pod is the smallest of the three described (approximately 320 metres x 72 metres) and by comparison is poorly exposed. A less well developed banding can be seen at 190°.

The banding, in the three large pods described is interpreted as being earlier than the F_1 deformational fabric and as representing an essentially unmodified igneous banding. Minor effects of the deformation

fig. 4.4 The Disposition of the Compositional Banding in the Ultramafites and Mafic gabbros of the Abhainn Easean Chais Pod.



can be seen both microscopically and megascopically. Microscopically the texture of the rock is essentially granoblastic, the hastingistic amphibole (M_1 granulite facies metamorphism) is in some cases alligned to give a nebulous linear element to this. Megascopically bands can seen to thin and pinch out and more competent bands develop transverse tensional joints. However, except in marginal areas, the degree of deformation in the ultramafites and mafic gabbros is relatively low. Interpreting the banding as of an early type poses the problem of its present orientation. Either its present position is indicative of its original position, or it has in some way been 'rotated' into its present orientation, possibly from a situation where it was parallel to the compositional banding of the anorthosite.

If the present thickness perpendicular to the strike of the banding is an indication of the original thickness of this horizon than this would vary from 1 Km - 8 metres in width (125 : 1). The contrast in size of the pods on either side of the complex possibly reflects an original size variation in the thickness of the horizon, and it may be that a combination of an original size variation and subsequent lateral attenuation could produce a thickness variation of this order. The table below shows the variation in present thickness (measured distance perpendicular to strike) related to the degree of discordance between the banding and the F_1 marginal foliation.

	Thickness perpendicular to strike (uncorrected for dip)	Discordance	Dip
Ha-Cleit Pod	1 Km.	60^o	60^o - 80^o
N.W. Easean Chais Pod	14 m.	parallel	46^o - 48^o
Central Easean Chais Pod	68 m.	35^o	42^o - 52^o
S.E. Easean Chais Pod	7½ m.	parallel	vertical

Working from the basis that the banding in the ultramafites and mafic gabbros was originally parallel to the compositional banding in the anorthosite, a feature that still persists in some areas, there are two possibilities:-

a) That the present disposition of the banding reflects its original orientation and that in some way this has remained unchanged. However, the banding in the anorthosite, with which it may have been originally parallel, has been reorientated during subsequent deformation. (perhaps during the F_2 folding phase).

b) That this banding has been rotated relative to that in the surrounding rocks, perhaps during the F_1 deformational period.

The occurrence of such an early discordant lithological banding is a common feature of the basic rocks throughout South Harris. The large mafic gabbro (meta-gabbro) sheets and lenses, of the Leverburgh meta-sedimentary belt, show an early banding, which is in many cases discordant to the margins of the sheets. Palmer (1971) described a discordant banding, striking at 40^{o}, along the southern margin of the Liuri - Rudh'an Teampuill mafic gabbro sheet. The attitude of the early banding within the Bayhead - Beinn Tharsiunn mafic gabbro sheet is variable. In the region of Bayhead the banding strikes at 40^{o} - 70^{o} and is markedly discordant to the margins of the sheet. (which strike at between 100^{o} - 110^{o}). However, in roadside exposures to the west of Beinn Tharsuinn the banding can be seen to be striking at approximately 110^{o}, parallel to the margins of the sheet.

On a small scale a discordant banding is sometimes obvious in numerous torpedo shaped boudins of mafic gabbro (rarely exceeding 10 metres in length). These are of common occurrence throughout the quartz gabbros of the anorthosite envelope, and are most abundant adjacent to the large ultramafite/mafic gabbro pods. The banding within these boundins strikes consistantly at60 - 70^{o} and terminates abruptly

against the F_1 foliation of the surrounding quartz gabbros. Similar structures have been described by Palmer (1971) from the Leverburgh meta-sedimentary belt and termed 'rotational boudins'. He described and figured examples of basic gneiss boudins from north of Geo Mor on the Chipaval peninsula.

In general the early banding in both large and small scale examples, strikes consistently between north and north-east, in marked contrast to the regional north-westerly strike in South Harris.

4.5 Folding of the Anorthosite Complex (F_2 Deformation)

It was suggested by Dearnley (1959, 1963) that the anorthosite was folded into an antiform (a fold which closes upwards). This observation is substantiated by the present work. The style of this fold is shown in fig. 4.10. Arrows indicating the facing direction of the anorthosite, in this diagram, are based on both field and chemical evidence which has been summarized in Chapter 2. The fold can be described as an antiformal syncline. The fold closure is neutral with the axis plunging at between 80° and the vertical. The 'nose' area of the fold, north-east of Leverburgh, is isoclinal, but on the south-west slopes of Roneval the fold limbs diverge and on the basis of the dihedral (interlimb) angle it is here better termed a tight syncline. The axial plane trace of this fold shows a broad curvature and the axial plane a variable dip. Dearnley (1959, 1963) who described the structure of the anorthosite as a north-westerly plunging antiform also noted such axial plane 'twists' and attributed them to cross-folding of late Laxfordian age.

Horizons within the anorthosite sequence, when traced from the central hinge zone into the limbs of the fold, become highly attenuated and show changes in both mineralogy and texture. Folding has created two distinct structural environments within the anorthosite complex (fig. 4.3):-

a) the central hinge zone, where:-

i) early M_1 granulite facies textures are preserved virtually unmodified (Table 2.1)

and ii) an F_1 (L-S) fabric is preserved

b) the fold limbs, where:-

i) the M_1 granulite facies textures are extensively modified (Table 2.1)

ii) M_1 mineral assemblages are amphibolitized

and iii) the F_1 fabric has been 'reworked'. For the most part the linear fabric developed along the fold limbs is more pronounced (especially along lithological boundaries in these areas) than the F_1 (L-S) fabric which characterizes the fold hinge. The new fabric developed along the fold limbs has a much enhanced S (planar) element, due to the allignment of newly formed platey minerals (chiefly biotite).

4.6 F_3 Deformation (early Laxfordian)

The F_1 and F_2 foliations turn into shears of F_3 type. These shears have a general N.N.W.-S.S.E. trend (fig. 4.6(a)) and are oblique to the north-west south-east axial plane trace of the F_2 fold. Thus as one would expect individual shears can be traced from the paragneisses across the gabbroic envelope and into the anorthosite, on both flanks of the complex. Several of these shears extend laterally for up to 500 metres and they vary in width from 22 metres down to a few centimetres. The predominant sense of movement, in the horizontal plane, along these shears is dextral. Very few sinistral shears have been recorded. Fig. 4.5 shows the distribution and effect of these F_3 shears in the nose area of the complex.

In several areas the outcrop pattern is such that these shears can be studied in the vertical plane, over distances varying from 10-15 metres, as well as in the horizontal plane. From these exposures it can be seen that:-

a) many of the shear planes are curved, being vertical at depth and turning over to dip either west or east, at as little as 35°, when traced upwards.

b) some of the shears which are vertical at depth become 'splayed-out' or fan-like when traced upwards.

c) the sense of vertical movement is also dextral in all of the shears studied in this manner. In some cases the vertical movement appears predominant over the observed horizontal movement.

The sheared rocks are highly amphibolitized and the anorthosite locally saussuritised. Anastomosing veins of pseudotachylite intrude the rocks adjacent to many of these shears.

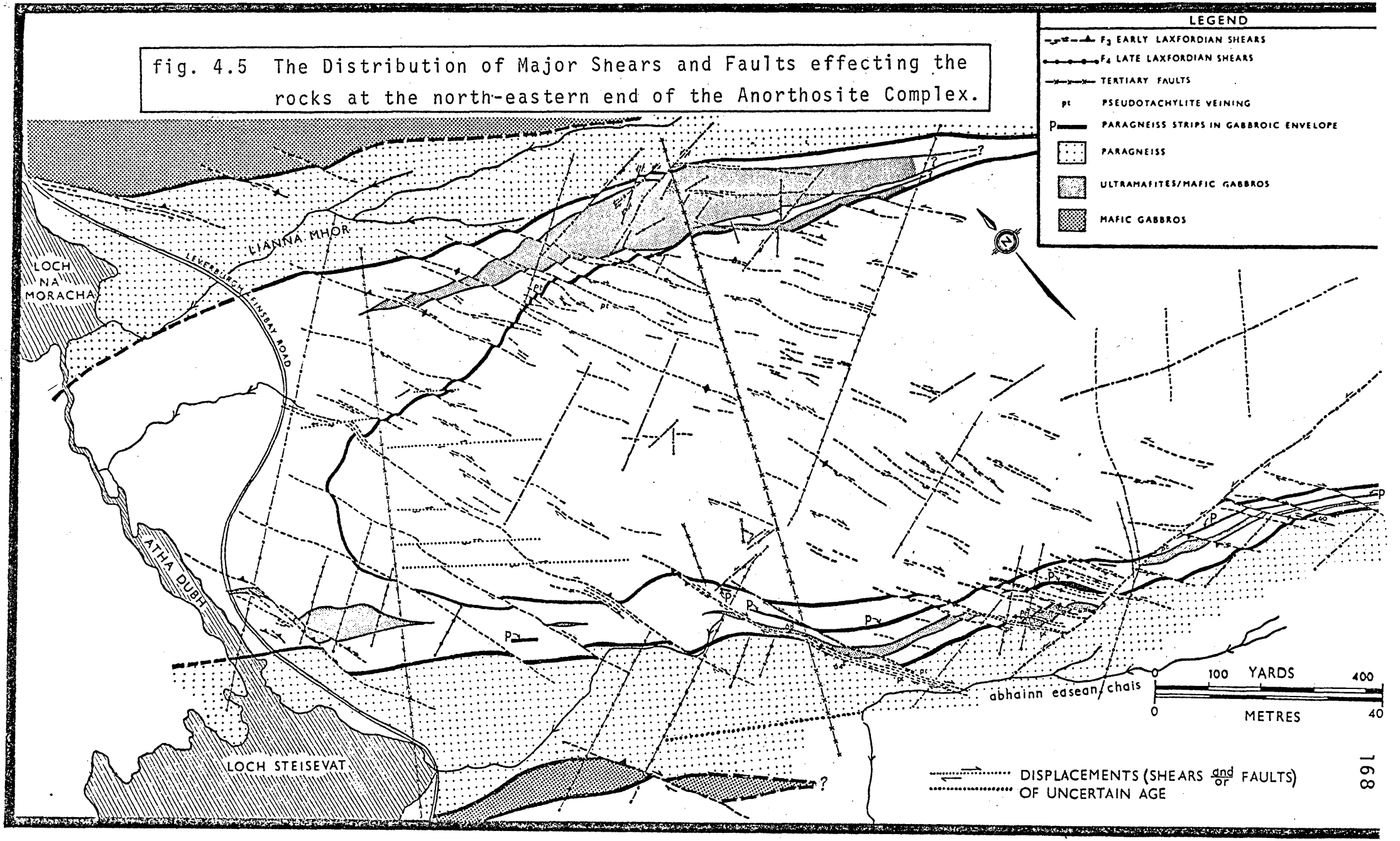
A certain degree of rotation appears to have occurred between pairs of shears of this age. Probably the best example of this can be seen on the south-western flank of the complex, north of the Abhainn Easean Chais. Here, a section of the Abhainn Easean Chais ultramafite/mafic gabbro pod and the surrounding quartz gabbros have been rotated anti-clockwise through approximately 20°, between two F_3 shears. This imparts a broad sygmoidal shape to the ultramafite/mafic gabbro pod (fig. 4.5, Map 3). This belt of rotation can be traced north-westwards through the anorthosite and in a south-easterly direction into the paragneisses.

Angular shear folds and boudins of the various differing lithologies effected, are a fairly common feature of these shears.

4.7 F_4 Deformation (late Laxfordian)

A number of shears occur closely associated with the large alkali pegmatites, which Dearnley (1959, 1963) has correlated with the northern granite-gneiss injection complex of late Laxfordian age. A rose plot of 108 recorded shears of this type is shown in fig. 4.6(b). Two distinct sets of late Laxfordian shears can be distinguished:-

fig. 4.5 The Distribution of Major Shears and Faults effecting the rocks at the north-eastern end of the Anorthosite Complex.



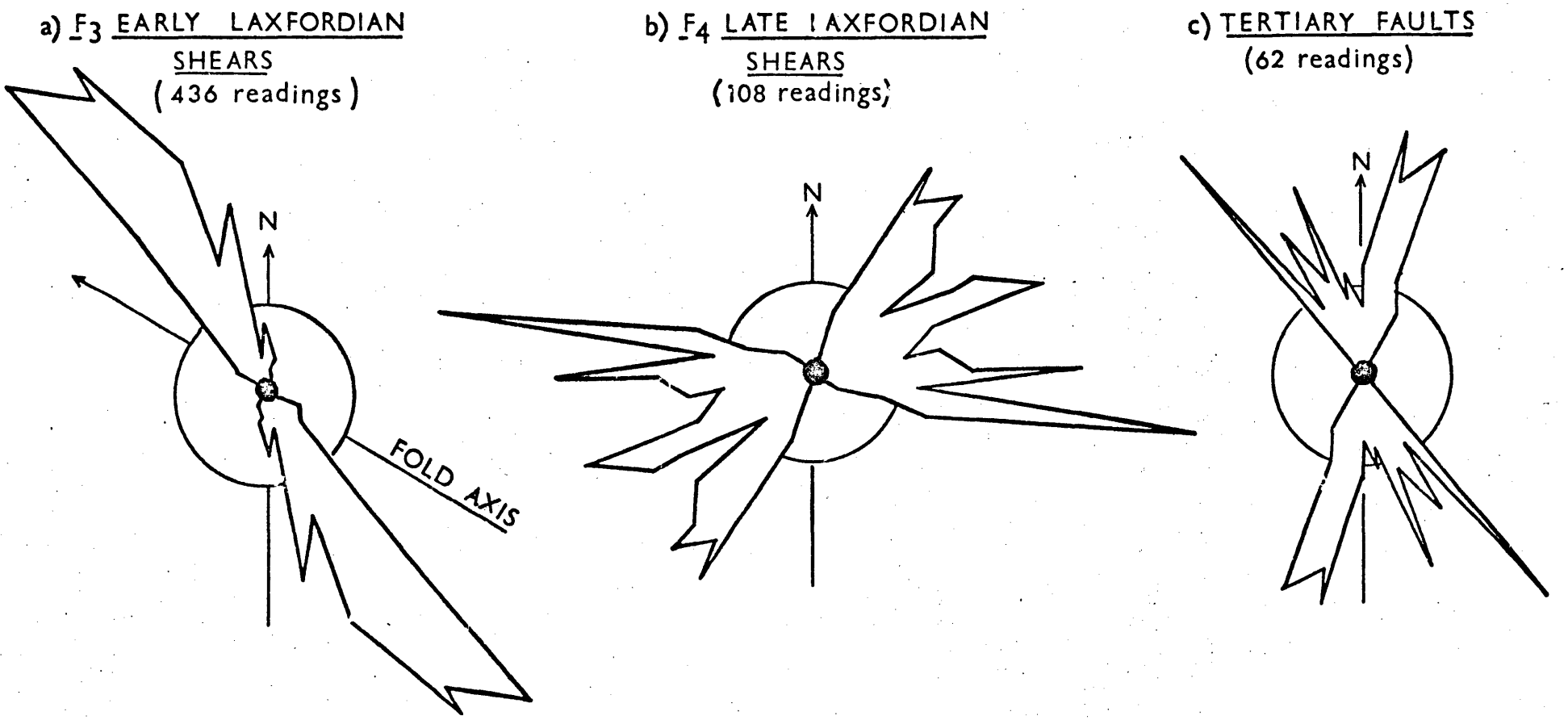


fig. 4.6 Rose diagrams illustrating the predominant trends of (a) the early Laxfordian shears; (b) the late Laxfordian shears; and (c) the Tertiary faults.

a) The most prominent set of F_4 shears trend east-west (90° - 105°). Many of these shears are of great lateral extent and can be traced over distances of up to 4½ Kms. The majority show sinistral movements, with recorded displacements of up to 140 metres.

b) Two sets of shears occur in a N.E.-S.W. direction, with maxima at 40° and 70°. These appear in some cases to be later than the first (east-west) set as they cut, without being displaced, obviously displacive east-west shears. Many form large-scale lineaments, visible on the aerial photographs of this area, but appear to have only minor sinistral or dextral displacements.

Dearnley has commented on the similarity in trend of these shears with those found at Loch Broom and Kyiesku, which are demonstrably of pre-Torridonian age.

The alkali pegmatites appear to have been, to some extent, later than the main shearing. The pegmatites appear to have been intruded along pre-existing shear-planes, along which only minor subsequent movement has taken place. Although, in many examples, there is a marked strike-swing into the margins of the pegmatites, the pegmatites themselves show only a slight peripheral granulation. The possibility of shear stresses controlling the orientation of minerals within the pegmatites has been investigated by Westoll (1967). He found that the feldspars of the pegmatites were crystographically orientated with respect to the long axis of the pegmatite body and suggested that this reflects crystal growth in a stress field (i.e. crystal growth contemporaneous with shearing).

4.8 The Coastal Thrusting

In the south-eastern part of the anorthosite complex between Rudha Vallarip and Lingarabay Island a set of small parallel thrusts, up to six in number and dipping between 30° and 60°, slice the anorthosite into overlapping 'schuppen' (fig. 4.7.). This thrust zone is best observed in exposures 360 metres south-east of Loch Na H-uamha (fig. 4.8),

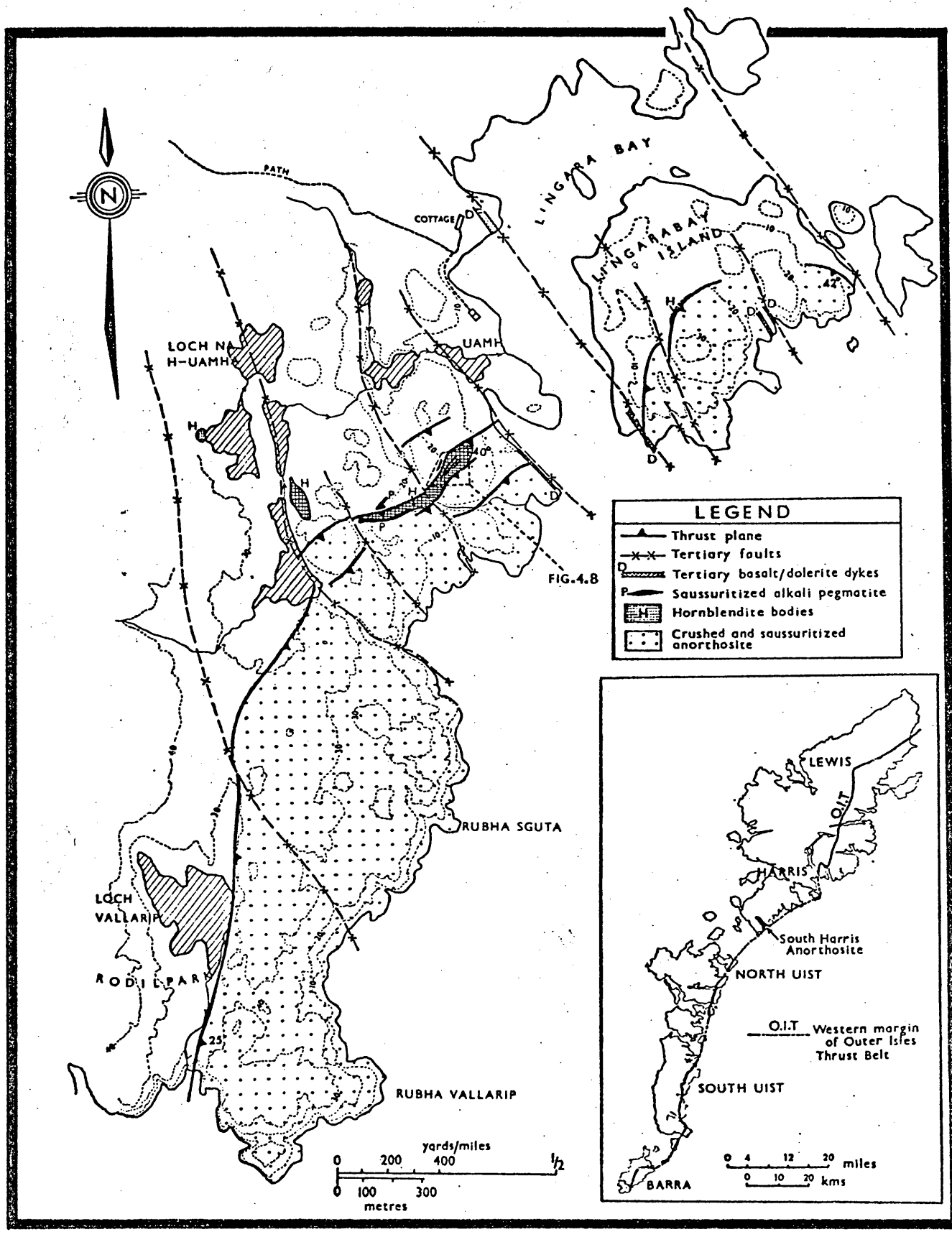


fig. 4.7 The coastal thrust zone in the anorthosite complex. The inset (bottom right) shows the western margin of the Outer Isles thrust belt.

fig. 4.8 THRUST ZONE; 360 metres south-east of Loch Na H-uamha

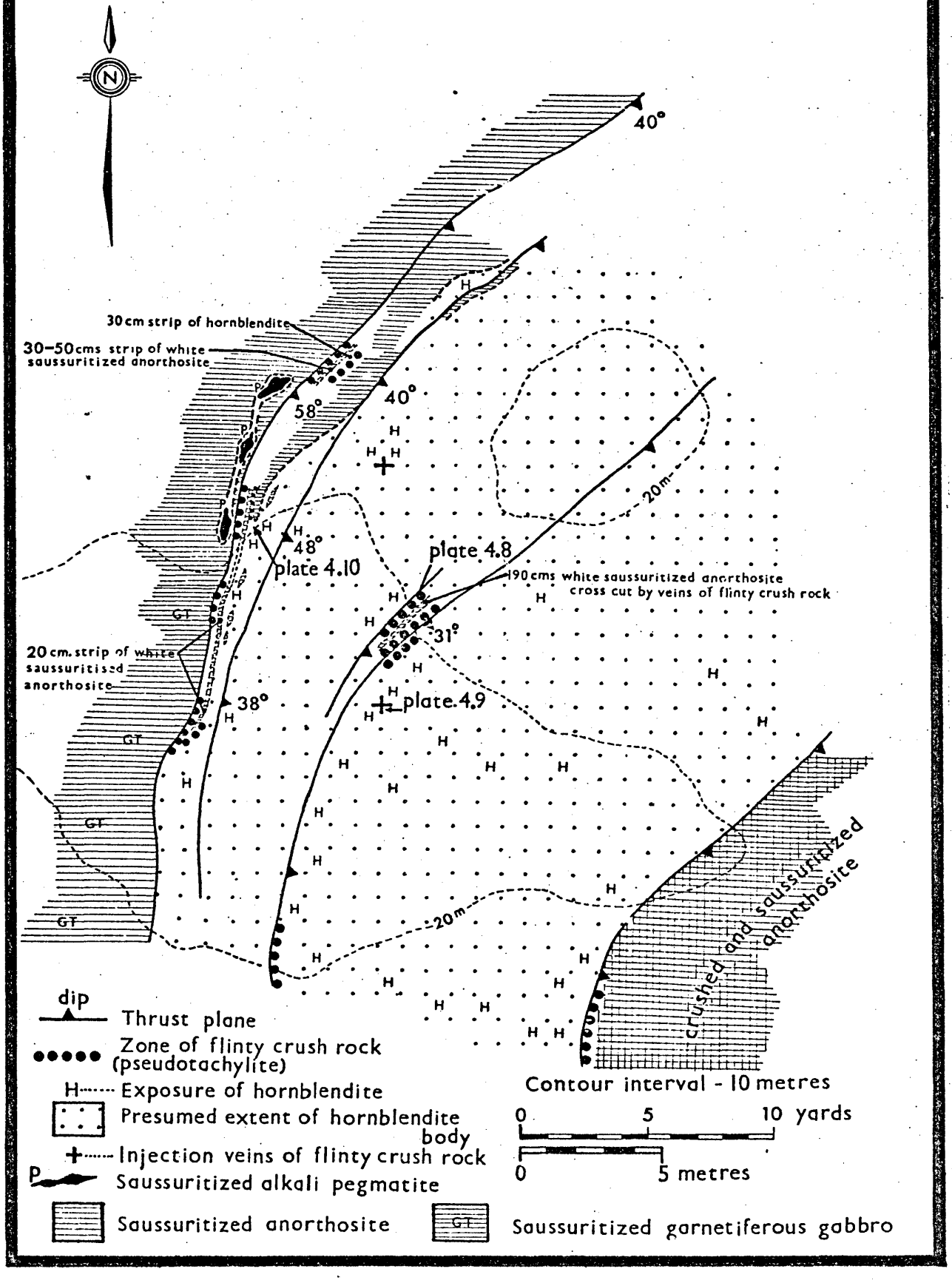




Plate 4.8 Zone of flinty crush rock (pseudotachylite) lining a subsiduary thrust plane. The fine grained pseudotachylite (brown weathering) contains rounded inclusions of hornblendite (pale-green, ovoid fragments) and saussuritised anorthosite (pale grey-white fragments).



Plate 4.9 Vein of flinty crush rock (pseudotachylite) intruding hornblendite. Note the well-rounded inclusions of hornblendite and saussuritised anorthosite within this vein.



Plate 4.10 Xenolithic strip of saussuritised anorthosite in hornblendite.



Plate 4.11 Fine anastomosing shears developed throughout the hornblendites. A biotite/epidote/sphene assemblage develops from the amphibole along the shear planes.

where six individual parallel thrusts can be mapped. The line of these thrusts is marked by zones, from 20-130 cms. in width, of pale green flinty crush rock containing sub-rounded fragments of saussuritised anorthosite, saussuritised alkali pegmatite and hornblendite (Plate 4.8). Veins of flinty crush rock are injected into the surrounding rocks, above and below the thrust in a 2 metre wide zone. The flinty crush rock or pseudotachylite is probably generated lower down the thrust planes and injected upwards into the thrust breccia. Small veins also penetrate the country rock, carrying with them fragments of the thrust breccia (Plate 4.9). A certain amount of reaction between the pseudotachylite and the smaller included rock fragments is indicated by the occurrence of narrow pale grey haloes around the latter.

Good examples of lineated thrust planes can be seen on the headland south of Loch Vallarip and on the east coast of Lingarabay Island.

The thrusting can be observed to be younger than the late Laxfordian alkali pegmatites, which are in many cases involved in the associated crushing, and the thrust planes are themselves displaced by Tertiary faults (fig. 4.7). However, other than defining these very broad limits no definate age can be given to the thrusting in this area.

Dearnley (1959, 1963) has attributed the saussuritisation of the anorthosite, south-east of the Rodil-Finsbay road, to dynamic retrograde metamorphism associated with movement along the thrust. The anorthosites which overlie the thrust zone are markedly different in character to those saussuritised types below the thrust. The degree of saussuritisation appears to be greater in these anorthosites and they take on a flinty, crushed appearance with no discernible structure or foliation.

At numerous localities along the thrust zone, the anorthosite is intruded by lenticular bodies of hornblendite. The petrology of these

	INTRUSIVE EVENTS	EFFECTS	REMARKS
Initial phase of movement along thrust		Crushing of rocks within and above thrust zone. Saussuritization of anorthosite and late Laxfordian alkali pegmatites above and below thrust.	
	Intrusion of hornblendite lenses, - the emplacement of many of these bodies is controlled by the pre-existing thrust zone. The hornblendite intrusions contain xenoliths of saussuritized anorthosite and saussuritized alkali pegmatite.		
Second phase of movement along thrust		EARLY: production of anastomosing shears in hornblendite bodies. (Plate 4.11).	These shears are thought to be produced subsequent to the intrusion of these bodies as they cut and displace the included xenolithic strips of saussuritized anorthosite. (Plate (4.10)
		LATE: production of pseudotachylite at depth - injected upwards along thrust planes and into surrounding rocks.	Veins of pseudotachylite cut obliquely across earlier shears. (plate 4.9)
Displacement of thrust zone by Tertiary faults			

Table 4.2 Proposed Sequence of Events for the Coastal Thrust Zone

hornblendites has been described in Chapter 2 (section 2.4.2). The confinement of many of these intrusions to the thrust zone implies some degree of tectonic control during their emplacement. The occurrence of rounded fragments of hornblendite within the flinty crush rock, which lines the thrust planes and also injects the hornblendite intrusions, would suggest emplacement of these bodies prior to, or contemporaneous with, movement along the thrust. However, the hornblendites are clearly uneffected by the saussuritisation process which has been attributed to movement along this thrust. To explain this apparently anomalous situation it is thought necessary to invoke two periods of movement along the thrust in this area (Table 4.2.).

4.9 F_5 Deformation (Tertiary)

The last recognizable set of faults trend a) between N-S and N.N.E.-S.S.W. and b) N.W.-S.E. A rose diagram of the recorded fault directions of this age is presented in fig. 4.6(c). These faults are responsible for the deeply eroded gullies seen in the south-eastern part of the anorthosite complex. A Tertiary age for these faults has been proposed by Dearnley (1959, 1963), who stated that these faults have a similar orientation to those which cut the Tertiary basalts of Skye. Faults of this age displace the coastal thrust and are closely associated with dykes of olivine basalt and olivine dolerite type (Table 2.3).

4.10 The Metamorphism of the Anorthosite Complex - An Introducation

The effects of two or possibly three major metamorphic events are discernible in the meta-igneous rocks of the anorthosite complex. An early Scourian (Badcallian) metamorphism, disignated M_1, was responsible for the production of medium pressure granulite facies assemblages. The earliest recognizable textures in the rocks of

the anorthosite complex are also thought to date from this event. The evidence in favour of the recognition of a late Scourian (or early Laxfordian) amphibolite or granulite facies metamorphism (M_2) will be discussed in a later section of this chapter. The final metamorphic event (M_3), to effect these rocks, occurred in late Laxfordian times and produced lower amphibolite facies assemblages.

4.11 M_1 Metamorphism

The earliest recognizable mineral assemblages in the anorthosite complex and associated meta-igneous rocks are characteristic of metamorphism at high pressures and high temperatures. These assemblages are summarized below:-

Gabbro-diorite

1) amp + opx + cpx + plag + qtz
2) gt + amp + plag + qtz
3) gt + amp + cpx + plag + qtz

Norite

4) amp + opx + cpx + plag + qtz
5) gt + amp + cpx + plag ± qtz
6) gt + amp + opx + cpx + plag

'Anorthosite'

7) gt + amp + cpx + plag ± qtz ± ilm
8) gt + amp + plag ± qtz ± ilm
9) amp + plag + qtz ± ilm
10) gt + amp + opx + cpx + plag ± qtz ± ilm
11) amp + cpx + plag + qtz
12) gt + plag + qtz

Mafic gabbros and Ultramafites

13) gt + amp + cpx + plag ± qtz
14) gt + amp + opx + plag ± qtz ± ilm
15) amp + opx + cpx + plag ± qtz
16) gt + amp + plag ± qtz ± ilm
17) amp + opx + plag ± qtz
18) gt + amp + cpx ± ilm
19) gt + amp + opx + cpx ± ilm

20) gt + cpx ± ilm
21) opx + cpx ± ilm
22) gt + opx + cpx ± ilm
23) amp ± plag
24) cpx ± ilm
25) amp + cpx ± ilm
26) gt + amp

These coarse grained assemblages develop stable granoblastic textures. In many ultramafites an inverse relationship between orthopyroxene and garnet has been observed; where orthopyroxene is abundant garnet is rare and vica versa.

In nearly all of the assemblages listed above an amphibole occurs together with the more typical granulite facies minerals. No biotite, produced during the early high-grade metamorphic event, has been observed in the meta-igneous rocks. These rocks would fall within the hornblende granulite sub-facies as defined by Fyfe et al. (1958).

A detailed subdivision of the granulite facies has been made by Waard (1965), who recognized two facies each comprising of three sub-facies;-

	PYROXENE GRANULITE FACIES		HORNBLENDE GRANULITE FACIES
	(SiO_2 excess system)		
High Load Pressure	Clinopyroxene-almandine subfacies	Isograd	Hornblende-clinopyroxene-almandine subfacies
	garnet isograd opx + anorthite ⟶ cpx + alm + qtz		
Medium Load Pressure	Orthopyroxene-plagioclase subfacies	Hornblende-Biotite	Hornblende-orthopyroxene-plagioclase subfacies
	cordierite isograd		cordierite isograd
Low Load Pressure	Cordierite-almandine subfacies		Biotite-cordierite-almandine subfacies

In the medium pressure portion of the granulite facies the assemblage orthopyroxene/plagioclase is stable in silica excess compositions and the assemblage orthopyroxene/clinopyroxene/garnet/plagioclase is stable in silica deficient compositions. At higher pressures the assemblage orthopyroxene/plagioclase becomes unstable, in silica excess compositions, and is replaced by garnet/clinopyroxene. Green et al. (1966) have demonstrated that the pressure/temperature conditions at which this reaction will take place, in basaltic rock types, is sensitive to the Mg/Fe and the Ca/Na ratio of the rock. At a given temperature an increase in the ratio 100 Mg/Mg + Fe will raise the pressure necessary for the forward reaction. Thus the assemblage orthopyroxene/ plagioclase rather than clinopyroxene/garnet will be stable at higher pressures in rocks of a more magnesian composition.

It should be noted, from the list above, that within the quartz-bearing meta-igneous rocks of this area, assemblages characteristic of both high pressure hornblende granulites (gt-cpx-qtz) and medium pressure hornblende granulites (opx-plag-qtz) can be found. This can be interpretted in two ways:-

a) either different parts of the meta-igneous complex recrystallized under differing P,T conditions.

or b) that the composition of the rocks in question also influenced the resulting assemblages.

The latter explanation is favoured. It seems likely that the early high-grade metamorphism took place at pressures intermediate between those for the medium and high pressure granulite fields, and that the mineral assemblage in a particular rock is a function of the prevailing P,T conditions and the composition (in particular the Mg/Fe ratio) of the rock type. The comparative lack of magnesian-rich rock types in the anorthosite complex would thus account for the relative rarity of orthopyroxene in the assemblages of these rocks.

4.12 M_2 Metamorphism

Within the anorthosite complex and the surrounding paragneisses large euhedral garnets occur overgrowing the F_1 foliation (defined by the M_1 amphibole and clinopyroxene). Garnet produced during the M_1 hornblende granulite facies metamorphism occurs within this foliation. The second generation of garnet often shows a nebulous alignment into parallel discontinuous trains which are oblique to the F_1 foliation. These garnets are only patchily developed and are characterized by a depletion rim composed solely of plagioclase feldspar. Garnets of this type are thought to be the product of a second high grade metamorphism designated M_2. In those rocks where M_2 garnets are developed there is possibly also a second generation of pargasitic amphibole which shows an alignment oblique to the M_1 amphibole and parallel to the trains of M_2 garnet. Further evidence for this metamorphic episode is lacking in the rocks of the anorthosite complex and it is not possible to decide whether the metamorphism was of garnet-amphibolite or hornblende-granulite facies.

Dickinson(1974) has described quartz bearing assemblages,from this area, which contain two generations of hypersthene. The first generation she ascribed to the early M_1 granulite facies event and the second to the breakdown of the M_1 garnet during a second high grade event. Dickinson noted that the second generation hyperstene was markedly less pleochroic than that produced during the M_1 event and concluded that this was a result of the lower alumina content of the second generation hypersthene - a consequence of its formation at the lower pressures which prevailed during the M_2 event.

The timing of the M_2 metamorphic episode is also in doubt. It definatly occurred after the formation of the F_1 foliation and prior to the M_3 amphibolite facies event. The ultramafite intrusions which are associated with the brecciated areas along and adjacent to the margins of the anorthosite also post-date the formation of the F_1 foliation and it is

possible that the assemblages of these ultramafites date from the M_2 metamorphic episode.

4.13 M_3 Metamorphism

The rocks of the anorthosite complex have been downgraded by a late Laxfordian amphibolite facies metamorphism. The effects of this metamorphic episode are seen throughout the complex but are locally more conspicuous adjacent to the large late Laxfordian shear zones. The effects of this regional downgrading have already been described at the beginning of Chapter 2. During this episode widespread potash metasomatism is also thought to have occurred throughout southern South Harris. In the anorthosite complex the introduction of potash is mainly confined to marginal areas and here is only of minor importance.

Dearnley (1959, 1963) correlated this period of regional retrogression with the formation of the granite-gneiss injection complex in northern South Harris and noted that the degree of retrogression increases when this injection complex is approached.

4.14 Summary

A proposed sequence of intrusive, metamorphic and deformational events for southern South Harris is shown in Table 4.3. The suggested correlation of the events in southern South Harris with the Scourian and Laxfordian time periods should be regarded as speculative. The Scourie dykes, in most Lewisian areas provide a marker by means of which the deformational and metamorphic events observed in any area can be related to the overall Lewisian chronology. The period of intrusion of such dykes is thought to represent a period of quiescence (both tectonic and metamorphic) from approximately 2200-1900 million years (Evans and Tarney, 1964). Within the anorthosite complex and its environs there are no intrusive bodies that can, with certainty, be recognized as Scourie dykes. The two mafic gabbro dyke suites, D_1 and D_2, are thought to be of early Scourian age, both types patchily retaining an early Scourian granulite facies mineralogy. The D_3 hornblendite dykes (and the 'Late dykes' intrusive into the gabbro-diorite; Palmer, 1971) are thought to be the only intrusive bodies recognized, that could be of Scourie dyke age.

An interpretation of the overall structure of southern South Harris is shown in fig. 4.9. Two factors have been considered in making this interpretation:-

a) A feature of the three major plutons in southern South Harris is that they all show very similar marginal relationships. Both flanks of the anorthosite are rimmed by mafic gabbros and ultramafites and a similar layered mafic gabbro rim is found along the southern contact of the gabbro-diorite and the northern contact of the norite. The northern contact of the gabbro-diorite is directly with meta-sediments of the Langavat belt. This is mirrored by the norite, the southern contact of which is directly with meta-sediments of the Ensay belt. Between these mafic gabbro sheets and the

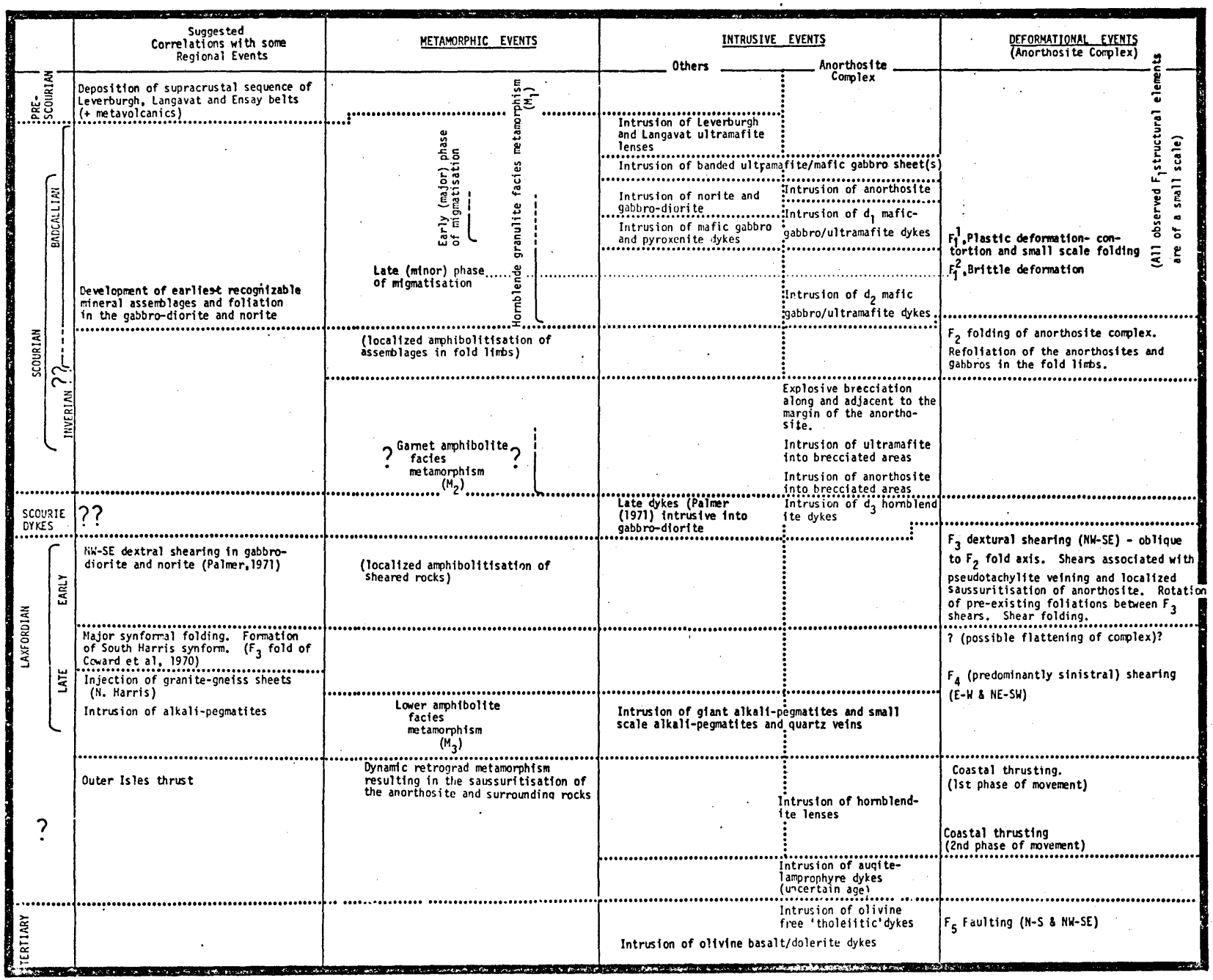


Table 4.3 A geological history for southern South Harris

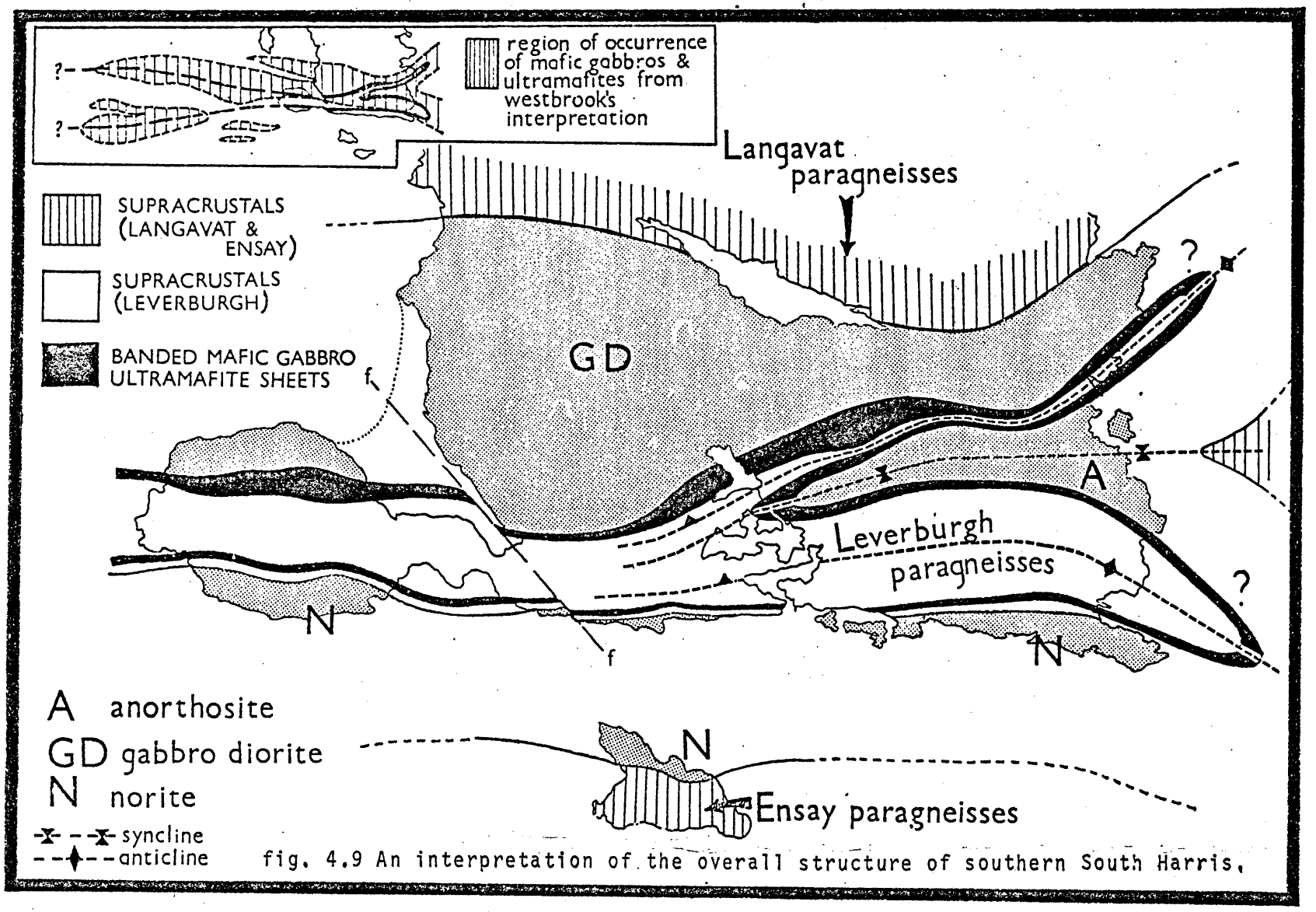


fig. 4.9 An interpretation of the overall structure of southern South Harris.

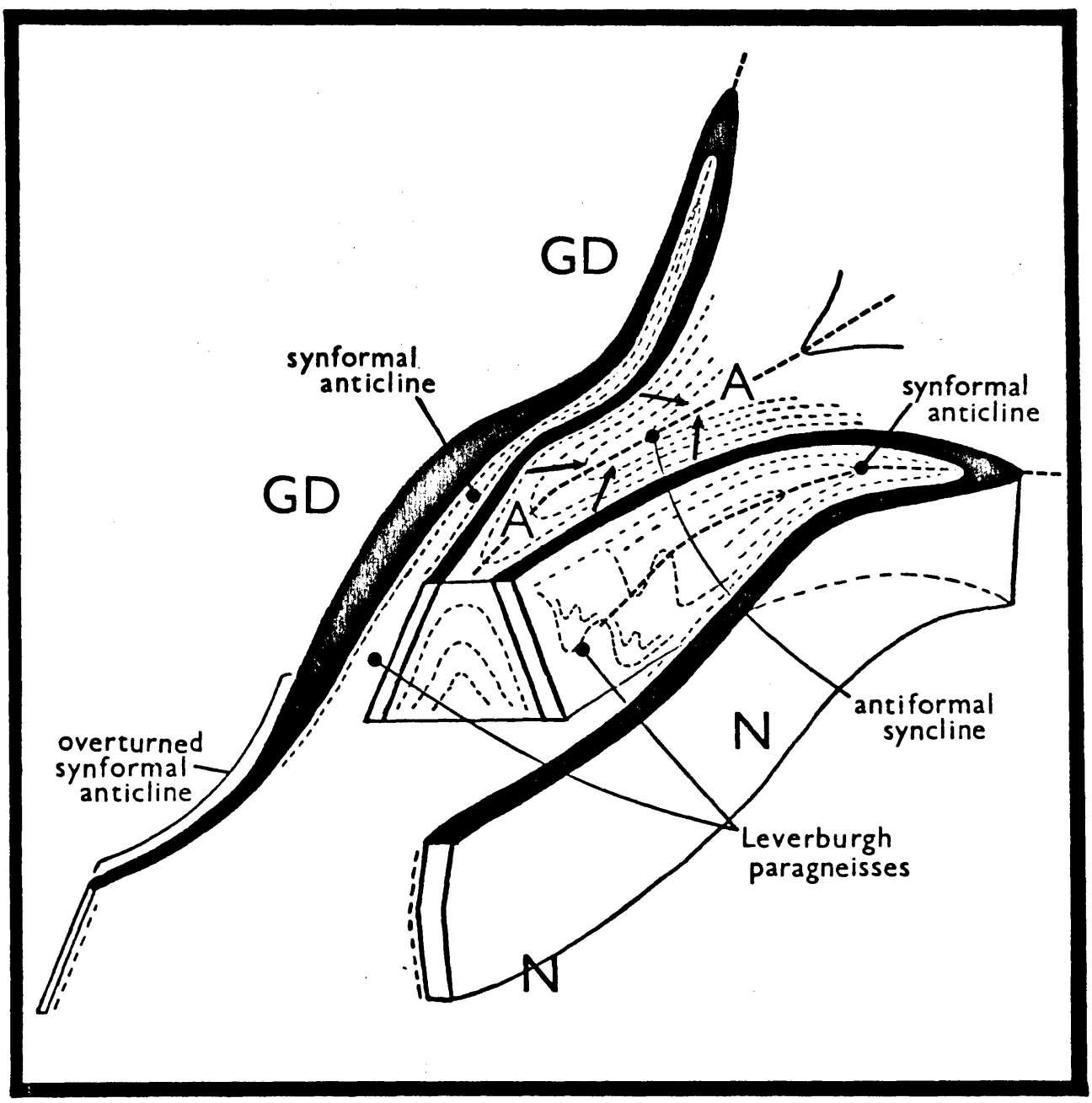


fig. 4.10 Block diagram to illustrate the style of folding within and adjacent to the anorthosite complex.
A - anorthosite
GD- gabbro-diorite
N - norite
Arrows indicate the facing direction of the anorthosite.

plutons discontinuous strips of quartzose paragneiss occur. From the previously discussed intrusive relationships it appears that the mafic gabbro sheets pre-date the intrusion of the gabbro-diorite, norite and anorthosite. It is tentatively suggested that the mafic gabbro sheets rimming the gabbro-diorite, norite and anorthosite are the exposed portions of one continuous sheet which is isoclinally folded. This layered mafic gabbro/ultramafite sheet is petrologically very similar to the layered basic gneiss sheets described by Davies (1974) from south of Loch Laxford, Sutherland.

b) A prominent feature of the aeromagnetic map of Great Britain is a north-westerly trending positive magnetic anomaly situated over South Harris. Westbrook (1974) has demonstrated the close relationship of this anomaly with the outcrop of the mafic gabbro sheets and this relationship has been borne in mind when making the present structural interpretation. He also noted that the magnetic anomaly, when traced in a north-westerly direction, becomes doubled and suggested that this may possibly be due to the mafic gabbros being situated on the limbs of a fold.

If the layered mafic gabbro sheet can be used as a marker horizon within the Lewisian basement it becomes possible to recognize three 'layers' within the basement in this area:-

③	Langavat and Ensay meta-sediments	↑ decreasing structural height
②	Gabbro-diorite Anorthosite Norite Layered Mafic gabbro (/ultramafite) sheets	
①	Leverburgh meta-sediments (and meta-volcanics)	

The folding responsible for the present disposition of the mafic gabbro sheets is thought to be a product of an earlier folding phase than that responsible for the large scale Laxfordian folds (the F_3 folds of Coward et al., 1970 - shown in fig. 4.1). The large Laxfordian folds show a similar trend to these early folds, but are of a differing style - they are upright cuspate folds with synformal structures closing towards the south-east and antiformal structures plunging gently north-west (i.e. in an opposite sense to the Roneval antiform). The overall disposition of the foliations in southern South Harris is synformal, with moderate (45^{o}) northerly dips in Ensay, vertical dips in the Leverburgh belt and moderate (50^{o} - 60^{o}) southerly dips in the Langavat belt. This dip evidence is cited by Palmer (1971) to support the recognition of a major Laxfordian synform which include the whole of southern South Harris. During this Laxfordian folding phase flattening and boudinage, of the previously folded igneous bodies, must have occurred.

Finally it should be noted that there are many similarities between the South Harris (Roneval) anorthosite and the anorthosite body which occurs at Ness, North Lewis (Watson, 1969). The Ness anorthosite is associated with a meta-sedimentary sequence of pelites, quartzites and calc-silicate rocks, very similar to the Leverburgh meta-sediments. Watson (1969) has demonstrated that this anorthosite has also been recrystallized by an early Scourian granulite facies metamorphism, a fact, which suggests to the present author, a similar age for the two anorthosite bodies.

CHAPTER 5

THE GEOCHEMISTRY OF THE ANORTHOSITE COMPLEX AND OF THE ASSOCIATED META-IGNEOUS ROCKS

5.1 General Introduction

Rock analyses were made by X-ray fluorescence spectrometry using a Phillips 1212 automatic spectrometer and using international standards for comparison. The major elements and selected trace elements were determined for a total of 155 samples. A detailed study of the trace elements and rare earths of these rocks is being undertaken by A. Heyes (Chelsea College, Univ. of London).

Bulk-rock analyses were made of samples taken from the following sources:-

	Rock Type	Number of Analyses
Meta-igneous rocks		
The Anorthosite Complex	The 'Anorthosite'	50 (14)*
	The gabbroic rim of the anorthosite complex	54 (21)
	Minor intrusives	29 (6)
	Gabbro-diorites	4
	Mafic gabbros from the Beinn Tharsuinn sheet	9 (1)
Meta-sedimentary rocks		
	Paragneisses from within and adjacent to the anorthosite complex	9 (1)
	total	155 (43)

* Bracketed figures refer to the number of analyses where Fe^{2+} determinations have been made.

Rock analyses performed by X-ray flourescence, yield a total iron value calculated as Fe^{3+}. Wet chemcial methods were used to determine the Fe^{2+} value for forty-three of the above analyses. A knowledge of the oxidation state of the iron has allowed the calculation of C.I.P.W. norms for these forty-three analyses. The calculation of the norm for analyses where the iron value is expressed as either total iron as Fe^{2+} or total iron as Fe^{3+}, leads to gross inaccuarcies. Only those normative ratios which are unaffected by the oxidation state of the iron, have been calculated for all the whole-rock analyses performed.

Where the oxidation state of the iron is known Fe^{2+} always exceeds Fe^{3+}. For this reason the iron values have been recalculated to total iron as FeO for the diagrams which follow in this chapter.

The rock analyses, together with C.I.P.W. norms (where applicable) and certain normative ratios are tabulated in Appendix 1. Rock analyses from previous geochemical studies of the meta-igneous rocks of South Harris are also quoted in Appendix 1 and are used for comparison in many diagrams which follow in this chapter. Included within these are twenty-five previously unpublished analyses of the anorthosite. The permission given by Robertson's Research, to quote this unpublished data is gratefully acknowledged.

5.2 Aims of the Geochemical Study

The rock analyses (and mineral analyses discussed in Chapter 6) were performed with the following aims in mind:-

a) To give a general picture of the bulk-rock and mineral chemistry of the rocks of the

anorthosite complex.

b) To determine whether igneous fractionation trends are preserved in these rocks.

c) If such igneous trends are preserved, to determine as much as possible about the igneous differentiation sequence.

d) To determine the geochemical relationships between the main rock types of the anorthosite complex and to compare the geochemistry of these rocks with the associated meta-igneous rocks, especially the gabbro-diorite and norite.

The compositions of metamorphic rocks should reflect fairly accurately their pre-metamorphic ones unless extensive metasomatism has taken place. Metamorphism will normally only result in the development of new minerals from the pre-existing assemblage and it may, in the case of some igneous rocks, cause rather more subtle changes in the chemistry of co-existing minerals (e.g. Fe : Mg ratios). The meta-igneous rock types of southern South Harris correspond closely in both major and trace element constituents with normal unmetamorphosed igneous rocks, a fact which strongly suggests the essentially isochemical nature of the Scourian high grade granulite facies metamorphism.

In a few instances the original pre-metamorphic chemical composition of the igneous rocks has been slightly modified by metasomatism associated with the late Laxfordian migmatization and the intrusion of granites in northern South Harris. This has resulted in the addition of limited amounts of alkalis (mainly K_2O) and water.

●	'ANORTHOSITES' (undifferentiated - includes rock types ranging from mafic gabbro → anorthosite)
	'ANORTHOSITES' (differentiated):-
▲	MAFIC GABBRO
●	GABBRO
◑	ANORTHOSITIC GABBRO
■	GABBROIC ANORTHOSITE
⊞	ANORTHOSITE
○	BANDED ULTRAMAFITES AND MAFIC GABBROS
◉	QUARTZ GABBROS
◆	ULTRAMAFITE AND MAFIC GABBRO DYKES, from the anorthosite complex.
△	ULTRAMAFITES associated with brecciated areas (Type 'A' and 'B' breccias), along and adjacent to the margin of the anorthosite body.
▽	GARNETITE NODULES from the above ultramafites
⊡	ANORTHOSITES associated with brecciated areas (Type 'B' breccia), along and adjacent to the margin of the anorthosite body.
◈	HORNBLENDITE intrusions, from the anorthosite complex.
X	ANORTHOSITIC GABBRO DYKES, from the anorthosite
♦	EPIDOTIC VEIN material, from the banded ultramafites and mafic gabbros
▼	GABBRO-DIORITES
✸	NORITES
✡	MAFIC GABBROS, Bayhead-Sletteval, Strondeval and Beinn Tharsuinn sheets.
⊖	ULTRAMAFITES, from the Langavat metasedimentary belt
⊕	ULTRAMAFITES, from the Leverburgh metasedimentary belt
□	PYROXENITE DYKES, intrusive into the norite.
✹	ULTRAMAFITE LENS, from the gabbro-diorite

Table 5.1 Key to Symbols used in plots of whole rock data. Unless otherwise stated, minerals are plotted with a symbol for their host rock (Chapter 6).

5.3 General Chemistry of the Anorthosite Complex

The compositional data for the anorthosite complex have been plotted on weight percent AFM projections (fig. 5.1). The three major components of the complex - the anorthosites, the banded ultramafites and mafic gabbros, and the quartz gabbros - are plotted on the left hand projection and the minor intrusives on the right-hand projection.

Both the ultramafites and mafic gabbros, and quartz gabbros form the gabbroic rim of the complex plot in elongate fields, parallel to the F-M join of the projection. A strong iron enrichment relative to MgO and alkalis is characteristic of both rock types. The anorthosites occupy a narrow field perpendicular to the F-M line, indicative of strong alkali enrichment and a slight overall increase in FeO relative to MgO. It is interesting to note that the rocks from the gabbroic rim of the complex show a degree of iron enrichment unmatched by any rocks from the anorthosite. An interpretation of this diagram will not be attempted until the detailed chemistry of these rocks has been discussed.

Average analyses of the three major rock types which comprise the anorthosite complex are shown in Table 5.2.

5.3.1 The "Anorthosites"

The chemistry of the anorthosites largely reflects their dominantly feldspathic nature. As would be expected Al_2O_3 values are high (24%-34%) and, in some cases, small amounts of corundum are present in the norm of the anorthosites. This implies an excess of alumina in the rock analyses over that required to combine with alkalis to form feldspars. Although corundum bearing anorthosites

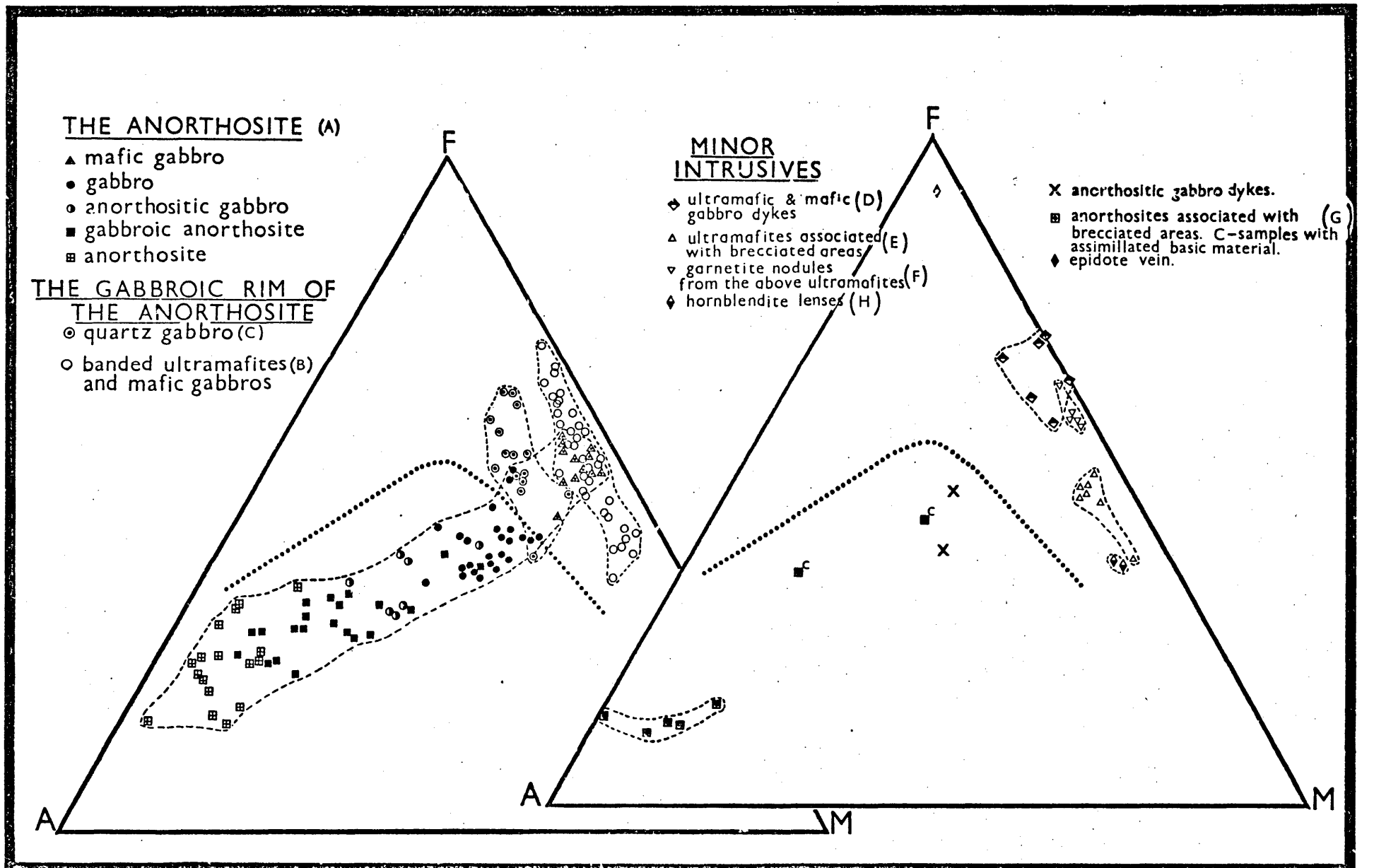


fig. 5.1 AFM projections for the rocks of the anorthosite complex. In weight percent, A = $Na_2O + K_2O$, F = total iron as FeO, M= MgO. The dotted line is that suggested by Irvine and Barager (1971) to separate tholeiitic (above) from calc-alkalic (below) rock suites.

	A		B		C	
OXIDES (wt.%)						
SiO_2	50.00		43.08		50.46	
TiO_2	0.23		0.86		1.07	
Al_2O_3	25.33		16.69		13.71	
Fe_2O_3	1.98		4.47		4.41	
FeO	2.92		9.32		8.31	
MnO	0.07		0.21		0.21	
MgO	3.71		9.36		7.00	
CaO	12.67		14.67		10.87	
Na_2O	2.74		1.00		2.82	
K_2O	0.39		0.15		0.47	
TOTAL	100.04		99.81		99.33	
Cr(p.p.m.)	110(18)		354(22)			
Sr(p.p.m.)	266(25)		88(5)			
Ni(p.p.m.)	-		40(1)			
Rb(p.p.m.)	18(8)		-			
C.I.P.W. Norm						
qtz	-		-		0.47	
or	2.30		0.88		2.78	
ab	22.08		6.13		23.86	
an	56.76		40.61		23.36	
ne	-		1.26		-	
di	5.78		26.09		24.86	
hyp(En)	9.45	(72.66)	-		15.57	(63.00)
ol (Fo)	0.35	(70.70)	16.72	(63.06)	-	
mt	2.87		6.48		6.39	
il	0.44		1.63		2.03	
Si unsat.	0.14		7.39		-	
Total Norm Feldspar	81.14		47.62		50.00	
Normative anorthite content of feldspar	69.95		85.27		46.72	

Table 5.2. Averaged analyses of the main rock types of the anorthosite complex

A	- average of 68 "anorthosite" analyses - the average Fe_2/ $Fe_2 + Fe_3$ ratio for fourteen analyses is used to calculate the FeO value for this average analysis. Saussuritised and highly retrogressed anorthosites were not included in the calculation of this average analysis.
B	- average of 37 analyses of the ultramafites and mafic gabbros from the gabbroic rim of the anorthosite complex - the average $Fe_2/Fe_2 + Fe_3$ ratio for twenty analyses is used to calculate the FeO value for this average analysis.
C	- average of 17 analyses of the quartz gabbros from the gabbroic rim of the complex - the average $Fe_2/Fe_2 + Fe_3$ ratio for three analyses is used to calculate the FeO value for this average analysis. Bracketed figures after trace element concentrations indicate the number of determinations used to provide the "average" figure.

have been reported from the Sittampundi complex, Madras (D. K. Hutt, pers. comm.), modal corundum has not been found in the South Harris anorthosites. This excess of Al_2O_3 may be due to either analytical error or non-stoichiometric excess of Al_2O_3 in the plagioclase feldspars. A non-stoichiometric excess of both SiO_2 and Al_2O_3 in natural feldspars has been demonstrated by Kracek and Neuvonen (1952) and Emmons (1953, 1955). It can be seen from Table 6.2 that many of the feldspars of the anorthosite exhibit a significant degree of departure from their stoichiometric formulae. This has been expressed by calculating the excess or deficiency of SiO_2 and Al_2O_3, relative to CaO, Na_2O, and K_2O. However, where a significant non-stoichiometric excess of Al_2O_3 is found (e.g. samples A15 and A45) in the analysed feldspar, this is not reflected by the appearance of corundum in the norms of the host rocks in question. It is possible that the small amounts of corundum, generated in the norms of some of these rocks, may represent a positive analytical error in Al_2O_3 determinations and/or a negative error in alkali or CaO determinations. However, the maximum analytical error involved in the measurement of Al_2O_3 is $\pm$ 0.1% - a similar figure can also be quoted for the precision of the Al_2O_3 determinations.

The occurrence of corundum (0.55 - 7.07%) in the norms of the saussuritised anorthosites may, to some extent, be explained by the breakdown of plagioclase feldspar to sericite or zoisite, accompanied by leaching of alkalis by intergranular fluids during saussuritisation.

Saussuritisation of the feldspar may be attributed to the reaction:-

$$\underbrace{4CaAl_2Si_2O_8}_{\text{labradorite}} + 3NaAlSi_3O_8 + 2H_2O \longrightarrow \underbrace{2Ca_2Al_3(SiO_4)_3(OH)}_{\text{zoisite}}$$

$$+ \underbrace{NaAl_2(AlSi_3)O_{10}(OH)_2}_{\text{paragonite}} + 2NaAlSi_3O_8 + 2SiO_2$$

excess albite quartz

If any leaching of the soda were to occur during the saussuritisation process it would lead to an excess of Al_2O_3 and SiO_2. Corundum and quartz would then be released and might appear in the norms of these rocks.

Mafic gabbros, gabbros and anorthositic gabbros from the anorthosite sequence, are in general olivine normative whilst the gabbroic anorthosites and anorthosites are quartz normative (see Fig. 5.3 and Appendix 1, Tables 15, 16, 17 and 18). Those samples which are quartz normative usually show small amounts of free quartz in thin section. Although olivine occurs in the norms of most of the gabbroic rock types it has never been observed in thin sections of the anorthosites. Similarly hypersthene is a common normative mineral, but only one 'anorthosite' with an undoubted occurrence of this mineral is recorded from the thin section studies made during the present work. The high oxidation ratio in these rocks (and in fact all the rocks of the complex) results in the appearance of appreciable amounts of magnetite in their C.I.P.W. norms.

The chemistry of two gravity stratified units from the base of the lower zone of the anorthosite sequence has been studied in detail (units 2 and 3, fig. 2.2). Fig. 5.2 shows diagramatically the changes in lithology within these two

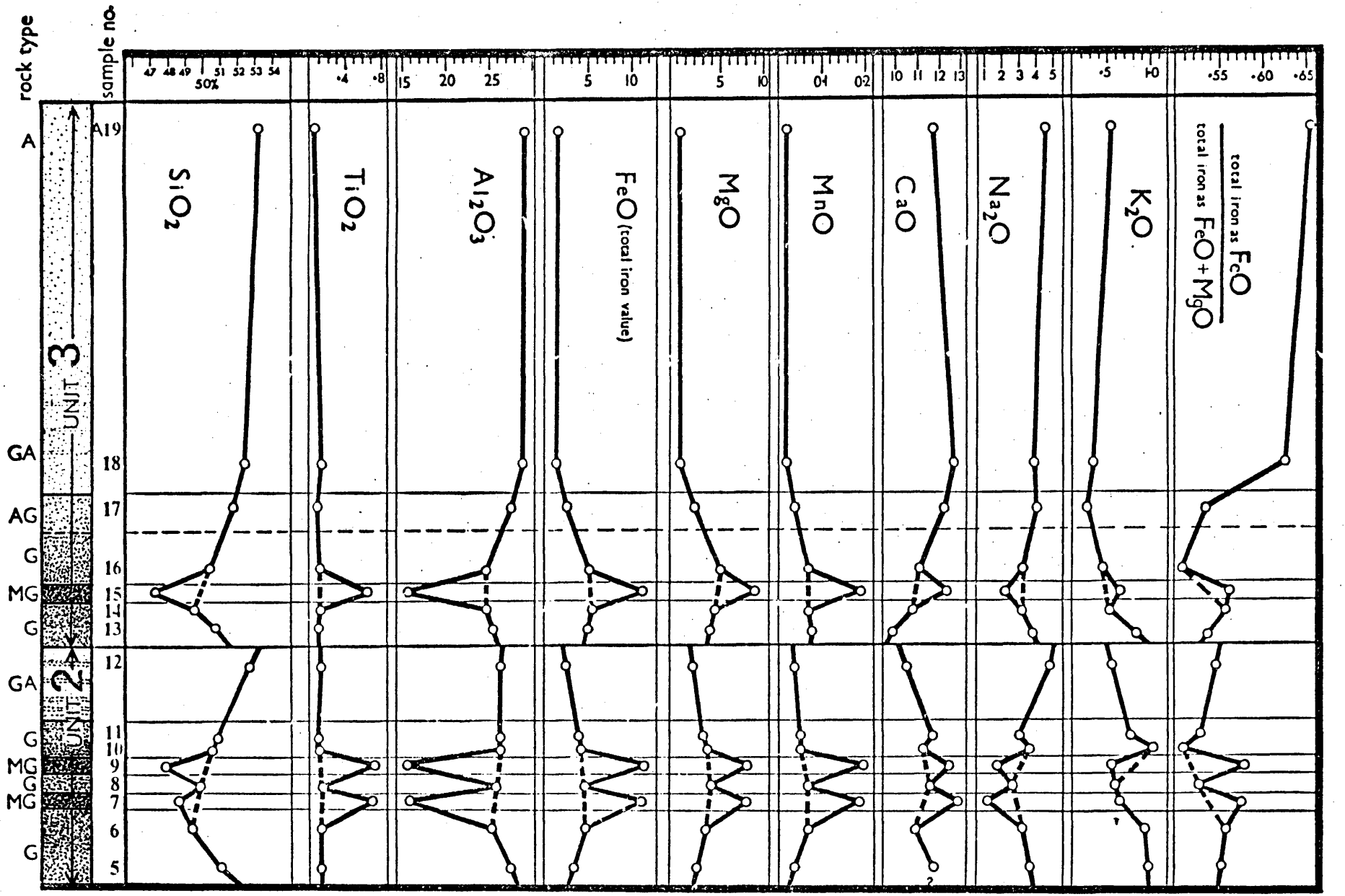


fig. 5.2 Oxide variation diagram for two gravity stratified units from the lower zone banded 'anorthosites' (measured section Y-Z)
A - anorthosite; AG - anorthositic gabbro; GA - gabbroic anorthosite; G - gabbro; MG - mafic gabbro.

units and the positions of the fifteen analysed samples. It is assumed that the leucocratic portions represent the top of each unit. The present mineralogy of the rocks of these two gravity stratified units has already been discussed in some detail and it would be advantageous, at this stage, to refer back to fig. 2.3 in Chapter 2. The variations in the normative mineral molecules for Unit 3 is shown in Figs. 5.3 and 5.4.

The variations in major element (oxide weight percent) concentrations are now considered and these are portrayed diagramatically on the right hand side of fig. 5.2. The variations in oxide concentrations correlate closely with changes in rock type. The outstanding feature of this diagram is the reversal of trend which takes place in almost all of the oxides either side of the mafic gabbro horizon(s) in each unit. With regard to the upper of the two figured units (unit 3), it can be seen that the gabbro at the base of this unit shows a decrease in SiO_2, Al_2O_3 and Na_2O. The decrease in these oxides culminates within the mafic gabbro horizon. Above the mafic gabbro horizon, SiO_2, Al_2O_3 and Na_2O show a consistant increase in amount upwards. This variation pattern is mirrored by the oxides of iron (total iron as FeO), magnesium and manganese.

The variation in the FeO/FeO + MgO ratio is generally considered to be a reliable guide to igneous differentiation processes. The variation in this ratio is shown on the far right hand side of fig. 5.2. Again considering the variation pattern in unit 3, the FeO/FeO + MgO ratio shows an increase (0.538 - 0.558) from the base of the unit upwards and into the mafic gabbro horizon. After an initial decrease immediately above the mafic gabbro it again shows an overall

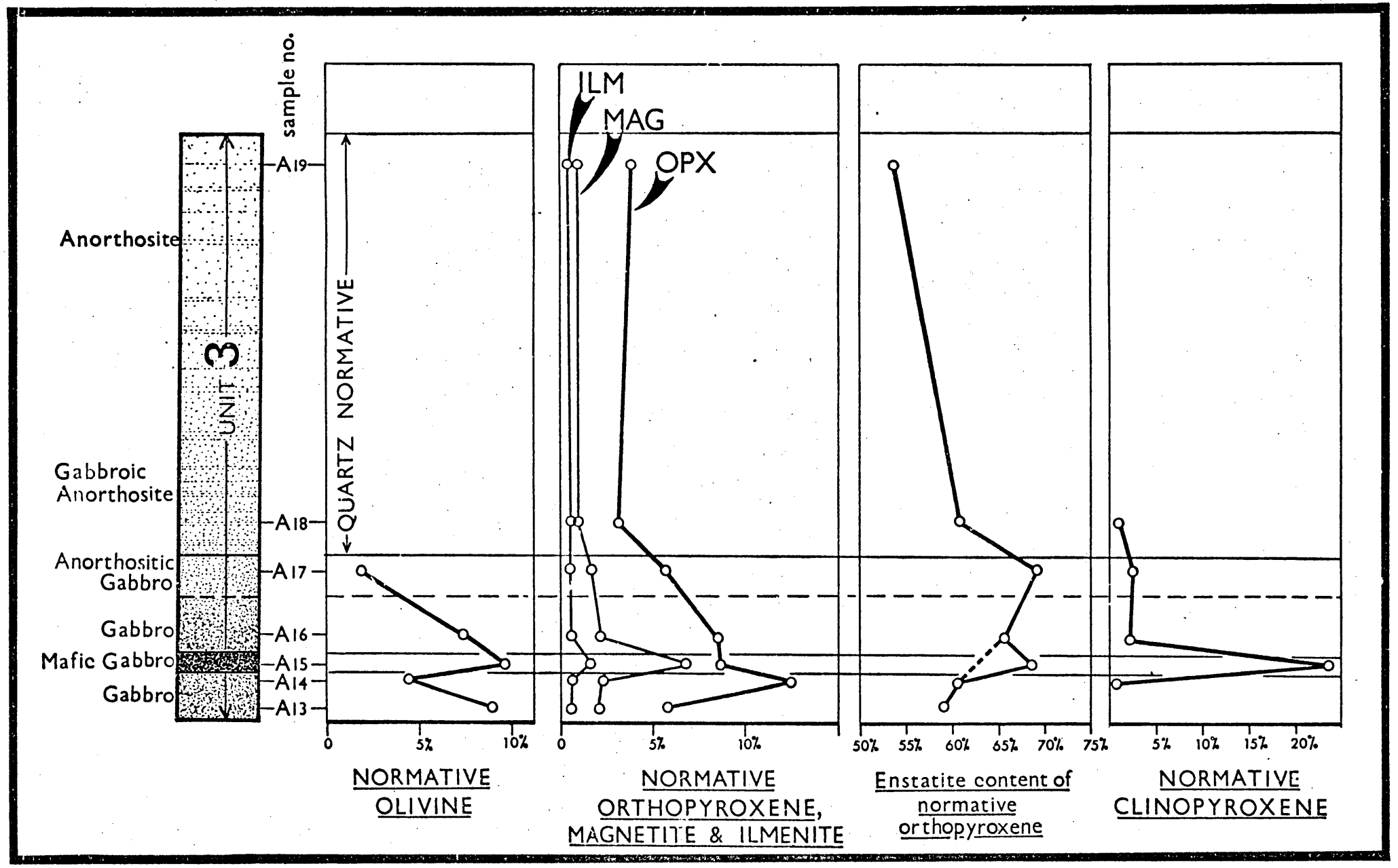


fig. 5.3 Variation of normative mineral molecules, within a single gravity stratified unit from the lower zone of banded 'anorthosites'.

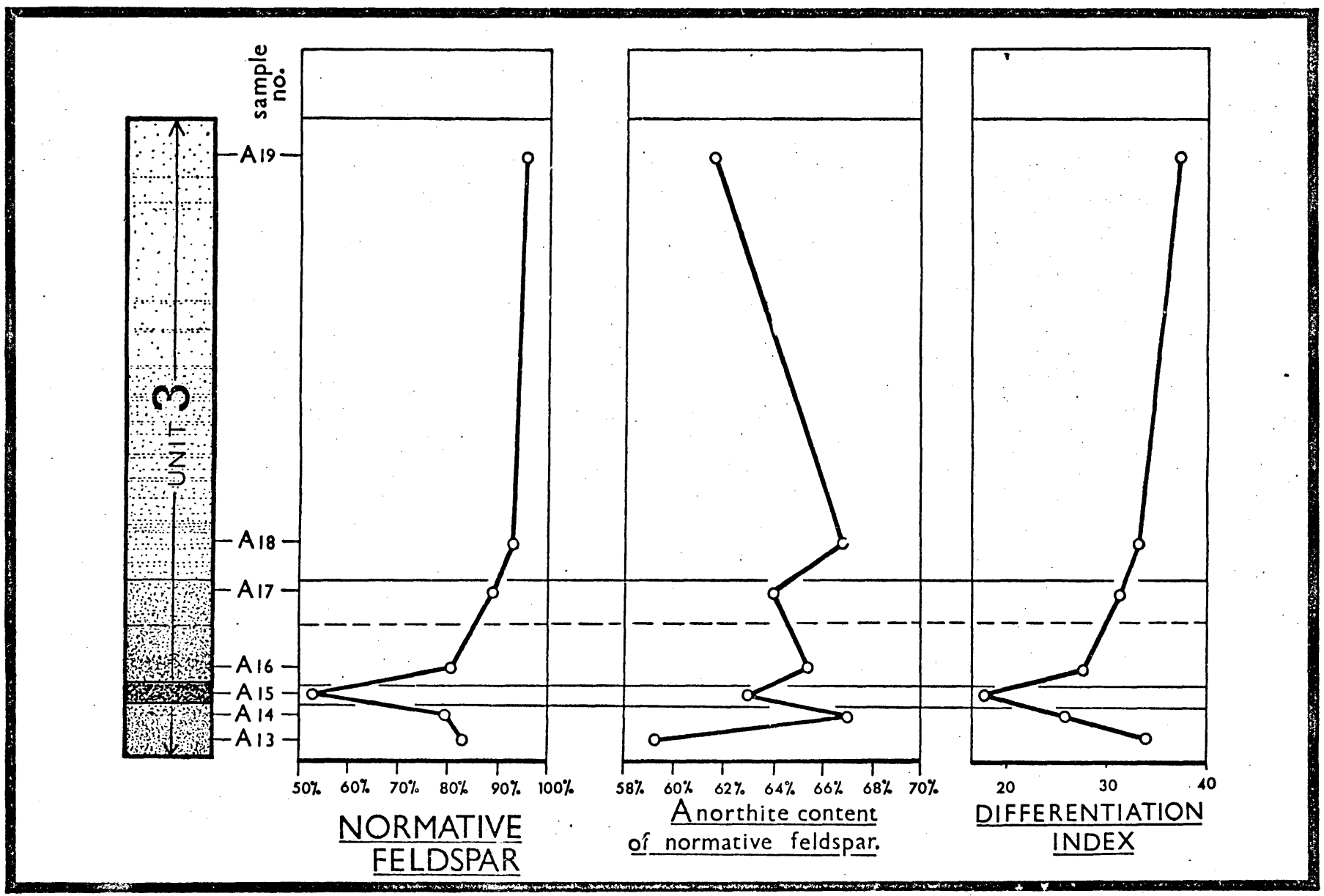


fig. 5.4 Variation of normative mineral molecules, within a single gravity stratified unit (cont.) The differentiation index (Thornton and Tuttle, 1960) is the sum of the normative components quartz, orthoclase, albite, nepheline, leucite and kaliophyllite.

increase (0,505 - 0,654) towards the top of this unit. This variation provides good evidence that igneous fractionation trends are still preserved within these layered rocks, despite the fact that they have been subjected to at least three metamorphic episodes. Such a variation in the FeO/FeO + MgO ratio would be very difficult to explain in terms of metamorphic processes as one might expect an equalization of the ratio during recrystallization and equilibration.

It appears reasonable to assume that each gravity stratified unit represents fractionation and accumulation from a common parent magma. The differences in composition of the magma which give rise to each unit were not large - compare analyses A5 and A13 (Appendix 1, Table 15).

The discussion will now be extended to include all the rocks which make up the anorthosite body. Fig. 5,5 shows that the range of calculated values for the ferrous iron-magnesia ratio (FeO/FeO + MgO) increases with increasing structural height in the anorthosite. The lower limit of this range is defined by the gabbros and the upper limit by the anorthosites. Values for the mafic gabbros in the lower zone are intermediate. As the gabbros form the base of the gravity-stratified units in each zone, it is thought that any variation in composition of these rocks, with structural height, may reflect a similar variation in the composition of the parent magma - which subsequently differentiated to produce the remainder of each unit. If this supposition is correct, it may be concluded that, with some fluctuations, the composition of the parent magma shows a slight enrichment in iron, relative to magnesium with structural height. If the anorthosites which occur at the

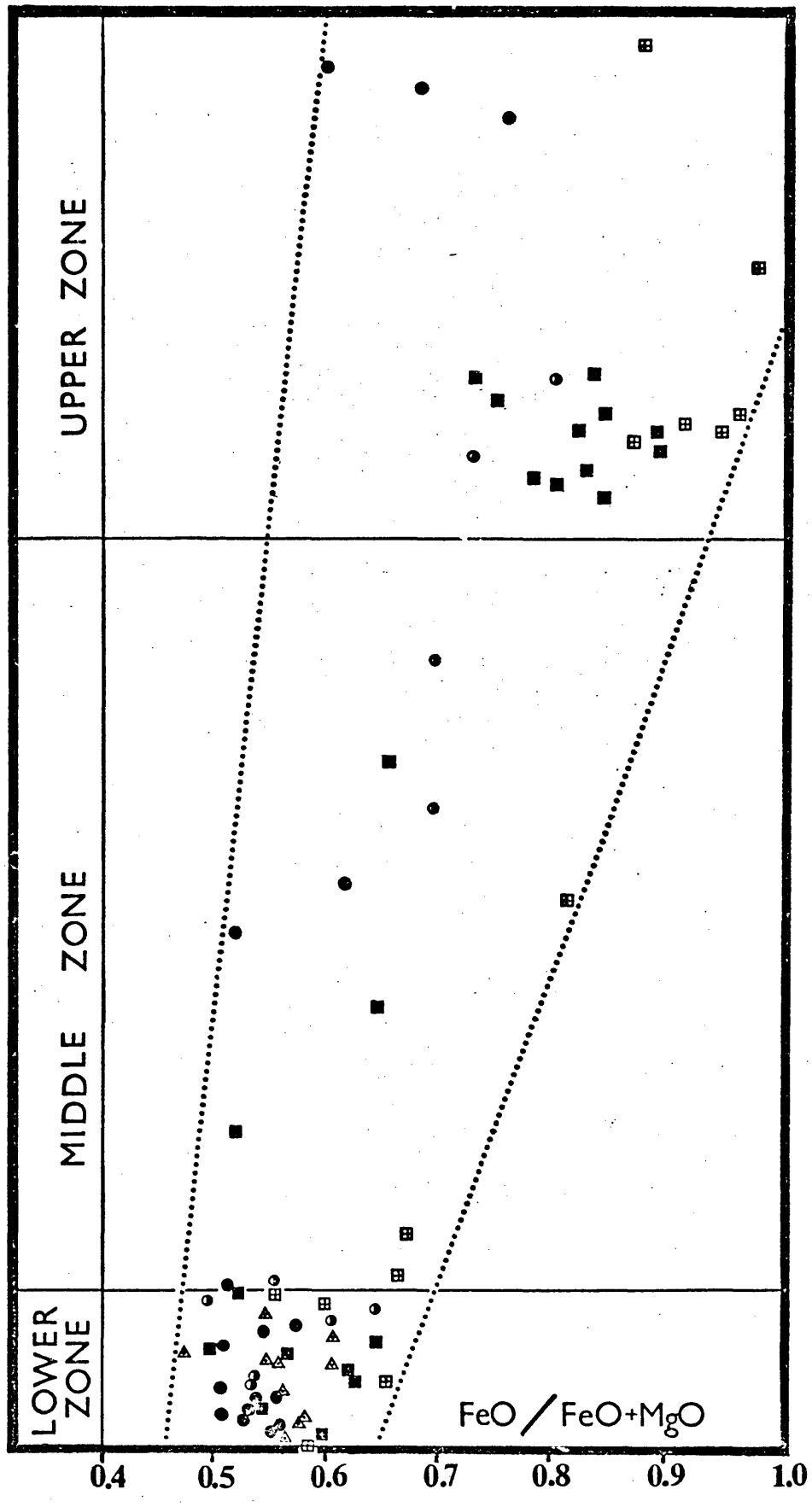


fig. 5.5 Variation of $\frac{\text{total iron as FeO}}{\text{total iron as FeO + MgO}}$ with structural height, for the rocks of the anorthosite body. For key to symbols see table 5.1.

top of each gravity-stratified unit are now considered, the variation in chemistry of these rocks should reflect the extent to which differentiation of the parent magma has taken place within each unit. Although, again, there are fluctuations there is a marked increase in the ferrous iron-magnesia ratio of the anorthosites with increasing structural height. This would suggest that anorthosite horizons at successively higher structural levels in the intrusion represent more extreme fractionation of the parent magma.

5.3.2 The Banded Ultramafites and Mafic Gabbros

These rocks are highly undersaturated with regard to silica and as a result are strongly olivine and nepheline normative. Calcium values in the ultramafites and mafic gabbros are high and result in the occurrence of up to 45% diopside in the norm of these rocks. The high CaO values, together with the low alkali concentrations, result in the high anorthite content of the normative feldspar.

The ultramafites and mafic gabbros are generally depleted in trace elements. Strontium (average 88 p.p.m.) appears to be astonishingly depleted considering the high calcium content of these rocks. Both chromium (average 354 p.p.m.) and nickel (average 40 p.p.m.) are anomalously low, bearing in mind the basicity of the rocks.

5.3.3 The Quartz Gabbros

The quartz gabbros form the bulk of the gabbroic rim of the anorthosite complex. These rocks are in fact gabbros and mafic gabbros which contain up to 12% modal quartz and which thus differ markedly from the banded ultramafites and mafic gabbros. The quartz gabbros also show higher total alkalis

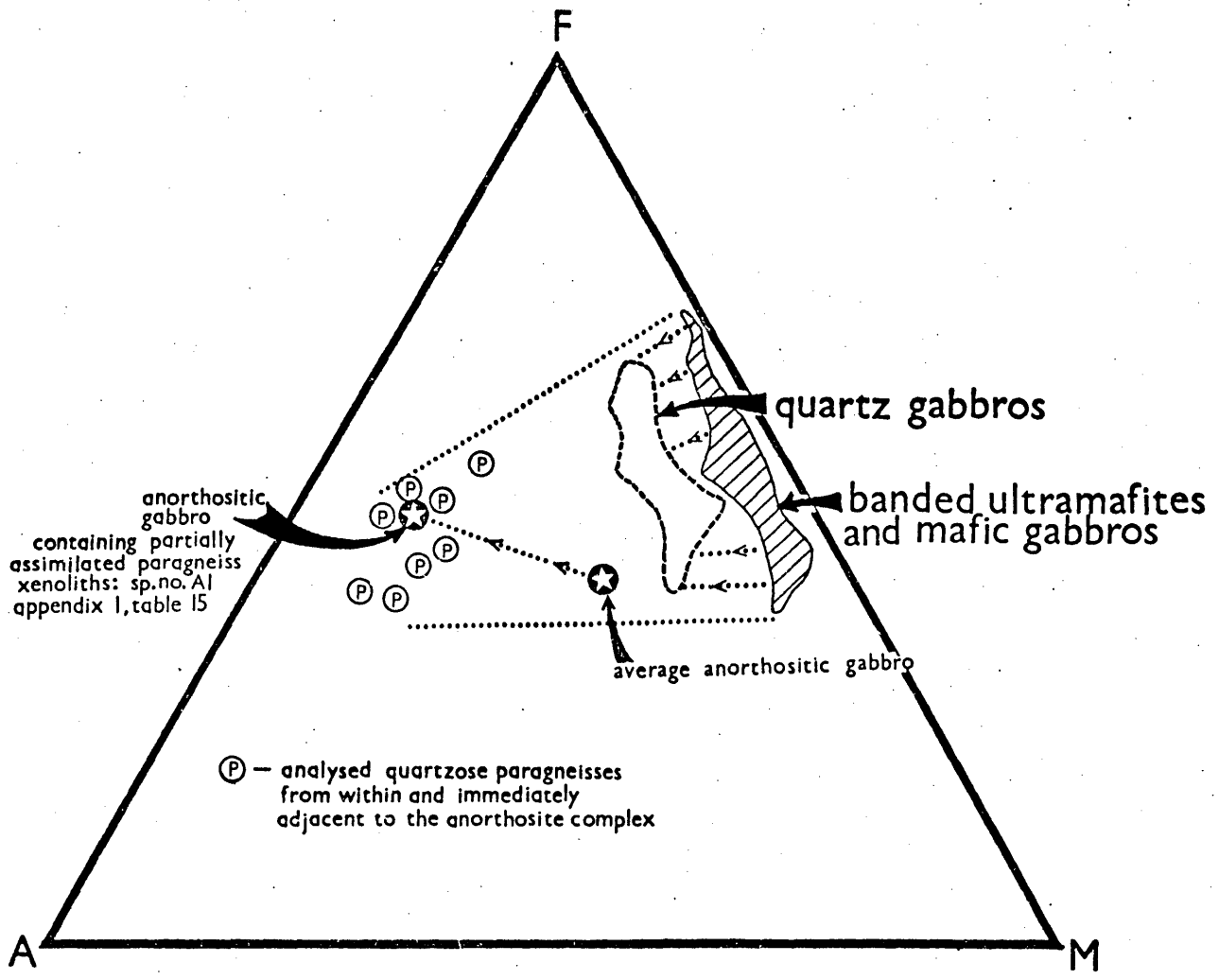


fig. 5.6 AFM projection to demonstrate the chemical effects of assimilation of the quartzose paragneisses (supracrustals) by the meta-igneous rocks of the anorthosite complex.

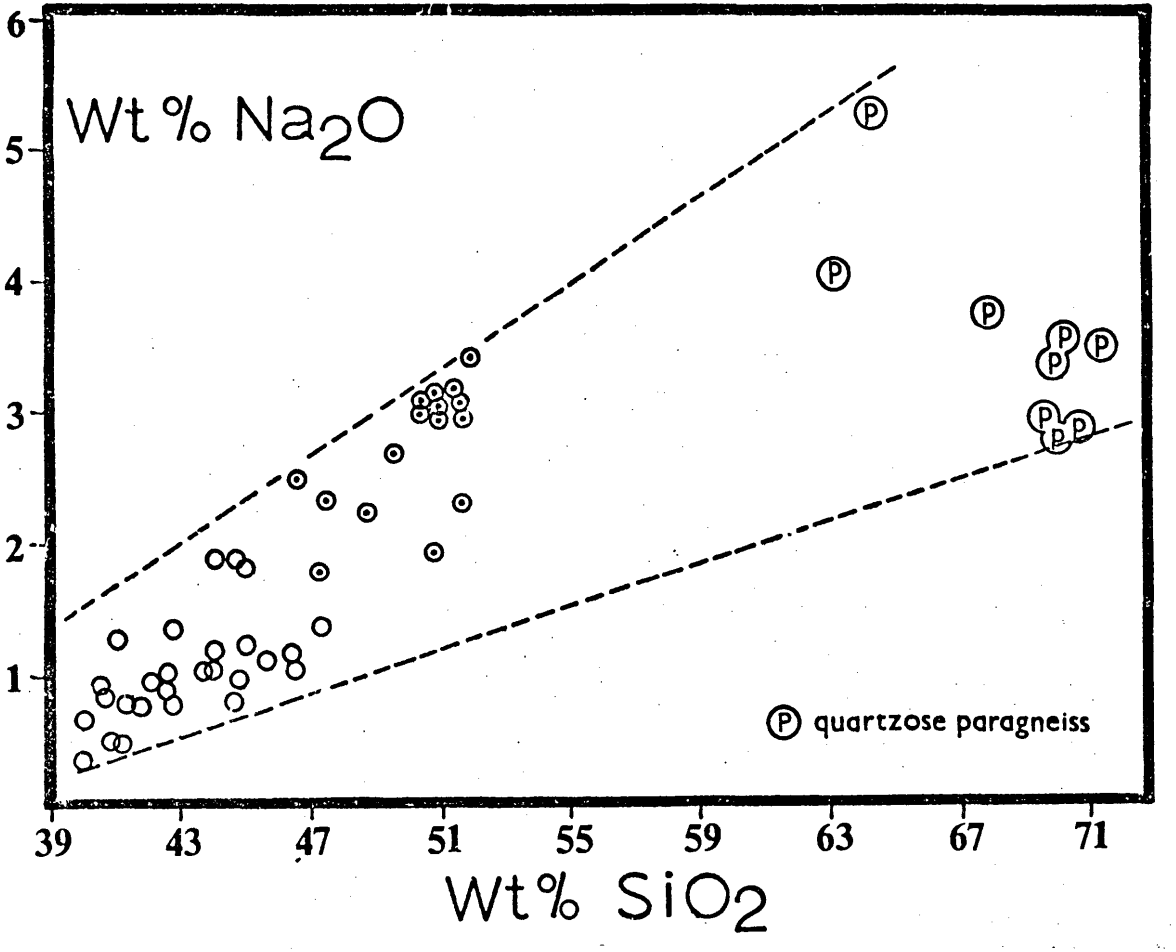


fig. 5.7 The relation between wt% Na_2O and wt% SiO_2 for the banded ultramafites/mafic gabbros, quartz gabbros and quartzose paragneisses from the gabbroic rim of the anorthosite complex. For the key to the symbols used see Table 5.1.

(Na_2O and K_2O) and lower CaO and Al_2O_3 contents, when compared to the ultramafites and mafic gabbros.

On the AFM projection the quartz gabbros plot in an elongate field, parallel to that of the banded ultramafites and mafic gabbros. But due to their higher total alkali content this field is offset from the latter, towards the alkali apex (fig. 5.6). Fig. 5.7 shows the relationship between weight percent SiO_2 and weight percent Na_2O, for the banded ultramafites/mafic gabbros, quartz gabbros and quartzose paragneisses. In both figs. 5.6 and 5.7, the quartz gabbros occupy an intermediate position between the paragneisses and ultramafites/mafic gabbros. The origin of the quartz gabbros is problematical, but it is thought that they represent hybrid rocks produced by assimilation of varying amounts of quartzose paragneiss by the parental liquid which differentiated to produce the ultramafite/mafic gabbro layered sequence.

The rocks which form the gabbroic rim of the anorthosite complex are thought to have been intruded as a sill-like body prior to the intrusion of the anorthosite. It is envisaged that the intrusion of this "hot" basic material into the supracrustals, locally produced a partial or total melting of the quartzose paragneisses. A co-mingling of these melt products and the basic magma, around the margin of the intrusion, produced the quartz gabbro sheath to this body. Parts of the paragneiss sequence evidently resisted melting and are preserved as both large and small xenolithic rafts in the quartz gabbros.

5.4 Metamorphism of the Anorthosite Complex

It was stated at the beginning of this chapter that the granulite facies metamorphism, which gives rise to the earliest recognizable mineral assemblages in the anorthosite, was thought to be isochemical. Hence the geochemistry of these rocks should accurately reflect their pre-metamorphic compositions. Thus, for any one rock analysis, a comparison of the calculated normative minerals with the modal minerals may throw some light on the various metamorphic reactions which yield the present granulite facies mineral assemblage.

As both chemical and modal analyses are available for the rocks of the two gravity stratified units from the base of the lower zone (units 2 and 3), they are used to illustrate the following discussion. These rocks show only slight effects of retrogression and the modal analyses of these samples include only granulite facies minerals. It is assumed, for the sake of this discussion, that the calculated normative molecules approximate, in type and proportion, to the original 'igneous' minerals of the rocks under review.

It can be demonstrated that a discrepancy exists between the figures for:-

a) total normative feldspar and modal feldspar, in any one sample

and b) the normative anorthite content of the feldspar and the anorthite content of the modal feldspar in the same sample,

These discrepancies are greatest with respect to the figures obtained for the mafic gabbros, and smallest with respect to those for the anorthosites. Although the reduction in anorthite content is in some cases considerable, it is not always sufficient to account for the apparent reduction in total feldspar. Thus there must also be a reduction in the

albite and/or orthoclase components of the feldspar to fully account for the observed reduction in total feldspar.

SAMPLE A15 - mafic gabbro			
Normative feldspar		Modal feldspar (granulite facies assemblage)	
or 3.96	total feldspar -	or 0.08	total feldspar -
ab 14.47	50.28%	ab 10.63	17.00%
an 31.85		an 6.29	
Normative An content - 63.35		Modal An content - 37.03	

SAMPLE A19 - anorthosite			
Normative feldspar		Modal feldspar (granulite facies assemblage)	
or 3.01	total fledspar-	or 1.66	total feldspar -
ab 33.26	95.06%	ab 34.00	92.00%
an 58.79		an 56.33	
Normative An content - 61.85		Modal An content - 61.23	

Either of the two postulated reactions below, for the formation of garnet in these rocks, would produce a less calcic feldspar (by reducing the anorthite component) and may also lead to an overall decrease in the modal feldspar content of the rock.

$$3Mg_2SiO_4 + 3CaAl_2Si_2O_8 \rightarrow \underbrace{2Mg_3Al_2Si_3O_{12}}_{\text{pyrope}} + \underbrace{Ca_3Al_2Si_3O_{12}}_{\text{grossular}} \quad \text{.....(1)}$$

olivine anorthite garnet

$$6MgSiO_3 + 3CaAl_2Si_2O_8 \rightarrow \underbrace{2Mg_3Al_2Si_3O_{12}}_{\text{pyrope}} + \underbrace{Ca_3Al_2Si_3O_{12}}_{\text{grossular}} + 3SiO_2 \quad \text{..(2)}$$

enstatite anorthite garnet quartz

Both reactions are thought to be responsible for the formation of garnet in these rocks. However, in those rocks where the formation of garnet is accompanied by the production of small amounts of quartz (which occurs as small blebs sieving the garnet grains), the reaction involving

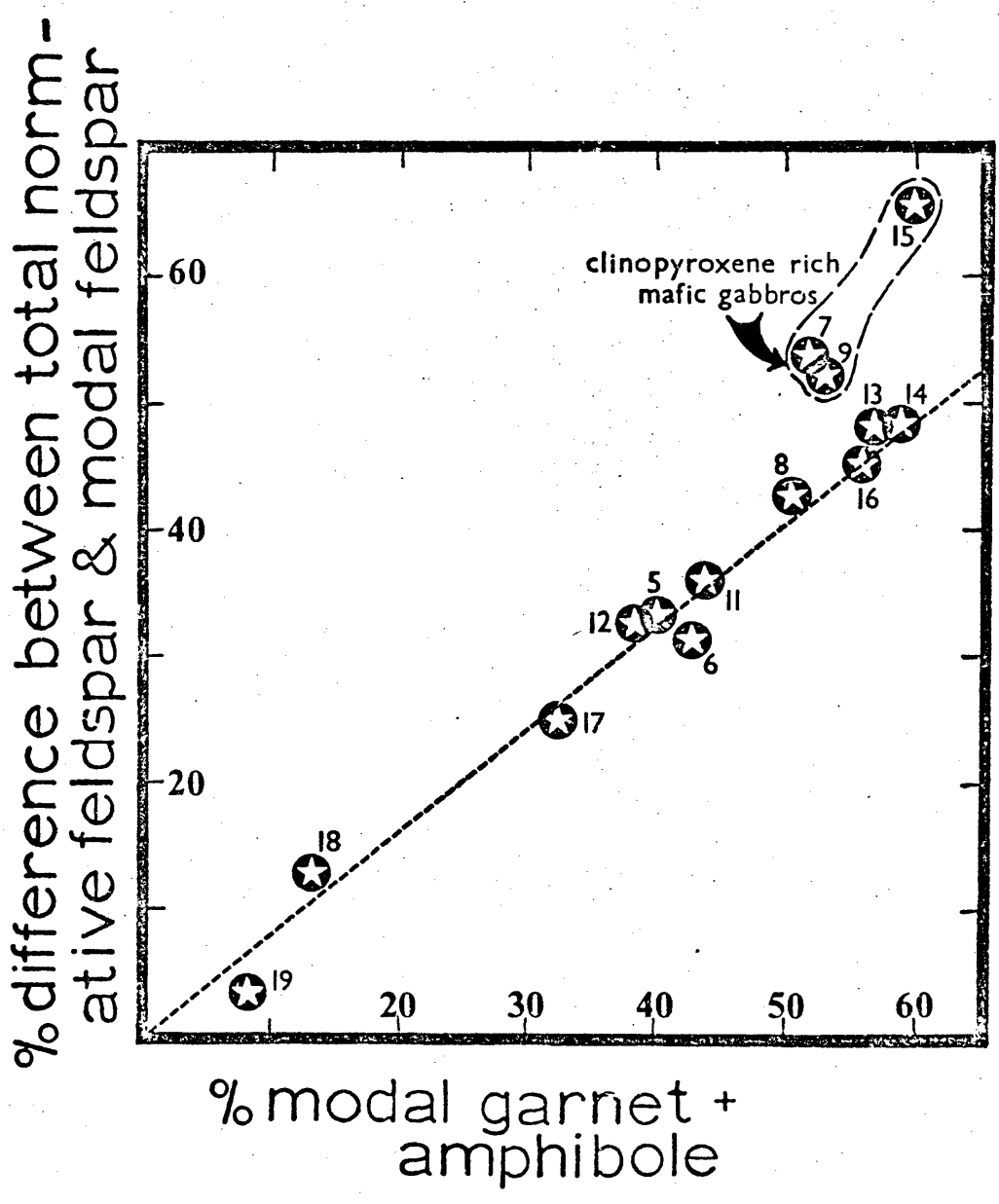


fig 5.8 The relation between the total modal % garnet + amphibole and the % difference between total normative feldspar and modal feldspar, for the analysed samples from gravity stratified units 2 & 3. The samples which lie on or adjacent to the dashed line (which has been drawn to pass through the origin of the graph) are all rocks which contain no modal clinopyroxene. Note that the clinopyroxene rich (greater than 20% modal cpx.) mafic gabbros plot well away from the dashed line.

enstatite is obviously favoured. The ratio pyrope : grossular (2 : 1) in both equations is reasonably consistant with garnet analyses from the anorthosite (Appendix 1, Tables 22, 23 and 24).

The two equations above neglect to take into account the formation of the iron rich garnet molecule - almandine. The almandine: pyrope ratio in the garnet analyses from the anorthosite varies from 1:1 to 4:1. As the Fe_2SiO_4 and $FeSiO_3$ components of the normative olivine and enstatite molecules are relatively low (Fe : Mg ratios 3 : 7 - 1 : 1), the formation of much of the garnet must have involved reaction with another iron-rich mineral - possibly magnetite and/or ilmenite?

The formation of the granulite facies pargasitic amphibole must also have involved reaction with the feldspar. In this case reactions will involve not only the anorthite component of the feldspar but also the albite and possibly the orthoclase components. For instance, pargasite may be generated by the following reaction:-

$$\underbrace{NaAlSi_3O_8 + CaAl_2Si_2O_8}_{\text{labradorite}} + 3MgSiO_3 + CaMgSi_2O_6 + H_2O \quad \text{....(3)}$$
$$\text{enstatite diopside}$$

$$\longrightarrow NaCa_2Mg_4Al_3Si_6O_{22}(OH)_2 + 4SiO_2$$
$$\text{pargasite}$$

If the feldspar were involved only in the formation of garnet and amphibole, then one might expect a reasonably good positive correlation between the sum of the modal garnet and amphibole and the percentage difference between total normative and modal feldspar in any one sample. This is in fact the case (fig. 5.8) in all analysed samples except the mafic gabbros. The mafic gabbros are also exceptional in that they contain over 20% modal clinopyroxene, whereas

the remainder of the horizons (in units 2 and 3) contain no modal clinopyroxene (fig.2.3). The high modal clinopyroxene content of the mafic gabbros is matched by an equally high normative clinopyroxene component. Small amounts of clinopyroxene also occur in the norms of the associated gabbros (fig. 5.3), but this is probably consumed in reactions producing the granulite facies pargasitic amphibole as no clinopyroxene appears in the mode of these rocks. It is possible that the modal clinopyroxene in the mafic gabbros is of primary igneous origin. However, in those rocks where clinopyroxene coexists with orthopyroxene, the distribution coefficient with reference to the Mg-Fe exchange ($K_{D\ (Mg\text{-}Fe)}$) between the pyroxene pair suggests that both are of metamorphic origin. Thus, where there is an excess of clinopyroxene in the original 'igneous' assemblage over that required in the formation of amphibole (equation 3), the original 'igneous' clinopyroxene may have reacted with the plagioclase feldspar (anorthite and albite components) to produce a metamorphic clinopyroxene which is:-

a) more calcic?

b) higher in Al_2O_3 - modal clinopyroxene Al_2O_3 values range from 2.8 - 7.1

c) higher in Na_2O - modal clinopyroxene Na_2O values range from 0.4 - 0.91

If we now refer back to fig. 5.8, we can see that the clinopyroxene-rich mafic gabbros (sample nos. A7, A9 and A15) ar anomalous in the respect that the percentage reduction from total normative feldspar values to observed modal feldspar values is greater than one would expect if the 'igneous' feldspars were only involved in reactions to form garnet

and amphibole. This diagram would thus tend to confirm the remarks made above on the derivation of the modal clinopyroxene.

To summarize, it may be said that:-

a) within the more mafic rock types of the anorthosite body, considerable amounts of feldspar have been consumed in metamorphic reactions to produce garnet, amphibole and clinopyroxene. Hence, metamorphism has effectively increased the mafic (or colour) index of these rocks and considerably altered the anorthite content of the remaining plagioclase feldspar.

b) In contrast, the highly feldspathic rock types, because of their low FeO and MgO contents, have a greatly reduced potential for the formation of new mafic minerals during metamorphism. Thus the mafic index of these rocks will show only a slight increase and the anorthite content of the plagioclase feldspar a slight decrease.

The contrast in rock types observed in the anorthosite body has been greatly exaggerated by metamorphism. The terminology adopted in this thesis to describe the rocks of the anorthosite body is based on modal analysis - either by point counting or by visual estimate. This method has proved perfectly satisfactory for field classification of these rocks, but it must be borne in mind that the original rock types of the anorthosite sequence were far more leucocratic. Even so, the overall pattern of variation of rock type remains unchanged - compare A and B Fig. 5.9.

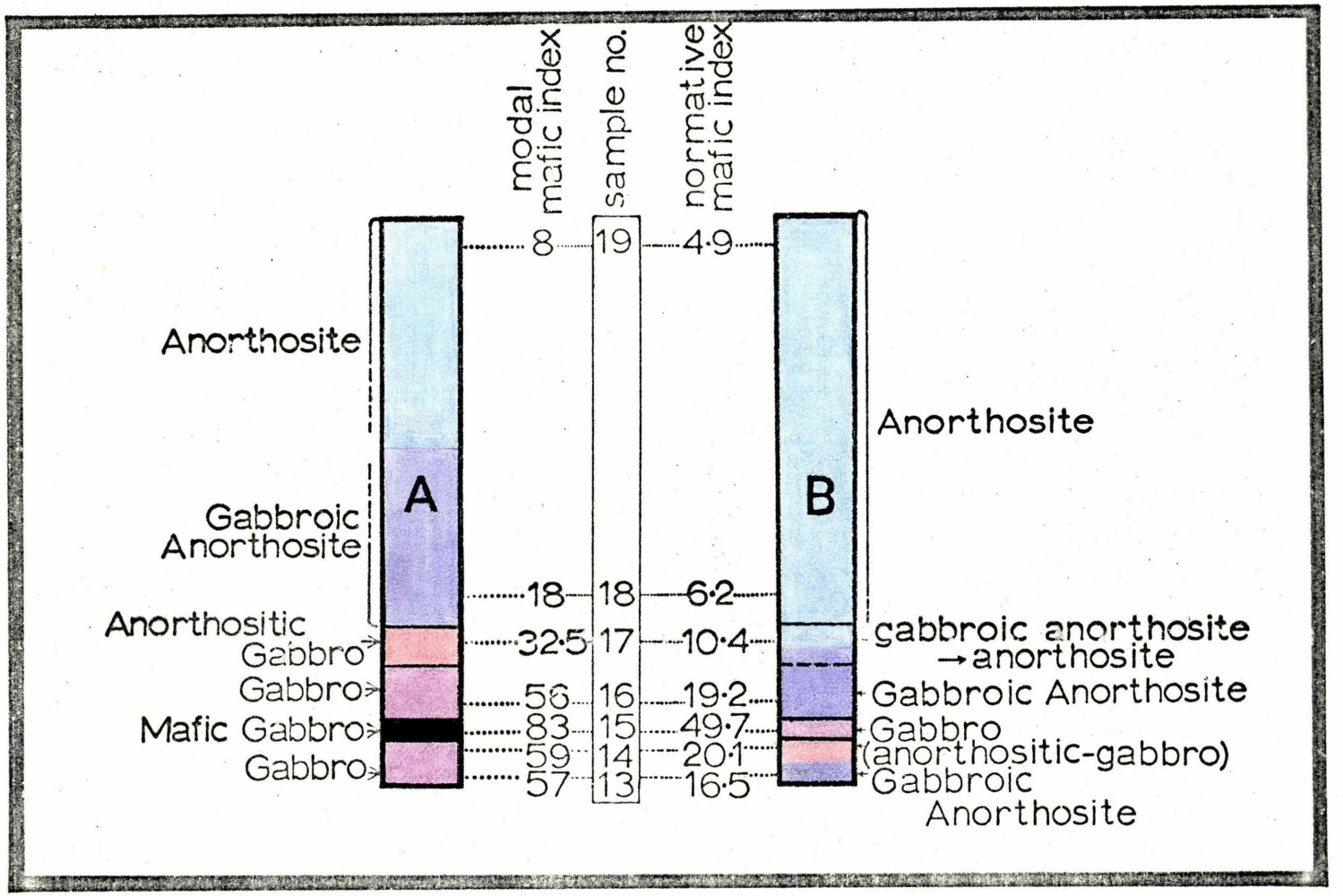


fig. 5.9 The contrast between:-
A - the observed variation in rock type within a single gravity stratified unit (unit 3) based on the modal mafic index, obtained by point-counting
B - possibly the original (pre-metamorphic) variation in rock type based on the normative mafic index, calculated from the bulk-rock analyses.

It will be noticed that the original rock types of the gravity stratified unit (B) are far more leucocratic, but the overall pattern of variation in rock types remains unchanged. The rock terminology adopted is that of Windley and Smith (1974) - see Table 1.2.

The change in composition of the feldspar which accompanied the high grade metamorphism would suggest a high degree of ionic exchange during recrystallization and equilibration. Ionic migrations, however, are thought to have taken place over only small distances - mostly less than the width of individual layers within the sequence - and would not, therefore, have affected the generally isochemical nature of the high-grade metamorphic event.

Turning now to the ultramafites and mafic gabbros from the gabbroic rim of the complex, a similar increase in the mafic index of these rocks is found to accompany metamorphic recrystallization. In some cases, a total normative feldspar content in excess of 50% is obtained from rocks which contain no modal feldspar (e.g. sample G5). However, unlike the anorthosite, the analyses of the modal feldspars from these rocks in most cases reflect the normative feldspar compositions.

Sample No.	Modal Anorthite Content of Plagioclase	Normative Anorthite Content of Plagioclase
G1	81.97	83.20
G2	84.71	84.56
G6	50.54	74.61
G10	77.73	86.55
G12	85.20	83.04

Bearing in mind the pattern of variation in the composition of the plagioclases demonstrated for the anorthosite, the highly calcic composition of these feldspars is surprising. Taking into account the high mafic index of

these rocks, it might have been expected that highly sodic plagioclase compositions would have resulted from metamorphic recrystallization. Metamorphic recrystallization of the plagioclases from the anorthosite has resulted in the removal of 1-80% of the anorthite component and proportionately lesser amounts of the albite and orthoclase components. Such a reduction in the anorthite content of these feldspars is uniform throughout any one sample (variation in modal An content is usually less than 1 mol.% in any one rock sample.) and does not just affect those feldspars immediately adjacent to newly formed amphibole and garnet. Whereas in the ultramafites and mafic gabbros it might seem reasonable to suggest that the feldspar components were only consumed on or adjacent to the sites of amphibole or garnet growth. Under these circumstances, one may expect the preservation of isolated patches of plagioclase which has recrystallized and retained its original composition. This is purely speculative but the observed differences in plagioclase composition must indicate a basic difference in the way in which these two portions of the complex reacted to the high grade metamorphic event.

5.5 The Differentiation of the Anorthosite Complex

If the rocks of the anorthosite complex are igneous in their parentage, it becomes possible to discuss the rocks of the complex in terms of fractional crystallization and to gain some insight into the evolution of the complex. It is thought that enough data are now available for some comments to be made on this subject.

The variation between the various oxide (weight percent) concentrations of the rocks of the anorthosite

Ⓐ

	SiO_2	TiO_2	Al_2O_3	**FeO	MnO	MgO	CaO	Na_2O	K_2O
SiO_2	*	-.30	.43	[-.51]	[-.85]	[-.75]	.20	[.71]	.29
TiO_2		*	[-.53]	[.50]	[.57]	[.55]	.26	-.39	.05
Al_2O_3			*	[-.91]	[-.73]	[-.85]	.21	[.69]	-.03
**FeO				*	[.90]	[.91]	-.24	[-.73]	-.10
MnO					*	[.86]	.22	[-.70]	-.09
MgO						*	-.26	[-.68]	-.12
CaO							*	-.07	[-.51]
Na_2O								*	.32
K_2O									*

Ⓑ

	SiO_2	TiO_2	Al_2O_3	**FeO	MnO	MgO	CaO	Na_2O	K_2O
SiO_2	*	[-.76]	.05	[-.84]	[-.62]	.38	[.68]	.37	.06
TiO_2		*	-.33	[.60]	.38	-.21	-.46	-.23	.01
Al_2O_3			*	-.33	-.22	[-.73]	.13	-.14	-.35
**FeO				*	[.76]	-.15	[-.62]	-.33	-.00
MnO					*	-.08	[-.55]	-.49	.30
MgO						*	.17	.17	.19
CaO							*	-.17	.31
Na_2O								*	[.79]
K_2O									*

Table 5.3 Correlation coefficients for oxides from the anorthosite complex

A - rocks from the anorthosite sequence (68 analyses) - saussuritized and highly retrogressed types not included.

B - the banded ultramafites and mafic gabbros from the gabbroic rim of the anorthosite complex (39 analyses) - excluding the quartz gabbros.

** FeO = total iron expressed as FeO.

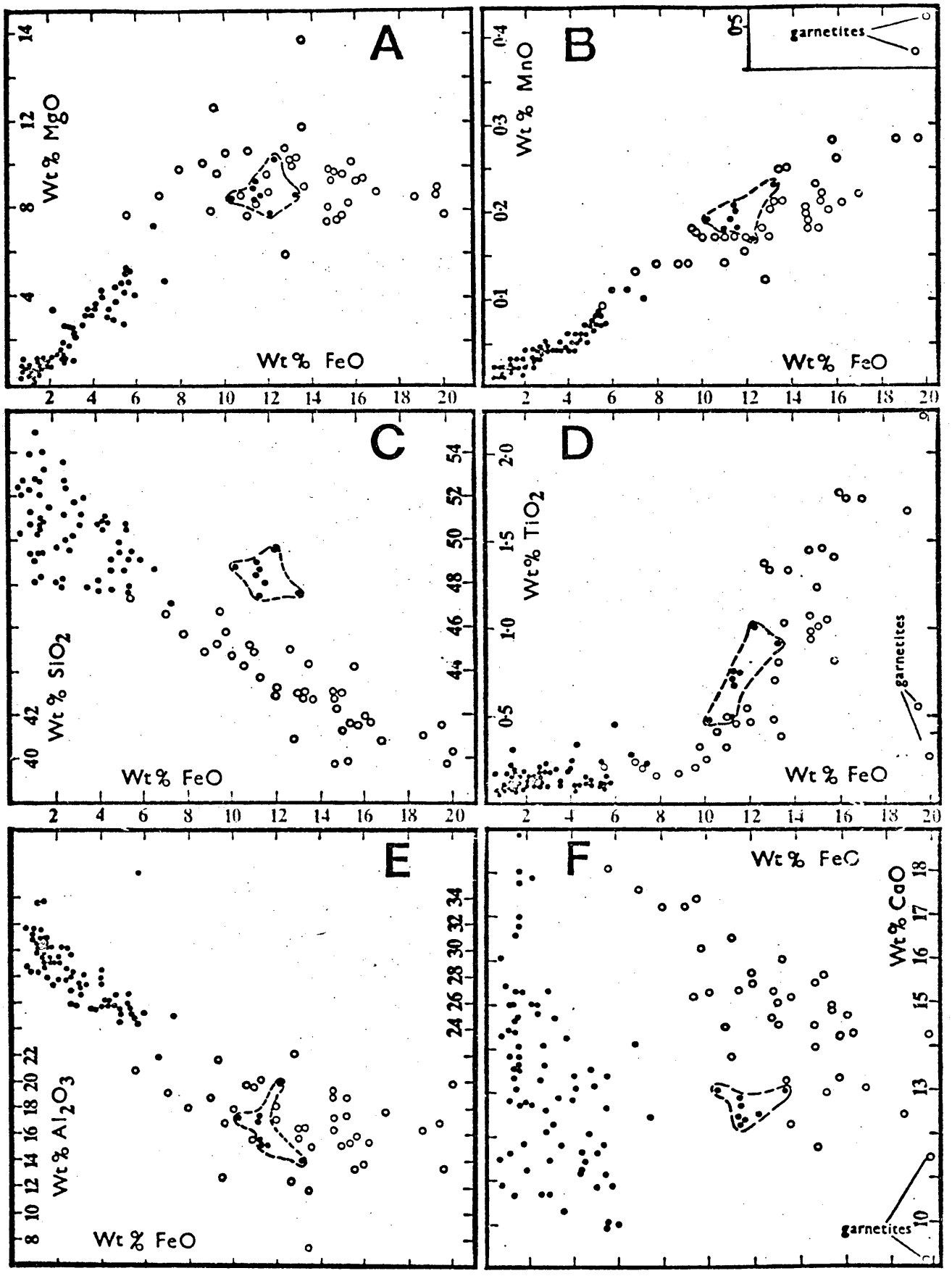


fig. 5.10 Harker variation diagrams for the rocks of the anorthosite complex. Oxides are plotted against FeO (total iron expressed as FeO). The compositional field of the mafic gabbros, from the lower zone of the anorthosite sequence, is shown in each plot. Open circles - ultramafites and mafic gabbros from the gabbroic rim of the complex. dots - 'anorthosites' (undifferentiated)

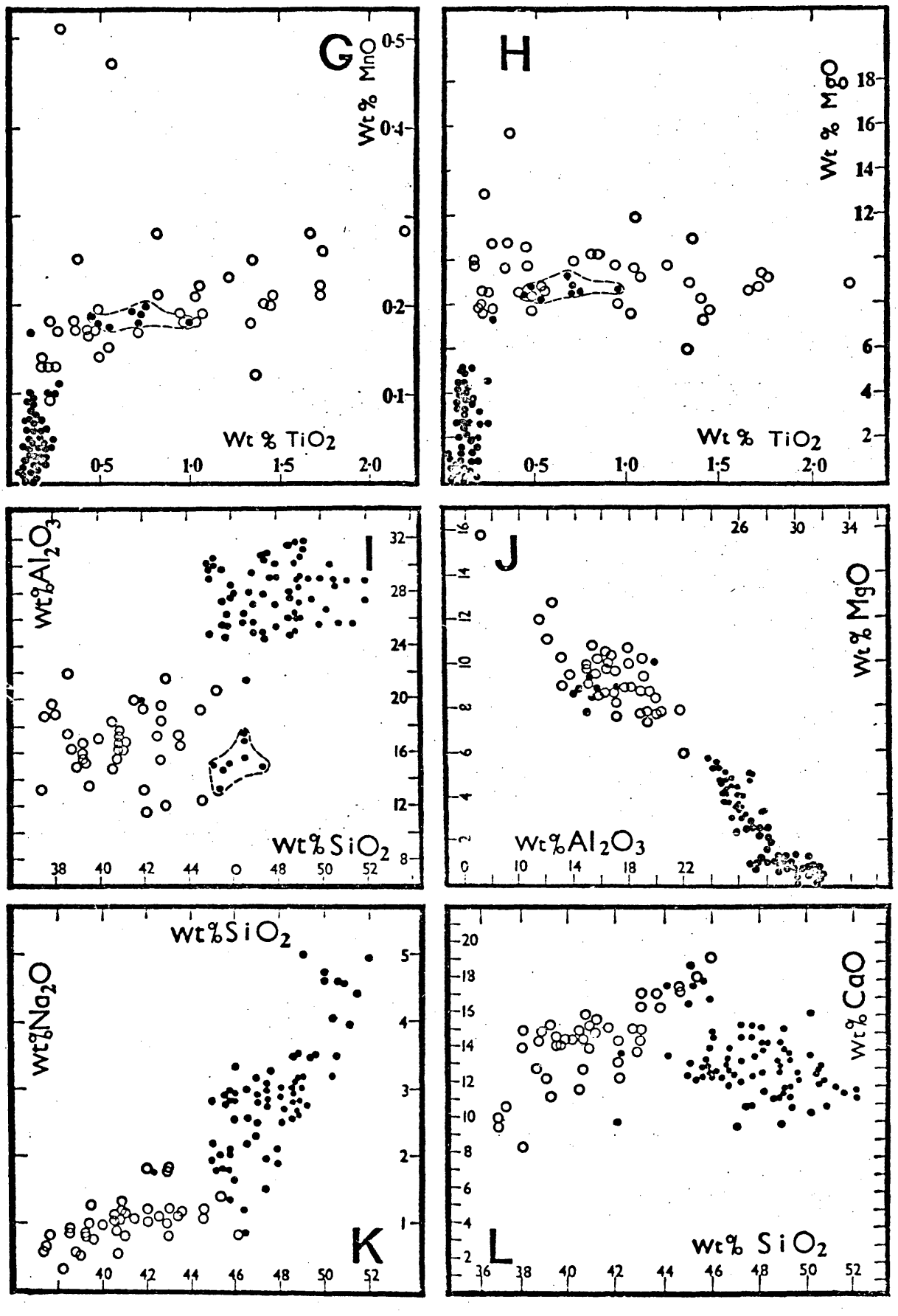


fig. 5.11 Harker variation diagrams for the rocks of the anorthosite complex. Oxides are plotted against (TiO_2 (G & H), SiO_2 (I, K & L) and Al_2O_3 (J). Open circles - ultramafites and mafic gabbros from the gabbroic rim of the complex. dots - 'anorthosites' (undifferentiated).

complex are shown in Harker variation diagrams (figs. 5.10 and 5.11). Table 5.3 gives correlation coefficients for all the oxide pairs, emphasizing those which show a significant correlation above the 5% confidence level. Significant correlations between oxide pairs appear to be more frequent in the anorthositic rocks than they do in the banded ultramafites and mafic gabbros from the gabbroic rim of the complex. There is also, in general, a higher degree of correlation (i.e. the correlation approaches closer to a perfect linear relationship) between the oxides of the anorthositic rocks than between those of the banded ultramafites and mafic gabbros.

Comparison of the two data sets shown in Table 5.3 reveals some interesting differences:-

a) Na_2O correlates with SiO_2, Al_2O_3, FeO (total iron as FeO), MnO and MgO in the anorthosites, but there is no significant correlation in the ultramafites and mafic gabbros from the gabbroic rim.

b) CaO correlates with SiO_2, FeO (total iron as FeO) and MnO in the ultramafites and mafic gabbros, but there is no significant correlation in the anorthosites.

c) the good FeO : MgO correlation (0.91) in the anorthosites is in contrast to the poor negative correlation (0.15) between these two oxides in the ultramafites and mafic gabbros.

These and other variations suggest that there were some significant differences in the factors controlling crystallization of the anorthosites and the gabbroic

(ultramafites and mafic gabbros) rocks which rim them.

Also is is of interest to note that the mafic gabbros, which form thin horizons in the lower part of the lower zone of the anorthosite sequence, show a greater chemical affinity to the banded ultramafites and mafic gabbros than they do to the remainder of the anorthosite sequence. This relationship is portrayed particularily well in those Harker variation diagrams where the oxides are plotted against FeO (fig. 5.10).

Although Harker variation diagrams are useful for demonstrating that some sort of relationship exists between the variables, Pearce (1968) has shown that these diagrams (and other ternary weight percent plots) distort genetic trends by changing their slopes. Pearce argued that '.....dividing two variables by a third parameter does not change the relationship between them if the third parameter is a constant.' This parameter must be constant in absolute terms, although its proportions relative to the other variables may change as the amounts of these variables change. This technique, advanced by Pearce (1968), has been successfully applied to investigate the differentiation of the Dundonald sill, Ontario (Pearce, 1969), the Palisade sill (Pearce, 1970) and the Losberg intrusion, Transvaal (Ferguson and Fripp, 1971). Before an attempt is made to apply this technique to the rocks of the South Harris anorthosite complex it will be useful to consider its application to a simple theoretical example to examine the significance of being able to portray the true relationships between the oxides. We will assume that fractionation of olivine alone is

sufficient to account for the chemical variations throughout the rocks of our theoretical differentiated body. In this case FeO, MgO and SiO_2 will be extracted from the system - or added in the case of olivine cumulate rock types. The rate at which these oxides are extracted (or added) will be dependent on the stoichiometry of the olivine. All other components (oxides) are neither added to nor subtracted from the system during differentiation, and thus they remain constant in equivalent amounts - although their concentration in the residual liquids will obviously increase as differentiation proceeds. Any of these oxides can thus be used as a constant to investigate the differentiation of the rocks in question. The relationship between absolute amounts (i.e. grammes) of MgO and SiO_2 will have the same slope as the relationship between, say, MgO/Al_2O_3 and SiO_2/Al_2O_3, if (and only if) Al_2O_3 was constant during the fractionation process - as it is in the hypothetical example. The slope of the relationship between MgO/Al_2O_3 and SiO_2/Al_2O_3 for the whole-rock data will, in this case, be controlled by the stoichiometry of the precipitating phase, olivine. The alumina ratio Mg : Si for the whole-rock data will produce a straight line graph, the slope of which is the same as that of the Mg : Si ratio of the olivine. The Mg : Si ratio of the olivine will, of course, vary with the composition of this phase. If the composition of the olivine changed during fractionation, then the plot of MgO/Al_2O_3 versus SiO_2/Al_2O_3 for the whole-rock oxides would be a curve and not a straight line. Such a curve could in fact be resolved into a series of straight lines, the slope of any one of these lines indicating the composition of the olivine fractionating at that stage. The

results of this technique obviously become more difficult to interpret as the number of minerals fractionating simultaneously increases.

It has been found, by inspection, that K_2O can be considered as a constant for the rocks of the anorthosite complex, although there are certain drawbacks in its use. It has already been mentioned that:-

a) a certain degree of potash metasomatism is thought to have accompanied the formation of the late Laxfordian granite-gneiss injection complex in northern South Harris.

and b) that a leaching of both soda and potash is suspected in the saussuritization of certain parts of the anorthosite.

Also it is now widely believed that anorthositic rocks are plagioclase crystal cumulates (Emslie, 1973). Although alkali feldspar does not occur as a separate phase in these rocks, small amounts of K_2O enter the plagioclase feldspar, and it is fairly safe to assume that this was a cumulate phase in the feldspathic rock types of the complex. This would argue against K_2O being constant in absolute terms, but, despite this seemingly serious limitation, it will be demonstrated that K_2O is effectively constant in this rock sequence.

Before considering the rocks of the anorthosite body (excluding at present the rocks of the gabbroic rim, which will be dealt with separately) two further assumptions can be made. Firstly, that a rock containing over 80% normative feldspar was likely to have been a simple plagioclase cumulate, and secondly, that with decreasing normative feldspar (i.e. less than 80%) there would have been more likelihood

		m		r		N
Anorthosites - excluding mafic gabbros from the lower zone.	Ca : Si	0.302	(0.301)[1] (0.300)[2]	0.83	(0.95)[1] (0.94)[2]	61
	Al : Si	0.355	(0.356)[1] (0.360)[2]	0.82	(0.97)[1] (0.93)[2]	60
	Na : Si	0.061	(0.062)[1]	0.72	(0.82)[1]	57
	K : Si	-	(0.00029)[1]	-	(0.81)[1]	(59)
	Fe+Mg : Si	0.00033		0.79		63
	Mg : Si	0.00010		0.80		64
	Mn : Si	0.00028		0.78		62
	Ti : Si	0.00065		0.81		61
		m		r		N
Mafic gabbros from the lower zone of the anorthosite sequence.	Ca : Si	0.297		0.98		8
	Al : Si	0.164		0.97		8
	Na : Si	0.028		0.78		8
	Fe+Mg : Si	0.500		0.99		8
	Fe : Si	0.228		0.99		8
	Mg : Si	0.272		0.97		8
	Mn : Si	0.0040		0.97		8
	Ti : Si	0.0079		0.97		8
		m		r		N
Ultramafites and mafic gabbros from the gabbroic rim of the anorthosite complex.	Ca : Si	0.423		0.98		32
	Al : Si	0.264		0.87		29
	Na : Si	0.022		0.85		28
	Mg : Si	0.393		0.96		32
	Fe+Mg : Si	0.602		0.97		9 (ultramafites)
	Fe+Mg : Si	0.515		0.99		9 (mafic gabbros)
	Ti : Si	0.034		0.86		16 (ultramafites)
	Ti : Si	0.007		0.93		17 (mafic gabbros)

Table 5.4

Table 5.4 Gradients of regression lines and correlation coefficients from the potash ratio diagrams for the rocks of the anorthosite complex.

() 1-m,r values from iron ratio diagrams
() 2-m,r values from magnesian ratio diagrams

m - gradient of regression line, calculated using the expression:

$$m = \frac{N \lesssim XY - \lesssim X \lesssim Y}{N \lesssim X^2 - (\lesssim X)^2}$$

r - linear correlation coefficient, calculated for each regression line, using expression:

$$r = \frac{N \lesssim XY - \lesssim X \lesssim Y}{\sqrt{N \lesssim X^2 - (\lesssim X)^2}\ \sqrt{N \lesssim Y^2 - (\lesssim Y)^2}}$$

This coefficient measures how closely the correlation approaches a linear relationship. A coefficient value equivalent to unity (1.0) denotes a perfect functional relationship. All calculated regression lines have correlation coefficients which are significant at the 5% confidence level.

X - independent variable (SiO_2 : K_2O or SiO_2 : FeO or SiO_2 : MgO)

Y - dependent variable

N - number of samples

$\lesssim$ - denotes that all the values or products that this sign refers to are summed.

that cumulus ferro-magnesian minerals were present. The validity of these assumptions will be discussed at a later stage. In those rocks containing in excess of 80% normative feldspar, FeO (or indeed MgO, MnO or TiO_2) can be considered as a constant on the assumption that no cumulate ferro-magnesian minerals were present. Figs. 5.12a and b, and 5.13a show the Ca : Si, Al : Si and Na : Si iron ratio plots for all of the analysed anorthosites with 80% or more normative feldspar - this effectively excludes only the mafic gabbros from the lower zone of the anorthosite sequence. It is thought that the slopes of the lines in these diagrams can be attributed to the fractionation of a single mineral phase, plagioclase feldspar. In this case, and assuming perfect solid solution in the plagioclase feldspars, the slopes of the lines will be indicative of the composition of the fractionating phase. Table 5.5 shows the calculated oxide values and the molecular proportions for two perfectly stoichiometric bytownites of composition An_{70} and An_{71}. A comparison of the Ca : Si, Al : Si and Na : Si ratios for these feldspars with the observed iron ratios for the anorthosites would require that the fractionating plagioclase should have a composition approximating to An_{71}. A direct comparison of these findings with the compositions of the modal feldspars of the anorthosite is not possible. It was previously shown that the composition of the modal feldspar was extensively modified during the early granulite facies metamorphism. As an alternative the normative compositions of the feldspars can be considered. A total of sixty-eight analyses of the anorthosite yield an average normative plagioclase of $An_{69.9}$ which is close to the theoretical composition of the

plagioclase feldspar required to satisfy the gradients of the regression lines in figs. 5.12a and b, and 5.13a.

One would also expect the subtraction or addition of K_2O from the system during the fractional crystallization of plagioclase feldspar. For example the fractionation of a plagioclase containing 0.10% (wt%) K_2O would theoretically produce a + 0.002 gradient to the regression line for the K_2O : SiO_2 ratio plot of the rocks involved. However, the almost zero (0.00029) slope for the K_2O/FeO : SiO_2/FeO oxide distribution plot (fig. 5.13b), for the anorthosites, would suggest that the K_2O remained effectively constant during the fractionation of plagioclase in these rocks.

Although there is some scatter in figs. 5.12a and b, and 5.13a the majority of data points in each diagram can best be related to a single straight line. This suggests that the composition of the fractionating plagioclase remained essentially unchanged throughout the differentiation of the anorthosite body. The small discrepancies between CaO : SiO_2 and Na_2O : SiO_2 iron ratios, for the whole rock data, and the Ca : Si and Na : Si ratios for the calculated An_{71} plagioclase feldspar are well within the limits of experimental error. However, the slightly larger discrepancy between Al_2O_3 : SiO_2 for the whole rock data and the Al : Si ratio for the plagioclase feldspar requires some further comment. Analyses of the modal feldspars from the anorthosite demonstrates that only in a few cases do they approach stoichiometry. In many analyses there is a significant non-stoichiometric excess of Al_2O_3 coupled with deficiency of SiO_2. If the fraction-

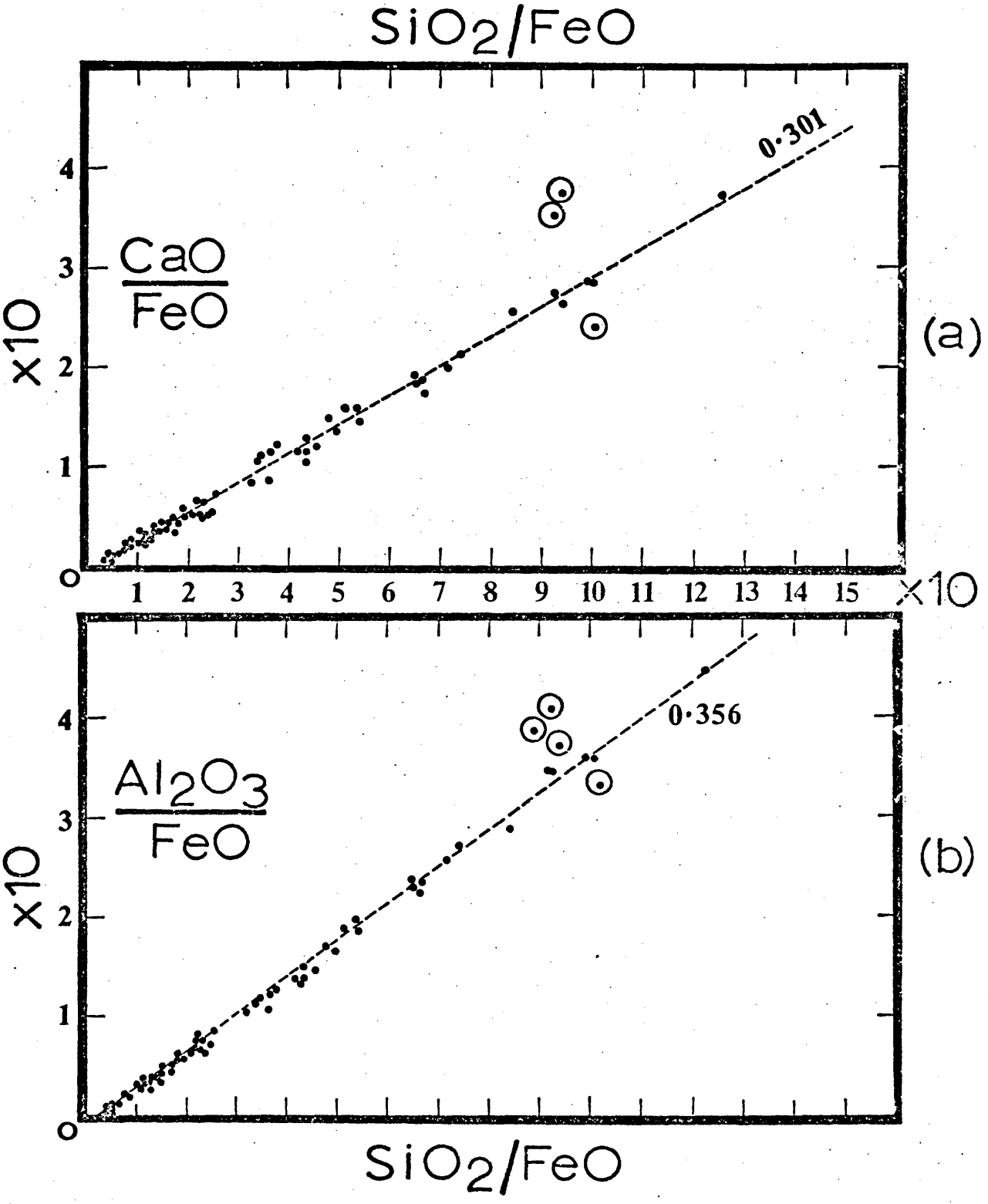


fig. 5.12 (a) CaO : SiO_2 and (b) Al_2O_3 : SiO_2 iron ratio diagrams (molecular) for those rocks of the anorthosie sequence which contain 80% or more normative feldspar. Saussuritised and highly retrogressed anorthosites are not plotted on these diagrams. The circled points, on each diagram, were not included in the regression analyses. FeO = total iron calculated as FeO.

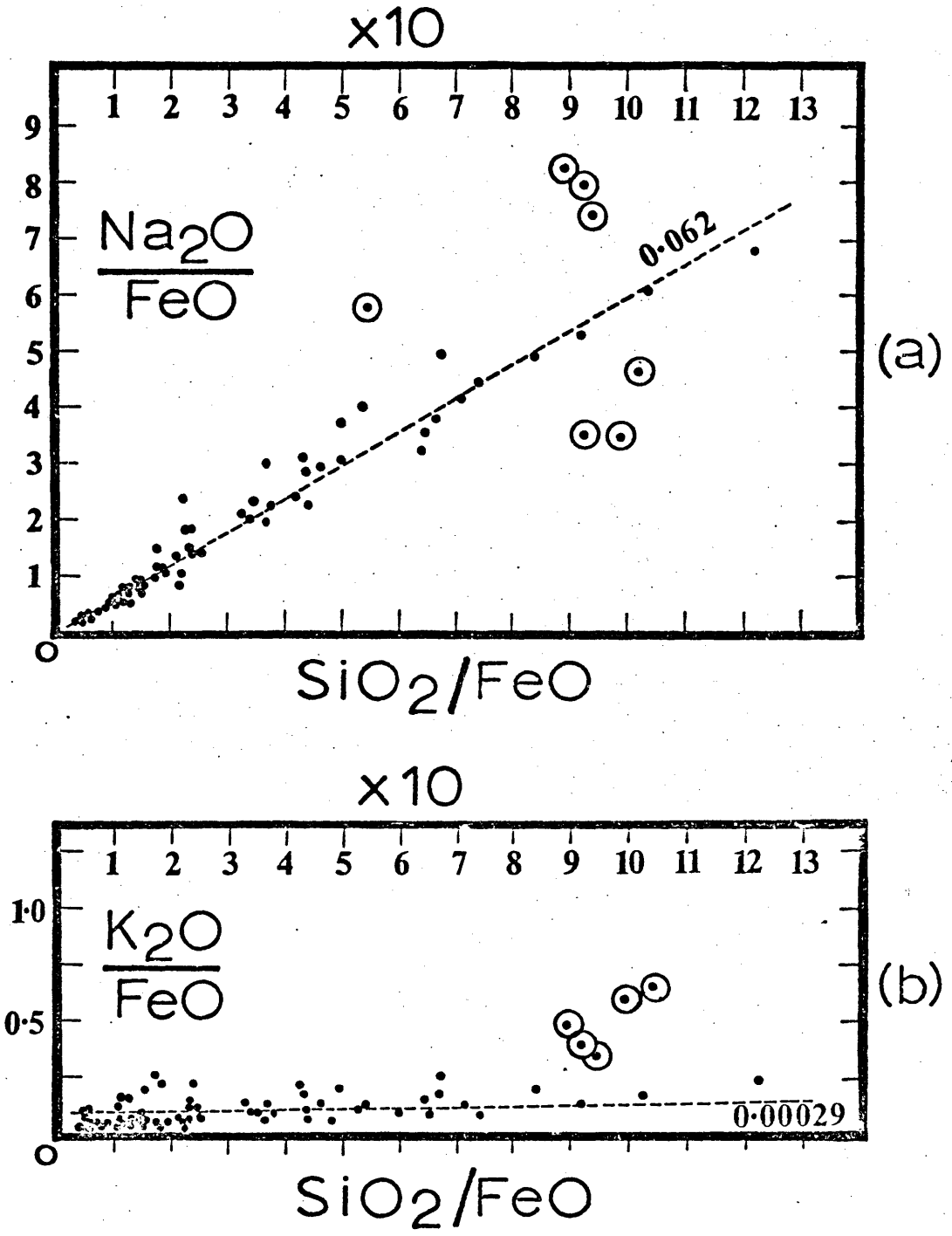


fig. 5.13 (a) Na_2O : SiO_2 and (b) K_2O : SiO_2 iron ratio diagrams (molecular) for those rocks of the anorthosite sequence which contain 80% or more normative feldspar. Saussuritised and highly retrogressed anorthosites are not plotted on these diagrams. The circled points, on each diagram, were not included in the regression analyses. FeO = total iron calculated as FeO.

ating feldspars displayed a similar departure from their stoichiometric formulae, this may be sufficient to explain the discrepancy between the gradient of the Al_2O_3/K_2O : SiO_2/K_2O regression line and the Al : Si ratio of the theoretical, stoichiometric, bytownite.

K_2O is now used as the constant parameter to investigate the validity of the two initial assumptions. The FeO+MgO : SiO_2 and MgO : SiO_2 potash ratio plots, for all the rocks of the anorthosite sequence, are shown in figs. 5.14a and b. It is immediately obvious from these two diagrams that two distinct trends are present. The rocks which plot on trend 1 in both diagrams comprise all those rock types with greater than 80% normative feldspar, and those which plot on trend 2 include those rocks which contain less than 80% normative feldspar - i.e. the mafic gabbros from the lower zone. The positive slopes for trend 1 are so small that for the purpose of this discussion they can be regarded as zero. This would confirm the view that a fractionating ferro-magnesian phase was absent from those rocks in the anorthosite sequence containing over 80% normative feldspar. This also justifies the use of FeO as a constant parameter to investigate the crystallization of these rocks.

The FeO + MgO : SiO_2 potash diagram is particularily revealing and leaves no doubt as to the presence of a fractionating ferro-magnesian mineral controlling the chemistry of the trend 2 rocks. The great advantage of this diagram is that the slope of the line produced is independent of the composition of the ferro-magnesian mineral involved, so that, even if metamorphism has altered the composition of individual grains of this mineral, the original fractionation trend will still be preserved. Assuming a state of ideal solid solution between the end

(A)	OXIDES (Wt. %)	
SiO_2	50.84	50.59
Al_2O_3	31.47	31.65
CaO	14.11	14.31
Na_2O	3.49	3.37
K_2O	0.08	0.08
Total	99.99	100.00
An	70.00	71.00
Ab	29.50	28.50
Or	0.50	0.50
	MOL. PROPS.	
Si	0.8461	0.8419
Al	0.3088	0.3104
Ca	0.2516	0.2552
Na	0.0562	0.0543
K	0.000898	0.00898
	ELEMENT RATIOS	
Ca : Si	0.297	0.303
Al : Si	0.365	0.368
Na : Si	0.066	0.064

(B)	Clinopyroxenes (average of 5 analyses)	Orthopyroxenes (one analysis)
Fe+Mg : Si	0.506	1.003
Mg : Si	0.380	0.643
**Fe : Si	0.126	0.360
Mn : Si	0.00169	0.00361
Na : Si	0.014	-
Al : Si	0.041	0.0256
Ca : Si	0.447	0.0119
Ti : Si	0.0071	0.0021

Table 5.5 A - element ratios for two theoretical, stoichiometric, bytownite feldspars.

B - average element ratios of the analysed clinopyroxenes and orthopyroxenes from the mafic gabbros at the base of the lower zone of the anorthosite sequence.

** total iron calculated as FeO

members in olivine and the pyroxenes, the Fe+Mg : Si ratios for those minerals can be calculated thus:-

		Fe + Mg : Si
olivine	Mg_2SiO_4 - Fe_2SiO_4	- 2.0
orthopyroxene	$Mg_2Si_2O_6$ - Fe_2SiO_6	- 1.0
Clinopyroxene	$CaMgSi_2O_6$ - $CaFeSi_2O_6$	- 0.5

The Fe + Mg : Si ratio for the trend 2 rocks is compatable with the fractionation of clinopyroxene. The theoretical value of 0.50 for the clinopyroxene compares to an average value of 0.506 for the analysed clinopyroxenes (Table 5.5) from the trend 2 rocks.

A comparison of the MgO : SiO_2 potash ratio of the trend 2 rocks and the calculated Mg : Si ratio of the analysed clinopyroxenes (Table 5.5) from these rocks, reveals a considerable discrepancy, suggesting a significant difference in the composition of the fractionating clinopyroxene and the analysed modal clinopyroxene. The Mn : SiO_2 potash ratio (fig. 5.15) for the trend 2 rocks is also at variance with the Mn : Si element ratio for the analysed clinopyroxenes. The theoretical fractionating clinopyroxene must have had a higher iron and manganese content and a complementary lower magnesium content than that suggested by the analyses of the modal clinopyroxenes from these rocks. The TiO_2 : SiO_2 potash ratio diagram (fig. 5.16) shows a good correlation between the slope for the trend 2, mafic gabbros, and the Ti : Si element ratio for the analysed clinopyroxenes.
A comparison of the element ratios and compositions of the theoretical fractionating clinopyroxene and the analysed

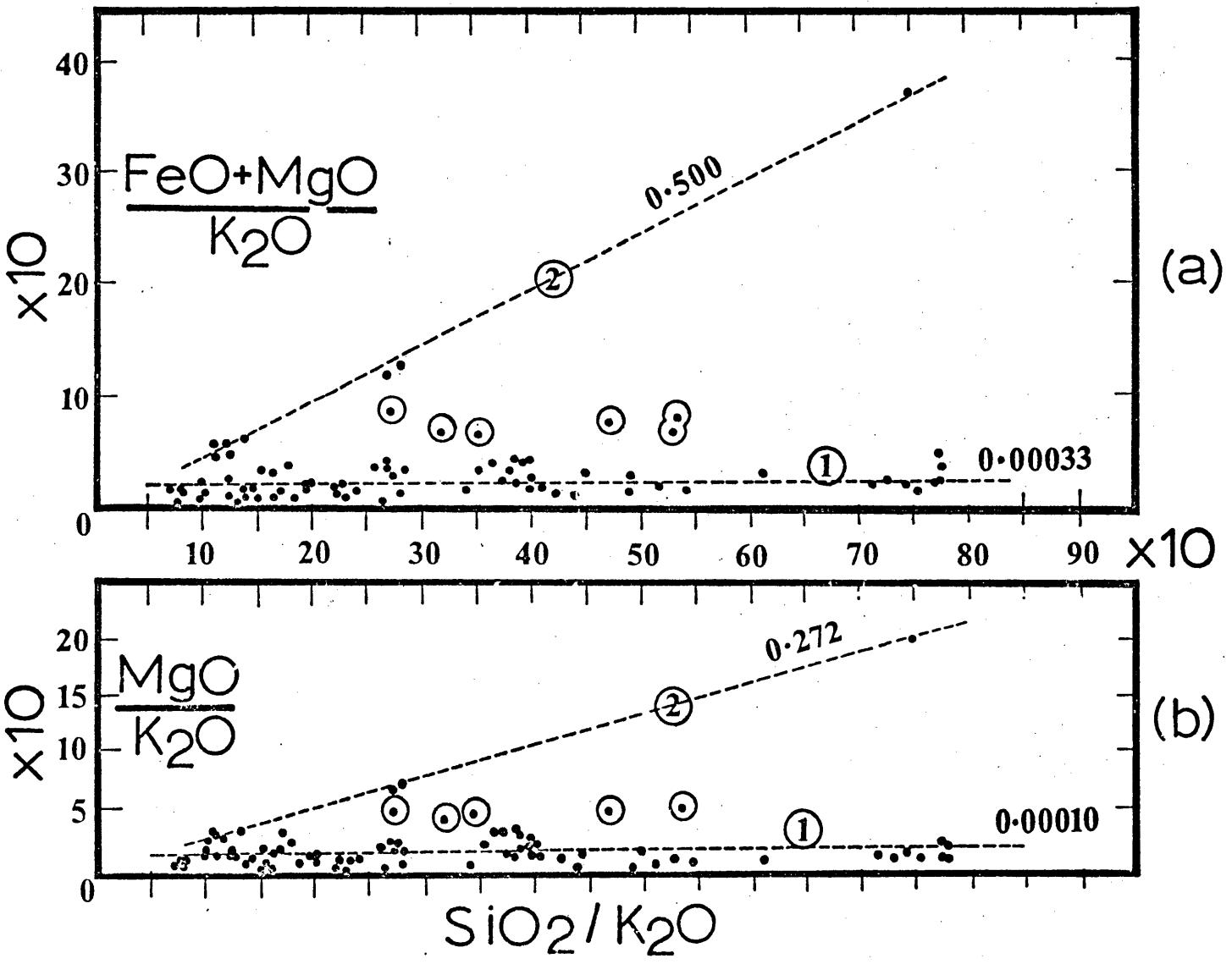


fig. 5.14 (a) FeO + MgO : SiO_2 and (b) MgO : SiO_2 potash ratio diagrams (molecular) for all the rocks of the anorthosite sequence. The circled points, on each diagram, were not included in the regression analyses. FeO = total iron calculated as FeO.

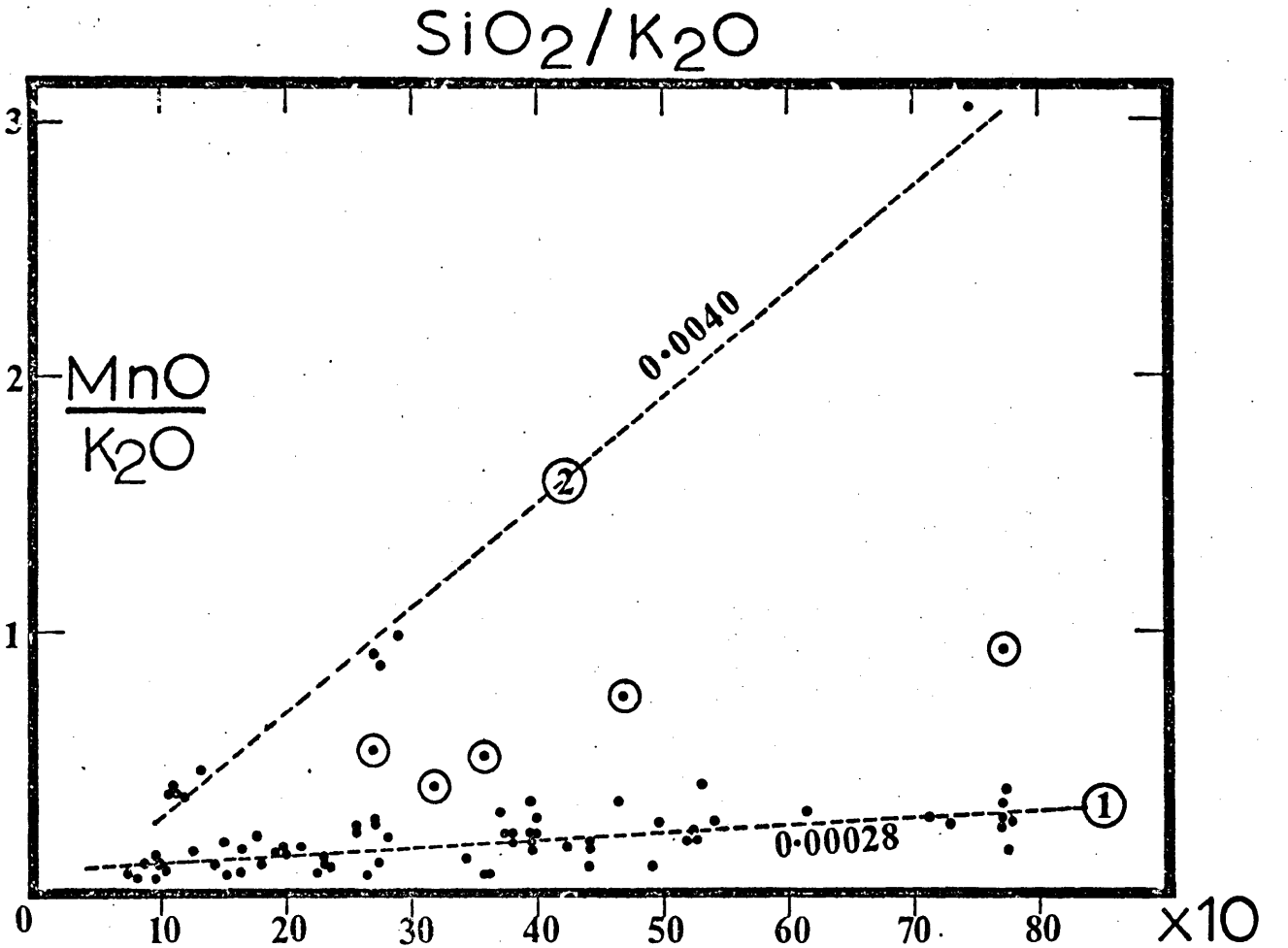


fig. 5.15 MnO : SiO_2 potash ratio diagram (molecular) for all the rocks from the anorthosite sequence. The circled points were not included in the regression analysis.

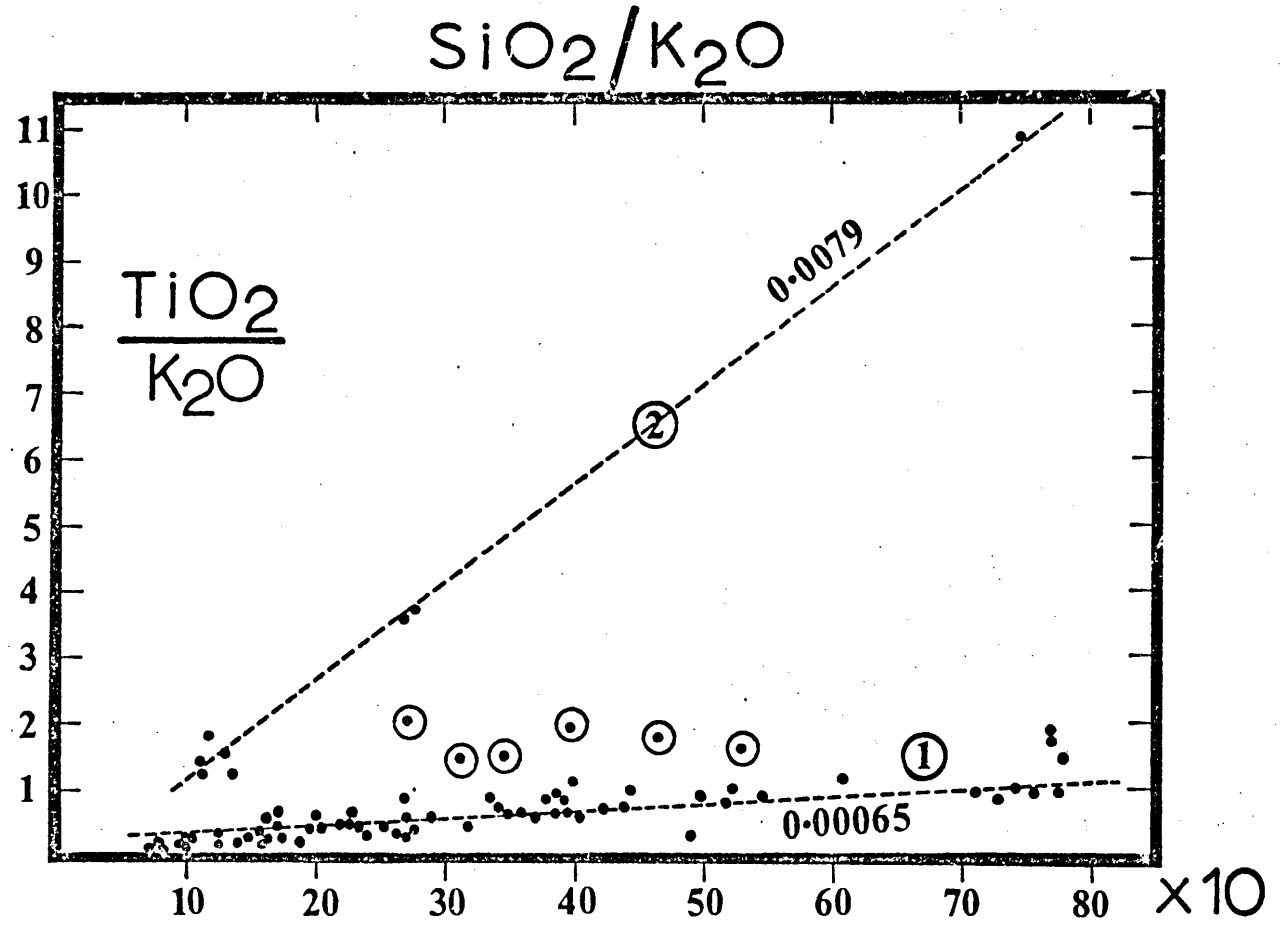


fig. 5.16 TiO_2 : SiO_2 potash diagram (molecular) for all the rocks from the anorthosite sequence. The circled points were not included in the regression analysis.

modal clinopyroxene is shown below:-

	Element ratios for fractionating clinopyroxene (obtained from Pearce variation diagrams)	Element ratios for analysed clinopyroxene (average of 5 analyses)
Mg : Si	0.272	0.380
Fe : Si	0.228	0.126
Fe+Mg : Si	0.500	0.506
Mn : Si	0.0040	0.00169
Ti : Si	0.0071	0.0079
	$En_{27}\ Fs_{23}\ (Wo_{50})$	$En_{38}\ Fs_{13}\ (Wo_{49})$

Finally the Al: Si and Na : Si oxide distribution patterns, for all of the rocks of the anorthosite body, will be considered using K_2O as the constant parameter. Both of these diagrams (figs. 5.17 and 5.18) show two distinct trends. Trend 1 again includes those rocks with greater than 80% normative feldspar and can be explained solely in terms of plagioclase fractionation - compare to fig. 5.12 a and b. However, the slope for the mafic gabbros, trend 2, is too high in both diagrams to be explained by the fractionation of clinopyroxene alone. The most likely explanation for this would involve the simultaneous fractionation of clinopyroxene and plagioclase feldspar.

The chemical variations displayed by the anorthosites can, for the most part, be explained solely by the fractionation of a bytownite feldspar (of composition An_{71}). However, the chemistry of the mafic gabbro horizons from the base of the anorthosite sequence indicates the simultaneous fractionation of both clinopyroxene (of composition En_{27}

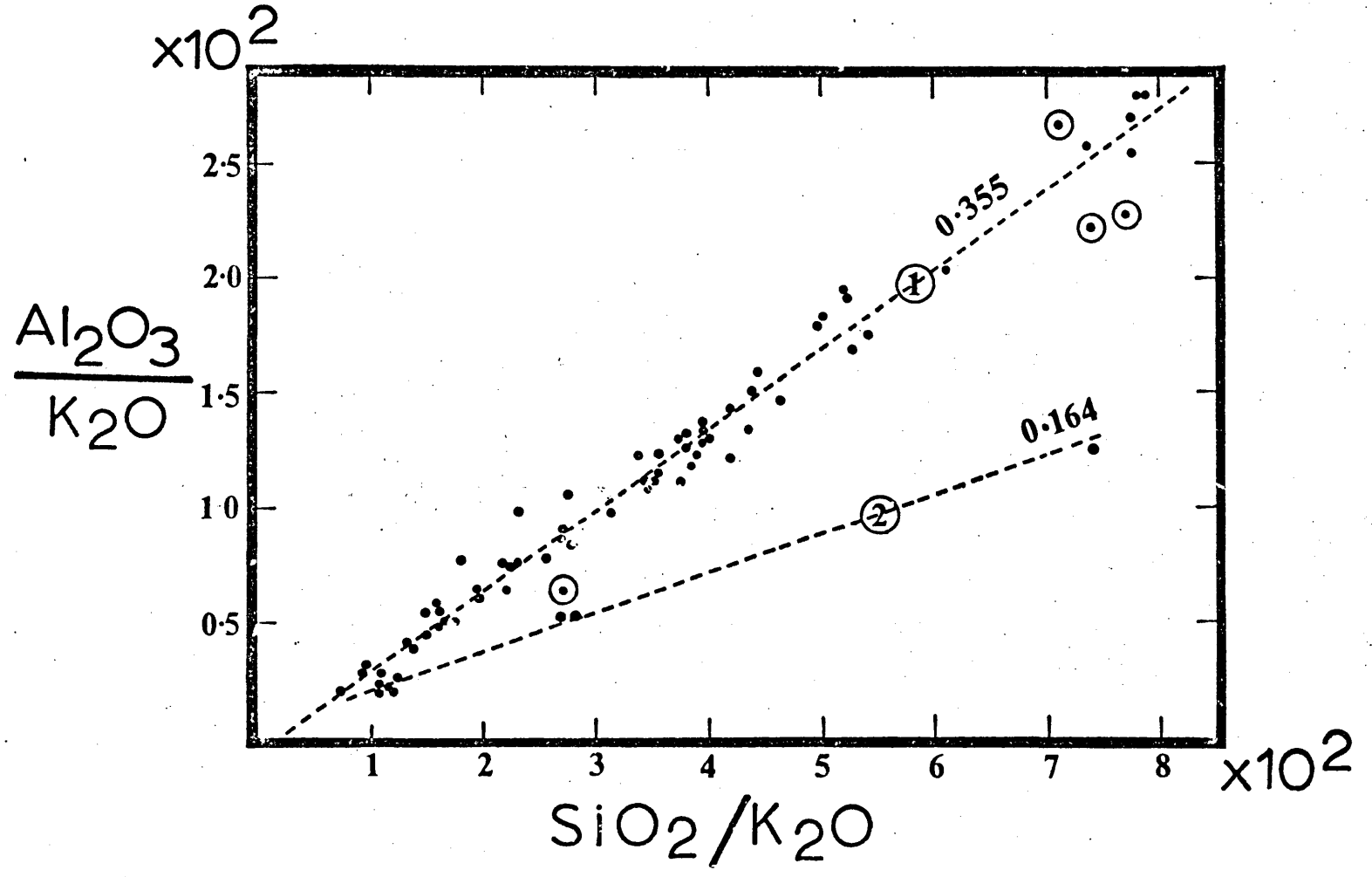


fig. 5.17 Al_2O_3 : SiO_2 potash ratio diagram (molecular) for all the rocks from the anorthosite sequence. The circled points were not included in the regression analysis.

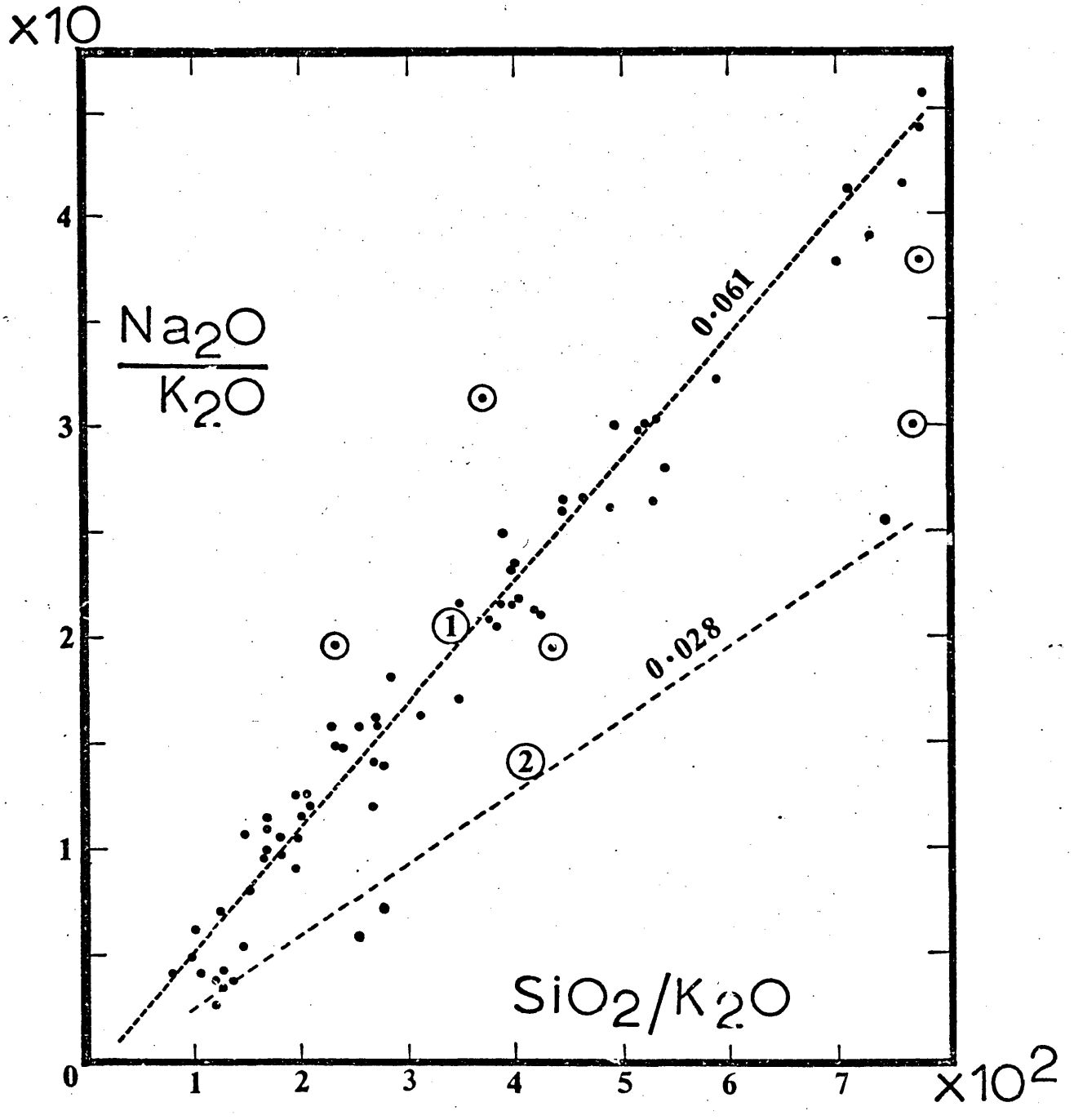


fig. 5.18 Na_2O : SiO_2 potash ratio diagram (molecular) for all the rocks from the anorthosite sequence. The circled points were not included in the regression analysis.

Fs_{23} Wo_{50}) and plagioclase feldspar.

The chemical consequences of plagioclase fractionation are quite definite and can, in fact, be calculated. Beginning with a set weight (or volume) of parental magma, various amounts of plagioclase can either be subtracted or added to simulate the various stages of fractionation. The resulting liquid (with or without the crystals) can be recalculated to 100%, to enable a direct comparison with the available data.

To illustrate this discussion the rock analyses from unit 3 at the base of the lower zone of the anorthosite sequence will be considered. The composition of the parental liquid for the rocks of this unit is taken to approach that of the gabbro (sample no. A13) at the base of this unit. The composition of liquids produced by the progressive fractionation and removal of plagioclase (An_{71}) crystals, from this parent magma, are shown in Table 5.6. The chemical variations produced by the addition of plagioclase crystals, to the parent magma - as would be the case in a plagioclase cumulate rock - are considered in Table 5.7.

The theoretical variations in absolute amounts of CaO and SiO_2 during fractionation of plagioclase are shown, using FeO as a constant parameter, in fig. 5.19. This diagram can be compared to fig. 5.20a, which shows the variation in absolute amounts of CaO and SiO_2 in unit 3 from the lower zone of the anorthosite sequence. The analysis A13 is taken to be the parent magma from which the rocks of this unit where derived. This rock has been described as a gabbro on the basis of its modal mafic index. However, it has already been pointed out that much of the original plagioclase feldspar of this rock has been consumed in the formation of new mafic minerals during the high grade granulite facies

A. Fractionation of Plagioclase (An_{71})

	Parent Magma (1000gms)	Amounts Subtracted	Resulting Amounts	Wt%	Mol. Prop.	Iron Ratio
STAGE 1						
SiO_2	508.46	-50.59	457.87	50.87	.84656	12.752
TiO_2	1.10		1.10	0.12	.00150	-
Al_2O_3	251.93	-31.65	220.28	24.48	.24014	3.617
Fe_2O_3	11.42		11.42	1.27	.00795	-
FeO	42.97		42.97	4.77	.06639	-
MnO	0.80		0.80	0.09	.00126	-
MgO	40.67		40.67	4.52	.11210	-
CaO	99.87	-14.31	85.56	9.51	.16958	2.554
Na_2O	34.46	- 3.37	31.09	3.45	.05566	0.838
K_2O	8.30	- 0.084	8.22	0.91	.00966	0.146
	999.99		899.98	99.99		
STAGE 2						
SiO_2	508.46	-101.18	407.28	50.91	.84722	11.336
TiO_2	1.10		1.10	0.14	.00175	-
Al_2O_3	251.93	-63.30	188.63	23.58	.23131	3.095
Fe_2O_3	11.42		11.42	1.43	.00895	-
FeO	42.97		42.97	5.37	.07474	-
MnO	0.80		0.80	0.10	.00141	-
MgO	40.67		40.67	5.08	.12599	-
CaO	99.87	-28.62	71.25	8.91	.15888	2.126
Na_2O	34.46	- 6.74	27.72	3.46	.05582	0.747
K_2O	8.30	- 0.168	8.13	1.02	.01082	0.145
	999.99		799.97	100.00		

Table 5.6 Chemical variations due to fractionation and removal of plagioclase (An_{71}) crystals.

B. Fractionation of Plagioclase (An_{71})

	Parent Magma (1000gms)	Amounts Added	Resulting Amounts	Wt%	Mol. Prop.	Iron Ratio
STAGE 3						
SiO_2	508.46	+101.18	609.64	50.80	.84539	16.969
TiO_2	1.10		1.10	0.09	.00112	-
Al_2O_3	251.93	+ 63.30	315.23	26.27	.25770	5.173
Fe_2O_3	11.42		11.42	0.95	.00595	-
FeO	42.97		42.97	3.58	.04982	-
MnO	0.80		0.80	0.07	.00099	-
MgO	40.67		40.67	3.39	.08407	-
CaO	99.87	+ 28.62	128.49	10.71	.19097	3.833
Na_2O	34.46	+ 6.74	41.20	3.43	.05533	1.111
K_2O	8.30	+ 0.168	8.47	0.70	.00743	0.149
	999.99		1199.99	99.99		
STAGE 4						
SiO_2	508.46	+202.36	710.82	50.77	.84489	19.773
TiO_2	1.10		1.10	0.08	.00100	-
Al_2O_3	251.93	+126.60	378.53	27.04	.26525	6.207
Fe_2O_3	11.42		11.42	0.82	.00513	-
FeO	42.97		42.97	3.07	.04273	-
MnO	0.80		0.80	0.06	.00084	-
MgO	40.67		40.67	2.91	.07217	-
CaO	99.87	+ 57.24	157.11	11.22	.20007	4.682
Na_2O	34.46	+ 13.48	47.94	3.42	.05517	1.291
K_2O	8.30	+ 0.336	8.64	0.62	.00658	0.154
	999.99		1400.00	100.01		
STAGE 5						
SiO_2	508.46	+809.44	1317.90	50.69	.84356	36.741
TiO_2	1.10		1.10	0.04	.00050	-
Al_2O_3	251.93	+506.40	758.33	29.17	.28614	12.463
Fe_2O_3	11.42		11.42	0.44	.00275	-
FeO	42.97		42.97	1.65	.02296	-
MnO	0.80		0.80	0.03	.00042	-
MgO	40.67		40.67	1.56	.03869	-
CaO	99.87	+228.96	328.83	12.65	.22557	9.824
Na_2O	34.46	+ 53.92	88.38	3.40	.05485	2.389
K_2O	8.30	+ 1.344	9.64	0.37	.00392	0.171
	999.99		2600.04	100.00		

Table 5.7. Chemical variations due to the fractionation and accumulation of plagioclase (An_{71}) feldspar - plagioclase cumulate rocks.

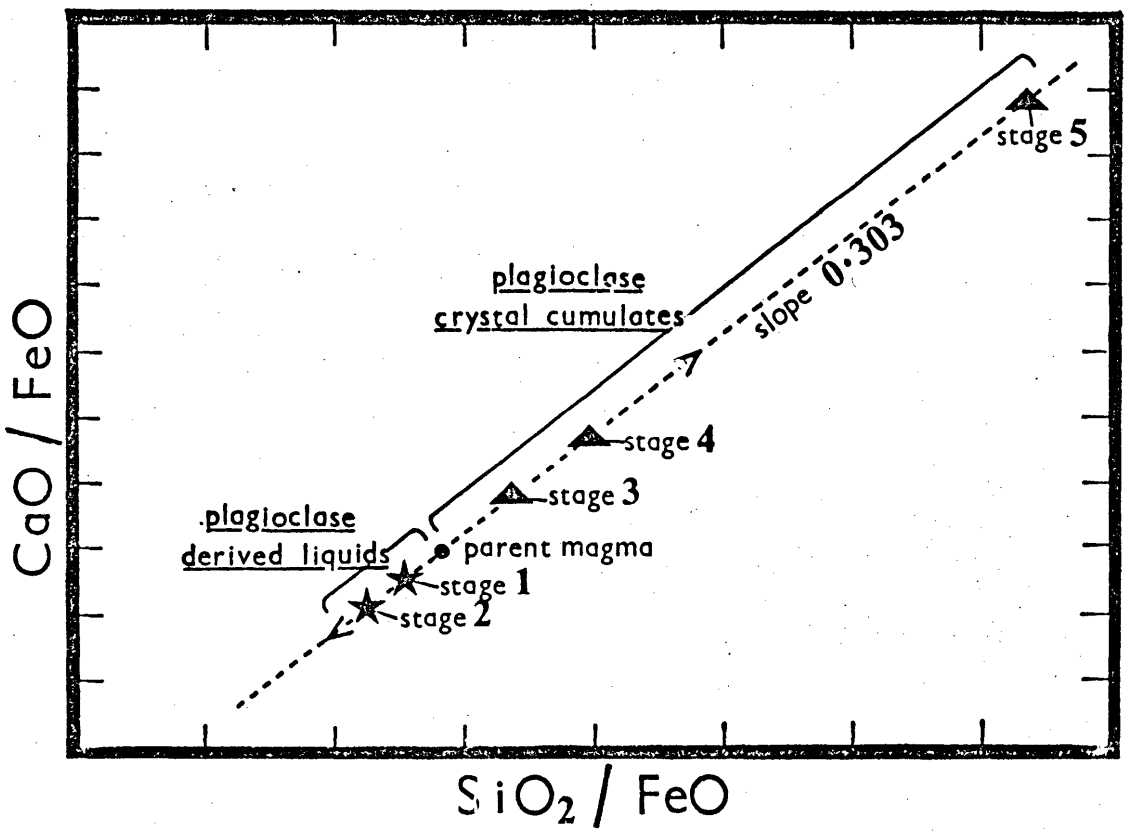


fig. 5.19 The theoretical variation of absolute amounts of CaO and SiO_2 during fractionation of plagioclase feldspar from the liquid pm (- the parent magma). ▲- indicates a cumulate rock. FeO is used as a constant parameter.

metamorphism, and the original mafic index of this rock was considerably lower than the modal mafic index. For our present purposes it will be of greater use if the rocks of this unit were considered in terms of their normative mafic index. The parent magma, in this case, can be more realistically referred to as a gabbroic anorthosite. The chemistry of those rocks which occur above the gabbro (previously referred to as a mafic gabbro on the basis of its modal mafic index) horizon in this unit, is consistant with them being plagioclase crystal cumulates. The fact that these rocks (sample nos. A16, 17, 18 and 19) plot sequentially must represent a progressive increase in the amount of cumulate plagioclase crystals upwards, towards the top of the unit.

Below the gabbro horizon the rock analyses represent liquids produced by the fractionation and removal of plagioclase feldspar. Again these rocks (sample nos. A14 and A15) plot sequentially, which must reflect the crystallization of liquids which are progressively depleted in the components which constitute the plagioclase feldspar. The progressive depletion of these oxides leads to a concentration of the remaining oxides (FeO, Fe_2O_3, MnO and MgO). This process culminates in the gabbro horizon, which is marked by the fractionation and accumulation of an iron-rich clinopyroxene.

This interpretation of the rocks from unit 3 from the lower zone anorthosites is summarized graphically in fig. 5.20b. It is not proposed to enter into a discussion on the processes which might have controlled the formation of such a rock sequence, but it is tempting to suggest that "plagioclase flotation" may have played a dominant role.

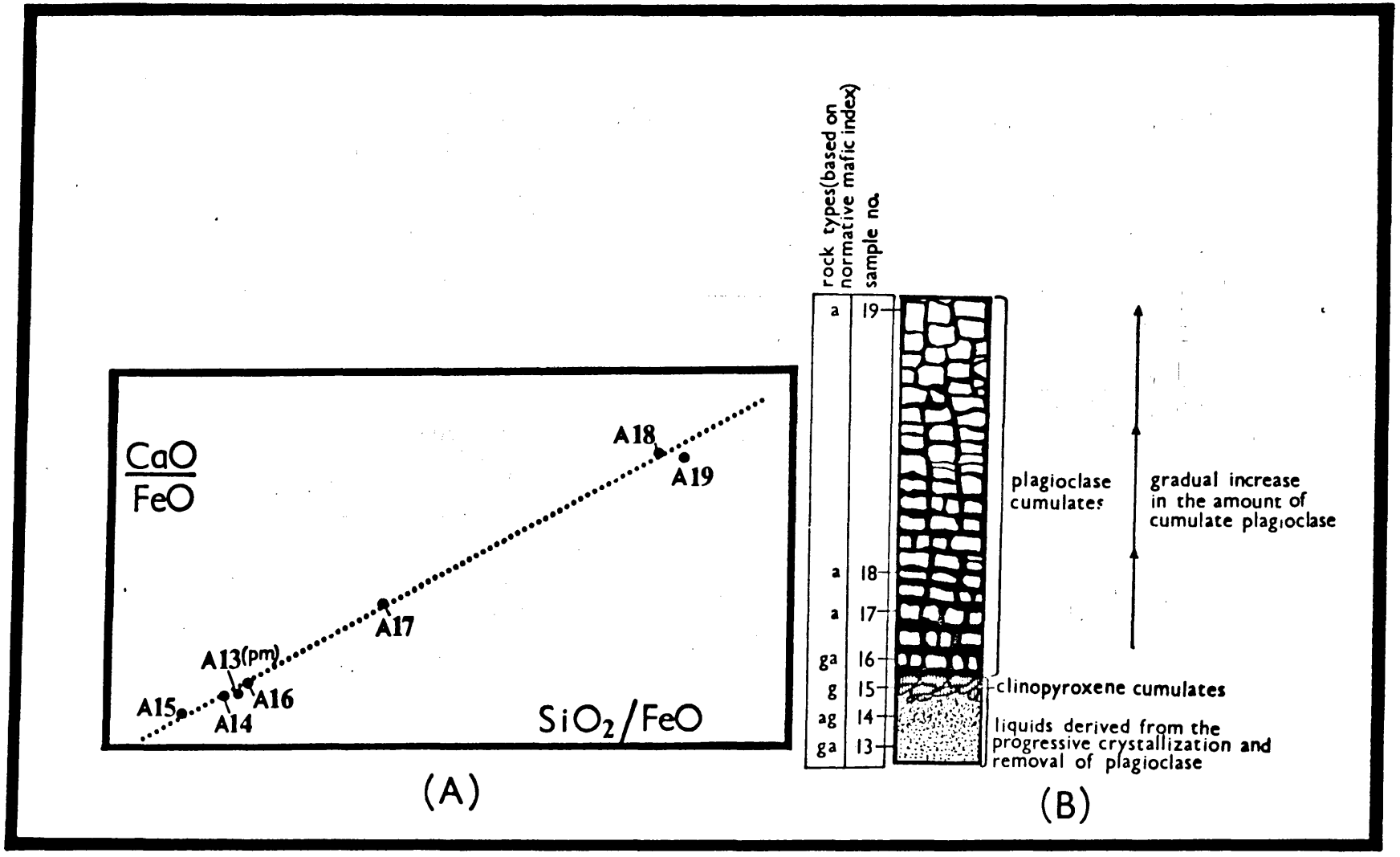


fig. 5.20 A - The variation in absolute amounts of CaO and SiO_2 in unit 3 from the base of the lower zone of the anorthosite sequence. FeO is used as a constant parameter.
B - An interpretation of the rock types from unit 3.
a - anorthosite; ga - gabbroic anorthosite; ag - anorthositic gabbro and g - gabbro

Whatever this process involved, the fact that it was cyclic in nature is beyond doubt. The differentiation pattern shown by the figured example is repeated over and over again throughout the anorthosite body. With increasing structural height, the plagioclase cumulate portion of this sequence is of progressively greater importance and size. Clinopyroxene cumulates are restricted in occurrence to certain thin horizons at the base of the anorthosite sequence.

The banded ultramafites and mafic gabbros from the gabbroic rim of the anorthosite complex are now considered using this technique. K_2O again is used as a constant factor to study the phases controlling the crystallization of these rocks. As these rocks are more basic than the rocks of the anorthosite sequence (indicated by higher normative colour indicies) it is now reasonable to expect the appearance of a fractionating ferro-magnesian phase. Inspection of the MgO : SiO_2 potash ratio plot (fig. 5.21) confirms this suspicion. The positive slope of 0.393 for the regression line in this diagram is compatible with the Mg : Si ratio of the analysed clinopyroxenes from these rocks (Table 5.8). The variation in the absolute amounts of MgO and SiO_2, in these rocks, can thus be satisfactorily explained by the fractionation of a calcium-rich pyroxene. The FeO + MgO : SiO_2 and TiO_2 : SiO_2 potash ratio plots (figs. 5.22 and 5.23) show two distinct trends. The first trend (trend 1), which comprises the ultramafite rock types, shows an FeO + MgO : SiO_2 ratio of 0.602 and a TiO_2 : SiO_2 ratio of 0.034. The second trend (trend 2), which comprises the mafic gabbros, shows both a lower FeO + MgO : SiO_2 ratio - 0.515 - and a lower TiO_2 : SiO_2 ratio - 0.007. The ratios for the second trend compare favourably with similar ratios

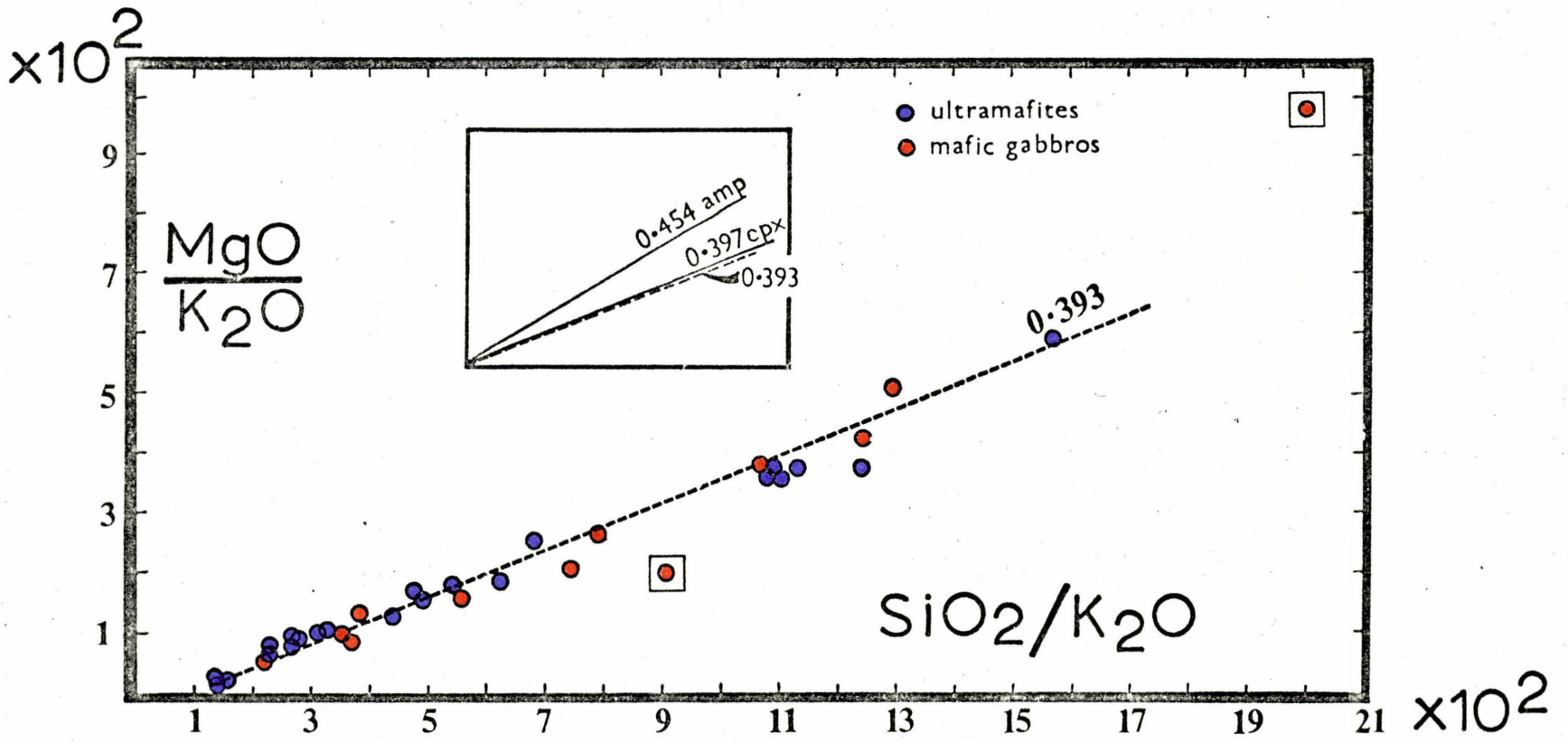


fig. 5.21 MgO : SiO_2 potash ratio diagram (molecular) for the banded ultramafites and mafic gabbros from the gabbroic rim of the anorthosite complex. The boxed points were not included in the regression analysis.

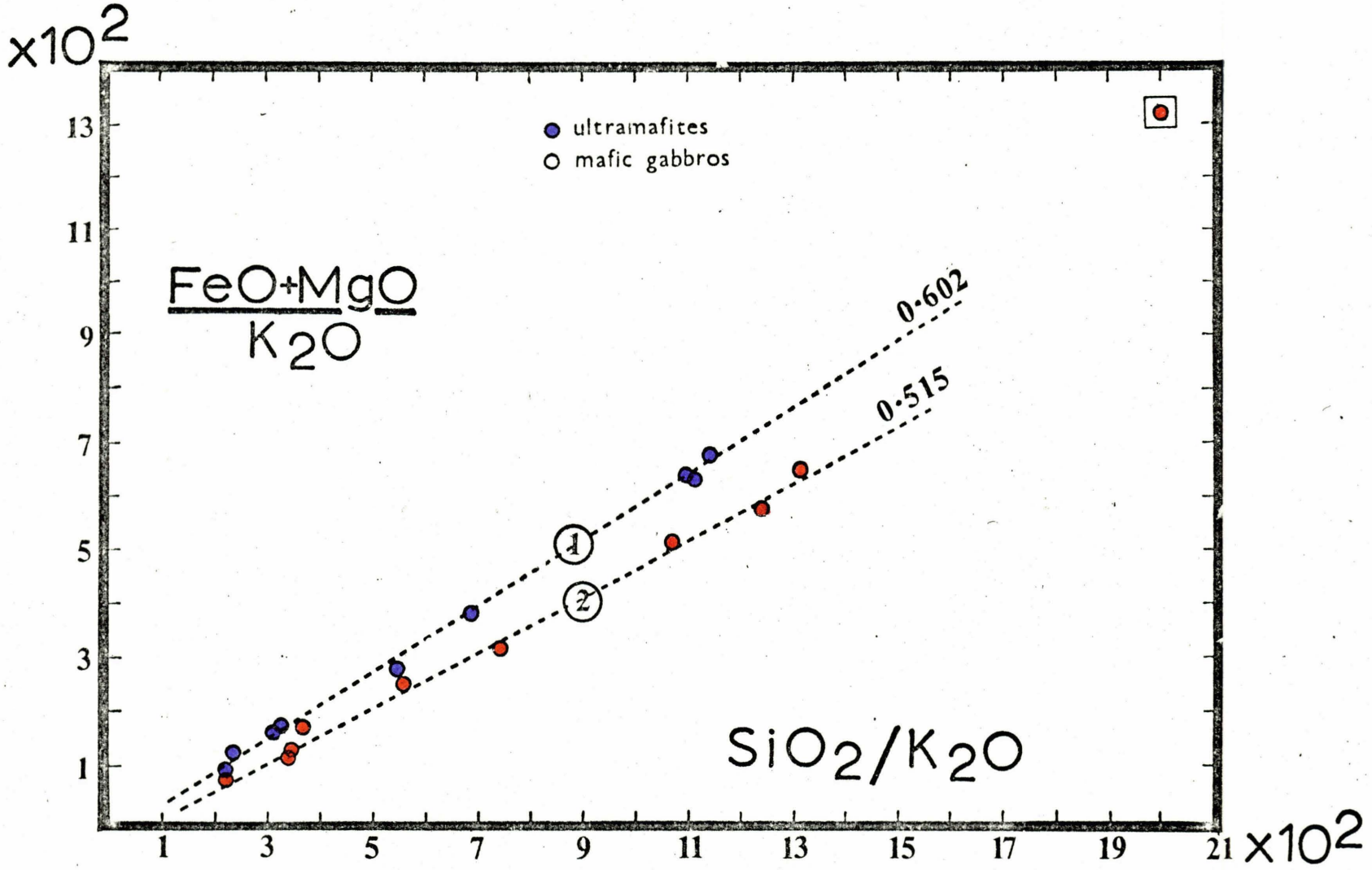


fig. 5.22 FeO + MgO : SiO_2 potash ratio diagram (molecular) for the banded ultramafites and mafic gabbros from the gabbroic rim of the anorthosite complex. The boxed point was not included in the regression analysis.

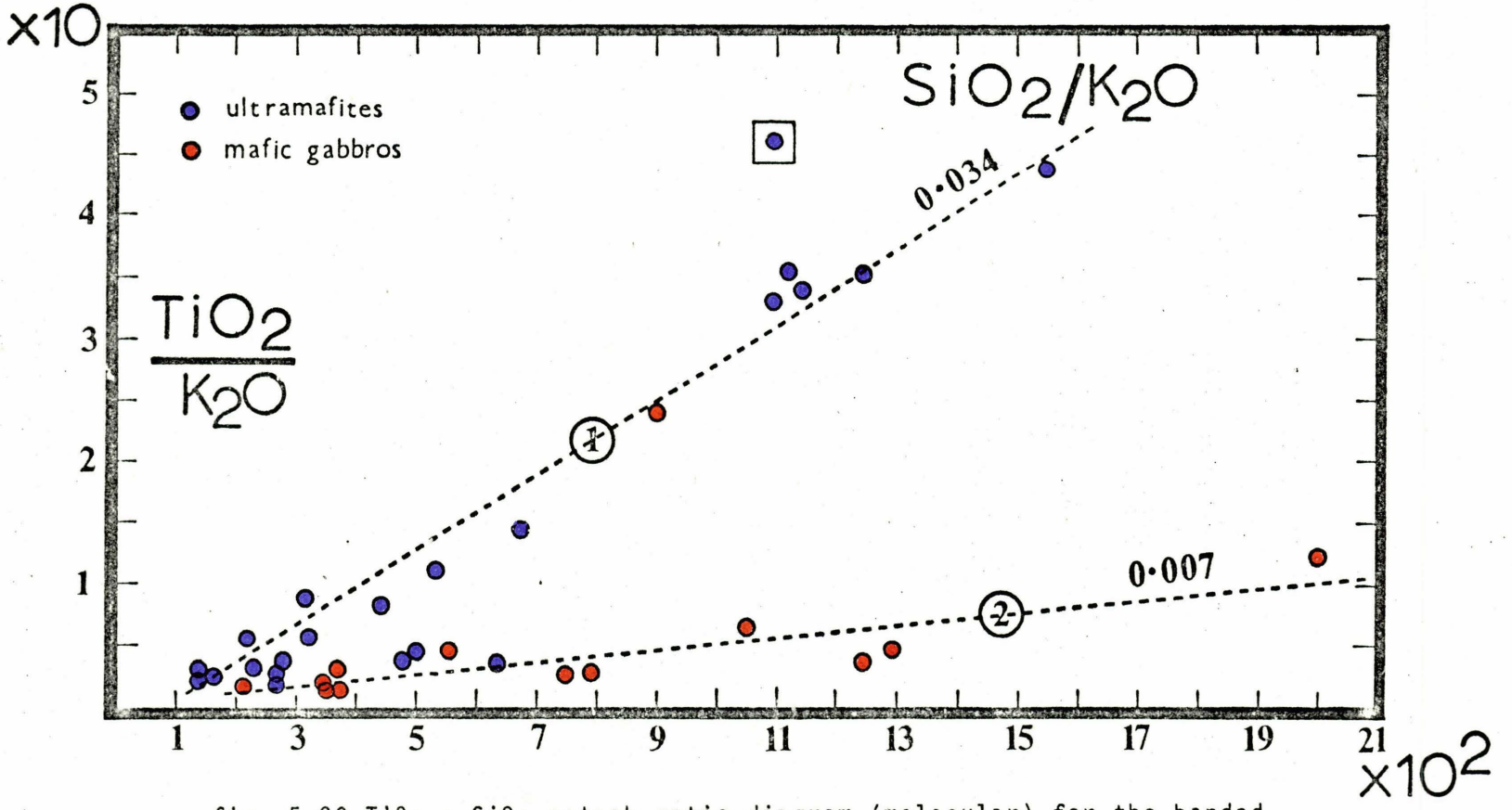


fig. 5.23 TiO_2 : SiO_2 potash ratio diagram (molecular) for the banded ultramafites and mafic gabbros from the gabbroic rim of the anorthosite complex. The boxed point was not included in the regression analysis.

calculated for the analysed clinopyroxenes (Table 5.8) - confirming the evidence for a fractionating calcium-rich pyroxene. However, the first trend needs some further investigation. The Fe + Mg : Si ratio of the clinopyroxene, on its own, is insufficient to produce the observed slope for the ultramafites (trend 1) in fig. 5.22. It is therefore necessary to introduce another fractionating iron-rich mineral which will not seriously affect the MgO : SiO_2 distribution in these rocks. It should also be borne in mind that this iron-rich mineral phase should also have an appreciable TiO_2 component - viz the much steeper slope shown by the ultramafites in the TiO_2 : SiO_2 potash ratio diagram (trend 1). Ilmenite is the only feasible choice. As the Fe + Mg : Si ratio (and the Ti : Si ratio) in ilmenite is infinitely large, only small amounts of this mineral would be sufficient to raise the FeO + MgO : SiO_2 and TiO_2 : SiO_2 ratios in the ultramafite rock types.

In view of the high iron content of most of the ultramafites and mafic gabbros only those analyses where the oxidation state of the iron has been determined are plotted in fig. 5.22.

If the relationship between absolute amounts of CaO and SiO_2 is examined (fig. 5.24), the observed positive slope to this distribution is slightly lower than might have been expected from a consideration of the Ca : Si ratio of the clinopyroxene. This may suggest that either:-

a) the fractionating clinopyroxene was less calcic than the analysed modal clinopyroxenes - which are of metamorphic origin.

or b) another, less calcic, phase may be fractionating. If, for example, two calcic minerals crystallized

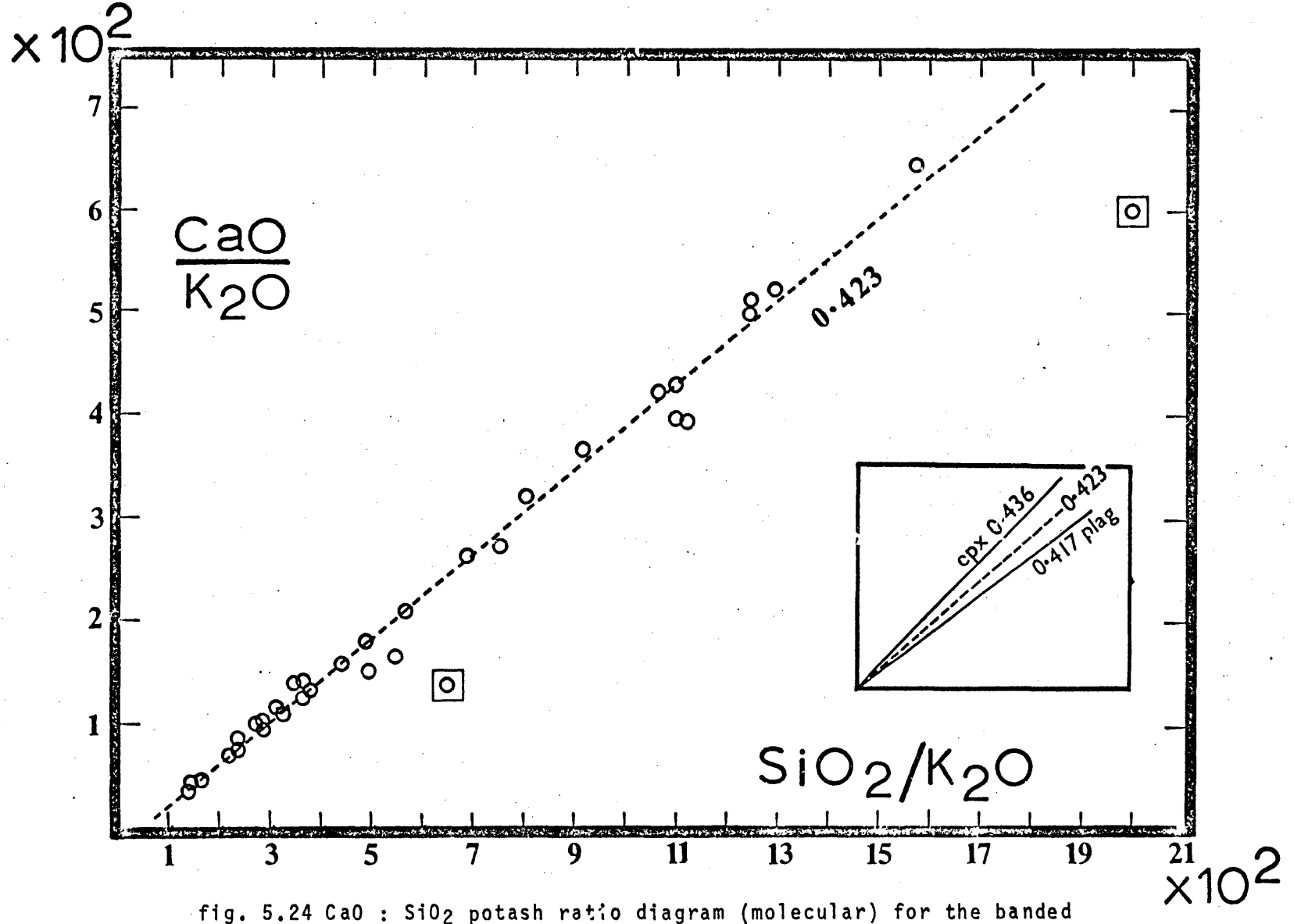


fig. 5.24 CaO : SiO_2 potash ratio diagram (molecular) for the banded ultramafites and mafic gabbros from the gabbroic rim of the anorthosite complex. The boxed points were not included in the regression analysis.

	Clinopyroxene (average of ten analyses)	Plagioclase Feldspar (An_{85})
Ca : Si	0.436	0.417
Al : Si	0.0757	0.4418
Na : Si	0.0159	0.0361
Mg : Si	0.397	-
Fe+Mg : Si	0.541*	-
Ti : Si	0.0069	-

Table 5.8 Banded ultramafites and mafic gabbros from the gabbroic rim of the anorthosite complex. Average element ratios for analysed clinopyroxenes and plagioclase feldspar.

* This value markedly exceeds the theoretical value (0.50) for a clinopyroxene. The iron value for the analysed clinopyroxenes is expressed as total iron as FeO. Although Fe_2O_3 values in the clinopyroxenes are probably low, even such a small value for Fe_2O_3 would effectively lower the value for the Fe^{2+} + Mg : Si ratio and bring this more in line with the theoretical value.

simultaneously, both would extract calcium from the liquid but at differing rates. The resultant slope of the regression line for the rock-data, would thus have a value intermediate between the ratios of these two oxides in the two calcic minerals involved.

The exact gradient of the slope would be dependent on the relative amounts of each phase crystallizing. Before proceeding further with this discussion, it will be of value to consider two more diagrams which demonstrate the relationship between Na_2O/K_2O : SiO_2/K_2O (fig. 5.25) and Al_2O_3/K_2O : SiO_2/K_2O (fig. 5.26). The gradients of the positive distribution slopes, in these diagrams, are clearly incompatible with what one would expect if clinopyroxene (and in the case of the ultramafites - ilmenite) were the only fractionating phase(s). The slopes of the lines in figs. 5.25 and 5.26 cannot be attributed to the fractionation of a single mineral phase but are compatible with the fractionation of clinopyroxene accompanied by a calcic plagioclase feldspar. The composition of such a plagioclase feldspar is taken to be approximately An_{85} - the average normative feldspar composition for these rocks. The average Ca : Si, Al : Si and Na : Si ratios for the analysed clinopyroxenes and an analysed bytownite (An_{85}) from these rocks, are given in Table 5.8. For the Al_2O_3/K_2O : SiO_2/K_2O plot, the slope of 0.264 is intermediate between the Al : Si ratio of the clinopyroxene (0.076) and the bytownite (0.442). The same is true for the Na_2O/K_2O : SiO_2/K_2O plot.

If the CaO : SiO_2 potash diagram is now re-examined, the reason for the slight discrepancy between the slope

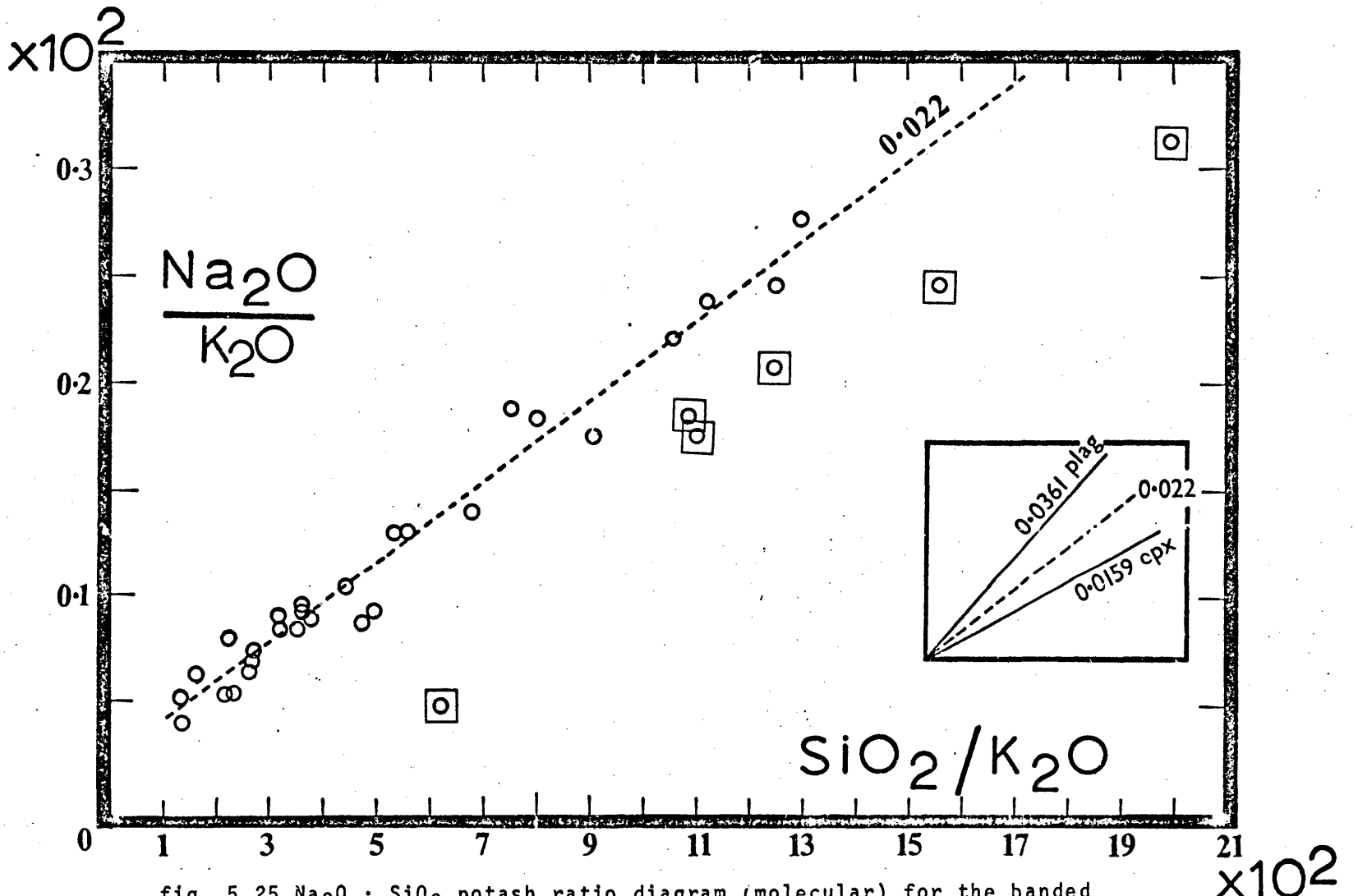


fig. 5.25 Na_2O : SiO_2 potash ratio diagram (molecular) for the banded ultramafites and mafic gabbros from the gabbroic rim of the anorthosite complex. The boxed points were not included in the regression analysis.

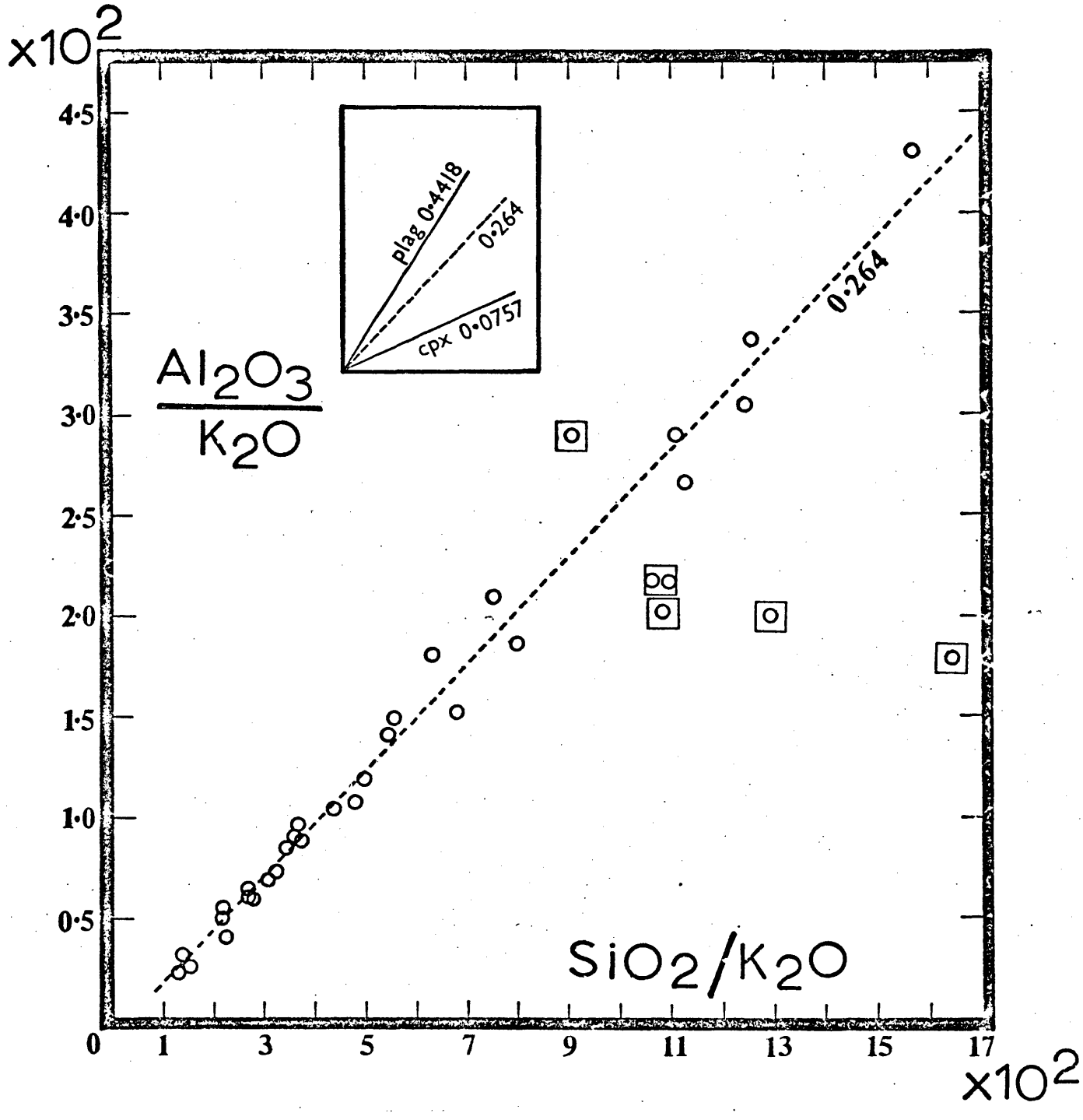


fig. 5.26 Al_2O_3 : SiO_2 potash ratio diagram (molecular) for the banded ultramafites and mafic gabbros from the gabbroic rim of the anorthosite complex. The boxed points were not included in the regression analysis.

of the line in this plot and the Ca : Si ratio of the clinopyroxene becomes apparent, and the second of the two alternative explanations for this discrepancy appears to be substantiated.

In summary, it can be said that the crystallization of the ultramafites of this sequence was controlled by the fractionation of clinopyroxene, plagioclase feldspar (bytownite An_{85}) and small amounts of ilmenite. On the other hand crystallization of the mafic gabbros was controlled by only two phases - clinopyroxene and plagioclase feldspar. There seems little or no evidence to postulate changes in the composition of the main fractionating phases with continued differentiation.

By applying a crude form of vector analysis to the data from the CaO : SiO_2 potash ratio diagram (fig. 5.24), it is possible to make a rough estimate of the original relative proportions of the two main fractionating minerals, clinopyroxene and plagioclase feldspar. The simultaneous crystallization of clinopyroxene and plagioclase in a ratio of 1 : 3 would result in the observed CaO : SiO_2 ratio for the whole rock data from both the ultramafites and mafic gabbros.

In contrast to the mafic gabbros from the anorthosite sequence, the composition of the modal clinopyroxene in these rocks reflects the composition of the theoretical fractionating clinopyroxene.

	Element ratios for fractionating clinopyroxene (obtained from Pearce variation diagrams	Element ratios for analysed clinopyroxene (averaged of 10 analyses)
Mg : Si	0.393	0.397
Fe : Si	0.122	0.144
Fe+Mg : Si	0.515	0.541
Ti : Si	0.007	0.0069
	$En_{39}\ Fs_{12}\ (Wo_{49})$	$En_{40}\ Fs_{14}\ (Wo_{46})$

5.6 General Chemistry of the South Harris Igneous Rock Suite

Anorthosites invariably show a close spatial relationship with a variety of rocks of intermediate to silic composition. The South Harris anorthosite complex is no exception.

The rocks associated with the anorthosite complex are plotted on an AFM (Na_2O + K_2O - total iron as FeO - MgO) weight percent triangular diagram (fig.5.27). The compositional fields of the rocks of the anorthosite complex are also indicated on this diagram. Similar diagrams, although with less data points, have been constructed by Dearnely (1959, 1963) and Palmer (1971). There is no doubt that many of the South Harris Igneous rocks are subalkaline, but up to now there has been no general agreement as to the chemical affinity of these rocks. Dearnley concluded that they were of tholeiitic affinity, and proposed that South Harris was an active plutonic centre during the intrusion of the tholeiitic "Scourie Dykes" - which are found throughout the Outer Hebrides and the Scottish mainland.

	Rock Types	Phases Controlling Crystallization
Gabbroic rim of anorthosite complex - the banded ultramafite/mafic gabbro sequence	Ultramafites	clinopyroxene ($En_{39}Fs_{12}$) + plagioclase feldspar (An_{85}) + ilmenite
	Mafic Gabbros	clinopyroxene ($En_{39}Fs_{12}$) + plagioclase feldspar (An_{85})
Anorthosites	Mafic Gabbro horizons from the lower zone of the anorthosite	clinopyroxene ($En_{27}Fs_{23}$) + plagioclase feldspar
	Remainder of anorthosite sequence	plagioclase feldspar (An_{71})

Table 5.9 Summary of phases controlling crystallization in the differentiated rock types of the anorthosite complex.

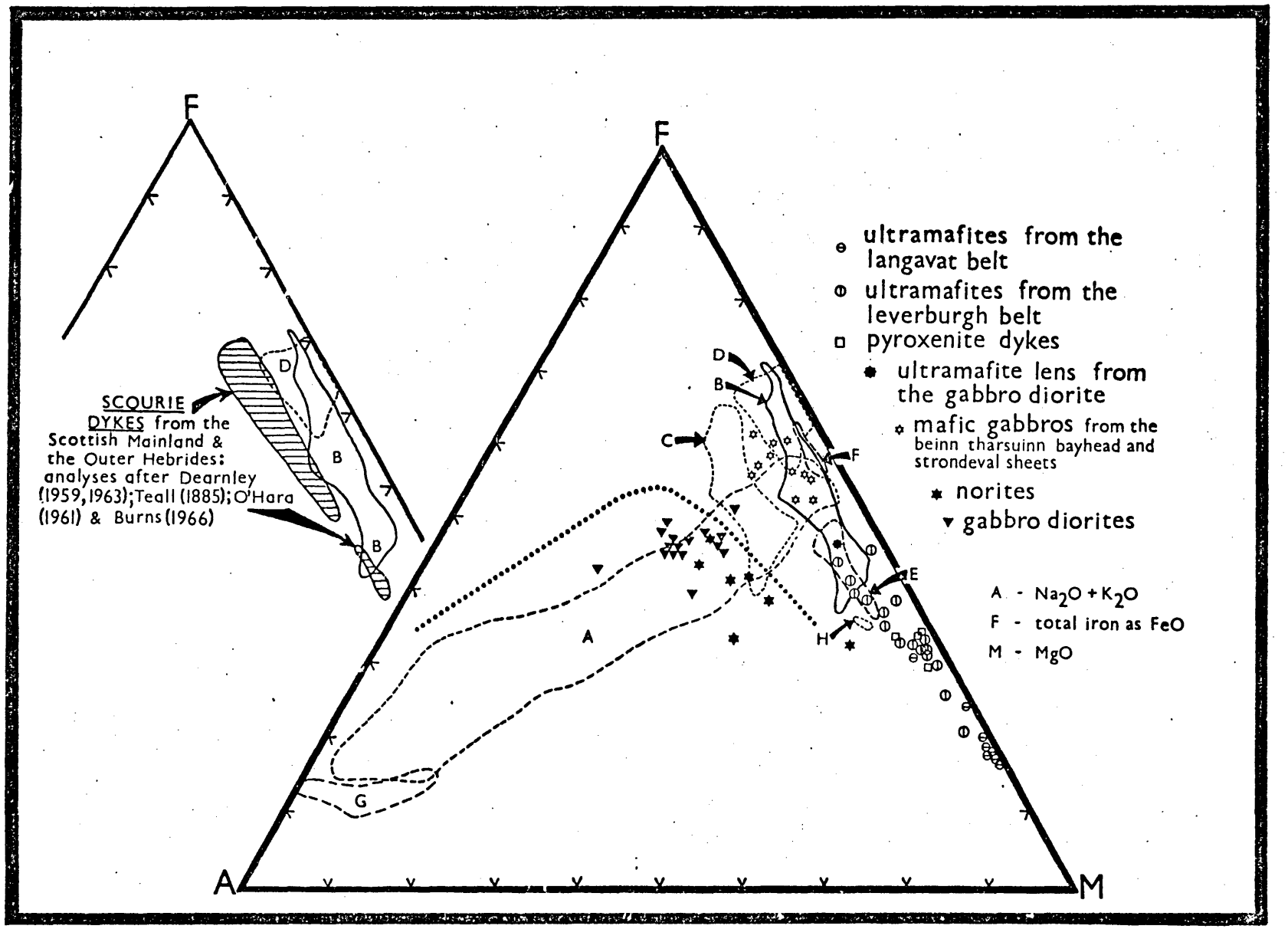


fig. 5.27 AFM projection for the rocks of the South Harris igneous suite. The compositional fields of the rocks from the anorthosite complex are indicated. (see fig. 5.1)

Palmer took the opposite view and regarded the anorthosite, norite and gabbro-diorite as calc-alkaline in affinity.

The AFM projection has come to be regarded as a simple technique for distinguishing calc-alkaline from tholeiitic suites. The dividing line used in fig. 5.27 is the line suggested by Irvine and Barager (1971) to separate tholeiitic (above) from calc-alkaline (below) suites. Special care must be exercised in the interpretation of such AFM diagrams when one is dealing with anorthositic rocks.

The vast majority of the analysed rocks from the South Harris anorthosite have been shown to be plagioclase crystal cumulates and, as such, will have a composition far removed from their original parent magma. A plagioclase cumulate will be selectively enriched in alkalis ($Na_2O + K_2O$) and Al_2O_3 relative to FeO and MgO. Thus, an analysis of a plagioclase cumulate rock will plot on an AFM projection somewhere along a line or curve which joins the alkali apex of the projection with the point at which the parent magma (for such a cumulate) would plot. A wholly plagioclase cumulate rock, of course, would plot at the alkali apex of the projection. To avoid any ambiguity in the interpretation of such projections, Emslie (1973) has suggested that all anorthositic rocks with Al_2O_3 contents greater than 20% should be omitted from the AFM diagram. However, in the case of the South Harris anorthosites this would mean the exclusion of those analyses which are thought to be representative of the parent magma composition. Also, although one can be reasonably sure of excluding most of the plagioclase cumulates by this method, it does not take into account those rocks which form from liquids

which have fractionated plagioclase feldspar (i.e. the plagioclase derived liquids). These liquids will be selectively depleted in alkalis and alumina, relative to iron and magnesia. To avoid any misinterpretation of the AFM projection, only those rocks from the anorthosite, which are thought to approximate in composition to the parent magma, are plotted on this projection (fig. 5.28). The eight plotted anorthosites all fall within the calc-alkaline field. The compositional field of the anorthosites overlaps those of the norite and gabbro-diorite which also fall within the calc-alkaline sector of the projection.

It is possible to recognise three distinct rock suites (fig. 5.28):-

1. An alkalic suite characterised by strong iron enrichment

   The rocks of the suite are undersaturated with respect to silica and contain between 10-20% normative olivine and up to 8% normative nepheline.

   This suite comprises:-

   a) the majority of the ultramafites found as lenses within the Leverburgh paragneisses.

   b) the mafic gabbros which form extensive sheets rimming the gabbro-diorite and norite.

   c) the banded ultramafites and mafic gabbros from the gabbroic rim of the anorthosite complex.

   d) the ultramafite and mafic gabbro minor intrusives within the anorthosite complex - the d_1 and d_2 dykes, the hornblendite lenses and dykes and the ultramafite intrusions associated with the brecciation along and adjacent to the margin of the anorthosite.

2. A highly aluminous calc-alkaline suite, which includes:-

   a) the gabbro diorite

   b) the norite

   c) the anorthosite (excluding its gabbroic rim).

3. A tholeiitic suite characterised by strong iron enrichment

   This suite includes all of those rock types referred

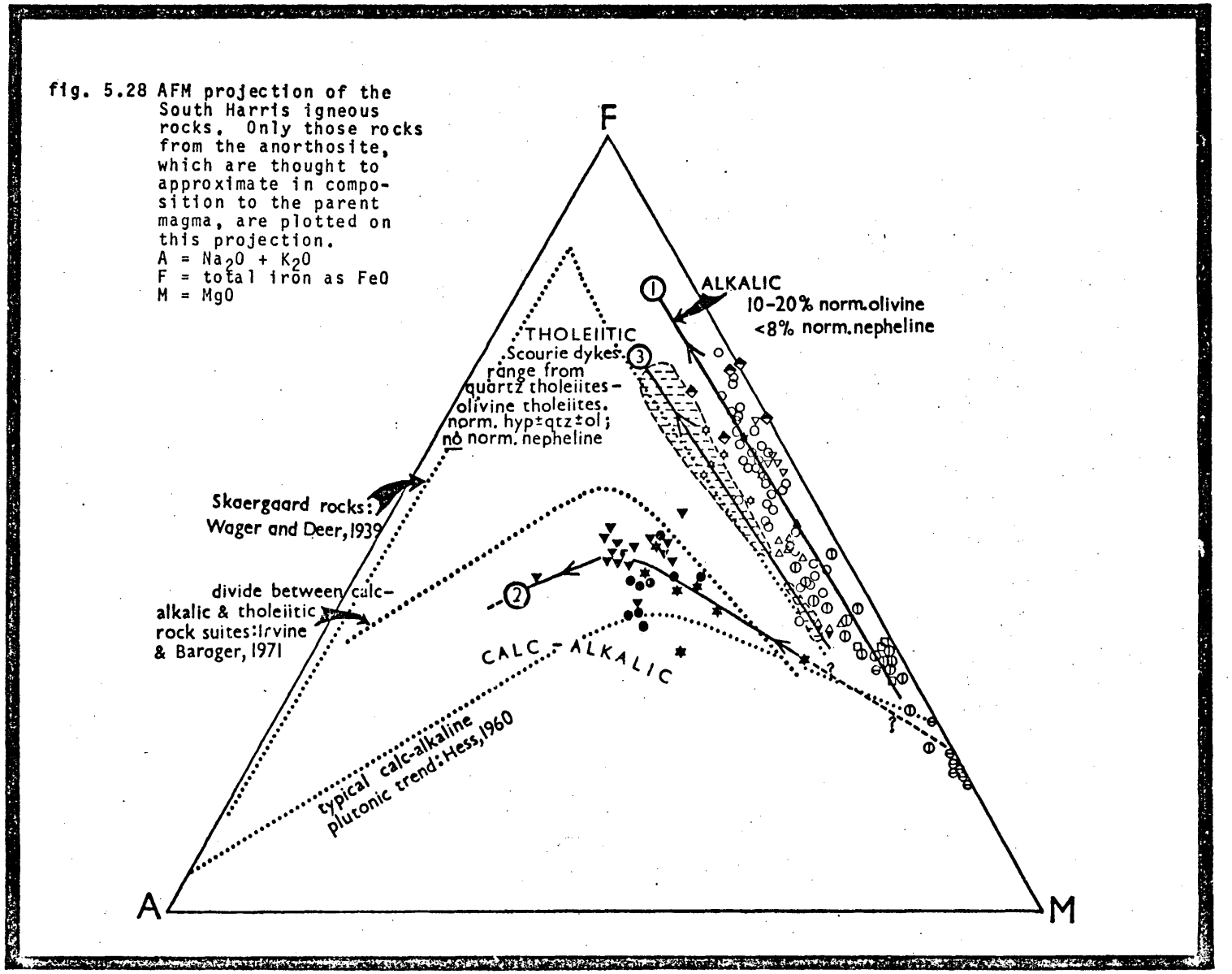


fig. 5.28 AFM projection of the South Harris igneous rocks. Only those rocks from the anorthosite, which are thought to approximate in composition to the parent magma, are plotted on this projection.
A = $Na_2O + K_2O$
F = total iron as FeO
M = MgO

to as "Scourie dykes".

Although no definite dykes of "Scourie dyke" type have been found in South Harris they occur abundantly throughout the remainder of the Outer Isles and on the Scottish mainland. The rocks of this suite range from olivine-tholeiite type (normative olivine and hypersthene) to tholeiite and quartz tholeitte (normative hypersthene : normative hypersthene and quartz).

Rocks of the alkalic suite occur as dyke or sill-like bodies of varying size. The larger of these bodies are thought to have differentiated in-situ and often retain only a slightly modified igneous layering. The strong iron enrichment shown by this suite (and the tholeiitic Scourie dykes) may reflect low partial oxygen pressures during crystallization. Osborn (1959, 1969) suggested that a low pO_2 would result in the suppression of magnetite during the early stages of crystallization, resulting in an enrichment of iron in successive liquids. On the other hand, when pO_2 is high iron is oxidized to its ferric state giving rise to the early crystallization of magnetite. In this case, as iron is extracted from the melt, iron enrichment is prevented and an enrichment of silica and alkalis takes place with the resultant calc-alkaline differentiation trend.

The high alumina nature of calc-alkaline rocks has been recognised by a number of investigators. Irvine and Barager (1971) have suggested a plot of weight percent Al_2O_3 against the normative ratio Anorthite/Anorthite + Albite, for distinguishing between tholeiitic and calc-alkaline suites. This plot is particularily suitable for mafic rocks of approximately basaltic composition, but

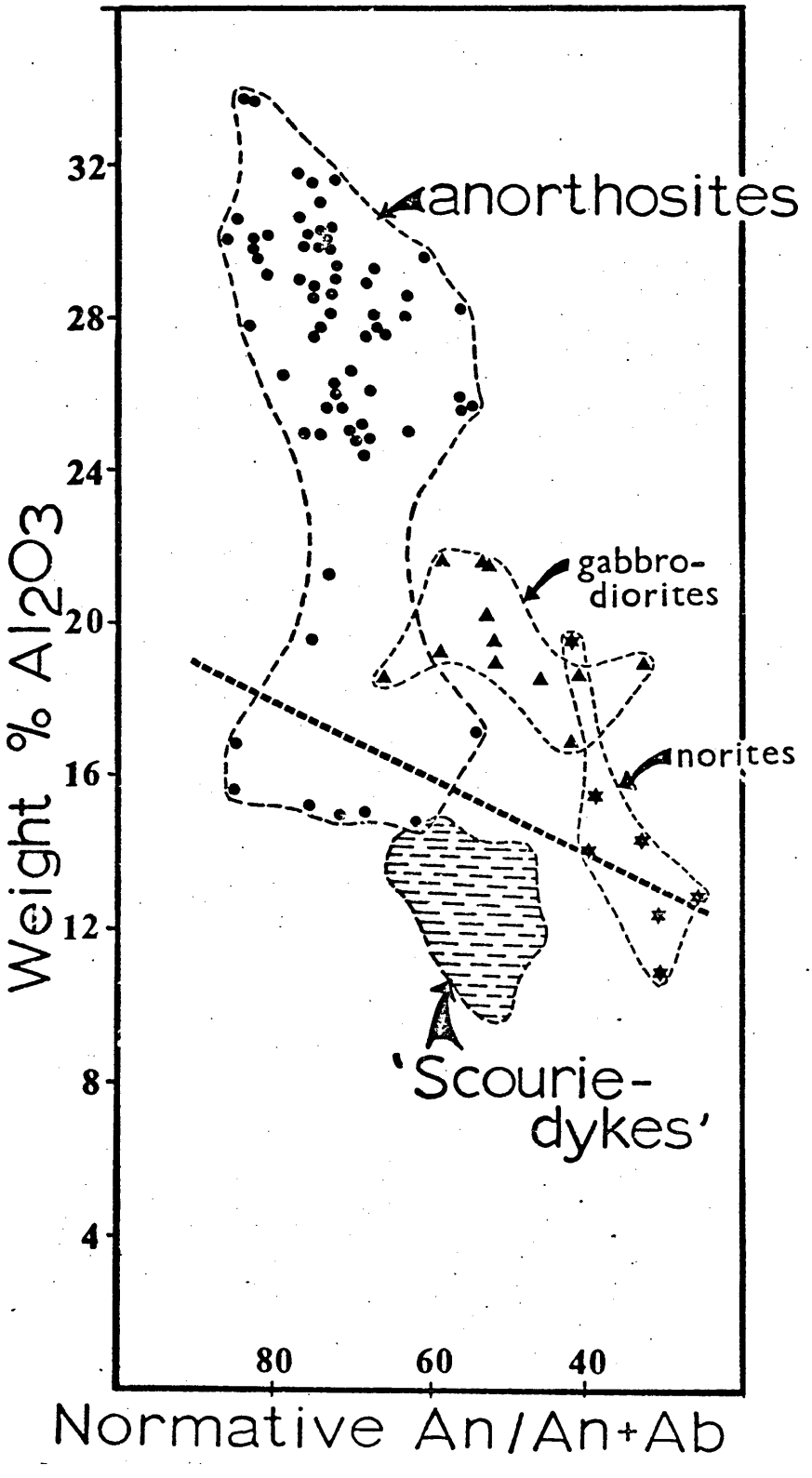


fig.5.29 Weight % Al_2O_3 vs. normative An/An+Ab. The dividing line shown is the one suggested by Irvine and Baragar (1971) for separating calc-alkaline (above) from tholeiitic (below) suites.

with careful interpretation it can be applied to the igneous rocks in South Harris (fig. 5.29).

It should be remembered that a plagioclase-rich rock, regardless of its parentage, will always have a high Al_2O_3 content, and thus plot in the calc-alkaline sector of the diagram. Similarily oxide-rich rocks, regardless of their parentage, will always plot in the lower tholeiitic field. The South Harris anorthosites plot in a broad field, which at its lower end straddles the divide used by Irvine and Barager. The scatter of data points from the anorthosite, parallel to the Al_2O_3 axis, is totally the result of plagioclase fractionation from the parental liquid containing approximately 24-25% Al_2O_3.

The divide between the two suites tends to be ineffective below An/An + Ab values of 35, where there is commonly a merging of the calc-alkalic and tholeiitic distributions. This effect may influence the shape of the compositional field of the norites. At higher An/An + Ab values (44-35) the norite field is situated in the upper calc-alkalic sector of the diagram. However, at lower An/An + Ab values (below 35) this field crosses the divide into the lower tholeiitic sector.

With these points in mind, this diagram gives a reasonably good separation between the tholeiitic and calc-alkaline rock suites, which is in agreement with the conclusions obtained from the AFM diagram.

The plot of the normative feldspar compositions (fig. 5.30) indicates that the majority of the South Harris igneous rocks are not strongly potassic, although they tend towards potash enrichment with decreasing anorthite content. The anorthosites (norm. % An 82-52) show the lowest normative

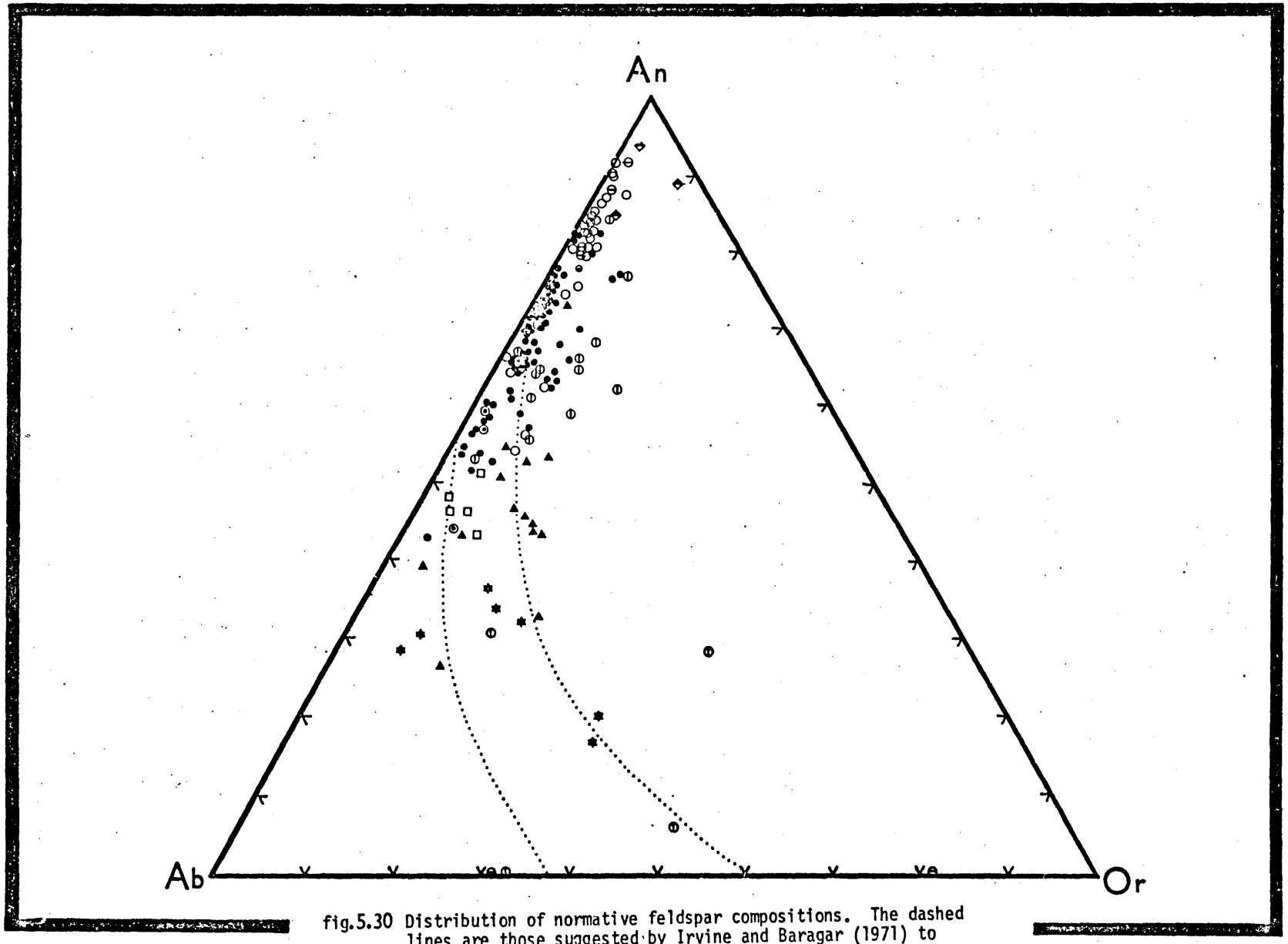


fig.5.30 Distribution of normative feldspar compositions. The dashed lines are those suggested by Irvine and Baragar (1971) to separate fields of sodic, 'normal', and potassic rocks.

potash feldspar content, whilst the norites (norm. % An 38-18) show the greatest enrichment in potash. The gabbro-diorites (norm. % An 73-28) have values between these two extremes.

This diagram is also thought to emphasize the susceptability of the smaller bodies of igneous rocks to potash metasomatism. For instance many of the ultramafites which occur as small lenses in the Leverburgh paragneisses, plot well within the potassic sector of this diagram. Potash metasomatism appears to have affected only the margins of the larger igneous bodies. Certainly the majority of the anorthosites have very low potash contents, although the highly retrogressed (amphibolitized) types show significantly higher normative potash feldspar values.

Finally, it is necessary to consider the compositional differences between the anorthosite, gabbro-diorite and norite. On the assumption that these rocks were originally igneous and that their original compositions have been little altered by metamorphism, plots of the oxides, from these three bodies, against the Thornton-Tuttle differentiation index (Thornton and Tuttle, 1960) have been made (figs. 5.31 and 5.32). This index is the sum of the normative components quartz, orthoclase, albite, nepheline, leucite and kaliophyllite, and is effectively a measure of the acidity of an igneous rock (i.e. the higher the index, the more "acid" the rock).

All of these plots emphasize the affinities of the gabbro-diorites and norites. The compositional differences between the anorthosite and the gabbro-diorite and norite probably reflect slight differences in the compositions of the parental liquids for each rock type. However, these differences are undoubtably exaggerated as a result of the predominant role played by plagioclase fractionation in the

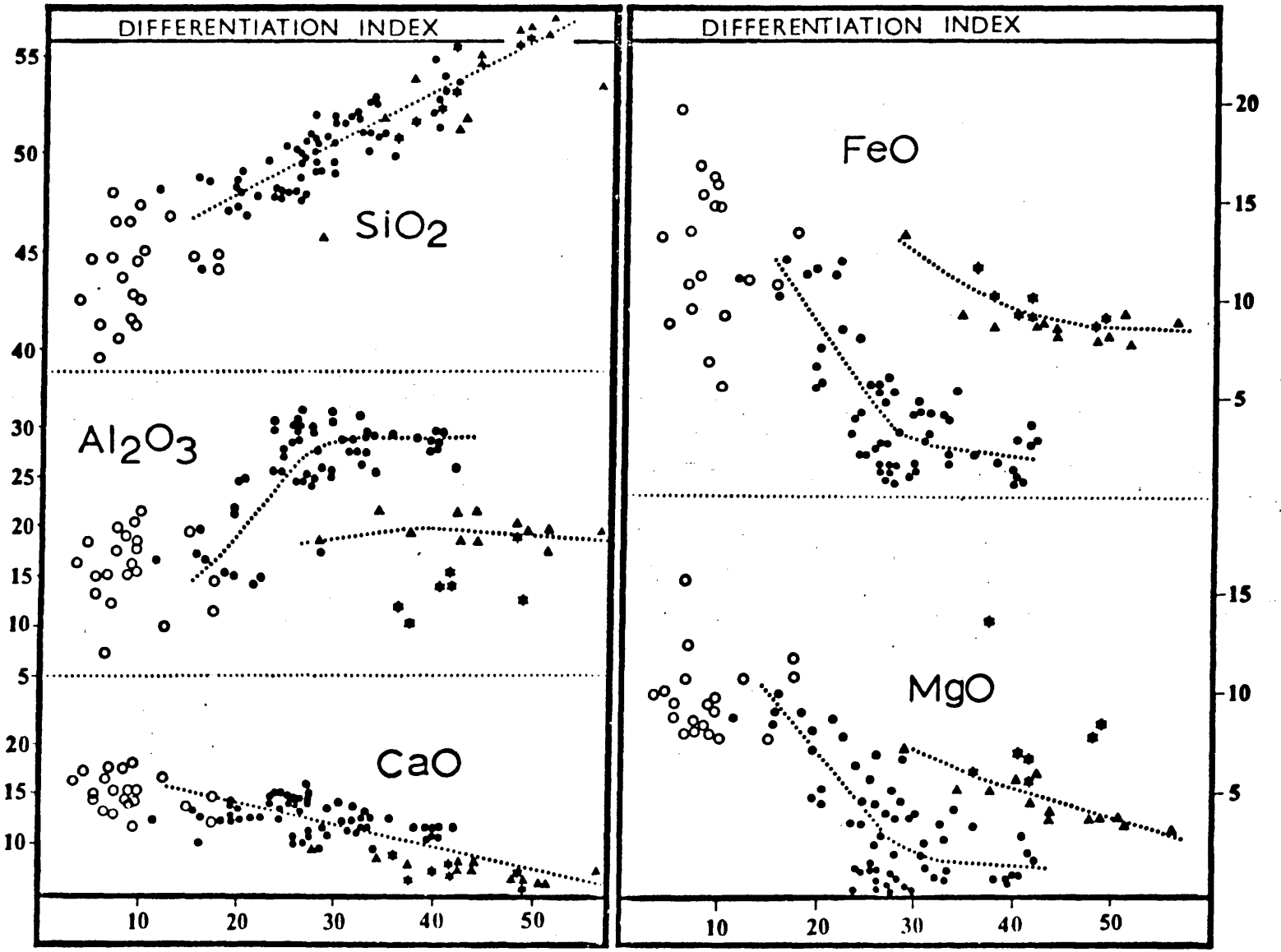


fig. 5.31 Differentiation index variation diagrams for the rocks of the anorthosite complex, the gabbro-diorite and the norite. The dotted lines are fitted by visual estimate. For the key to the symbols used see table 5.1.

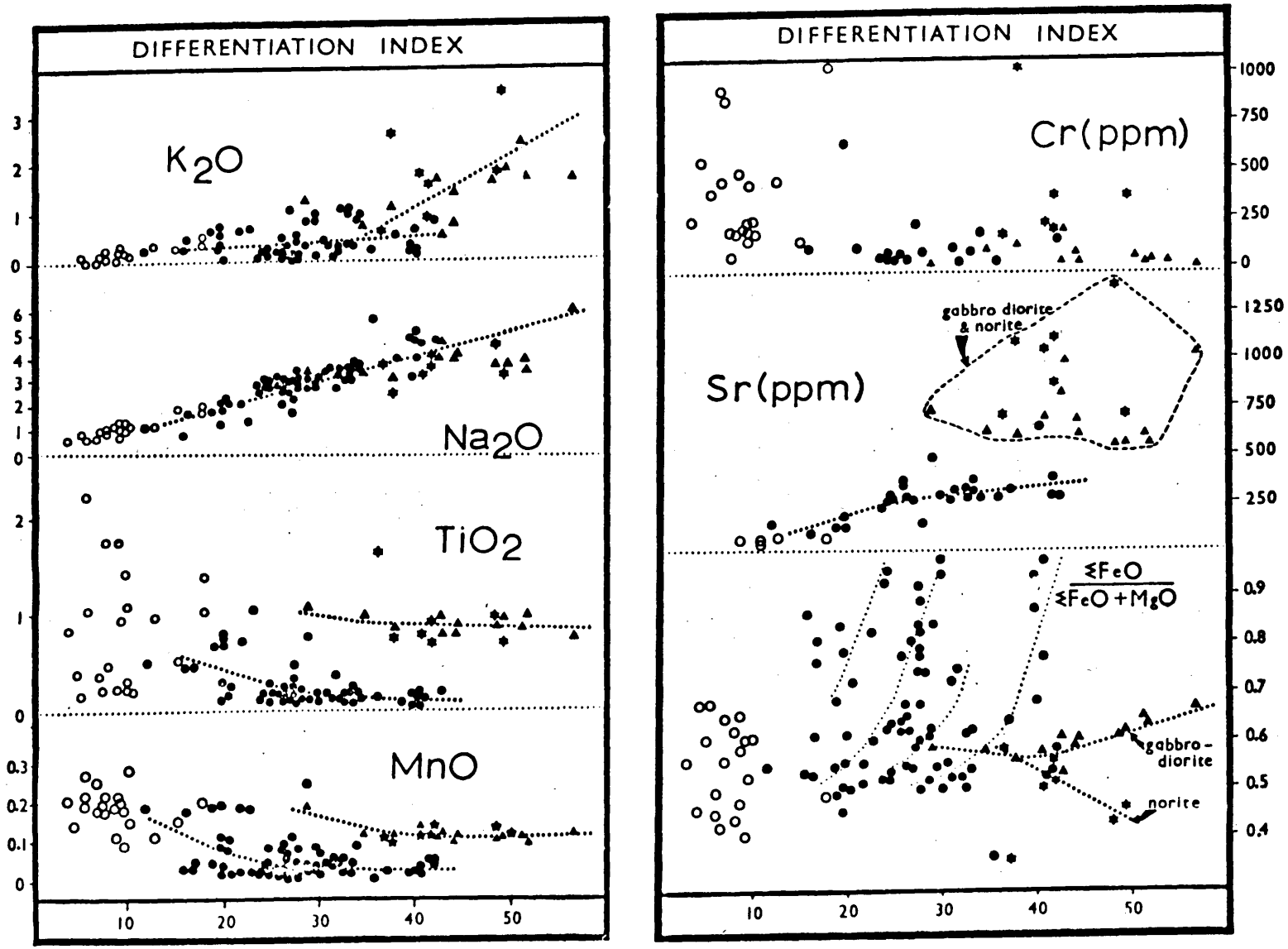


fig. 5.32 Differentiation index variation diagrams for the rocks of the anorthosite complex, the gabbro-diorite and the norite. The dotted lines are fitted by visual estimate. For the key to the symbols used, see table 5.1 . 98-104 points are plotted on each diagram, except for Sr - 54 points, and Cr - 55 points.

differentiation of the anorthosite body.

These plots show normal "igneous" differentiation trends in the oxides : MgO and CaO decrease with increase of differentiation index ; total iron, MnO and TiO_2 also tend to decrease, reflecting the overall decrease in mafic content of later differentiates.

SiO_2, K_2O and Na_2O all increase with the differentiation index, but this increase is implicit in the calculation of the index and is not necessarily significant.

Chromium values are uniformally low in all three rock types. Strontium values in the anorthosite are low, but show an overall increase with the differentiation index. In contrast strontium values from the gabbro-diorites and norites are markedly higher, but show no coherent relationship with the differentiation index.

The most interesting of these diagrams is the plot of the ratio FeO/FeO + MgO. The scatter of points, for the anorthosites, in this plot is thought to represent the cyclic enrichment in FeO relative to MgO, which has already been demonstrated for these rocks. The gabbro-diorites show a slight, but straightforward, increase in FeO relative to MgO. The norites, however, appear to be selectively enriched in MgO relative to FeO, although this observation is based on only six data points. The straightforward, linear type variation in the FeO/FeO + MgO ratio of the gabbro-diorites and norites is thought, possibly, to demonstrate the lack of any cyclic differentiation process in the formation of these rocks.

5.7 The Significance of the Meta-igneous Rock Suites of South Harris

Garson et al. (1973) have suggested that the association of meta-igneous and meta-sedimentary rock types occurring in South Harris represents a slice of oceanic crust which has either overthrust or obducted continental crust (represented by the Lewisian grey gneisses). Subsequently this oceanic slice was intricately interfolded with the continental gneisses. They propose that the compositions of the Langavat and Leverburgh meta-sediments can be correlated with pelagic sediments of Layer 1 of the oceanic crust and they equate the kyanite-garnet gneisses, which occur in the Leverburgh belt, with early Pre-Cambrian grey-wackes, possibly deposited within an Archean arc system.

I will now consider the meta-igneous rock types and their possible place in such an interpretation. It is thought that three major rock suites can be distinguished in the Outer Isles. Rocks of alkalic and high alumina calc-alkalic type are present in southern South Harris, and throughout the remainder of the Outer Hebrides and Scottish mainland tholeiitic "Scourie dykes" are abundant. A similar association of alkali poor tholeiite, high alumina basalt and alkalic basalt has been described by Kuno (1966) from the Japanese arc system. Kuno proposed that there was a definite link between the depth of the earthquake foci and the basalt magma type in this area. He suggested that the variety of basalt types present reflects differences in the depth of partial melting of the mantle related to the inclined zone of earthquake foci. It appears an almost established fact that the spectrum of

basalt types from quartz-normative tholeiites, passing though high alumina basalts to nepheline-normative alkali basalts represents successive depths of generation in the mantle (Green et al., 1967). However, there is still some uncertainty regarding the actual depths of their generation. These basalt magma types may be generated either by fractional crystallization of a more primative olivine tholeitic or picritic basalt magma (Green, 1969) or by direct melting of the mantle iherzolite.

From a comparison with the magma types in the Japanese island arc it is possible that in South Harris we are dealing with the remnants of an Archean arc system. The chronological sequence of intrusion in South Harris suggests a successively shallower depth of magma generation.

Magma Type	SCOURIAN Scourie dyke LAXFORDIAN	Depth of magma segregation
ALKALIC		35 - 60 Kms
HIGH-ALUMINA CALC ALKALIC		15 - 35 Kms
THOLEIITIC		0 - 15 Kms

The estimates for the depths of magma segregation, on the right hand side of the above table, are taken from Green et al., (1967).

The dunites, peridotites and pyroxenites, within the Langavat meta-sedimentary belt, have been likened to rhythmically layered "Alpine type" or orogenic peridotites by Livingstone (1963). In view of their tectonic setting they would fall in the orogenic "root-zone" peridotite class of den Tex (1965).

Their original form may have been that of a transgressive sill, but subsequent deformation has boundinaged this body into a series of isolated lenses. Gabbroic, dioritic and granitic rocks have been recognized as co-magmatic with alpine-peridotites in at least ten areas. The chemical relations between the various members of this alpine mafic magma series suggest a magnesian differentiation trend near to the typical calc-alkaline plutonic trend (Thayer, 1967). It is tempting to suggest that the anorthosite, gabbro-diorite, norite and Langavat ultramafites constitute such an 'Alpine-suite'. This interpretation, however, requires considerable care in its application, especially where, as in this area, more than one magma series is known to be present.

Osborn (1969) has suggested that alpine peridotites and orogenic andesites represent complimentary fractions of a more primative olivine basalt magma, which has differentiated by crystal fractionation. It has also been demonstrated by Green et al (1967) that fractional crystallization of olivine and low alumina orthopyroxene from either olivine tholeiite, olivine basalt or alkali olivine basalt, at depths between 15-35 Km, would lead to the production of alumina enriched liquids.

It is tentatively suggested that the peridotites, dunites and pyroxenites from the Langavat metasedimentary belt may represent a refractory olivine/orthopyroxene residuum, produced by crystal fractionation, from a parental olivine basalt magma. The complimentary high alumina basaltic liquid may have undergone further fractional crystallization at shallower levels giving rise to three separate high alumina magma types, now represented by the gabbro-diorite, norite and anorthosite. Green et al. point out that

relatively large amounts of ultramafite would be generated in the production of high alumina basalts by such a method (olivine + orthopyroxene ultramafite : high alumina basalt 3 : 1). The relative scarcity of such ultramafites in South Harris (fig. 1.2) would thus be a drawback to this proposed petrogenetic model.

CHAPTER 6

MINERAL GEOCHEMISTRY OF THE ANORTHOSITE COMPLEX AND ASSOCIATED META-IGNEOUS ROCKS

6.1 General Introduction

Mineral analyses were made on a modified (semi-automated) Cambridge electron microprobe ('Geoscan'), using natural and synthetic standards. A total of 111 new microprobe analyses of the major mineral phases of the rocks of the anorthosite complex have been made. All microprobe analyses have been recalculated from metal to oxide values. Structural formulae for these analyses have been calculated to the numbers of oxygens used by Deer et al., (1963). Amphibole analyses have been re-calculated on the basis of twenty-three oxygen atoms, as the water content of these minerals is unknown. Microprobe analyses yield a total iron value that is usually expressed as Fe^{2+}. This total iron value has been re-calculated into Fe^{2+} and Fe^{3+} for all of the garnet analyses and the single ilmenite analysis performed. This theoretical splitting of the iron value was achieved using the computer program FERRIC, based on a method proposed by Finger (1972). In the case of the garnet analyses, such a calculation improves the summations for the R^{+2} and R^{+3} cation sites and increases the percentage of cations that can be assigned to theoretical end-member molecules.

Mineral analyses and further details of analytical technique and data processing methods are presented in Appendix 1. A description of the chemistry of the main mineral phases, followed by some comments on the inter-element distributions between co-existing minerals, is given in this chapter.

The mineral analyses were made mainly with the object of showing general compositions of the main mineral phases in the rock types of the anorthosite complex.

6.2 Clinopyroxenes

Although clinopyroxene is a relatively abundant mineral in the rocks of the anorthosite complex, it appears to be particularily susceptible to the effects of retrogression. Even in the freshest rocks examined the clinopyroxene shows some degree of alteration to a pale blue/green magnesio-hornblende or actionolitic-hornblende. This alteration has effectively limited the number of clinopyroxenes suitable for analysis. Twenty-one clinopyroxene analyses from the rocks of the anorthosite complex are presented (Appendix 1, Tables 5, 19, 20 and 37), together with three analyses from the Leverburgh ultramafite lenses (quoted from Livingstone, 1953). All of the analysed clinopyroxenes show equilibrium textures and there is no trace of exsolution of calcium-poor lamellae. The composition of these clinopyroxenes, in terms of their end-members, is shown in fig 6.1. The four clinopyroxene which co-exist with orthopyroxene are joined by tie-lines in fig. 6.1.

Many of the clinopyroxene are weakly zoned. The variations in major oxide concentrations (wt%) across two clinopyroxene grains are shown in fig. 6.2. The two main changes in chemistry which occur from the centre to the rim in these grains are:-

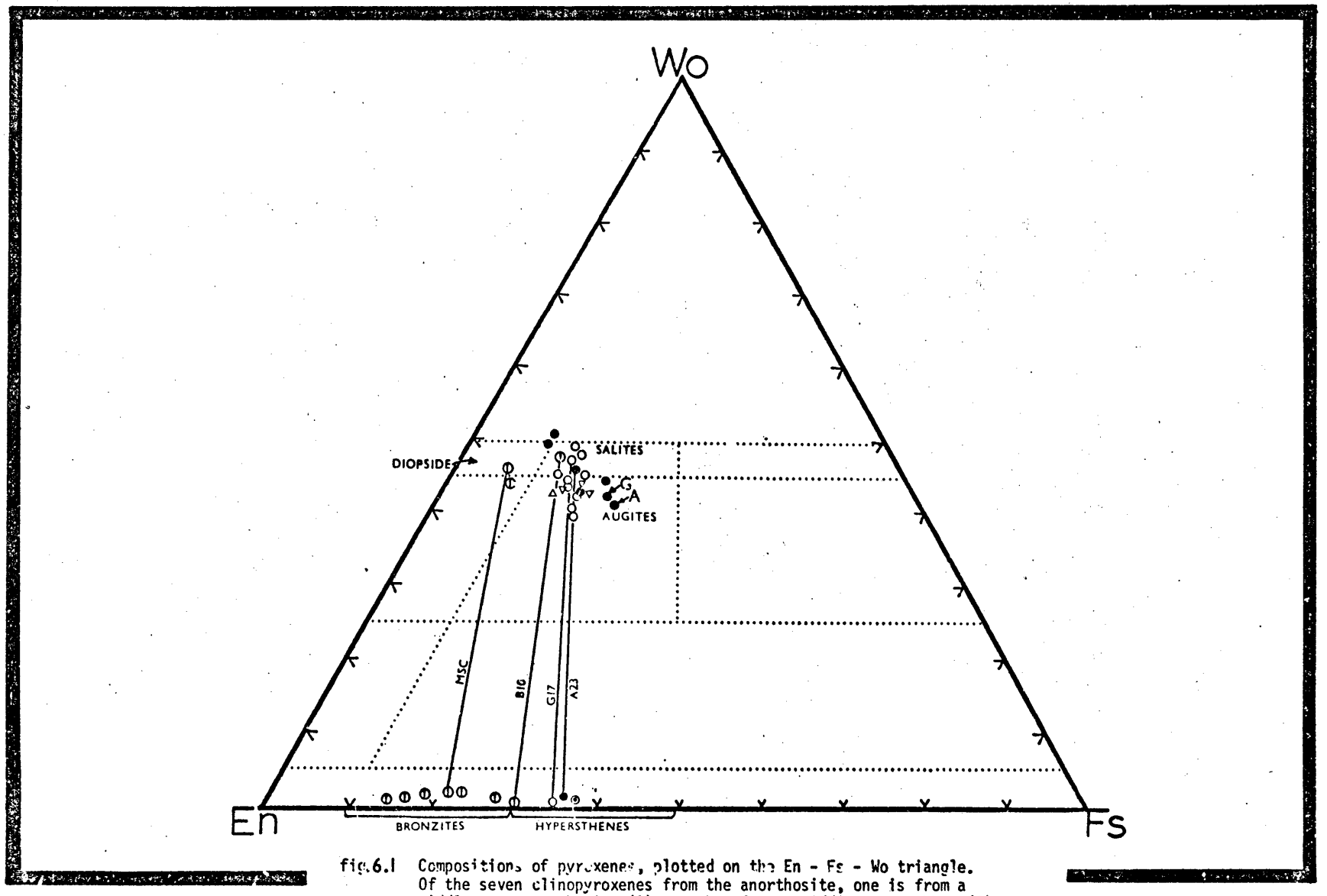


fig.6.1 Compositions of pyroxenes, plotted on the En - Fs - Wo triangle. Of the seven clinopyroxenes from the anorthosite, one is from a middle zone anorthosite (A), another from a middle zone gabbro (G) and the remaining five from mafic gabbro horizons in the lower zone.

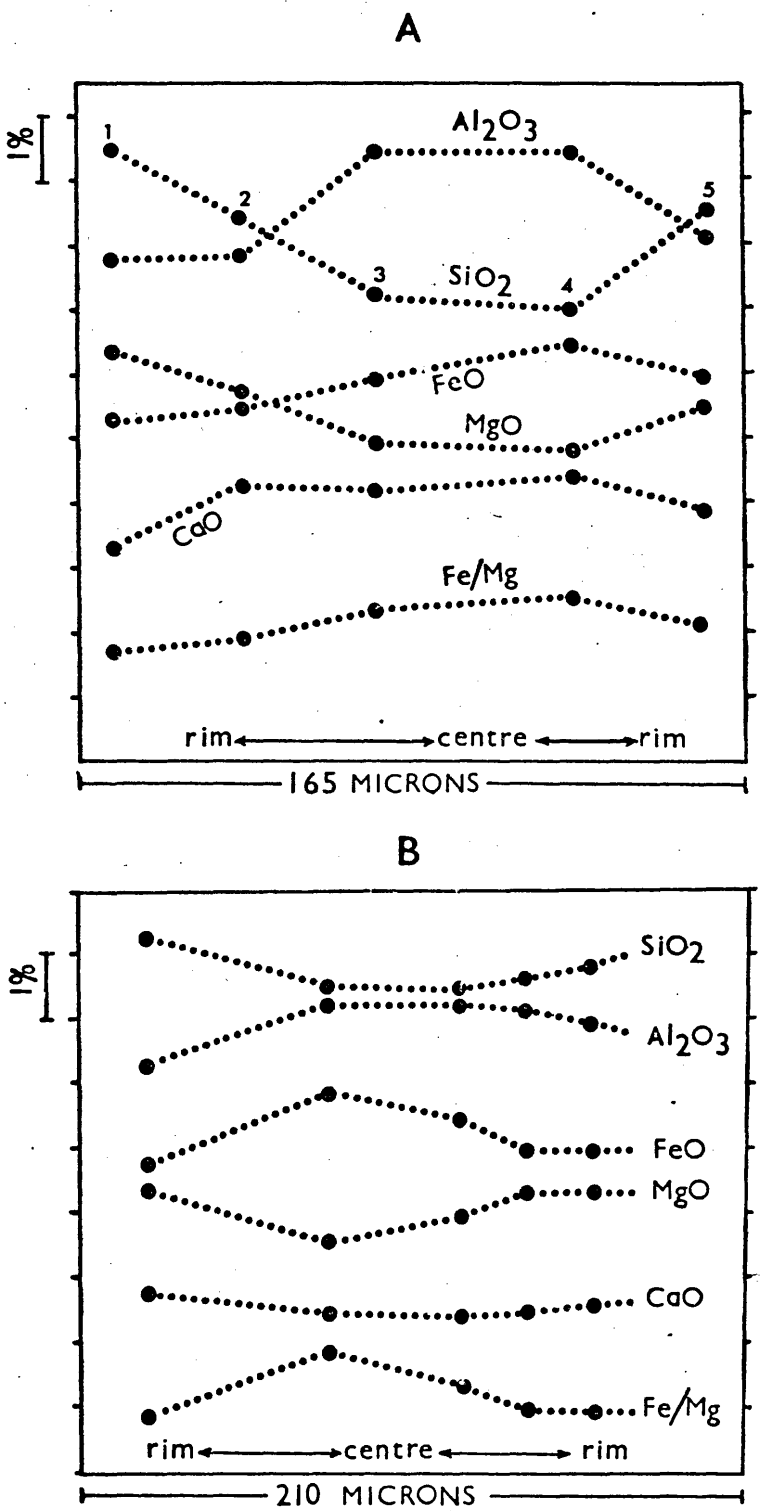


fig.6.2 Major element variations across two clinopyroxene grains.
A - clinopyroxene from mafic gabbro A15
B - clinopyroxene from mafic gabbro A23.

a) a gradual decrease in Al_2O_3 accompanied by an increase in SiO_2, and

b) a decrease in FeO (total iron as FeO) accompanied by an increase in MgO.

Several of the oxides show a variation in concentration (expressed as wt%) relative to the iron content of the clinopyroxene (fig. 6.3a, b, c). For example, with a progressive increase in the iron (ferrosilite) content of the clinopyroxenes:-

a) CaO shows an overall decrease (fig. 6.3a)

b) TiO_2 increases (fig. 6.3b)

The Na_2O and Al_2O_3 contents of the clinopyroxenes are highly variable. The Al_2O_3 content of the clinopyroxenes varies from 2.9% - 7.9%. It is generally agreed that the amount of Al^{3+} in six-fold co-ordination increases in amount with pressure, whilst Al^{3+} in four-fold co-ordination increases with temperature. Hence the Al_2O_3 content of the clinopyroxene may be taken as diagnostic of metamorphic grade. The percentage of Tschermak's molecule is a direct measure of Al^{3+} in four-fold co-ordination, and the percentage of jadeite a measure of Al^{3+} in six-fold co-ordination (coupled with Na_2O content). White (1964) has suggested a plot of percent jadeite against percent Tschermakite to distinguish eclogitic from granulitic clinopyroxenes. The clinopyroxenes from the South Harris igneous rocks have been assigned to the hypothetical end-member molecules : acmite ($NaFe^{3+}Si_2O_6$)/jadeite ($NaAlSi_2O_6$), Tschermakite ((CaMg) Al_2SiO_6), hedenbergite and diopside, in this order, according to the procedure described by Yoder and Tilley (1962). Modifications to this scheme, suggested by White (1964) have also been adopted. These modifications enable a

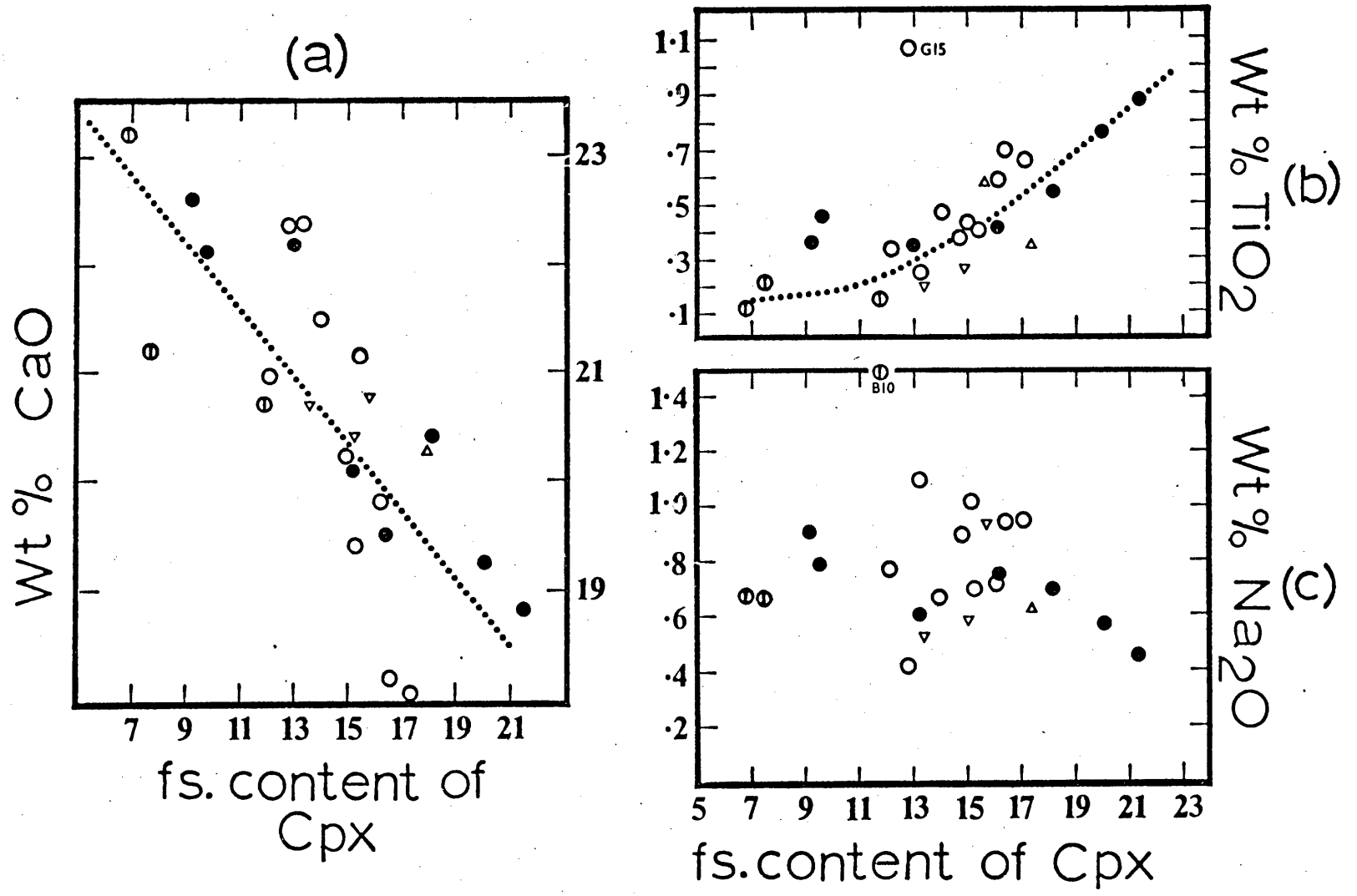


fig. 6.3 The relation between the ferrosilite (Fs) component of the clinopyroxenes and wt% a) CaO; b) TiO_2 and c) Na_2O. Each clinopyroxene is plotted with a symbol for its host rock (Table 5.1). Anomolous points are labelled with their sample numbers. Note that many of the scales do not begin at zero. The dotted lines were inserted by eye.

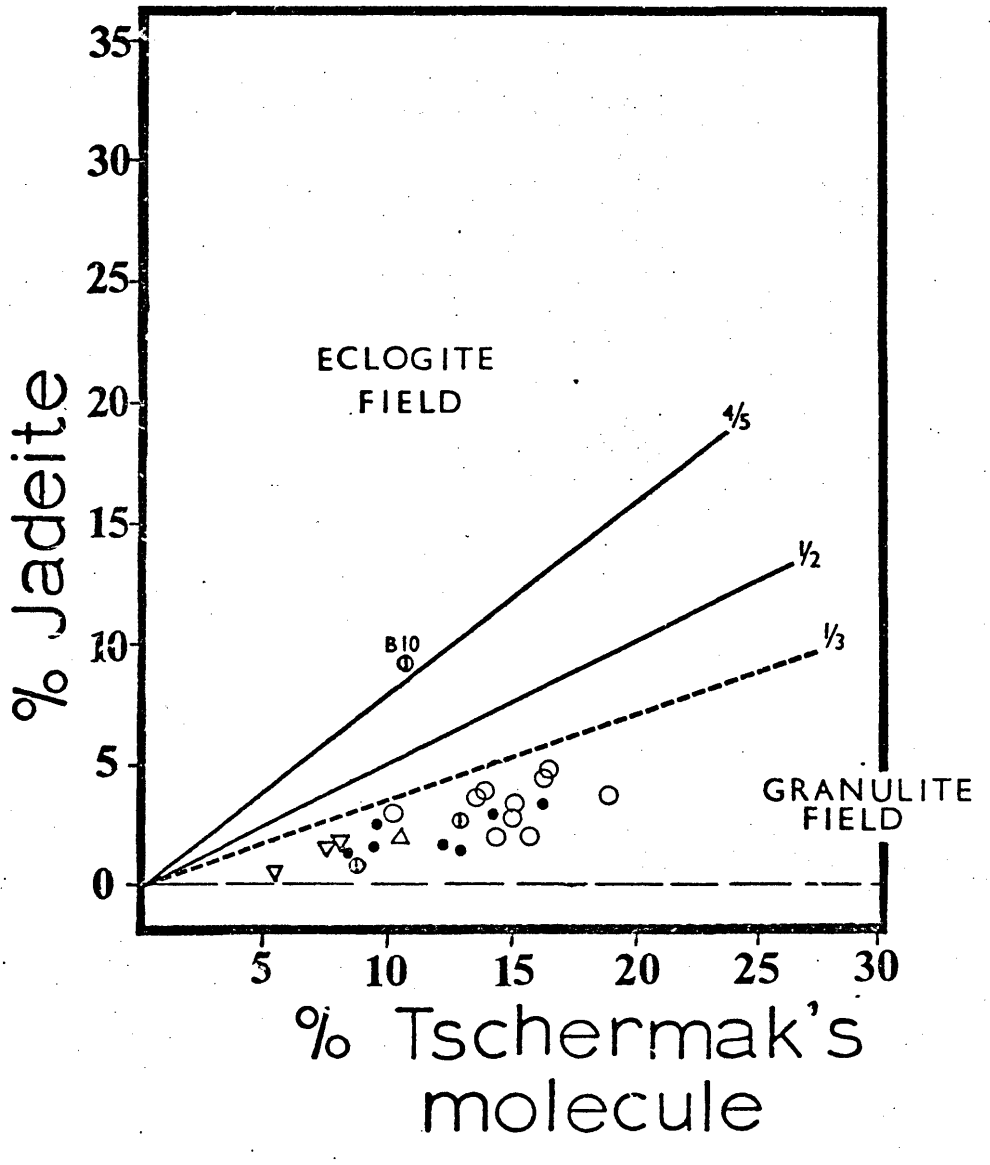


fig. 6.4 Plot of mol.% jadeite against Tschermaks molecule for the South Harris clinopyroxenes.

distinction to be made between the acmite and jadeite molecules. To allow this calculation to be made, theoretical Fe^{3+} values for all the clinopyroxenes were calculated by the method proposed by Finger (1972). Fig. 6.4 shows that all of the South Harris clinopyroxenes fall within the granulite field, except the analysis BIO (Livingstone, 1967) which falls in the eclogitic clinopyroxene field.

The iron (Ferrosilite) content of the clinopyroxenes is dependent on the Fe/Fe + Mg ratio of their respective host rocks (fig. 6.5a). The Fe/Fe + Mg ratio of the clinopyroxenes is, in all cases, lower than that of their equivalent host rocks. There is some evidence to suggest that the difference between the Fe/Fe + Mg ratio of the clinopyroxenes and that of their host rocks increases within increasingly iron-rich rocks.

6.3 Orthopyroxenes

Orthopyroxene bearing assemblagesare rare in the rocks of the anorthosite complex; only three samples have yielded orthopyroxene grains suitable for analysis. These, together with seven analyses of the orthopyroxenes from the magnesium-rich ultramafites of the Leverburgh metasedimentary belt (quoted from Livingstone, 1963), are presented in Appendix 1, Tables 5, 12, 19 and 31. The orthopyroxenes from the anorthosite complex are technically hypersthenes, whilst those from the Leverburgh ultramafites are bronzites.

It is of concern to determine whether the orthopyroxene in these rocks is a strictly metamorphic mineral, or whether it has recrystallized from an original igneous

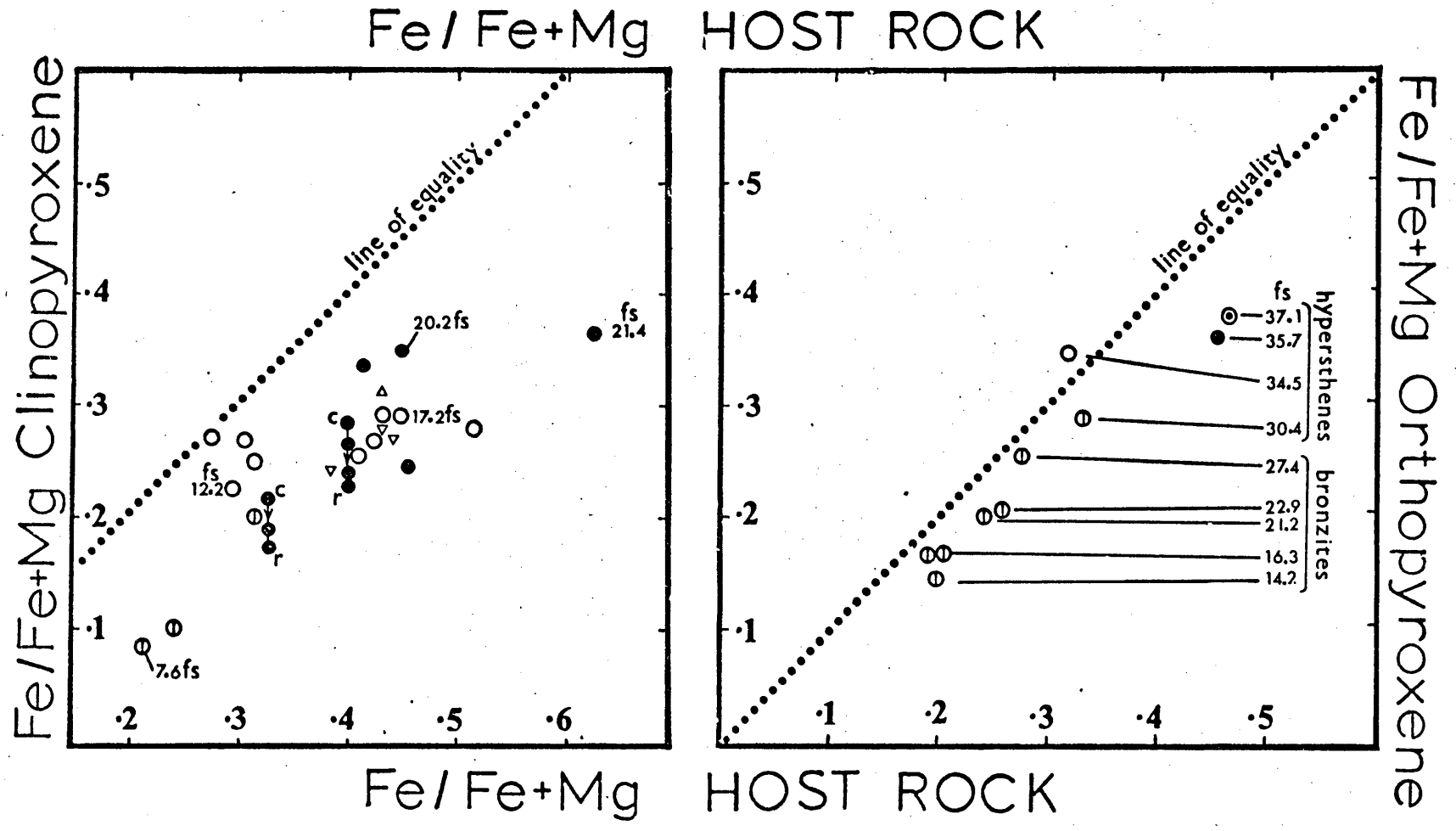


fig. 6.5 (a) - the relation between the atomic ratio Fe/Fe+Mg of the clinopyroxenes and their respective host rocks. c= grain centre, r= grain rim. Ferrosilite (Fs) values are indicated for some of the clinopyroxenes.
(b) - the relation between the atomic ratio Fe/Fe+Mg of the orthopyroxenes and their respective host rocks. Ferrosilite (Fs) values are indicated for all of the orthopyroxenes.

Each mineral is plotted with a symbol for its host rock (Table 5.1)

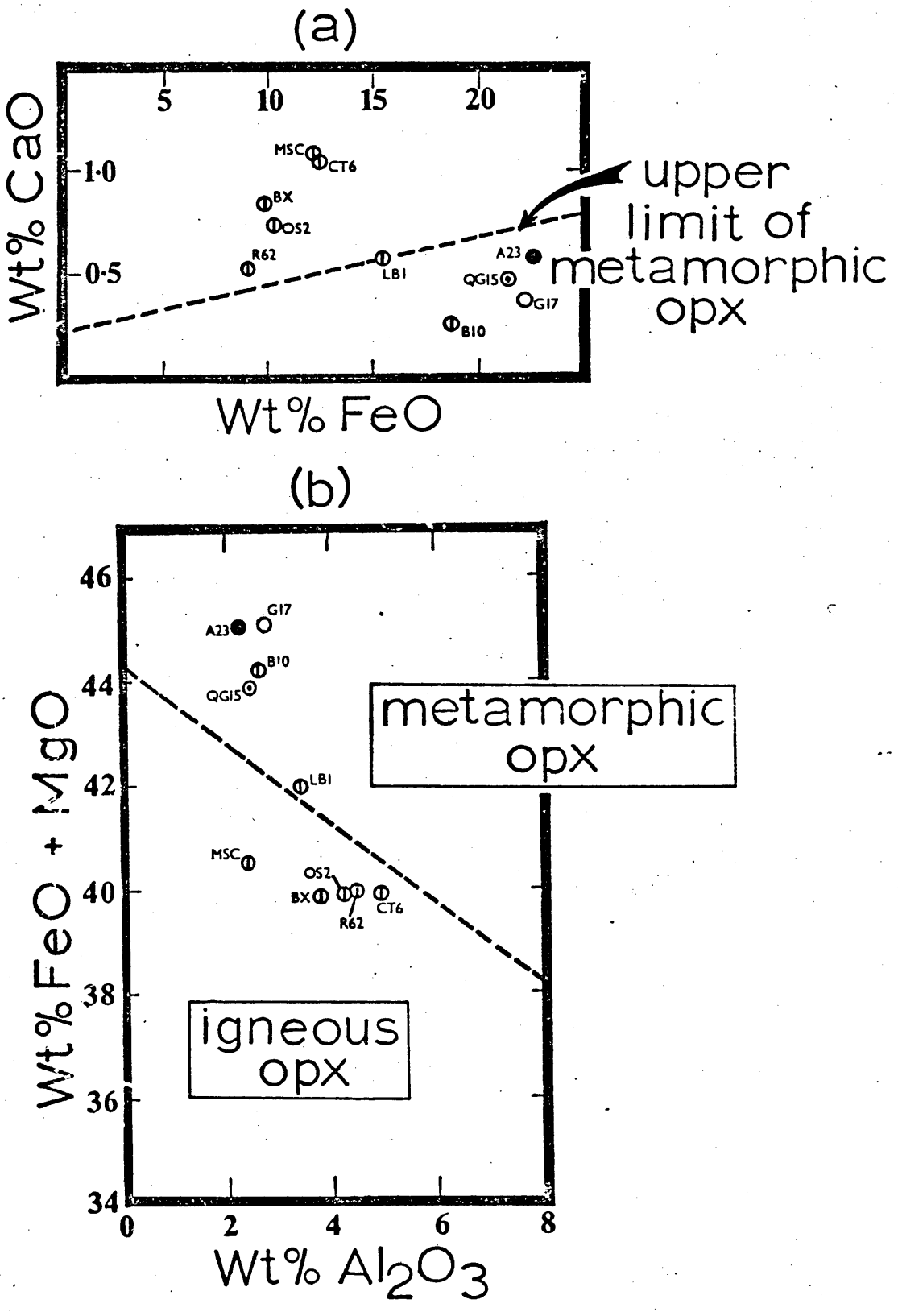


fig. 6.6 a) The relation between wt% CaO and FeO in the orthopyroxenes. The dashed line defines the field for metamorphic orthopyroxenes (Howie and Smith, 1966).
b) The relation between wt% FeO+MgO and Al_2O_3.
The dashed line is that suggested by Bhattacharyya (1971), to separate the fields of metamorphic (above) and igneous (below) orthopyroxenes.
Each orthopyroxene is plotted with a symbol for its host rock (Table 5.1).

orthopyroxene.

Fig. 6.6a shows a plot of weight percent CaO against weight percent FeO (total iron). The dashed line on this diagram, which defines the upper limit of metamorphic orthopyroxenes, is taken from Howie and Smith (1966). Bhattacharyya (1971) has suggested a plot of weight percent Al_2O_3 against weight percent FeO + MgO, for distinguishing metamorphic from igneous orthopyroxenes (fig. 6.6b). A scatter of points is obvious in both of these diagrams. However, it should be noted that the same samples, on each diagram, plot in comparable positions relative to the suggested dividing lines. Both of these diagrams are difficult to interpret, but it is thought that the scatter of points in both may indicate that the orthopyroxenes were originally igneous and have suffered varying degrees of recrystallization and re-equilibration during the high grade metamorphism.

An alternative explanation for this spread of data for the orthopyroxenes must also be considered. The analyses quoted from Livingstone are bulk concentrate analyses made by classical wet chemical methods. If individual grains contained exsolved lamellae of calcium-rich pyroxene this would have effectively raised the calcium oxide values for these analyses and lowered the FeO and MgO values. The net effect of these changes would be to bias these data points towards the "igneous orthopyroxene fields" in both plots shown in fig. 6.6. It is noteworthy, in this connection, that the microprobe point-analyses of orthopyroxenes from the anorthosite complex fall well within the metamorphic fields. Exsolution features have not been observed in any of the orthopyroxenes examined, but the above comments should be borne in mind as an alternative

explanation for the distribution of data points in figs. 6.6a and 6.6b.

The iron content of the orthopyroxenes, like the clinopyroxenes, is dependant upon the Fe/Mg ratio of their host rocks (fig. 6.5b). In all but one case the Fe/Fe + Mg ratio of the orthopyroxene is slightly lower than that of its host rock.

6.4 Garnets

Only those garnets which are attributable to the early high-grade (granulite) facies metamorphism have been analysed. Insufficient time was available to undertake a comparative study of those garnets which grow across the early foliation (F_1), defined by the granulite facies minerals.

Source of garnet analyses:-

Symbol	No. of Analyses	Host Rock Type	Analyst
⊕	1	Ultramafite from Leverburgh paragneiss belt.	Livingstone (1963, 1967)
○	15	Banded Ultramafites and mafic gabbros from the gabbroic rim of the anorthosite complex.	*
○	2	Ultramafites from the gabbroic rim of the anorthosite ("eclogite and metagabbro").	Davidson (1943)
●	18	Anorthosite	*
▽	2	Ultramafites associated with brecciation in anorthosite.	*
Total	38	* analyses by present author	

A theoretical Fe_2O_3 value has been calculated for all of the new garnet analyses. The calculated ferric iron values usually do not exceed 3% and, in some cases, the stoichiometry of the garnet does not allow the presence of any Fe^{3+} in the formula. Such a calculation improves the summations for the R^{+2} and R^{+3} cation sites and increases the percentage of cations that can be assigned to end-member molecules. Titanium has been arbitarily assigned to the R^{+3} cation site (substituting for Al^{3+} of Fe^{3+}). There is some evidence, however, that TiO_4 tetrahedra play a comparable role to the SiO_4 tetrahedra in the garnet structure (Deer et al., v.1, 1963). For the calculation into end-member molecules, the scheme of Rickwood (1968) has been adopted. All of the garnets can be recalculated into a maximum of seven end-member molecules. The percentage number of cations which can be allocated to end-member molecules is suggested by Rickwood as a figure useful for the assessment of analytical quality. The m ajority of these analyses (95%) can be recast into end-member molecules utilizing in excess of 97% of the available cations.

The garnet compositions are dominated by the almandine ($Fe_3Al_2Si_3O_{12}$) and pyrope ($Mg_3Al_2Si_3O_{12}$) components, with almandine usually in excess of pyrope (fig.6.7). Spessartine ($Mn_3Al_2Si_3O_{12}$) values are low ($<1.5\%$) even in those garnets which have an appreciable almandine content. The grossular ($Ca_3Al_2Si_3O_{12}$) component shows a range of values from 3-33%. As a general rule garnets coexisting with appreciable amounts of calcium-rich pyroxene yield low grossular contents, whilst the grossular content of those garnets which co-exist with relatively minor amounts of clinopyroxene are considerably greater.

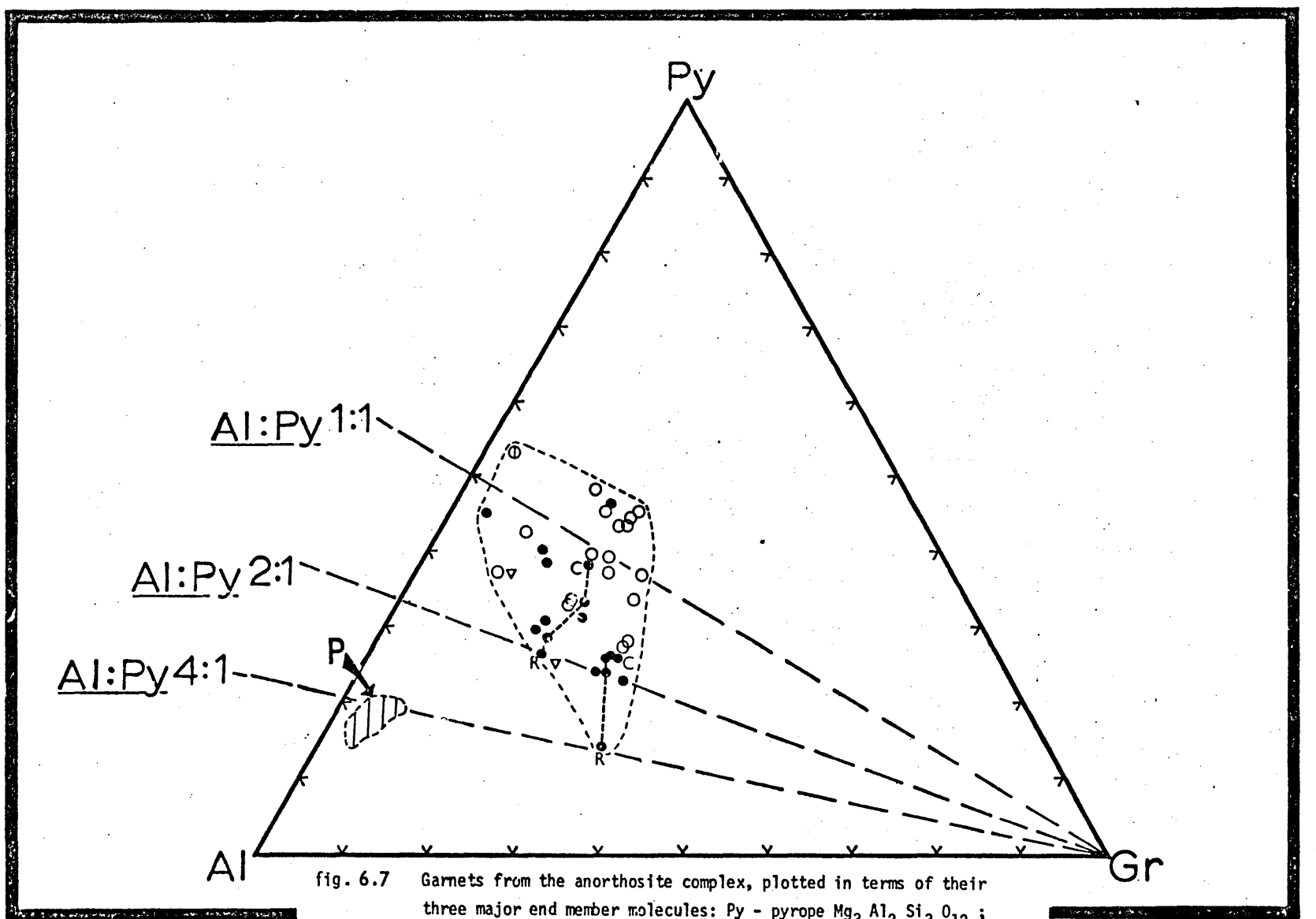


fig. 6.7 Garnets from the anorthosite complex, plotted in terms of their three major end member molecules: Py - pyrope $Mg_3 Al_2 Si_3 O_{12}$; Al - almandine $Fe_3 Al_2 Si_3 O_{12}$; Gr - grossular $Ca_3 Al_2 Si_3 O_{12}$. Each garnet is plotted with a symbol for its host rock (see table 5.1) The dashed lines indicate the range of compositions, from centre (C) to rim (R) within a single zoned grain. The compositional field (P) of seven garnets froms the Leverburgh paragneisses is also shown (analyses from Dickinson (1974)).

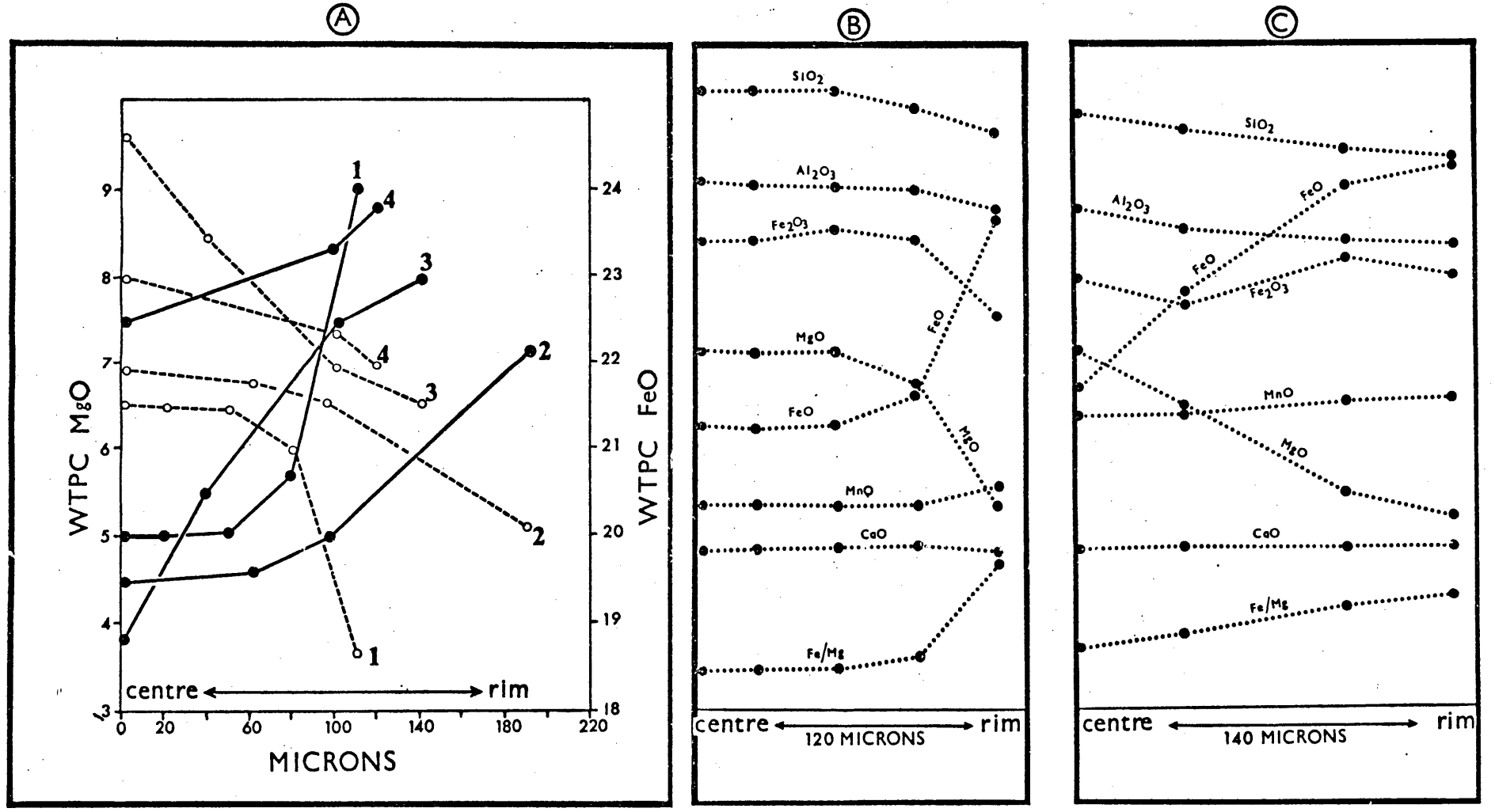


fig. 6.8 Major element variations across individual garnet grains.

A.- Variation of FeO (solid circles and solid lines) and MgO (open circles and dashed lines), from grain centre to grain rim, in four garnets.

1. garnet from rock A46 - middle zone anorthosite
2. " " " A47 - middle zone gabbro
3. " " " A47 - middle zone gabbro
4. " " " A9 - lower zone mafic gabbro

B. Major element variations across garnet A46
C. " " " " " A47

In B & C the Fe_2O_3 values are calculated by the method proposed by Finger (1972).

Chromium oxide values are low (average 0.05%) in all of the garnet analyses, except for sample G17 which contains 0.4% Cr_2O_3. Nickel has been detected in only one garnet; sample G15 shows a nickel concentration $>$ 1000p.p.m. Sodium values range from 0-1000p.p.m. The sample G15 is again anomalous, yielding an Na value approximating to 2500p.p.m.

The blood-red garnets, which characterize the igneous rocks of South Harris, are chemically quite distinct from the lilac garnets which occur throughout the meta-sediments. The compositional field of the latter, defined by seven analyses from Dickinson (1974), is shown in fig. 6.7. The lilac garnets show a significantly higher almandine : pyrope ratio than the red garnets from the igneous rocks. Also the spessartine component of these garnets is four to five times greater than that of the red garnets.

All of the analysed garnets show some degree of zonation. The observed major element variations across the garnets are illustrated in fig. 6.8. These variations, from the grain centre to the grain rim, can be summarized as follows:-

a) a decrease in wt% SiO_2 and Al_2O_3.

b) an increase in wt% FeO and MnO and a complimentary decrease in wt% MgO.

c) wt% CaO values are constant.

The almandine-pyrope ratio of the analysed garnets appears to be dependent on the Fe/Fe + Mg ratio of the equivalent host rock (fig. 6.9a). The Fe/Fe + Mg ratio of the garnets is usually greater than that of their host rocks. This latter relationship has been demonstrated by Buddington (1952) in the Adirondack gabbroic rocks, whilst Subramanium (1956) has shown that the converse relationship is true in the case of garnets from eclogites. In the

South Harris igneous rocks, the relationship between the Fe/Fe + Mg ratio of the garnets and their equivalent host rocks varies in relation to the iron content of the host rock. Garnets which occur in iron-poor rocks (i.e. rocks whith a low Fe/Fe + Mg ratio) show a considerably higher Fe/Fe + Mg ratio than their host rock. However, the positive difference between the Fe/Fe + Mg ratio of the garnets and their equivalent host rocks decreases with increasing iron content of the host rock (i.e. with increasing Fe/Fe + Mg values). A point is reached where the Fe/Fe + Mg ratio of the garnet equals that of its host rock - this takes place at an Fe/Fe + Mg value of approximately 0.62. Garnets, suitable for analysis, were not available from the very iron-rich rocks (Fe/Fe + Mg ratios greater than 0.62), but it would appear, from an extrapolation of the measured data, that these garnets would have lower Fe/Fe + Mg ratios than their host rocks. A further complication results from the strong zonation of many of the analysed garnets. Zonation of the garnets is probably the cause of the scatter points in fig. 5.9a. The zonation shown by the garnets has been studied in two thin sections. In both cases, reconnaisance traverses were made across all the garnet grains in either slide in order to determine which grains showed the most extreme zonation of the major oxides. A number of point analyses were then made across these grains. This method of approach is very time consuming and could not be applied to all those samples where the garnets were analysed. In all other cases, the garnet analysis, for any one example, is an average figure calculated from a random selection of up to

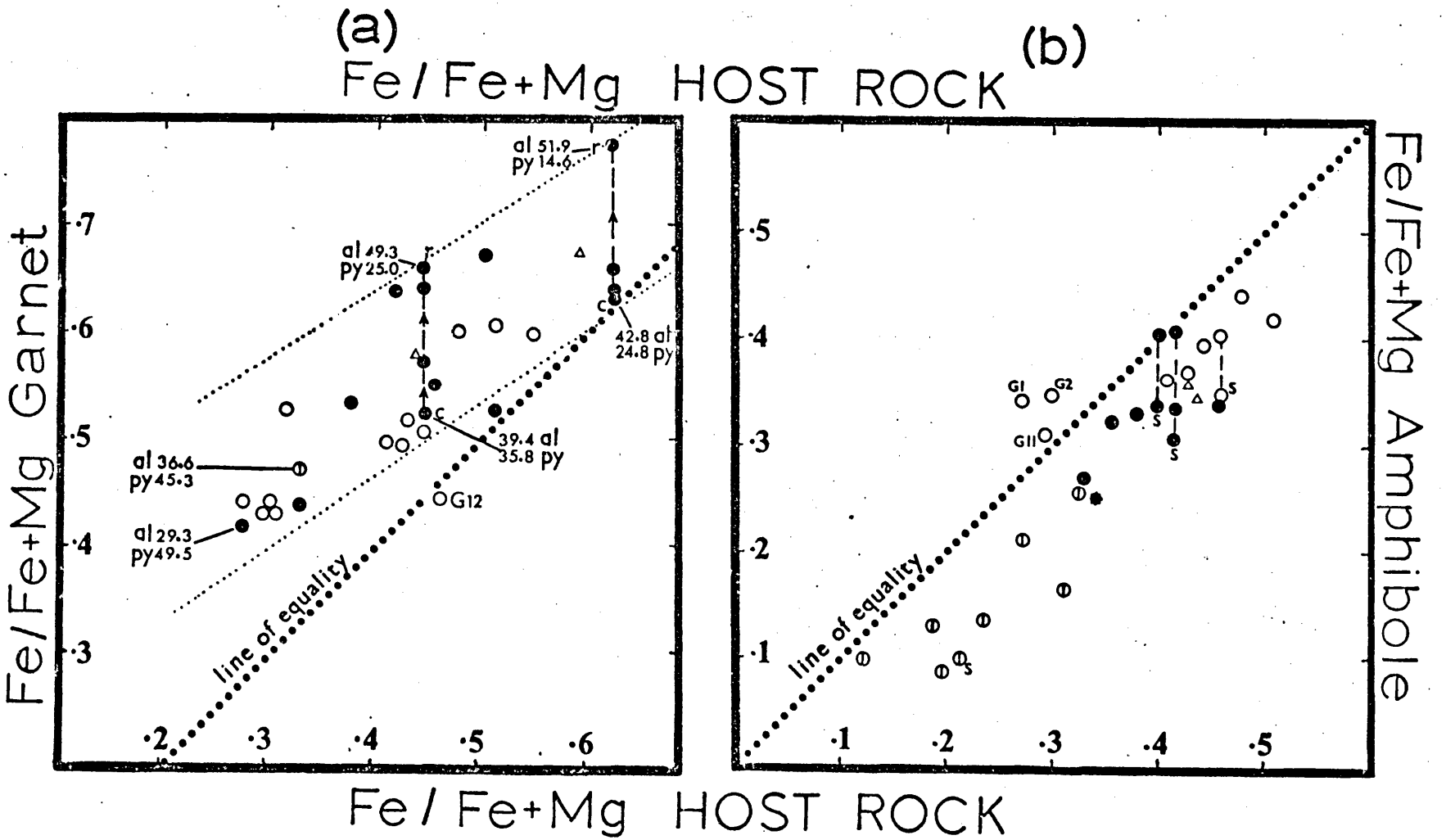


fig. 6.9 (a) - the relation between the atomic ratio Fe/Fe+Mg of the garnets and their respective host rocks. c= grain centre, r= grain rim. The values for the theoretical end members almandine (al) and pyrope (py) are indicated for some of the garnets.
(b) - the relation between the atomic ratio Fe/Fe+Mg of the amphiboles and their respective host rocks.

Each mineral is plotted with a symbol for its host rock (table 5.1). Anomolous points are labelled with their sample number.

nine individual grains. Point analyses were made at the centre and rim of each grain. Although quick and convenient, the scatter of points in fig. 5.9a for these "averaged" garnet compositions is thought to emphasize the inadequacies of this latter method.

6.5 Amphiboles

Amphibole is a common mineral phase throughout the rocks of the anorthosite complex. High-grade (granulite facies) amphiboles are of two types:-

a) An olive-green amphibole; pleochroism X yellow-green; Y brown-green; Z dark brown. These amphiboles occur throughout the mafic gabbros, ultramafites and quartz gabbros of the gabbroic rim of the complex, and within mafic gabbro horizons of the lower zone anorthosites.

b) A straw-green amphibole; pleochroism X pale green-straw; Y green; Z blue-green. These characterize the gabbros, anorthositic-gabbros and the highly felsic rock types of the anorthosite sequence.

In addition to these high-grade amphiboles a pale-green blue amphibole is a common product of the retrograde (amphibole facies) metamorphism of high-grade mafic minerals.

Source of amphibole analyses:-

Symbol used in plots	Number of analyses		Host Rock Type	Analyst
	granulite facies amphiboles	amphibolite facies amphiboles		
⊕	7	1	Ultramafites (peridotites and pyroxenites) occurring as lenses within the Leverburgh metasediments.	Livingstone (1963)
✹	1	-	Ultramafite pod from the gabbro-diroite	Dearnley (1959,1963)
●	7	2	'Anorthosites'	*
○	9	1	Banded ultramafites and mafic gabbros from the gabbroic rim of the anorthosite complex	*
▽	2	-	Ultramafites associated with brecciated areas along and adjacent to the margin of the anorthosite.	*
total	26	4		

* Analyses by present author

6.5.1 Classification of the Amphiboles

The analysed amphiboles can be broadly classified as hornblendes. Owing to the complex chemistry of the amphiboles three alternate classificatory schemes are employed. Each scheme uses differing parameters and each brings out certain features common to all of the amphiboles and also important differences in chemistry between certain groups of amphiboles.

Firstly, the high-grade calciferous amphiboles can be classified with respect to the diagram given by Leake (1968). In this diagram (fig. 6.10) Si atoms are plotted against niggli mg (the atomic ratio Mg/Mg + Fe + Mn). None of the analysed amphiboles have niggli mg values below 0.5. This diagram applies to amphiboles with greater than 2.5 atoms (Ca + Na + K) and less than 0.5 atoms of titanium per unit formula. The latter criterion is satisfied by all of the South Harris amphiboles, whilst the former is broken by two of the high-grade amphiboles which contain only slightly less than the required 2.5 atoms (Ca + Na + K) and are included on this diagram. However, amphiboles formed during the retrograde metamorphism have markedly less than the prescribed 2.5 atoms (Ca + Na + K) and are thus not plotted on this diagram. These, according to the classificatory scheme of Leake, would be actinolitic-hornblendes (sample no. SH2) and magnesio-hornblendes (sample nos. G12, A9 and A15).

The amphibole terminology used throughout this thesis is based on Leake's classification.

It is apparent from fig. 6.10 that an extensive substitution of Al for Si takes place, up to a maximum of

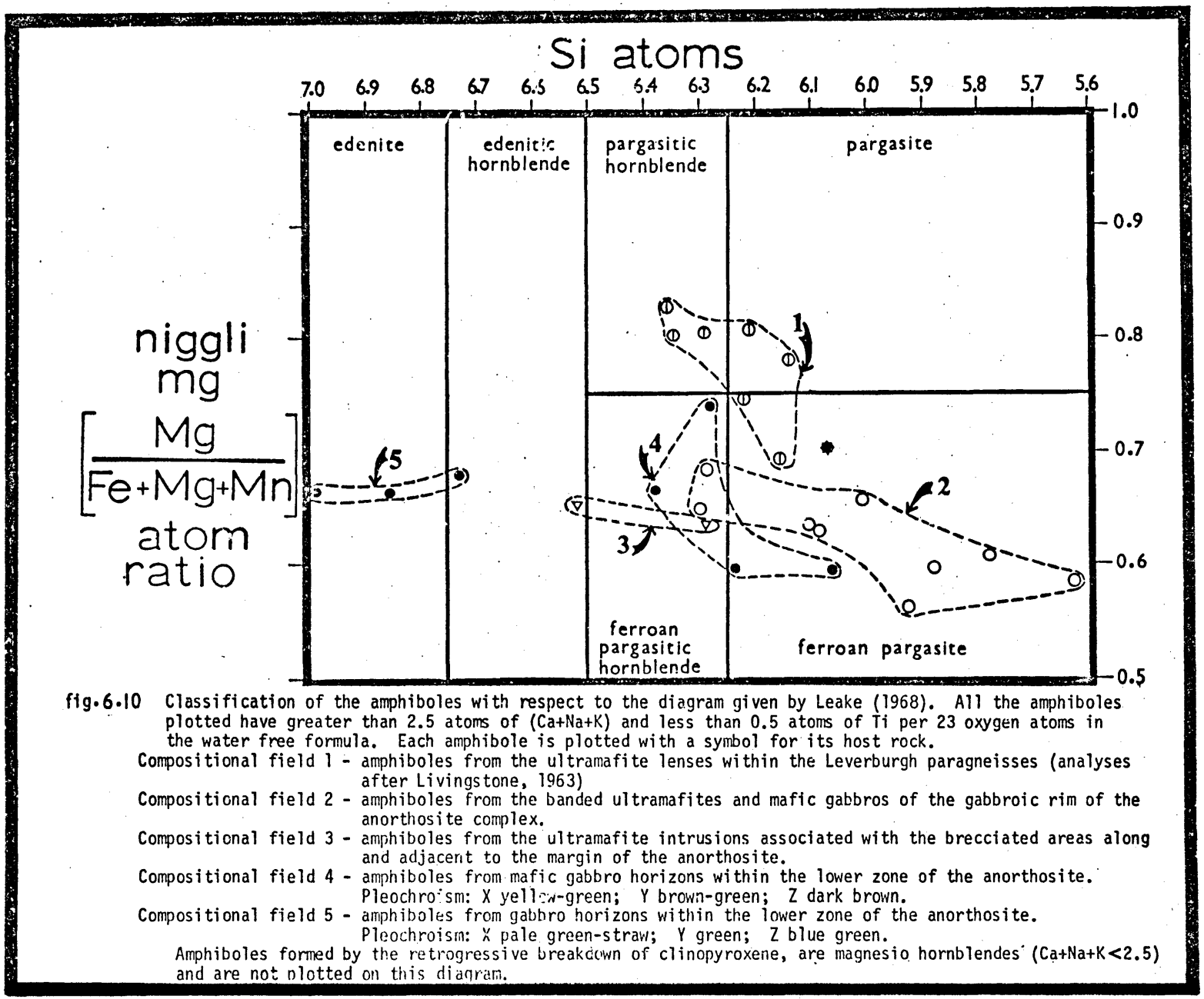


fig.6.10 Classification of the amphiboles with respect to the diagram given by Leake (1968). All the amphiboles plotted have greater than 2.5 atoms of (Ca+Na+K) and less than 0.5 atoms of Ti per 23 oxygen atoms in the water free formula. Each amphibole is plotted with a symbol for its host rock.

Compositional field 1 - amphiboles from the ultramafite lenses within the Leverburgh paragneisses (analyses after Livingstone, 1963)

Compositional field 2 - amphiboles from the banded ultramafites and mafic gabbros of the gabbroic rim of the anorthosite complex.

Compositional field 3 - amphiboles from the ultramafite intrusions associated with the brecciated areas along and adjacent to the margin of the anorthosite.

Compositional field 4 - amphiboles from mafic gabbro horizons within the lower zone of the anorthosite. Pleochroism: X yellow-green; Y brown-green; Z dark brown.

Compositional field 5 - amphiboles from gabbro horizons within the lower zone of the anorthosite. Pleochroism: X pale green-straw; Y green; Z blue green.

Amphiboles formed by the retrogressive breakdown of clinopyroxene, are magnesio hornblendes (Ca+Na+K<2.5) and are not plotted on this diagram.

of 2.37 Al^{IV} atoms per unit formula. It is of interest to note that the amphibole (G5) exhibiting this high Al^{IV} content co-exists with a clinopyroxene containing 18.3% Tschermak's molecule. Tschermak's molecule is effectively a measure of the amount of tetrahedral Al present in the clinopyroxene unit formula and the value quoted above is the highest recorded from the South Harris clinopyroxenes.

The alumina content of the amphibole increases during the transition from clinopyroxene-bearing to garnet-bearing assemblages. This, however, is mainly due to an increase in octahedral aluminium (Al^{VI}) and is not apparent from the diagram in question. Also the amphiboles from the plagioclase-rich rocks tend to show much lower Al^{IV} and Al^{VI} values than those from ultramafites and mafic gabbros. Thus, the pargasites and pargasitic hornblendes (average Al^{IV} - 1.84; average Al^{VI} - 0.59) of the ultramafites and mafic gabbros give way to edenites (average Al^{IV} - 1.13; average Al^{VI} - 0.42) in the more felsic gabbros and anorthositic gabbros of the anorthosite sequence.

Fig. 6.11 shows the amphiboles plotted with respect to tetrahedral Al and (Na + K) atoms per unit formula. The number of tetrahedral Al atoms is obtained by adding Al to Si until eight tetrahedral atoms are reached. In all of the amphiboles plotted on this diagram Na atoms exceed the number of K atoms. Reference points for ideal tremolite, edenite, tschermakite and pargasite are shown on this diagram. The two outer dashed lines show the compositional limits of the hornblendic-amphiboles suggested by Deer et al. (1963). Both the granulite facies and amphibolite facies amphiboles are plotted on this diagram.

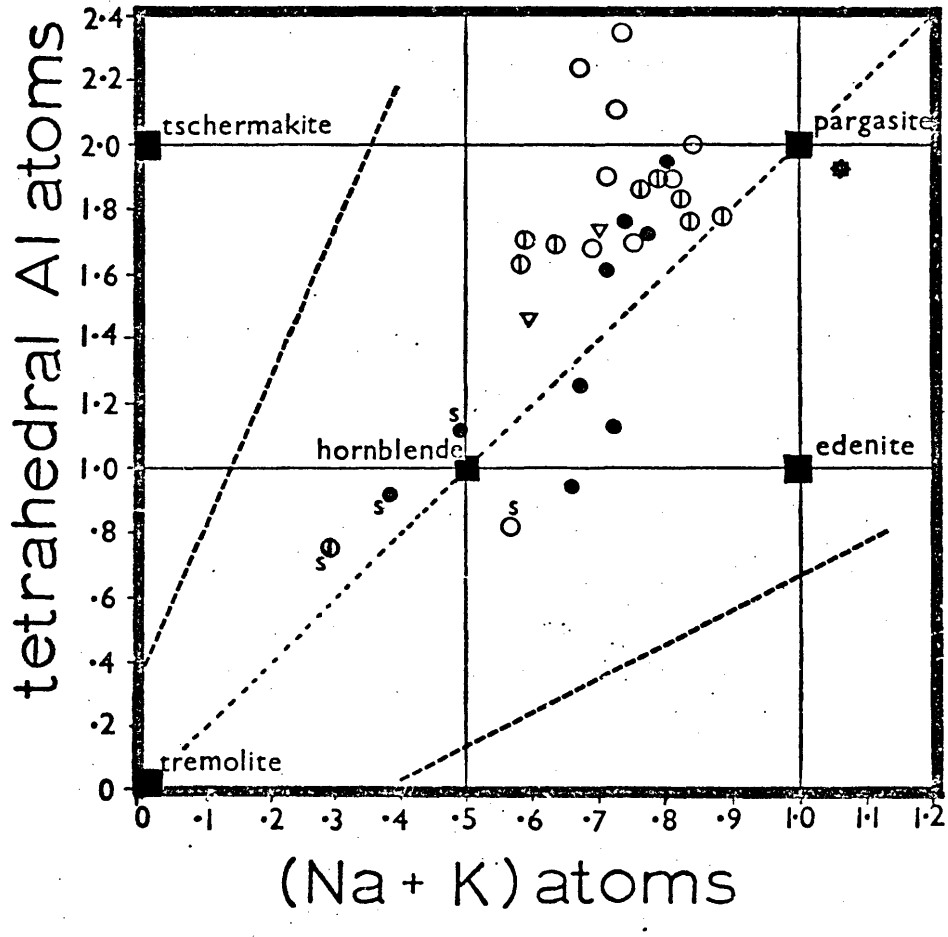


fig. 6.11 Classification of the amphiboles with respect to the number of tetrahedral Al and (Na+K) atoms (after Deer et al, 1963, V.2). The number of atoms are specified with respect to 23 oxygens in the water free unit formula. Each amphibole is plotted with a symbol for its host rock (Table 5.1). Deer et al. S - denotes amphiboles formed by the retrogressive breakdown of clinopyroxene.

The latter are plotted with a symbol for their host rock and are distinguished by the addition of an 's' adjacent to the symbol. These four analyses are all of amphiboles derived from and rimming granulite facies clinopyroxenes. The two basic differences between the granulite facies and amphibolite facies amphiboles are brought out by this diagram:

a) The lower total alkali (Na + K) content of the amphibolite facies amphiboles.

	granulite facies amphiboles		amphibolite facies amphiboles	
	average value	range of values	average value	range of values
Na	0.60	0.96 - 0.35	0.40	0.53 - 0.24
K	0.15	0.35 - 0.01	0.06	0.09 - 0.01
(Na + K)	0.75	1.07 - 0.58	0.46	0.63 - 0.30

b) The lower total Al content of the amphibolite facies amphiboles.

	granulite facies amphiboles		amphibolite facies amphiboles	
	average value	range of values	average value	range of values
Al^{IV}	1.75	2.37 - 0.97	0.84	1.10 - 0.68
Al^{VI}	0.50	0.85 - 0.19	0.45	0.64 - 0.12
total Al	2.25	3.18 - 1.36	1.29	1.65 - 0.80

The lower total Al content of the amphibolite facies amphiboles is due mainly to a decrease in Al^{IV}. This is in line with the conclusions of Zakrutkin (1961) and Kostyuk and Sobolev (1969).

Finally the amphiboles are classified with respect to a diagram (fig. 6.12) given by Ernst (1968) and subsequently modified by Windley and Smith (1974). This diagram gives a

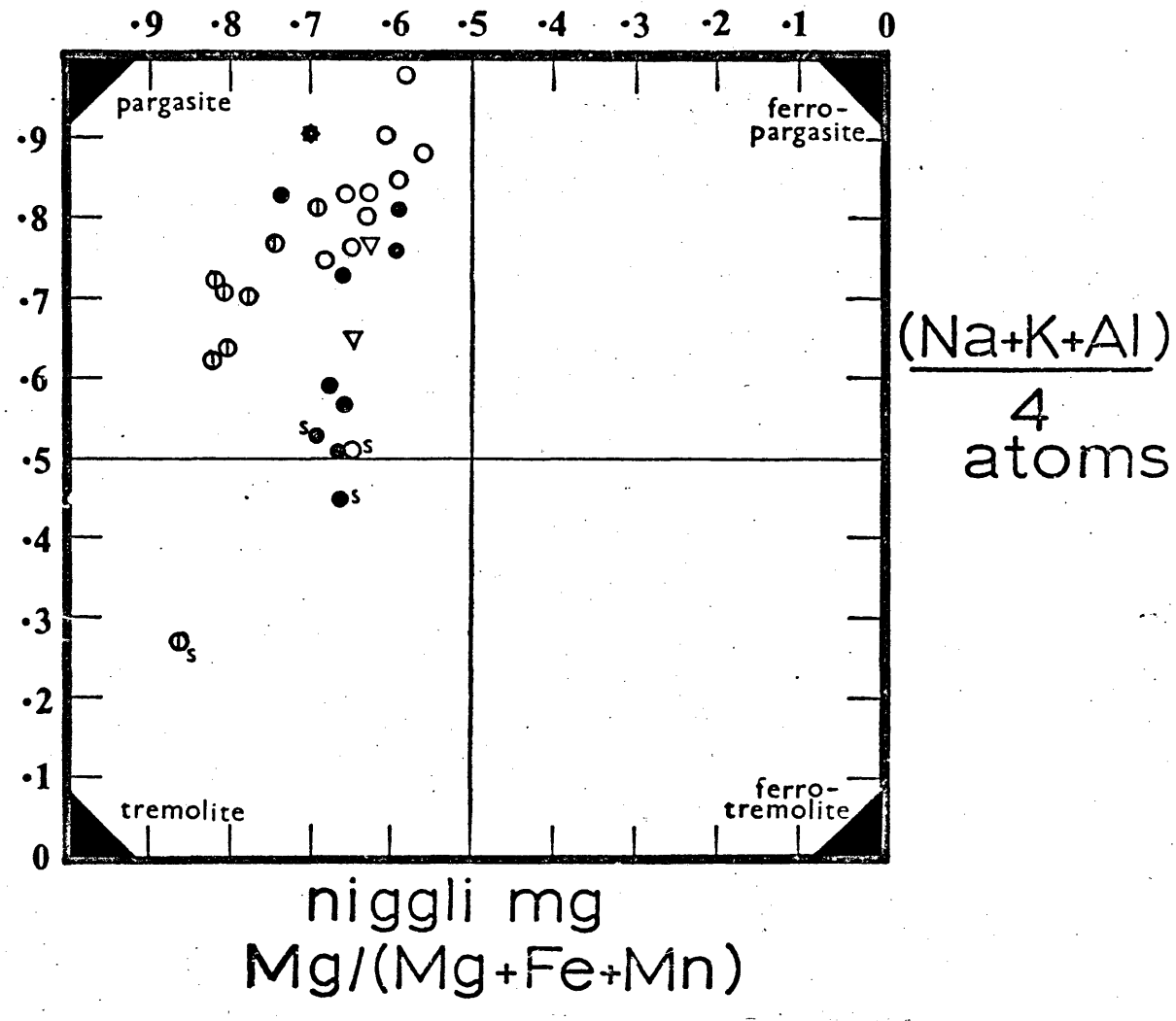


fig. 6.12 Classification of the South Harris amphiboles with respect to a diagram given by Ernst (1968, Fig 10), modified by Windley and Smith (1974). This modification takes into account the fact that microprobe analyses do not yield a value for ferric iron. Windley and Smith added potassium to sodium so that the ordinate is (Na+K+Al) rather than (Na+Al+Fe^3) as suggested by Ernst.
Each amphibole is plotted with a symbol for its host rock (table 5.1).

classification of the amphiboles in terms of pargasite and tremolite end-members and their iron-rich equivalents.

6.5.2 Element Variations within the Amphiboles

Kostyuk and Sobolev (1969), in a general survey of calciferous amphiboles from metamorphic rocks, have demonstrated several coherent relationships between element pairs within those amphiboles from the same paragenetic province. These linear relationships result from isomorphous substitution during metamorphism.

Fig. 6.13 a and b show that both SiO_2 - Al_2O_3 and FeO - MgO show good negative correlations. On both of these diagrams all of the data points lie well within two standard errors of the dashed lines. Crystal chemistry also predicts a positive correlation between MnO - FeO. However, as can be seen from fig. 6.14, there is virtually no correlation between these two oxides. The values of MnO within the South Harris amphiboles are low (less than 0.2%) and this relationship may be highly sensitive to the oxidation state of the iron. Alternatively the lack of correlation between MnO and FeO, in the high grade amphiboles, may reflect a state of partial disequilibrium in the host rock, brought about by the low grade amphibolite facies metamorphism.

The relation between Wt% Cr_2O_3 - FeO and wt% TiO_2 - FeO is shown in fig. 6.15 a and 6.15b. In both of these diagrams there is almost a complete segregation of the amphiboles depending on the nature of their host rock. Chromium values in the amphiboles from the anorthosite complex are very low, reflecting the anomalously low Cr_2O_3 values in the bulk-rock analyses of these rocks. TiO_2 and FeO show a weak positive correlation. It is noticeable from this diagram that TiO_2 values for the granulite facies amphiboles are significantly

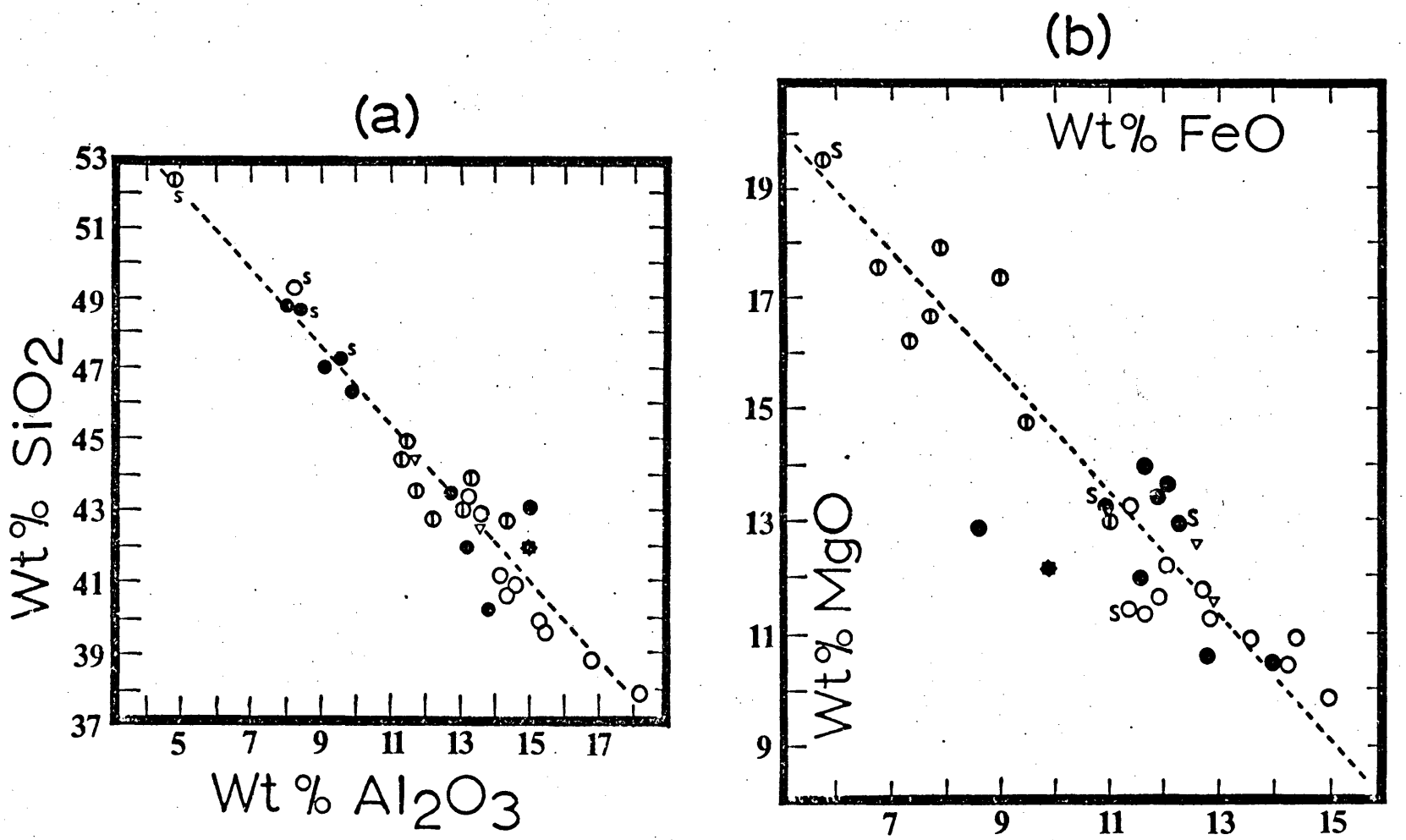


fig. 6.13 (a) - the relation between wt% SiO_2 and Al_2O_3 in the amphiboles.
(b) - the relation between wt% MgO and FeO (total iron as FeO) in the amphiboles.
Each amphibole is plotted with a symbol for its host rock (see table 5.1). S - denotes amphiboles derived from and rimming clinopyroxenes (amphiboles formed during retrogression). Note that the scales do not begin at zero. The dashed lines were fitted by eye.

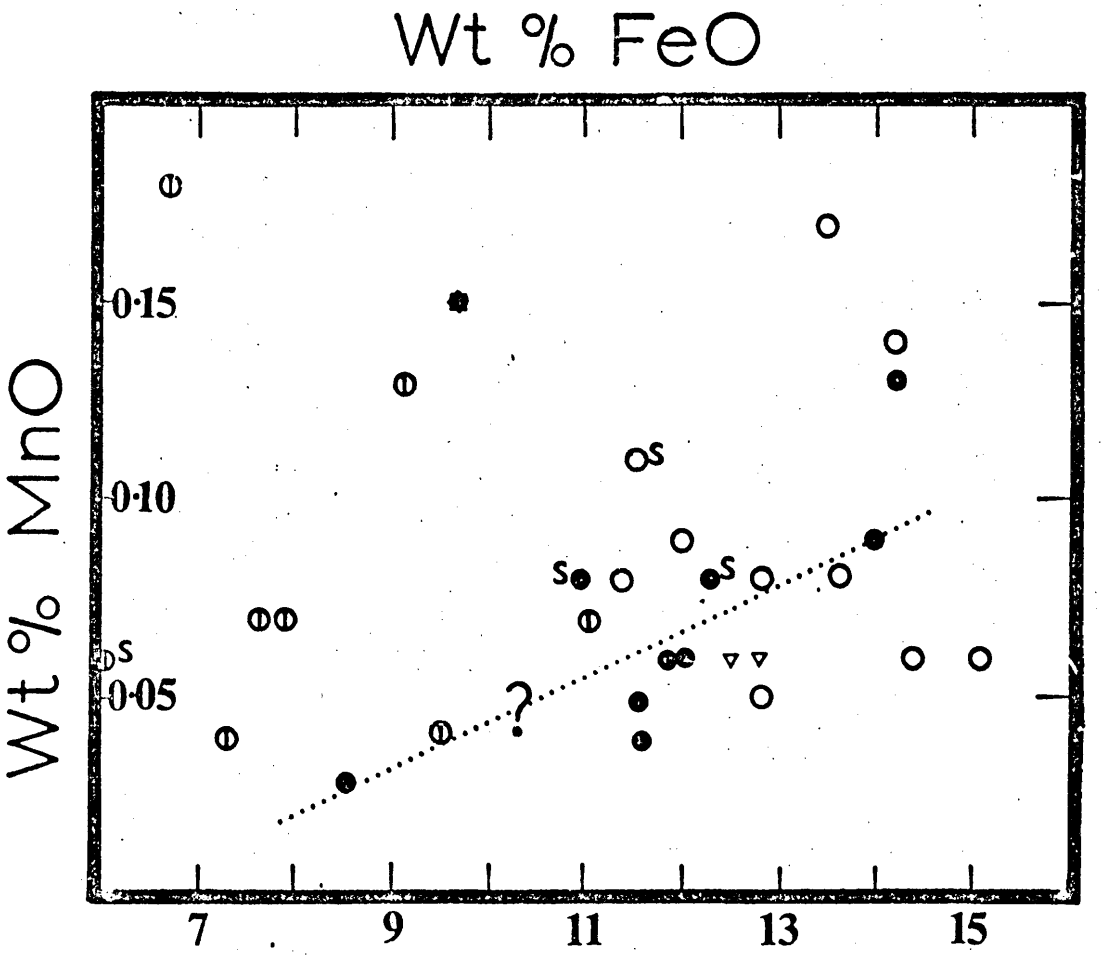


fig. 6.14 The relation between wt% FeO and MnO in the amphiboles. (FeO = total iron calculated as FeO). Each amphibole is plotted with a symbol for its host rock (Table 5.1). S - denotes amphiboles derived from and rimming clinopyroxenes (amphiboles formed during retrogression).

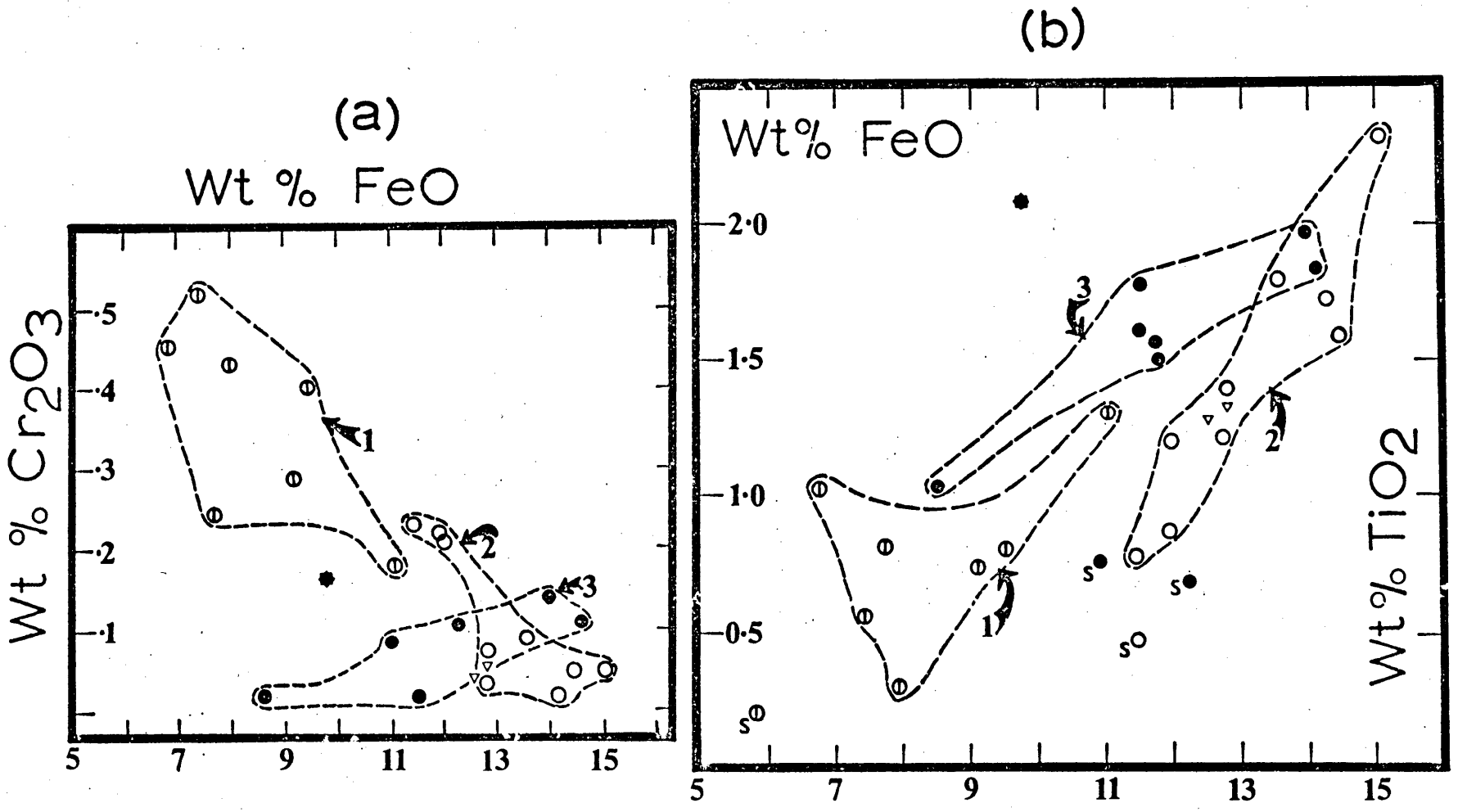


fig. 6.15 (a) - the relation between wt% Cr_2O_3 and FeO (total iron as FeO) in the amphiboles.
(b) - the relation between wt% TiO_2 and FeO (total iron as FeO) in the amphiboles.
Each amphibole is plotted with a symbol for its host rock (table 5,1).
S - denotes amphiboles derived from and rimmed clinopyroxenes.
Field 1 - amphiboles from ultramafites, occuring as lenses within the Leverburgh metasediments.
Field 2 - amphiboles from banded ultramafites and mafic gabbros from the gabbroic rim of the anorthosite complex.
Field 3 - amphiboles from the 'anorthosites'.

higher than those for the amphibolite facies amphiboles : average TiO_2 (26 analyses) for granulite facies amphiboles - 1.33% ; average TiO_2 (4 analyses) for amphibolite facies amphibole - 0.05%.

The Fe/Fe + Mg ratio of the high-grade amphiboles is dependent upon the composition of the host rock (fig. 6.9b). In general the Fe/Fe + Mg ratio of these amphiboles is equal to or only slightly less than that of the host rock. The Fe/Fe + Mg ratio of the low-grade (amphibolite facies) amphibole is also lower than that of the host rock and significantly lower than that of the high-grade amphibole from the same rock.

	Fe/Fe + Mg		
Sample No.	Host Rock	High Grade Amphibole (Granulite Facies)	Low Grade Amphibole (Amphibolite Facies)
G 12	0.463	0.404	0.344
A 9	0.416	0.405	0.329
A 15	0.403	0.402	0.302

6.6 Plagioclase Feldspar

Analyses have revealed a compositional range for the plagioclase feldspar from the anorthosite complex of An_{14} to An_{85} (Table 6.1). Firstly, dealing with the plagioclases from the anorthosite, the anorthite content of these feldspars appear to be dependent on the mafic index of the rock. The highly felsic rock types contain calcic plagioclase (up to $An_{71.6}$), whilst the mafic rock types contain sodic plagioclase (An_{39} - An_{37}). It is thought that the original (pre-metamorphic) composition of the plagioclases from the anorthosites was fairly constant (An_{69-71}, regardless of the mafic index of the rock)

and that the observed variation in composition is attributable to metamorphic recrystallization.

The plagioclases from the banded ultramafites and mafic gabbros, with one exception, are considerably more calcic (An_{77} - An_{85}), and are thought to have undergone little change in composition during metamorphic recrystallization.

Partial chemical analyses of twenty-two plagioclase feldspars, from the quartz gabbros, have also been made. In the majority of these, calcium (or calcium and sodium) values only were determined. These rocks contain plagioclase feldspar of widely varying composition - An_{14} to An_{56} - which includes the most sodic plagioclase recorded from the complex.

The plagioclase feldspars vary in colour from purple - pink - mottled pink/white - white. Minor elements have been analysed in some of the plagioclases to try and determine the cause of the colour variation in this mineral. Quantitative and semi-quantitative determinations of the FeO, MgO, MnO and TiO_2 concentrations of both the pink and white feldspars have been made:

	White Plagioclase Feldspar	Pink Plagioclase Feldspar
FeO (total iron)	<0.14%	0.6 - 1.2%
MnO	<0.04%	>0.2%
MgO	n.d.	n.d.
TiO_2	n.d.	n.d. except for one sample which yielded a value of 0.3%

Anorthosite	Mafic gabbro	$An_{37}Ab_{62.5}Or_{0.5} \leftrightarrow An_{39}Ab_{60}Or_1$
	Gabbro	$An_{44}Ab_{55}Or_1 \longleftrightarrow An_{52}Ab_{47}Or_1$
	Gabbroic-anorthosite	$An_{56}Ab_{43}Or_1 \longleftrightarrow An_{69}Ab_{29}Or_2$
	Anorthosite	$Ab_{64}Ab_{33}Or_2 \longleftrightarrow An_{72}Ab_{27}Or_1$
Banded ultramafites and mafic gabbros from the gabbroic rim of the anorthosite complex.		$An_{85}Ab_{15}Or_0 \longleftrightarrow An_{78}Ab_{22}Or_0$
Quartz gabbros from the gabbroic rim of the anorthosite complex	Quartz gabbros (3-4% modal quartz)	An_{53} - An_{56}*
	Quartz gabbros (4-12% modal quartz)	An_{14} - An_{30}*

* partial chemical analyses - Ca only determined.

Table 6.1 The compositions of plagioclase feldspars from the rocks of the anorthosite complex.

In thin section, the pink feldspars are crowded with tiny brownish-red rods and laths. From the minor element determinations, this included or exsolved material is concluded to be either haematite or, in one case, titano-haematite. The haematite rods may represent iron (and titanium) exsolved from the feldspar structure during the high-grade metamorphism. Some feldspars seem to be zoned, with a higher concentration of haematite rods at their margins than internally.

Compositional zoning of the feldspars is rare. Even where a zonation is apparent, a decrease in anorthite content of no more than 3-5 mol. percent from grain centre to grain rim, has been measured. Some plagioclase grains show exsolution lamellae ; a coarse set of lamellae (up to 2 microns in width) and a second later set of very fine lamallae (B. Wood, Manch. Univ., pers. comm.).

The stoichiometry of the plagioclase feldspars is such that the concnetration of each element is strictly controlled by the overall composition of the mineral. Thus the weight percent values of CaO, Na_2O and K_2O will predict the amounts of SiO_2 and Al_2O_3 and the SiO_2 : Al_2O_3 ratio. The analysed plagioclase feldspars show varying degrees of departure from their stoichiometric formulae. The degree of non-stoichiometry, shown by each analysed plagioclase, has been calculated in terms of either a deficiency in or an excess of Al_2O_3 and SiO_2, relative to the weight percent concentration of CaO, Na_2O and K_2O (Table 6.2). A deficiency or excess of either SiO_2 or Al_2O_3 at the 0.05% level is well within the limits of experimental error, however an excess or deficiency of up to 6.0% clearly is significant and would require an

Sample No.	SiO_2	Al_2O_3
A 9	+ 0.33%	- 0.85%
A 12	+ 0.07%	+ 0.78%
A 15	- 1.26%	+ 3.29%
A 18	+ 0.66%	+ 0.77%
A 19	- 2.15%	+ 0.17%
A 23	- 0.04%	- 0.09%
A 45	- 6.63%	+ 3.08%
A 46	+ 0.03%	- 0.05%
A 47	+ 0.04%	- 0.04%
A 50	- 0.29%	- 0.13%
G 1	+ 0.66%	+ 0.51%
G 2	+ 2.16%	+ 0.03%
G 6	- 2.07%	- 2.02%
G 10	- 1.38%	- 0.40%
G 12	- 2.34%	- 0.97%

Table 6.2 Non-stoichiometry in the analysed plagioclase feldspars. Departure from stoichiometry is calculated in terms of an excess of or deficiency in SiO_2 and Al_2O_3 relative to CaO, Na_2O and K_2O.

explanation.

6.7 Epidotes

Minerals from the epidote group occur throughout the highly retrogressed and saussuritised rocks of the anorthosite complex. A number of thin epidote veins also occur cross cutting the banded ultramafite/mafic gabbro sequence of the gabbroic rim of the complex. The epidote within these veins occur in large, 8 - 10 mm., anhedral grains. The variety of interference colours displayed by these grains was thought to be indicative of a strong zonation. Several of the epidotes from these veins were analysed to determine the nature of and the extent of the zoning.

The variation of interference colours of the epidotes shows a good correlation with the replacement of Al^{3+} by Fe^{3+} (fig. 6.16). It is possible that the break in linearity of this relationship is related to the replacement of Al^{3+} in the AlO_6 and $AlO_4(OH)_2$ octahedral chains, in addition to the replacement of Al outside these chains (Deer et al., 1963).

6.8 Chemical Distribution Between Co-existing Minerals

The interelement distributions between co-existing ferro-magnesian minerals will be considered in this section Insufficient data precludes an investigation of the element distribution between the amphiboles and plagioclase feldspars.

An evaluation of the element partitioning between co-existing ferro-magnesian phases may permit estimates of the degree of equilibration and, in some cases, allow

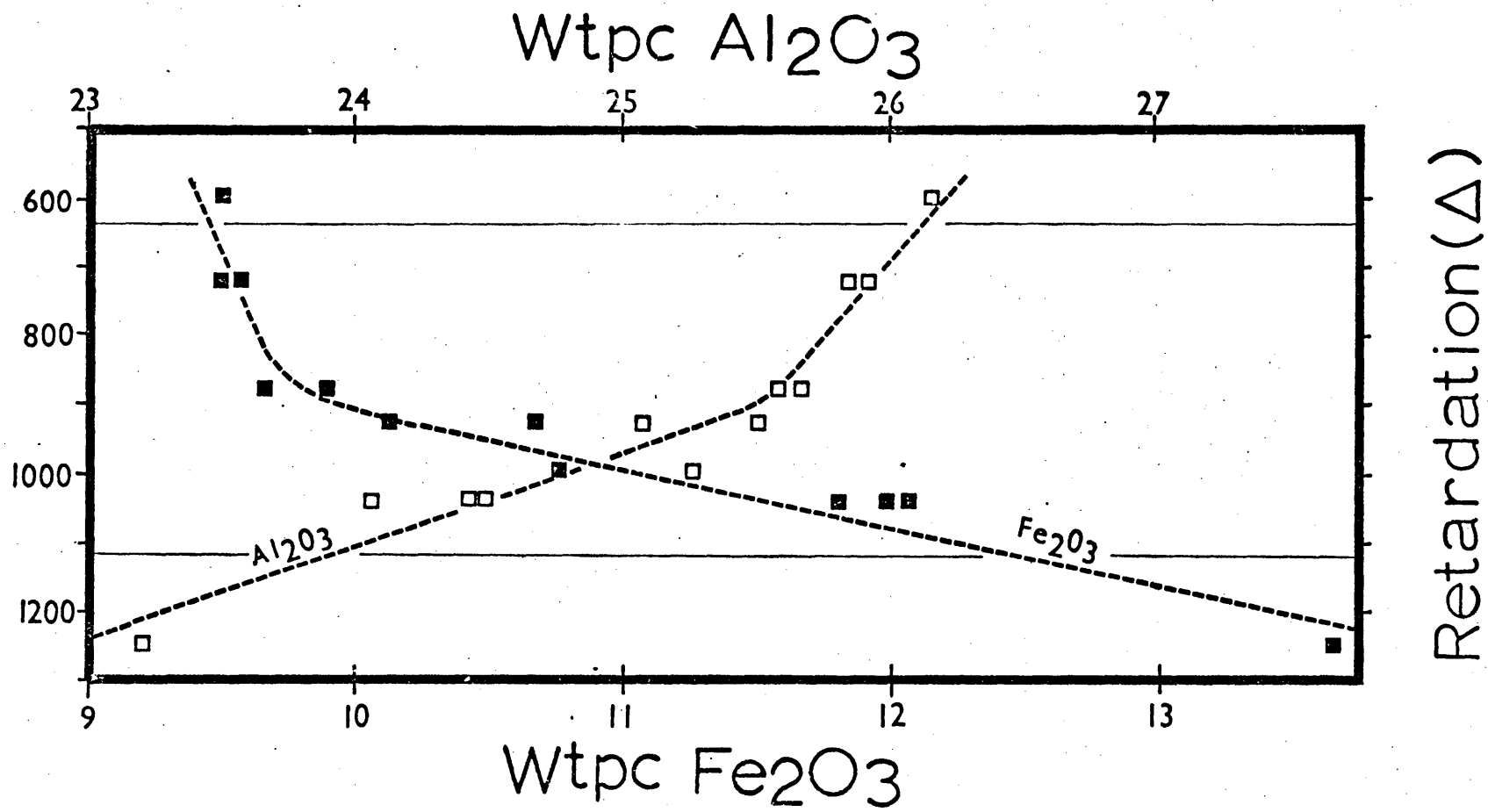


fig. 6.16 The relation between wt% Fe_2O_3, Al_2O_3 and retardation (estimated from interference colours) in epidotes. Open squares - Al_2O_3 Solid squares - Fe_2O_3. Dashed lines fitted by eye.

estimates of temperature conditions to be made.

Fig. 6.17 shows the Fe/Mg distribution between co-existing ferro-magnesian phases. The variation between Fe/Mg ratios of the individual phases and the Fe/Mg ratio of their respective host rocks has already been considered (figs. 6.5 and 6.9). From fig. 6.17 it can be seen that the order of preference of magnesium, in these phases, is clinopyroxene, amphibole, orthopyroxene and finally garnet. This order is in agreement with that expected from equilibration during solid-state metamorphic reactions.

The distribution coefficients of iron and magnesian between co-existing garnet and clinopyroxene ($K'_{(Mg-Fe)}$) fall within the range of values (K' = 7.8-3.5) found for intermediate pressure granulite facies rocks by Chappell and White (1970). The garnet-clinopyroxene pair from the rock B10 also falls within this field. This is interesting, as the clinopyroxene from this rock, on the basis of the ratio percent jadeite : percent Tschermakite, would indicate an eclogitic paragenesis.(fig.6.4). There is some evidence that equilibrium between Fe and Mg was attained during the high grade metamorphism. The partitioning of Fe and Mg between co-existing ortho- and clinopyroxenes, under equilibrium conditions, can be considered in terms of the distribution coefficient $K_{D(Mg-Fe)}$. Assemblages containing co-existing ortho- and clinopyroxenes are relatively rare in the South Harris igneous rocks. The distribution coefficients ($K_{D(Mg-Fe)}$) have been calculated for four pyroxene pairs and the results are presented in Table 6.3A. All of these values fall within the range of $K_{D(Mg-Fe)}$ for high-grade metamorphic rocks found by Kretz (1963). Fe^{3+} values for the samples A23 and G17 are not

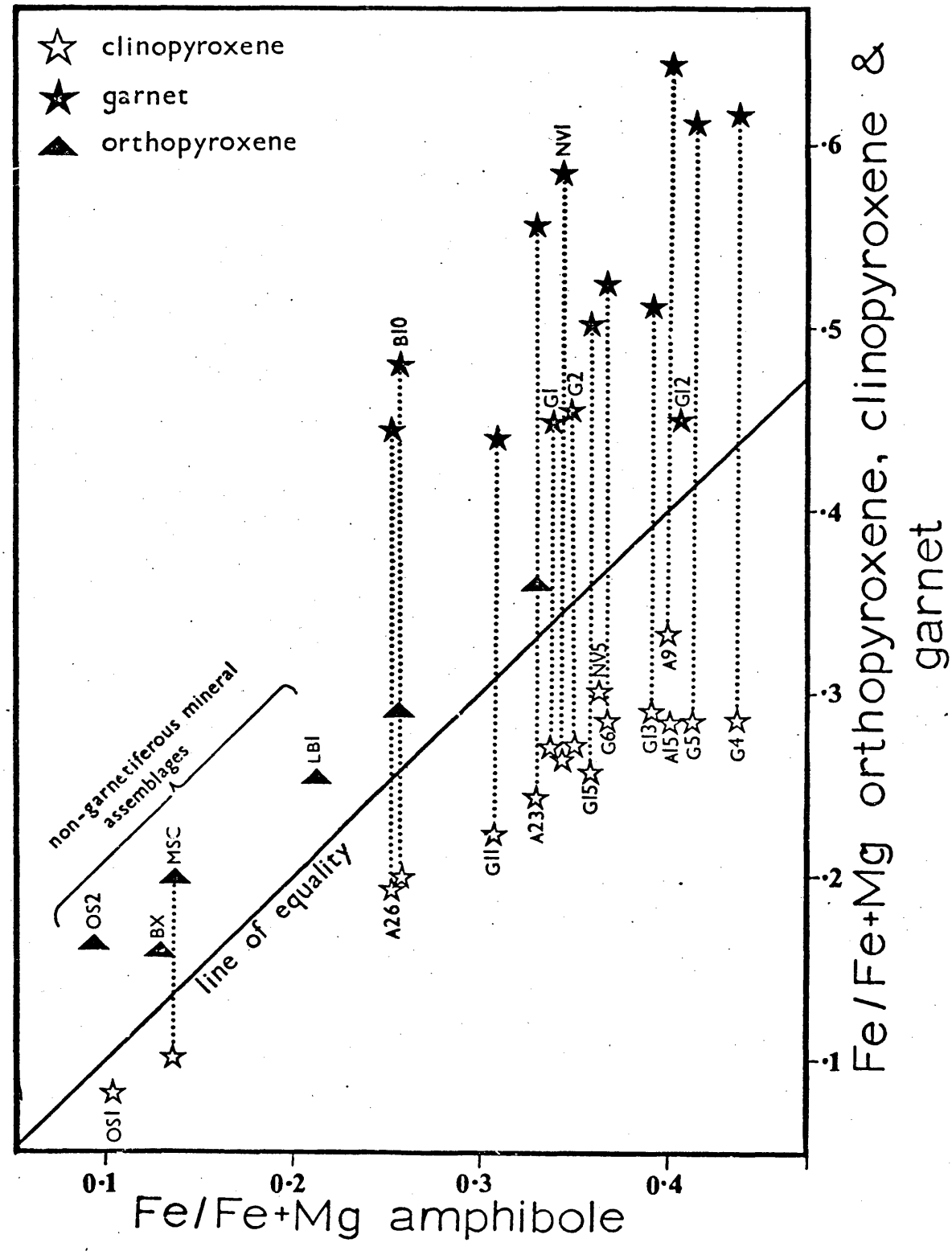


fig. 6.17 Distribution of iron and magnesium (expressed as the atomic ratio Fe/Fe+Mg) between orthopyroxene, clinopyroxene and garnet, with respect to co-existing amphibole. Co-existing mineral phases have been joined by dotted lines. Note that both scales do not begin at zero.

known and "total iron as FeO" values were substituted for Fe^{2+} in the calculation of the K_D value. Where Fe^{3+} values are low this will not make a significant difference to the result. The Mg-Fe distribution between co-existing pyroxenes in the South Harris igneous rocks indicates equilibration under metamorphic conditions.

The co-existing pyroxene pairs, from the samples A23, G17, B10 and MSC, have enabled an estimate of temperature to be made using the method of Wood and Banno (1973). This method gives the temperature of equilibration and is generally accurate to within 70°c for co-existing pyroxenes at the magnesian end of the solid solution series. The temperature estimations for samples A23 and G17 are probably less accurate than the above figure suggests, as the Fe^{3+} values for these pyroxenes is unknown. The calculated temperatures (Table 6.3B) of between 1131° to 1314° C are clearly too high for equilibration under metamorphic conditions. Dickinson (1974) has estimated temperatures of between 700-800° C (at pressures 7.5 - 10 Kbars) for the high-grade, granulite facies, metamorphism in this area. The K_D values for these pyroxenes are clearly indicative of metamorphic equilibration; however, the temperature estimates, from the same pyroxene pairs, are more in line with igneous crystallization. It is thought particularily significant that the highest calculated temperature - 1314° C from sample MSC - is from the most magnesian-rich rock.

The distribution of Al, Cr, Ti and Mn between co-existing ferro-magnesian minerals is shown in fig. 6.18. There is a weak positive correlation between Al in the clinopyroxenes and amphiboles. The distribution of Ti

Ⓐ

Sample No.	Opx ($XMgSiO_3$ = Mg/Mg + Fe)	Cpx ($XMgCaSi_2O_6$ = Mg/Mg + Fe)	K_D(Mg-Fe)
A 23	0.501	0.639	0.567
G 17	0.513	0.625	0.632
B 10	0.559	0.661	0.650
MSC	0.671	0.790	0.542

Ⓑ

Sample No.	cpx $a_{Mg_2Si_2O_6}$	opx $a_{Mg_2Si_2O_6}$	X^{opx}_{Fe}	Calculated Temperature (°C)
A 23	0.256	0.384	0.359	1134°
G 17	0.240	0.410	0.335	1131°
B 10	0.228	0.462	0.287	1148°
MSC	0.361	0.580	0.196	1314°

Table 6.3 A - Distribution of Mg and Fe^{2+} between co-existing clinopyroxene and orthopyroxene (Kretz, 1963). The distribution coefficeint is defined as:-

$$K_{D(Mg-Fe)} \equiv \frac{XMgSiO_3}{1-XMgSiO_3} \cdot \frac{1-XMgCaSi_2O_6}{XMgSi_2O_6}$$

B - Temperature estimates from co-existing pyroxenes using the method of Wood and Banno (1973). The temperature is derived from the following semi-empirical equation:-

$$T^oK \left[\ln \frac{a^{cpx}_{Mg_2Si_2O_6}}{a^{opx}_{Mg_2Si_2O_6}}\right] - 7.65\, X^{opx}_{Fe} + 3.88\, (X^{opx}_{Fe})^2 - 4.6 = \frac{-10202}{}$$

where $X^{opx}_{Fe} = Fe^{2+}/Fe^{2+} + Mg^{2+}$ (opx)

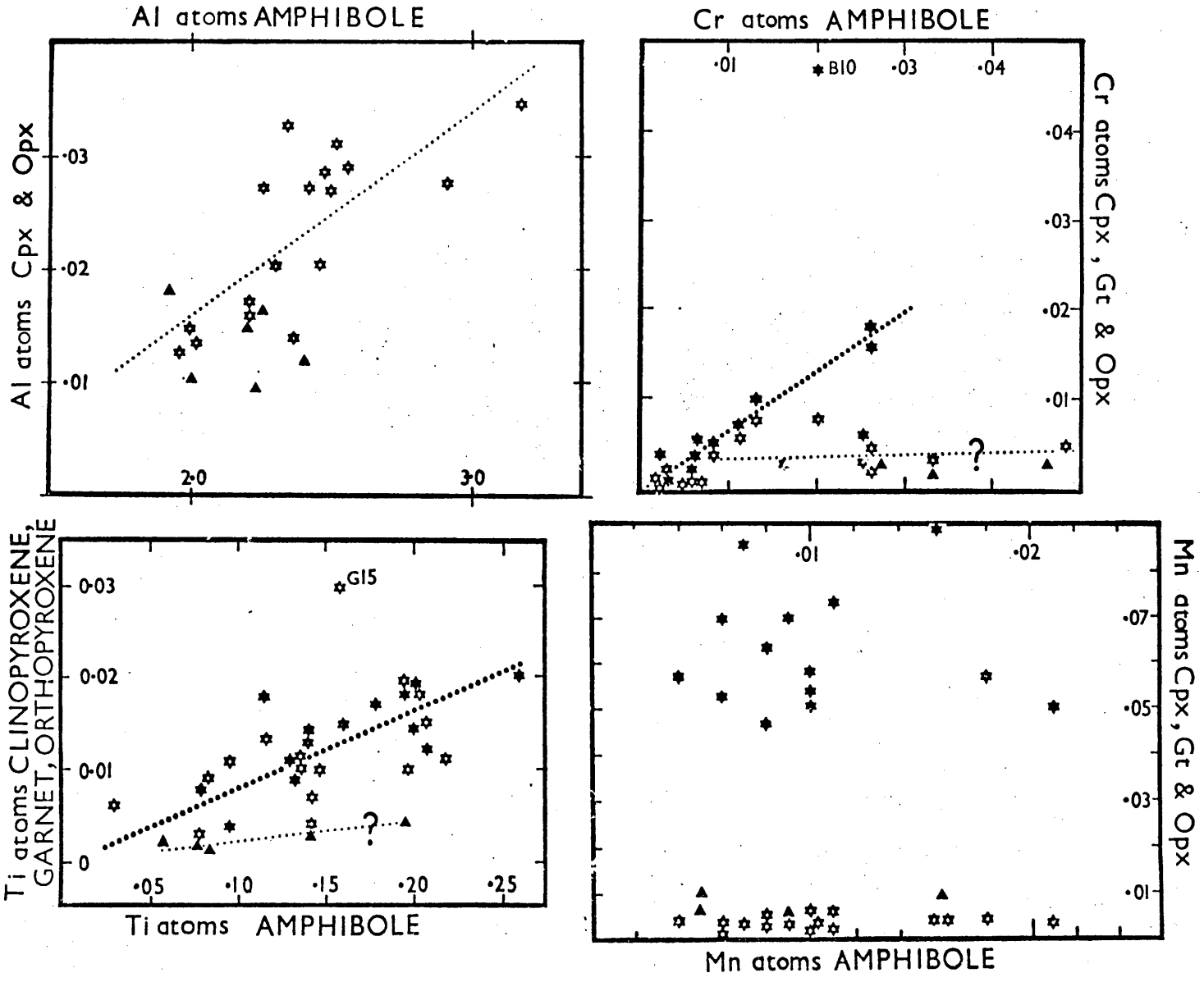
and $aMgSiO_6$ $(Mg^{2+}/Mg^{2+} + Fe^{2+} + Ca^{2+} + Mn^{2+} + Na^{+})_{M2}$ X

$(Mg^{2+}/Mg^{2+} + Fe^{2+} + Fe^{3+} + Al^{3+} + Cr^{3+} + Ti^{4+})$ MI

$^oK - 273.16 = {}^oC$

fig.6.18 Relation between Al, Cr, Ti and Mn atoms of clinopyroxenes, orthopyroxenes, garnets and coexisting amphiboles. The number of atoms was calculated with respect to 6 atoms of oxygen in the pyroxenes, 24 atoms of oxygen in the garnets and 23 atoms for water free amphibole analyses.

Solid stars - garnet; Open stars - clinopyroxene; Solid triangles - orthopyroxene. Dotted lines were inserted by eye. Anomolous points are labelled with their sample numbers.



between amphibole-clinopyroxene and amphibole-garnet shows a reasonably good positive correlation. Except for the sample B10, a good positive correlation for Cr exists between the garnets and amphiboles. Mn shows no obvious correlations.

There is good evidence that equilibration between Mg and Fe was obtained during the high grade metamorphism:-

a) the systematic variation of the Fe/Mg ratio of the ferro-magnesian minerals with the Fe/Mg ratio of their respective host rocks.

b) the $K_{D(Mg-Fe)}$ values for pyroxene pairs fall within the range of values for metamorphic rocks.

However, the partitioning of Al, Ti, Cr and in particular Mn between the co-existing ferro-magnesian phases would suggest that these elements were comparatively insensitive to change during metamorphic recrystallization.

Summary and Conclusions

The main conclusions from the present study of the Roneval anorthosite complex and the associated meta-igneous rocks have been summarized at the end of each chapter. These conclusions are now brought together and presented in the form of a list.

The Anorthosite

1) The anorthosite body is thought to be a basin or sill-like intrusion formed by gravity differentiation of a basic magma.
2) It was intruded into the meta-sedimentary cover sequence during the early Scourian and is of a similar age to the Ness anorthosite in North Lewis.
3) The anorthosite sequence comprises of a great number of gravity stratified units. Each unit has a gabbroic base and an anorthositic top. Within the lower zone of the anorthosite the basal gabbroic portion of these units is predominant. Higher within the anorthosite sequence (the upper zone) the anorthositic portion of these units is predominant.
4) The entire differentiation pattern shown by the rocks of the anorthosite body can be satisfactorily attributed to plagioclase feldspar (and clinopyroxene at the base of the sequence) fractionation as the natural chemical data of these rocks fall on or very close to the theoretical curves for this mineral.
5) The anorthosite displays features, both on the scale of a single gravity stratified unit and on the scale of the entire body, which favour a 'plagioclase flotation ' model.
6) The parent magma for the anorthosite body was a high-alumina calc alkalic (anhydrous) gabbroic anorthosite.
7) The generally smooth liquid lines of descent, in the Pearce variation diagrams, indicate that only one magma pulse is necessary to explain this rhythmically layered sequence.

The Gabbroic rim of the Anorthosite

1) Despite the close spatial relationship of the gabbros of the gabbroic rim and the anorthosite body, they are concluded to have been derived from two seperate intrusions. The gabbroic rim of the anorthosite complex is thought to represent a basic sill-like body intruded into the meta-sedimentary cover sequence prior to the intrusion of the anorthosite.
2) Along the upper and lower surfaces of this intrusion the basic material underwent a large scale in situ assimilation of the quartzose paragneisses which produced the hybridized sheath of quartz gabbros.
3) Centrally within the intrusion the unmodified basic magma differentiated under the influence of gravity to produce a layered sequence.

4) The layering is defined on a large scale by an alternation of mafic gabbros and ultramafites. Within these rock layers a small-scale rhythmic layering is developed.
5) The differentiation pattern displayed by the layered gabbros from the central part of the gabbroic envelope can be ascribed to the fractional crystallization of plagioclase feldspar (bytownite An_{85}) and clinopyroxene, in the case of the mafic gabbros, and plagioclase feldspar, clinopyroxene and ilmenite, in the case of the ultramafites.

General

1) The earliest mineral assemblages and textures recognized in the rocks of the anorthosite complex date from an early Scourian (Badcallian) hornblende granulite facies metamorphism. The preservation of igneous differentiation trends within the rocks of the anorthosite complex suggests that this metamorphism was essentially isochemical.
2) The anorthosite complex and its cover sequence were compressed into a neutral isoclinal syncline, the anorthosite forms the observed core to this fold. The resultant double-layered complex was further flattened during the major Laxfordian folding of the Outer Isles.
3) Within the anorthosite complex and its environs there are no intrusive bodies that can, with certainty, be recognized as Scourie dykes.
4) Three rock suites (representing three seperate magma types) can be recognized in the Outer Isles:-
   a) A high-alumina calc alkalic suite. The anorthosite, gabbro-diorite, norite and Langavat ultramafites (dunites,peridotites and pyroxenites) are thought to constitute a calc alkalic 'Alpine suite'. The dunites, peridotites and pyroxenites from the Langavat belt are thought to represent a refractory olivine/orthopyroxene residuum produced by fractional crystallization from a parental olivine basalt magma. The complimentary high alumina basaltic liquid may have undergone further fractional crystallization at shallower levels giving rise to three seperate high-alumina magmas now represented by the anorthosite, gabbro-diorite and norite.
   b) A nepheline normative alkalic suite, represented by a variety of Scourian and Laxfordian basic intrusions in South Harris.
   c) A tholeiitic suite represented by the Scourie dykes, which, although not identified in South Harris, are abundant throughout the remainder of the Outer Isles.

   Comparisons are drawn with the magma types described from the Japanese arc system and it is concluded that the recognition of these three rock suites

from the Outer Isles supports the interpretation of this area as an Archean arc system.

5) The chronological sequence of intrusion in South Harris suggests a successively shallower depth of magma generation.

REFERENCES

Bhattacharyya, C. 1971: An evaluation of the chemical differences between igneous and metamorphic orthopyroxenes. Amer. Miner, 56, 499-506.

Bowes, D.R. 1968: An orogenic interpretation of the Lewissian of Scotland. 23rd Int. Geol. Congress, 4, 225-236.

Buddington, A.F. 1952: Chemical petrology of some metamorphosed Adirondack gabbroic, syenitic and quartz syenitic rocks. Amer. J. Sci. (Bowen Volume), 37-84.

Burns, D.J. 1966: Chemical and mineralogical changes associated with the Laxfordian metamorphism of dolerite dykes in the Scourie-Loch Laxford area, Sutherland, Scotland. Geol. Mag., 103, 19-35.

Chappell, B.W. and White, A.J.R. 1970: Further data on an eclogite from the Sittampundi complex, India. Mineralog. Mag., 37, 555-560.

Coward, M.P., Francis, P.J., Graham, R.H., Myers, J.S. and Watson, J. 1969: Remnants of an early metasedimentary assemblage in the Lewisian complex of the Outer Hebrides. Proc. Geol. Assoc. Lond., 80, 387-408.

Coward, M.P., Francis, P.J., Graham, R.H. and Watson, J. 1970: Large-scale Laxfordian structures of the Outer Hebrides in relation to those of the Scottish mainland. Tectonophys., 10, 425-435.

Davidson, C.F. 1943: The Archaean rocks of the Rodil district, South Harris, Outer Hebrides. Trans. Roy. Soc. Edin., 61, 71-112.

Davies, F.B. 1974: A layered basic complex in the Lewisian, south of Loch Laxford, Sutherland. J. Geol. Soc. Lond., 130, 279-284.

Dearnley, R. 1959: Metamorphic petrology and histroy of the Lewisian rocks of South Harris, Outer Hebrides. PhD thesis, Univ. of Leeds.

Dearnley, R. 1962: An outline of the Lewisian complex of the Outer Hebrides in relation to that of the Scottish mainland. Q.J. Geol. Soc. Lond., 118, 143-176.

Dearnley, R. 1963: The Lewisian complex of South Harris. Q.J. Geol. Soc. Lond., 119, 243-312.

Deer, W.A., Howie, R.A. and Zussman, J. 1963: Rock forming minerals. 5 volumes. London, Longmans.

Dickinson, B.B. 1974: The metamorphic evolution of the Leverburgh supracrustal belt, South Harris, with special reference to the textural variations. Unpubl. PhD thesis, Univ. of London, Imperial College.

Emmons, R.C. 1953: Selected petrogenic relationships of plagioclase. Mem. Geol. Soc. Amer., 52, 142pp.

Emmons, R.C. 1955: Plagioclase silica. Bull. Geol. Soc. Amer., 66, 1061-1062.

Emslie, R.F. 1973: Some chemical characteristics of anorthositic suites and their significance. Can. J. Earth Sci., 10, 54-71.

Ernst, W.G. 1968: Amphiboles. New York: Springer-Verlag.

Evans, C.R. 1965: Geochronology of the Lewisian basement near Lochinver, Sutherland. Nature, Lond., 207, 54-56.

Ferguson, J. and Fripp, R.E.P. 1971: Differentiation in the Losberg intrusion, Fochville, Transvaal. Trans. Geol. Soc. S. Afr., 74, 25-31.

Finger, L.W. 1972: The uncertainty in the calculated ferric iron content of a microprobe analysis. Ann. Rep. Dir. Geophys. Lab. Carnegie Institute, 71, 600-603.

Fleuty, M.J. 1964: The description of folds. Proc. Geol. Ass., 75, 461-492.

Fyfe, W.S., Turner, F.J. and Verhoogen, J. 1958: Metamorphic reactions and metamorphic facies. Mem. Geol. Soc. Am., No. 73.

Garson, M.S. and Livingstone, A. 1973: Is the South Harris complex in north Scotland a Pre-cambrian overthrust slice of oceanic crust and island arc? Nature (Phy-Sci), 243 (127), 74-76.

Graham, R.H. 1969: A structural analysis of Lewisian rocks in parts of North Uist and the Sound of Harris, Outer Hebrides. PhD thesis, Univ. of London, Imperial College.

Green, D.H. and Ringwood, A.E. 1966: An experimental investigation of the gabbro to eclogite transformation and its petrological implications. Publ. No. 444. Department of Geophysics and Geochemistry, Australian National University, Canberra, 1-59.

Green, T.H., Green, D.H. and Ringwood, A.E. 1967: The origin of high alumina basalts and their relationships to quartz tholeiites and alkali basalts. Earth and Planetary Science Letters, 2, 41-51.

Green, D.H. 1969: The origin of basaltic and nephelinitic magmas in the earth's mantle. Tectonophysics (Special Issue: Deep-seated foundations of geological phenomena), 7, 409-422.

Heddle, M.F. 1878: Chapters on the mineralogy of Scotland - IV. Augite, hornblende and serpentinous change. Trans. Roy. Soc. Edin., 28, 453-555.

Hess, H.H. 1960: Stillwater igneous complex, Montana. Mem. Geol. Soc. Am., 80, 230pp.

Howie, R.A. and Smith, J.V. 1966: X-ray emission microanalysis of rock forming minerals. V-Orthopyroxenes. J. Geol., 74, 443-462.

Howie, R.A. and Subramaniam, A.P. 1957: The paragenesis of garnet in charnockite, enderbite and related granulites. Mineralog. Mag., 31, 565-586.

Howley, J.A. 1966: The South Harris anorthosite complex. Robertson Research Internal Report no. 71.

Hutt, D.K. 1974: The geology and geochemistry of part of the Fiskenaesset anorthosite complex, West Greenland. PhD thesis. Univ. of London, Imperial College.

Irvine, T.N. and Barager, W.R.A. 1971: A guide to the chemical classification of the common volcanic rocks. Can. J. Earth Sci., 8, 523-548.

Jehu, T.J. and Craig, R.M. 1927: Geology of the Outer Hebrides - Part IV. South Harris. Trans. Roy. Soc. Edin., 55, 457-488.

Kelsey, C.H. 1965: Calculation of the C.I.P.W. norm. Mineralog. Mag., 34, 276-282.

von Knorring, O. and Dearnley, R. 1960: The Lewisian pegmatites of South Harris, Outer Hebrides. Mineralog. Mag., 32, 366-378.

Kostyuk, E.A. and Sobolev, V.S. 1969: Paragenetic types of calciferous amphiboles of metamorphic rocks. Lithos 2, 67-81.

Kracek, F.C. and Neuvonen, K.J. 1952: Thermochemistry of plagioclase and alkali feldspars. Amer. J. Sci. (Bowen Volume), 293-318.

Kretz, R. 1963: The distribution of magnesium and iron between orthopyroxene and calcic pyroxene in natural mineral assemblages. Journel of Geol., 71, 773-785.

Kuno, H. 1966: Lateral variation of basalt magma types across continental margins and island arcs. Bull. Volcanol., 29, 195-222.

Leake, B.E. 1968: A catalog of analysed calciferous and sub-calciferous amphiboles together with their nomenclature and associated minerals. Geol. Soc. Amer. Spec. Pap. 98, 210pp.

Livingstone, A. 1963: Geochemical studies of ultrabasic rocks from the Outer Hebrides. Unpub. PhD thesis, Univ. of Manchester.

Livingstone, A. 1967: A garnet peridotite and a garnet-amphibole pyroxenite from South Harris, Outer Hebrides, and their bearing on the South Harris eclogite facies status. Miner. Mag., 36, 380-388.

Mason, P.K., Frost, M.T. and Reed, S. 1969: British Museum - Imperial College - National Physical Laboratory, computer programs for calculating corrections in quantitative X-ray microanalysis. Nat. Phys. Lab., Dir. of Inorg. and Mett. Struct., IMS Rep., 1, 91pp.

Moorbath, S., Welke, H. and Gale, N.H. 1969: The significance of lead isotope studies in ancient high-grade metamorphic basement complexes, as exemplified by the Lewisian rocks of North-West Scotland. Earth Planet. Sci. Lett., 6, 245-256.

Myers, J.S. 1968: The tectonic and metamorphic history of the Lewisian migmatite complex of Western Harris, Outer Hebrides, Scotland. PhD thesis, Univ. of London, Imperial College.

Myers, J.S. 1970: Gneiss types and their significance in the repeatedly deformed and metamorphosed Lewisian complex of Western Harris, Outer Hebrides. Scott. J. Geol., 6, 186-199.

Newman, D. 1971: Recent developments in mineral exploration in the north-west highlands and islands of Scotland. Trans. Ist. of Mining and Metallurgy, 80, B276-B280.

Nockolds, S.R. 1954: Average chemical composition of some igneous rocks. Bull. Geol. Soc. Am., 65, 1007-1032.

O'Hara, M.J. 1961: Petrology of the Scourie dykes, Sutherland. Mineralog. Mag., 32, 848-865.

Osborn, E.F. 1959: Role of oxygen pressure in the crystallization and differentiation of basaltic magma. Amer. J. Sci., 257, 609-647.

Osborn, E.F. 1969: The complementariness of orogenic andeites and alpine peridotite. Geochim and Cosmoch. Acta., 33, 307-324.

Palmer, K.F. 1971: A comparative study of two Pre-cambrian gneiss areas - The Suportoq region, East Greenland and South Harris, Outer Hebrides - and their bearing on Pre-cambrian crustal evolution. PhD thesis Univ. of Birmingham.

Park R.G. 1970: Observations on Lewisian chronology. Scott. J. Geol., 6, 379-399.

Pearce, T.H. 1968: A contribution to the theory of variation diagrams. Contr. Miner. and Petrol., 19, 142-157.

Pearce, T.H. 1969: Some comments on the differentiation of the Dundonald sill, Ontario. Can.J. Earth Sci., 6, 75-80.

Pearce, T.H. 1970: Chemical variations in the Palisade Sill. J. Pet., 11, 15-32.

Ramsay, J.G. 1967: Folding and fracturing of rocks. McGraw-Hill, New York.

Rickwood, P.C. 1968: On recasting analyses of garnet into end member molecules. Contr. Miner. and Petrol., 18, 175-198.

Sorensen, H. 1953: The ultrabasic rocks at Torqussaq west Greenland. A contribution to the peridotite problem. Medd. Gronland, 136(4), 1-47.

Subramaniam, A.P. 1956: Mineralogy and petrology of Sittampundi complex, Salem District, Madras State, India. Bull. Geol. Soc. Amer., 67, 317-390.

Tarney, J. 1964: The basic and ultrabasic intrusions of the Assynt area, north-west Scotland. PhD Thesis, Univ. of Durham.

Teall, J.J.H. 1885: The metamorphism of dolerite into hornblende schist. Q.J. Geol. Soc. Lond., 41, 133-144.

den Tex, E. 1965: Metamorphic lineages of orogenic plutonism. Geologie en Mijnbouw, 44, 105-132.

Thayer, T.P. 1967: Chemical and structural relations of ultramafic and feldspathic rocks in alpine intrusive complexes. In: Ultramafic and Related Rocks, edited by P.J. Wyllie. John Wiley, New York, N.Y., pp. 222-239.

Thornton, C.P. and Tuttle, O.F. 1960: Chemistry of igneous rocks, 1 - The differentiation index. Amer. J. Sci., 258, 664-684.

de Waard, D. 1965: A proposed subdivision of the granulite facies. Am. J. Sci., 263, 455-461.

Wager, L.R. and Deer, W.A. 1939: Geological investigations in east Greenland, Part III. The petrology of the Skaergaard intrusion, Kangerdlugssuaq, east Greenland. Medd. Gronland, 105(4), 1-352.

Walker, G.P.L. 1962: Low-potash gismondine from Ireland and Iceland. Miner. Mag., 33, 187-201.

Watson, J. 1969: The Pre-Cambrian gneiss complex of Ness, Lewis, in relation to the effects of Laxfordian regeneration. Scott. J. Geol., 5, 269-285.

Watson, J.(in press): The Pre-Cambrian. Geol. Soc. Sp. Report Series.

Watson, J. and Lisle, R.J. 1973: The Pre-Laxfordian complex of the Outer Hebrides. The early Pre-Cambrian of Scotland and related rocks of Greenland. Edited by R.G. Park and J. Tarney. Univ. of Keele, 1973.

Westbrook, G.K. 1974: The South Harris magnetic anomaly. Proc. Geol. Ass., 85(1), 1-12.

Westoll, N.D.S. 1967: The anorthosite complex, Rodil Estate, South Harris. Robertson Research Internal Report, no. 154.

White, A.J.R. 1964: Clinopyroxenes from eclogites and basic granulites. Amer. Mineralog., 49, 883-888.

Windley, B.F., Herd, R.K. and Bowden, A.A. 1973: The Fiskenaesset complex, West Greenland, Part 1. A preliminary study of the stratigraphy, petrology and whole rock chemistry from Qeqertarssuatsiaq. Gronlands Gelogiske Undersogelse, Bull 106, 80pp.

Windley, B.F. and Smith, J.V. 1974:
The Fiskenaesset complex, West Greenland, Part II. General mineral chemistry from Qeqertarssuatsiaq. Gronlands Geologiske Undersogelse, Bull. 108, 54pp.

Wood, B.J. and Banno, S. 1973:
Garnet-orthopyroxene and orthopyroxene-clinopyroxene relationships in simple and complex systems. Contr. Miner. and Petrol., 42, 109-124.

Yoder, H.S. and Tilley, C.E. 1962:
Origin of basalt magmas: and experimental study of natural and synthetic rock systems. J. Pet., 3, 342-532.

Zakrutkin, V.V. 1961: A comparative characteristic of the amphiboles from the rocks the amphibolite and granulite facies of the Anabar shield. Geologiya i Geofizika, N9 (in Russian).

APPENDIX 1

WHOLE ROCK AND MINERAL ANALYSES

WHOLE-ROCK AND MINERAL ANALYSES

A BRIEF NOTE ON ANALYTICAL METHOD AND DATA PROCESSING TECHNIQUES

WHOLE-ROCK ANALYSES

Major elements, and selected trace elements, were determined with the Phillips 1212 automatic X-ray flourescence spectrometer. Ferrous iron oxide values for forty-three analyses were determined by wet chemical methods. For major element oxides the values obtained should be accurate to within ± 1% and minor element oxide values accurate to between 3-5%.

Rock analyses were recalculated into C.I.P.W. normative molecules, using the computer program LEMNORM (written by R. W. Le Maitre). This program uses the norm calculation procedure suggested by Kelsey (1965) and, in addition, produces and plots a number of normative ratios.

MINERAL ANALYSES

All mineral analyses were made on polished thin sections using a semi-automated Cambridge electron microprobe. Elements were analysized in pairs using beam currents up to 0.1 micro-amps. The following natural and synthetic standards were used for analysis:-

natural wollastonite (WOLL).....for Ca and Si
synthetic titanium oxide (TIOX).....for Ti
synthetic spinel (MGALOX).....for Al (and Mg)
synthetic iron oxide (FE203).....for Fe
synthetic fosterite (FORST).....for Mg (and Si)
natural rhodonite (RHODON).....for Mn
natural jadeite (JAD).....for Na
synthetic potassium tantallate (KTANT)....for K
synthetic chrome oxide (CR203).....for Cr
synthetic nickel oxide (NIOXID).....for Ni
synthetic cobalt oxide.....for Co

Corrections to the raw data were made by a version of the computer program designed by Mason et al. (1969) with extensive modifications made by Hutt (1974). Major element oxide values should in general be accurate to ± 2% and minor element oxide values to ± 5%.

Each mineral analysis is an average of numerous point analyses made on different parts of a number of grains in each thin section.

Mineral analyses have been recalculated into a structural (unit) formula by the computer program RECAL (written by I. Rucklidge). Garnet and ilmenite analyses were initially processed through the program FERRIC (written by L. Finger). This program calculates a hypothetical ferric iron value for the analysis and readjusts the original ferrous iron oxide value (Finger, 1972). End member molecules for garnet analyses are calculated by the scheme devised by Rickwood (1968). The recasting of garnet analyses, into end member molecules, was achieved using the program GARNET (written by A. Peckett, Univ. of Durham). The percentage number of cations which can be allocated to garnet molecules, is suggested by Rickwood, as a figure useful for assessment of analytical quality. All 38 garnet analyses can be recast into a maximum of seven end members.

ABBREVIATIONS

(i) MINERAL ANALYSES

opx	orthopyroxene
cpx	clinopyroxene
amp	amphibole
gt	garnet
plag	plagioclase feldspar
ilm	ilmenite
scap	scapolite
ppm	parts per million
S.G.	specific gravity
av.	average e.g. av. 10 average of 10 point analyses
Fe/Mg	$\frac{Fe + Mn}{Mg}$ (cation ratio)
Fe/Fe+Mg	$\frac{Fe + Mn}{Fe + Mn + Mg}$ (cation ratio)
niggli mg	$\frac{Mg}{Fe^3 + Fe^2 + Mn + Mg}$ (cation ratio for amphiboles)
Me %	$\frac{100\ (Ca + Mg + Fe + Mn + Ti)}{(Na + K + Ca + Mg + Fe + Mn + Ti)}$ (cation ratio for scapolites)

Ab	albite molecule	End member molecules for feldspars
An	anorthite molecule	
Or	orthoclase molecule	
En	enstatite molecule	End member molecules for pyroxenes
Fs	ferrosilite molecule	
Wo	wollastonite molecule	

Uvarovite	$Ca_3 Cr_2 Si_3 O_{12}$	End member molecules for garnets (Rickwood, 1968)
Pyrope	$Mg_3 Al_2 Si_3 O_{12}$	
Almandine	$Fe_3 Al_2 Si_3 O_{12}$	
Spessartine	$Mn_3 Al_2 Si_3 O_{12}$	
Grossular	$Ca_3 Al_2 Si_3 O_{12}$	
Andradite	$Ca_3 Fe_2 Si_3 O_{12}$	
Schorlomite	$Ca_3 Ti_2(Fe_2Ti) O_{12}$	

(ii) WHOLE ROCK ANLAYSES

n.d.	not detected	
L.O.I.	loss on ignition	
S.G.	specific gravity	
ppm	parts per million	
Wt %	weight percent	
$Fe_2/Fe_2 + Fe_3$	$\frac{FeO + MnO + NiO}{(FeO + MnO + NiO)+(0.8998 \times Fe_2O_3)}$	(Weight percent ratio)
$\leqslant FeO/\leqslant FeO + MgO$	$\frac{\text{Total Wt \% Fe as FeO}}{\text{Total Wt \% Fe as FeO + MgO}}$	(Weight percent ratio)
DIFF. IND.	Thornton - Tuttle differentiation Index (Thornton and Tuttle, 1960) Sum of the normative components quartz, orthoclase, albite, nepheline, leucite and kaliophyllite.	
SI. UNSAT.	Silica undersaturation - where there is insufficent silica to combine with all the other relevant oxides, to give the highly silicic minerals of the norm, a value for the silica deficency or silica undersaturation of the rock is given.	

Normative mineral molecules:-

qtz	Quartz	SiO_2
c	Corundum	Al_2O_3
or	Orthoclase	$K_2O.Al_2O_3.6SiO_2$
ab	Albite	$Na_2O.Al_2O_3.6SiO_2$
an	Anorthite	$CaO.Al_2O_3.2SiO_2$
lc	Leucite	$K_2O.Al_2O_3.4SiO_2$
ne	Nepheline	$Na_2O.Al_2O_3.2SiO_2$
kp	Kaliophilite	$K_2O.Al_2O_3.2SiO_2$
ac	Acmite	$Na_2O.Fe_2O_3.4SiO_2$
ns	Sodium metasilicate	$Na_2O.SiO_2$
ks	Potassium metasilicate	$K_2O.SiO_2$
di	Diopside	$CaO.(Mg,Fe)O.2SiO_2$
wo	Wollastonite	$CaO.SiO_2$
hyp	Hypersthene	$(Mg,Fe)O.SiO_2$
ol	Olivine	$2(Mg,Fe)O.SiO_2$
cs	Dicalcium silicate	$2CaO.SiO_2$
mt	Magnetite	$FeO.Fe_2O_3$
cm	Chromite	$FeO.Cr_2O_3$
il	Ilemite	$FeO.TiO_2$
hm	Hematite	Fe_2O_3
sph	Sphene	$CaO.TiO_2.SiO_2$
pf	Perovskite	$CaO.TiO_2$
ru	Rutile	TiO_2
ap	Apatite	$3CaO.P_2O_5.\frac{1}{3}CaF$
cc	Calcite	$CaO.CO_2$

(En) enstatie content of normative hypersthene

(Fo) fosterite content of normative olivine

CATALOGUE OF SAMPLE NUMBERS

THE SLIDE NUMBERS REFER TO THIN SECTIONS
AND PROBE SECTIONS IN THE IMPERIAL COLLEGE COLLECTION

SAMPLE NUMBER USED IN THESIS	X.R.F. NUMBER	SLIDE NUMBER	FIELD NUMBER
G1	GW4950	43333	FG1
G2	GW4930	43102	FG2
G3	GW4940	42580	FG3
G4	GW4960	42581	FG4
G5	GW4970	42582	FG5
G6	GW5780	43332	X2
G7	GW5010	43334	FG8,2
G8	GW4980	-	FG6,L
G9	GW4990	42593	FG6,M
G10	GW5000	42584	FG7
G11	GW5770	43331	X1
G12	GW5030	42586	FG9
G13	GW5040	42587	FG10
G14	GW5050	42588	FG11
G15	GW5060	42589	FG12
G16	GW5070	42590	FG13
G17	GW5080	43101	FG14
G18	GW5730	-	P10
G20	GW5790	-	X5,1
G21	GW5300	-	X5,2
G22	GW5870	-	X4
G23	GW5700	-	P3
G24	GW5810	-	P1,1
G25	GW5710	-	P4
G26	GW5830	-	P5
G27	GW5840	-	P7
G28	GW5720	-	P8
G29	GW5690	-	P2
G30	GW5100	-	FG24
G32	HB1660	38112	1A2
G33	HB1490	39299	1B
G40	GW5170	-	FG41
G41	GW5160	-	FG40
G42	GW5180	-	FG42

SAMPLE NUMBER USED IN THESIS	X.R.F. NUMBER	SLIDE NUMBER	FIELD NUMBER
G43	HB1570	40832	R110
G44	HB1770	-	2B
G45	GW5190	-	FG43
BT1	GW5570	42597	BT1
BT2	GW5580	42591	BT2
BT3	GW5620	42592	BT3
BT4	GW5630	42593	BT4
BT5	GW5640	42594	BT5,1
BT6	GW5650	-	BT5,2
BT7	GW5660	42598	BT6,1
BT8	GW5670	-	BT6,2
BT9	GW5680	42595	BT7
QG1	GW5410	43107	LG1
QG2	GW5420	43108	LG2
QG3	GW5430	43109	LG3
QG4	GW5450	43110	LG4,1
QG5	GW5440	-	LG4,2
QG6	GW5460	43111	LG5
QG7	GW5490	43094	MG1,1
QG8	GW5500	-	MG1,2
QG9	GW5510	43095	MG2
QG10	GW5520	43096	MG3
QG11	GW5530	43097	MG4
QG12	GW5540	43098	MG5
QG13	GW5550	43099	MG6
QG14	GW5560	43100	MG7
QG15	HB1820	41345	S14
QG16	GW5150	-	FG30
QG17	GW4920	43102	2FG
T1	HB1670	-	T1
T4	GW3610	-	T4
T5	HB1620	-	T5
T7	GW3560	-	T7
A1	GW5250	43113	AP10

SAMPLE NUMBER USED IN THESIS	X.R.F. NUMBER	SLIDE NUMBER	FIELD NUMBER
A2	HB1560	39298 / 40841	2C
A3	GW5480	-	M2
A4	HB1430	39989	1A
A5	AZ840	39990	3A
A6	AZ810	39991	5A
A7	GW3420	40825	6A
A8	GW3510	40826	7A
A9	GW3450	40000	8A
A10	GW3740 / GW3430	39995	9A
A11	GW3470	39997 / 40827	11A
A12	GW3390	40005	13A
A13	HB1850	40003	14L
A14	HB1600	40004	14U
A15	AZ790	39993	15A
A16	GW3570	40830	18L
A17	HB1630	40829	18U
A18	HB1610	40007	19A
A19	GW3730	40006	21A
A20	GW3350	40836	D2
A21	GW3630	40837	E2
A22	GW5470	-	M1
A23	GW3580	40001 / 41342	F1
A24	GW3750	41343	S60
A25	GW3720	39999	F2
A26	HB1790	39998	F3
A27	GW3440	40002	F5
A28	GW3330	-	R40
A29	GW3500	-	R41
A30	GW3690	-	R42
A31	GW3700	41335	R24
A32	GW3520	41332	R22
A33	GW3340	41331	R21
A34	HB1690	41333	J1
A35	AZ780	39994	J2

SAMPLE NUMBER USED IN THESIS	X.R.F. NUMBER	SLIDE NUMBER	FIELD NUMBER
A36	GW3360	-	R103
A37	GW3530	-	R102
A38	GW5240	-	1J
A39	GW3410	-	R18
A40	GW3380	-	R180
A41	GW3710	-	R181
A42	GW3550	-	R121
A43	GW3540	38113/4	1L
A44	HB1810	38105	1M
A45	GW5230	39308/9	1N
A46	AZ850	38104	I03
A47	AZ860	38103	I02
A48	AZ800	-	IP3
A49	GW5880	38115/6	7A2
A50	AZ820	38101/2	3C2
NV1	GW5740	43104	NV1
NV2	GW5750	43105	NV2
NV3	GW5760	43106	W7
NV4	GW5140	-	FG23
NV5	GW5110	43103	FG21,1
NV6	GW5200	-	FG50,1
NV7	GW5210	-	FG50,2
NV8	GW5120	-	FG22,1
NV9	GW5130	-	FG22,2
NV10	GW5090	-	FG21,2
NV11	GW5220	-	FG27
R60	HB1520	-	R60,1
R61	HB1650	-	R60,2
ED1	GW5850	-	ED1
ED2	GW5860	-	ED2
ED3	GW5890	-	P16
ED4	GW3600	39996	10A
ED5	GW3620	-	S61
ED6	GW3640	-	D12

	X.R.F. NUMBER	SLIDE NUMBER	FIELD NUMBER
AD1	HB1580	-	S4
AD2	HB1640	39307	8A2
Epidotic Vein	HB1480	40008	R9
SA1	AZ2870	38117	4C2
SA2	GW3370	-	R90
SA3	GW5270	-	W22
SA4	GW3680	-	R92
SA5	GW3590	-	R100
SA6	HB1500	40838	12A
SA7	GW3320	-	R105
PP1	GW5320	-	H1
PP2	GW5330	-	H2
PP3	GW5340		PP3
PP4	GW5350	-	PP4
PP5	GW5360	-	PP8
PP6	GW5370	-	PP9
PP7	GW5380	42596	BT10
PP8	GW3400	-	R30
PP9	GW5390	-	PP7
	QUARTZ GABBROS		
		38765(1-5)	1E
		S12	S12
		S15	S15
	ANORTHOSITES		
		40833	F4
		41337	R20
		41334	R23
		41336	R25
		41339	R26
		41340	R27
		40843	3J
		38465	S45
		38466	S46
		SLIDE NUMBER	FIELD NUMBER
		39304	S50
		39306	S51
		38107/6/8	1K
		39305	7C
		39300	1D
		39301	2D
		MAFIC GABBRO DYKES	
		39992	4A
		43335	P18
		38469	S95
		38461	S40
		38462	S41
		39390	S2C
		39293	S20
		PARAGNEISSES	
		38460	S11
		38476	S36
		38471	S31
		38473	S33
		38458	S8
		S10	S10
		UNMETAMORPHOSED BASIC DYKES	
		43329	D5
		43330	D6

WHOLE-ROCK & MINERAL ANALYSES

	WHOLE ROCK ANALYSES	MINERAL ANALYSES	SAMPLE LOCALITIES
(1.) ULTRAMAFITES AND MAFIC GABBROS	APPENDIX 1		
A) ULTRAMAFITES AND MAFIC GABBROS FROM THE GABBROIC RIM OF THE ANORTHOSITE	Tables 1, 2, 3, 4	5, 6, 7, 8 & 9	Fig 1 (appendix 2)
B) MAFIC GABBROS	Table 10		Fig 2 (appendix 2)
C) QUARTZ GABBROS FROM THE GABBROIC RIM OF THE ANORTHOSITE	Tables 11 & 12	12	Fig 5 (appendix 2)
(2.) GABBROS			
A) GABBRO-DIORITE	Table 13		Fig 3 (appendix 2)
B) NORITE	Table 14		
(3.) ANORTHOSITES	Tables 15, 16, 17, 18, 26, 27, & 28	19, 20, 21, 22, 23, 24 & 25	Fig 2.1, Map 4
(4.) MINOR INTRUSIVES			
A) ULTRAMAFITES			
a) Ultramafite lenses from the Leverburgh metasediments	Tables 29 & 30	31, 32 & 33	
b) Ultramafite lens within the gabbro-diorite	Table 30	32	
c) Ultramafite (pyroxenite) dykes intrusive into the norite	Table 30		
d) Ultramafite (hornblendite) lenses intrusive into the anorthosite complex	Table 34		Fig 4 (appendix 2)
e) Ultramafite lenses within the Lanagavat metasediments	Table 35		
f) Ultramafites associated with brecciated areas, along and adjacent to the margin of the anorthosite	Table 36	37, 38 & 39	Fig 5 (appendix 2)
B) MAFIC GABBROS (AND ULTRAMAFITES)			
a) Mafic gabbro and ultramafite dykes (d_1 & d_2) intrusive into the anorthosite	Table 40		Map 4
C) OTHERS			
a) Anorthositic-gabbro dykes, intrusive into the anorthosite	Table 41		Fig 5 (appendix 2)
b) Epidote veins, cutting the banded ultramafites and mafic gabbros	Table 41	41	
c) Anorthosite intrusions associated with brecciated areas, along and adjacent to the margin of the anorthosite	Table 41	42	Fig 5 (appendix 2)
(5.) PARAGNEISS	Table 43		Fig 5 (appendix 2)

① ULTRAMAFITES AND MAFIC GABBROS

Sample No.	Rock Type	Mineral Analyses: Cpx	Opx	Gt	Amp	Plag
(i) Abhainn Easean Chais Pod						
Measured section A-B						
G1	Mafic Gabbros	*		*	*	*
G2		*		*	*	*
G3		*				
G4	Ultramafites			*	*	
G5		*		*	*	
G6		*		*	*	*
G7	Mafic Gabbros					
G8						
G9	Ultramafite					
G10	Mafic Gabbro	*		*		*
G11		*		*	*	*
G12				*	*	
G13		*		*	*	
G14	Ultramafites					
G15		*		*	*	
G16						
G17		*	*	*		
G18	Mafic Gabbro					
Measured section C-D						
G20						
G21	Ultramafites					
G22						
G23	Mafic Gabbro					
G24	Ultramafites					
G25						
G26	Mafic Gabbro					
G27						
G28	Ultramafites					
G29						
G30	Amphibolitized ultramafite interbanded with paragneiss					

Mineral assemblages for samples G1-G29 (Figs 2.7* 2.8*)

Sample No.	Rock Type	Mineral Analyses: Gt
(ii) Steisevat Pod		
G32	Ultramafite (amphibole-clinopyroxenite)	
G33	Ultramafite (clinopyroxene-garnetite)	
(iii) Ha-Cleit Pod		
G40	Mafic Gabbro	
G41	Ultramafite (garnet-amphibole-clinopyroxenite)	
G42	Ultramafite (amphibole-garnetite)	
G43	Mafic Gabbro	*
G44	Ultramafite (hornblendite)	
G45	Ultramafite	
	Dearnley - garnet/clinopyroxene/plagioclase/amphibole rock Ha-Cleit summit	
	Davidson - garnet/clinopyroxene/scapolite rock Rodilpark	*

A. Ultramafites and mafic gabbros from the gabbroic rim of the anorthosite

	G1	G2	G3	G4	G5	G6	G7	G8	G9	G10	G11	G12	
OXIDES (Wt %)													
SiO_2	47.25	46.45	39.50	41.40	40.48	44.82	44.89	45.09	44.85	43.66	46.55	42.52	SiO_2
TiO_2	0.23	0.24	2.22	1.74	1.74	0.50	0.18	0.21	0.36	0.46	0.23	1.09	TiO_2
Al_2O_3	20.55	19.12	13.29	15.32	17.75	19.59	18.51	21.75	18.26	20.06	12.42	18.90	Al_2O_3
Fe_2O_3	2.16	2.74	9.26	6.86	5.81	3.69	3.34	2.82	4.45	3.44	3.70	5.81	Fe_2O_3
FeO	3.59	4.45	11.54	10.01	11.61	7.63	5.84	6.67	6.93	8.18	6.29	9.45	FeO
MnO	0.09	0.13	0.18	0.21	0.22	0.14	0.14	0.14	0.17	0.17	0.18	0.19	MnO
MgO	7.84	8.57	8.95	9.48	8.70	7.86	10.16	7.97	10.72	8.30	12.53	9.23	MgO
CaO	18.03	17.61	14.37	14.36	13.04	13.81	17.23	15.15	16.55	15.37	17.40	11.78	CaO
Na_2O	1.33	1.15	0.64	1.27	0.90	1.82	0.77	1.20	0.96	1.04	1.03	1.04	Na_2O
K_2O	0.21	0.06	0.06	0.21	0.06	0.32	0.06	0.09	0.07	0.12	0.06	0.12	K_2O
TOTAL	101.28	100.52	100.11	100.86	100.31	100.18	101.12	101.09	100.32	100.80	100.39	100.13	TOTAL
Cr(ppm)	401	464	360	185	33	104	506	210	429	164	841	163	Cr(ppm)
C.I.P.W. NORM.													
or	1.24	0.35	0.35	1.24	0.35	1.89	0.35	0.53	0.41	0.71	0.35	0.71	or
ab	5.79	6.39	5.03	3.98	6.73	10.59	2.25	8.92	4.63	4.91	4.26	8.80	ab
an	49.49	46.84	33.22	35.49	44.22	44.34	46.88	53.70	37.13	49.72	29.09	46.55	an
ne	2.96	1.81	0.21	3.66	0.48	2.60	2.31	0.67	1.89	2.11	2.41	-	ne
di	31.80	32.33	30.77	28.84	16.71	19.60	30.89	17 37	36.04	21.56	45.66	9.62	di
hyp(En)	-	-	-	-	-	-	-	-	-	-	-	9.57(67.6)	hyp(En)
ol (Fo)	6.44(79.8)	8.37(66.9)	12.89(66.6)	14.40(67.0)	20.09(58.3)	14.84(63.3)	13.25(74.4)	15.41(65.2)	13.09(72.8)	15.93(61.9)	12.81(77.0)	14.38(65.5)	ol (Fo)
mt	3.13	3.97	13.42	9.95	8.42	5.35	4.84	4.09	6.45	4.99	5.36	8.42	mt
il	0.44	0.46	4.22	3.30	3.30	0.95	0.34	0.40	0.68	0.87	0.44	2.07	il
Fe_2/Fe_2+Fe_3	.654	.650	.587	.624	.694	.701	.666	.729	.639	.730	.660	.648	Fe_2/Fe_2+Fe_3
∑FeO/∑FeO+MgO	.414	.446	.689	.631	.659	.582	.465	.536	.505	.576	.434	.614	∑FeO/∑FeO+MgO
DIFF. IND.	9.99	8.56	5.59	8.89	7.56	15.09	4.92	10.12	6.94	7.73	7.03	9.51	DIFF. IND.
SI. UNSAT.	5.08	4.85	5.10	8.63	7.88	7.82	7.16	6.42	6.73	7.77	7.12	5.48	SI. UNSAT.
TOTAL NORMATIVE FELDSPAR	56.52	53.58	38.60	40.71	51.31	56.83	49.49	63.15	42.17	55.34	33.70	56.06	TOTAL NORMATIVE FELDSPAR
NORMATIVE ANORTHITE CONTENT OF FELDSPAR	83.20	84.56	85.58	79.97	85.39	74.61	90.51	84.14	84.26	86.55	80.55	83.04	NORMATIVE ANORTHITE CONTENT OF FELDSPAR

Table 1 Banded ultramafites and mafic gabbros from the gabbroic rim of the anorthosite - whole rock analyses and C.I.P.W. norms.

	G13	G14	G15	G16	G17	G18	G20	G21	G22	G23	G24	G25	
OXIDES (Wt %)													
SiO_2	42.79	41.39	42.60	41.38	48.21	44.51	42.71	43.01	42.61	45.62	39.76	39.56	SiO_2
TiO_2	0.95	1.06	0.81	1.42	0.39	0.26	0.55	0.48	0.71	0.17	1.48	1.46	TiO_2
Al_2O_3	16.21	15.32	16.46	15.87	7.30	17.94	18.03	17.00	15.68	17.99	18.82	19.26	Al_2O_3
Fe_2O_3	5.37	5.75	5.20	6.61	3.99	4.91	13.23	13.29	14.54	8.82	16.93	16.08	Fe_2O_3
FeO	9.84	10.22	8.51	9.84	9.84	5.68							FeO
MnO	0.19	0.22	0.21	0.20	0.25	0.17	0.15	0.17	0.17	0.14	0.21	0.20	MnO
MgO	9.94	9.78	10.23	8.22	15.87	10.62	8.81	9.77	10.11	9.92	7.82	7.38	MgO
CaO	14.05	14.85	16.06	14.23	13.22	15.29	15.45	15.72	14.53	17.19	14.88	15.45	CaO
Na_2O	1.16	0.80	0.53	1.02	0.77	1.11	1.07	1.13	1.17	1.11	0.80	0.64	Na_2O
K_2O	0.21	0.09	0.001	0.29	0.04	0.19	0.25	0.25	0.24	0.09	0.05	0.04	K_2O
TOTAL	100.71	99.48	100.61	99.08	99.88	100.68	100.25	100.82	99.76	101.05	100.75	100.07	TOTAL
Cr(ppm)	193	158	237	126	893								Cr(ppm)
C.I.P.W. NORM.													
or	1.24	0.53	—	1.71	0.24	1.12							or
ab	6.04	2.95	2.56	6.07	6.51	6.60							ab
an	38.41	37.95	42.54	37.87	16.35	43.41							an
ne	2.04	2.07	1.04	1.39	—	1.51							ne
di	25.34	28.96	29.91	26.53	39.56	25.82							di
hyp(En)	—	—	—	—	19.33(72.4)	—							hyp(En)
ol(Fo)	18.04(64.4)	16.67(64.2)	15.48(69.0)	13.23(64.1)	11.37(70.5)	14.60(79.8)							ol(Fo)
mt	7.79	8.34	7.54	9.58	5.78	7.12							mt
il	1.80	2.01	1.54	2.70	0.74	0.49							il
Fe_2/Fe_2+Fe_3	.675	.667	.651	.628	.738	.570							Fe_2/Fe_2+Fe_3
ΣFeO/ΣFeO+MgO	.596	.612	.563	.658	.458	.487	.575	.550	.564	.444	.661	.662	ΣFeO/ΣFeO+MgO
DIFF. IND.	9.33	5.55	3.60	9.17	6.75	9.24							DIFF. IND.
SI. UNSAT.	8.58	8.07	6.86	6.19	4.42	7.11							SI. UNSAT.
TOTAL NORMATIVE FELDSPAR	45.69	41.43	45.10	45.65	23.10	51.14							TOTAL NORMATIVE FELDSPAR
NORMATIVE ANORTHITE CONTENT OF FELDSPAR	80.46	87.24	92.19	80.51	70.77	82.46							NORMATIVE ANORTHITE CONTENT OF FELDSPAR

Table 2 Banded ultramafites and mafic gabbros from the gabbroic rim of the anorthosite - Whole rock analyses and C.I.P.W. norms (cont.)

	G26	G27	G28	G29	G30	G32	G33	G40	G41	G42	G43	G44	
SiO_2	40.58	42.45	41.73	41.09	42.73	44.90	41.34	45.76	42.87	40.04	44.05	44.13	SiO_2
TiO_2	1.35	1.35	1.76	1.24	1.01	1.38	0.56	0.34	0.48	0.28	0.43	1.04	TiO_2
Al_2O_3	22.04	14.94	13.61	15.15	17.29	12.04	16.88	16.59	16.37	19.95	19.70	11.42	Al_2O_3
Fe_2O_3	14.16	15.31	17.82	16.61	16.87	14.08	21.84	10.84	14.52	22.33	11.75	15.06	Fe_2O_3
FeO													FeO
MnO	0.18	0.25	0.26	0.23	0.18	0.12	0.47	0.18	0.20	0.51	0.17	0.21	MnO
MgO	5.92	9.02	9.22	9.84	7.58	10.99	8.44	9.70	10.31	7.87	3.49	11.94	MgO
CaO	15.30	15.19	14.72	15.65	12.99	14.65	11.42	16.26	15.02	8.42	14.48	12.23	CaO
Na_2O	0.81	0.86	0.73	0.51	1.33	1.78	0.75	1.13	0.78	0.33	1.20	1.81	Na_2O
K_2O	0.07	0.01	0.06	0.008	0.48	0.54	0.13	0.03	0.14	0.10	0.19	0.43	K_2O
TOTAL	100.41	99.38	99.91	100.33	100.46	100.48	101.83	100.83	100.69	99.83	100.46	98.27	TOTAL
Cr (ppm)	–	–	–	–	–	430	470	–	–	–	100	1160	Cr (ppm)
Sr (ppm)	–	–	–	–	–	85	25	–	–	–	222	63	Sr (ppm)
Rb (ppm)	–	–	–	–	–	3	n.d.	–	–	–	41	4	Rb (ppm)
ΣFeO/ΣFeO+MgO	.683	.604	.635	.603	.667	.535	.699	.501	.559	.718	.555	.532	ΣFeO/ΣFeO+MgO

Table 3 Banded ultramafites and mafic gabbros from the gabbroic rim of the anorthosite - Whole rock analyses (cont.)

	G45	DEARNLEY -HA CLEIT SUMMIT	DAVIDSON- RODILPARK	
SiO_2	42.05	44.06	40.78	SiO_2
TiO_2	0.99	0.82	1.68	TiO_2
Al_2O_3	17.17	13.15	16.16	Al_2O_3
Fe_2O_3	16.33	2.67	4.17	Fe_2O_3
FeO		13.48	14.81	FeO
MnO	0.18	0.28	0.28	MnO
MgO	8.04	10.31	8.42	MgO
CaO	14.56	13.31	12.52	CaO
Na_2O	0.99	1.02	0.53	Na_2O
K_2O	0.15	0.30	0.06	K_2O
TOTAL	100.46	100.39	99.64	TOTAL
Cr(ppm)	–	150	–	Cr(ppm)
Sr(ppm)	–	45	–	Sr
Rb(ppm)	–	–	–	Rb(ppm)
Ni(ppm)	–	40	–	Ni(ppm)
V(ppm)	–	600	–	V(ppm)
S.G.	–	–	3.45	S.G.
C.I.P.W. NORM.				
or		1.77	.35	or
ab		7.91	4.48	ab
an		30.42	41.54	an
ne		.39	–	ne
di		29.30	17.04	di
hyp		–	6.41(49.4)	hyp
ol		24.17(51.7)	20.35(46.8)	ol
mt		3.87	6.05	mt
il		1.56	3.19	il
Fe_2/Fe_2+Fe_3	–	.851	.801	Fe_2/Fe_2+Fe_3
∑FeO/∑FeO+MgO	.646	.606	.688	∑FeO/∑FeO+MgO
DIFF. IND.		10.07	4.84	DIFF. IND.
SI. UNSAT.		9.11	7.26	SI. UNSAT.

Table 4 Banded ultramafites and mafic gabbros from the gabbroic rim of the anorthosite - Whole rock analyses and C.I.P.W. norms (cont.)

	CLINOPYROXENES										ORTHO-PYROXENE	
	G1 av.10	G2 av.7	G3 av.13	G5 av.8	G6 av.18	G10 av.9	G11 av.14	G13 av.12	G15 av.8	G17	G17	
SiO_2	49.90	49.98	50.10	49.19	50.01	50.25	50.33	50.27	50.11	51.21	51.77	SiO_2
TiO_2	0.38	0.43	0.59	0.70	0.41	0.47	0.33	0.66	1.07	0.22	0.09	TiO_2
Al_2O_3	7.17	7.60	5.71	7.93	6.18	6.72	6.22	6.30	6.57	3.92	2.80	Al_2O_3
FeO	8.68	8.71	9.74	9.45	9.22	8.12	7.17	9.93	7.58	8.15	22.19	FeO
MnO	0.19	0.16	0.20	0.13	0.11	0.04	0.06	0.10	0.12	0.04	0.25	MnO
MgO	13.31	13.31	14.08	13.68	13.10	12.29	13.81	13.81	12.47	13.56	23.42	MgO
CaO	20.17	19.42	19.81	18.28	21.15	21.50	20.99	18.05	22.39	22.44	0.38	CaO
Na_2O	0.90	1.02	0.73	0.95	0.71	0.68	0.78	0.95	0.42	1.10	-	Na_2O
Cr_2O_3	0.12	-	0.04	0.04	0.05	0.21	0.17	0.21	0.13	0.16	0.06	Cr_2O_3
TOTAL	100.82	100.63	101.00	100.35	100.94	100.28	99.86	100.28	100.86	100.80	100.96	TOTAL
UNIT FORMULA												
Si	1.838	1.839	1.850	1.817	1.849	1.859	1.861	1.860	1.844	1.896	1.908	Si
Al^4	.162 2.000	.161 2.000	.150 2.000	.183 2.000	.151 2.000	.141 2.000	.139 2.000	.140 2.000	.156 2.000	.104 2.000	.092 2.000	Al^4
Al^6	.149	.168	.099	.163	.118	.152	.133	.135	.129	.067	.030	Al^6
Ti	.011	.012	.016	.019	.011	.013	.009	.018	.030	.006	.002	Ti
Cr	.003	-	.001	.001	.001	.006	.005	.006	.004	.005	.002	Cr
Mg	.731 2.017	.730 2.021	.775 2.035	.753 2.024	.722 2.030	.678 2.003	.761 2.019	.762 2.015	.684 1.997	.748 2.049	1.287 2.028	Mg
Fe^{2+}	.267	.268	.301	.292	.285	.251	.222	.307	.233	.252	.648	Fe^{2+}
Mn	.006	.005	.006	.004	.003	.001	.002	.003	.004	.001	.008	Mn
Ca	.796	.765	.784	.724	.838	.852	.832	.716	.883	.890	.015	Ca
Na	.064	.073	.052	.068	.051	.049	.056	.068	.030	.079	-	Na
O	6.000	6.000	6.000	6.000	6.000	6.000	6.000	6.000	6.000	6.000	6.000	O
Fe/Mg	.374	.374	.396	.393	.400	.373	.294	.408	.347	.339	.538	Fe/Mg
Fe/Fe+Mg	.272	.272	.284	.282	.286	.271	.227	.290	.257	.253	.350	Fe/Fe+Mg
En	40.73	41.39	41.68	42.59	39.13	38.05	41.95	42.68	38.00	39.58	64.80	En
Fs	14.90	15.20	16.18	16.51	15.45	14.10	12.22	17.22	12.96	13.35	34.45	Fs
Wo	44.37	43.41	42.15	40.91	45.42	47.85	45.83	40.10	49.04	47.08	0.76	Wo

Table 5. Pyroxene analyses - Banded ultramafites and mafic gabbros from the gabbroic rim of the anorthosite.

	G1	G2	G4	G5	G6	G11	G12	G13	G15	** G12	
	av.6	av.7	av.8	av.14	av.7	av.8	av.5	av.8	av.8	av.6	
SiO_2	40.88	42.87	39.79	37.87	40.67	43.27	39.46	38.71	41.09	49.32	SiO_2
TiO_2	0.85	1.21	2.33	1.74	1.20	0.76	1.59	1.81	1.42	0.45	TiO_2
Al_2O_3	14.45	13.62	15.19	18.16	14.23	13.18	15.22	16.62	14.15	8.20	Al_2O_3
FeO	12.00	11.97	15.05	14.29	12.78	11.41	14.46	13.54	12.81	11.57	FeO
MnO	0.09	0.08	0.06	0.14	0.05	0.08	0.06	0.17	0.08	0.11	MnO
MgO	13.12	12.63	10.80	11.45	12.34	14.25	11.96	11.91	12.79	12.39	MgO
CaO	12.30	12.23	11.91	11.86	12.40	12.47	12.55	12.12	12.41	12.00	CaO
Na_2O	1.98	1.85	2.29	2.34	1.81	2.16	2.06	1.82	2.11	1.88	Na_2O
K_2O	1.13	0.89	0.97	0.32	1.38	0.75	0.69	0.77	0.51	0.49	K_2O
Cr_2O_3	0.21	0.22	0.05	0.02	0.04	0.23	0.05	0.09	0.07	-	Cr_2O_3
TOTAL	97.01	97.57	98.44	98.19	96.95	98.56	98.10	97.56	97.44	96.41	TOTAL
UNIT FORMULA											
Si	6.093	6.310	5.930	5.626	6.094	6.297	5.888	5.778	6.100	7.223	Si
Al^4	1.907 8.000	1.690 8.000	2.070 8.000	2.374 8.000	1.906 8.000	1.703 8.000	2.112 8.000	2.222 8.000	1.900 8.000	.777 8.000	Al^4
Al^6	.631	.672	.598	.807	.617	.558	.565	.702	.576	.639	Al^6
Fe^{2+}	1.496	1.473	1.876	1.776	1.602	1.389	1.805	1.690	1.590	1.417	Fe^{2+}
Mn	.011	.010	.008	.018	.006	.010	.008	.021	.010	.014	Mn
Mg	2.915 5.173	2.771 5.086	2.399 5.147	2.536 5.332	2.756 5.121	3.091 5.157	2.660 5.222	2.650 5.277	2.830 5.173	2.705 4.824	Mg
Cr	.025	.026	.006	.002	.005	.026	.006	.011	.008	-	Cr
Ti	.095	.134	.261	.194	.135	.083	.178	.203	.159	.050	Ti
Ca	1.964 1.964	1.929 1.929	1.902 1.902	1.888 1.888	1.991 1.991	1.945 1.945	2.007 2.007	1.938 1.938	1.974 1.974	1.883 1.883	Ca
Na	.572	.528	.662	.674	.526	.610	.596	.527	.607	.534	Na
K	.215 .787	.167 .695	.184 .846	.061 .735	.264 .790	.139 .749	.131 .727	.147 .673	.097 .704	.092 .625	K
O	23.000	23.000	23.000	23.000	23.000	23.000	23.000	23.000	23.000	23.000	O
Fe/Mg	.517	.535	.785	.707	.583	.452	.681	.646	.565	.529	Fe/Mg
Fe/Fe+Mg	.341	.349	.440	.414	.368	.311	.405	.392	.361	.346	Fe/Fe+Mg
niggli mg	.659	.651	.560	.586	.632	.688	.595	.608	.634	.654	niggli mg

Table 6 Amphibole analyses - Banded ultramafites and mafic gabbros from the gabbroic rim of the anorthosite.
** indicates amphibole derived from, and rimming clinopyroxene.

	G.1		G.2			G.4			G.5			G.6		G10		
	av.16		av.9 CENTRE		av.9 RIM	av.6 CENTRE		av.6 RIM	av.7 CENTRE		av.5 RIM	av.9		av.11		
SiO_2	39.93		39.92		40.01	39.34		39.49	39.41		39.21	39.26		39.36		SiO_2
TiO_2	.04		0.11		0.09	0.15		0.20	0.16		0.16	0.09		0.12		TiO_2
Al_2O_3	22.57		21.43		21.97	20.27		20.16	22.21		22.59	21.41		21.56		Al_2O_3
Fe_2O_3	*2.28		*2.05		*2.22	*2.29		*2.37	*0.02		*0.03	*2.79		*2.53		Fe_2O_3
FeO	15.08		15.87		15.22	20.90		20.54	19.53		19.52	17.16		15.86		FeO
MnO	.58		0.43		0.41	0.48		0.50	0.48		0.41	0.41		0.32		MnO
MgO	10.64		10.89		10.98	7.45		7.80	7.21		7.09	8.95		8.96		MgO
CaO	9.63		9.45		9.90	9.51		9.40	10.61		10.57	10.49		11.72		CaO
Cr_2O_3	.05		0.12		0.15	0.04		0.05	-		-	n.d.		0.03		Cr_2O_3
TOTAL	100.80		100.27		100.95	100.43		100.51	99.63		99.58	100.56		100.46		TOTAL
Na(ppm)	350		-		-	-		-	-		-	130		-		Na(ppm)
UNIT FORMULA																
Si	5.925	6.000	5.975	6.000	5.937	6.031	6.031	6.038	6.038	6.017	6.017	5.986	6.000	5.928	6.000	5.928	6.000	Si
Al	.075		.025		.063							.014		.072		.072		Al
Al	3.873	4.138	3.756	4.013	3.780	3.663	3.949	3.633	3.935	3.997	4.017	4.051	4.073	3.739	4.066	3.755	4.059	Al
Cr	.006		.014		.018	.055		.006		-		-		-		.004		Cr
Ti	.004		.012		.010	.017		.023		.018		.018		.010		.014		Ti
Fe^{3+}	.255		.231		.248	.264		.273		.002		.003		.317		.287		Fe^{3+}
Mg	2.353	5.829	2.430	5.986	2.429	1.702	6.006	1.778	6.009	1.641	5.932	1.613	5.888	2.015	5.931	2.011	5.941	Mg
Fe^{2+}	1.871		1.987		1.889	2.680		2.627		2.494		2.492		2.167		1.998		Fe^{2+}
Mn	.073		.055		.052	.062		.065		.062		.053		.052		.041		Mn
Ca	1.531		1.516		1.574	1.562		1.540		1.736		1.729		1.697		1.891		Ca
O	24.000		24.000		24.000	24.000		24.000		24.000		24.000		24.000		24.000		O
Fe/Mg	.826		.840		.799	1.601		1.514		1.558		1.578		1.102		1.014		Fe/Mg
Fe/Fe+Mg	.452		.457		.444	.617		.602		.609		.612		.524		.503		Fe/Fe+Mg
GARNET MOLECULES (RICKWOOD 1968)																		
Uvarovite	0.15		0.36		0.44	0.12		0.15	-		-	-		0.09				Uvarovite
Andradite	6.55		5.60		6.15	6.72		6.97	0.06		0.09	7.97		7.01				Andradite
Pyrope	40.38		40.59		40.87	28.87		30.30	27.66		27.40	33.97		33.86				Pyrope
Spessartine	1.25		0.91		0.87	1.06		1.10	1.05		0.90	0.88		0.69				Spessartine
Grossular	19.56		19.18		19.78	19.65		19.12	29.20		29.28	20.60		24.50				Grossular
Almandine	32.11		33.18		31.78	43.59		42.36	42.04		42.33	36.54		33.62				Almandine
Schorlomite	-		0.19		0.10	-		-	-		-	0.05		0.23				Schorlomite
% cations assigned to garnet molecules	97.35		99.78		99.06	98.38		97.91	99.08		98.37	97.78		99.02				% cations assigned to garnet molecules

* - denotes calcalated Fe_2O_3 value

Table 7 Garnet analyses - Banded ultramafites and mafic gabbros from the gabbroic rim of the anorthosite.

	G11 av.12		G12 av.14		G13 av.13		G15 av.11		G17 av.10		G43 av.10		Davidson - garnet from 'eclogite' Rodil Park		Davidson - garnet from 'metagabbro' Rodil Park		
SiO_2	39.88		39.45		39.57		39.49		39.24		40.24		38.72		38.86		SiO_2
TiO_2	0.07		0.15		0.12		0.13		0.11		0.13		0.34		0.50		TiO_2
Al_2O_3	21.82		21.51		21.08		20.76		21.26		21.98		19.74		20.45		Al_2O_3
Fe_2O_3	*2.57		*2.17		*2.59		*3.14		*2.45		*0.25		1.43		3.19		Fe_2O_3
FeO	15.90		15.99		17.75		16.56		20.12		16.67		21.02		21.38		FeO
MnO	0.46		0.36		0.39		0.41		0.65		0.04		0.46		0.48		MnO
MgO	11.71		11.19		9.69		9.37		10.16		11.76		7.75		8.32		MgO
CaO	8.10		8.59		9.37		10.66		6.35		8.24		10.32		6.47		CaO
Cr_2O_3	0.15		0.05		0.06		0.04		0.04		-		-		-		Cr_2O_3
TOTAL	100.66		99.46		100.62		100.56		100.74		99.32		99.82		99.45		TOTAL
Ni(ppm)	-		-		-		1096		-		-		-		-		Ni(ppm)
Na(ppm)	254		100		-		2484		220		-		-		-		Na(ppm)
UNIT FORMULA																	
Si	5.932	6.000	5.946	6.000	5.964	6.000	5.958	6.000	5.931	6.000	6.030	6.030	5.994	6.000	5.996	6.000	Si
Al	.068		.054		.036		.042		.069				.006		0.004		Al
Al	3.758		3.768		3.708		3.650		3.718		3.882		3.595		3.715		Al
Cr	.018		.006		.007		.005		.048		-		-		-		Cr
Ti	.008	4.071	.017	4.037	.014	4.023	.015	4.027	.013	4.057	.015	3.925	.040	3.801	.035	4.120	Ti
Fe^{3+}	.288		.246		.293		.357		.279		.028		.167		.370		Fe^{3+}
Mg	2.596		2.514		2.177		2.107		2.289		2.627		1.788		1.914		Mg
Fe^{2+}	1.978		2.016		2.238		2.090		2.543		2.090		2.721		2.759		Fe^{2+}
Mn	.058	5.923	.046	5.963	.050	5.977	.052	5.973	.083	5.943	.005	6.045	.060	6.281	.063	5.805	Mn
Ca	1.291		1.387		1.513		1.723		1.028		1.323		1.712		1.070		Ca
O	24.000		24.000		24.000		24.000		24.000		24.000		24.000		24.000		O
Fe/Mg	.784		.820		1.051		1.017		1.147		.797		1.555		1.475		Fe/Mg
Fe/Fe+Mg	.440		.451		.512		.504		.534		.444		.609		.596		Fe/Fe+Mg
GARNET MOLECULES (RICKWOOD, 1968)																	
Uvarovite	0.45		0.15		0.18		0.12		1.21		-		-		-		Uvarovite
Andradite	7.28		5.91		7.14		8.71		6.82		0.72		4.42		9.57		Andradite
Pyrope	43.83		42.16		36.42		35.28		38.52		44.79		31.64		32.97		Pyrope
Spessartine	0.98		0.77		0.83		0.88		1.40		0.09		1.07		1.08		Spessartine
Grossular	14.06		16.92		17.76		19.78		9.06		21.83		25.86		8.86		Grossular
Almandine	33.39		33.80		37.43		34.99		42.78		32.57		37.01		47.53		Almandine
Schorlomite	-		0.29		0.23		0.24		.21		-		-		-		Schorlomite
% cations assigned to garnet molecules	98.76		99.39		99.62		96.55		99.05		97.77		93.72		97.20		% cations assigned to garnet molecules

* - denotes calculated Fe_2O_3 value

Table 8 Garnet analyses (continued from table 7.)

	G1	G2	G6	G10	G12	
	av.30	av.34	av.26	av.32	av.26	
SiO_2	48.04	48.28	55.31	48.08	46.21	SiO_2
Al_2O_3	34.11	33.66	27.75	33.22	34.64	Al_2O_3
FeO	0.141	0.109	0.123	0.138	0.058	FeO
MnO	n.d.	n.d.	0.015	0.041	0.028	MnO
CaO	16.64	16.94	10.98	16.15	17.99	CaO
Na_2O	2.01	1.67	5.86	2.55	1.72	Na_2O
K_2O	0.02	0.03	0.12	0.01	0.01	K_2O
TOTAL	100.96	100.69	100.16	100.19	100.66	TOTAL
UNIT FORMULA						
Si	8.720	8.780	9.981	8.800	8.465	Si
Al	7.298	7.216	5.903	7.167	7.479	Al
Fe^{2+}	.021	.071	.018	.021	.009	Fe^{2+}
Mn	–	–	.003	.006	.005	Mn
Ca	3.236	3.301	2.123	3.167	3.531	Ca
Na	.707	.589	2.051	.905	.611	Na
K	.005	.007	.028	.002	.002	K
O	32.000	32.000	32.000	32.000	32.000	O
Ab	17.92	15.11	48.81	22.21	14.74	Ab
An	81.97	84.71	50.54	77.73	85.20	An
Or	0.12	0.18	0.66	0.06	0.06	Or
average grain centre Ab		14.48	46.74			Ab average grain centre
average grain centre An		85.41	52.61			An average grain centre
average grain centre Or		0.12	0.65			Or average grain centre
average grain rim Ab		16.97	49.31			Ab average grain rim
average grain rim An		82.91	49.31			An average grain rim
average grain rim Or		0.12	0.54			Or average grain rim

Table 9 Feldspar analyses - Banded ultramafites and mafic gabbros from the gabbroic rim of the anorthosite.

	BEINN THARSUINN MAFIC GABBROS									STRONDEVAL MAFIC GABBRO	MAFIC GABBRO SHEET IN GABBRO-DIORITE, N. OF BAYHEAD	
	BT1	BT2	BT3	BT4	BT5	BT6	BT7	BT8	BT9	F2878	F2882	
OXIDES (Wt%)												
SiO_2	44.97	45.16	45.53	45.96	45.82	44.57	47.59	47.99	45.32	44.1	44.2	SiO_2
TiO_2	1.25	0.99	1.05	1.38	1.01	1.00	0.79	0.73	1.21	1.25	0.25	TiO_2
Al_2O_3	13.34	13.21	13.45	12.84	13.99	13.22	13.86	13.69	13.00	9.12	16.0	Al_2O_3
Fe_2O_3	15.59	14.12	14.15	16.78	15.96	17.95	11.93	4.83	16.98	18.7	15.3	Fe_2O_3
FeO								6.92				FeO
MnO	0.20	0.21	0.20	0.27	0.23	0.30	0.16	0.21	0.26	0.22	0.17	MnO
MgO	9.38	10.32	9.68	7.38	8.23	9.35	6.31	6.43	8.41	11.8	9.8	MgO
CaO	14.17	15.58	14.39	14.24	13.85	13.74	18.08	17.93	13.75	12.2	13.1	CaO
Na_2O	1.39	1.24	1.79	1.98	1.85	1.22	2.13	1.96	1.71	1.4	1.1	Na_2O
K_2O	0.35	0.06	0.20	0.05	0.04	0.008	0.03	0.03	0.06	0.09	0.09	K_2O
TOTAL	100.61	100.89	100.44	100.88	100.98	101.36	100.87	100.72	100.70	98.89	100.01	TOTAL
Cr(ppm)										90	14	Cr(ppm)
Ni(ppm)										138	180	Ni(ppm)
Sr(ppm)										47	58	Sr(ppm)
Rb(ppm)										0	2	Rb(ppm)
S(ppm)										393	350	S(ppm)
C.I.P.W. NORM.												
or								0.18				or
ab								12.19				ab
an								28.47				an
ne								2.38				ne
di								43.95				di
ol(Fo)								0.16 (65.1)				ol(Fo)
mt								7.00				mt
il								1.39				il
Fe_2/Fe_2+Fe_3								.621				Fe_2/Fe_2+Fe_3
$\leq FeO/\leq FeO+MgO$	.599	.552	.568	.672	.636	.633	.630	.637	.645	.588	.584	$\leq FeO/\leq FeO+MgO$
DIFF. IND.								14.75				DIFF. IND.
SI. UNSAT.								2.07				SI. UNSAT.
TOTAL NORMATIVE FELDSPAR								40.84		26.09	45.22	TOTAL NORMATIVE FELDSPAR
NORMATIVE ANORTHITE CONTENT OF FELDSPAR								65.88		64.06	82.02	NORMATIVE ANORTHITE CONTENT OF FELDSPAR

Table 10 Mafic gabbros from the Beinn Tharsuinn, Strondeval and Sletteval/Bayhead sheets - Whole rock analyses. Analyses F2878 and F2882 after Palmer (1971).

C. Quartz gabbros

	(a) cont.			
	QG12	QG13	QG14	QG15
OXIDES (Wt%)				
SiO_2	52.02	49.68	46.47	51.74
TiO_2	0.94	0.85	1.60	0.61
Al_2O_3	14.42	13.22	13.37	11.72
Fe_2O_3	12.09	14.36	18.01	10.35
FeO				
MnO	0.19	0.21	0.26	0.17
MgO	6.15	7.72	6.46	10.93
CaO	10.56	10.85	11.32	10.60
Na_2O	3.36	2.69	2.51	2.26
K_2O	0.55	0.69	0.32	1.10
TOTAL	100.28	100.27	100.32	99.48
Cr(ppm)	-	-	-	1020
Sr(ppm)	-	-	-	186
Rb(ppm)	-	-	-	42
$\Sigma FeO/\Sigma FeO+MgO$	.639	.626	.715	.460

QG15 ORTHO-PYROXENE		
52.25		
0.03		
2.50		
21.28		
0.52		
22.73		
0.48		
0.13		
n.d.		
99.92		
1100		
-		
-		
UNIT FORMULA		
Si	1.948	2.000
Al^4	.052	
Al^6	.058	1.998
Ti	.001	
Cr	.008	
Mg	.709	
Fe	1.183	
Mn	.016	
Ca	.019	
Na	.004	
O	6.000	
Fe/Mg	.613	
Fe/Fe+Mg	.380	
En	61.90	
Fs	37.10	
Wo	1.00	

(b)		
QG16	QG17	
47.34	50.87	SiO_2
0.48	0.27	TiO_2
17.23	19.92	Al_2O_3
10.78	2.25	Fe_2O_3
	4.69	FeO
0.17	0.11	MnO
8.05	6.92	MgO
15.07	11.91	CaO
1.76	3.07	Na_2O
0.18	0.23	K_2O
101.06	100.25	TOTAL
-	-	Cr(ppm)
-	-	Sr(ppm)
-	-	Rb(ppm)
C.I.P.W. NORM		
	1.36	or
	25.97	ab
	39.90	an
	15.42	di
	7.30(72.7)	hyp(En)
	6.51(70.3)	ol (Fo)
	3.26	mt
	0.51	il
	.703	Fe_2/Fe_2+Fe_3
.547	.492	$\Sigma FeO/\Sigma FeO+MgO$
	27.33	DIFF. IND.
	2.53	SI. UNSAT.
	67.23	TOTAL NORMATIVE FELDSPAR
	59.34	NORMATIVE ANORTHITE CONTENT OF FELDSPAR

Table 12 Quartz gabbros - Whole rock analyses and C.I.P.W. norms.
(a) - quartz gabbros with 4-12% modal quartz
(b) - quartz gabbros with 0-4% modal quartz

② GABBROS

OXIDES (Wt %)	T_1	T_4	T_5	T_7	DEARNLEY ANAL. 10	DEARNLEY ANAL. 16	T1518	T1519	T1520	T1521	T1522	T1523	T1524	T1525	T1526	T2880	
SiO_2	56.37	54.33	59.13	59.47	55.11	56.13	53.90	51.90	53.50	56.60	57.80	51.10	56.40	51.90	54.80	45.70	SiO_2
TiO_2	0.77	0.73	0.76	0.75	0.88	0.83	0.82	0.77	0.70	0.90	0.94	0.96	0.86	0.95	0.79	1.09	TiO_2
Al_2O_3	17.95	18.69	17.86	17.65	18.54	17.17	19.40	13.60	19.10	19.30	19.70	21.30	20.30	21.70	21.60	18.50	Al_2O_3
Fe_2O_3	8.12	8.92	7.03	6.75	1.63	2.97	2.76	2.98	4.52	3.46	3.53	3.36	3.11	2.70	2.82	11.74	Fe_2O_3
FeO					5.39	4.98	4.55	4.41	3.03	3.42	2.98	4.12	3.49	5.15	3.97		FeO
MnO	0.12	0.13	0.10	0.10	0.11	0.10	0.11	0.12	0.12	0.10	0.09	0.11	0.10	0.11	0.10	0.18	MnO
MgO	5.14	5.64	4.22	3.82	4.33	3.95	5.31	6.00	3.36	3.90	3.42	4.48	3.84	5.10	4.15	6.74	MgO
CaO	7.50	8.38	7.27	6.56	7.91	6.35	8.00	8.28	7.62	6.75	6.34	7.85	6.77	8.53	7.80	9.50	CaO
Na_2O	3.14	3.27	3.51	2.98	4.04	3.74	3.02	4.73	5.93	3.48	3.29	3.82	3.44	3.30	3.83	3.05	Na_2O
K_2O	0.92	0.79	1.25	1.97	.79	2.41	1.07	0.50	1.64	1.91	1.77	1.68	1.65	0.74	1.43	1.20	K_2O
P_2O_5	-	-	-	-	1.13	0.17	0.25	0.26	0.55	0.29	0.24	0.40	0.26	0.40	0.30	0.43	P_2O_5
TOTAL	100.03	100.88	101.13	100.05	99.86	98.80	99.19	98.55	100.07	100.11	100.10	99.18	100.22	100.58	101.59	98.13	TOTAL
Sr(ppm)	544	693	589	680	600	600	605	987	1072	563	560	830	558	628	690	724	Sr(ppm)
Rb(ppm)	4	1	13	44	-	-	7	12	38	36	30	38	39	4	21	25	Rb(ppm)
Cr(ppm)	180	-	160	-	35	30	101	195	15	51	23	24	26	73	64	16	Cr(ppm)
Ni(ppm)	n.d.	-	n.d.	-	6	2	20	106	19	14	9	12	10	19	26	22	Ni(ppm)
Zr(ppm)	47	34	75	118	16	65	81	90	170	198	247	232	202	84	180	109	Zr(ppm)
Ba(ppm)	-	-	-	-	300	600	705	436	476	972	888	856	709	505	667	651	Ba(ppm)
C.I.P.W. NORM																	
qtz					5.42	5.23	6.04	-	-	8.66	13.35	-	9.39	2.45	3.24		qtz
c					-	-	-	-	-	-	1.42	-	1.17	.92	.29		c
or					4.67	14.24	6.32	2.96	9.69	11.29	10.46	9.93	9.75	4.37	8.45		or
ab					34.18	31.64	25.55	40.02	42.99	29.44	27.84	32.32	29.11	27.92	32.41		ab
an					30.13	22.95	36.22	28.05	20.66	31.41	29.89	36.02	31.89	39.71	36.74		an
ne					-	-	-	-	3.89	-	-	-	-	-	-		ne
di					1.42	6.05	1.47	9.06	10.66	.15	-	.25	-	-	-		di
hyp(En)					17.39 (59.4)	12.40 (64.2)	17.44 (72.6)	4.15 (76.2)	-	11.76 (82.7)	9.69 (89.2)	9.47 (76.3)	12.17 (78.8)	18.56 (68.7)	14.18 (72.4)		hyp(En)
ol(Fo)					-	-	-	7.93 (74.4)	3.01 (89.8)	-	-	3.57 (74.6)	-	-	-		ol(Fo)
mt					2.36	4.31	4.00	4.32	6.55	5.02	5.12	4.87	4.51	3.91	4.09		mt
il					1.67	1.58	1.56	1.46	1.33	1.71	1.78	1.82	1.63	1.80	1.50		il
hap					2.67	.40	.59	.61	1.30	.68	.57	.94	.61	.94	.71		hap
Fe_2/Fe_2+Fe_3	-	-	-	-	.790	.655	.652	.628	.437	.531	.492	.583	.562	.684	.616	-	Fe_2/Fe_2+Fe_3
ΣFeO/ΣFeO+MgO	.587	.588	.600	.614	.613	.659	.570	.542	.679	.628	.643	.614	.621	.598	.611	.611	ΣFeO/ΣFeO+MgO
DIFF. IND.					44.27	51.12	37.91	42.98	56.57	49.39	51.65	42.25	48.25	34.74	44.10		DIFF. IND.
SI UNSAT.					-	-	-	3.12	4.54	-	-	1.41	-	-	-		SI UNSAT.

Table 13 Gabbro-diorites - Whole rock analyses and C.I.P.W. norms. Analyses T1518 - T2880 after Palmer (1971). Analyses 10 & 16 after Dearnley (1963).

	865	866	N2872	N2873	N2874	N2871	N2875	N2876	N2877	D.2	
OXIDES(Wt %)											
SiO_2	52.6	53.3	50.9	51.6	55.9	55.9	52.6	55.4	51.3	56.49	SiO_2
TiO_2	0.75	0.66	1.6	0.74	0.89	0.85	0.67	0.71	0.92	0.65	TiO_2
Al_2O_3	14.1	15.5	12.3	10.6	14.2	19.5	10.2	15.5	15.2	12.98	Al_2O_3
Fe_2O_3	3.35	3.05	10.2	8.7	8.80	7.08	8.02	9.07	8 92	1.73	Fe_2O_3
FeO	4.67	4.81								6.08	FeO
MnO	0.12	0.12	0.11	0.11	0.12	0.11	0.11	0.12	0.11	0.11	MnO
MgO	7.18	6.71	6.15	13.7	5.9	8.08	-	-	-	8.73	MgO
CaO	7.90	8.10	9.0	6.7	7.0	7.13	7.4	6.5	9.5	5.49	CaO
Na_2O	3.26	3.76	3.85	2.55	4.16	4.52	-	-	-	3.38	Na_2O
K_2O	1.86	1.62	0.62	2.72	0.82	1.70	2.3	2.8	0.78	3.48	K_2O
P_2O_5	0.41	0.39	0.09	0.3	0.2	0.4	0.25	0.28	0.32	0.26	P_2O_5
H_2O+	-	-	-	-	-	-	-	-	-	0.67	H_2O+
H_2O-	-	-	-	-	-	-	-	-	-	0.15	H_2O-
TOTAL	96.20	98.02	94.82	97.74	97.99	105.27	← partial analyses →			100.20	TOTAL
Sr(ppm)	1035	832	721	1049	1098	1396	995	998	1340	700	Sr(ppm)
Rb(ppm)	17	10	10	36	9	19	38	38	4	-	Rb(ppm)
Cr(ppm)	226	367	151	1204	192	-	413	1408	168	350	Cr(ppm)
Ni(ppm)	38	93	528	828	59	-	1264	1588	41	180	Ni(ppm)
Zr(ppm)	91	79	39	47	133	67	81	50	60	12	Zr(ppm)
Ba(ppm)	1483	1247	228	1764	553	-	1334	1564	554	1200	Ba(ppm)
C.I.P.W. NORM											
qtz	1.78	.16								-	qtz
or	10.99	9.58								20.57	or
ab	27.58	31.81								28.60	ab
an	18.35	20.64								9.97	an
di	14.49	13.62								12.54	di
hyp(En)	15.77(78.5)	15.64 (75.0)								20.23(70.9)	hy(En)
ol (Fo)	-	-								3.14(68.8)	ol(Fo)
mt	4.86	4.42								2.51	mt
il	1.42	1.25								1.23	il
hap	.97	.92								.61	hap
Fe_2/Fe_2+Fe_3	.614	.642								.799	Fe_2/Fe_2+Fe_3
‹FeO/‹FeO+MgO	.517	.529	.599	.364	.573	.441				.467	‹FeO/‹FeO+MgO
DIFF. IND.	40.36	41.55								49.17	DIFF. IND.
SI UNSAT.	-	-								1.21	SI UNSAT.

Table 14 Norites - Whole rock analyses and C.I.P.W. norms. Analyses 865 & 866 and N2872 → N2877 after Palmer (1971). Analysis D2 after Dearnley (1963).

③. ANORTHOSITES

Sample No.	A1	A2	A3	A4	A5	A6	A7	A8	A9	A10	A11	A12	A13	A14	Sample No.
Rock Type	A.G.	A.	M.G.	G.A.	G.	G.	M.G.	G.	M.G.	G.	G.	G.A.	G.	G.	Rock Type
Available Mineral Analyses					Amp				Gt Cpx Amp Feld			Feld	Amp		Available Mineral Analyses
OXIDES (Wt%)															
SiO_2	50.53	52.30	47.87	53.51	51.01	49.45	48.60	49.94	47.95	50.65	50.88	52.62	50.76	49.52	SiO_2
TiO_2	0.09	0.10	0.72	0.18	0.13	0.13	0.72	0.13	0.75	0.10	0.10	0.13	0.11	0.12	TiO_2
Al_2O_3	27.40	30.02	14.58	25.66	27.27	25.22	15.69	25.69	15.14	26.12	26.01	25.85	25.15	24.76	Al_2O_3
Fe_2O_3	4.54	1.04	3.94	3.04	3.76	5.34	12.49	5.35	12.81	4.61	4.58	3.03	1.14	1.20	Fe_2O_3
FeO			7.75										4.29	4.51	FeO
MnO	0.04	0.01	0.18	0.04	0.04	0.07	0.19	0.07	0.20	0.05	0.05	0.04	0.08	0.07	MnO
MgO	1.00	0.66	8.85	1.85	2.75	3.86	8.35	4.33	8.46	4.05	3.67	2.30	4.06	4.45	MgO
CaO	13.18	12.81	12.74	11.47	11.87	10.98	12.93	11.67	12.42	11.26	11.71	10.72	9.97	10.91	CaO
Na_2O	3.44	4.06	2.07	4.45	3.21	2.79	0.81	2.10	1.30	3.10	2.61	4.54	3.44	2.73	Na_2O
K_2O	0.62	0.31	0.66	0.80	1.00	0.97	0.67	0.62	0.58	1.06	0.79	0.58	0.83	0.51	K_2O
P_2O_5	-	-	-	-	n.d.	0.02	-	-	-	-	-	-	-	-	P_2O_5
TOTAL	100.84	101.31	99.36	101.00	101.04	98.83	100.45	99.90	99.61	101.00	100.40	99.81	99.83	98.78	TOTAL
Sr(ppm)	-	429	-	285	311	298	139	314	130	293	-	289	286	281	Sr(ppm)
Rb(ppm)	-	54	-	13	-	-	-	-	-	-	-	-	33	20	Rb(ppm)
Zr(ppm)	-	-	-	12	9	4	21	9	19	6	5	5	10	-	Zr(ppm)
Cr(ppm)	-	350	-	130	-	-	-	-	-	-	-	-	150	10	Cr(ppm)
C.I.P.W. NORM															
qtz			-										-	-	qtz
c			-										0.47	-	c
or			3.90										4.91	3.01	or
ab			17.51										29.11	23.10	ab
an			28.55										49.46	53.81	an
di			28.00										-	0.26	di
hyp(En)			3.04(68.5)										5.96(59.4)	12.47(60.6)	hyp(En)
ol(Fo)			11.28(66.4)										8.07(57.1)	4.16(58.2)	ol(Fo)
mt			5.71										1.65	1.74	mt
il			1.37										0.21	0.23	il
Fe_2/Fe_2+Fe_3			.691										.810	.809	Fe_2/Fe_2+Fe_3
∑FeO/∑FeO+MgO	.803	.586	.561	.597	.552	.555	.574	.526	.577	.506	.529	.542	.538	.557	FeO/ FeO+MgO
DIFF. IND.			21.41										34.01	26.11	DIFF. IND.
SI. UNSAT.			4.31										2.99	1.55	SI. UNSAT.
TOTAL NORMATIVE FELDSPAR			49.96	89.53	90.19	82.77	48.01		48.36	86.56		91.54	83.48	79.92	TOTAL NORMATIVE FELDSPAR
NORMATIVE ANORTHITE CONTENT OF FELDSPAR			57.14	53.09	63.24	64.55	77.48		70.04	62.46		53.79	59.2	67.33	NORMATIVE ANORTHITE CONTENT OF FELDSPAR

Table 15 'Anorthosites' - Whole rock analyses and C.I.P.W. norms. A - anorthosite; G.A. - gabbroic anorthosite; A.G. - anorthositic-gabbro; G - gabbro; M.G. - mafic gabbro.

Sample No.	A15	A16	A17	A18	A19	A20	A21	A22	A23	A24	A25	A26	A27	A28	Sample No.
Rock Type	M.G.	G.	A.G.	G.A.	A.	A.G.	G.A.	M.G.	Opx.M.G.	M.G.	G.A.	M.G.	G.A.	G.	Rock Type
Available Mineral Analyses	Cpx Amp Feld	Amp		Feld	Feld				Gt Cpx Amp Feld Opx	Gt		Gt Cpx Amp			Available Mineral Analyses
OXIDES (Wt%)															OXIDES (Wt%)
SiO_2	47.23	50.46	51.77	52.49	53.13	51.91	52.53	47.42	48.36	48.41	49.60	48.42	52.34	50.75	SiO_2
TiO_2	0.69	0.11	0.10	0.13	0.09	0.11	0.16	0.92	0.49	0.45	0.16	0.28	0.22	0.11	TiO_2
Al_2O_3	15.21	24.78	27.43	28.99	28.92	25.43	28.56	13.98	16.84	17.33	27.92	21.24	26.56	26.03	Al_2O_3
Fe_2O_3	3.96	1.13	0.99	0.44	0.52	] 4.06	] 1.52	] 14.63	3.52	] 11.37	] 2.84	1.48	] 2.93	] 4.69	Fe_2O_3
FeO	7.79	4.26	2.07	1.04	1.01	]	]	]	8.02	]	]	5.25	]	]	FeO
MnO	0.19	0.07	0.04	0.02	0.02	0.05	0.02	0.23	0.18	0.19	0.04	0.11	0.04	0.06	MnO
MgO	9.13	5.18	2.59	0.85	0.86	3.17	0.84	8.62	8.83	8.58	1.98	7.34	2.65	4.12	MgO
CaO	12.29	11.19	12.31	12.86	11.85	10.39	13.05	13.04	12.46	13.11	13.60	14.08	12.09	11.45	CaO
Na_2O	1.71	2.97	3.50	3.43	3.93	4.72	3.41	1.76	1.14	0.85	3.26	2.12	3.14	3.13	Na_2O
K_2O	0.67	0.45	0.29	0.35	0.51	0.22	0.24	0.10	0.27	0.28	0.39	0.28	0.41	0.48	K_2O
P_2O_5	0.01	-	-	-	-	-	-	-	-	-	-	-	-	-	P_2O_5
TOTAL	98.88	100.60	101.09	100.60	100.84	100.06	100.33	100.70	100.11	100.57	99.79	100.60	100.38	100.82	TOTAL
Sr(ppm)	126	147	316	361	311	373	329	–	148	–	262	189	330	–	Sr(ppm)
Rb(ppm)	–	–	14	7	–	–	–	–	1	–	–	n.d.	–	–	Rb(ppm)
Zr(ppm)	14	5	4	3	11	27	5	–	42	–	26	6	1	–	Zr(ppm)
Cr(ppm)	–	–	70	50	–	–	–	–	–	–	–	620	–	–	Cr(ppm)
C.I.P.W. NORM.															C.I.P.W. NORM
qtz	-	-	-	1.99	0.79				0.37			-			qtz
c	–	–	–	–	0.36				–			–			c
or	3.96	2.66	1.71	2.07	3.01				1.60			1.65			or
ab	14.47	25.13	29.61	29.02	33.26				9.65			17.75			ab
an	31.85	52.96	58.29	62.68	58.79				40.04			47.62			an
ne	–	–	–	–	–				–			0.10			ne
di	23.51	2.07	2.25	0.92	–				17.65			17.95			di
hyp(En)	8.62(68.9)	8.52(65.4)	5.89(69.0)	3.04(60.7)	4.00(53.5)				24.78(66.0)			–			hyp(En)
ol(Fo)	9.41(66.8)	7.41(63.1)	1.71(66.9)	–	–				–			12.85(67.2)			ol(Fo)
mt	5.74	1.64	1.44	0.64	0.75				5.10			2.15			mt
il	1.31	0.21	0.19	0.25	0.17				0.93			0.53			il
Fe_2/Fe_2+Fe_3	.691	.810	.703	.728					.721			.801			Fe_2/Fe_2+Fe_3
FeO/ΣFeO+MgO	.558	.505	.533	.628	.654	.535	.620	.604	.559	.544	.563	.473	.499	.506	ΣFeO/ΣFeO+MgO
DIFF. IND.	18.43	27.79	31.33	33.08	37.06				11.61			19.51			DIFF. IND.
SI. UNSAT.	3.61	2.80	0.66	–	–				–			5.01			SI. UNSAT.
TOTAL NORMATIVE FELDSPAR	50.28	80.75	89.61	93.77	95.06	89.64	94.79		51.28	51.41	92.61	67.02		85.13	TOTAL NORMATIVE FELDSPAR
NORMATIVE ANORTHITE CONTENT OF FELDSPAR	63.35	65.59	65.04	66.84	61.85	53.99	65.00		78.08	82.79	66.98	70.94		65.56	NORMATIVE ANORTHITE CONTENT OF FELDSPAR

Table 16 'Anorthosites' - Whole rock analyses and C.I.P.W. norms
A - anorthosite; G.A. - gabbroic anorthosite; A.G. - anorthositic gabbro; G - gabbro; M.G. - mafic gabbro.

Sample No.	A29	A30	A31	A32	A33	A34	A35	A36	A37	A38	A39	A40	A41	A42	Sample No.
Rock Type	A.G.	M.G.	G.	G.	A.G.	M.G.	G.A.	A.	G.A.	A.G.	A.G	G.	A.G.	A.	Rock Type
Available Mineral Aanalyses		Cpx													Available Mineral Analyses
OXIDES (wt%)															
SiO_2	51.57	49.47	48.58	49.07	50.59	44.12	50.09	51.20	50.26	49.44	49.53	47.84	48.11	54.10	SiO_2
TiO_2	0.19	1.02	0.10	0.16	0.20	0.12	0.15	0.08	0.05	0.08	0.13	0.11	0.20	0.16	TiO_2
Al_2O_3	28.98	14.78	25.99	25.82	28.03	19.77	30.22	31.13	31.75	30.80	30.81	26.54	27.88	27.14	Al_2O_3
Fe_2O_3	2.11	13.55	5.74	5.09	3.55	13.51	0.43	1.05	0.51	0.89	1.39	5.88	4.36	1.97	Fe_2O_3
FeO							2.00								FeO
MnO	0.03	0.18	0.07	0.06	0.04	0.17	0.03	0.02	0.01	0.01	0.02	0.08	0.06	0.02	MnO
MgO	1.04	7.88	4.36	3.41	2.09	10.15	1.31	0.63	0.47	0.64	1.15	5.03	3.16	0.89	MgO
CaO	12.80	12.57	11.97	12.13	12.90	10.08	14.07	13.84	14.36	15.44	15.35	12.70	12.82	11.22	CaO
Na_2O	3.45	1.48	2.56	2.84	2.84	1.74	2.87	2.72	2.69	3.02	1.99	2.07	2.63	4.90	Na_2O
K_2O	0.35	0.66	0.24	0.20	0.20	0.24	0.21	0.11	0.16	0.10	0.10	0.21	0.28	0.38	K_2O
P_2O_5	-	-	-	-	-	-	0.02	-	-	-	-	-	-	-	P_2O_5
TOTAL	100.52	101.39	99.61	98.78	100.44	99.90	101.40	100.78	100.26	100.42	100.47	100.46	99.50	100.78	TOTAL
Sr(ppm)						106	345								Sr(ppm)
Rb(ppm)						n.d.	-								Pb(ppm)
Zr(ppm)						6	8								Zr(ppm)
Cr(ppm)						80	-								Cr(ppm)
C.I.P.W. NORM.															
or							1.24								or
ab							24.28								ab
an							68.96								an
di							0.70								di
hyp(En)							3.19(51.1)								hyp(En)
ol(Fo)							2.10(48.6)								ol(Fo)
mt							0.62								mt
il							0.28								il
Fe_2/Fe_2+Fe_3							.840								Fe_2/Fe_2+Fe_3
ΣFeO/ΣFeO+MgO	.646	.604	.542	.573	.604	.545	.646	.600	.494	.556	.521	.513	.554	.666	ΣFeO/ΣFeO+MgO
DIFF. IND.							25.52								DIFF. IND.
SI. UNSAT.							0.76								SI. UNSAT.
TOTAL NORMATIVE FELDSPAR	75.05	48.19	85.35		89.11	61.57	94.49	93.37			86.87	81.63	86.40		TOTAL NORMATIVE FELDSPAR
NORMATIVE ANORTHITE CONTENT OF FELDSPAR	66.07	66.04	71.80		76.18	73.79	72.99	74.63			81.95	76.95	72.26		NORMATIVE ANORTHITE CONTENT OF FELDSPAR

Table 17 'Anorthosites' - Whole rock analyses and C.I.P.W. norms. A - anorthosite; G.A. - gabbroic anorthosite; A.G. - anorthositic gabbro; G - gabbro; M.G. - mafic gabbro.

Sample No.	A43	A44	A45	A46	A47	A48	A49	A50	Sample No.
Rock Type	G.A.	A.	G	A	G	A	A.G.	A	Rock Type
Available Mineral Analyses			Gt Feld	Gt Feld Scap Cpx	Gt Feld Cpx	Gt		Feld	Available Mineral Analyses
OXIDES (Wt%)									
SiO_2	50.10	50.80	49.05	50.64	46.97	49.45	48.44	50.76	SiO_2
TiO_2	0.24	0.13	0.16	0.11	0.25	0.10	0.13	0.20	TiO_2
Al_2O_3	27.10	28.98	24.85	31.84	24.99	30.96	26.35	30.11	Al_2O_3
Fe_2O_3	3.14	1.84	2.08	1.05	8.07	1.29	1.32	0.62	Fe_2O_3
FeO			3.68				3.28	0.83	FeO
MnO	0.05	0.03	0.07	0.01	0.10	0.02	0.06	0.02	MnO
MgO	2.62	0.90	5.18	0.21	4.52	0.62	3.04	0.28	MgO
CaO	15.36	15.35	13.42	14.43	12.57	14.68	13.57	14.07	CaO
Na_2O	1.89	2.79	2.33	2.54	2.15	3.01	3.00	2.64	Na_2O
K_2O	0.20	0.13	0.10	0.18	0.17	0.15	0.28	0.19	K_2O
P_2O_5	-	-	-	0.02	0.02	0.02	-	0.02	P_2O_5
TOTAL	100.70	100.95	100.91	101.03	99.81	100.30	99.47	99.74	TOTAL
Sr(ppm)		262							Sr(ppm)
Rb(ppm)		5							Rb(ppm)
Cr(ppm)		50							Cr(ppm)
C.I.P.W. NORM.									
qtz			-				-	3.79	qtz
or			0.59				1.65	1.12	or
ab			19.71				22.17	22.34	ab
an			57.06				57.61	69.76	an
di			7.65				7.92	0.04	di
hyp(En)			8.60(72.4)				-	1.40(49.2)	hyp(En)
ol (Fo)			3.98(70.5)				6.22(58.7)	-	ol (Fo)
mt			3.02				1.91	0.90	mt
il			0.30				0.25	0.38	il
Fe_2/Fe_2+Fe_3			.667					.604	Fe_2/Fe_2+Fe_3
ΣFeO/ΣFeO+MgO	.519	.648	.517	.818	.616	.652	.576	.832	ΣFeO/ΣFeO+MgO
DIFF. IND.			20.30					27.25	DIFF. IND.
SI. UNSAT.			1.54				3.79		SI. UNSAT.
TOTAL NORMATIVE FELDSPAR			77.36	94.15	77.24	96.41	81.43	93.21	TOTAL NORMATIVE FELDSPAR
NORMATIVE ANORTHITE CONTENT OF FELDSPAR			73.75	76.04	75.15	72.96	70.75	74.83	NORMATIVE ANORTHITE CONTENT OF FELDSPAR

Table 18 'Anorthosites' - Whole rock analyses and C.I.P.W. norms
A - anorthosite; G.A. - gabbroic anorthosite; A.G. - anorthositic gabbro; G - gabbro; M.G. - mafic gabbro.

	CLINOPYROXENES										ORTHOPYROXENE		
	A9 av.8		A15 av.9		A23 av.6		A26 av.9		A30 av.4		A23 av.6		
SiO_2	51.15		51.69		51.11		51.00		50.70		52.20		SiO_2
TiO_2	0.54		0.41		0.35		0.46		0.36		0.13		TiO_2
Al_2O_3	4.66		4.73		3.59		6.87		7.11		2.27		Al_2O_3
FeO	10.65		9.45		7.78		5.57		5.24		22.47		FeO
MnO	0.13		0.06		0.16		0.12		0.03		0.23		MnO
MgO	12.01		13.33		13.80		13.24		12.74		22.53		MgO
CaO	20.37		19.50		22.21		22.12		22.61		0.58		CaO
Na_2O	0.71		0.77		0.61		0.79		0.91		-		Na_2O
K_2O	0.09		0.18		-		-		0.03		n.d.		K_2O
Cr_2O_3	0.28		0.10		0.03		0.11		0.13		-		Cr_2O_3
TOTAL	100.60		100.22		99.64		100.28		99.87		100.42		TOTAL
UNIT FORMULA													
Si	1.904		1.914		1.908		1.867		1.864		1.936		Si
Al^4	.096	2.000	.086	2.000	.092	2.000	.133	2.000	.136	2.000	.064	2.000	Al^4
Al^6	.109		.120		.066		.163		.172		.035		Al^6
Ti	.015		.011		.010		.013		.010		.004		Ti
Cr	.008		.003		.001		.003		.004		-		Cr
Mg	.666		.736		.768		.722		.698		1.245		Mg
Fe	.332	2.002	.293	2.002	.243	2.025	.170	1.999	.161	2.004	.697	2.011	Fe
Mn	.004		.002		.005		.004		.001		.007		Mn
Ca	.812		.774		.888		.867		.891		.023		Ca
Na	.051		.055		.045		.056		.065		-		Na
K	.004		.009		-		-		.002		-		K
O	6.000		6.000		6.000		6.000		6.000		6.000		O
Fe/Mg	.504		.400		.323		.241		.233		.566		Fe/Mg
Fe/Fe+Mg	.335		.286		.244		.194		.189		.361		Fe/Fe+Mg
En	36.79		40.82		40.34		41.03		39.89		63.13		En
Fs	18.34		16.25		13.03		9.69		9.20		35.70		Fs
Wo	44.86		42.93		46.64		49.28		50.92		1.17		Wo

Table 19 Pyroxene analyses - Mafic gabbro layers from the lower zone anorthosites.

	A15					A46	A47	
	POINT 1	POINT 2	POINT 3	POINT 4	POINT 5			
SiO_2	53.43	52.44	51.25	51.02	52.50	49.13	49.06	SiO_2
TiO_2	0.09	0.21	0.15	0.18	0.22	0.88	0.76	TiO_2
Al_2O_3	2.80	2.84	4.45	4.42	3.23	5.96	6.39	Al_2O_3
FeO	8.30	8.53	8.93	9.48	9.05	12.29	11.72	FeO
MnO	0.10	0.08	0.08	0.08	0.07	0.02	0.05	MnO
MgO	15.38	14.72	13.94	13.84	14.50	11.80	12.15	MgO
CaO	19.30	20.32	20.22	20.42	19.93	18.78	19.26	CaO
Na_2O	0.40	0.81	0.57	0.80	0.79	0.47	0.58	Na_2O
TOTAL	99.80	99.95	99.59	100.24	100.29	99.33	99.97	TOTAL
UNIT FORMULA								
Si	1.967	1.943	1.908	1.897	1.940	1.858	1.843	Si
Al^4	.033 (2.000)	.057 (2.000)	.092 (2.000)	.103 (2.000)	.060 (2.000)	.142 (2.000)	.157 (2.000)	Al^4
Al^6	.089	.067	.104	.090	.081	.124	.126	Al^6
Ti	.002	.006	.004	.005	.006	.033	.021	Ti
Mg	.844	.813	.774	.767	.798	.665	.680	Mg
Fe	.256 (1.984)	.264 (2.018)	.278 (2.010)	.295 (2.030)	.279 (2.011)	.389 (2.009)	.368 (2.014)	Fe
Mn	.003	.003	.003	.003	.002	.001	.002	Mn
Ca	.761	.307	.807	.813	.789	.761	.775	Ca
Na	.029	.058	.041	.058	.056	.035	.042	Na
O	6.000	6.000	6.000	6.000	6.000	6.000	6.000	O
Fe/Mg	.306	.328	.363	.388	.352	.586	.544	Fe/Mg
Fe/Fe+Mg	.235	.247	.266	.279	.260	.370	.352	Fe/Fe+Mg
En	45.28	43.08	41.57	40.84	42.76	36.64	37.30	En
Fs	13.89	14.15	15.09	15.87	14.95	21.43	20.19	Fs
Wo	40.83	42.77	43.34	43.29	42.28	41.93	42.51	Wo

Table 20. (i) Point analyses across the clinopyroxene A15
(ii) Clinopyroxene analyses from middle zone anorthosites

	A5		A9		A13		A15		A16		A23		A26		** A9		** A15		
	av.5		av.9		av.6		av.8		av.8		av.8		av.9		av.5		av.6		
SiO_2	47.02		40.13		48.92		41.90		46.39		43.40		43.06		48.79		47.26		SiO_2
TiO_2	1.55		1.83		1.52		1.94		1.61		1.79		1.04		0.67		0.75		TiO_2
Al_2O_3	9.10		13.75		8.01		13.14		9.99		12.86		14.91		8.23		9.61		Al_2O_3
FeO	11.94		14.16		12.06		14.03		11.67		11.54		8.55		12.25		10.97		FeO
MnO	0.06		0.13		0.06		0.09		0.04		0.05		0.03		0.07		0.07		MnO
MgO	13.46		11.66		13.62		11.51		13.99		13.03		13.89		13.99		14.23		MgO
CaO	11.97		11.85		12.17		11.99		12.22		11.74		12.20		12.07		11.92		CaO
Na_2O	2.11		1.74		2.10		1.81		1.97		1.88		1.48		1.26		1.70		Na_2O
K_2O	0.52		1.52		0.37		1.14		0.51		0.95		1.87		0.18		0.07		K_2O
Cr_2O_3	-		0.11		-		0.14		-		0.02		0.02		0.11		0.09		Cr_2O_3
TOTAL	97.73		96.88		98.83		97.69		98.39		97.26		97.05		97.62		96.67		TOTAL
UNIT FORMULA																			
Si	6.864	8.000	6.067	8.000	7.031	8.000	6.241	8.000	6.725	8.000	6.383	8.000	6.282	8.000	7.071	8.000	6.895	8.000	Si
Al^4	1.136		1.933		.969		1.759		1.275		1.617		1.718		.929		1.105		Al^4
Al^6	.430	4.993	.517	5.172	.388	4.925	.548	5.097	.432	5.051	.613	5.095	.846	5.030	.477	5.078	.547	5.081	Al^6
Fe^{2+}	1.458		1.790		1.449		1.748		1.415		1.419		1.043		1.485		1.338		Fe^{2+}
Mn	.007		.017		.007		.011		.005		.006		.004		.009		.009		Mn
Mg	2.928		2.628		2.917		2.556		3.023		2.857		3.021		3.022		3.094		Mg
Cr	-		.013		-		.016		-		.002		.002		.013		.010		Cr
Ti	.170		.208		.164		.217		.176		.198		.114		.073		.082		Ti
Ca	1.872	1.872	1.920	1.920	1.874	1.874	1.914	1.914	1.898	1.898	1.850	1.850	1.907	1.907	1.874	1.874	1.863	1.863	Ca
Na	.597	.716	.510	.803	.585	.653	.523	.739	.554	.674	.536	.714	.419	.767	.354	.387	.481	.494	Na
K	.119		.293		.068		.217		.120		.178		.348		.033		.013		K
O	23.000		23.000		23.000		23.000		23.000		23.000		23.000		23.000		23.000		O
Fe/Mg	.498		.688		.497		.688		.468		.499		.347		.494		.435		Fe/Mg
Fe/Fe+Mg	.332		.407		.332		.408		.319		.333		.257		.331		.303		Fe/Fe+Mg
niggli mg	.666		.593		.667		.592		.680		.667		.743		.669		.697		niggli mg

Table 21 Amphibole analyses - from the lower zone anorthosites.
** indicates amphiboles derived from and rimming clinopyroxene.

	A9 av.11		A23 av.6		A24 av.13		A26 av.8		
SiO_2	39.10		39.63		39.18		40.83		SiO_2
TiO_2	0.10		0.17		0.14		0.16		TiO_2
Al_2O_3	21.36		21.57		21.17		22.44		Al_2O_3
Fe_2O_3	*1.04		*1.29		*1.82		*0.90		Fe_2O_3
FeO	23.32		21.27		20.26		17.03		FeO
MnO	0.69		0.55		0.49		0.46		MnO
MgO	7.42		9.71		9.86		12.22		MgO
CaO	7.49		6.56		6.75		7.56		CaO
Cr_2O_3	0.08		0.03		0.08		0.01		Cr_2O_3
TOTAL	100.60		100.78		99.74		101.61		TOTAL
UNIT FORMULA									
Si	5.994	6.000	5.986	6.000	5.973	6.000	5.992	6.000	Si
Al	.006		.014		.027		.008		Al
Al	3.853	3.995	3.826	3.995	3.777	4.011	3.873	3.991	Al
Cr	.010		.004		.010		.001		Cr
Ti	.012		.019		.016		.018		Ti
Fe^{3+}	.120		.146		.208		.099		Fe^{3+}
Mg	1.695	6.005	2.186	6.005	2.241	5.989	2.673	6.009	Mg
Fe^{2+}	2.990		2.687		2.583		2.090		Fe^{2+}
Mn	.090		.070		.063		.057		Mn
Ca	1.230		1.062		1.103		1.189		Ca
O	24.000		24.000		24.000		24.000		O
Fe/Mg	1.816		1.261		1.181		.803		Fe/Mg
Fe/Fe+Mg	.645		.558		.541		.445		Fe/Fe+Mg
GARNET MOLECULES (RICKWOOD, 1968)									
Uvarovite	0.24		0.09		0.24		0.03		Uvarovite
Andradite	3.01		3.67		4.96		2.50		Andradite
Pyrope	28.34		36.53		37.41		44.75		Pyrope
Spessartine	1.50		1.18		1.06		0.96		Spessartine
Grossular	17.31		13.97		12.94		17.38		Grossular
Almandine	49.61		44.56		43.12		34.39		Almandine
Schorlomite	-		-		0.27		-		Schorlomite
% cations assigned to garnet molecules	99.73		99.76		99.81		99.55		% cations assigned to garnet molecules

* denotes calculated Fe_2O_3 value

Table 22 Garnet analyses - Mafic gabbro layers from the lower zone anorthosites.

	A41		A45		A46		A47		A48		
	av.3		av.6		av.21		av.11		av.15		
SiO_2	39.60		39.15		38.72		39.36		39.32		SiO_2
Al_2O_3	22.06		21.75		21.17		21.64		20.64		Al_2O_3
Fe_2O_3	*1.03		*3.21		*2.18		*1.71		*1.19		Fe_2O_3
FeO	17.21		21.06		20.33		21.23		21.27		FeO
MnO	0.10		0.20		0.36		0.44		0.39		MnO
MgO	13.14		10.59		5.91		7.81		5.74		MgO
CaO	7.77		4.77		11.76		8.95		11.80		CaO
TOTAL	100.91		100.73		100.44		101.14		100.35		TOTAL
UNIT FORMULA											
Si	5.875	6.000	5.907	6.000	5.955	6.000	5.968	6.000	6.057	6.057	Si
Al^{4}	.125		.093		.045		.032				Al^{4}
Al^{6}	3.733	3.848	3.775	4.139	3.792	4.045	3.836	4.031	3.748	3.885	Al^{6}
Fe^{3+}	.115		.364		.253		.195		.137		Fe^{3+}
Mg	2.906	6.290	2.382	5.837	1.355	5.955	1.765	5.969	1.318	6.058	Mg
Fe	2.136		2.658		2.615		2.693		2.741		Fe
Mn	.013		.026		.047		.057		.051		Mn
Ca	1.235		.771		1.938		1.454		1.948		Ca
O	24.000		24.000		24.000		24.000		24.000		O
Fe/Mg	.739		1.127		1.965		1.557		2.118		Fe/Mg
Fe/Fe+Mg	.425		.530		.663		.609		.679		Fe/Fe+Mg
GARNET MOLECULES (RICKWOOD, 1968)											
Andradite	2.94		9.37		6.36		4.90		3.55		Andradite
Pyrope	49.46		40.81		22.75		29.58		22.62		Pyrope
Spessartine	0.21		0.44		0.79		0.95		0.87		Spessartine
Grossular	18.09		3.85		26.19		19.46		29.87		Grossular
Almandine	29.30		45.54		43.91		45.11		43.09		Almandine
Schorlomite	-		-		-		-		-		Schorlomite
% cations assigned to garnet molecules	97.09		97.42		99.25		99.47		97.14		% cations assigned to garnet molecules

* denotes calculated Fe_2O_3 value

Table 23 Garnet analyses - Middle zone anorthosites.

	A46					A47				
	CENTRE ←				RIM	CENTRE ←			RIM	
	Point 1	Point 2	Point 3	Point 4	Point 5	Point 1	Point 2	Point 3	Point 4	
SiO_2	39.24	39.21	39.21	38.93	38.45	39.77	39.51	39.18	39.00	SiO_2
Al_2O_3	21.62	21.50	21.47	21.48	21.11	22.09	21.75	21.56	21.44	Al_2O_3
Fe_2O_3	*1.52	*1.55	*1.77	*1.56	*0.08	*1.81	*1.36	*2.19	*1.95	Fe_2O_3
FeO	20.10	20.03	20.08	20.68	24.00	18.77	20.45	22.42	22.98	FeO
MnO	0.35	0.34	0.32	0.34	0.62	0.30	0.33	0.55	0.56	MnO
MgO	6.52	6.48	6.47	5.97	3.67	9.56	8.40	6.94	6.54	MgO
CaO	11.59	11.68	11.67	11.62	11.56	8.93	8.97	8.98	8.92	CaO
TOTAL	100.93	100.79	100.99	100.58	99.49	101.23	100.77	101.82	101.40	TOTAL
UNIT FORMULA										
Si	5.973	5.979	5.971	5.969	6.041	5.950	5.982	5.946	5.957	Si
Al	.027 — 6.000	.021 — 6.000	.029 — 6.000	.031 — 6.000	6.041	.050 — 6.000	.018 — 6.000	.054 — 6.000	.043 — 6.000	Al
Al	3.853	3.843	3.826	3.851	3.909	3.846	3.863	3.803	3.818	Al
Fe^{3+}	.174 — 4.026	.178 — 4.021	.203 — 4.028	.180 — 4.031	.010 — 3.919	.204 — 4.050	.155 — 4.018	.250 — 4.054	.225 — 4.042	Fe^{3+}
Mg	1.479	1.473	1.469	1.364	.859	2.132	1.896	1.570	1.489	Mg
Fe^{2+}	2.559	2.554	2.557	2.652	3.153	2.349	2.589	2.845	2.936	Fe^{2+}
Mn	.045 — 5.974	.044 — 5.979	.041 — 5.972	.044 — 5.969	.083 — 6.041	.038 — 5.950	.042 — 5.982	.071 — 5.947	.072 — 5.958	Mn
Ca	1.890	1.908	1.904	1.909	1.946	1.432	1.455	1.460	1.460	Ca
O	24.000	24.000	24.000	24.000	24.000	24.000	24.000	24.000	24.000	O
Fe/Mg	1.760	1.764	1.769	1.976	3.765	1.119	1.388	1.857	2.020	Fe/Mg
Fe/Fe+Mg	.638	.638	.639	.664	.790	.528	.581	.650	.669	Fe/Fe+Mg
GARNET MOLECULES (RICKWOOD 1968)										
Uvarovite	-	-	-	-	-	-	-	-	-	Uvarovite
Anadradite	4.37	4.46	5.10	4.52	0.24	5.14	3.89	6.31	5.64	Andradite
Pyrope	24.77	24.64	24.60	22.86	14.62	35.83	31.69	26.40	25.00	Pyrope
Spessartine	0.76	0.73	0.69	0.74	1.40	0.64	0.71	1.19	1.22	Spessartine
Grossular	27.28	27.46	26.80	27.46	32.87	18.92	20.44	18.25	18.86	Grossular
Almandine	42.83	42.71	42.82	44.42	51.87	39.47	43.27	47.85	49.28	Almandine
Schorlomite	-	-	-	-	-	-	-	-	-	Schorlomite
% cations assigned to garnet molecules	99.55	99.64	99.52	99.48	97.96	99.17	99.69	99.10	99.29	% cations assigned to garnet molecules

Table 24 Point analyses across two garnets from the middle zone anorthosites.

*- denotes calculated Fe_2O_3 value

	A9	A12	A15	A18	A19	A23	A45	A46	A46			
	av.14	av.22	av.9	av.21	av.12	av.12	av.17	av.15	CENTRE	MID	RIM	
SiO_2	58.86	54.86	56.68	54.01	50.98	58.23	50.61	50.22	50.49	50.04	51.65	SiO_2
Al_2O_3	25.55	29.03	28.95	30.62	31.64	26.37	33.06	31.90	32.23	31.52	31.25	Al_2O_3
CaO	8.09	11.15	7.62	12.13	13.52	8.20	10.73	14.60	14.81	14.33	13.73	CaO
Na_2O	6.93	5.17	7.11	4.52	3.95	6.89	5.76	3.17	3.15	3.24	3.74	Na_2O
K_2O	0.25	0.23	0.08	0.29	0.32	0.18	0.21	0.13	0.13	0.12	0.13	K_2O
TOTAL	99.68	100.44	100.44	101.57	100.41	99.87	100.37	100.02	100.81	99.25	100.50	TOTAL
Sr(ppm)	–	–	–	–	–	793	–	–	–	–	–	
UNIT FORMULA												
Si	10.555	9.853	10.095	9.625	9.246	10.429	9.155	9.149	9.129	9.182	9.339	Si
Al	5.402	6.147	6.079	6.433	6.766	5.568	7.051	6.851	6.870	6.819	6.661	Al
Ca	1.555	2.146	1.454	2.316	2.627	1.574	2.08	2.850	2.869	2.817	2.660	Ca
Na	2.409	1.800	2.455	1.562	1.389	2.393	2.02	1.120	1.104	1.153	1.311	Na
K	.057	.053	.018	.066	.074	.041	.048	.030	.030	.029	.030	K
O	32.000	32.000	32.000	32.000	32.000	32.000	32.000	32.000	32.000	32.000	32.000	O
Z	15.96	16.00	16.17	16.06	16.01	16.00	16.21	16.00	16.00	16.00	16.00	Z
X	4.02	4.00	3.93	3.94	4.09	4.01	4.15	4.00	4.00	4.00	4.00	X
Ab	59.92	45.02	62.52	39.60	33.23	59.71	48.70	27.99	27.58	28.84	32.77	Ab
An	38.66	53.66	37.03	58.72	64.23	39.27	50.14	71.25	71.67	70.44	66.48	An
Or	1.42	1.32	0.45	1.67	1.81	1.02	1.16	0.76	0.75	0.72	0.75	Or

	A47	A50
	av.11	av.7
SiO_2	53.25	51.49
Al_2O_3	30.18	31.61
CaO	12.47	14.06
Na_2O	4.49	3.67
K_2O	0.11	0.09
TOTAL	100.50	100.92
Si	9.592	9.260
Al	6.409	6.716
Ca	2.407	2.715
Na	1.568	1.282
K	.025	.021
O	32.000	32.000
Z	16.00	16.00
X	4.00	4.02
Ab	39.20	31.91
An	60.17	67.57
Or	0.63	0.52

SCAPOLITE
A46 av.9

SiO_2	45.46	Si	6.805	11.491
Al_2O_3	26.56	Al	4.686	
FeO	.22	Ti	.003	3.899
MnO	.013	Fe	.028	
MgO	.004	Mn	.001	
CaO	17.36	Ca	2.785	
Na_2O	3.40	Na	.987	
K_2O	.50	K	.095	
TiO_2	.027	O	24.000	
TOTAL	93.54			
		Me%	72.25	

Table 25 Feldspar and scapolite analyses - from the 'anorthosites'.

Table 26 Anorthosites. - Whole rock analyses and C.I.P.W. norms. Analyses 856 - 864 and 2879 & 2881 after Palmer (1971). Analyses DAV3 & DAV4 after Davidson (1943). ★-indicates saussuritised type.

	856	858	859	860	862	863	864	2879	2881	DAV 3	DAV 4 ★	
OXIDES(Wt %)												
SiO_2	48.0	48.1	47.7	49.7	47.7	47.8	47.6	51.1	48.8	53.90	52.24	SiO_2
TiO_2	0.14	0.15	0.11	0.12	0.11	0.19	0.25	0.17	0.75	nil	0.17	TiO_2
Al_2O_3	27.8	28.4	27.5	29.3	24.4	25.6	25.5	29.5	17.2	28.08	27.80	Al_2O_3
Fe_2O_3	1.0	1.37	1.26	1.90	1.82	1.49	1.16	2.74	12.5	0.31	0.24	Fe_2O_3
FeO	1.12	1.11	1.16	0.33	3.12	2.43	2.87			0.62	0.09	FeO
MnO	0.02	0.03	0.03	0.01	0.05	0.04	0.04	0.03	0.24	nil	nil	MnO
MgO	1.13	1.40	1.33	3.46	2.81	3.42	3.54	0.98	6.8	trace	0.07	MgO
CaO	15.04	14.86	15.02	12.7	13.2	14.2	13.4	10.7	9.8	11.64	16.02	CaO
Na_2O	2.96	3.32	2.93	5.53	3.07	2.85	2.82	5.0	3.18	3.88	1.58	Na_2O
K_2O	0.17	0.20	0.19	0.22	0.29	0.14	0.16	0.20	0.35	0.62	1.10	K_2O
H_2O+	–	–	–	–	–	–	–	–	–	0.30	0.74	H_2O+
H_2O-	–	–	–	–	–	–	–	–	–	0.10	–	H_2O-
CO_2	–	–	–	–	–	–	–	–	–	–	0.06	CO_2
P_2O_5	0.01	0.01	0.01	0.01	0.09	0.01	0.02	0.02	0.21	–	–	P_2O_5
TOTAL	97.39	98.95	97.24	103.28	96.66	98.17	97.36	100.44	99.83	99.45	100.11	TOTAL
Sr(ppm)	260	352	255	276	262	230	288	668	496			Sr(ppm)
Cr(ppm)	20	45	18	9	15	36	30	17	58			Cr(ppm)
Ni(ppm)	37	27	36	3	75	162	165	26	16			Ni(ppm)
Zr(ppm)	16	28	16	17	64	20	26	31	74			Zr(ppm)
Ba(ppm)	74	108	67	112	183	69	98	163	269			Ba(ppm)
C.I.P.W. NORM												
qtz	–	–	–	–	–	–	–			3.69	7.50	qtz
or	1.00	1.18	1.12	1.30	1.71	.83	.95			3.66	6.50	or
ab	21.70	20.04	20.82	20.25	23.93	20.92	22.66			32.83	13.37	ab
an	62.07	62.01	61.33	54.49	51.95	56.65	56.46			57.38	65.52	an
ne	1.81	4.36	2.15	14.38	1.11	1.73	.65			–	–	ne
di	8.02	8.86	8.96	6.58	10.54	11.02	7.99			.33	.38	di
wo	1.04	.20	.80	–	–	–	–			–	5.37	wo
hyp(En)	–	–	–	–	–	–	–			.71(–)	–	hyp(En)
ol(Fo)	–	–	–	3.90(98.9)	4.37(60.7)	4.48(71.9)	6.46(66.6)			–	–	ol(Fo)
mt	1.45	1.99	1.83	.75	2.64	2.16	1.68			.45	–	mt
hm	–	–	–	1.38	–	–	–			–	.24	hm
il	.27	.28	.21	.23	.21	.36	.47			–	.19	il
sph	–	–	–	–	–	–	–			–	.17	sph
hap	.02	.02	.02	.02	.21	.02	.05			–	–	hap
cc	–	–	–	–	–	–	–			–	.14	cc
Fe_2/Fe_2+Fe_3	.559	.481	.512	.166	.659	.648	.736			.690	.294	Fe_2/Fe_2+Fe_3
∑FeO/∑FeO+MgO	.641	.626	.633	.371	.629	.524	.525	.695	.623		.789	∑FeO/∑FeO+MgO
DIFF. IND	24.52	25.58	24.10	35.93	26.75	23.48	24.25			40.18	27.37	DIFF. IND.
SI UNSAT.	1.53	3.69	1.82	13.83	2.58	3.21	3.03			–	–	SI UNSAT.

	PINK ANORTH.	WHITE ANORTH. ★	NW3 ★	NW6 ★	NW8 ★	NW10 ★	NW11 ★	NW12 ★	NW14	NW9	NW15	NW17	
OXIDES (Wt %)													
SiO_2	49.1	48.2	52.6	52.0	48.0	54.8	47.4	49.0	50.9	50.1	50.9	50.4	SiO_2
TiO_2	0.11	0.10	0.08	0.06	0.17	0.16	0.23	0.46	0.35	0.33	0.16	0.13	TiO_2
Al_2O_3	29.7	29.8	28.2	28.4	30.6	27.6	28.7	25.1	28.5	29.2	30.4	31.6	Al_2O_3
Fe_2O_3	0.50	0.62	0.39	0.49	0.96	0.96	2.5	2.9	2.9	0.96	0.89	0.56	Fe_2O_3
FeO	0.50	0.58	0.30	0.09	0.21	0.40	3.1	3.3	1.6	0.32	0.55	0.62	FeO
MnO	0.02	0.02	0.02	0.02	0.02	0.02	0.08	0.11	0.05	0.02	0.02	0.02	MnO
MgO	0.40	0.40	1.1	0.60	0.33	0.50	2.5	4.0	1.3	1.0	0.44	0.1	MgO
CaO	15.0	14.7	10.9	11.5	15.1	10.7	10.0	10.0	11.2	14.4	13.5	13.3	CaO
Na_2O	13.5	2.58	4.6	4.6	2.8	3.1	2.0	2.5	2.5	3.0	3.0	3.0	Na_2O
K_2O	0.10	0.10	0.25	0.35	0.20	0.25	0.15	0.15	0.10	0.20	0.10	0.15	K_2O
L.O.I.	1.0	2.8	1.7	1.7	1.1	1.6	3.0	2.2	0.48	0.24	0.35	0.45	L.O.I.
H_2O-	-	-	0.06	0.10	0.05	0.18	0.11	0.11	0.06	0.04	0.03	0.05	H_2O-
TOTAL	99.92	99.90	100.20	99.91	99.54	99.27	99.77	99.83	99.94	99.81	100.34	100.38	TOTAL
Sr(ppm)	-	-	50	200	500	1000	1000	200	100	50	1000	200	Sr(ppm)
Cr(ppm)	-	-	-	-	-	-	-	200	-	-	-	-	Cr(ppm)
Ni(ppm)	-	-	-	-	3	10	100	120	100	3	15	5	Ni(ppm)
Zr(ppm)	-	-	-	-	-	-	-	30	-	-	-	-	Zr(ppm)
Ba(ppm)	-	-	100	-	50	500	200	50	50	-	50	-	Ba(ppm)
C.I.P.W. NORM													
qtz	-	1.27	-	-	-	12.24	8.49	5.08	10.01	.79	3.52	3.50	qtz
c	-	-	.55	-	-	2.78	7.07	2.64	3.92	-	.81	2.32	c
or	.59	.59	1.48	2.07	1.18	1.48	.89	.89	.59	1.18	.59	.89	or
ab	24.09	21.83	38.92	36.62	21.69	26.23	16.92	21.15	21.15	25.38	25.38	25.38	ab
an	65.04	69.44	54.08	55.82	70.34	53.09	49.61	49.61	55.57	65.63	66.98	65.99	an
ne	2.99	-	-	1.25	1.08	-	-	-	-	-	-	-	ne
di	2.86	2.81	-	.96	1.77	-	-	-	-	4.53	-	-	di
wo	2.43	-	-	-	.96	-	-	-	-	-	-	-	wo
hyp(En)	-	.07(69.2)	2.29(95.7)	-	-	1.25(100.0)	9.62(65.4)	13.07(76.2)	3.29(99.3)	.39(100.0)	1.14(97.0)	.75(34.6)	hyp(En)
ol(Fo)	-	-	.41(95.3)	.73(100.0)	-	-	-	-	-	-	-	-	ol(Fo)
mt	.72	.90	.57	.18	.25	.89	3.62	4.20	4.20	.14	1.29	.81	mt
hm	-	-	-	.36	.79	.35	-	-	-	.86	-	-	hm
il	.19	.19	.15	.11	.22	.30	.44	.87	.66	.63	.30	.25	il
Fe_2/Fe_2+Fe_3	.536	.518	.477	.200	.210	.327	.586	.567	.387	.283	.416	.560	Fe_2/Fe_2+Fe_3
ΣFeO/ΣFeO+MgO	.926	.939	.776	.882	.964	.948	.682	.596	.763	.899	.951	.983	ΣFeO/ΣFeO+MgO
DIFF IND.	27.67	23.69	40.40	39.93	23.95	39.94	26.30	27.11	31.75	27.35	29.49	29.77	DIFF. IND.
SI UNSAT.	2.53	-	.17	1.37	.92	-	-	-	-	-	-	-	SI UNSAT.
MODE													
Quartz			1	1	3	4	1	1	1	1	1	-	Quartz
Feldspar			19	18	8	9	8	7	63	66	91	97	Feldspar
Sericite			19	3	23	18	7	8	1	1	1	1	Sericite
Epidote			1	1	1	2	-	-	-	1	-	-	Epidote
Zoisite			13	30	53	33	38	28	2	1	-	-	Zoisite
Clinozoisite			2	2	1	2	2	10	2	2	1	1	Clinozoisite
Others			44	41	11	32	44	47	31	30	7	1	Others

Table 27 Anorthosites - Whole rock analyses, C.I.P.W. norms and modal analyses. All analyses after Westoll and Howley (Robertson's Research) * - indicates saussuritised types.

	RHC601	RHC602	RHC603	RHC604	RHC605	RHC606	RHC607	RHC608	RHC609	RHC610	RHC611	RHC612	RHC613	
OXIDES (Wt %)														
SiO_2	47.7	48.9	48.7	47.2	47.3	52.1	47.0	47.0	46.1	45.9	43.9	47.0	44.8	SiO_2
TiO_2	0.11	0.18	0.13	0.12	0.10	0.10	0.14	0.08	0.13	0.12	0.07	0.10	0.22	TiO_2
Al_2O_3	29.5	28.1	30.0	30.3	28.9	29.2	29.2	29.7	30.5	33.7	33.7	30.2	30.0	Al_2O_3
Fe_2O_3 FeO	1.5	3.4	2.9	2.6	1.5	1.5	2.3	1.5	1.5	1.5	1.4	1.5	1.4	Fe_2O_3 FeO
MnO	0.02	0.04	0.04	0.03	0.03	0.03	0.04	0.03	0.03	0.03	0.02	0.02	0.02	MnO
MgO	0.35	1.0	0.95	1.1	0.3	0.25	0.6	0.2	0.25	0.45	0.35	0.50	0.25	MgO
CaO	17.0	14.7	12.6	13.3	18.1	13.6	17.9	18.9	17.8	13.8	13.5	16.8	16.6	CaO
Na_2O	1.75	2.9	3.75	3.6	1.85	2.45	1.9	1.8	2.9	4.35	3.9	2.8	3.6	Na_2O
K_2O	0.5	0.4	0.35	0.15	0.05	0.15	0.05	0.05	0.05	0.4	0.3	0.1	0.25	K_2O
L.O.I.	1.39	1.94	2.63	2.00	0.82	1.13	0.71	1.01	0.76	3.00	2.57	1.00	2.61	L.O.I.
H_2O-	0.04	0.03	0.09	0.11	0.06	0.09	0.05	0.09	0.01	0.13	0.19	-	0.08	H_2O-
TOTAL	99.86	99.99	100.24	100.21	100.41	100.30	99.89	99.91	100.23	100.18	99.90	100.02	99.83	TOTAL
$\Sigma FeO/\Sigma FeO+MgO$	.794	.754	.733	.680	.818	.844	.775	.871	.844	.750	.783	.730	.834	$\Sigma FeO/\Sigma FeO+MgO$
MODE														
Quartz	17.0	6.2	15.3	2.7	3.1	2.6	5.5	2.6	4.1	4.1	0.5	4.5	1.8	Quartz
Feldspar	1.6	5.8	38.8	11.4	17.0	8.6	19.3	5.0	26.1	20.7	4.6	10.1	11.1	Feldspar
Sericite	5.6	6.1	41.3	11.0	6.4	30.0	9.4	1.9	15.4	36.9	39.8	10.9	30.1	Sericite
Epidote	0.7	10.9	2.1	2.2	0.7	4.8	1.0	1.7	3.9	2.5	2.5	1.8	1.2	Epidote
Zoisite	75.0	70.0	0.3	71.0	70.6	52.1	64.6	86.9	49.4	32.8	52.0	72.5	54.1	Zoisite
Clinozoisite	-	0.9	-	1.2	2.1	1.3	-	0.2	1.1	1.1	0.2	0.1	0.8	Clinozoisite
Calcite	-	-	-	-	-	-	-	0.4	1.7	1.7	-	-	-	Calcite
Chlorite	-	-	-	1.4	0.15	1.0	-	-	-	-	-	-	-	Chlorite
Sphene	-	-	-	-	-	-	-	-	-	-	-	0.1	0.4	Sphene

Table 28 Anorthosites from the quarry area. - Whole rock and modal analyses. All analyses after Cummings (Robertson's Research).

Possibly all saussuritised types

④ MINOR INTRUSIVES

SAMPLE NO.	MINERAL ASSEMBLAGES OF ANALYSED ROCKS ( ) - MODAL % OF EACH COMPONENT	MINERAL ANALYSES TABLES 31, 32 & 33			
		Opx	Cpx	Amp	Gt
a) ULTRAMAFITE LENSES WITHIN THE LEVERBURGH METASEDIMENTS					
	(i) Amphibole Peridotites				
‡ MSC3	Opx(33), Amp(28), Cpx(15), Ol(13), Spinel(11)				
‡ BX	Opx(43), Amp(28), Ol(15), Cpx(7), Spinel(7)	*		*	
‡ OS1	Cpx/Ol/Amp/Spinel		*	*	
‡ OS2	Opx(44), Amp(29), Ol(13), Spinel(12), Cpx(2)	*		*	
‡‡ DAV1	Opx/Amp/Ol/Spinel				
	(ii) Garnet Amphibole Peridotite				
‡ X	Opx(40), Amp(30), Ol(15), Symp(10), Spinel(4), Gt(1)				
	(iii) Amphibole Pyroxenites, Garnet Amphibole Pyroxenites and Hornblendites				
‡ BIO	Cpx(45), Gt(22), Amp(17), Opx(10), Bi(5)	*	*	*	*
‡ BI	Amp(74), Cpx(20), Opx(5)				
‡ LBI	Amp(65), Opx(22), Cpx(11)	*		*	
‡ CTI	Amp/Cpx/Gt/Opx				
‡ CT6	Amp(64), Opx(22), Cpx(10)	*			
‡ 5001	Amp/Cpx/Opx/Gt			*	
‡ MSC	Amp(51), Opx(26), Cpx(19), Spinel(4)	*	*	*	
‡ Q2	Amp(36), Opx(31), Cpx(29), Spinel(5)				
‡ QB	Opx/Cpx/Bi/Amp				
‡ SH2	Opx/Cpx/amp			*	
‡ ENE	Opx/Cpx/Bi/Amp				
b) ULTRAMAFITE LENS FROM WITHIN THE GABBRO-DIORITE					
● D1	Cpx(40), Opx(27), Amp(21), Spinel(6), Plag (3)			*	
c) ULTRAMAFITE (PYROXENITE) DYKES INTRUSIVE INTO THE NORITE					
X U919 X U920 X U921 X U922 X U923	Cpx(60-70), Opx(40-30), Amp				
d) ULTRAMAFITE (HORNBLENDITE) LENSES INTRUSIVE INTO THE ANORTHOSITE COMPLEX					
R60 R61	Amp (99-100), Bi (1)				

‡‡ Davidson (1943)
X Palmer (1971)
● Dearnley (1959)
‡ Livingstone (1963, 1967)

Table 29.[a] Ultramafites from the Leverburgh metasedimentary belt - Whole rock analyses and C.I.P.W. Norms

OXIDES(Wt %)	MSC3	BX	OS1	OS2	DAV.1	X	B10	B1	LB1	CT1	CT6	500I	MSC	
SiO_2	44.12	42.66	44.02	42.70	44.69	42.52	45.26	43.76	44.15	44.70	43.98	43.67	44.22	SiO_2
TiO_2	0.41	0.22	0.42	0.68	0.49	0.32	0.72	0.53	0.92	0.71	0.45	1.37	0.65	TiO_2
Al_2O_3	7.04	10.40	4.24	7.46	8.66	10.41	10.88	12.45	11.27	9.06	11.52	6.87	9.12	Al_2O_3
Fe_2O_3	6.42	3.76	5.74	5.97	5.23	3.11	2.26	1.91	3.39	5.29	3.65	6.95	5.43	Fe_2O_3
FeO	5.02	6.97	4.84	6.25	7.44	6.25	9.88	8.96	8.52	6.79	7.31	10.06	6.73	FeO
MnO	0.14	0.11	0.14	0.11	0.27	0.12	0.17	0.15	0.11	0.15	0.29	0.14	0.22	MnO
MgO	22.28	24.07	19.10	24.53	23.56	25.14	13.38	14.43	16.60	14.51	16.67	18.91	19.68	MgO
CaO	9.53	7.40	16.01	9.51	8.54	6.86	13.72	12.64	11.25	14.46	11.41	8.71	10.46	CaO
Na_2O	0.84	0.54	1.44	0.91	0.38	0.87	1.76	1.83	1.69	1.69	1.28	0.67	1.72	Na_2O
K_2O	0.19	0.46	0.44	0.06	0.12	0.56	0.63	0.58	0.34	0.36	0.95	0.33	0.20	K_2O
H_2O+	2.77	3.32	2.87	1.47	0.33	3.05	1.02	1.76	1.49	1.35	2.49	1.37	1.53	H_2O+
H_2O-	0.21	0.17	0.21	0.16	0.10	0.27	0.06	0.13	0.12	0.30	0.28	-	0.04	H_2O-
P_2O_5	trace	0.03	-	0.04	-	-	0.02	0.15	0.06	-	-	-	0.09	P_2O_5
Cr_2O_3	0.40	0.52	0.44	0.32	-	0.47	0.32	0.32	0.32	0.27	0.39	0.36	0.29	Cr_2O_3
S	-	-	-	-	-	-	-	0.14	-	-	-	-	-	S
TOTAL	99.37	100.63	99.91	100.17	99.81	99.95	100.08	99.79	100.23	99.64	100.67	99.41	100.38	TOTAL
Ni(ppm)	1090	870	1090	1160		1390	160	200	550	60	870	840	360	Ni(ppm)
Sr(ppm)	157	66	67	67		68	81	93	n.d.	87	29	47	47	Sr(ppm)
Rb(ppm)	4	15	12	n.d.		n.d.	11	2	8	9	n.d.	8	n.d.	Rb(ppm)
S.G.	3.28	3.14	3.21	3.29	3.28	3.21	3.33	3.18	3.24	3.21	3.20	3.32	3.23	S.G.
C.I.P.W. NORM														
or	1.12	2.72	—	.35	.71	3.31	3.72	3.43	2.01	2.13	5.61	1.95	1.18	or
ab	7.11	4.57	—	7.70	3.22	7.36	4.05	3.09	9.36	5.82	5.19	5.67	11.91	ab
an	14.88	24.60	3.81	16.10	21.57	22.85	19.93	24.05	22.16	16.07	22.89	14.77	16.58	an
ne	—	—	6.60	—	—	—	5.87	6.71	2.68	4.59	3.05	—	1.43	ne
lc	—	—	2.04	—	—	—	—	—	—	—	—	—	—	lc
ns	—	—	—	—	—	—	—	—	—	—	—	—	—	ns
di	25.38	9.42	55.55	24.21	16.44	8.82	38.77	30.31	26.54	44.14	26.84	22.61	27.42	di
hyp(En)	14.42(95.7)	11.26(87.9)	—	2.52(93.1)	21.91(88.1)	4.20(89.2)	—	—	—	—	—	22.53(82.7)	—	hyp(En)
ol(Fo)	22.81(95.3)	37.87(86.9)	17.58(93.9)	37.15(92.5)	27.02(86.9)	44.28(88.3)	21.49(66.6)	25.58(69.8)	28.60(77.6)	15.82(82.6)	27.60(79.8)	17.31(81.1)	30.55(86.7)	ol(Fo)
cs	—	—	1.48	—	—	—	—	—	—	—	—	—	—	cs
mt	9.31	5.45	8.32	8.66	7.58	4.51	3.28	2.77	4.91	7.67	5.29	10.08	7.87	mt
cm	.59	.77	.65	.47	—	.69	.47	.47	.47	.40	.57	.53	.43	cm
il	.78	.42	.80	1.29	.93	.61	1.37	1.01	1.75	1.35	.85	2.60	1.23	il
hap	—	.07	—	.09	—	—	.05	.35	.14	—	—	—	.21	hap
Fe_2/Fe_2+Fe_3	.472	.677	.491	.542	.621	.695	.832	.841	.739	.593	.698	.620	.587	Fe_2/Fe_2+Fe_3
ΣFeO/ΣFeO+MgO	.326	.301	.344	.322	3[illegible]	.265	.471	.424	.461	.443	.377	.463	.371	ΣFeO/ΣFeO+MgO
DIFF. IND.	8.23	7.29	8.64	8.05	3.92	10.67	13.65	13.23	14.04	12.54	13.86	7.62	14.52	DIFF. IND.
SI UNSAT.	9.56	15.45	14.00	15.43	11.02	18.17	13.20	15.59	13.61	10.28	13.6[illegible]	6.94	13.71	SI UNSAT.

Table 30. a) Ultramafites from the Leverburgh metasedimentary belt (cont.)
b) Ultramafite lens from the gabbro-diorite
c) Ultramafite dykes from the norite

Whole rock analyses and C.I.P.W. Norms.

	(a)				(b)	(c)					
	Q2	QB	SH2	ENE	D1	U919	U920	U921	U922	U923	
OXIDES(Wt%)											
SiO_2	46.99	48.03	51.35	47.89	48.40	53.4	55.0	51.7	53.7	53.9	SiO_2
TiO_2	0.28	0.56	0.15	1.57	.70	0.27	0.25	0.43	0.25	0.25	TiO_2
Al_2O_3	7.77	2.64	0.54	4.27	7.40	3.24	3.3	5.5	2.8	2.8	Al_2O_3
Fe_2O_3	2.67	2.08	1.66	2.11	3.20	9.92	7.8	9.5	9.9	10.0	Fe_2O_3
FeO	8.20	7.99	4.88	10.11	11.10						FeO
MnO	0.17	0.15	0.11	0.15	-	0.19	0.16	0.17	0.20	0.21	MnO
MgO	20.91	20.57	23.73	18.49	14.50	17.5	16.1	15.8	17.6	17.8	MgO
CaO	10.71	12.94	14.58	11.04	12.70	12.8	16.3	13.7	13.3	13.2	CaO
Na_2O	0.91	0.70	0.87	0.62	1.60	0.69	0.61	1.15	0.61	0.59	Na_2O
K_2O	0.21	1.12	0.16	1.30	0.10	0.17	0.09	0.19	0.06	0.04	K_2O
H_2O+	0.75	1.91	1.49	1.62	0.30						H_2O+
H_2O-	0.15	0.16	0.11	0.09	-						H_2O-
P_2O_5	0.04	n.d.	0.03	-	-	0.01	0.02	0.01	0.03	0.01	P_2O_5
Cr_2O_3	0.52	0.36	0.57	0.40	0.15	0.09	0.05	0.06	0.09	0.10	Cr_2O_3
TOTAL	100 28	99.21	100.23	99.46	100.15	98.28	99.68	98.21	98.54	98.90	TOTAL
Ni(ppm)	890		n.d.		850	174	443	189	197	175	Ni(ppm)
Sr(ppm)	47		50		40	64	89	88	60	54	Sr(ppm)
Rb(ppm)	6		n.d.		-	3	2	1	1	1	Rb(ppm)
S.G.	3.19	3.13	3.15	3.28							
C.I.P.W NORM											
or	1.24	6.62	.95	7.68	.59						or
ab	7.70	5.92	1.89	5.25	13.54						ab
an	16.50	.75	-	5.03	12.72						an
ac	-	-	4.60	-	-						ac
ns	-	-	.01	-	-						ns
di	28.94	50.48	56.96	39.81	40.63						di
hyp(En)	12.63(81.4)	2.55(81.7)	13.66(87.9)	13.96(76.2)	8.46(68.6)						hyp(En)
ol (Fo)	27.11(79.8)	26.21(79.9)	19.18(86.8)	19.77(74.4)	17.80(66.5)						ol(Fo)
mt	3.87	3.02	-	3.06	4.64						mt
cm	.77	.53	.84	.59	-						cm
il	.53	1.06	.28	2.60	1.33						il
hap	.09	-	.07	-	-						hap
$Fe_2/Fe_2 + Fe_3$	.777	.813	.770	.844	.794						$Fe_2/Fe_2 + Fe_3$
∑FeO/∑FeO+MgO	.336	.324	.212	.394	.491	.338	.304	.351	.336	.336	∑FeO/∑FeO+MgO
DIFF. IND.	8.94	12.54	2.83	12.93	14.13						DIFF. IND.
SI UNSAT.	10.84	10.48	7.85	7.77	6.81						SI UNSAT.

	CLINOPYROXENES			ORTHOPYROXENES							
	MSC	OS1	B10	MSC	BY	OS2	R62	B10	LB1	CT6	
SiO_2	50.65	52.60	51.22	52.90	53.59	53.58	53.63	50.36	50.81	51.59	SiO_2
TiO_2	0.11	0.21	0.13	0.09	0.09	-	0.19	0.15	0.05	-	TiO_2
Al_2O_3	3.05	2.91	6.20	2.44	3.84	4.31	4.53	2.69	3.49	5.03	Al_2O_3
Fe_2O_3	1.38	2.09	0.91	1.67	2.16	-	1.54	2.09	2.26	2.84	Fe_2O_3
FeO	3.29	2.65	5.67	12.32	9 94	10.32	9.07	18.48	15.69	12.28	FeO
MnO	0.14	0.09	0.10	0.28	0.21	-	0.25	0.17	0.32	0.27	MnO
MgO	17.09	16.74	12.67	28.24	29.13	29.27	30.31	25.80	26.38	27.22	MgO
CaO	23.22	21.15	20.71	1.09	0.85	0.73	0.53	0.23	0.59	1.08	CaO
Na_2O	0.68	0.68	1.55	0.07	0.09	-	0.02	0.08	0.07	0.05	Na_2O
K_2O	0.33	0.29	0.10	0.02	0.18	-	-	-	0.02	n.d.	K_2O
P_2O_5	-	-	0.02	-	-	-	-	-	-	-	P_2O_5
Cr_2O_3	0.12	0.17	0.27	0.06	-	0.09	-	-	0.12	0.23	Cr_2O_3
TOTAL	100.06	99.58	99.55	99.18	100.08	98.30	100.07	100.05	99.80	100.59	TOTAL
S.G.	3.33	-	3.36	3.47	3.37	3.39	-	-	3.46	3.38	S.G.
Si	1.868	1.925	1.892	1.911	1.896	1.914	1.883	1.860	1.859	1.844	Si
Al^4	0.132 (2.000)	0.075 (2.000)	0.108 (2.000)	0.089 (2.000)	0.104 (2.000)	.086 (2.000)	0.117 (2.000)	0.117 (1.977)	0.141 (2.000)	0.156 (2.000)	Al^4
Al^6	0.001	0.050	0.162	0.015	0.056	.096	.071	-	0.010	0.056	Al^6
Fe^{3+}	0.038	0.058	0.025	0.045	0.058	-	.041	0.058	0.062	0.076	Fe^{3+}
Fe^{2+}	0.101	0.081	0.175	0.372	0.294	.308	.266	0.571	0.480	0.367	Fe^{2+}
Mn	0.004	0.003	0 003	0.009	0.006	-	.007	0.005	0.010	0.008	Mn
Mg	0.940 (2.073)	0.913 (2.006)	0.698 (2.010)	1.521 (2.014)	1.536 (2.000)	1.559 (1.994)	1.597 (1.998)	1.420 (2.074)	1.439 (2.034)	1.451 (2.010)	Mg
Ca	0.918	0.829	0.820	0.042	0.032	.028	.020	0.009	0.023	0.041	Ca
Na	0.049	0.048	0.111	0.005	0.006	-	.001	0.006	0.005	0.003	Na
K	0.016	0.014	0.005	0.001	0.008	-	-	-	0.001	-	K
Ti	0.003	0.006	0.004	0.002	0.002	-	.005	0.004	0.001	-	Ti
Cr	0.003	0.005	0.008	0.002	-	.003	-	-	0.003	0.007	Cr
O	6.000	6.000	6.000	6.000	6.000	6.000	6.000	6.000	6.000	6.000	O
Fe/Mg	0.113	0.092	0.256	0.250	0.196	.198	.173	.406	.341	.259	Fe/Mg
Fe/Fe + Mg	0.101	0.084	0.204	0.200	0.164	.165	.147	.289	.254	.206	Fe/Fe+Mg
En	47.1	48.4	40.5	76.8	79.7	82.2	84.71	69.2	71.4	75.0	En
Fs	6.9	7.6	11.9	21.2	18.6	16.27	14.22	30.4	27.4	22.9	Fs
Wo	46.0	44.0	47.6	2.0	1.7	1.47	1.06	.4	1.2	2.1	Wo

Table 31 Pyroxene analyses - Ultramafite lenses from the Leverburgh metasedimentary belt. All analyses after Livingstone (1963).

	BX	OS1	OS2	BIO	LB1	500I	MSC	SH2	D1	
SiO_2	43.95	43.60	44.57	42.82	43.05	44.89	42.78	52.54	41.95	SiO_2
TiO_2	0.54	0.27	0.80	1.31	0.79	1.15	0.73	0.19	2.07	TiO_2
Al_2O_3	13.22	11.78	11.40	14.27	13.09	11.50	12.14	4.85	14.92	Al_2O_3
Fe_2O_3	3.08	4.55	5.06	2.62	2.18	0.44	4.49	1.72	2.15	Fe_2O_3
FeO	4.62	3.86	3.13	8.65	7.52	6.38	5.08	4.25	7.85	FeO
MnO	0.04	0.07	0.07	0.07	0.04	0.18	0.13	0.06	0.15	MnO
MgO	17.21	18.92	17.69	14.02	15.74	18.57	18.44	20.51	13.20	MgO
CaO	12.03	11.81	12.68	11.73	11.98	13.19	11.43	12.99	11.93	CaO
Na_2O	1.25	2.31	2.17	2.36	2.66	1.79	2.56	0.88	3.40	Na_2O
K_2O	1.34	1.36	0.20	0.95	0.47	0.50	0.29	0.32	0.61	K_2O
Cr_2O_3	0.52	0.43	0.24	0.18	0.40	0.45	0.29	n.d.	0.15	Cr_2O_3
TOTAL	97.80	98.96	98.01	98.98	97.92	99.04	98.36	98.31	98.38	TOTAL
H_2O+	2.42	1.57	2.20	1.50	2.01	1.83	2.03	1.86	1.38	H_2O+
H_2O-	0.06	0.06	0.05	n.d.	0.03	–	0.04	0.03	0.15	H_2O-
P_2O_5	0.12	0.02	–	0.03	0.02	–	0.08	n.d.	—	P_2O_5
S.G.	3.117	3.154	3.112	3.189	3.188	3.145	3.126	3.062	—	S.G.
Si	6.291	6.216	6.353	6.168	6.233	6.364	6.138	7.322	6.075	Si
Al^4	1.709 (8.000)	1.784 (8.000)	1.647 (8.000)	1.832 (8.000)	1.767 (8.000)	1.636 (8.000)	1.862 (8.000)	.678 (8.000)	1.925 (8.000)	Al^4
Al^6	.521	.195	.268	.591	.466	.286	.192	.119	.621	Al^6
Fe^{3+}	.332	.488	.543	.284	.238	.047	.485	.180	.234	Fe^{3+}
Fe^{2+}	.553 (5.200)	.460 (5.250)	.373 (5.064)	1.042 (5.099)	.911 (5.148)	.756 (5.209)	.610 (5.357)	.495 (5.082)	.951 (4.916)	Fe^{2+}
Mn	.005	.008	.008	.009	.005	.022	.016	.007	.018	Mn
Mg	3.672	4.021	3.759	3.010	3.397	3.924	3.944	4.261	2.849	Mg
Cr	.059	.048	.027	.020	.046	.050	.033		.017	Cr
Ti	.058	.029	.086	.142	.086	.123	.079	.020	.225	Ti
Ca	1.845 (1.845)	1.804 (1.804)	1.937 (1.937)	1.811 (1.811)	1.858 (1.858)	2.004 (2.004)	1.757 (1.757)	1.940 (1.940)	1.851 (1.851)	Ca
Na	.347 (.592)	.639 (.886)	.600 (.636)	.659 (.834)	.747 (.834)	.492 (.583)	.712 (.765)	.238 (.295)	.955 (1.067)	Na
K	.245	.247	.036	.175	.087	.090	.053	.057	.113	K
O	23.000	23.000	23.000	23.000	23.000	23.000	23.000	23.000	23.000	O
Fe/Mg	.152	.117	.102	.349	.269	.198	.159	.118	.340	Fe/Mg
Fe/Fe + Mg	.132	.104	.092	.259	.212	.165	.137	.105	.254	Fe/Fe+Mg
niggli mg	.805	.808	.802	.693	.746	.827	.780	.862	.703	niggli mg

Table 32 Amphibole analyses - Ultramafite lenses from the Leverburgh metasedimentary belt. All analyses after Livingstone (1963), except D1 which is after Dearnley (1959).

	B10	
SiO_2	37.49	
TiO_2	0.12	
Al_2O_3	21.03	
Fe_2O_3	4.12	
FeO	18.46	
MnO	0.54	
MgO	11.42	
CaO	5.92	
Na_2O	0.12	
Cr_2O_3	0.39	
K_2O	0.06	
TOTAL	99.67	
S.G.	3.946	
UNIT FORMULA		
Si	5.741	6.000
Al	.259	
Al	3.537	4.073
Cr	.047	
Ti	.014	
Fe^{3+}	.475	
Mg	2.607	6.013
Fe^{2+}	2.364	
Mn	.070	
Ca	.971	
O	24.000	
Fe/Mg	.934	
Fe/Fe+Mg	.483	
GARNET MOLECULES (RICKWOOD 1968)		
Uvarovite	1.23	
Andradite	12.14	
Pyrope	45.30	
Spessartine	1.22	
Grossular	3.27	
Almandine	36.60	
Schorlomite	0.24	
% cations assigned to garnet molecules	95.41	

Table 33 Garnet analysis - Ultramafite lens from the Leverburgh metasedimentary belt. After Livingstone (1963, 1967)

(d)

	R60	R61
OXIDES (Wt%)		
SiO_2	43.74	44.27
TiO_2	1.56	1.53
Al_2O_3	12.84	12.69
Fe_2O_3	4.69	4.72
FeO	5.49	5.53
MnO	0.10	0.10
MgO	15.06	15.60
CaO	12.96	13.66
Na_2O	2.18	1.99
K_2O	0.65	0.65
TOTAL	99.27	100.74
Sr(ppm)	245	257
Rb(ppm)	3	3
Cr(ppm)	270	260
C.I.P.W. NORM.		
or	3.84	3.84
ab	3.45	1.92
an	23.33	23.78
ne	8.12	8.08
di	32.22	34.60
ol(Fo)	18.54 (91.0)	18.77 (91.3)
mt	6.80	6.84
il	2.96	2.91
Fe_2/Fe_2+Fe_3	.570	.570
∑FeO/∑FeO+MgO	.392	.385
DIFF. IND.	15.41	13.84
SI. UNSAT.	14.54	14.60
TOTAL NORMATIVE FELDSPAR	30.63	29.54
NORMATIVE ANORTHITE CONTENT OF FELDSPAR	60.22	63.20

Table 34 d) Hornblendites, intrusive into the anorthosite - Whole rock analyses and C.I.P.W. norms

e) ULTRAMAFITES FROM THE LANGAVAT METASEDIMENTARY BELT

(DUNITES - AMPHIBOLE PERIDOTITES)

SAMPLE NO.	ROCK TYPE
MLL	Amphibole - phlogopite peridotite
NLLAI	Dunite - olivine rock with minor amounts of chlorite, tremolite (developing from the olivine) and anthophyllite. Accessory magnetite (or chromite) and carbonate.
LL8	Amphibole peridotite - olivine/tremolite rock.
LLBS(A)	Amphibolite band from a layered ultramafite sequence at the southern end of the Scara Ruadh lens. - Tremolite anthophyllite, Chlorite rock.
LLBS(S)	Serpentinite band from a layered ultramafite sequence at the southern end of the Scara Ruadh lens. - Serpentine (with remnants of olivine), tremolite, chlorite, magnetite rock.
LL2	Serpentinite from east side of Scara Ruadh lens.
LLIS	Chlorite rich rock from a layered ultramafite series at the N.E. margin of the Scara Ruadh lens.
SNS4	Actinolite/chlorite rock rimming the Sqeir nan Sgarbh lens.

All analyses after Livingstone (1963)

Table 35 e) Ultramafites from the Langavat metasedimentary belt - Whole rock analyses and C.I.P.W. NORMS

	MLL	NLLAI	LL8	LLBS(A)	LLBS(S)	LLIS	LL2	SNS4	
OXIDES(Wt %)									
SiO_2	36.35	36.37	44.16	47.36	34.99	38.31	36.52	45.58	SiO_2
TiO_2	0.31	n.d.	0.24	0.12	0.14	0.11	0.05	0.24	TiO_2
Al_2O_3	5.91	0.69	2.81	5.29	3.07	10.51	3.49	14.85	Al_2O_3
Fe_2O_3	4.03	2.94	5.37	2.15	9.03	1.70	7.26	0.77	Fe_2O_3
FeO	4.69	6.69	2.95	4.24	3.67	5.40	2.14	8.26	FeO
MnO	0.09	0.13	0.13	0.12	0.09	0.15	0.09	0.11	MnO
MgO	40.33	45.56	30.35	26.93	36.88	31.76	38.11	19.01	MgO
CaO	n.d.	0.70	5.38	6.81	0.94	2.01	n.d.	6.02	CaO
Na_2O	0.22	0.05	0.18	0.20	0.04	0.26	0.03	1.01	Na_2O
K_2O	0.70	0.01	0.03	0.03	0.01	0.03	0.01	0.07	K_2O
H_2O+	6.45	5.95	7.24	5.56	10.48	9.03	11.40	3.37	H_2O+
H_2O-	0.43	–	0.20	0.20	0.33	–	0.42	0.08	H_2O-
P_2O_5	trace	–	0.03	–	–	–	0.04	–	P_2O_5
Cr_2O_3	0.36	1.26	1.09	0.55	0.78	1.43	1.14	0.37	Cr_2O_3
TOTAL	99.87	100.35	100.16	99.56	100.45	100.70	100.15	99.74	TOTAL
NI (ppm)	–	2490	–	–	–	–	–	–	NI (ppm)
S.G.	2.95	2.99	2.86	2.88	2.86	2.75	2.61	–	S.G.
C.I.P.W NORM.									
c	4.79	–	–	–	1.28	6.40	3.43	2.17	c
or	4.14	–	.18	.18	.06	.18	.06	.41	or
ab	1.86	–	1.52	1.69	.34	2.20	.25	8.55	ab
an	–	1.63	6.77	13.45	4.66	9.97	–	29.87	an
ne	–	.23	–	–	–	–	–	–	ne
kp	–	.03	–	–	–	–	–	–	kp
di	–	–	15.35	15.97	–	–	–	–	di
hyp (En)	4.33(97.1)	–	36.98(98.9)	42.04(93.1)	17.45(100.0)	23.98(91.8)	26.52(100.0)	32.44(77.5)	hyp(En)
ol (Fo)	70.91(96.7)	86.47(92.5)	22.07(98.8)	16.32(92.6)	52.14(100.0)	44.17(91.1)	47.86(100.0)	20.74(75.6)	ol(Fo)
cs	–	.57	–	–	–	–	–	–	cs
mt	5.84	4.26	7.57	3.12	10.53	2.46	5.31	1.12	mt
cm	.53	1.86	1.60	.81	1.15	2.11	1.68	.54	cm
hm	–	–	.15	–	1.77	–	3.60	–	hm
il	.59	–	.46	.23	.27	.21	.09	.46	il
hap	–	–	.07	–	–	–	.09	–	hap
Fe_2/Fe_2+Fe_3	.569	.721	.389	.693	.316	.784	.254	.924	Fe_2/Fe_2+Fe_3
$\Sigma FeO/\Sigma FeO+MgO$	.111	.170	.200	.187	.243	.179	.185	.320	$\Sigma FeO/\Sigma FeO+MgO$
DIFF. IND.	6.0	.26	1.70	1.87	.40	2.38	.31	8.96	DIFF. IND.
SI UNSAT.	29.83	37.07	9.42	6.79	22.26	18.32	20.44	8.18	SI UNSAT.

f) Ultramafites associated with brecciated areas, along and adjacent to the margin of the anorthosite

Sample Nos.	Rock Type	Mineral Analyses			
		Cpx	Gt	Amp	Ilm
(i) Ultramafites - clinopyroxenites and garnet clinopyroxenites					
NV2	clinopyroxenite (plus minor Scapolite)	*			
NV4	garnet clinopyroxenites				
NV8					
NV9					
NV10					
NV11					
(ii) Garnetite nodules from the ultramafites					
NV1	clinopyroxene garnetites	*	*	*	*
NV3		*	*		
NV5		*		*	
NV6					
NV7					

	NV2	NV4	NV3	NV9	NV10	NV11	NV1	NV3	NV5	NV6	NV7	
OXIDES (Wt%)												
SiO_2	48.87	47.36	45.22	45.56	46.51	47.55	42.70	43.84	43.36	43.77	43.38	SiO_2
TiO_2	0.60	1.19	1.31	1.19	1.44	1.23	0.89	0.64	0.78	0.92	0.94	TiO_2
Al_2O_3	6.37	8.26	10.35	9.96	9.71	10.40	14.26	13.60	13.41	13.02	13.21	Al_2O_3
Fe_2O_3	8.73	12.17	13.46	13.16	13.32	13.15	19.94	7.20	17.26	17.25	17.43	Fe_2O_3
FeO								8.39				FeO
MnO	0.09	0.11	0.13	0.15	0.17	0.15	0.37	0.28	0.31	0.32	0.31	MnO
MgO	12.39	12.06	11.35	11.52	11.31	9.44	10.11	10.61	10.31	10.97	10.72	MgO
CaO	21.86	17.26	15.32	16.14	17.79	16.05	12.39	13.92	14.06	14.14	14.12	CaO
Na_2O	1.10	1.31	1.36	1.78	1.05	1.58	0.71	0.73	0.73	0.80	0.79	Na_2O
K_2O	n.d.	0.22	0.35	0.23	0.02	0.24	0.02	0.10	0.005	0.13	0.14	K_2O
TOTAL	100.01	99.94	100.35	99.95	101.32	99.79	101.39	99.31	100.23	101.32	101.04	TOTAL
Cr(ppm)	–	–	–	–	–	–	106	–	–	–	–	Cr(ppm)
C.I.P.W. NORM												
or								0.59				or
ab								6.18				ab
an								33.54				an
di								28.47				di
hyp(En)								11.65(75.0)				hyp(En)
ol (fo)								7.23(73.1)				ol (fo)
mt								10.44				mt
il								1.22				il
Fe_2/Fe_2+Fe_3								.572				Fe_2/Fe_2+Fe_3
∑FeO/∑FeO+MgO	.388	.476	.505	.507	.514	.556	.640	.584	.601	.586	.594	∑FeO/∑FeO+MgO
DIFF. IND.								6.77				DIFF. IND.
SI. UNSAT.								2.83				SI. UNSAT.
TOTAL NORMATIVE FELDSPAR								40.31				TOTAL NORMATIVE FELDSPAR
NORMATIVE ANORTHITE CONTENT OF FELDSPAR								83.21				NORMATIVE ANORTHITE CONTENT OF FELDSPAR

Table 36 Ultramafites associated with brecciated areas, along and adjacent to the margin of the anorthosite - Whole rock analyses and C.I.P.W. norm

	CLINOPYROXENES			
	NV1 av.5	NV3 av.9	NV2 av.7	NV5 av.10
SiO_2	51.92	50.65	52.70	51.19
TiO_2	0.25	0.58	0.19	0.34
Al_2O_3	3.21	3.78	2.65	3.09
Fe_2O_3 / FeO	9.21	9.59	8.31	10.61
MnO	0.09	0.09	0.06	0.13
MgO	14.26	13.77	15.10	13.45
CaO	20.42	20.75	20.66	20.29
Na_2O	0.59	0.94	0.52	0.63
K_2O	-	-	-	-
Cr_2O_3	0.02	0.23	0.02	0.05
TOTAL	99.97	100.38	100.21	99.78
UNIT FORMULA				
Si	1.930	1.889	1.945	1.922
Al^4	.070	.111	.055	.078
	2.000	2.000	2.000	2.000
Al^6	.071	.055	.061	.059
Ti	.007	.016	.005	.010
Cr	.001	.007	.001	.001
Mg	.790	.765	.831	.753
	2.014	2.042	2.010	2.022
Fe^{2+}	.286	.299	.257	.333
Mn	.003	.003	.002	.004
Ca	.813	.829	.817	.816
Na	.043	.068	.037	.046
O	6.000	6.000	6.000	6.000
Fe/Mg	.366	.394	.311	.448
Fe/Fe+Mg	.268	.283	.237	.309
En	41.81	40.42	43.62	39.57
Fs	15.15	15.79	13.47	17.51
Wo	43.04	43.78	42.91	42.91

Table 37 Clinopyroxene analyses - Ultramafite intrusions.

	NV1		NV5	
	av.9		av.9	
SiO_2	44.31		42.54	
TiO_2	1.26		1.32	
Al_2O_3	11.56		13.59	
FeO	12.58		12.79	
MnO	0.06		0.06	
MgO	13.54		12.62	
CaO	11.49		11.81	
Na_2O	2.05		2.38	
K_2O	0.04		0.13	
Cr_2O_3	0.04		0.05	
TOTAL	96.93		97.29	
UNIT FORMULA				
Si	6.530	8.000	6.282	8.000
Al^4	1.470		1.718	
Al^6	.537		.647	
Fe^{2+}	1.550		1.580	
Mn	.007		.008	
Mg	2.974	5.214	2.778	5.164
Cr	.005		.006	
Ti	.140		.147	
Ca	1.814	1.814	1.869	1.869
Na	.586	.593	.681	.706
K	.008		.024	
O	23.000		23.000	
Fe/Mg	.524		.571	
Fe/Fe+Mg	.344		.364	
niggli mg	.656		.636	

Table 38 Amphibole analyses - Ultramafite intrusions.

	GARNETS				ILMENITE	
	NV3 av.12		NV1 av. 9		NV1 av.12	
SiO_2	39.07		38.64		0.017	
TiO_2	0.13		0.11		50.08	
Al_2O_3	21.69		20.38		0.015	
Fe_2O_3	-		*2.99		*4.65	
FeO	24.15		21.32		43.73	
MnO	0.63		0.66		0.33	
MgO	6.48		8.73		0.54	
CaO	8.14		6.83		0.02	
Cr_2O_3	0.23		0.02		0.02	
TOTAL	100.52		99.68		99.41	
Na(ppm)	970		95			
UNIT FORMULA						
Si	6.008	6.008	5.960	6.000	Al .001	
Al			.040		Fe^{3+} .177	2.089
Al	3.931		3.665		Ti 1.910	
Cr	.028	3.974	.002	4.027	Mg .041	
Ti	.015		.013		Fe 1.855	1.911
Fe^{3+}			.347		Mn .014	
Mg	1.485		2.007		Ca .001	
Fe	3.106		2.751		O 6.000	
Mn	.082	6.015	.082	5.973		
Ca	1.341		1.129			
O	24.000		24.000			
Fe/Mg	2.146		1.413			
Fe/Fe+Mg	.682		.586			
GARNET MOLECULES (RICKWOOD, 1968)						
Uvarovite	0.71		0.06			
Andradite			8.51			
Pyrope	25.01		33.61			
Spessartine	1.38		1.44			
Grossular	21.88		10.12			
Almandine	51.02		46.05			
Schorlomite	-		0.21			
% cations assigned to garnet molecules	99.00		99.54			

★ – denotes calculated Fe_2O_3 value

Table 39 Garnet and ilmenite analyses - Ultramafite intrusions.

B. Mafic gabbros

	ED1	ED2	ED3	ED4	ED5	ED6	
OXIDES (Wt%)							
SiO_2	47.28	49.26	48.69	45.85	46.51	47.81	SiO_2
TiO_2	1.17	1.51	0.90	1.16	1.89	1.41	TiO_2
Al_2O_3	12.95	12.09	14.37	15.25	14.13	15.04	Al_2O_3
Fe_2O_3	6.07	17.39	13.79	16.33	18.79	17.53	Fe_2O_3
FeO	9.06						FeO
MnO	0.25	0.25	0.21	0.24	0.27	0.26	MnO
MgO	7.86	6.07	8.20	8.55	7.30	6.75	MgO
CaO	13.01	11.06	12.49	12.73	12.67	12.30	CaO
Na_2O	1.63	1.76	1.26	0.13	0.22	0.06	Na_2O
K_2O	0.14	0.10	0.03	0.61	0.10	0.24	K_2O
TOTAL	99.42	99.49	99.94	100.85	101.88	101.40	TOTAL
C.I.P.W. NORM.							
qtz	1.02						qtz
or	0.83						or
ab	13.79						ab
an	27.61						an
di	29.94						di
hyp(En)	15.21(64.0)						hyp(En)
mt	8.80						mt
il	2.22						il
Fe_2/Fe_2+Fe_3	.630						Fe_2/Fe_2+Fe_3
∢FeO/∢FeO+MgO	.649	.721	.602	.632	.698	.700	∢FeO/∢FeO+MgO
DIFF. IND.	15.64						DIFF. IND.
SI. UNSAT.	-						SI. UNSAT.
TOTAL NORMATIVE FELDSPAR	42.23						TOTAL NORMATIVE FELDSPAR
NORMATIVE ANORTHITE CONTENT OF FELDSPAR	65.38						NORMATIVE ANORTHITE CONTENT OF FELDSPAR

Table 40 Mafic gabbro and ultramafite dykes (d_1 & d_2) intrusive into the anorthosite - Whole rock analyses and C.I.P.W. norm

C. Others

	(a)	
	AD1	AD2
OXIDES (Wt%)		
SiO_2	54.22	54.76
TiO_2	0.40	0.57
Al_2O_3	20.87	22.17
Fe_2O_3	7.73	1.23
FeO		3.81
MnO	0.11	0.07
MgO	4.45	4.20
CaO	9.32	9.57
Na_2O	3.45	3.83
K_2O	0.35	0.22
TOTAL	100.90	100.43
Sr(ppm)	655	1229
Rb(ppm)	n.d.	2
Cr(ppm)	80	100
C.I.P.W. NORM.		
qtz		3.56
or		1.30
ab		32.41
an		42.66
ne		–
di		3.90
hyp(En)		13.74(67.35)
ol (Fo)		–
mt		1.78
il		1.08
Fe_2/Fe_2+Fe_3		.778
ΣFeO/ΣFeO+MgO	.610	.539
DIFF. IND. SI. UNSAT.		37.26
TOTAL NORMATIVE FELDSPAR		76.36
NORMATIVE ANORTHITE CONTENT OF FELDSPAR		55.86

	(b)		
	EPIDOTE		
EPIDOTIC VEIN	CENTRE	RIM	
38.51	38.10	38.31	
0.21	-	-	
26.06	26.14	24.49	
9.41	9.54	12.09	
0.10	0.11	0.08	
0.44	0.06	0.06	
26.23	23.89	23.91	
0.33	-	-	
0.10	-	-	
101.39	97.84	98.94	
1008			
2			
300			
UNIT FORMULA			
Si 3.116	3.116	3.126	3.126
Al			
Al 2.520		2.355	
Fe^{3+} .587	3.107	.742	3.097
Mg .007		.007	
Ca 2.093	2.108	2.090	2.103
Mn .008		.006	
O 13.000		13.000	
.951			

							(c)	
SA1	SA2	SA3	SA4	SA5	SA6	SA7		
53.15	53.91	54.25	53.88	55.06	56.18	50.88	SiO_2	
0.10	0.07	0.03	0.03	0.08	0.09	0.17	TiO_2	
29.24	28.26	28.65	29.03	25.04	25.13	27.23	Al_2O_3	
0.27	0.72	0.88	0.75	4.38	1.34	4.04	Fe_2O_3	
0.47							FeO	
0.01	0.01	0.02	0.02	0.11	0.02	0.08	MnO	
0.02	0.49	0.59	0.63	1.79	1.15	2.40	MgO	
11.87	10.95	11.59	11.54	7.86	9.43	11.55	CaO	
4.56	5.12	4.87	4.30	5.83	5.59	2.48	Na_2O	
0.36	0.17	0.16	0.16	0.40	0.26	0.23	K_2O	
100.05	99.70	101.04	100.34	100.55	99.19	99.06	TOTAL	
948	925	–	–	–	1065	–	Sr(ppm)	
–	–	–	–	–	3	–	Rb(ppm)	
–	–	–	–	–	80	–	Cr(ppm)	
C.I.P.W. NORM.								
–							qtz	
2.13							or	
38.04							ab	
58.26							an	
0.29							ne	
0.55							di	
–							hyp(En)	
0.19(10.64)							ol (Fo)	
0.39							mt	
0.19							il	
.664							Fe_2/Fe_2+Fe_3	
.973	.569	.573	.517	.688	.512	.602	ΣFeO/ΣFeO+MgO	
40.46							DIFF. IND. SI. UNSAT.	
0.31								
98.43							TOTAL NORMATIVE FELDSPAR	
59.02							NORMATIVE ANORTHITE CONTENT OF FELDSPAR	

Table 41 a) Anorthositic-gabbro dykes from the anorthosite complex. Whole rock analyses and C.I.P.W. norm.
b) Epidote veins cutting the banded ultramafites and mafic gabbros from the gabbroic rim of the anorthosite. Whole rock analysis and mineral analyses of epidote.
c) Anorthosite intrusions associated with brecciated areas along and adjacent to the margin of the anorthosite. Whole rock analyses and C.I.P.W. norm.

	PLAGIOCLASE FELDSPAR		SCAPOLITE		
	SA1			SA1	
	av.18			av.3	
SiO_2	48.43		SiO_2	54.35	
Al_2O_3	34.68		Al_2O_3	25.09	
CaO	12.48		FeO	0.113	
Na_2O	4.73		MnO	0.016	
K_2O	0.15		MgO	0.033	
TOTAL	100.47		CaO	13.22	
			Na_2O	3.73	
UNIT FORMULA			K_2O	0.25	
Si	8.794		TOTAL	96.80	
Al	7.424				
Ca	2.428		UNIT FORMULA		
Na	1.665		Si	7.624	11.774
K	.035		Al	4.150	
O	32.000		Fe	.001	3.057
			Mn	.002	
Z	16.22		Mg	.007	
X	4.13		Ca	1.987	
			Na	1.015	
Ab	40.33		K	.045	
An	58.82		O	24.000	
Or	0.85				
			Me%	65.32	

Table 42 Feldspar and Scapolite analyses from the anorthosite intrusions

⑤ PARAGNEISSES

	PP1	PP2	PP3	PP4	PP5	PP6	PP7	PP8	PP9	
OXIDES (Wt%)										
SiO_2	70.49	72.33	72.17	72.63	73.55	72.34	65.07	66.58	71.84	SiO_2
TiO_2	0.44	0.37	0.32	0.50	0.53	0.47	0.56	0.13	0.32	TiO_2
Al_2O_3	14.10	13.63	13.48	12.71	12.65	12.83	16.56	19.85	13.61	Al_2O_3
Fe_2O_3	1.42	4.76	5.16	4.18	3.81	3.45	5.12	1.50	5.11	Fe_2O_3
FeO	2.83									FeO
MnO	0.09	0.10	0.06	0.04	0.03	0.03	0.10	0.02	0.06	MnO
MgO	0.77	0.87	1.38	1.07	1.25	1.20	1.80	0.99	1.46	MgO
CaO	4.45	4.46	4.35	4.08	3.08	3.53	4.94	6.63	4.38	CaO
Na_2O	3.70	3.33	2.67	2.78	3.42	3.70	4.01	5.28	2.87	Na_2O
K_2O	0.36	0.23	0.53	0.18	1.12	0.42	1.88	0.43	0.53	K_2O
TOTAL	98.65	100.08	100.12	98.37	99.44	97.97	100.04	101.41	100.18	TOTAL
C.I.P.W. NORM.										
qtz	35.60									
or	2.13									
ab	31.31									
an	20.81									
di	1.07									
hyp	4.84									
mt	2.06									
il	0.84									
Fe_2/Fe_2+Fe_3	.696									
∑FeO/∑FeO+MgO	.842									
TOTAL NORMATIVE FELDSPAR	54.24									
NORMATIVE ANORTHITE CONTENT OF FELDSPAR	38.36									

Table 43 Paragneisses (garnet-biotite quartzites) - Whole rock analyses and C.I.P.W. norm

APPENDIX 2

SAMPLE LOCALITIES FOR ANALYSED ROCKS

fig. 1. ULTRAMAFITES & MAFIC GABBROS FROM THE GABBROIC RIM OF THE ANORTHOSITE

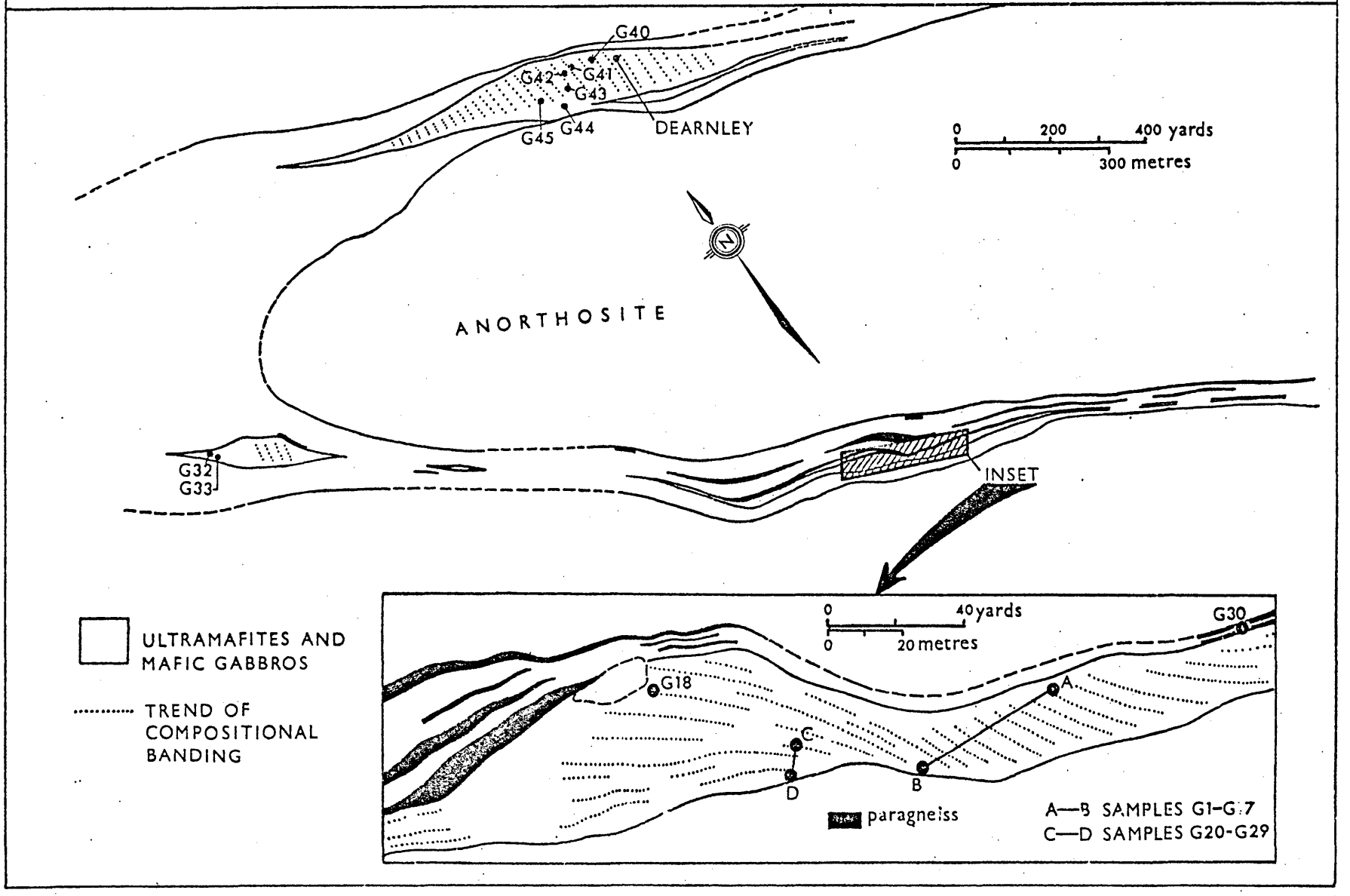
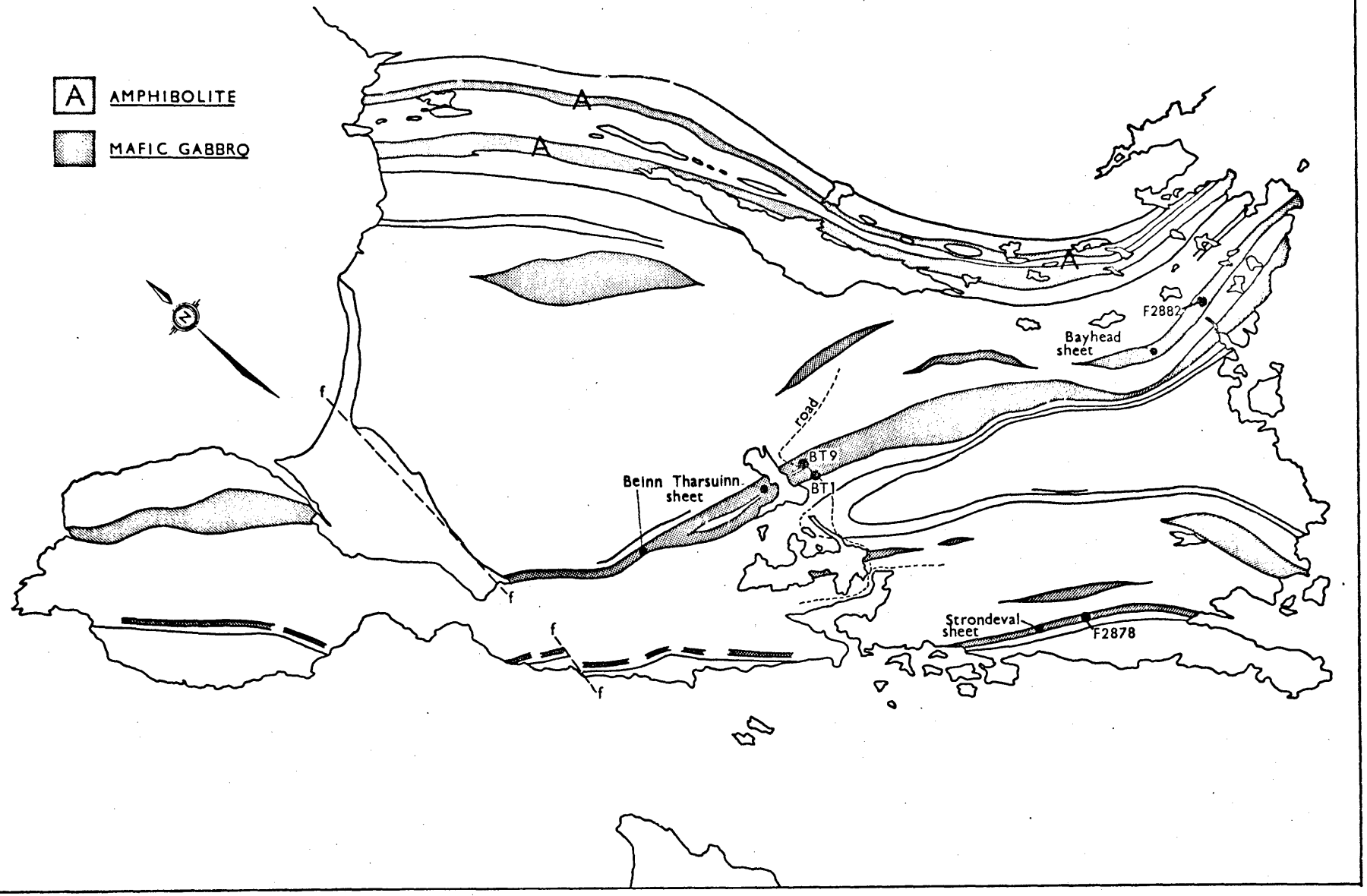


fig. 2 MAFIC GABBRO SHEETS



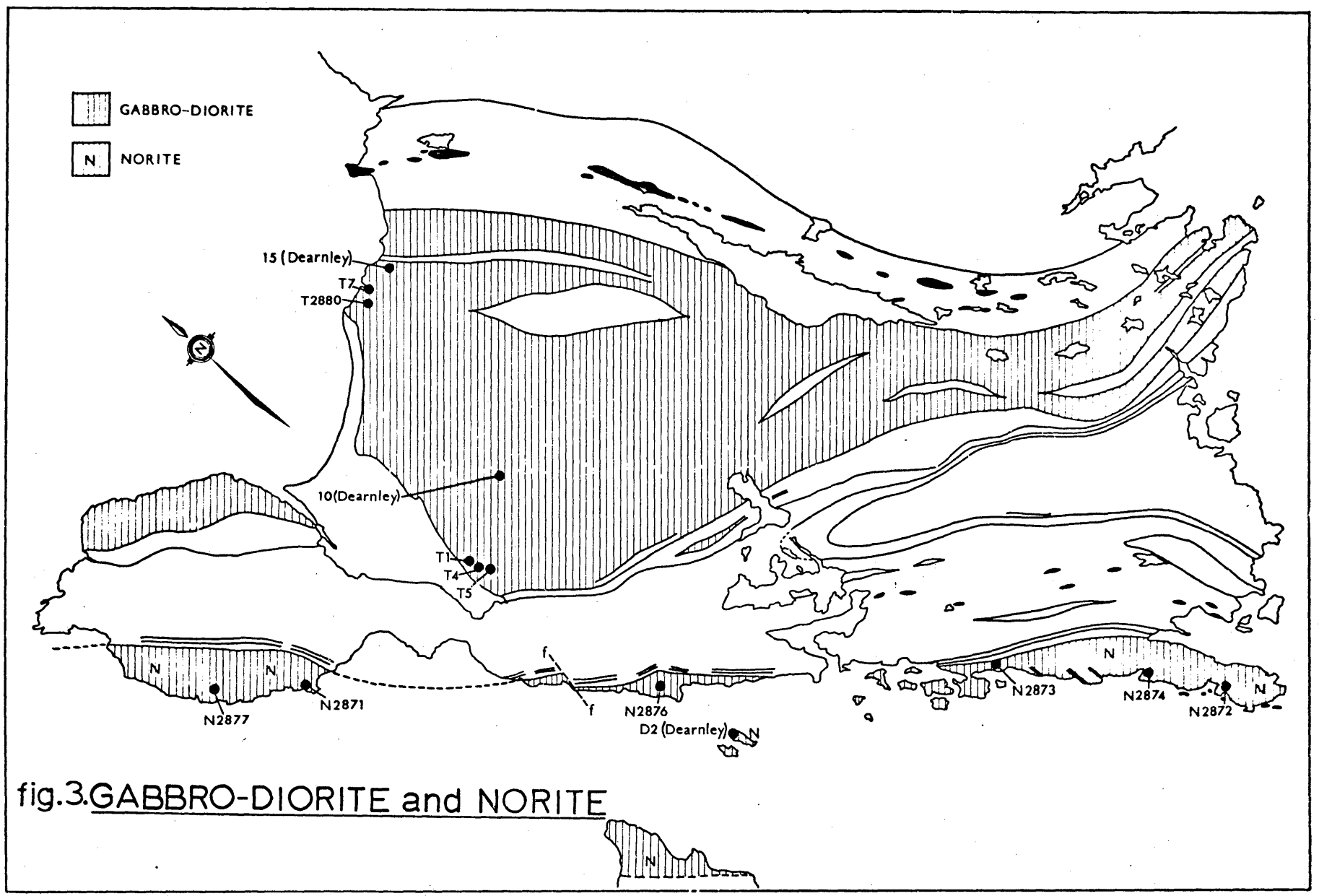
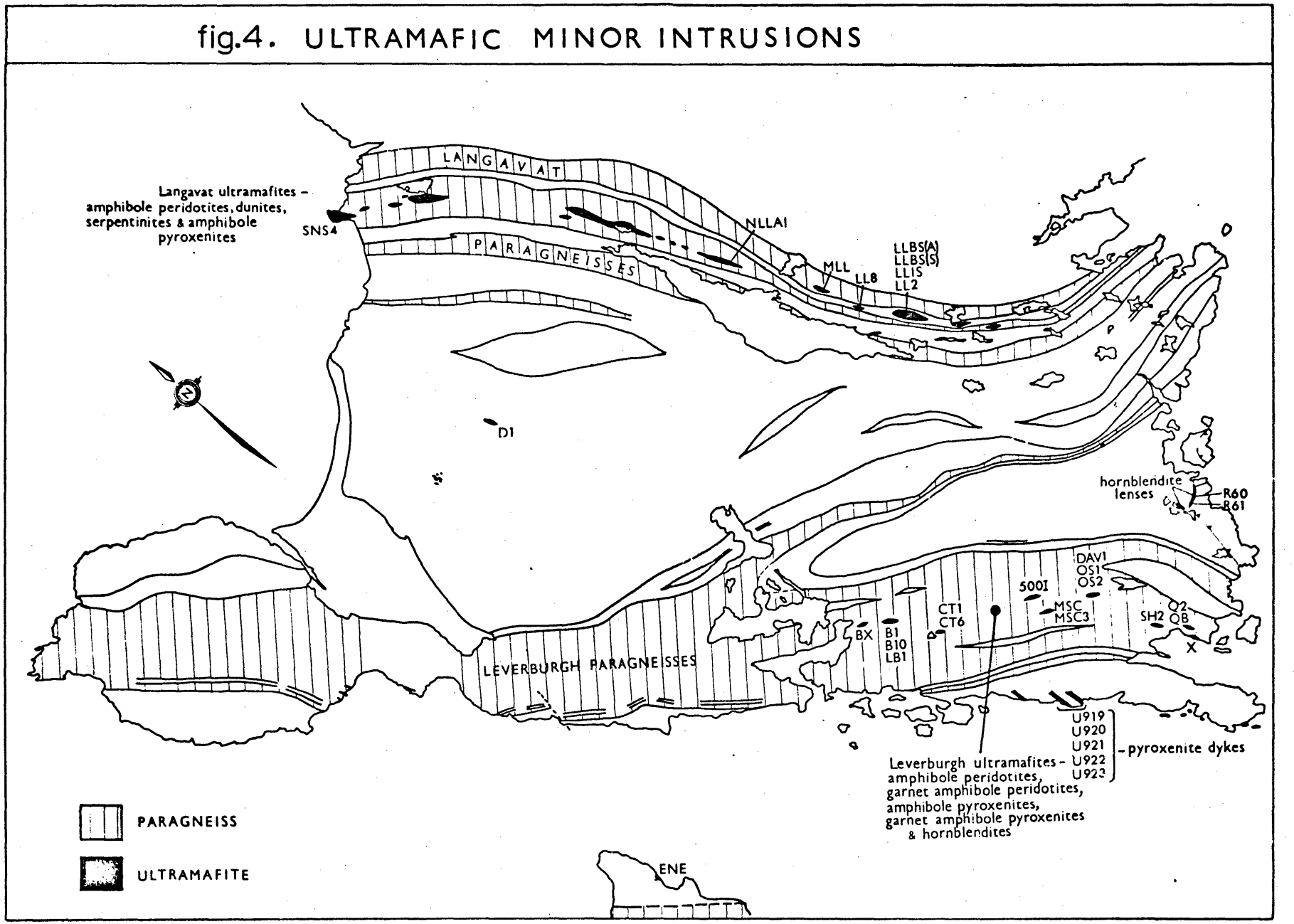


fig.3.GABBRO-DIORITE and NORITE

fig.4. ULTRAMAFIC MINOR INTRUSIONS



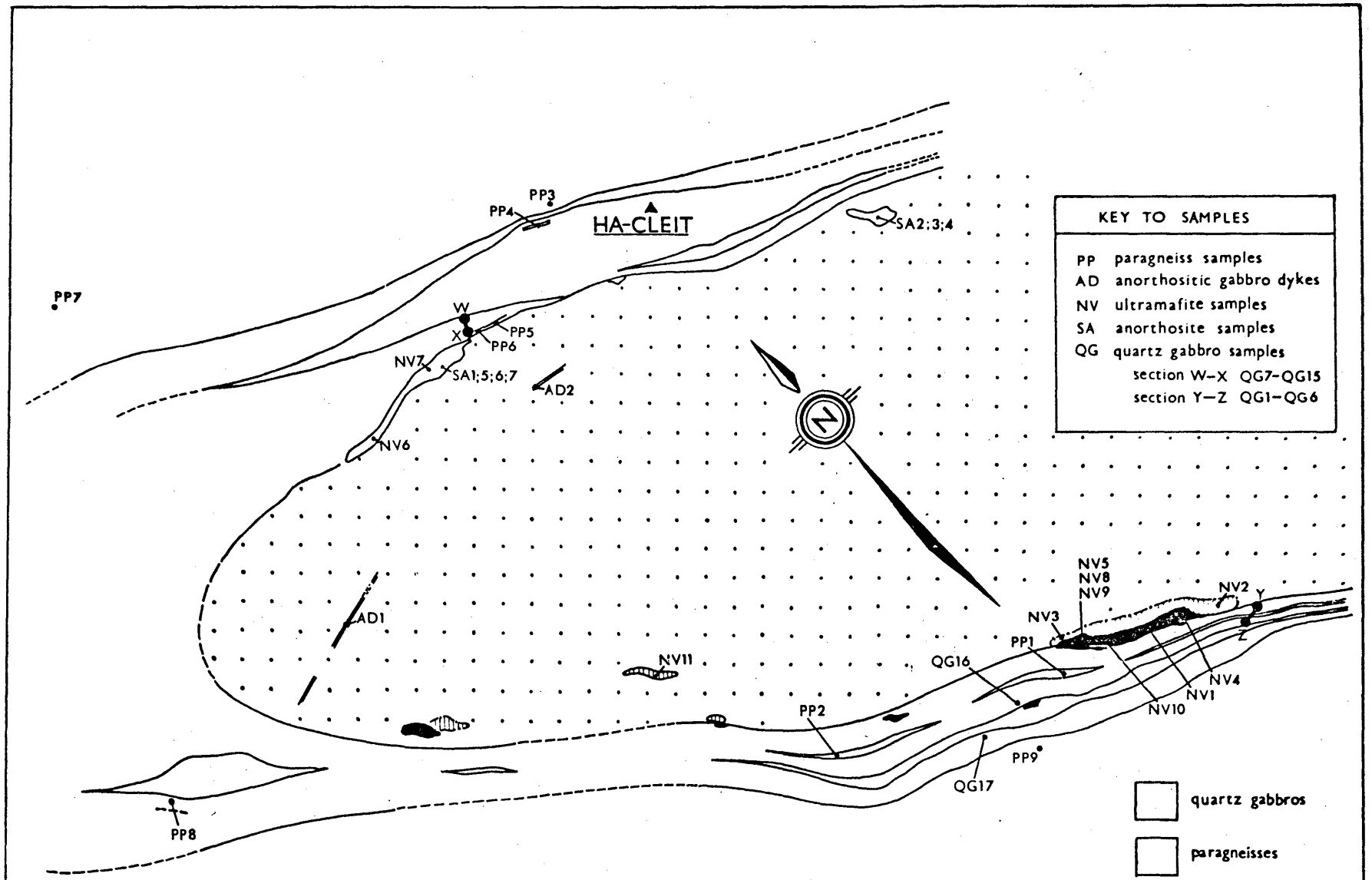
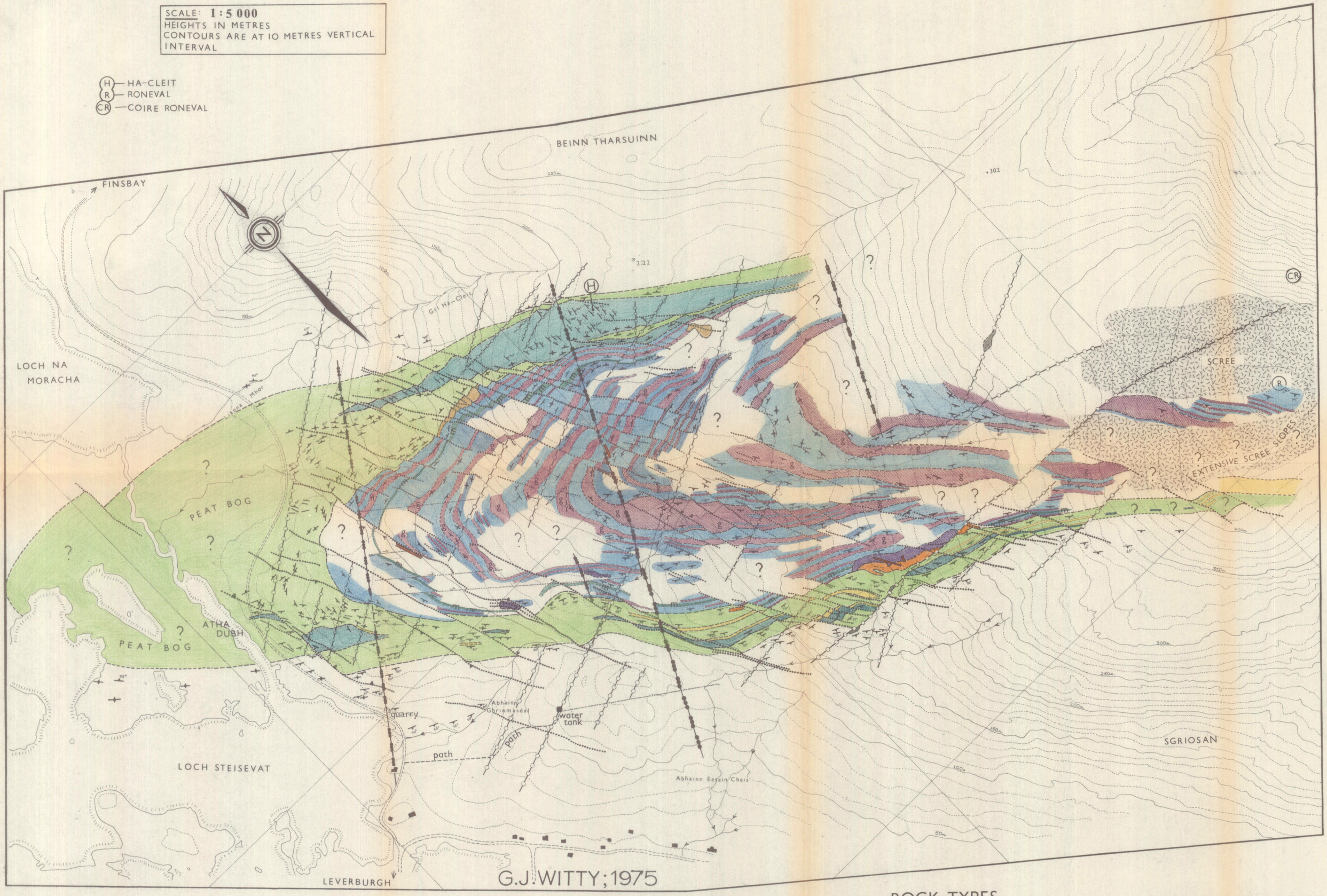


fig.5. QUARTZ GABBROS, PARAGNEISSES & MINOR INTRUSIVES.
north-east end of anorthosite complex

MAP 1. THE ANORTHOSITE COMPLEX north east of RONEVAL SUMMIT

SCALE: 1:5 000
HEIGHTS IN METRES
CONTOURS ARE AT 10 METRES VERTICAL INTERVAL

(H) — HA-CLEIT
(R) — RONEVAL
(CR) — COIRE RONEVAL



G.J. WITTY; 1975

BASE MAP:— ORDANANCE SURVEY 1:10 000

LEGEND

- LITHOLOGICAL CONTACT - OBSERVED
- LITHOLOGICAL CONTACT - INFERRED CERTAIN
- LITHOLOGICAL CONTACT - INFERRED UNCERTAIN
- DIP & STRIKE OF FOLIATIONS
- VERTICAL FOLIATIONS
- DIP & STRIKE OF BANDING
- F_3 EARLY LAXFORDIAN SHEARS
- F_4 LATE LAXFORDIAN SHEARS
- F_5 TERTIARY FAULTS
- DISPLACEMENTS (FAULTS OR SHEARS) OF UNCERTAIN AGE

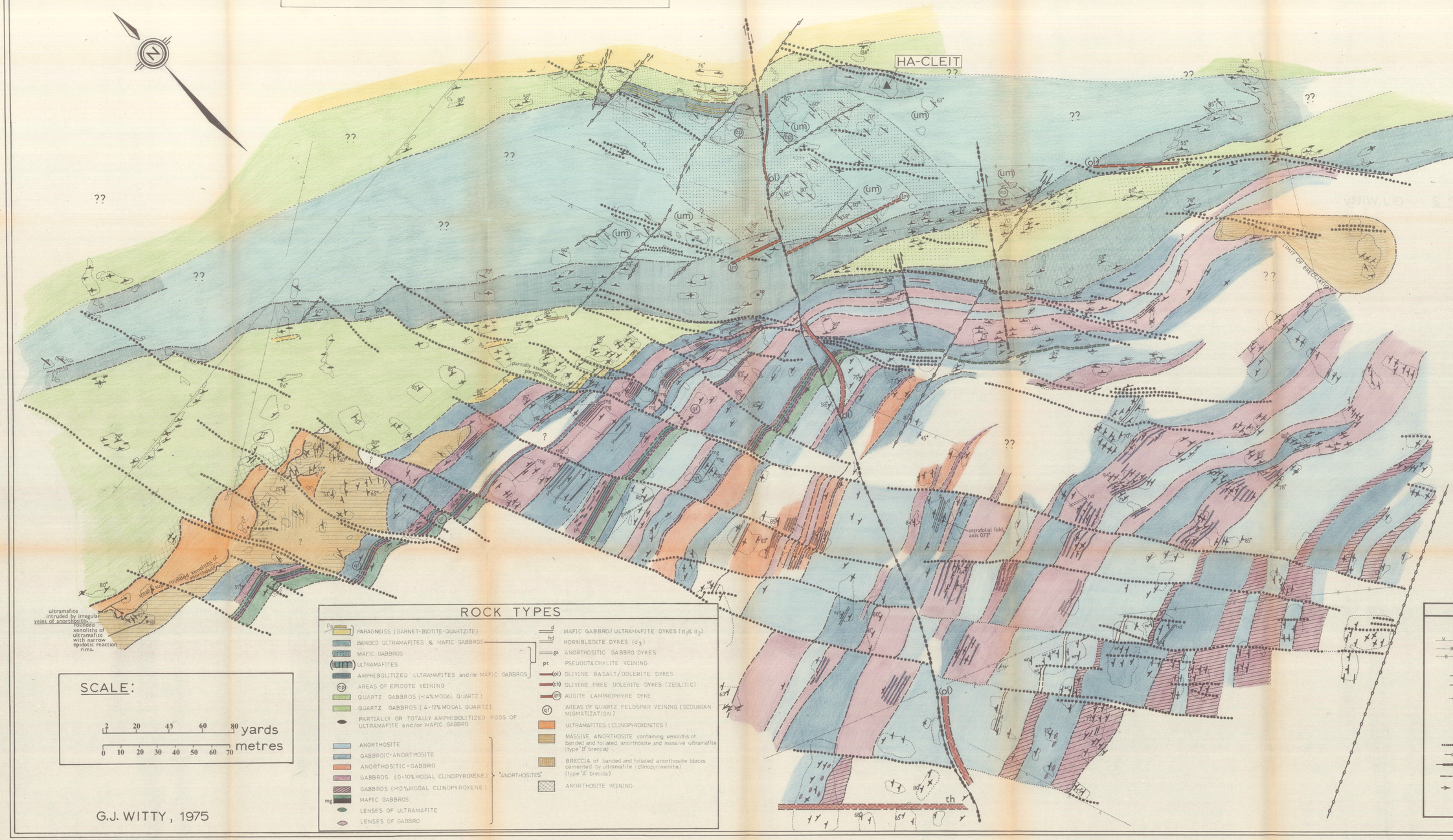
ROCK TYPES

- GARNET BIOTITE QUARTZITE (PARAGNEISS)
- BANDED ULTRAMAFITES & MAFIC GABBROS
- QUARTZ GABBROS
- INTRUSIONS OF MASSIVE ULTRAMAFITE (CLINOPYROXENITES & GARNET CLINOPYROXENITES) CONTAINING GARNETITE NODULES
- TYPE 'A' BRECCIA
- TYPE 'B' BRECCIA
- TERTIARY DOLERITE DYKES
- ALKALI PEGMATITES

THE ANORTHOSITE BODY

- ANORTHOSITES & GABBROIC ANORTHOSITES — a
- GABBROS & ANORTHOSITIC GABBROS
  - Cpx < 10 % — g
  - Cpx > 10 % — g
- MAFIC GABBROS — m

MAP 2 THE ANORTHOSITE COMPLEX
east and south-east of HA-CLEIT SUMMIT



ROCK TYPES

- Pg PARAGNEISS (GARNET-BIOTITE-QUARTZITE)
- BANDED ULTRAMAFITES & MAFIC GABBROS
- MAFIC GABBROS
- (um) ULTRAMAFITES
- AMPHIBOLITIZED ULTRAMAFITES and/or MAFIC GABBROS
- (ep) AREAS OF EPIDOTE VEINING
- QUARTZ GABBROS (<4% MODAL QUARTZ)
- QUARTZ GABBROS (4-12% MODAL QUARTZ)
- PARTIALLY OR TOTALLY AMPHIBOLITIZED PODS OF ULTRAMAFITE and/or MAFIC GABBRO

"ANORTHOSITES"
- ANORTHOSITE
- GABBROIC-ANORTHOSITE
- ANORTHOSITIC-GABBRO
- GABBROS (0-10% MODAL CLINOPYROXENE)
- GABBROS (>10% MODAL CLINOPYROXENE)
- mg MAFIC GABBROS
- LENSES OF ULTRAMAFITE
- LENSES OF GABBRO

- d1 MAFIC GABBRO/ULTRAMAFITE DYKES (d_1 & d_2)
- hd HORNBLEDITE DYKES (d_3)
- ga ANORTHOSITIC GABBRO DYKES
- pt PSEUDOTACHYLITE VEINING
- (ol) OLIVINE BASALT/DOLERITE DYKES
- (th) OLIVINE FREE DOLERITE DYKES (ZEOLITIC)
- (lm) AUGITE LAMPROPHYRE DYKE
- (qf) AREAS OF QUARTZ FELDSPAR VEINING (SCOURIAN MIGMATIZATION)
- ULTRAMAFITES (CLINOPYROXENITES)
- MASSIVE ANORTHOSITE containing xenoliths of banded and foliated anorthosite and massive ultramafite (type 'B' breccia)
- BRECCIA of banded and foliated anorthosite blocks cemented by ultramafite (clinopyroxenite) (type 'A' breccia)
- ANORTHOSITE VEINING

SCALE:

2 20 40 60 80 yards

0 10 20 30 40 50 60 70 metres

G.J. WITTY, 1975

KEY TO SYMBOLS

- sp SAMPLE LOCALITY
- V V HOLLOW BREAK OF SLOPE
- X X HOLLOW
- II RIDGE
- OUTLINE OF EXPOSURE
- LITHOLOGICAL CONTACT - OBSERVED
- LITHOLOGICAL CONTACT - INFERRED CERTAIN
- LITHOLOGICAL CONTACT - INFERRED UNCERTAIN
- 59° DIP & STRIKE OF FOLIATION
- VERTICAL FOLIATION
- 57° DIP & STRIKE OF BANDING
- F_3 EARLY LAXFORDIAN SHEARS
- F LATE LAXFORDIAN SHEARS
- F_5 TERTIARY FAULTS
- LIMIT OF AMPHIBOLITISATION; BANDED ULTRAMAFITES & MAFIC GABBROS
- FOLDS & FOLD STYLES

ROCK TYPES

Pa — Paragneiss (garnet-biotite quartzite)

Banded ultramafites & mafic gabbros

Mafic gabbros

Clinopyroxene rich ultramafites

Garnet and/or amphibole rich ultramafites

Amphibolitized ultramafites and or mafic gabbros

Quartz gabbros (<4% modal quartz)

Quartz gabbros (4-12% modal quartz)

partially or totally amphibolitized pods of ultramafite and/or mafic gabbro

ql — quartz lenses

pt — pseudotachylite veining

sa — saussuritized rocks

Ultramafites (clinopyroxenites & garnet clinopyroxenites containing garnetite nodules)

Anorthosite breccia (type 'A' breccia cemented by ultramafite)

Mafic gabbro

Gabbro

Gabbroic anorthosite — lower zone 'anorthosites'

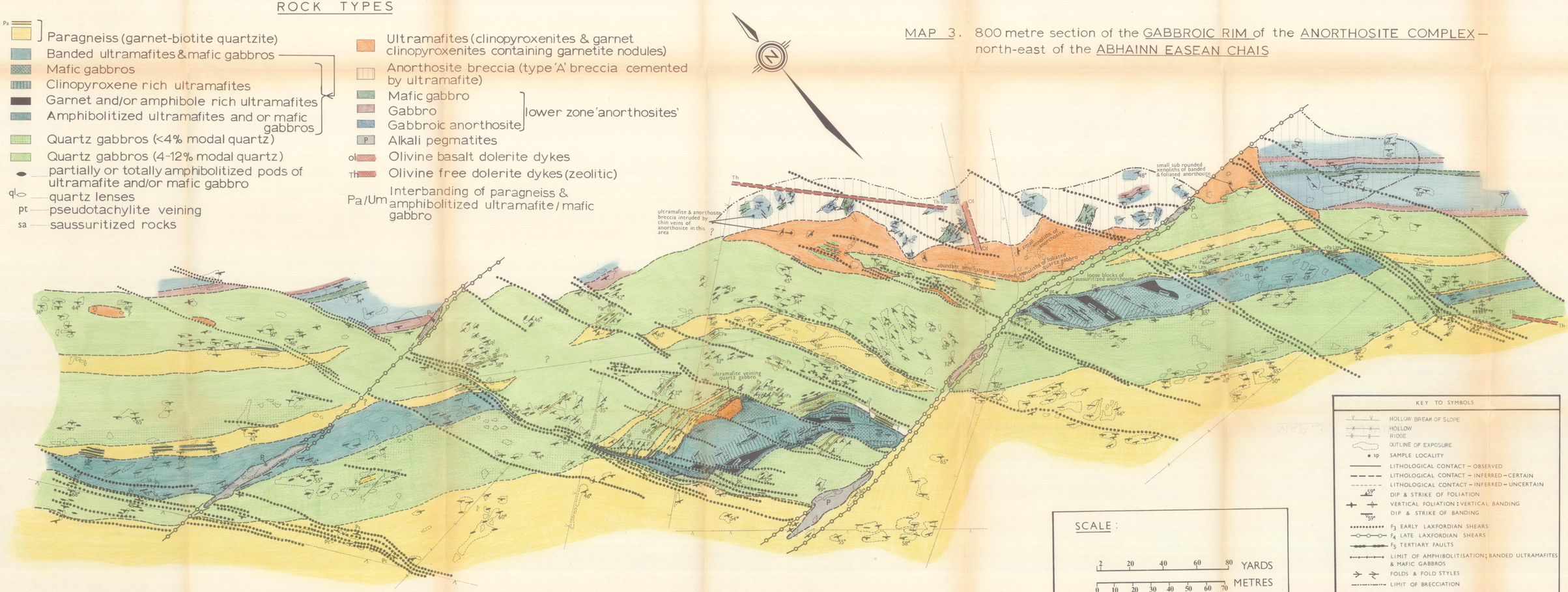
P — Alkali pegmatites

ol — Olivine basalt dolerite dykes

Th — Olivine free dolerite dykes (zeolitic)

Pa/Um — Interbanding of paragneiss & amphibolitized ultramafite / mafic gabbro

MAP 3. 800 metre section of the GABBROIC RIM of the ANORTHOSITE COMPLEX — north-east of the ABHAINN EASEAN CHAIS



G.J. WITTY, 1975

ROCK TYPES

- anorthosite : 0-10% mafic minerals
- gabbroic anorthosite : 10-20% mafic minerals
- anorthositic gabbro : 20-35% mafic minerals
- amphibole gabbros
- clinopyroxene gabbros
  (35-65% mafic minerals)
- mafic gabbro : 65-90% mafic minerals
- mafic gabbro bands > 30cms
- d — mafic gabbro dykes (d_1 & d_2)
- hb/d — hornblendite dykes (d_3)
- ultramafite lenses
- gabbro lenses

MAP 4

THE ANORTHOSITE - sample localities - east & south-east of Ha-Cleit summit. (Scale 1:88)

